A new computational approach for fluid-structure interaction of slender bodies immersed in three-dimensional flows

Fabien Lespagnol

POLITECNICO DI MILANO
DEPARTMENT OF MATHEMATICS
MOX LABORATORY

SORBONNE UNIVERSITÉ
LABORATOIRE JACQUES-LOUIS LIONS
INRIA PARIS

A NEW COMPUTATIONAL APPROACH FOR FLUID-STRUCTURE INTERACTION OF SLENDER BODIES IMMERSED IN THREE-DIMENSIONAL FLOWS

Doctoral Dissertation presented by **Fabien Lespagnol**,
publicly defended on **June 26, 2024**,
supported by **Università Italo Francese, Bando Vinci 2019**.

Reviewers:
Astrid DECOENE (Université de Bordeaux)
Alexander POPP (Universität der Bundeswehr München)

Defense committee:

Xavier CLAEYS (Sorbonne Université)	*Examiner*
Astrid DECOENE (Université de Bordeaux)	*Reviewer*
Lucia GASTALDI (Università degli studi di Brescia)	*Examiner*
Luca FORMAGGIA (Politecnico di Milano)	*Chairman of the committee*
Alexander POPP (Universität der Bundeswehr München)	*Reviewer*

Co-supervisors:
Miguel A. FERNANDEZ (Sorbonne Université / Inria Paris)
Paolo ZUNINO (Politecnico di Milano)

Co-advisors:
Muriel BOULAKIA (Université Versailles Saint-Quentin-en-Yvelines)
Céline GRANDMONT (Sorbonne Université / Inria Paris / Université Libre de Bruxelles)

Mathematical Models and Methods in Engineering – 2024 - - Cycle XXXVI

SUMMARY. This PhD dissertation aims to develop a new modelling and computational approach for the simulation of slender bodies immersed in three dimensional flows (3D). Thanks to the special geometric configuration of the slender structures, we can model this problem by mixed-dimensional coupled equations in which the solid balance equations are formulated in a one-dimensional (1D) domain. Addressing these types of problems presents several challenges. From a mathematical perspective, the main two difficulties involve defining well-posed trace operators of co-dimension two (from the 3D to the 1D domain) and ensuring the accuracy of solutions obtained with the mixed-dimensional formulation when compared to the fully 3D one. From a computational point of view, the non-standard mathematical formulation of the coupled problem makes it difficult to guarantee the convergence of the discrete solutions with standard numerical approaches. The main advantages of the approach we present in this manuscript lies in its strong mathematical basis. Indeed, while many standard mixed-dimensional formulations yield solutions with poor regularity due to ill-posed trace operators, our reduced order method generates solutions within standard Hilbert spaces. This facilitates the application of Galerkin projection-based approximation methods such as the finite element method (FEM).

In the second chapter, we establish the continuous formulation of the 3D fluid-structure interaction coupled problem using incompressible Navier-Stokes equations for the description of the fluid dynamics and a linear Timoshenko beam model for modeling the response of the slender structure. These two models are coupled with a mixed-dimensional version of fluid-structure interface conditions, combining the fictitious domain (FD) approach with the projection of kinematic coupling conditions onto a finite-dimensional Fourier space via Lagrange multipliers. We then develop a discrete formulation based on the finite element method and a semi-implicit treatment of the Dirichlet-Neumann coupling conditions, employing a partitioned procedure for the resolution of the fluid-structure interaction problem. We establish the energy stability of the scheme and provide extensive numerical evidence of the accuracy and robustness of the discrete formulation, notably with respect to a full order model with standard coupling conditions.

In the third and fourth chapter we conduct a mathematical analysis on the approximation error of our reduced order coupled method, examining both the modeling and numerical approximation errors resulting from the mixed-dimensional formulation and the fictitious domain finite element method, respectively. We explore these aspects in two simplified frameworks. We first consider a two-dimensional Poisson problem (2D) with a fixed immersed boundary and non-homogeneous Dirichlet boundary conditions. We then extend this analysis to the 2D stationary Stokes problem with rigid-body Dirichlet boundary conditions on the immersed interface. In both cases, after proving the existence of solutions for the reduced order problem, we prove its convergence, when the size of the obstacle is small, to the full order problem with standard Dirichlet boundary conditions. In

particular, our estimates highlight the need to consider enough Fourier modes to achieve convergence on the Lagrange multipliers, which is an essential aspect in addressing the fluid-structure interaction coupled problem. Subsequently, the numerical discretization of the reduced order problem is analyzed. As standard for this family of methods, the convergence obtained with the fictitious domain finite element method is sub-optimal, due to the discontinuity of the solution at the interface. Furthermore, the stability and accuracy of the scheme depend on the ratio between the mesh size and the obstacle size, which can be restrictive for very small obstacles. To address the limitations of the fictitious domain approach, we propose and analyze two modified finite element method, one stabilized and one augmented. Finally, we develop a 2D fluid-structure interaction formulation where small particles are immersed in a Stokesian flow, applying reduced order interface coupling conditions. The properties of the reduced order model and the corresponding numerical methods are illustrated by some numerical experiments.

Using a semi-implicit scheme for the resolution of the 3D fluid-structure interaction problem requires to iterate over the fluid and solid solvers multiple times, which can be computationally expensive. The most efficient approach for the time discretization of the fluid-structure interaction problem would be to adopt an explicit coupling scheme, solving this way the fluid and structure sub-problems only once per time step. However, for standard (Dirichlet-Neumann) explicit coupling schemes, a large fluid/solid density ratio combined with a slender and lengthy geometry gives rise to unconditional numerical instability. Subsequently, in the last chapter, we introduce a Robin-based loosely coupled scheme specifically designed for 3D mixed-dimensional formulation and prove its unconditional stability. We also provide numerical evidence of the accuracy of the explicit scheme through several test cases.

RÉSUMÉ Ce projet de doctorat a pour objectif de développer une nouvelle approche computationnelle pour la simulation de corps élancés immergés dans un écoulement tridimensionnel (3D). Grâce à la configuration géométrique particulière des structures élancées, nous pouvons modéliser ce problème par des équations couplées en dimensions mixtes pour lesquelles les équations d'équilibre du solide sont formulées dans un domaine unidimensionnel (1D). Ce type de problèmes pose plusieurs difficultés à surmonter. D'un point de vue mathématique, ils impliquent de définir des opérateurs de trace bien posés de codimension deux (du domaine 3D au domaine 1D) mais aussi de garantir que les solutions obtenues avec la formulation mixte sont proches de celles obtenues avec une formulation complètement 3D. D'un point de vue computationnel, la formulation mathématique non classique du problème couplé rend également difficile de garantir la convergence des solutions discrètes avec des approches numériques classiques. Les principaux avantages de l'approche que nous présentons dans ce manuscrit résident dans sa solide base mathématique. En effet, tandis que de nombreuses formulations mixtes donnent des solutions avec une faible régularité en raison d'opérateurs de trace mal posés, notre méthode réduite génère des solutions dans des espaces de Hilbert classiques. Cela facilite l'application de méthodes d'approximation basées sur la projection de Galerkin telles que la méthode des éléments finis (MEF).

Dans le deuxième chapitre, nous établissons la formulation continue du problème couplé 3D d'interaction fluide-structure en considérant les équations de Navier-Stokes incompressibles pour la description de la dynamique du fluide et un modèle de poutre linéaire de Timoshenko pour la modélisation de la réponse de la structure élancée. Ces modèles sont couplés avec une version en dimensions mixtes des conditions d'interface fluide-structure, associant l'approche de domaine fictif (DF) avec la projection des conditions de couplage cinématique sur un espace de Fourier de dimension finie via des multiplicateurs de Lagrange. Nous développons ensuite une formulation discrète basée sur la méthode des éléments finis et un traitement semi-implicite des conditions de couplage Dirichlet-Neumann, en utilisant une procédure partitionnée pour la résolution du problème d'interaction fluide-structure. Nous établissons la stabilité énergétique du schéma et fournissons des preuves numériques détaillées sur la précision et la robustesse de la formulation discrète, notamment par rapport à un modèle complet avec des conditions de couplage fluide-structure classiques.

Dans les troisième et quatrième chapitres, nous effectuons une analyse mathématique sur l'erreur d'approximation de notre méthode réduite couplée, en examinant les erreurs de modélisation et d'approximation numériques résultant respectivement de la formulation en dimensions mixtes et de la méthode des éléments finis avec domaine fictif. Nous explorons ces aspects dans deux cadres simplifiés. Nous considérons d'abord un problème de Poisson 2D avec une frontière immergée statique et des conditions aux bords de Dirichlet non homogènes. Nous étendons ensuite cette analyse au problème de Stokes bidimen-

sionnel stationnaire avec des conditions aux bords de type solides rigides sur l'interface immergée. Dans les deux cas, après avoir prouvé l'existence de solutions pour le problème réduit, nous prouvons sa convergence, lorsque la taille de l'obstacle tend vers zéro, vers le problème complet avec des conditions aux bords de Dirichlet classiques. En particulier, nos estimations mettent en évidence la nécessité de considérer suffisamment de modes de Fourier pour obtenir une convergence sur les multiplicateurs de Lagrange, ce qui est un aspect essentiel pour l'analyse du problème couplé d'interaction fluide-structure. Ensuite, nous analysons la discrétisation numérique du problème réduit. De façon assez classique pour cette famille de méthodes, la convergence obtenue avec la méthode des éléments finis avec domaine fictif est sous-optimale, en raison de la discontinuité de la solution à l'interface. De plus, la stabilité et la convergence du schéma dépend du rapport entre la taille du maillage et la taille de l'obstacle, ce qui peut être contraignant pour des obstacles de très petite taille. Pour pallier les limites de l'approche domaine fictif, nous proposons et analysons deux méthodes éléments finis alternatives, une méthode stabilisée et une méthode enrichie. Enfin, nous développons une formulation d'interaction fluide-structure 2D où de petites particules sont immergées dans un écoulement de Stokes, en appliquant des conditions de couplage d'interface réduites. Les propriétés du modèle réduit et des méthodes numériques correspondantes sont illustrées par des exemples numériques.

L'utilisation d'un schéma semi-implicite pour la résolution du problème d'interaction fluide-structure 3D exige d'itérer de nombreuses fois sur les solveurs fluide et solide, ce qui peut être coûteux en termes de temps de calcul. L'approche la plus efficace pour la discrétisation temporelle du problème d'interaction fluide-structure consisterait à adopter un schéma de couplage explicite, permettant ainsi de résoudre les sous-problèmes fluide et solide une seule fois par pas de temps. Cependant, pour les schémas de couplage explicite classiques (Dirichlet-Neumann), un rapport élevé entre la densité du fluide et la densité du solide associé à une géométrie mince amène souvent à de l'instabilité numérique. Par conséquent, dans le dernier chapitre, nous introduisons un schéma faiblement couplé qui repose sur des conditions d'interface de Robin spécifiquement conçu pour une formulation 3D en dimensions mixtes et prouvons sa stabilité inconditionnelle. Nous fournissons également des preuves numériques de la précision du schéma explicite par plusieurs cas test.

SOMMARIO Questa tesi di dottorato ha come obiettivo lo sviluppo di un nuovo approccio computazionale per la simulazione di corpi slanciati immersi in un flusso tridimensionale (3D). Sfruttando la particolare configurazione geometrica delle strutture slanciate, è possibile modellizzare il problema tramite equazioni accoppiate con dimensioni miste, in cui le equazioni di bilancio del solido sono formulate in un dominio unidimensionale (1D). Questo tipo di problemi presenta diverse difficoltà. Da un punto di vista matematico, si tratta di definire degli operatori di traccia ben definiti di codimensione due (dal dominio 3D al dominio 1D) oltre al garantire che le soluzioni ottenute con la formulazione in dimensioni miste siano vicine a quelle ottenute con una formulazione completamente 3D. Dal punto di vista computazionale, la formulazione matematica non convenzionale del problema accoppiato rende difficile garantire la convergenza delle soluzioni discrete con approcci numerici classici. In effeti, molte formulazioni miste producono soluzioni con scarsa regolarità a causa di operatori di tracia mal definiti, il nostro metodo ridotto genera soluzioni in spazi di Hilbert classici. Questo facilita l'applicazione di metodi di approssimazione basati sulla proiezione di Galerkin come il metodo degli elementi finiti (MEF)

Nel secondo capitolo, presentiamo la formulazione continua del problema accoppiato 3D di interazione fluido-struttura, considerando le equazioni di Navier-Stokes incomprimibili per la descrizione della dinamica del fluido e un modello di trave lineare di Timoshenko per la modellizzazione della risposta dinamica della struttura sottile. Questi modelli sono accoppiati con una versione delle condizioni di interfaccia fluido-struttura in dimensioni miste, che associa l'approccio del dominio fittizio (FD) con la proiezione delle condizioni di accoppiamento cinematico su uno spazio di Fourier a dimensioni finite tramite moltiplicatori di Lagrange. Successivamente, sviluppiamo una formulazione discreta basata sul metodo degli elementi finiti e un trattamento semi-implicito delle condizioni di accoppiamento Dirichlet-Neumann, utilizzando una procedura partizionata per la risoluzione del problema di interazione fluido-struttura. Stabilizziamo il regime di energia dello schema e forniamo numerose prove numeriche dell'accuratezza e della robustezza della formulazione discreta, in particolare rispetto a un modello classico (ALE) con condizioni di accoppiamento fluido-struttura convenzionali.

Nei capitoli terzo e quarto, presentiamo l'analisi matematica dell'errore di approssimazione del metodo accoppiato e ridotto, esaminando sia gli errori di modellizzazione che di approssimazione numerica derivanti rispettivamente dalla formulazione a dimensioni miste e dal metodo degli elementi finiti con dominio fittizio (FEM). Esploriamo questi aspetti in due contesti semplificati. Iniziamo col considerare un problema di Poisson 2D con una frontiera immersa fissa e condizioni al bordo di Dirichlet non omogenee. Estendiamo poi questa analisi al problema di Stokes 2D stazionario con condizioni al bordo di tipo solido rigido sull'interfaccia immersa. In entrambi i casi, dopo aver dimostrato l'esistenza della soluzione per il problema ridotto, ne proviamo la convergenza, quando le dimen-

sioni dell'ostacolo tendono a zero, al problema completamente risolto con condizioni al bordo di Dirichlet standard. In particolare, le stime ricavate evidenziano la necessità di considerare abbastanza modi di Fourier per ottenere una convergenza sui moltiplicatori di Lagrange, che è un aspetto fondamentale per l'analisi del problema accoppiato di interazione fluido-struttura. Successivamente, analizziamo la discretizzazione numerica del problema ridotto. Come è consuetudine per questa famiglia di metodi, la convergenza ottenuta con il metodo degli elementi finiti di dominio fittizio è subottimale, a causa della discontinuità della soluzione all'interfaccia. Inoltre, la stabilità e l'accuratezza dello schema dipendono dal rapporto tra la dimensione caratteristica della griglia del fluido e la dimensione dell'ostacolo, il che può essere limitante per ostacoli molto piccoli. Per superare le limitazioni dell'approccio del dominio fittizio, proponiamo e analizziamo due metodi degli elementi finiti alternativi, un metodo stabilizzato e un metodo arricchito. Infine, sviluppiamo una formulazione dell'interazione fluido-struttura 2D in cui piccole particelle sono immerse in un flusso di Stokes, applicando condizioni di accoppiamento ridotte all'interfaccia. Le proprietà del modello ridotto e dei metodi numerici corrispondenti sono illustrate da alcuni esempi numerici.

L'uso di uno schema semi-implicito per la risoluzione del problema di interazione fluido-struttura 3D richiede di iterare più volte sui solvers fluido e solido, il che può essere costoso in termini di tempo di calcolo. L'approccio più efficiente per la discretizzazione temporale del problema di interazione fluido-struttura è lo schema di accoppiamento esplicito, che consente di risolvere i sotto-problemi fluido e solido solo una volta per time step. Tuttavia, per gli schemi di accoppiamento esplicito standard (Dirichlet-Neumann), l'alto rapporto fra la densità del fluido e del solido insieme alla geometria slanciata causa spesso instabilità numerica. Nell'ultimo capitolo, introduciamo uno schema debolmente accoppiato basato su condizioni di interfaccia di Robin specificamente progettato per una formulazione 3D a dimensioni miste e ne dimostriamo la stabilità incondizionata. Forniamo inoltre prove numeriche della precisione dello schema esplicito attraverso diversi esempi.

ACKNOWLEDGEMENTS. I would like express my deepest gratitude to my thesis supervisors Miguel, Paolo, Muriel and Céline for your dedication and availability throughout this thesis. Your expertise and your many contributions to this manuscipt were essential to the completion of this PhD project.

I also extend my thanks to the reviewers of this PhD thesis, Astrid Decoene and Alexander Popp, for their interest in my work, the time devoted to reading it, their detailed and thorough reports, and their numerous constructive comments and suggestions for improvement.

I thank all the members of the jury for agreeing to participate in the thesis committee.

Contents

CHAPTER 1

Introduction

1.1 Motivations

The study of slender structures immersed in three-dimensional (3D) flows is of great importance in a variety of engineering disciplines. For instance, it offers valuable insights on phenomena such as vortex vibrations induced by ocean currents or waves impacting submerged industrial structures [Wu et al., 2012], see Figure 1.1a. Specifically, in the context of long-submerged ocean risers, these vibrations can result in considerable deflection and, in severe cases, fatigue-induced failure within the riser system. Understanding the underlying mechanisms and behaviors of these vibrations is essential to design effective control strategies that may limit the impact of these vibrations [Hong and Shah, 2018]. In an other context, such studies contribute to understanding how aquatic vegetation interacts with the surrounding flow. Indeed, aquatic vegetation plays a crucial role in controlling the mean and turbulent flow [Dijkstra and Uittenbogaard, 2010], affecting therefore the transport of sediments and pollutants [Nepf and Vivoni, 2000, Luhar et al., 2008]. In particular, recent studies have highlighted the beneficial effects of aquatic vegetation, including its role in reducing riverbed erosion [Wang et al., 2015], see Figure 1.1b. Interest in investigating the interaction between slender structures and ambient flow also extends to biomedical applications, such as the design of vascular stents [Zunino et al., 2016]. For instance, modeling stents aids in comprehending how variations in blood pressure affect the risk of fatigue

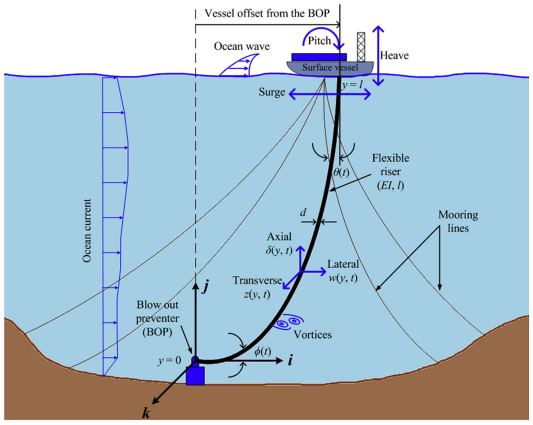

(a) *Schematic of a subsea production system - Source: [Hong and Shah, 2018]*

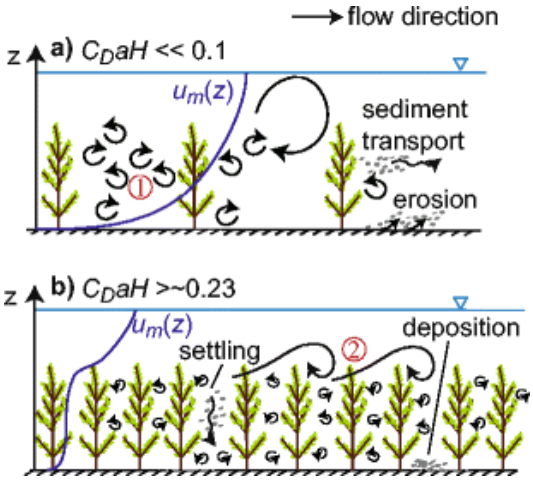

(b) *Effect of vegetation on the turbulent flow structure and sediment transport - Source: [Västilä and Järvelä, 2018]*

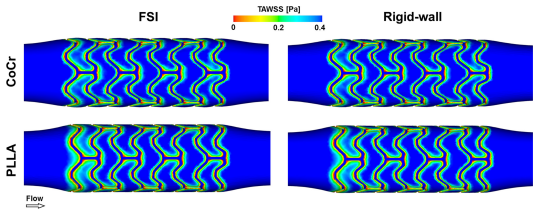

(c) *Contour maps of TAWSS (time averaged WSSS) along the fluid-structure interface - Source: [Chiastra et al., 2014]*

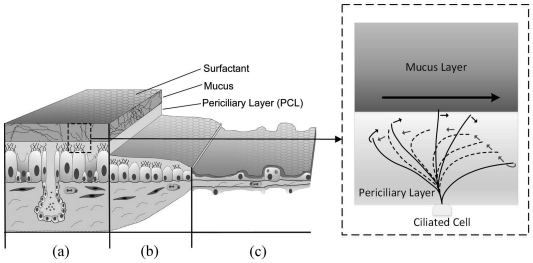

(d) *Muco-ciliary clearance - Source: [Vanaki et al., 2020]*

fracture, thereby enhancing their longevity [Li et al., 2010, Marrey et al., 2006]. It also impacts fundamental quantities, such as wall shear stress, WSS, which may be source to various diseases [Chiastra et al., 2014], see Figure 1.1c. Finally, it also has application in understanding microorganisms, examples include the simulation of ciliated cells that cover the lung and play a crucial role in the muco-ciliary clearance [Liron and Mochon, 1976, Smith et al., 2007], see Figure 1.1d, or the prediction of the motion of microswimmers [Lauga and Powers, 2009, Alouges et al., 2013].

1.2 Modelling assumptions

As we have seen in the previous section, the physical characteristics of the problem under study can take on various forms. In the next section, we comment on the modelling assumptions made in this manuscript on the physical properties of the two subsystems involved, namely the slender structures and the surrounding fluid, as well as the coupling

conditions enforced between these two sub-systems.

1.2.1 Fluid modeling assumptions

In this document, we assume that the fluid can be described as a Newtonian fluid. However, it is worth noting that certain biological fluids, such as mucus, exhibit non-Newtonian characteristics with properties spanning between those of viscous fluids and elastic solids [Lai et al., 2009]. Similarly, blood, due to its complex composition and the presence of suspended particles (such as red blood cells) and macromolecules (such as proteins) exhibits non-Newtonian effects [Chen et al., 2006]. Under the Newtonian assumption, the constitutive equation between the stress tensor and the strain rate tensor is linear, and the momentum conservation equation yield the Navier-Stokes equations. In our study, we further assume a constant fluid density, implying incompressibility. This assumption holds true for liquids where compressibility effects are negligible and serves as a reasonable approximation for gases with low Mach numbers. In addition, we presume isothermal flow conditions, ensuring that viscosity remains constant throughout the system.

An important parameter for characterizing the behavior of fluids is the Reynolds number. It serves as a dimensionless quantity representing the ratio of inertial forces to viscous forces within the flow. When the Reynolds number is low, indicating either high viscosity or small characteristic dimensions, the inertial terms in the Navier-Stokes equations become negligible. This leads to the emergence of stationary Stokes equations, particularly useful in scenarios involving biological applications characterized by small length scales and highly viscous fluids.

1.2.2 Solid modeling assumptions

In simulating fluid-structure interaction, the second key consideration is to accurately model slender structures. A classical approach for this purpose is beam theory, offering a simplified approach to understand and predict the behavior of such structures under varying loads. The aim is to simplify the analysis of beam behavior by only examining the distribution of forces and deformations along the beam centerline, neglecting variations in other dimensions such as width or depth. Several beam theories have emerged on the basis of different assumptions, each offering varying levels of accuracy. These theories are typically categorized into three groups [Eugster, 2015, Meier et al., 2019]:

- **Induced beam theories:** The one dimensional model is directly derived from the three dimensional theory, either by considering an asymptotic expansion with respect to the beam thickness, or imposing additional constraints on specific functions space, which aligns to the expected behavior of slender bodies (e.g., imposing rigid and planar cross-sections). We can find for example the planar linearized Euler-Bernouilli and Timoshenko beam theory [Timoshenko, 1921, Timoshenko, 1922].

- **Intrinsic beam theories:** The beam is considered a generalized one-dimensional continuum. Consequently, the one-dimensional representation of beam dynamics is decoupled from the three-dimensional theory. This enables one-dimensional quantities to satisfy some fundamental mechanical principles such as the balance of forces and moments, conservation of energy, or the existence of work-conjugated stress-strain pairs. However, as intrinsic theories do not prescribe specific constitutive laws, many choices are allowed, often justified through empirical validation and experimentation. Examples include the work of Kircchoff [Kirchhoff, 1850] or Cosserat and Cosserat [Cosserat and Cosserat, 1909].

- **Semi-induced beam theories:** This approach represents a compromise between induced and intrinsic theories, as it postulates only the constitutive law while deriving the remaining kinetic and kinematic from the three-dimensional continuum theory. We can find for example the non linear beam formulations such as the Kirchhof-Love beam theory with reference to Kirchhof [Kirchhoff, 1859] and Love [Love, 2013], or the Simo-Reisness beam theory with reference to Reissner [Reissner, 1972] and Simo [Simo, 1985].

One of the simplest and most practical theories first described by Euler and Bernouilli around 1750 is commonly called Euler-Bernoulli beam theory. The foundational assumption of this theory is that the beam's cross-sections are rigid and during deformation, the cross-section stay normal to the beam centerline. A possible enrichment of the Euler-Bernoulli model is the Timoshenko model [Timoshenko, 1921, Timoshenko, 1922], which still assumes undeformable sections but can eventually not be perpendicular to the beam centerline. In particular, unlike the case of the Bernoulli beam, the shear influence on the deformation is considered; in particular, it assumes an equivalent constant shear stress in the entire cross section. The various beam theories can be introduced through different perspectives, one of which revolves around their ability to accurately represent the geometric nonlinearity of beams, encompassing large deformations and rotations.

In particular, when deriving and computing the 1D beam formulations, we need necessarily to consider a reference frame for the formulation. We can consider three alternatives reference frames:

- **Fixed global frame of reference:** This approach is particular adapted to linear analysis involving small displacements and strains. It keeps the initial global reference frame as fixed, simplifying integration and differentiation operations performed within this frame. We find for example the planar Euler-Bernouilli and Timoshenko beam theory [Timoshenko, 1921, Timoshenko, 1922] or the linearization of the Simo-Reissner [Simo, 1985, Reissner, 1972] for small displacement derived for example in [Arunakirinathar and Reddy, 1993], corresponding to the extension of the planar Timoshenko beam theory to three dimensions.

- **Corotational frame of reference:** Corotational transformations are ideal for large displacement-small strain problems, see for example [Krenk, 2009]. This formulation separates the motion of each beam element into two parts- a rigid motion associated with the element-based frame of reference (rotation and translation) and a deformation of the element within this frame of reference. The main advantage of this formulation is that the displacements and the rotations within the local frame of reference are small. Therefore, the deformation of the beam can be modeled by approximate linear beam theory.

- **Geometrically exact frame of reference :** This formulation is suitable for addressing large displacement and large strain problems. Specifically, it aims to accurately handle rotations, which can often be challenging due to their nonlinear nature. Geometrically exact 3D beam theory has been used as a basis for development of a variety of finite element formulations, and many formulations with many different approaches can be found in the literature. See for example the seminal work of Simo [Simo, 1985] and the subsequent work by Simo and Vu-Quoc [Simo and Vu-Quoc, 1986].

1.2.3 Coupling methods

Coupled systems in which 2D flows interact with 1D beams can be efficiently simulated by identifying the beam centerline with the fluid-structure interface and by neglecting the interface thickness in the beam coupling (see, e.g., [Baaijens, 2001, Boilevin-Kayl et al., 2019]). However, for problems in which 3D flows meet 1D beams, the situation is much more delicate. The difference in dimensionality complicates the formulation of load and motion transfer conditions and also calls for innovative numerical techniques to bridge the gap between local fluid dynamics near the beam and the global behavior of the system. In fact, three distinct modeling approaches can be found in the literature:

- **Coupling on the reconstructed 2D beam interface:** In this approach, coupling conditions for kinematics and dynamics are enforced on the 2D interface of the beam, defined as the union of the cross-sections of the one-dimensional beam model. Widely adopted in industrial context, this approach simplifies the problem to a fluid-structure interaction with a co-dimension one at the interface. This category of problems have been extensively studied, particularly in the context of the interaction between a fluid and a shell. The kinematic coupling conditions are typically based on the assumption that the fluid particles do not penetrate the fluid-structure interface and do not adhere to the structure surface, thereby enforcing velocity equality between the fluid and the structure. As for the dynamic coupling conditions, following Newton's third law, under the assumption of rigid and planar cross-sections, the resultant forces and moments acting on each cross-section are typically taken equal to

the integral of the fluid stress and the moment of the fluid stress (see e.g., [Maniyeri and Kang, 2012, Huang et al., 2021, Ausas et al., 2022a, Wang et al., 2022]).

This approach corresponds to the standard treatment of the coupling conditions where the dimensional reduction has only been applied on the solid model. Given that in this manuscript, the case of a 3D beam model has not been treated, this model will be often referred to as the *full order model*. Note that another categorization proposed in [Steinbrecher et al., 2020] in the context of solid-solid interaction is is to refer to them as *surface-to-volume coupling schemes*.

- **Coupling on the centerline of the beam:** One of the main limitations of writing the coupled equations on the 2D beam interface is that it involves some restrictive conditions on the size of the fluid mesh in the vicinity of the slender bodies, which can be computationally expensive, especially when dealing with complex networks. Since the radius of the slender structures is small with respect to their longitudinal length, another solution is to ignore this 2D interface. On a computational standpoint, this strategy is really efficient and enables the simulation of a large number of beams [Griffith and Lim, 2012, Wiens and Stockie, 2015, Wang et al., 2019, Hagmeyer et al., 2022, Hagmeyer et al., 2023] allowing this way the computation of real-world scenarios. However, on a continuous level, two questions naturally emerge. The first one is if the continuous problem associated with this solution is well-posed. Indeed, imposing kinematic and dynamic coupling conditions on the beam centerline requires the introduction of a trace operator of codimension two, thereby demanding regularity for the solution within the fluid domain. However, these conditions simultaneously introduce a one-dimensional Dirac operator on the right-hand side of the fluid equations, often preventing the solution from reaching the desired regularity. The second question is the accuracy of the model, whether imposing coupling conditions on the centerline is a good approximation or not of the full order problem when the thickness of the slender body tends to 0.

- **Mixed-dimensional coupling with projection operator:** This method can be seen as an intermediate between the first two methods introduced above. It consists in projecting the kinematic constraint defined on the 2D fluid-structure interface onto a finite-dimensional space lying on the beam centerline [Heltai and Zunino, 2023]. An example includes replacing the original kinematic constraints on each cross section of the beam by a constraint which acts only on the average of the velocity. To some extent, this approach could be seen as a bridge, rectifying certain disparities among the mentioned sets of fluid-beam interaction methodologies, whether employing a 2D or 1D representation of the interface, and aims to be a compromise between accuracy, computational cost, and robustness. Such method has recently been used in other contexts such as structure-structure interaction [Khristenko et al., 2021] , coupling

of two elliptic equations [Kuchta et al., 2021a] or coupled problems in multiscale elasticity [Belponer et al., 2023]. The basic idea of my PhD project was to adapt and analyse such methods in the case of fluid-structure interaction.

1.3 Numerical methods for fluid-structure interaction

In this section, we provide a non-exhaustive review of the techniques employed to couple the fluid model and the solid model.

1.3.1 Eulerian and Lagrangian formulations

We usually distinguish two frameworks for the formulation of the solid and fluid equations, the Lagrangian and Eulerian approaches. The Lagrangian method involves tracking the motion of individual particles over time and space within a global reference frame. This approach is particularly favored in solid mechanics due to the historical dependency of stress, usually necessitating the specification of an undeformed configuration. It focuses on analyzing the system's energy, known as the Lagrangian, and derives equations of motion through the principle of least action. Conversevely, the Eulerian approach is mostly used in fluid dynamics, where, as opposed to tracking individual particles, the focus is made on observing the flow or deformation at fixed points in space as time progresses. The fluid is considered as a continuum, and conservation equations are developed based on control volumes, analyzing how quantities such as velocity, pressure, and stress change over time and space within a specified domain. The ALE framework, a hybrid approach, aims to take advantage of the best of the two approaches. It is widely used in FSI (Fluid-Structure Interaction) simulations where it provides a formulation suited for fluid equations written in a moving domain.

1.3.2 Space discretization

For systems characterized by low-to-moderate interface deflection, employing fitted mesh techniques is widespread. These techniques often rely on the arbitrary Lagrangian-Eulerian (ALE) description of the fluid, as pioneered by Hirt and co-authors [Hirt et al., 1974] and further developed by Donea and Huerta [Donea et al., 1982]. A key advantage of this approach lies in its ability to facilitate the time discretization of quantities associated with moving domains, achieved through an ALE map that parametrized the evolving fluid domain (see, e.g, [Liu et al., 2012, Wang and Xiao, 2016], for the use of ALE techniques in the context of 3D-1D fluid-structure interaction problems). However, for large interface displacements, the ALE formalism can become cumbersome. In this case, a preferred approach consists of combining an Eulerian description of the fluid and a Lagrangian description of the structure with unfitted meshes such that the fluid mesh does not match to the fluid-structure interface. Among this type of approaches, we can mention

the Immersed Boundary Method (IB) introduced by Peskin [Peskin, 1972], where interaction between the two meshes is accomplished using source terms (or forcing functions) in the governing equations in order to reproduce the effect of a boundary (see, e.g, [Griffith and Lim, 2012, Wiens and Stockie, 2015, Tschisgale and Fröhlich, 2020, Wang et al., 2019, Maxian and Peskin, 2020] for the application of IB method on 3D-1D fluid structure interaction problems). Another approach, also relying on unfitted meshes, is the fictitious domain method where Lagrange multipliers are used in place of delta functions, [Glowinski et al., 1994, Glowinski et al., 1999a, Boffi and Gastaldi, 2015]. However, in non-fitted approaches, the discrete approximation spaces for the pressure and velocity do not allow for weak and strong discontinuities across the interface. Consequently, the IB and the FD are often sub-optimal and suffer from mass conservation issues. A widely used strategy to circumvent these issues is based on the Cut-FEM approaches which attain optimal accuracy by integrating equations only in the physical region [Groß and Reusken, 2007, Haslinger and Renard, 2009, Burman and Hansbo, 2014]. However, these methods require mesh-cutting techniques, which can be challenging to implement, especially for complex geometries and moving interfaces. Moreover, when elements are badly cut, cut-FEM approaches face instability issues resulting in ill-conditioning of the associated algebraic system. Consequently, stabilization terms often need to be added to discrete formulation [Burman, 2010, Burman and Hansbo, 2014]. Finally, let us mention another solution frequently adopted in the context of bioengineering applications involving viscous Stokasian flow: the slender-body theory (see, e.g. [Bouzarth and Minion, 2011, Bringley and Peskin, 2008, Tornberg and Shelley, 2004, Tornberg and Gustavsson, 2006, Cortez et al., 2005, Mori et al., 2018, Decoene et al., 2023]). This theory adopts a one-way approach, approximating the slender body through a one-dimensional force density defined along its centerline. By doing so, the slender-body theory offers an integral form approximation for the Stokes problem in an unbounded domain based on this one-dimensional force.

1.3.3 Time discretization

To couple the fluid solver and the solid solver, it is generally necessary to impose three coupling conditions:

- The kinematic condition corresponding to the equality of the fluid and structure velocities at the fluid-structure interface,
- The dynamic conditions ensuring the continuity of the stress at the fluid-structure interface,
- The geometric condition, which guarantees compatibility between the fluid domain and the solid domain. In an Eulerian model, it guarantees the application of kinematic and dynamic coupling conditions at the fluid-structure interface. In an ALE

framework, it further ensures that the deformation of the fluid domain corresponds to the deformation of the solid domain at the interface

We can basically distinguish two families of algorithms to solve fluid-structure interaction problems. The first family is made of monolithic procedures for which the fluid and solid solver are gathered in a unique system of equations, see e.g [Badia et al., 2008b, Gee et al., 2011, Muddle et al., 2012, Richter, 2015]. Monololitic approaches are known to be accurate and stable, however, they are often poorly flexible and involve high computational cost, notably, they do not enable the use of separate fluid and structure solvers. The second family is the partitioned procedures which separate the solid and fluid solver as two distinct softwares, see e.g. [Fernández and Moubachir, 2005a, Badia et al., 2008a, Degroote et al., 2008, Van Brummelen, 2011, Baek and Karniadakis, 2012]. In a partitioned scheme, information is exchanged between the two solvers. For instance, in a classical Dirichlet-Neumann FSI coupled model, the velocity of the structure at each time step is transmitted to the fluid solver, which solves the boundary conditions of a Dirichlet problem at the fluid-structure interface. Subsequently, the fluid solver returns the fluid stress to the solid solver, which then solves a Neumann problem.

For the partitioned approach, the time coupling mechanism dictates the sequence in which these information exchanges occur between the two solvers. The scheme is defined as strongly coupled if the interface conditions are still satisfied after time discretisation; conversely, it is defined as weakly coupled (or loosely coupled) if some spurious numerical power may appear at the fluid-structure interface. The implicit coupling is known to be accurate and unconditionally stable, but it can also increase computational cost as it requires to solve a non-linear coupled scheme at each time step. Conversely, loosely coupled schemes are much more efficient from a computational standpoint; however, for a small ratio between solid and fluid density or for slender structures, they are known to suffer from instability, emerging from the so-called added mass effect [Nobile, 2001]. Many strategies have been explored to counteract these instability issues, involving alternative coupling algorithms than the classical Dirichlet-Neumann method. Among them we find the Robin-Neumann methods [Fernández et al., 2013, Fernández et al., 2015b, Tuković et al., 2019] or Robin-Robin method [Burman et al., 2022b, Burman et al., 2022a, Burman et al., 2023].

This PhD project focuses on the development and analysis of mixed-dimensional coupling conditions built on averaged operators for fluid-structure interaction problems. Additionally, we aim to develop effective and accurate numerical methods to resolve the resulting coupled problem.

1.4 Overview on thesis content

In the context of the modeling and mathematical background discussed in the previous sections, we provide here a detailed description of the main original contributions of each chapter of this thesis, with the objective of describing the role of each chapter within the thesis and describing a clear vision of the unity of the entire work.

1.4.1 Chapter 2: A mixed-dimensional formulation for the simulation of slender structures immersed in an incompressible flow

In the first chapter, we propose a new mathematical and computational framework for fluid-structure interaction systems in which a 3D fluid mechanically interacts with an immersed slender structure defined in a 1D domain. We establish the continuous formulation using the Navier-Stokes equations for the fluid and the linear Timoshenko beam model for the structure, we complement these models with a reduced order version of the fluid-structure interface coupling conditions. The basic idea consists of combining a fictitious domain approach with a projection of the kinematic coupling conditions onto a finite-dimensional space $\boldsymbol{F}_N$ defined within the 1D structure domain. Specifically, in each cross section, the original kinematic coupling conditions are replaced by their projection on the first N modes of the Fourier expansion at the reconstructed 2D fluid-structure interface. To this purpose,, we consider Ω a bounded domain in $\mathbb{R}^3$ and $\widehat{\omega}^\varepsilon$ a free-stress reference configuration for the beam. We assume that $\widehat{\omega}^\varepsilon$ is an elliptic cylinder of length L, with a centerline aligned with the z-axis and elliptic cross sections of size proportional to ε. We denote by $\widehat{\omega}^\varepsilon(s)$ the cross-section centered in $s\boldsymbol{e}_z$ and by (s,ν) the elliptic cylindrical surface coordinate defined in $\partial\widehat{\omega}^\varepsilon$. The current beam configuration, given by $\omega^\varepsilon(t)$, is defined in terms of a deformation map $\boldsymbol{\phi} : \widehat{\omega}^\varepsilon \times \mathbb{R}^+ \to \mathbb{R}^3$ such that $\omega^\varepsilon(t) = \boldsymbol{\phi}(\widehat{\omega}^\varepsilon, t)$. Subsequently, we denote by $\Sigma^\varepsilon(t) = \partial\omega^\varepsilon(t)\backslash\partial\Omega$ and $\Omega(t) = \Omega\backslash\Sigma^\varepsilon(t)$ the current position of the fluid-structure interface and the domain occupied by the fluid, respectively. The reduced order formulation we consider is introduced in Section 2.2 as follows: find $\boldsymbol{u} : \Omega \to \mathbb{R}^+$, $p : \Omega \to \mathbb{R}^+$ the velocity and pressure of the fluid, and $\boldsymbol{r} : (0,L)\times\mathbb{R}^+ \to \mathbb{R}^3$,

$\boldsymbol{\theta} : (0, L) \times \mathbb{R}^+ \to \mathbb{R}^3$ the displacement and rotation of the beam such that

Fluid sub-problem:

$$\begin{cases} \rho_{\mathrm{f}} \partial_t \boldsymbol{u} + \rho_{\mathrm{f}} \boldsymbol{u} \cdot \boldsymbol{\nabla} \boldsymbol{u} - \operatorname{div} \boldsymbol{\sigma}(\boldsymbol{u}, p) = \boldsymbol{0} & \text{in} \quad \Omega(t), \\ \operatorname{div} \boldsymbol{u} = 0 & \text{in} \quad \Omega(t), \\ \boldsymbol{u} = \boldsymbol{0} & \text{on} \quad \Gamma. \end{cases} \tag{1.4.1}$$

Structure sub-problem:

$$\begin{cases} \rho_{\mathrm{b}} \boldsymbol{A} \partial_t^2 \boldsymbol{r} - \boldsymbol{G} \partial_s \big(\partial_s \boldsymbol{r} - \boldsymbol{\theta} \wedge \boldsymbol{e}_z \big) = \boldsymbol{f} & \text{in} \quad (0, L) \times \mathbb{R}^+, \\ \rho_{\mathrm{b}} \boldsymbol{I} \partial_t^2 \boldsymbol{\theta} - \boldsymbol{E} \partial_s^2 \boldsymbol{\theta} - \boldsymbol{e}_z \wedge \boldsymbol{G} \big(\partial_s \boldsymbol{r} - \boldsymbol{\theta} \wedge \boldsymbol{e}_z \big) = \boldsymbol{m} & \text{in} \quad (0, L) \times \mathbb{R}^+. \end{cases} \tag{1.4.2}$$

Reduced order coupling conditions:

$$\begin{cases} \boldsymbol{\phi}(\widehat{\boldsymbol{x}}, t) = s \boldsymbol{e}_z + \boldsymbol{r}(s, t) + \boldsymbol{\Lambda}(s, t)(\widehat{\boldsymbol{x}} - s \boldsymbol{e}_z), \; s = \widehat{\boldsymbol{x}} \cdot \boldsymbol{e}_z, \; (\widehat{\boldsymbol{x}}, t) \in \widehat{\omega}^\varepsilon \times \mathbb{R}^+, \\ \boldsymbol{\Pi}_N(\boldsymbol{u}) = \boldsymbol{\Pi}_N(\partial_t \boldsymbol{\phi} \circ \boldsymbol{\phi}_t^{-1}) \quad \text{on} \quad \Sigma^\varepsilon(t), \\ \boldsymbol{f}(s) = - \displaystyle\int_{\Sigma^\varepsilon(t) \cap \partial\omega^\varepsilon(s,t)} \boldsymbol{\lambda}_N \quad \forall s \in (0, L), \\ \boldsymbol{m}(s) = - \displaystyle\int_{\Sigma^\varepsilon(t) \cap \partial\omega^\varepsilon(s,t)} (\boldsymbol{I}_3 - \boldsymbol{r}(s, t) - (\boldsymbol{\phi}_t^{-1} \cdot \boldsymbol{e}_z) \boldsymbol{e}_z) \wedge \boldsymbol{\lambda}_N \quad \forall s \in (0, L), \\ \boldsymbol{\lambda}_N = \big(\boldsymbol{\sigma}(\boldsymbol{u}, p)^+ \boldsymbol{n}^+ - \boldsymbol{\sigma}(\boldsymbol{u}, p)^- \boldsymbol{n}^- \big) \in \boldsymbol{F}_N. \end{cases} \tag{1.4.3}$$

where $\boldsymbol{\Lambda} : (0, L) \times \mathbb{R}^+ \to SO(3)$ is the orthogonal rotation matrix associated to the rotation vector $\boldsymbol{\theta}$ and $\boldsymbol{\Pi}_N$ is the L^2 projector on the space

$$\boldsymbol{F}_N(t) \stackrel{\text{def}}{=} \Bigg\{ \widehat{\boldsymbol{v}} \circ \boldsymbol{\phi}_t^{-1} \in \boldsymbol{L}^2(\Sigma^\varepsilon(t)) \;\Bigg|\; \widehat{\boldsymbol{v}}(s, \nu) = \boldsymbol{a}_0(s) + \sum_{k=1}^{N} (\boldsymbol{a}_k(s) \cos(k\nu) + \boldsymbol{b}_k(s) \sin(k\nu)), \boldsymbol{a}_k, \boldsymbol{b}_k \in \boldsymbol{L}^2(0, L) \Bigg\} \tag{1.4.4}$$

Considering a Dirichlet-Neumann partitioned approach, the reduced order coupled model (1.4.1)-(1.4.3) consists for the fluid sub-problem to solve Navier-Stokes equations in the whole domain $\Omega(t)$ (hence the denomination fictitious domain) where the kinematic conditions are projected on the finite dimensional $\boldsymbol{F}_N(t)$ via Lagrange multipliers. Typically for $N = 0$, on each cross section of the beam, we impose the equality of the average velocity of the fluid and structure. For the structure sub-problem, it consists in solving a Neumann problem where the external forces and torques on the right-hand side are computed from the fluid Lagrange multiplier.

In Section 2.3, we present the discretization of the coupled problem (1.4.1)-(1.4.3) using a $\mathbb{P}_1/\mathbb{P}_1$ stabilized finite element method on Ω for the discretization of the fluid velocity-pressure pair $\boldsymbol{u}/p$, and $\mathbb{P}_1/\mathbb{P}_1$ finite elements method on $(0, L)$ for the discretization of the pair $\boldsymbol{r}/\boldsymbol{\theta}$. We denote by $\boldsymbol{V}_h$ and Q_h the discrete spaces for the approximation of the fluid velocity $\boldsymbol{u}$ and pressure p respectively, $\boldsymbol{Y}_h$ the discrete space for the approximation of the beam displacement $\boldsymbol{r}$ and rotation $\boldsymbol{\theta}$, and $\boldsymbol{F}_{N,H}^n$ a discretization of $\boldsymbol{F}_N(t)$ where the coefficients $\boldsymbol{a}_k, \boldsymbol{b}_k$ are taken in $\boldsymbol{Y}_H$. For the time discretization, we consider an explicit treatement of the geometric coupling condition given by the deformation map $\boldsymbol{\phi}_H^n$ and an implicit treatement of the kinematic and dynamics coupling conditions. The fully discrete formulation of the strongly coupled problem (1.4.1)-(1.4.3) writes: find $(\boldsymbol{u}_h^n, p_h^n, \boldsymbol{\lambda}_{N,H}^n, \boldsymbol{r}_H^n, \boldsymbol{\theta}_H^n) \in \boldsymbol{V}_h \times Q_h \times \boldsymbol{F}_{N,H}^n \times \boldsymbol{Y}_H \times \boldsymbol{Y}_H$ with $\dot{\boldsymbol{r}}_H^{n-\frac{1}{2}} = \partial_\tau \boldsymbol{r}_H^n$ and $\dot{\boldsymbol{\theta}}_H^{n-\frac{1}{2}} = \partial_\tau \boldsymbol{\theta}_H^n$ such that

$$
\begin{cases}
\boldsymbol{\phi}_H^n = (\boldsymbol{I}_3 \cdot \boldsymbol{e}_z)\boldsymbol{e}_z + \overline{\boldsymbol{r}_H^{n-1}} + \overline{\boldsymbol{\Lambda}_h^{n-1}}\big(\boldsymbol{I}_3 - (\boldsymbol{I}_3 \cdot \boldsymbol{e}_z)\boldsymbol{e}_z\big) \quad \text{in} \quad \widehat{\omega}^\varepsilon, \\
\Sigma^{\varepsilon,n} = \boldsymbol{\phi}_H^n(\widehat{\Sigma}^\varepsilon), \\
\rho_{\mathrm{f}}(\partial_\tau \boldsymbol{u}_h^n, \boldsymbol{v}_h)_\Omega + a_{\Omega,h}^{\mathrm{f}}\big(\boldsymbol{u}_h^{n-1}; (\boldsymbol{u}_h^n, p_h^n), (\boldsymbol{v}_h, q_h)\big) \\
\quad + \rho_{\mathrm{b}}\big(\boldsymbol{A}\partial_\tau \dot{\boldsymbol{r}}_H^n, \delta\boldsymbol{r}_H\big)_{(0,L)} + \rho_{\mathrm{b}}\big(\boldsymbol{I}\partial_\tau \dot{\boldsymbol{\theta}}_H^n, \delta\boldsymbol{\theta}_H\big)_{(0,L)} \\
\quad + a_H^{\mathrm{b}}\big((\boldsymbol{r}_H^{n-\frac{1}{2}}, \boldsymbol{\theta}_H^{n-\frac{1}{2}}), (\delta\boldsymbol{r}_H, \delta\boldsymbol{\theta}_H)\big) \\
\quad - \big(\boldsymbol{\lambda}_{N,H}^n, \overline{\delta\boldsymbol{r}_H} + \overline{\delta\boldsymbol{\theta}_H} \wedge (\boldsymbol{I}_3 - \overline{\boldsymbol{r}_H^{n-1}} \circ (\boldsymbol{\phi}_H^n)^{-1} - ((\boldsymbol{\phi}_H^n)^{-1} \cdot \boldsymbol{e}_z)\boldsymbol{e}_z)\big)_{\varepsilon,n} \\
\quad + \big(\boldsymbol{\mu}_{N,H}, \boldsymbol{u}_h^n - \partial_\tau \boldsymbol{\phi}_H^{n+1} \circ (\boldsymbol{\phi}_H^n)^{-1}\big)_{\varepsilon,n} = 0
\end{cases}
\tag{1.4.5}
$$

for all $(\boldsymbol{v}_h, q_h, \boldsymbol{\mu}_{N,H}, \delta\boldsymbol{r}_H, \boldsymbol{\theta}_H) \in \boldsymbol{V}_h \times Q_h \times \boldsymbol{F}_{N,H}^n \times \boldsymbol{Y}_H \times \boldsymbol{Y}_H$, where $a_{\Omega,h}^{\mathrm{f}}$ and a_H^{b} are the bilinear forms associated to the fluid and solid sub-problems, respectively. In the same section, we also prove the unconditional stability of the reduced order coupled problem (1.4.5) under the assumption of small rotations. Finally, to illustrate the accuracy of the proposed strategy, in Section 2.4 we compare it with two other approaches, a full order model based on the ALE approach and another reduced mixed-dimensional model with coupling conditions on the beam centerline. More specifically, we investigate the influence of the Reynolds number, of the fluid mesh refinement, and of the number of Fourier modes taken for the Lagrange multiplier space. In particular, when full order approaches usually require the background fluid mesh to correctly resolve the reconstructed 2D beam interface, we show that our method gives good result, as least qualitatively, for a beam thickness close to the mesh size. On the other side, we give numerical evidence that its mathematical derivation from a full order formulation also ensures the convergence of the discrete formulation for small mesh size. Finally, to show the robustness of our reduced order formulation, we extend it to the case of multiple beams with a nonlinear beam model and contact model, see Figure 1.2.

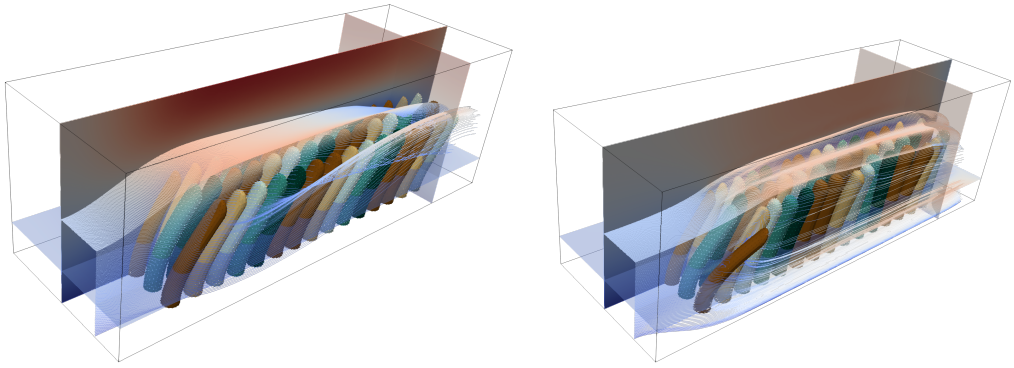

(a) *Stokesian flow* **(b)** *Navier-Stokasian flow*

Figure 1.2: *Snapshots of the fluid velocity magnitude for multiple beams immersed in a Stokesian (left) and Navier-Stokes (right) using discrete formulation* (1.4.5)

1.4.2 Chapter 3: Mathematical and numerical analysis of reduced order interface conditions and augmented finite element method for mixed-dimensional problems

In this chapter, we perform a rigorous analysis of the 2D Problem (1.4.1)-(1.4.3) that arises by studying a transversal section of the problem introduced in Chapter 2. Instead of dealing with a two-way interaction, we focus on the obstacle problem such that the kinematic coupling conditions are substituted with a non-homogeneous Dirichlet condition on a fixed circular internal boundary $\partial\omega^\varepsilon$. We also make a drastic simplification of the fluid model, stepping back to the scalar Poisson equation. More specifically, introducing F_N defined by

$$F_N \overset{\text{def}}{=} \{v \in L^2(\partial\omega^\varepsilon) : \\ v(\varepsilon)(\theta) = a_0 + \sum_{k=1}^{N}(a_k\cos(k\theta) + b_k\sin(k\theta)), \quad a_k, b_k \in \mathbb{R}\}, \quad (1.4.6)$$

the problem we consider in Chapter 3 is formulated as follows: find $(u_N^\varepsilon, \lambda_N^\varepsilon) \in H_0^1(\Omega) \times F_N$ such that

$$\begin{cases} (\nabla u_N^\varepsilon, \nabla v)_\Omega - (\lambda_N^\varepsilon, v)_\varepsilon = (f, v)_\Omega & \forall v \in H_0^1(\Omega), \\ (\mu_N, u_N^\varepsilon)_\varepsilon = (\mu_N, u_\mathrm{b})_\varepsilon & \forall \mu_N \in F_N, \end{cases} \quad (1.4.7)$$

with $(u_\mathrm{b}, f) \in H^{\frac{1}{2}}(\partial\omega^\varepsilon) \times L^2(\Omega)$, $\mathrm{supp} f \cap \omega^\varepsilon = \varnothing$ and $(\cdot,\cdot)_\varepsilon$ is the L^2 rescaled scalar product on $\partial\omega^\varepsilon$. Note that many works exist on the mathematical analysis and numerical approximation of the Poisson problem with small inclusions (see the introduction of Chapter 3 for a non exhaustive review). Our objective is not, in this case, to compete with

these methods, but to understand the strenghts and weaknesses of the reduced order model introduced in Chapter 2, and possibly propose improvements. In Section 3.3, in a first part, we prove the well-posedness of Problem 1.4.7 and provide uniform a-priori estimates on the solution $(u_N^\varepsilon, \lambda_N^\varepsilon)$ with respect to ε. This leads to the following theorem.

Restated Theorem 3.3.1. *Problem* (1.4.7) *admits a unique solution* $(u_N^\varepsilon, \lambda_N^\varepsilon)$ *in* $H_0^1(\Omega) \times F_N$. *Moreover, this solution satisfies the following energy bound:*

$$\|u_N^\varepsilon\|_{1,\Omega} + \|\lambda_N^\varepsilon\|_{-\frac{1}{2},\varepsilon} \lesssim \|u_{\mathrm{b}}\|_{\frac{1}{2},\varepsilon} + \|f\|_\Omega. \tag{1.4.8}$$

This theorem implies that the solution of the reduced order problem continuously depends on the data and the continuity constant does not dependent on ε and N. In a second part, we consider the convergence of Problem 1.4.7, as $\varepsilon \to 0$, towards the following full order Poisson problem: find $(u^\varepsilon, \lambda^\varepsilon) \in H_0^1(\Omega) \times H^{-\frac{1}{2}}(\partial\omega^\varepsilon)$ such that

$$\begin{cases} (\nabla u^\varepsilon, \nabla v)_\Omega - \langle \lambda^\varepsilon, v \rangle_{-\frac{1}{2},\partial\omega^\varepsilon} = (f, v)_{\Omega^\varepsilon} & \forall v \in H_0^1(\Omega), \\ \langle \mu, u^\varepsilon \rangle_{-\frac{1}{2},\partial\omega^\varepsilon} = \langle \mu, u_{\mathrm{b}} \rangle_{-\frac{1}{2},\partial\omega^\varepsilon} & \forall \mu \in H^{-\frac{1}{2}}(\partial\omega^\varepsilon). \end{cases} \tag{1.4.9}$$

As mentioned in the previous section, since the reduced order model is derived from the original full order one, we expect, at least in the simplified framework we consider here, to be able to derive some convergence estimates when ε is small. The main result on the ε-convergence is given in Theorem 3.3.4.

Restated Theorem 3.3.4. *Let* $(u^\varepsilon, \lambda^\varepsilon) \in H^1(\Omega) \times H^{-\frac{1}{2}}(\partial\omega^\varepsilon)$ *be a solution of* (1.4.9) *and* $(u_N^\varepsilon, \lambda_N^\varepsilon) \in H_0^1(\Omega) \times F_N$ *solution of* (1.4.7)*, with* $u_{\mathrm{b}} \in F_N$*, we have for all* $\varepsilon \in (0, \rho)$*,*

$$\|u_N^\varepsilon - u^\varepsilon\|_{1,\Omega^\varepsilon} + \varepsilon \|\lambda_N^\varepsilon - \lambda^\varepsilon\|_{-\frac{1}{2},\varepsilon} \lesssim \left(\frac{\varepsilon}{\rho}\right)^{N+1} (\|u_{\mathrm{b}}\|_{\frac{1}{2},\varepsilon} + \|f\|_\Omega) \tag{1.4.10}$$

Note that Theorem 3.3.4 implies that, for a given ε, by increasing the number of Fourier modes, we can increase the accuracy with respect to the solution of Problem (1.4.9). It also highlights the necessity of considering a minimum number of modes $N \geqslant 1$ to achieve convergence of the Lagrange multipliers for the rescaled norm $\|\cdot\|_{-\frac{1}{2},\varepsilon}$. This is an important aspect of the method since for the 3D problem introduced in Chapter 2, the Lagrange multiplier is related to the forces that are exchanged at the interface, see (1.4.3). In Section 3.4, we introduce the discretization of Problem (1.4.7). To be consistent with Chapter 2, we investigate a fictitious domain method with a mesh that does not match to the internal boundary $\partial\omega^\varepsilon$. Setting $X_h^k(\Omega)$ the space of $\mathbb{P}_k$ continuous finite element in Ω and $V_h^k \overset{\text{def}}{=} X_h^k(\Omega) \cap H_0^1(\Omega)$ the space for the discrete approximation of u_N^ε, the standard finite element approximation of Problem (1.4.7) writes: find $(u_{N,h}^\varepsilon, \lambda_{N,h}^\varepsilon) \in V_h^k \times F_N$ such that

$$(\nabla u_{N,h}^\varepsilon, \nabla v_h)_\Omega - (\lambda_{N,h}^\varepsilon, v_h)_\varepsilon + (\mu_N, u_{N,h}^\varepsilon - u_{\mathrm{b}})_\varepsilon = (f, v_h)_\Omega \tag{1.4.11}$$

for all $(v_h, \mu_N) \in V_h^k \times F_N$. Under the assumption $N \leqslant k$, we establish the following general a-priori estimates for the discrete error of Problem (1.4.11) :

$$\|u_N^\varepsilon - u_{N,h}^\varepsilon\|_{1,\Omega} \lesssim |\log(\varepsilon)|^{\frac{1}{2}}(1+\frac{h}{\varepsilon})^N \inf_{v_h \in V_h^k} \|u_N^\varepsilon - v_h\|_{1,\Omega},$$

$$\|\lambda_N^\varepsilon - \lambda_{N,h}^\varepsilon\|_{-\frac{1}{2},\varepsilon} \lesssim |\log(\varepsilon)|^{\frac{1}{2}}(1+\frac{h}{\varepsilon})^{2N} \inf_{v_h \in V_h^k} \|u_N^\varepsilon - v_h\|_{1,\Omega},$$

As expected, the approximation with standard finite element suffers from a locking effect when $N \geqslant 1$, where the inf-sup condition, and consequently, the constant associated with the approximation error explodes, when the ratio ε/h is small. This phenomenon increases with higher values of N. To eliminate the constraint $N \leqslant k$ and mitigate the locking effect when $N \geqslant 1$, we propose a stabilized version of Problem (1.4.11) by adding the following term to the variational formulation:

$$s_h(\mu_N, \lambda_N) = \gamma_\lambda \left(\frac{h}{\varepsilon}\right) \varepsilon^{-1}(\mu_N, \lambda_N)_\varepsilon \quad \forall (\mu_N, \lambda_N) \in F_N,$$

with $\gamma > 0$ a user-defined parameter. We then obtained the following a priori estimate in terms of the approximation error:

$$\|(u_N^\varepsilon - u_{N,h}^\varepsilon, \lambda_N^\varepsilon - \lambda_{N,h}^\varepsilon)\|_\varepsilon \lesssim |\log(\varepsilon)|^{\frac{1}{2}} \inf_{v_h \in V_h^k} \|u_N^\varepsilon - v_h\|_{1,\Omega} + \varepsilon^{-\frac{1}{2}} \left(\frac{h}{\varepsilon}\right)^{\frac{1}{2}} \|\lambda_N^\varepsilon\|_\varepsilon.$$

where

$$\|(v_h, \mu)\|_\varepsilon \overset{\text{def}}{=} \left(\|v_h\|_{1,\Omega}^2 + \|\mu\|_{-\frac{1}{2},\varepsilon}^2 + \left(\frac{h}{\varepsilon}\right)\varepsilon^{-1}\|\mu\|_\varepsilon^2\right)^{\frac{1}{2}} \quad \forall\, (v_h, \mu) \in V_h^k \times F_N\,.$$

Although the stabilized method helps to limit the phenomenon of numerical locking, in both the standard and the stabilized discrete formulations, the convergence rate of the finite element methods is limited by the low regularity of the solution u_N^ε. Indeed, due to the gradient jump of u_N^ε across $\partial\omega^\varepsilon$, u_N^ε is not more regular than $H^{\frac{3}{2}-\eta}(\Omega)$, and consequently for any interpolation operator Π_h^k on $X_h^k(\Omega)$, we have at best

$$\|u_N^\varepsilon - \Pi_h^k u_N^\varepsilon\|_\Omega + h\|\nabla(u_N^\varepsilon - \Pi_h^k u_N^\varepsilon)\|_\Omega \lesssim h^{\frac{3}{2}-\eta}\|u_N^\varepsilon\|_{\frac{3}{2}-\eta,\Omega} \quad \forall k \in \mathbb{N}^\star.$$

Furthermore, for $s \geqslant 1$ and some specific boundary conditions,

$$\|u_N^\varepsilon\|_{s,\Omega} \sim \frac{1}{\varepsilon^{s-1}} \text{ when } \varepsilon \to 0, \tag{1.4.12}$$

such that the discrete approximation error explodes as ε/h is small. To address the sub-optimality of the standard finite element method, we propose to enrich the finite element

space by adding well-chosen functions solutions of the Poisson problem. These additional functions aim at improving the approximation of the jump at the interface and the singular behavior of u_N^ε described in (1.4.12). The resulting variational formulation is given by: find $(\tilde{u}_{N,h}^\varepsilon, \tilde{\lambda}_{N,h}^\varepsilon) \in V_{N,h}^k \times F_N$ such that

$$\begin{cases} (\nabla \tilde{u}_{N,h}^\varepsilon, \nabla v_h)_\Omega + (\tilde{\lambda}_{N,h}^\varepsilon, v_h)_\varepsilon = (f, v_h)_\Omega \quad \forall v_h \in V_{N,h}^k, \\ (\mu_N, \tilde{u}_{N,h}^\varepsilon)_\varepsilon = (\mu, u_{\mathrm{b}})_\varepsilon \quad \forall \mu_N \in F_N. \end{cases} \tag{1.4.13}$$

where $V_{N,h}^k$ is the augmented finite element space. Subsequently, we prove that this augmented finite element approach restores optimal convergence, as asserted in Theorem 3.4.6.

Restated Theorem 3.4.6. *Let $k \in \mathbb{N}^*$. We assume that f belongs to $H^{k-1}(\Omega)$. Let $(u_N^\varepsilon, \lambda_N^\varepsilon)$ be the solution of problem* (1.4.7) *and $(\tilde{u}_{N,h}^\varepsilon, \tilde{\lambda}_{N,h}^\varepsilon)$ be the solution of problem* (1.4.13)*. Then, we have*

$$\|u_N^\varepsilon - \tilde{u}_{N,h}^\varepsilon\|_{1,\Omega} + \|\lambda_N^\varepsilon - \tilde{\lambda}_{N,h}^\varepsilon\|_{-\frac{1}{2},\varepsilon} \lesssim |\log(\varepsilon)|^{\frac{1}{2}} h^k \left(\|f\|_{k-1,\Omega} + \|u_{\mathrm{b}}\|_{\frac{1}{2},\varepsilon} \right). \tag{1.4.14}$$

Theorem 3.4.6 proves that the augmented finite element method enables to derive a numerical error estimate of any order in h and to reduce considerably the interdependence between the mesh size and the obstacle size. Finally, the previous results are supported by several numerical experiments in Section 3.5, see for example Figure 1.3 for some numerical evidence of the convergence rate of the augmented finite element method given by Theorem 3.4.6.

1.4.3 Chapter 4: A new computational approach for the simulation of small particles in a two-dimensional Stokesian flow: formulation and error analysis

This chapter keeps the overall structure of Chapter 3 while extending the analysis to the stationary Stokes problem. It pays special attention to small inclusions and the convergence of the Lagrange multipliers, which constitute a critical aspect when addressing coupled problems. While, in a first part, for the mathematical analysis, we still consider the obstacle problem, we also introduce in a second part the 2D fluid-structure interaction model for rigid particles immersed in a Stokesian fluid. While the Poisson problem essentially serves as a theoretical basis for the 3D one, its extension to the Stokes equations coupled with small particles via reduced order coupling conditions has an intrinsic value. Nonetheless, many other numerical methods are available for addressing such problem. In the introduction of Chapter 4, we provide a non exhaustive review of existing solutions in this domain. This chapter aims at bridging the gap, at least partially, between Chapter 2 and Chapter 4, the main objective being to lay the mathematical foundation for extending our analysis to a 3D framework in a future work. Specifically, on a continuous level, in

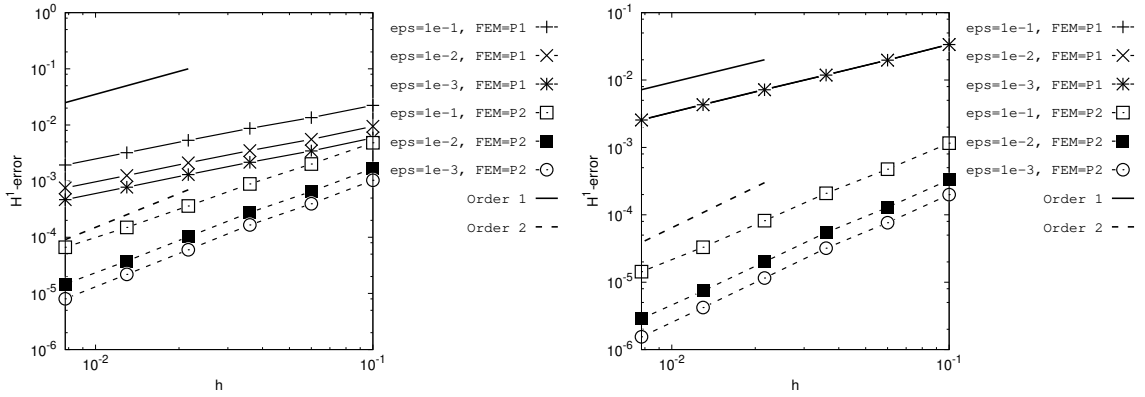

(a) H^1 *rel. err.* $\tilde{u}^{\varepsilon}_{N,h},\ N=0$, *augmented FEM.*

(b) H^1 *rel. err.* $\tilde{u}^{\varepsilon}_{N,h},\ N=1$, *augmented FEM.*

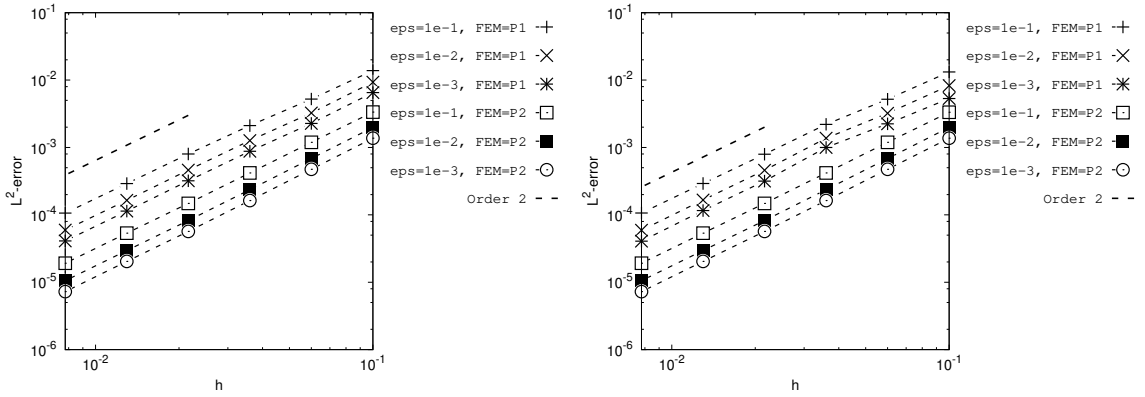

(c) L^2 *rel. err.* $\tilde{\lambda}^{\varepsilon}_{N,h},\ N=0$, *augmented FEM.*

(d) L^2 *rel. err.* $\tilde{\lambda}^{\varepsilon}_{N,h},\ N=1$, *augmented FEM.*

Figure 1.3: *Numerical error for the augmented finite element method*

Section 4, we consider the following stationary Stokes problem with reduced order Dirichlet boundary conditions: find $(\boldsymbol{u}^{\varepsilon}_N, p^{\varepsilon}_N, \boldsymbol{\lambda}^{\varepsilon}_N,) \in \boldsymbol{V} \times Q \times \boldsymbol{F}_N$ such that

$$\begin{cases} 2(\boldsymbol{\varepsilon}(\boldsymbol{u}^{\varepsilon}_N), \boldsymbol{\varepsilon}(\boldsymbol{v}))_\Omega - (p^{\varepsilon}_N, \operatorname{div} \boldsymbol{v})_\Omega - (\boldsymbol{\lambda}^{\varepsilon}_N, \operatorname{div} \boldsymbol{v})_\Omega = 0 \quad \forall \boldsymbol{v} \in \boldsymbol{V}, \\ (q, \operatorname{div} \boldsymbol{u}^{\varepsilon}_N)_\Omega = 0 \quad \forall q \in Q, \\ (\boldsymbol{\mu}_N, \boldsymbol{u}^{\varepsilon}_N)_\varepsilon = (\boldsymbol{\mu}_N, \boldsymbol{v}_{\mathrm{b}} + \varepsilon w_{\mathrm{b}} \boldsymbol{e}_\theta)_\varepsilon \quad \forall \boldsymbol{\mu}_N \in \boldsymbol{F}_N, \end{cases} \tag{1.4.15}$$

with $\boldsymbol{v}_{\mathrm{b}} \in \mathbb{R}^3$, , $w_{\mathrm{b}} \in \mathbb{R}$ and where $\boldsymbol{F}_N$ is the vector counterpart of the space F_N given in (1.4.6) such that

$$\boldsymbol{F}_N \overset{\text{def}}{=} \Big\{ \boldsymbol{v} \in \boldsymbol{L}^2(\partial\omega^{\varepsilon}) \ : \\ \boldsymbol{v}(\varepsilon)(\theta) = \boldsymbol{a}_0 + \sum_{k=1}^{n} (\boldsymbol{a}_k \cos(k\theta) + \boldsymbol{b}_k \sin(k\theta)), \quad \boldsymbol{a}_k,\ \boldsymbol{b}_k \in \mathbb{R}^2 \Big\}.$$

The corresponding full order Stokes problem with standard Dirichlet boundary conditions reads: find $(\boldsymbol{u}^\varepsilon, p^\varepsilon, \boldsymbol{\lambda}^\varepsilon) \in \boldsymbol{V} \times Q \times \boldsymbol{H}_\star^{-\frac{1}{2}}(\partial\omega^\varepsilon)$ such that

$$\begin{cases} 2(\boldsymbol{\varepsilon}(\boldsymbol{u}^\varepsilon), \boldsymbol{\varepsilon}(\boldsymbol{v}))_\Omega - (p^\varepsilon, \operatorname{div} \boldsymbol{v})_\Omega + (q, \operatorname{div} \boldsymbol{u}^\varepsilon)_\Omega - \langle \boldsymbol{\lambda}^\varepsilon, \boldsymbol{v} \rangle_{-\frac{1}{2},\partial\omega^\varepsilon} \\ \qquad + \langle \boldsymbol{\mu}^\varepsilon, \boldsymbol{u}^\varepsilon - \boldsymbol{v}_\mathrm{b} - w_\mathrm{b}\boldsymbol{e}_\theta \rangle_{-\frac{1}{2},\partial\omega^\varepsilon} = \boldsymbol{0} \end{cases} \tag{1.4.16}$$

for all $(\boldsymbol{v}, q, \boldsymbol{\mu}) \in \boldsymbol{V} \times Q \times \boldsymbol{H}_\star^{-\frac{1}{2}}(\partial\omega^\varepsilon)$. The well-posedness of Problem (1.4.15) and its ε-convergence towards the Problem (1.4.16) are stated in Theorem 4.2.1 and Theorem 4.2.5, respectively.

Restated Theorem 4.2.1. *Problem* (1.4.16) *admits a unique solution* $(\boldsymbol{u}_N^\varepsilon, p_N^\varepsilon, \boldsymbol{\lambda}_N^\varepsilon)$ *in* $\boldsymbol{V} \times Q \times \boldsymbol{F}_N$*. Moreover, the following a priori estimate holds:*

$$\|\boldsymbol{u}_N^\varepsilon\|_{1,\Omega} + |\log(\varepsilon)|^{-\frac{1}{2}}\|p_N^\varepsilon\|_\Omega + \|\boldsymbol{\lambda}_N^\varepsilon\|_{-\frac{1}{2},\varepsilon} \lesssim |\boldsymbol{v}_\mathrm{b}| + \varepsilon|w_\mathrm{b}|. \tag{1.4.17}$$

Restated Theorem 4.2.5. *Let* $(\boldsymbol{u}^\varepsilon, p^\varepsilon, \boldsymbol{\lambda}^\varepsilon) \in \boldsymbol{V} \times Q \times \boldsymbol{H}^{-\frac{1}{2}}(\partial\omega^\varepsilon)$ *and* $(\boldsymbol{u}_N^\varepsilon, p_N^\varepsilon, \boldsymbol{\lambda}_N^\varepsilon) \in \boldsymbol{V} \times Q \times \boldsymbol{F}_N$ *be solution of* (1.4.15) *and* (1.4.16)*, respectively. There exists* $0 < \tilde{\rho} < \rho$ *such that for all* $\varepsilon \in (0, \tilde{\rho})$*, we have*

$$\begin{aligned} \|\boldsymbol{u}_N^\varepsilon - \boldsymbol{u}^\varepsilon\|_{1,\Omega} + \varepsilon\|\boldsymbol{\lambda}_N^\varepsilon - \boldsymbol{\lambda}^\varepsilon\|_{-\frac{1}{2},\varepsilon} + |\log(\varepsilon)|^{-\frac{1}{2}}\|p_N^\varepsilon - p^\varepsilon\|_\Omega \\ \lesssim (1+N)\left(\frac{\varepsilon}{\rho}\right)^{N+1}(|\boldsymbol{v}_\mathrm{b}| + \varepsilon|w_\mathrm{b}|). \end{aligned} \tag{1.4.18}$$

Similarly to the Poisson case, we observe that the convergence order in ε of the reduced order Stokes problem is equal to the number of Fourier modes $N+1$. Furthermore, at least $N \geqslant 1$ Fourier modes are necessary to ensure the convergence of the Lagrange multipliers with the rescaled norm $\|\cdot\|_{-\frac{1}{2},\varepsilon}$. At the discrete level, similarly to Chapter 3, we introduce in Section 4.3 two numerical methods based on finite element discretization and unfitted mesh. The first method employs a low-order stabilized finite element approach using a $\mathbb{P}_1/\mathbb{P}_1$ discretization for the pair $(\boldsymbol{u}_N^\varepsilon, p_N^\varepsilon)$. Denoting by $\boldsymbol{V}_h$ and Q_h the discrete spaces for the approximation of $\boldsymbol{u}_N^\varepsilon$ and p_N^ε, respectively, it reads: find $(\boldsymbol{u}_{N,h}^\varepsilon, p_{N,h}^\varepsilon, \boldsymbol{\lambda}_{N,h}^\varepsilon) \in \boldsymbol{V}_h \times Q_h \times \boldsymbol{F}_N$ such that

$$\begin{cases} 2(\boldsymbol{\varepsilon}(\boldsymbol{u}_{N,h}^\varepsilon), \boldsymbol{\varepsilon}(\boldsymbol{v}_h))_\Omega - (p_{N,h}^\varepsilon, \operatorname{div} \boldsymbol{v}_h)_\Omega - (\boldsymbol{\lambda}_{N,h}^\varepsilon, \boldsymbol{v}_h) = 0 & \forall \boldsymbol{v}_h \in \boldsymbol{V}_h, \\ (q_h, \operatorname{div} \boldsymbol{u}_{N,h}^\varepsilon)_\Omega + \gamma_p|\log(\varepsilon)|h^2(\nabla q_h, \nabla p_{N,h}^\varepsilon)_\Omega = 0 & \forall q_h \in Q_h, \\ (\boldsymbol{\mu}_N, \boldsymbol{u}_{N,h}^\varepsilon) + \gamma_\lambda\left(\dfrac{h}{\varepsilon}\right)\varepsilon^{-1}(\boldsymbol{\mu}_N, \boldsymbol{\lambda}_{N,h}^\varepsilon)_\varepsilon = (\boldsymbol{\mu}_N, \boldsymbol{v}_\mathrm{b} + \varepsilon w_\mathrm{b}\boldsymbol{e}_\theta)_\varepsilon & \forall \boldsymbol{\mu}_N \in \boldsymbol{F}_N, \end{cases} \tag{1.4.19}$$

where $\gamma_\lambda, \gamma_p > 0$ are user-defined parameters uniformly independent of N, h and ε. We

then derive the following a priori error bounds:

$$\|(\boldsymbol{u}_N^\varepsilon - \boldsymbol{u}_{N,h}^\varepsilon, p_N^\varepsilon - p_{N,h}^\varepsilon, \boldsymbol{\lambda}_N^\varepsilon - \boldsymbol{\lambda}_{N,h}^\varepsilon)\|_\varepsilon \\ \lesssim |\log(\varepsilon)|^{\frac{1}{2}} h^{\frac{1}{2}-\eta} \|\boldsymbol{u}_N^\varepsilon\|_{\frac{3}{2}-\eta,\Omega} + |\log(\varepsilon)|^{\frac{1}{2}} h^{\frac{1}{2}-\eta} \|p_N^\varepsilon\|_{\frac{1}{2}-\eta,\Omega} + \varepsilon^{-\frac{1}{2}} \left(\frac{h}{\varepsilon}\right)^{\frac{1}{2}} \|\lambda_N^\varepsilon\|_\varepsilon,$$

where

$$\|(\boldsymbol{v}_h, q_h, \boldsymbol{\mu}_N)\|_\varepsilon \overset{\text{def}}{=} \\ \left(\|v_h\|_{1,\Omega}^2 + |\log(\varepsilon)|^{-\frac{1}{2}} \|p_h\|_\Omega^2 + \|\boldsymbol{\mu}_N\|_{-\frac{1}{2},\varepsilon}^2 + h^2 |\log(\varepsilon)| \|\nabla p_h\|_\Omega^2 + \left(\frac{h}{\varepsilon}\right) \varepsilon^{-1} \|\boldsymbol{\mu}_N\|_\varepsilon^2\right)^{\frac{1}{2}}$$

for all $(\boldsymbol{v}_h, q_h, \boldsymbol{\mu}_N) \in \boldsymbol{V}_h \times Q_h \times \boldsymbol{F}_N$. This estimate emphasize that, similar to the Poisson problem introduced in Chapter 3, the stabilized finite element method introduced in (1.4.19) is sub-optimal and the maximum h-convergence rate for both the velocity and pressure unknowns is of order $\frac{1}{2} - \eta$. Moreover, we can show that the $H^{\frac{3}{2}-\eta}$ norm of $\boldsymbol{u}_N^\varepsilon$ and the $H^{\frac{1}{2}-\eta}$ norm of p_N^ε are expected to behave as $\varepsilon^{-\frac{1}{2}+\eta}$ as ε goes to 0. Consequently, the error bounds may explode as $h/\varepsilon \to 0$. Subsequently, we propose a high-order finite element method designed to address both of the aforementioned issues. Again, similarly to Chapter 3, it consists in enriching the finite element spaces $\boldsymbol{V}_h$ and Q_h with an explicit solution of the Stokes problem for correctly approximating the singular part of $\boldsymbol{u}_N^\varepsilon$ and p_N^ε. The specificity of the Stokes equations is that we need to enrich both the velocity and the pressure space. Moreover, we consider an inf-sup sable pair of conforming elements $(\boldsymbol{V}_h^k, \tilde{Q}_h^{k-1})$ for the approximation of the velocity and pressure space such that $\operatorname{div}(\boldsymbol{V}_h^k) \subset \tilde{Q}_h^{k-1}$. The discrete formulation of the augmented finite element method reads: find $(\tilde{\boldsymbol{u}}_{N,h}^\varepsilon, \tilde{p}_{N,h}^\varepsilon, \tilde{\boldsymbol{\lambda}}_{N,h}^\varepsilon) \in \boldsymbol{V}_{N,h}^k \times \tilde{Q}_{N,h}^{k-1} \in \boldsymbol{F}_N$ such that

$$2(\boldsymbol{\varepsilon}(\tilde{\boldsymbol{u}}_{N,h}^\varepsilon), \boldsymbol{\varepsilon}(\tilde{\boldsymbol{v}}_{N,h}))_\Omega - (\tilde{p}_{N,h}^\varepsilon, \operatorname{div}; \tilde{\boldsymbol{v}}_{N,h})_\Omega - (\tilde{\boldsymbol{\lambda}}_{N,h}^\varepsilon, \tilde{\boldsymbol{v}}_{N,h})_\varepsilon \\ + (\tilde{q}_{N,h}, \operatorname{div} \tilde{\boldsymbol{u}}_{N,h}^\varepsilon) + (\boldsymbol{\mu}_N, \tilde{\boldsymbol{u}}_{N,h}^\varepsilon)_\varepsilon = (\boldsymbol{\mu}_N, \boldsymbol{v}_\mathrm{b} + w_\mathrm{b} \boldsymbol{e}_\theta)_\varepsilon \quad (1.4.20)$$

for all $(\tilde{\boldsymbol{v}}_{N,h}, \tilde{q}_{N,h}, \boldsymbol{\mu}_N) \in \boldsymbol{V}_{N,h}^k \times \tilde{Q}_{N,h}^{k-1} \times \boldsymbol{F}_N$. The approximation properties of the augmented finite element method (1.4.20) are given in Theorem 4.3.8.

Restated Theorem 4.3.8. *Let $k \geqslant 1$. Let $(\boldsymbol{u}_N^\varepsilon, p_N^\varepsilon, \boldsymbol{\lambda}_N^\varepsilon)$ be the solution of problem* (1.4.15) *and $(\tilde{\boldsymbol{u}}_{N,h}^\varepsilon, \tilde{p}_{N,h}^\varepsilon, \tilde{\boldsymbol{\lambda}}_{N,h})$ be the solution of Problem* (1.4.19)*. Then we have the following,*

$$\|\boldsymbol{u}_N^\varepsilon - \tilde{\boldsymbol{u}}_{N,h}^\varepsilon\|_{1,\Omega} + |\log(\varepsilon)|^{-\frac{1}{2}} \|p_N^\varepsilon - \tilde{p}_{N,h}^\varepsilon\|_\Omega + \|\boldsymbol{\lambda}_N^\varepsilon - \tilde{\boldsymbol{\lambda}}_{N,h}^\varepsilon\|_{-\frac{1}{2},\varepsilon} \\ \lesssim |\log(\varepsilon)|^{\frac{1}{2}} h^k (|\boldsymbol{v}_\mathrm{b}| + \varepsilon |w_\mathrm{b}|)$$

The convergence rate obtained for the Stokes case is similar to the Poisson case. In particular, it enables to restore the optimal convergence in h and to considerably reduce the dependence of the convergence constant with the ratio h/ε. In Section 4.4, we introduce a fully discrete formulation for the reduced order coupled model of small particles immersed in a two-dimensional Stokesian flow. For the time discretization, we consider an explicit treatment of the deformation map $\boldsymbol{\phi}_H^n$ and an implicit treatment of the kinematic and dynamic coupling conditions. The fully discrete strongly coupled model writes: Find $(\boldsymbol{u}_{N,h}^{\varepsilon,n}, p_{N,h}^{\varepsilon,n}, \boldsymbol{\lambda}_{N,h}^{\varepsilon,n}, \boldsymbol{r}^n, \theta^n) \in \boldsymbol{V}_h \times Q_h^n \times \boldsymbol{F}_{N,h}^n \times \mathbb{R}^2 \times \mathbb{R}$ with $\dot{\boldsymbol{r}}^n = \partial_\tau \boldsymbol{r}^n$ and $\dot{\theta}^n = \partial_\tau \theta^n$ such that

$$\begin{cases} \boldsymbol{\phi}_h^n(\widehat{\boldsymbol{x}}) = \boldsymbol{r}^{n-1} + \boldsymbol{\Lambda}^{n-1}\widehat{\boldsymbol{x}} \quad \forall \widehat{\boldsymbol{x}} \in \widehat{\omega}^\varepsilon, \quad \omega^{\varepsilon,n} = \boldsymbol{\phi}_h^n(\widehat{\omega}^\varepsilon), \\ a_\Omega^{\mathrm{f}}\big((\boldsymbol{u}_{N,h}^{\varepsilon,n}, p_{N,h}^{\varepsilon,n}), (\boldsymbol{v}_h, q_h)\big) - 1/\mu_{\mathrm{f}} s_h^p(q_h, p_{N,h}^{\varepsilon,n}) - 1/\mu_{\mathrm{f}} s_h^\lambda(\boldsymbol{\mu}_N, \boldsymbol{\lambda}_{N,h}^{\varepsilon,n}) \\ \quad + I\partial_\tau \dot{\theta}^n \delta\theta + M\partial_\tau \dot{\boldsymbol{r}}^n \cdot \delta\boldsymbol{r} \\ \quad - \big(\boldsymbol{\lambda}_{N,h}^n, \boldsymbol{v}_h - \delta\boldsymbol{r} - \delta\theta(\boldsymbol{I}_2 - \boldsymbol{r}^{n-1})^\perp\big)_{\varepsilon,n} \\ \quad + \big(\boldsymbol{\mu}_{N,h}, \boldsymbol{u}_N^{\varepsilon,n} - \dot{\boldsymbol{r}}^{n-1} - \dot{\theta}^{n-1}(\boldsymbol{I}_2 - \boldsymbol{r}^{n-1})^\perp\big)_{\varepsilon,n} = 0 \end{cases} \tag{1.4.21}$$

for all $(\boldsymbol{v}_h, q_h, \boldsymbol{\mu}_N, \delta\boldsymbol{r}, \delta\theta) \in \boldsymbol{V}_h^n \times Q_h^n \times \boldsymbol{F}_{N,h}^n \times \mathbb{R}^2 \times \mathbb{R}$, where the bilinear form $a_\Omega^{\mathrm{f}} : (\boldsymbol{V}_h \times Q_h^n) \times (\boldsymbol{V}_h \times Q_h^n) \to \mathbb{R}$ is defined by

$$a_\Omega^{\mathrm{f}}((\boldsymbol{u}_h, p_h), (\boldsymbol{v}_h, q_h)) \stackrel{\mathrm{def}}{=} 2\mu_{\mathrm{f}}(\boldsymbol{\varepsilon}(\boldsymbol{u}_h), \boldsymbol{\varepsilon}(\boldsymbol{v}_h))_\Omega - (p_h, \operatorname{div} \boldsymbol{v}_h)_\Omega + (q_h, \operatorname{div} \boldsymbol{u}_h)_\Omega$$

In Section 4.5, we illustrate with numerical experiments the results presented above. We also analyse similarly to the numerical experiments implemented in Chapter 2 the role of the Lagrange multiplier space on the fluid and solid dynamics. In Figure 1.4, we provide some snapshots of the velocity magnitude for a falling elliptical particle in a Stokesian flow obtained with the discrete formulation (1.4.21) using $N = 1$ modes. We can observe that both the translation and rotation dynamics are captured by the reduced order scheme.

1.4.4 Chapter 5: Loosely coupled Robin-Robin scheme for the simulation of slender bodies immersed in an incompressible flow

In this last chapter, we return to the analysis of the 3D addressed in Chapter 2. The main objective of defining the reduced order coupling conditions (1.4.3) is to propose an approach that enables the simulation of complex systems, possibly including a large number of slender structures, by reducing the cost associated to the computation of the coupling conditions. In Chapter 2, the time discretization of the coupling conditions is based on a semi-implicit scheme, with an explicit treatment of the geometric coupling conditions and an implicit treatment of the kinematics and dynamics coupling conditions. As mentioned in Section 1.3.3, one of the main advantages of this approach is that it delivers unconditional stability. However, it also requires a large number of iterations at each time step to

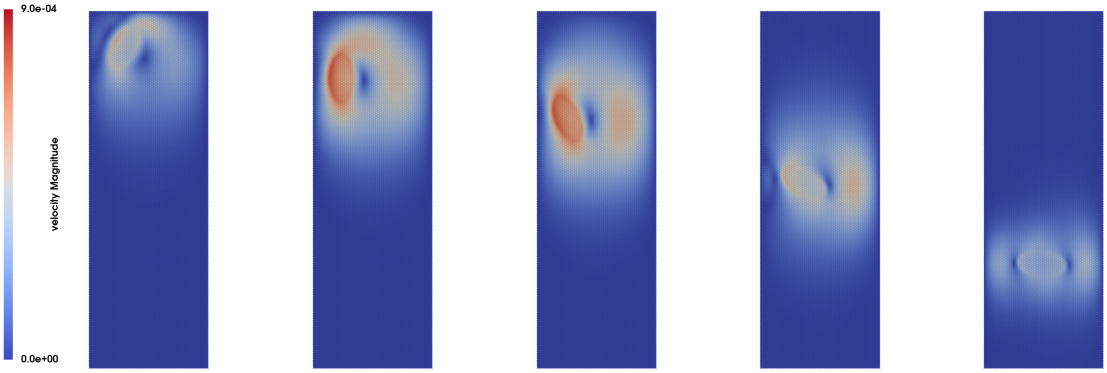

Figure 1.4: *Snaphots of the fluid velocity magnitude at time* $t \in \{0, 500, 1000, 2000, 4000\}$ *for a falling elliptical particle in a Stokesian flow obtained with formulation* (1.4.21) *and* $N = 1$

solve the non-linear coupled system, which can be computationally expensive. Ideally, explicitly solving the fluid and structure sub-problems, meaning addressing them only once per time step, would significantly reduce the computational cost of the resolution of the overall system. Unfortunately, in scenarios with highly slender structures or a low ratio between the structures and fluid density, standard explicit methods often suffer from instability. Subsequently, in this final chapter, we introduce a stable loosely coupled scheme, based on Robin-type coupling conditions for the fluid and solid sub-problems, specifically developed for the simulation of structures defined on domain of co-dimension two with respect to the fluid domain. To this purpose, we introduce $\widehat{\boldsymbol{F}}_{0,H}$ and $\widehat{\boldsymbol{F}}_{N^\star,H}$ such that

$$\begin{aligned}
\widehat{\boldsymbol{F}}_{0,H} &\overset{\text{def}}{=} \big\{\widehat{\boldsymbol{v}}_H \in \boldsymbol{L}^2(\partial\widehat{\omega}^\varepsilon) \ : \ \widehat{\boldsymbol{v}}_H(s,\nu) = \boldsymbol{a}_{0,H}(s), \quad \boldsymbol{a}_{0,H} \in \boldsymbol{Y}_H\big\}.\\
\widehat{\boldsymbol{F}}_{N^\star,H} &\overset{\text{def}}{=} \big\{\widehat{\boldsymbol{v}}_H \in \boldsymbol{L}^2(\partial\widehat{\omega}^\varepsilon) : \\
&\qquad \widehat{\boldsymbol{v}}_H(s,\nu) \overset{\text{def}}{=} \sum_{k=0}^{N} \boldsymbol{a}_{k,H}\cos(k\nu) + \boldsymbol{b}_{k,H}\sin(k\nu), \quad \boldsymbol{a}_{k,H}, \boldsymbol{b}_{k,H} \in \boldsymbol{Y}_H\big\},
\end{aligned}$$

and $\widehat{\boldsymbol{\Pi}}_{0,H}$, $\widehat{\boldsymbol{\Pi}}_{N^\star,H}$ the L^2 orthogonal projector on $\widehat{\boldsymbol{F}}_{0,H}$ and $\widehat{\boldsymbol{F}}_{N^\star,H}$ respectively. If we neglect the rotation contributions in the kinematic and dynamic coupling conditions, the coupling conditions for the Robin-Robin loosely coupled scheme write for the fluid and structure sub-problems, respectively:

$$\begin{aligned}
-(\boldsymbol{\lambda}^n_{0,H}, \overline{\delta\boldsymbol{r}_H})_{\hat{\varepsilon}} + \alpha(\overline{\dot{\boldsymbol{r}}_H^{\,n-\frac{1}{2}}}, \overline{\delta\boldsymbol{r}_H})_{\hat{\varepsilon}} \\
= \alpha(\boldsymbol{u}_h^{n-1}\circ\boldsymbol{\phi}_H^{n-1}, \overline{\delta\boldsymbol{r}_H})_{\hat{\varepsilon}} - (\boldsymbol{\lambda}^{n-1}_{0,H}, \overline{\delta\boldsymbol{r}_H})_{\hat{\varepsilon}} \quad \forall \delta\boldsymbol{r}_H \in \boldsymbol{Y}_h
\end{aligned} \tag{1.4.22}$$

and

$$\begin{cases} -(\boldsymbol{\mu}_{0,H}, \boldsymbol{\lambda}_{0,H}^n)_{\widehat{\varepsilon}} + \alpha(\boldsymbol{\mu}_{0,H}, \boldsymbol{u}_h^n \circ \boldsymbol{\phi}_H^n)_{\widehat{\varepsilon}} \\ \qquad\qquad = \alpha(\boldsymbol{\mu}_{0,H}, \overline{\dot{\boldsymbol{r}}_H^{n-\frac{1}{2}}})_{\widehat{\varepsilon}} - (\boldsymbol{\mu}_{0,H}, \boldsymbol{\lambda}_{0,H}^{n-1})_{\widehat{\varepsilon}} \quad \forall \boldsymbol{\mu}_{0,H} \in \widehat{\boldsymbol{F}}_{0,H} \\ (\boldsymbol{\mu}_{N^\star,H}, \boldsymbol{u}_h \circ \boldsymbol{\phi}_H^n)_{\widehat{\varepsilon}} = 0 \quad \forall \boldsymbol{\mu}_{N^\star,H} \in \widehat{\boldsymbol{F}}_{N^\star,H}, \end{cases} \tag{1.4.23}$$

The fully discrete formulation of the coupled problem (2.2.4),(2.2.21) with Lagrange multiplier space (1.4.4) and Robin-Robin coupling conditions (1.4.22)-(1.4.23) is given in Section 5.2 by the following algorithm: $\forall n \geqslant 0$

Solid sub-problem:

Find $(\boldsymbol{r}_H^n, \boldsymbol{\theta}_H^n) \in \boldsymbol{Y}_H \times \boldsymbol{Y}_H$ such that $(\dot{\boldsymbol{r}}_H^{n-\frac{1}{2}}, \dot{\boldsymbol{\theta}}_H^{n-\frac{1}{2}}) = (\partial_\tau \boldsymbol{r}_H^n, \partial_\tau \boldsymbol{\theta}_H^n)$ and

$$\begin{cases} \rho^{\mathrm{b}}\big(\boldsymbol{A}\partial_\tau \dot{\boldsymbol{r}}_H^n, \delta\boldsymbol{r}_H\big)_{(0,L)} + \rho^{\mathrm{b}}\big(\boldsymbol{I}\partial_\tau \dot{\boldsymbol{\theta}}_H^n, \delta\boldsymbol{\theta}_H\big)_{(0,L)} \\ + a_H^{\mathrm{b}}\big((\boldsymbol{r}_H^{n-\frac{1}{2}}, \boldsymbol{\theta}_H^{n-\frac{1}{2}}), (\delta\boldsymbol{r}_H, \delta\boldsymbol{\theta}_H)\big) \\ + \alpha(\overline{\dot{\boldsymbol{r}}_H^{n-\frac{1}{2}}} - \boldsymbol{u}_h^{n-1} \circ \boldsymbol{\phi}_H^{n-1}, \overline{\delta\boldsymbol{r}_H})_{\widehat{\varepsilon}} = -\big(\boldsymbol{\lambda}_{0,H}^{n-1}, \overline{\delta\boldsymbol{r}_H}\big)_{\widehat{\varepsilon}} \end{cases} \tag{1.4.24}$$

Deformation map:

$$\boldsymbol{\phi}_H^n = (\boldsymbol{I}_3 \cdot \boldsymbol{e}_z)\boldsymbol{e}_z + \overline{\boldsymbol{r}_H^n} + \overline{\boldsymbol{\Lambda}_H^n}\big(\boldsymbol{I}_3 - (\boldsymbol{I}_3 \cdot \boldsymbol{e}_z)\boldsymbol{e}_z\big) \quad \text{in} \quad \widehat{\omega}^\varepsilon. \tag{1.4.25}$$

Fluid sub-problem:

Find $(\boldsymbol{u}_h^n, p_h^n, \boldsymbol{\lambda}_{N,H}^n) \in \boldsymbol{V}_h \times Q_h \times \widehat{\boldsymbol{F}}_{N,H} \times \boldsymbol{Y}_H \times \boldsymbol{Y}_H$ such that

$$\begin{cases} \rho^{\mathrm{f}}(\partial_\tau \boldsymbol{u}_h^n, \boldsymbol{v}_h)_\Omega + a_{\Omega,h}^{\mathrm{f}}\big(\boldsymbol{u}_h^{n-1}; (\boldsymbol{u}_h^n, p_h^n), (\boldsymbol{v}_h, q_h)\big) - (\boldsymbol{\lambda}_{N,H}^n, \boldsymbol{v}_h \circ \boldsymbol{\phi}_H^n)_{\widehat{\varepsilon}} \\ + \alpha(\boldsymbol{\mu}_{0,H}, \boldsymbol{u}_h^n \circ \boldsymbol{\phi}_H^n - \overline{\dot{\boldsymbol{r}}_H^{n-\frac{1}{2}}})_{\widehat{\varepsilon}} + (\boldsymbol{\mu}_{0,H}, \boldsymbol{\lambda}_{0,H}^n - \boldsymbol{\lambda}_{0,H}^{n-1})_{\widehat{\varepsilon}} \\ + (\boldsymbol{\mu}_{N^\star,H}, \boldsymbol{u}_h^n \circ \boldsymbol{\phi}_H^n)_{\widehat{\varepsilon}} = 0, \\ \boldsymbol{\lambda}_{0,H}^{n-1} = \widehat{\boldsymbol{\Pi}}_{0,H}(\boldsymbol{\lambda}_{N,H}^{n-1}), \quad \boldsymbol{\lambda}_{0,H}^n = \widehat{\boldsymbol{\Pi}}_{0,H}(\boldsymbol{\lambda}_{N,H}^n). \end{cases} \tag{1.4.26}$$

for all $(\boldsymbol{v}_h, q_h, \boldsymbol{\mu}_{N,H}, \delta\boldsymbol{r}_H, \boldsymbol{\theta}_H) \in \boldsymbol{V}_h \times Q_h \times \widehat{\boldsymbol{F}}_{N,H} \times \boldsymbol{Y}_H \times \boldsymbol{Y}_H$ with $(\boldsymbol{\mu}_{0,H}, \boldsymbol{\mu}_{N^\star,H}) = (\widehat{\boldsymbol{\Pi}}_{0,H}(\boldsymbol{\mu}_{N,H}), \widehat{\boldsymbol{\Pi}}_{N^\star,H}(\boldsymbol{\mu}_{N,H}))$. The stability of Algorithm (1.4.24)-(1.4.26) is proved in Section 5.2.2 as stated in Theorem 5.2.1.

Restated Theorem 5.2.1. *Let* $\{(\boldsymbol{u}_h^n, p_h^n, \boldsymbol{\lambda}_{N,H}^n, \boldsymbol{r}_H^n, \boldsymbol{\theta}_H^n)\}$ *be given by Algorithm* (1.4.24)-(1.4.26)*. There holds*

$$\mathfrak{E}^n + \sum_{m=1}^{n} \mathfrak{D}^m \leqslant \mathfrak{E}^0 \quad \forall n \geqslant 0, \tag{1.4.27}$$

where the discrete mechanical energy $\mathfrak{E}^n$ of the system is defined by

$$\begin{aligned}\mathfrak{E}^n \overset{\text{def}}{=}& \rho^{\mathrm{f}}\|\boldsymbol{u}_h^n\|_{\Omega}^2 + \rho^{\mathrm{b}}\|\dot{\boldsymbol{r}}_H^n\|_{\boldsymbol{A},(0,L)}^2 + \rho^{\mathrm{b}}\|\dot{\boldsymbol{\theta}}_H^n\|_{\boldsymbol{I},(0,L)}^2 + \|(\boldsymbol{r}_H^n,\boldsymbol{\theta}_H^n)\|_{\mathrm{b},H}^2 \\ &+ \tau\alpha\|\widehat{\boldsymbol{\Pi}}_{0,H}(\boldsymbol{u}_h^n \circ \boldsymbol{\phi}_H^n)\|_{\hat{\varepsilon}}^2 + \frac{\tau}{\alpha}\|\boldsymbol{\lambda}_{0,H}^n\|_{\hat{\varepsilon}}^2 \\ \mathfrak{D}^n \overset{\text{def}}{=}& 2\mu_{\mathrm{f}}\tau\|\boldsymbol{\varepsilon}(\boldsymbol{u}_h^n)\|_{\Omega}^2 + \rho^f\|\boldsymbol{u}_h^n - \boldsymbol{u}_h^{n-1}\|_{\Omega}^2 + 2\alpha\tau\|\overline{\dot{\boldsymbol{r}}_H^{n-\frac{1}{2}}} - \widehat{\boldsymbol{\Pi}}_{0,H}(\boldsymbol{u}_h^{n-1} \circ \boldsymbol{\phi}_H^{n-1})\|_{\hat{\varepsilon}}^2.\end{aligned}$$

with

$$\|\cdot\|_{\boldsymbol{A},(0,L)} \overset{\text{def}}{=} \sqrt{(\boldsymbol{A}\,\cdot,\cdot)_{(0,L)}}, \quad \|\cdot\|_{\boldsymbol{I},(0,L)} \overset{\text{def}}{=} \sqrt{(\boldsymbol{I}\,\cdot,\cdot)_{(0,L)}},$$
$$\|\cdot,\cdot\|_{\mathrm{b},H} \overset{\text{def}}{=} \sqrt{a_H^{\mathrm{b}}\big((\cdot,\cdot),(\cdot,\cdot)\big)}.$$

Finally, in Section 5.3, we consider some numerical tests used in Section 2.4 of Chapter 2 and compare the solutions obtained with the semi-implicit coupled scheme (1.4.5) and the Robin-Robin loosely coupled scheme (1.4.24)-(1.4.26) validating in this way the accuracy of the proposed algorithm. In particular, we consider the multiple beams test case presented in Figure 1.2 with Navier-Stokes equations for fluid model. Snapshots of the velocity magnitude at time $t = 0.06$ for the semi-implicit and Robin-Robin loosely coupled scheme are provided in Figure 1.5.

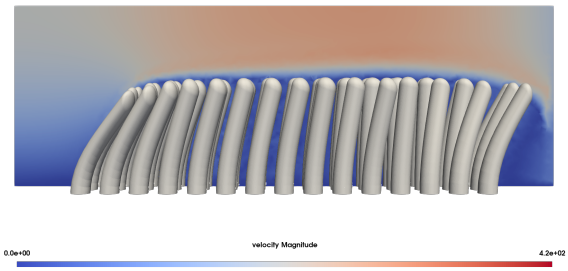

Formulation (1.4.24)-(1.4.26), $N = 2$

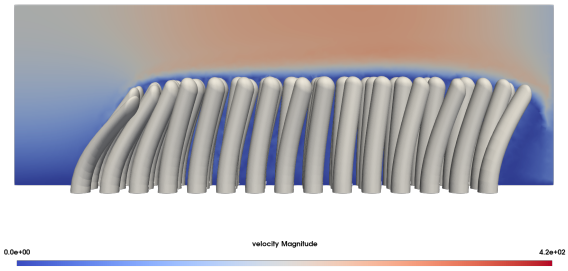

Formulation (1.4.5), $N = 2$

Figure 1.5: *Snapshots of the fluid velocity magnitude for multiple beams immersed in a Navier-Stokes flow with formulation* (1.4.24)-(1.4.26) *(up) and formulation* (1.4.5) *(down),* $N = 2$ *at time* $t = 0.06$.

CHAPTER 2

A mixed-dimensional formulation for the simulation of slender structures immersed in an an compressible flow

Corresponding to the preprint [Lespagnol et al., 2023].

2.1 Introduction

In this chapter, we introduce a new modelling and computational framework for the simulation of slender structures immersed in a three-dimensional (3D) flow. Slender structures are characterized by a low ratio between the transversal size and the longitudinal length. Owing to the geometrical properties of slender structures, many models have exploited the mixed-dimensional nature of these coupled systems with the purpose of developing more efficient computational approaches, in which the solid balance equations are written in a one-dimensional domain (1D). A specific case we explore in this context is the use of beam theory for the solid balance equations, resulting in a particular case of fluid-structure interaction problems also known as fluid-beam interaction, (see Section 1.2.2 for an overview on beam theory). A widely used modeling simplification when coupling general media featuring a dimensional gap of one, viz., 2D-1D or 3D-2D coupling consists in identifying

the beam centerline with the fluid-structure interface by neglecting the beam thickness (see e.g [Baaijens, 2001, Boilevin-Kayl et al., 2019]). These models were proved to be a good approximation of the original fully 3D or 2D problem when the thickness of the slender body tends to 0 (see, e.g., [Chapelle and Ferent, 2003, Landajuela et al., 2017]). However, in cases where 3D flows interact with 1D beams, the situation is much more delicate. Such dimensional gap lead to ill-posed trace operators, complicating the formulation of the load and motion transfer conditions. It also calls for innovative numerical techniques to bridge the gap between local fluid dynamics near the beam and global behavior of the system. Two distinct modeling approaches can be found in the literature. A first family of methods is based on the formulation of the interface coupling conditions on the physical (2D) reconstructed surface of the beam (see, e.g., [Maniyeri and Kang, 2012, Huang et al., 2019, Ausas et al., 2022b]), while the second one reduces the complexity of the problem by considering the interface as the (1D) centerline of the beam (see, e.g., [Griffith and Lim, 2012, Wiens and Stockie, 2015, Wang et al., 2019, Hagmeyer et al., 2022, Hagmeyer et al., 2023]). The strengths and weaknesses of each formulation as well as a review of some existing numerical methods for the discretization of 3D-1D fluid-structure interaction coupled problems are given in Sections 1.2.3 and 1.3.2, respectively.

In this chapter, we consider another modeling approach which the basic idea consists in combining a fictitious domain methodology with a projection of the kinematic constraint onto a finite-dimensional space lying on the beam centerline. More precisely, on each cross section of the beam, the original kinematic constraint is replaced by a constraint which acts only on the first N modes of the Fourier expansion of the velocity at the interface (see [Khristenko et al., 2021] for a similar idea in the context of reinforced materials). This method has been used in [Kuchta et al., 2021b] for $N = 0$ for stationary elliptic problems (use of averaged porjection operators). Notably, the work demonstrated the well-posedness of both the continuous and discrete models within the framework of the finite element method. To some extent, this approach could be seen as a bridge, rectifying certain disparities among the aforementioned sets of fluid-beam interaction methodologies, whether employing a 2D or a 1D representation of the interface and aims to be a compromise between accuracy, computational cost and robustness.

In order to illustrate the accuracy of the proposed strategy, we compare it with two others approaches, a full order model based on the ALE approach with couplings conditions on the reconstructed 2D interface and another reduced mixed-dimensional model with coupling conditions on the beam centerline. In particular, we will investigate the influence of the Reynolds number, of the fluid mesh refinement, or of the number of Fourier modes taken for the Lagrange multiplier space.

The rest of the chapter is organized as follows. In Section 2.2, we describe the fluid and solid models, as well as the coupling conditions for the full order ALE coupled model and two reduced mixed-dimensional coupled models. The discrete formulation of the proposed model is provided in Section 2.3. A few computer implementation details of

the considered solution procedure are also given. Section 2.4 is devoted to the numerical experiments, where we investigate how different model parameters impact the accuracy and robustness of the proposed approach. Finally, a summary of the results of this chapter together with some research perspectives are drawn in Section 2.5.

2.2 Continuous setting and mathematical formulation

In this section, we briefly present the beam and fluid models considered in this chapter. We choose a linear Timoshenko beam formulation for the solid and the fluid is assumed to satisfied the incompressible Navier-Stokes equations. Our approach will be presented in Section 2.2.2.5 for the fluid and in Section 2.2.3.4 for the coupling conditions.

2.2.1 Timoshenko beam model

Let $(\boldsymbol{e}_x, \boldsymbol{e}_y, \boldsymbol{e}_z)$ be a given right-handed Cartesian frame. We consider a reference straight beam of length L and elliptical cross-sections orthogonal to its centerline, denoted by $\widehat{\omega}^\varepsilon \overset{\text{def}}{=} \varepsilon\mathcal{E}(a,1) \times (0,L)$. Here $\mathcal{E}(a,b)$ stands for an elliptical region in the (xOy) plane with major axis of length a and a minor axis of length b, and ε is a parameter related to the thickness of the beam. For $s \in (0,L)$, we denote by $\widehat{\omega}^\varepsilon(s) \overset{\text{def}}{=} \varepsilon\mathcal{E}(a,1) \times \{s\}$ the cross-section centered in $s\boldsymbol{e}_z$, such that $\widehat{\omega}^\varepsilon = \bigcup_{s\in(0,L)} \widehat{\omega}^\varepsilon(s)$ (see Figure 2.1). For the sake of simplicity, we assume that $\widehat{\omega}^\varepsilon$ corresponds to the position of a beam at the initial time. The motion of the beam is given in terms of the map $\boldsymbol{\phi} : \widehat{\omega}^\varepsilon \times \mathbb{R}^+ \to \mathbb{R}^3$, so that the current configuration of the beam $\omega^\varepsilon(t)$ is given by $\omega^\varepsilon(t) = \boldsymbol{\phi}(\widehat{\omega}^\varepsilon, t)$ (see Figure 2.2). In what follows, we consider a Timoshenko beam model, such that the cross-sections are supposed to remain undeformable but may not necessarily remain perpendicular to the beam centerline. The motion of the beam can hence be parametrized in the following way:

$$\boldsymbol{\phi}(\widehat{\boldsymbol{x}}, t) = s\boldsymbol{e}_z + \boldsymbol{r}(s,t) + \boldsymbol{\Lambda}(s,t)(\widehat{\boldsymbol{x}} - s\boldsymbol{e}_z), \quad s = \widehat{\boldsymbol{x}} \cdot \boldsymbol{e}_z, \quad (\widehat{\boldsymbol{x}}, t) \in \widehat{\omega}^\varepsilon \times \mathbb{R}^+, \quad (2.2.1)$$

where $\boldsymbol{r} : (0,L) \times \mathbb{R}^+ \to \mathbb{R}^3$ stands for the displacement of the centerline and $\boldsymbol{\Lambda} : (0,L) \times \mathbb{R}^+ \to SO(3)$ describes the rotation of the cross-sections. Here, $SO(3)$ stands for the Special Orthogonal group given by

$$SO(3) \overset{\text{def}}{=} \{\boldsymbol{\Lambda} \in \mathbb{R}^{3\times 3} \ : \ \boldsymbol{\Lambda}^{\mathrm{T}}\boldsymbol{\Lambda} = \boldsymbol{I}_3, \quad \det \boldsymbol{\Lambda} = 1\}, \quad (2.2.2)$$

where $\boldsymbol{I}_3$ denotes the identity matrix in $\mathbb{R}^{3\times 3}$. Note, in particular, that the centerline $\mathcal{B}(t)$ and the cross-sections $(\omega^\varepsilon(s,t))_{s\in(0,L)}$ of the current configuration of the beam are given respectively by

$$\mathcal{B}(t) \overset{\text{def}}{=} \boldsymbol{\phi}\big(\widehat{\mathcal{B}}, t\big), \quad \widehat{\mathcal{B}} \overset{\text{def}}{=} \{0\} \times \{0\} \times (0,L), \quad \omega^\varepsilon(s,t) \overset{\text{def}}{=} \boldsymbol{\phi}(\widehat{\omega}^\varepsilon(s), t).$$

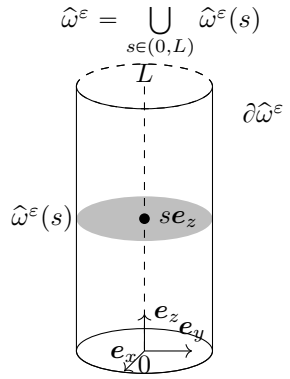

(a) *Reference configuration of the beam.*

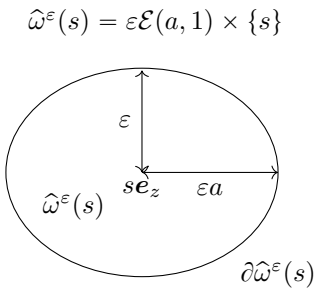

(b) *Elliptical cross-section of the beam in the reference configuration.*

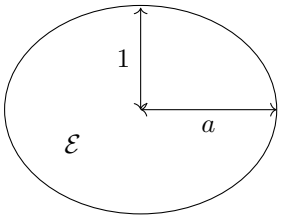

(c) *Reference ellipse.*

Figure 2.1: *Geometrical configuration of the beam and notations.*

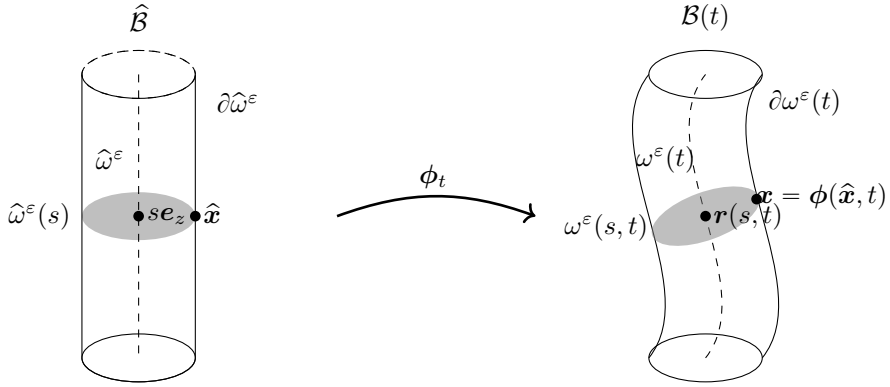

Figure 2.2: *The deformation map.*

Due to the orthogonality of the rotation matrix $\boldsymbol{\Lambda}$, it can be given only in terms of three independent parameters. One option is to consider the rotational vector, defined by

$$\boldsymbol{\theta} \stackrel{\text{def}}{=} \theta \boldsymbol{n}^\perp,$$

where $\boldsymbol{n}^{\perp}$ is a unit vector defining the axis of rotation and $\theta = \sqrt{\boldsymbol{\theta}\cdot\boldsymbol{\theta}}$ is the angle of rotation. We set $\boldsymbol{\Theta}$ the skew symetric matrix associated to the vector $\boldsymbol{\theta}$ such that for all $\boldsymbol{v} \in \mathbb{R}^3$,

$$\boldsymbol{\Theta}\boldsymbol{v} = \boldsymbol{\theta} \wedge \boldsymbol{v},$$

where the symbol $\wedge$ denotes the cross product in three dimensions. Using Rodrigues' rotation formula (see, e.g., [Dai, 2015]), the relation between the rotation matrix and the rotational vector is then given by

$$\boldsymbol{\Lambda} = \boldsymbol{I}_3 + \frac{\sin\theta}{\theta}\boldsymbol{\Theta} + \frac{1-\cos\theta}{\theta^2}\boldsymbol{\Theta}^2. \tag{2.2.3}$$

Consequently, the dynamics of the beam will be given in terms of $\boldsymbol{r}$ and $\boldsymbol{\theta}$, which will here be described by a variant of the linear elastic model introduced in [Arunakirinathar and Reddy, 1993] for the static case. The model accounts for bending, shear, torsion, and membrane effects within a small displacements and rotations framework. More precisely, the dynamics of the beam are described by the following balance equations:

$$\begin{cases} \rho_{\mathrm{b}}\boldsymbol{A}\partial_t^2\boldsymbol{r} - \boldsymbol{G}\partial_s\big(\partial_s\boldsymbol{r} - \boldsymbol{\theta}\wedge\boldsymbol{e}_z\big) = \boldsymbol{f} & \text{in} \quad (0,L)\times\mathbb{R}^+, \\ \rho_{\mathrm{b}}\boldsymbol{I}\partial_t^2\boldsymbol{\theta} - \boldsymbol{E}\partial_s^2\boldsymbol{\theta} - \boldsymbol{e}_z\wedge\boldsymbol{G}\big(\partial_s\boldsymbol{r} - \boldsymbol{\theta}\wedge\boldsymbol{e}_z\big) = \boldsymbol{m} & \text{in} \quad (0,L)\times\mathbb{R}^+, \end{cases} \tag{2.2.4}$$

where the matrices $\boldsymbol{A}$, $\boldsymbol{I}$, $\boldsymbol{E}$ and $\boldsymbol{G}$ are given by

$$\boldsymbol{A} \overset{\text{def}}{=} \begin{bmatrix} A & 0 & 0 \\ 0 & A & 0 \\ 0 & 0 & A \end{bmatrix}, \qquad \boldsymbol{I} \overset{\text{def}}{=} \begin{bmatrix} I_x & 0 & 0 \\ 0 & I_y & 0 \\ 0 & 0 & J \end{bmatrix},$$

$$\boldsymbol{G} \overset{\text{def}}{=} \begin{bmatrix} GA\kappa & 0 & 0 \\ 0 & GA\kappa & 0 \\ 0 & 0 & EA \end{bmatrix}, \qquad \boldsymbol{E} \overset{\text{def}}{=} \begin{bmatrix} EI_x & 0 & 0 \\ 0 & EI_y & 0 \\ 0 & 0 & GJ \end{bmatrix},$$

and the symbols ρ_{b}, E, G, I_x, I_y, J, A and κ, respectively, denote the linear density, Young's modulus, the shear modulus, the principal moments of inertia in x and y, the second moment of inertia, the cross-sectional area and the shear correction factor.

2.2.2 Navier-Stokes fluid model

In this paper, the fluid is modeled by the incompressible Navier-Stokes equations, written with full or reduced formulations that will lead to different numerical schemes. For the sake of simplicity we present the different models and strategies in the case where homogeneous Dirichlet boundary conditions are prescribed on the fluid boundary that is not the fluid-structure interface. We assume here that $\boldsymbol{r}$ and $\boldsymbol{\Lambda}$ are regular enough and that for all

t, $\boldsymbol{\phi}_t \stackrel{\text{def}}{=} \boldsymbol{\phi}(\cdot, t) : \widehat{\omega}^\varepsilon \to \omega^\varepsilon(t)$ is one to one. The beam is supposed to move within a fixed and smooth bounded domain $\Omega \subset \mathbb{R}^3$ and we assume that it is surrounded by a fluid which occupies $\widehat{\Omega}_{\mathrm{f}}^\varepsilon \stackrel{\text{def}}{=} \Omega \backslash \overline{\widehat{\omega}^\varepsilon}$ in the reference configuration and at each time t the time-dependent domain

$$\Omega_{\mathrm{f}}^\varepsilon(t) \stackrel{\text{def}}{=} \Omega \backslash \overline{\omega^\varepsilon}(t) \subset \mathbb{R}^3$$

in the current configuration. In what follows, $\Sigma^\varepsilon(t) \stackrel{\text{def}}{=} \partial\Omega_{\mathrm{f}}^\varepsilon(t) \cap \partial\omega^\varepsilon(t)$ denotes the current configuration of the fluid-solid interface. The fluid domain boundary is partitioned as $\partial\Omega_{\mathrm{f}}^\varepsilon(t) = \Sigma^\varepsilon(t) \cup \Gamma$, with $\Gamma \subset \partial\Omega$. Furthermore, we can introduce the trajectory of the fluid domain as the non-cylindrical space-time domain:

$$\mathcal{O} \stackrel{\text{def}}{=} \bigcup_{t \in \mathbb{R}^+} \Omega_{\mathrm{f}}^\varepsilon(t) \times \{t\}. \tag{2.2.5}$$

2.2.2.1 Eulerian formalism

The fluid equations in the Eulerian formalism read: find the fluid velocity $\boldsymbol{u} : \mathcal{O} \to \mathbb{R}^3$ and fluid pressure $p : \mathcal{O} \to \mathbb{R}$ such that

$$\begin{cases} \rho_{\mathrm{f}} \partial_t \boldsymbol{u} + \rho_{\mathrm{f}} \boldsymbol{u} \cdot \boldsymbol{\nabla} \boldsymbol{u} - \boldsymbol{\nabla} \cdot \boldsymbol{\sigma}(\boldsymbol{u}, p) = \boldsymbol{0} & \text{in} \quad \Omega_{\mathrm{f}}^\varepsilon(t), \\ \boldsymbol{\nabla} \cdot \boldsymbol{u} = 0 & \text{in} \quad \Omega_{\mathrm{f}}^\varepsilon(t), \\ \boldsymbol{u} = \boldsymbol{0} & \text{on} \quad \Gamma, \\ \boldsymbol{u} = \boldsymbol{u}_{\mathrm{b}} & \text{on} \quad \Sigma^\varepsilon(t) \end{cases} \tag{2.2.6}$$

Here, ρ_{f} stands for the fluid density, μ_{f} for the dynamic viscosity of the fluid, and $\boldsymbol{\sigma}(\boldsymbol{u}, p)$ denotes the Cauchy stress tensor given by

$$\boldsymbol{\sigma}(\boldsymbol{u}, p) \stackrel{\text{def}}{=} 2\mu_{\mathrm{f}} \boldsymbol{\varepsilon}(\boldsymbol{u}) - p \boldsymbol{I}_3, \quad \boldsymbol{\varepsilon}(\boldsymbol{u}) \stackrel{\text{def}}{=} \frac{1}{2}\big(\boldsymbol{\nabla} \boldsymbol{u} + (\boldsymbol{\nabla} \boldsymbol{u})^{\mathrm{T}}\big). \tag{2.2.7}$$

Lastly, $\boldsymbol{u}_{\mathrm{b}}$ denotes the Eulerian velocity of the beam, which will be linked to the beam unknowns in Section 2.2.3 below.

2.2.2.2 ALE formalism

In the ALE formalism, the fluid domain $\Omega_{\mathrm{f}}^\varepsilon(t)$ is parametrized by a one-to-one mapping $\boldsymbol{\mathcal{A}} : \widehat{\Omega}_{\mathrm{f}}^\varepsilon \times \mathbb{R}^+ \to \mathbb{R}^3$ such that $\Omega_{\mathrm{f}}^\varepsilon(t) = \boldsymbol{\mathcal{A}}(\widehat{\Omega}_{\mathrm{f}}^\varepsilon, t)$, for $t \in \mathbb{R}^+$. We also set $\boldsymbol{\mathcal{A}}_t(\cdot) = \boldsymbol{\mathcal{A}}(\cdot, t)$. We can hence defined the ALE time derivative

$$\partial_t|_{\boldsymbol{\mathcal{A}}} \boldsymbol{u}(\boldsymbol{x}, t) = \frac{\mathrm{d}}{\mathrm{d}t}\big(\boldsymbol{u}(\boldsymbol{\mathcal{A}}(\widehat{\boldsymbol{x}}, t), t)\big), \quad \widehat{\boldsymbol{x}} = \boldsymbol{\mathcal{A}}_t^{-1}(\boldsymbol{x}).$$

By a simple use of the chain rule, we obtain the following relation

$$\partial_t \boldsymbol{u} = \partial_t|_{\boldsymbol{\mathcal{A}}} \boldsymbol{u} - (\widehat{\boldsymbol{w}}_{\mathrm{f}} \circ \boldsymbol{\mathcal{A}}_t^{-1}) \cdot \boldsymbol{\nabla} \boldsymbol{u}, \tag{2.2.8}$$

where $\widehat{\boldsymbol{w}}_{\mathrm{f}} \overset{\text{def}}{=} \partial_t \boldsymbol{\mathcal{A}}$ is the fluid domain velocity. In what follows, when dealing with equations expressed in the ALE formalism, for any function $\widehat{\boldsymbol{v}}$ defined in $\widehat{\omega}_{\mathrm{f}}^{\varepsilon}$, we will denote by $\boldsymbol{v} = \widehat{\boldsymbol{v}} \circ (\boldsymbol{\mathcal{A}}_t)^{-1}$ its Eulerian counterpart. The fluid equations (2.2.6) admit the following equivalent formulation: find the fluid velocity $\boldsymbol{u} : \mathcal{O} \to \mathbb{R}^3$ and fluid pressure $p : \mathcal{O} \to \mathbb{R}$ such that

$$\begin{cases} \rho_{\mathrm{f}} \partial_t|_{\boldsymbol{\mathcal{A}}} \boldsymbol{u} + \rho_{\mathrm{f}} (\boldsymbol{u} - \boldsymbol{w}_{\mathrm{f}}) \cdot \boldsymbol{\nabla} \boldsymbol{u} - \boldsymbol{\nabla} \cdot \boldsymbol{\sigma}(\boldsymbol{u}, p) = \boldsymbol{0} & \text{in} \quad \Omega_{\mathrm{f}}^{\varepsilon}(t), \\ \boldsymbol{\nabla} \cdot \boldsymbol{u} = 0 & \text{in} \quad \Omega_{\mathrm{f}}^{\varepsilon}(t), \\ \boldsymbol{u} = \boldsymbol{0} & \text{on} \quad \Gamma, \\ \boldsymbol{u} = \boldsymbol{u}_{\mathrm{b}} & \text{on} \quad \Sigma^{\varepsilon}(t). \end{cases} \tag{2.2.9}$$

The main advantage of (2.2.9) with respect of (2.2.8) is that it facilitates the discretization in time.

2.2.2.3 Fictitious domain approach

In what follows, for any Lipschitz domain $\mathcal{D}$ in $\mathbb{R}^d$, $d \in \{2, 3\}$, we will make use of the standard Sobolev spaces $H^s(\mathcal{D})$ and $L^m(\mathcal{D})$ ($s \in \mathbb{R}$, $m \in \mathbb{N} \cap [1, +\infty[$). We also denote by $H^1_{\mathcal{S}}(\mathcal{D})$ the closed subspace of the functions in $H^1(\mathcal{D})$ with zero trace on $\mathcal{S}$, and by $L^2_0(\mathcal{D})$ the subspace of the functions in $L^2(\mathcal{D})$ with zero mean in $\mathcal{D}$. When $\mathcal{S} = \partial\mathcal{D}$, we will use the notation $H^1_0(\mathcal{D})$ for the space $H^1_{\mathcal{S}}(\mathcal{D})$. The scalar product in $L^2(\mathcal{D})$ is denoted by $(\cdot, \cdot)_{\mathcal{D}}$ and the associated norm by $\| \cdot \|_{\mathcal{D}}$. The bold notation will be used for vector Sobolev spaces. In the fictitious domain approach, the fluid equations (2.2.6) are solved in the whole domain Ω while enforcing the kinematic constraint $(2.2.6)_4$ on $\Sigma^{\varepsilon}(t)$ through Lagrange multipliers:

$$\langle \boldsymbol{\mu}, \boldsymbol{u}(t) \rangle_{\Sigma^{\varepsilon}(t)} = \langle \boldsymbol{\mu}, \boldsymbol{u}_{\mathrm{b}}(t) \rangle_{\Sigma^{\varepsilon}(t)} \quad \forall \boldsymbol{\mu} \in \boldsymbol{H}^{-\frac{1}{2}}(\Sigma^{\varepsilon}(t)) \quad \forall t \in \mathbb{R}^+, \tag{2.2.10}$$

where $\langle \cdot, \cdot \rangle_{\mathcal{S}}$ denotes the duality pairing between $\boldsymbol{H}^{-\frac{1}{2}}(\mathcal{S})$ and $\boldsymbol{H}^{\frac{1}{2}}(\mathcal{S})$. One of the advantages of the fictitious domain methods is that it allows the use of arbitrary fluid meshes constant in time; for further details on this approach, refer to [Girault and Glowinski, 1995, Girault et al., 2002]. Let $\boldsymbol{V} \overset{\text{def}}{=} \boldsymbol{H}^1_0(\Omega)$ and $Q \overset{\text{def}}{=} L^2_0(\Omega)$ be the functional spaces for the fluid velocity and pressure, respectively, the considered fictitious domain formulation of the fluid problem (2.2.6) reads: we look for $(\boldsymbol{u}, p, \boldsymbol{\lambda})$ such that $(\boldsymbol{u}(t), p(t), \boldsymbol{\lambda}(t)) \in \boldsymbol{V} \times Q \times \boldsymbol{H}^{-\frac{1}{2}}(\Sigma^{\varepsilon}(t))$ a.e. $t \in \mathbb{R}^+$ and

$$\rho_{\mathrm{f}} (\partial_t \boldsymbol{u}, \boldsymbol{v})_{\Omega} + a^{\mathrm{f}}_{\Omega}\big(\boldsymbol{u}; (\boldsymbol{u}, p, (\boldsymbol{v}, q)\big) - \langle \boldsymbol{\lambda}, \boldsymbol{v} \rangle_{\Sigma^{\varepsilon}(t)} + \langle \boldsymbol{\mu}, \boldsymbol{u} - \boldsymbol{u}_{\mathrm{b}} \rangle_{\Sigma^{\varepsilon}(t)} = 0 \tag{2.2.11}$$

for all $(\boldsymbol{v}, q, \boldsymbol{\mu}) \in \boldsymbol{V} \times Q \times \boldsymbol{H}^{-\frac{1}{2}}(\Sigma^\varepsilon(t))$, and where

$$a_\Omega^{\mathrm{f}}\big(\boldsymbol{z}; (\boldsymbol{u}, p), (\boldsymbol{v}, q)\big) \stackrel{\text{def}}{=} c_\Omega\big(\boldsymbol{z}; (\boldsymbol{u}, \boldsymbol{v})\big) + a_\Omega\big((\boldsymbol{u}, p), (\boldsymbol{v}, q)\big), \tag{2.2.12}$$

$$c_\Omega\big(\boldsymbol{z}; (\boldsymbol{u}, \boldsymbol{v})\big) \stackrel{\text{def}}{=} \rho_{\mathrm{f}}(\boldsymbol{z} \cdot \boldsymbol{\nabla}\boldsymbol{u}, \boldsymbol{v})_\Omega, \tag{2.2.13}$$

$$a_\Omega\big((\boldsymbol{u}, p), (\boldsymbol{v}, q)\big) \stackrel{\text{def}}{=} 2\mu_{\mathrm{f}}(\boldsymbol{\varepsilon}(\boldsymbol{u}), \boldsymbol{\varepsilon}(\boldsymbol{v}))_\Omega - (p, \boldsymbol{\nabla} \cdot \boldsymbol{v})_\Omega + (q, \boldsymbol{\nabla} \cdot \boldsymbol{u})_\Omega. \tag{2.2.14}$$

2.2.2.4 Fictitious domain approach with kinematic constraint on the beam centerline

We present here a first reduced model based on a fictitious domain approach. This formulation is inspired by the reduced models reported in [Hagmeyer et al., 2022, Hagmeyer et al., 2023] (see also [Griffith and Lim, 2012, Wiens and Stockie, 2015, Wang et al., 2019]) and assumes that, owing to the small thickness of the beam ε, the kinematic constraint can be simply enforced on the beam centerline. The Dirichlet boundary conditions $\boldsymbol{u}_{\mathrm{b}}$ are then enforced with Lagrange multipliers defined on the beam centerline as follows:

$$(\boldsymbol{\mu}, \boldsymbol{u}(t))_{\mathcal{B}(t)} = (\boldsymbol{\mu}, \boldsymbol{u}_{\mathrm{b}}(t))_{\mathcal{B}(t)} \quad \forall\, \boldsymbol{\mu} \in \boldsymbol{L}^2(\mathcal{B}(t)) \quad \forall t \in \mathbb{R}^+. \tag{2.2.15}$$

This approach reduces the size of the problem by passing for the boundary conditions from a two-dimensional constraint on the beam interface to a one-dimensional constraint on the beam centerline. The weak form of the fluid equations then writes: we look for $(\boldsymbol{u}, p, \boldsymbol{\lambda})$ such that $(\boldsymbol{u}(t), p(t), \boldsymbol{\lambda}(t)) \in \boldsymbol{V} \times Q \times \boldsymbol{L}^2(\mathcal{B}(t))$ a.e. $t \in \mathbb{R}^+$ and

$$\rho_{\mathrm{f}}(\partial_t \boldsymbol{u}, \boldsymbol{v})_\Omega + a_\Omega^{\mathrm{f}}\big(\boldsymbol{u}; (\boldsymbol{u}, p), (\boldsymbol{v}, q)\big) - (\boldsymbol{\lambda}, \boldsymbol{v})_{\mathcal{B}(t)} + (\boldsymbol{\mu}, \boldsymbol{u} - \boldsymbol{u}_{\mathrm{b}})_{\mathcal{B}(t)} = 0 \tag{2.2.16}$$

for all $(\boldsymbol{v}, q, \boldsymbol{\mu}) \in \boldsymbol{V} \times Q \times \boldsymbol{L}^2(\mathcal{B}(t))$. It should be noted that the relation (2.2.15) is only well-defined for $\boldsymbol{u} \in \boldsymbol{H}^{1+\eta}(\Omega)$, with $\eta > 0$. Nevertheless, in the context of problem (2.2.16), this minimum regularity for $\boldsymbol{u}$ might not be attained (due to the singularity induced by the term $(\boldsymbol{\lambda}(t), \boldsymbol{v})_{\mathcal{B}(t)}$). This prevents us from establishing both the well-posedness of the continuous problem (2.2.16) and the accuracy of the associated numerical methods, which is a major drawback.

2.2.2.5 Fictitious domain approach with reduced order kinematic condition

In this section, we introduce our method, which is also based on a fictitious domain approach with Lagrange multipliers, following a similar approach to (2.2.11) and (2.2.16). Our objective, similar to (2.2.16), is to take advantage of the slenderness of the beam to reduce the size of the problem. To do so, we replace the Lagrange multiplier space $\boldsymbol{H}^{-\frac{1}{2}}(\Sigma^\varepsilon(t))$ by a reduced-order space denoted as $\boldsymbol{F}_N(t)$. In order to define the space $\boldsymbol{F}_N(t)$, we first introduce a local coordinate ν on each cross-section of the reference configuration of the fluid-solid interface so that any point $\widehat{\boldsymbol{x}}$ on $\widehat{\Sigma}^\varepsilon$ can be parametrized as

$$\widehat{\boldsymbol{x}} = s\boldsymbol{e}_z + \varepsilon(\cos(\nu)\boldsymbol{e}_x + a\sin(\nu)\boldsymbol{e}_y). \tag{2.2.17}$$

In particular, any function $\widehat{\boldsymbol{v}}$ defined on $\widehat{\Sigma}^\varepsilon$ can be expressed as follows:

$$\widehat{\boldsymbol{v}}(s,\nu) \stackrel{\text{def}}{=} \boldsymbol{v}(s\boldsymbol{e}_z + \varepsilon(\cos(\nu)\boldsymbol{e}_x + a\sin(\nu)\boldsymbol{e}_y)) \quad \forall (s,\nu) \in (0,L)\times(0,2\pi).$$

Let $\boldsymbol{\mathcal{F}}_N$ be a finite dimensional subspace of $\boldsymbol{L}^2(0,2\pi)$, where the dimension varies with N, we set for all $t \in \mathbb{R}^+$, the space $\boldsymbol{F}_N(t) \subset \boldsymbol{L}^2(\Sigma^\varepsilon(t))$ defined by

$$\boldsymbol{F}_N(t) \stackrel{\text{def}}{=} \left\{ \widehat{\boldsymbol{v}} \circ \boldsymbol{\phi}_t^{-1} \ : \ \widehat{\boldsymbol{v}}(s,\nu) = \sum_{k=0}^{N} \alpha_k(s)\boldsymbol{g}_k(\nu),\ \alpha_k \in L^2(0,L),\ \boldsymbol{g}_k \in \boldsymbol{\mathcal{F}}_N \right\}. \quad (2.2.18)$$

The idea of (2.2.18) is to take advantage of the tensorization of $\widehat{\Sigma}^\varepsilon$ by $(0,L)\times(0,2\pi)$ to discretize the space $\boldsymbol{L}^2(0,2\pi)$ using the finite dimensional space $\boldsymbol{\mathcal{F}}_N$. The expression reduced order comes from the fact that any function $\boldsymbol{v} \in \boldsymbol{F}_N(t)$ is now uniquely determined by the set of functions $\{\alpha_k\}_{0\leqslant k\leqslant N} \subset L^2(0,L)$, thus passing from a functional space $\boldsymbol{H}^{-\frac{1}{2}}(\Sigma^\varepsilon(t))$ originally defined in a two-dimensional domain to a set of $N+1$ functions defined on a 1D domain. In particular, the reduced-order interface conditions on $\Sigma^\varepsilon(t)$ read as follows:

$$(\boldsymbol{\mu}_N, \boldsymbol{u}(t))_{\varepsilon,t} = (\boldsymbol{\mu}_N, \boldsymbol{u}_{\rm b}(t))_{\varepsilon,t} \quad \forall \boldsymbol{\mu}_N \in \boldsymbol{F}_N(t) \quad \forall t \in \mathbb{R}^+, \quad (2.2.19)$$

where $(\cdot,\cdot)_{\varepsilon,t}$ denotes the re-scaled L^2 inner-product on $\Sigma^\varepsilon(t)$:

$$(\boldsymbol{u},\boldsymbol{v})_{\varepsilon,t} \stackrel{\text{def}}{=} \int_{\Sigma_\varepsilon(t)} (\boldsymbol{u}\cdot\boldsymbol{v})\widehat{h}\circ\boldsymbol{\phi}_t^{-1}, \quad \widehat{h}(s,\nu) \stackrel{\text{def}}{=} \left(\varepsilon\sqrt{a^2\cos^2(\nu)+\sin^2(\nu)}\right)^{-1} \quad (2.2.20)$$

Note that (2.2.19) reduces (2.2.10) by enforcing $2N+1$ scalar constraints on each cross-section of the interface when (2.2.15) reduces (2.2.10) by neglecting the thickness of the beam and enforcing a single vector constraint on the beam centerline. The associated reduced weak formulation reads: we look for $(\boldsymbol{u}, p, \boldsymbol{\lambda}_N)$ such that $(\boldsymbol{u}(t), p(t), \boldsymbol{\lambda}_N(t)) \in \boldsymbol{V}\times Q \times \boldsymbol{F}_N(t)$ a.e. $t \in \mathbb{R}^+$ and

$$\rho_{\rm f}(\partial_t\boldsymbol{u},\boldsymbol{v})_\Omega + a_\Omega^{\rm f}\big(\boldsymbol{u};(\boldsymbol{u},p,(\boldsymbol{v},q)\big) - (\boldsymbol{\lambda}_N,\boldsymbol{v})_{\varepsilon,t} + (\boldsymbol{\mu}_N, \boldsymbol{u}-\boldsymbol{u}_{\rm b})_{\varepsilon,t} = 0 \quad (2.2.21)$$

for all $(\boldsymbol{v}, q, \boldsymbol{\mu}_N) \in \boldsymbol{V}\times Q\times \boldsymbol{F}_N(t)$.

2.2.3 Coupled problems: interface coupling conditions

In this section, we provide the interface coupling conditions between the beam model (2.2.4) and the different fluid modeling options given by (2.2.9), (2.2.16) or (2.2.21). The numerical approximation of the resulting coupled problems is addressed in Section 2.3. In what follows, we shall make extensive use of an extension operator from the beam centerline, $\{0\}\times\{0\}\times(0,L)$, to the bean reference domain $\widehat{\omega}^\varepsilon$, defined as follows: for any

vector field $\boldsymbol{v} : (0, L) \times \mathbb{R}^+ \to \mathbb{R}^3$ we define the vector field $\bar{\boldsymbol{v}} : \widehat{\omega}^\varepsilon \times \mathbb{R}^+ \to \mathbb{R}^3$ by the relation

$$\bar{\boldsymbol{v}}(\widehat{\boldsymbol{x}}, t) = \boldsymbol{v}(s, t), \quad s = \widehat{\boldsymbol{x}} \cdot \boldsymbol{e}_z \quad \forall (\widehat{\boldsymbol{x}}, t) \in \widehat{\omega}^\varepsilon \times \mathbb{R}^+.$$

In other words, functions defined on the centerline of the beam are lifted to the whole beam reference domain by using a projection operator which links each point of the beam to the cross-section to which it belongs. Notice that, using (2.2.1), we can express the deformation map $\boldsymbol{\phi}$ as:

$$\boldsymbol{\phi} = (\boldsymbol{I}_3 \cdot \boldsymbol{e}_z)\boldsymbol{e}_z + \bar{\boldsymbol{r}} + \bar{\boldsymbol{\Lambda}}\big(\boldsymbol{I}_3 - (\boldsymbol{I}_3 \cdot \boldsymbol{e}_z)\boldsymbol{e}_z\big). \tag{2.2.22}$$

2.2.3.1 ALE formalism for the fluid

In this section, we introduce the coupling conditions associated to the ALE formulation introduced in Section 2.2.2.2. In what follows, the symbol $\boldsymbol{\mathcal{L}}$ denotes a given lifting operator from $\widehat{\Sigma}^\varepsilon$ to $\widehat{\Omega}_{\mathrm{f}}^\varepsilon$ which vanishes on $\partial\Omega$. Note that the extension provided by $\boldsymbol{\mathcal{L}}$ is arbitrary inside $\widehat{\Omega}_{\mathrm{f}}^\varepsilon$. The interface coupling conditions between the solid sub-problem (2.2.4) and the fluid sub-problem (2.2.9) are given by

$$\begin{cases} \boldsymbol{\phi} = (\boldsymbol{I}_3 \cdot \boldsymbol{e}_z)\boldsymbol{e}_z + \bar{\boldsymbol{r}} + \bar{\boldsymbol{\Lambda}}\big(\boldsymbol{I}_3 - (\boldsymbol{I}_3 \cdot \boldsymbol{e}_z)\boldsymbol{e}_z\big) \quad \text{in} \quad \widehat{\omega}^\varepsilon, \\ \boldsymbol{\mathcal{A}} = \boldsymbol{\mathcal{L}}(\boldsymbol{\phi}), \quad \widehat{\boldsymbol{w}}_{\mathrm{f}} = \partial_t \boldsymbol{\mathcal{A}}, \quad \Omega_{\mathrm{f}}^\varepsilon(t) = \boldsymbol{\mathcal{A}}(\widehat{\Omega}_{\mathrm{f}}^\varepsilon, t), \\ \boldsymbol{u}_{\mathrm{b}} = \partial_t \boldsymbol{\phi} \circ \boldsymbol{\phi}_t^{-1} \quad \text{on} \quad \Sigma^\varepsilon(t), \\ (\boldsymbol{f}, \delta\boldsymbol{r})_{(0,L)} = -\big(\boldsymbol{\sigma}(\boldsymbol{u}, p)\boldsymbol{n}^+, \overline{\delta\boldsymbol{r}} \circ \boldsymbol{\mathcal{A}}_t^{-1}\big)_{\Sigma^\varepsilon(t)}, \\ (\boldsymbol{m}, \delta\boldsymbol{\theta})_{(0,L)} = -\big(\boldsymbol{\sigma}(\boldsymbol{u}, p)\boldsymbol{n}^+, \overline{\delta\boldsymbol{\theta}} \circ \boldsymbol{\mathcal{A}}_t^{-1} \wedge (\boldsymbol{I}_3 - \bar{\boldsymbol{r}} \circ \boldsymbol{\mathcal{A}}_t^{-1} - (\boldsymbol{\mathcal{A}}_t^{-1} \cdot \boldsymbol{e}_z)\boldsymbol{e}_z)\big)_{\Sigma^\varepsilon(t)}, \end{cases} \tag{2.2.23}$$

for all $\delta\boldsymbol{r}$, $\delta\boldsymbol{\theta} \in \boldsymbol{Y}$, with $\boldsymbol{Y}$ the space of admissible displacements and rotations of the beam (typically $\boldsymbol{H}^1(0, L)$ or a subspace of it), and $\boldsymbol{n}^+$ stands for the exterior unit normal to $\partial\Omega_{\mathrm{f}}^\varepsilon(t)$. The coupling conditions of (2.2.23) respectively express the geometric compatibility, kinematic coupling and dynamic balance between the fluid and the beam at the interface. Let $\boldsymbol{F} \overset{\text{def}}{=} \boldsymbol{\nabla}\boldsymbol{\mathcal{A}}$ and $J \overset{\text{def}}{=} \det \boldsymbol{F}$ denote, respectively, the gradient and Jacobian of $\boldsymbol{\mathcal{A}}$. Using the Piola transform, the last two equalities of (2.2.23) reduce to

$$\begin{aligned} \boldsymbol{f}(s) &= -\int_{\widehat{\Sigma}^\varepsilon \cap \partial\widehat{\omega}^\varepsilon(s)} J\boldsymbol{\sigma}(\boldsymbol{u}, p) \circ \boldsymbol{\mathcal{A}}\, \boldsymbol{F}^{-\mathrm{T}} \widehat{\boldsymbol{n}}^+, \\ \boldsymbol{m}(s) &= -\int_{\widehat{\Sigma}^\varepsilon \cap \partial\widehat{\omega}^\varepsilon(s)} J(\boldsymbol{\mathcal{A}} - \boldsymbol{r}(s) - s\boldsymbol{e}_z) \wedge \boldsymbol{\sigma}(\boldsymbol{u}, p) \circ \boldsymbol{\mathcal{A}}\, \boldsymbol{F}^{-\mathrm{T}} \widehat{\boldsymbol{n}}^+, \end{aligned}$$

for any $s \in (0, L)$ and where $\widehat{\boldsymbol{n}}^+$ denotes the exterior unit normal to $\partial\widehat{\Omega}_{\mathrm{f}}^\varepsilon$. In other words, for a given $s \in (0, L)$, the forcing terms $\boldsymbol{f}(s)$ and $\boldsymbol{m}(s)$, acting on the beam system (2.2.4), are given as the cross-section resultant of the fluid force and torque in the reference configuration.

2.2.3.2 Fictitious domain approach

In this approach, the coupling conditions are transferred through the Lagrange multipliers. The interface coupling conditions between the solid sub-problem (2.2.4) and the fluid sub-problem (2.2.11) are given by:

$$\begin{cases} \boldsymbol{\phi} = (\boldsymbol{I}_3 \cdot \boldsymbol{e}_z)\boldsymbol{e}_z + \bar{\boldsymbol{r}} + \bar{\boldsymbol{\Lambda}}\big(\boldsymbol{I}_3 - (\boldsymbol{I}_3 \cdot \boldsymbol{e}_z)\boldsymbol{e}_z\big) \quad \text{in} \quad \widehat{\omega}^\varepsilon, \\ \boldsymbol{u}_\mathrm{b} = \partial_t \boldsymbol{\phi} \circ \boldsymbol{\phi}_t^{-1} \quad \text{on} \quad \Sigma^\varepsilon(t), \\ (\boldsymbol{f}, \delta\boldsymbol{r})_{(0,L)} = -\langle \boldsymbol{\lambda}_N, \overline{\delta\boldsymbol{r}} \circ \boldsymbol{\phi}_t^{-1} \rangle_{\Sigma^\varepsilon(t)} \quad \forall \delta\boldsymbol{r} \in \boldsymbol{Y}, \\ (\boldsymbol{m}, \delta\boldsymbol{\theta})_{(0,L)} = -\langle \boldsymbol{\lambda}_N, \overline{\delta\boldsymbol{\theta}} \circ \boldsymbol{\phi}_t^{-1} \wedge (\boldsymbol{I}_3 - \bar{\boldsymbol{r}} \circ \boldsymbol{\phi}_t^{-1} - (\boldsymbol{\phi}_t^{-1} \cdot \boldsymbol{e}_z)\boldsymbol{e}_z) \rangle_{\Sigma^\varepsilon(t)} \quad \forall \delta\boldsymbol{\theta} \in \boldsymbol{Y}. \end{cases} \tag{2.2.24}$$

2.2.3.3 Fictitious domain approach with coupling conditions on the beam centerline

In this approach, the fluid-structure interface is identified with the beam centerline and thickness effects are neglected in the interface coupling (see, e.g., [Hagmeyer et al., 2022, Hagmeyer et al., 2023]). In particular, no rotational velocity is defined on the beam centerline, so that the fluid torque acting on the beam is null. As a result, the interface coupling conditions between the solid sub-problem (2.2.4) and the fluid sub-problem (2.2.16) are given by:

$$\begin{cases} \boldsymbol{\phi} = (\boldsymbol{I}_3 \cdot \boldsymbol{e}_z)\boldsymbol{e}_z + \bar{\boldsymbol{r}} \quad \text{in} \quad \widehat{\mathcal{B}}, \\ \boldsymbol{u}_\mathrm{b} = \partial_t \boldsymbol{\phi} \circ \boldsymbol{\phi}_t^{-1} \quad \text{in} \quad \mathcal{B}(t), \\ (\boldsymbol{f}, \delta\boldsymbol{r})_{(0,L)} = -(\boldsymbol{\lambda}, \delta\boldsymbol{r})_{\mathcal{B}(t)} \quad \forall \delta\boldsymbol{r} \circ \phi_t^{-1} \in \boldsymbol{Y}, \\ \boldsymbol{m} = \boldsymbol{0}. \end{cases} \tag{2.2.25}$$

Note that the last relation completely neglects the rotational dynamics. In the next section, we propose an alternative reduced coupled model which overcomes this issue, as illustrated in the numerical experiments of Section 2.3.

2.2.3.4 Fictitious domain approach with reduced order interface coupling conditions

In this section, we introduce the coupling conditions associated to our method, which corresponds to the fictitious domain formulation introduced in Section 2.2.2.5. As finite dimensional space $\boldsymbol{\mathcal{F}}_N \subset \boldsymbol{L}^2(0, 2\pi)$ in (2.2.18), we consider

$$\boldsymbol{\mathcal{F}}_N = \mathrm{span}\big\{ \sin(k\nu)\boldsymbol{e}_j, \cos(k\nu)\boldsymbol{e}_j \big\}_{0 \leqslant k \leqslant N, j \in \{x,y,z\}}.$$

We hence get the following reduced Lagrange multiplier space: for $t \in \mathbb{R}^+$,

$$\boldsymbol{F}_N(t) = \Big\{ \widehat{\boldsymbol{v}} \circ \boldsymbol{\phi}_t^{-1} \in L^2(\Sigma^\varepsilon(t)) \ : \\ \widehat{\boldsymbol{v}}(s,\nu) = \boldsymbol{a}_0(s) + \sum_{k=1}^{N} (\boldsymbol{a}_k(s)\cos(k\nu) + \boldsymbol{b}_k(s)\sin(k\nu)), \boldsymbol{a}_k, \boldsymbol{b}_k \in \boldsymbol{L}^2(0,L) \Big\} \quad (2.2.26)$$

The interface coupling conditions between the solid sub-problem (2.2.4) and the fluid sub-problem (2.2.21) read as

$$\begin{cases} \boldsymbol{\phi} = (\boldsymbol{I}_3 \cdot \boldsymbol{e}_z)\boldsymbol{e}_z + \bar{\boldsymbol{r}} + \bar{\boldsymbol{\Lambda}}\big(\boldsymbol{I}_3 - (\boldsymbol{I}_3 \cdot \boldsymbol{e}_z)\boldsymbol{e}_z\big) \quad \text{in} \quad \widehat{\omega}^\varepsilon, \\ \boldsymbol{u}_\mathrm{b} = \partial_t \boldsymbol{\phi} \circ \boldsymbol{\phi}_t^{-1} \quad \text{on} \quad \Sigma^\varepsilon(t), \\ (\boldsymbol{f}, \delta\boldsymbol{r})_{(0,L)} = -(\boldsymbol{\lambda}_N, \overline{\delta\boldsymbol{r}} \circ \boldsymbol{\phi}_t^{-1})_{\varepsilon,t} \quad \forall \delta\boldsymbol{r} \in \boldsymbol{Y}, \\ (\boldsymbol{m}, \delta\boldsymbol{\theta})_{(0,L)} = -\big(\boldsymbol{\lambda}_N, \overline{\delta\boldsymbol{\theta}} \circ \boldsymbol{\phi}_t^{-1} \wedge (\boldsymbol{I}_3 - \bar{\boldsymbol{r}} \circ \boldsymbol{\phi}_t^{-1} - (\boldsymbol{\phi}_t^{-1} \cdot \boldsymbol{e}_z)\boldsymbol{e}_z)\big)_{\varepsilon,t} \quad \forall \delta\boldsymbol{\theta} \in \boldsymbol{Y}. \end{cases} \quad (2.2.27)$$

Remark 1. It should be noted that, given that the fluid computational domain is the whole domain Ω, the relation $\boldsymbol{\lambda}_N = \boldsymbol{\sigma}(\boldsymbol{u},p)\boldsymbol{n}$ does not hold. Instead, $\boldsymbol{\lambda}_N$ corresponds to the jump of the fluid stress across $\Sigma^\varepsilon(t)$, viz.,

$$\boldsymbol{\lambda}_N = \big(\boldsymbol{\sigma}(\boldsymbol{u},p)^+\boldsymbol{n}^+ - \boldsymbol{\sigma}(\boldsymbol{u},p)^-\boldsymbol{n}^-\big) \quad \text{on} \quad \Sigma^\varepsilon(t).$$

Here, the indices $+$ and $-$ denote trace values on $\Sigma^\varepsilon(t)$ taken from $\Omega_\mathrm{f}^\varepsilon(t)$ and $\omega^\varepsilon(t)$, respectively. Nevertheless, numerical evidence provided in Section 2.4, suggests that the contribution of the internal fluid stress is negligible when the size ε of the cross-section is small.

2.2.1 Energy estimate (small rotational velocity) The purpose of the last part of this section is to provide an energy estimate for the coupled reduced model (2.2.4), (2.2.21), (2.2.27). To do so, we first give an explicit expression of the Lagrangian velocity of the beam $\widehat{\boldsymbol{u}}_\mathrm{b} \overset{\text{def}}{=} \partial_t\boldsymbol{\phi}$ according to the beam unknowns. From (2.2.1) we get

$$\widehat{\boldsymbol{u}}_\mathrm{b} = \overline{\partial_t \boldsymbol{r}} + \overline{\partial_t \boldsymbol{\Lambda}}(\boldsymbol{I}_3 - (\boldsymbol{I}_3 \cdot \boldsymbol{e}_z)\boldsymbol{e}_z) \quad (2.2.28)$$

On the other hand, from (2.2.1) and the orthogonality of $\boldsymbol{\Lambda}$, we have

$$\boldsymbol{I}_3 - (\boldsymbol{I}_3 \cdot \boldsymbol{e}_z)\boldsymbol{e}_z = \bar{\boldsymbol{\Lambda}}^\mathrm{T}(\boldsymbol{\phi} - \bar{\boldsymbol{r}} - (\boldsymbol{I}_3 \cdot \boldsymbol{e}_z)\boldsymbol{e}_z),$$

By inserting this expression into (2.2.28) we obtain

$$\widehat{\boldsymbol{u}}_\mathrm{b} = \overline{\partial_t \boldsymbol{r}} + \overline{\partial_t \boldsymbol{\Lambda}\boldsymbol{\Lambda}}^\mathrm{T}\big(\boldsymbol{\phi} - \bar{\boldsymbol{r}} - (\boldsymbol{I}_3 \cdot \boldsymbol{e}_z)\boldsymbol{e}_z\big). \quad (2.2.29)$$

From the orthogonality of $\boldsymbol{\Lambda}$, we infer that the matrix $\partial_t \boldsymbol{\Lambda}\boldsymbol{\Lambda}^{\mathrm{T}}$ is skew symmetric, so that there exists a vector field $\boldsymbol{w}$ in $(0,L)\times\mathbb{R}^+$, termed angular velocity vector, such that

$$\partial_t \boldsymbol{\Lambda}\boldsymbol{\Lambda}^{\mathrm{T}}\boldsymbol{v} = \boldsymbol{w}\wedge\boldsymbol{v} \quad \forall \boldsymbol{v}\in\mathbb{R}^3.$$

Hence the relation (2.2.29) can be equivalently re-written as

$$\widehat{\boldsymbol{u}}_{\mathrm{b}} = \overline{\partial_t \boldsymbol{r}} + \overline{\boldsymbol{w}} \wedge \big(\boldsymbol{\phi} - \overline{\boldsymbol{r}} - (\boldsymbol{I}_3\cdot\boldsymbol{e}_z)\boldsymbol{e}_z\big) \tag{2.2.30}$$

and we deduce that

$$\boldsymbol{u}_{\mathrm{b}} = \overline{\partial_t \boldsymbol{r}}\circ\boldsymbol{\phi}_t^{-1} + \overline{\boldsymbol{w}}\circ\boldsymbol{\phi}_t^{-1} \wedge \big(\boldsymbol{I}_3 - \overline{\boldsymbol{r}}\circ\boldsymbol{\phi}_t^{-1} - (\boldsymbol{\phi}_t^{-1}\cdot\boldsymbol{e}_z)\boldsymbol{e}_z\big).$$

Note that the velocity of the beam corresponds to a rigid-body velocity per cross-section. To retrieve the desired energy estimate, we need to assume that the beam undergoes small rotations. This assumption is needed to cope with the mismatch between the treatment of the geometrical non-linearities in the solid (linear) and in the fluid (non-linear). We hence consider a variant of the kinematic coupling condition $(2.2.27)_2$ in which the Eulerian velocity of the beam, $\boldsymbol{u}_{\mathrm{b}}$ given by (2.2.1), is taken with a linearized angular velocity, namely,

$$\boldsymbol{w} = \partial_t \boldsymbol{\theta}, \tag{2.2.31}$$

which yields

$$\boldsymbol{u}_{\mathrm{b}} = \partial_t \boldsymbol{r}\circ\boldsymbol{\phi}_t^{-1} + \overline{\partial_t\boldsymbol{\theta}}\circ\boldsymbol{\phi}_t^{-1} \wedge (\boldsymbol{I}_3 - \overline{\boldsymbol{r}}\circ\boldsymbol{\phi}_t^{-1} - (\boldsymbol{\phi}_t^{-1}\cdot\boldsymbol{e}_z)\boldsymbol{e}_z). \tag{2.2.32}$$

Note in particular that in this case the relation $\boldsymbol{u}_{\mathrm{b}} = \partial_t\boldsymbol{\phi}\circ\boldsymbol{\phi}_t^{-1}$ does not hold anymore. The relations (2.2.31) and (2.2.32) are only valid in a small rotational velocity framework. The resulting problem in weak form read as follows: we look for $(\boldsymbol{u}, p, \boldsymbol{\lambda}_N, \boldsymbol{r}, \boldsymbol{\theta})$ such that $(\boldsymbol{u}(t), p(t), \boldsymbol{\lambda}_N(t), \boldsymbol{r}(t), \boldsymbol{\theta}(t)) \in \boldsymbol{V}\times Q\times \boldsymbol{F}_N(t)\times\boldsymbol{Y}\times\boldsymbol{Y}$ a.e. $t\in\mathbb{R}^+$ and

$$\begin{cases} \boldsymbol{\phi} = (\boldsymbol{I}_3\cdot\boldsymbol{e}_z)\boldsymbol{e}_z + \overline{\boldsymbol{r}} + \overline{\boldsymbol{\Lambda}}\big(\boldsymbol{I}_3 - (\boldsymbol{I}_3\cdot\boldsymbol{e}_z)\boldsymbol{e}_z\big) \quad \text{in} \quad \widehat{\omega}^{\varepsilon}, \\ \rho_{\mathrm{f}}(\partial_t\boldsymbol{u},\boldsymbol{v})_{\Omega} + a^{\mathrm{f}}_{\Omega}\big(\boldsymbol{u};(\boldsymbol{u},p),(\boldsymbol{v},q)\big) \\ \quad + \rho_{\mathrm{b}}(\boldsymbol{A}\partial_t^2\boldsymbol{r},\delta\boldsymbol{r})_{(0,L)} + \rho_{\mathrm{b}}(\boldsymbol{I}\partial_t^2\boldsymbol{\theta},\delta\boldsymbol{\theta})_{(0,L)} + a^{\mathrm{b}}\big((\boldsymbol{r},\boldsymbol{\theta}),(\delta\boldsymbol{r},\delta\boldsymbol{\theta})\big) \\ \quad - \big(\boldsymbol{\lambda}_N, \boldsymbol{v} - \overline{\delta\boldsymbol{r}}\circ\boldsymbol{\phi}_t^{-1} - \overline{\delta\boldsymbol{\theta}}\circ\boldsymbol{\phi}_t^{-1}\wedge\big(\boldsymbol{I}_3 - \overline{\boldsymbol{r}}\circ\boldsymbol{\phi}_t^{-1} - (\boldsymbol{\phi}_t^{-1}\cdot\boldsymbol{e}_z)\boldsymbol{e}_z\big)\big)_{\varepsilon,t} \\ \quad + \big(\boldsymbol{\mu}_N, \boldsymbol{u} - \overline{\partial_t\boldsymbol{r}}\circ\boldsymbol{\phi}_t^{-1} - \overline{\partial_t\boldsymbol{\theta}}\circ\boldsymbol{\phi}_t^{-1}\wedge(\boldsymbol{I}_3 - \overline{\boldsymbol{r}}\circ\boldsymbol{\phi}_t^{-1} - (\boldsymbol{\phi}_t^{-1}\cdot\boldsymbol{e}_z)\boldsymbol{e}_z)\big)_{\varepsilon,t} = 0 \end{cases} \tag{2.2.33}$$

for all $(\boldsymbol{v}, q, \boldsymbol{\mu}_N, \delta\boldsymbol{r}, \delta\boldsymbol{\theta}) \in \boldsymbol{V}\times Q\times\boldsymbol{F}_N(t)\times\boldsymbol{Y}\times\boldsymbol{Y}$. Here, the bilinear form a^{b} represents the weak form of the beam elastic operator given by

$$a^{\mathrm{b}}\big((\boldsymbol{r},\boldsymbol{\theta}),(\delta\boldsymbol{r},\delta\boldsymbol{\theta})\big) \stackrel{\mathrm{def}}{=} (\boldsymbol{E}\partial_s\boldsymbol{\theta},\partial_s\delta\boldsymbol{\theta})_{(0,L)} + \big(\boldsymbol{G}(\partial_s\boldsymbol{r} - \boldsymbol{\theta}\wedge\boldsymbol{e}_z),(\partial_s\delta\boldsymbol{r} - \delta\boldsymbol{\theta}\wedge\boldsymbol{e}_z)\big)_{(0,L)}.$$

The energy stability of (2.2.33) is stated in the next result.

Theorem 2.2.1. *Let $(\boldsymbol{u}, p, \boldsymbol{\lambda}_N, \boldsymbol{r}, \boldsymbol{\theta})$ be a regular enough solution of the reduced order coupled problem* (2.2.33)*. There holds*

$$\mathfrak{E}(t) \leqslant \mathfrak{E}(0) \quad \forall t \in \mathbb{R}^+, \tag{2.2.34}$$

where the mechanical energy of the system $\mathfrak{E}(t)$ is defined by

$$\mathfrak{E}(t) \stackrel{\text{def}}{=} \frac{\rho_{\mathrm{f}}}{2}\|\boldsymbol{u}(t)\|_{\Omega}^2 + \frac{\rho_{\mathrm{b}}}{2}\|\partial_t \boldsymbol{r}(t)\|_{\boldsymbol{A},(0,L)}^2 + \frac{\rho_{\mathrm{b}}}{2}\|\partial_t \boldsymbol{\theta}(t)\|_{\boldsymbol{I},(0,L)}^2 + \frac{1}{2}\big\|(\boldsymbol{r}(t), \boldsymbol{\theta}(t))\big\|_{\mathrm{b}}^2,$$

with

$$\|\cdot\|_{\boldsymbol{A},(0,L)} \stackrel{\text{def}}{=} \sqrt{(\boldsymbol{A}\,\cdot,\cdot)_{(0,L)}}, \quad \|\cdot\|_{\boldsymbol{I},(0,L)} \stackrel{\text{def}}{=} \sqrt{(\boldsymbol{I}\,\cdot,\cdot)_{(0,L)}},$$
$$\|\cdot,\cdot\|_{\mathrm{b}} \stackrel{\text{def}}{=} \sqrt{a^{\mathrm{b}}\big((\cdot,\cdot),(\cdot,\cdot)\big)}.$$

Proof. By testing (2.2.33) with

$$(\boldsymbol{v}, q, \delta\boldsymbol{r}, \delta\boldsymbol{\theta}, \boldsymbol{\mu}_N) = (\boldsymbol{u}, p, \partial_t \boldsymbol{r}, \partial_t \boldsymbol{\theta}, \boldsymbol{\lambda}_N),$$

we get

$$\rho_{\mathrm{f}}(\partial_t \boldsymbol{u}, \boldsymbol{u})_{\Omega} + \rho_{\mathrm{b}}(\boldsymbol{A}\partial_t^2 \boldsymbol{r}, \partial_t \boldsymbol{r})_{(0,L)} + \rho_{\mathrm{b}}(\boldsymbol{I}\partial_t^2 \boldsymbol{\theta}, \partial_t \boldsymbol{\theta})_{(0,L)} + a_{\Omega}^{\mathrm{f}}\big(\boldsymbol{u}; (\boldsymbol{u}, p), (\boldsymbol{u}, p)\big) + a^{\mathrm{b}}\big((\boldsymbol{r}, \boldsymbol{\theta}), (\partial_t \boldsymbol{r}, \partial_t \boldsymbol{\theta})\big) = 0. \tag{2.2.35}$$

Using integration by parts and the boundary conditions on $\boldsymbol{u}$, we have

$$a_{\Omega}^{\mathrm{f}}\big(\boldsymbol{u}; (\boldsymbol{u}, p), (\boldsymbol{u}, p)\big) = 2\mu\|\boldsymbol{\varepsilon}(\boldsymbol{u})\|_{\Omega}^2.$$

Since the remaining terms of (2.2.35) are inner-products, we finally get

$$\frac{\mathrm{d}}{\mathrm{d}t}\left(\frac{\rho_{\mathrm{f}}}{2}\|\boldsymbol{u}\|_{\Omega}^2 + \frac{\rho_{\mathrm{b}}}{2}\|\partial_t \boldsymbol{r}\|_{\boldsymbol{A},(0,L)}^2 + \frac{\rho_{\mathrm{b}}}{2}\|\partial_t \boldsymbol{\theta}\|_{\boldsymbol{I},(0,L)}^2 + \frac{1}{2}\|(\boldsymbol{r}, \boldsymbol{\theta})\|_{\mathrm{b}}^2\right) \leqslant 0.$$

The estimate (2.2.34) then follows by integrating this bound over $(0, t)$, which completes the proof. □

Remark 2. For the coupled problem (2.2.4), (2.2.9), (2.2.23) with an ALE formalism in the fluid, the above mentioned mismatch between $\boldsymbol{u}_{\mathrm{b}}$ and $\partial_t \boldsymbol{\phi} \circ \boldsymbol{\phi}^{-1}$ prevents from establishing the energy estimate (2.2.34). In order to guarantee energy stability for this model, one simple option is to update the fluid domain from a linearized version of (2.2.1) with $\boldsymbol{\Lambda} \approx \boldsymbol{I}_3 + \boldsymbol{\Theta}$. Another option would be to directly consider a non-linear model for the balance equations of the beam model.

2.3 Numerical method

In this section, we introduce a numerical scheme for the approximation of the coupled problem (2.2.4), (2.2.21), (2.2.27). In what follows, we denote by $\tau > 0$ the time-step length and, for $n \in \mathbb{N}$, we set $t^n \overset{\text{def}}{=} n\tau$. For any time-dependent function $\boldsymbol{v}$, $\boldsymbol{v}^n$ stands for an approximation of $\boldsymbol{v}(t^n)$. We also introduce the standard notations

$$\partial_\tau \boldsymbol{v}^n \overset{\text{def}}{=} \frac{1}{\tau}(\boldsymbol{v}^n - \boldsymbol{v}^{n-1}), \quad \boldsymbol{v}^{n-\frac{1}{2}} \overset{\text{def}}{=} \frac{1}{2}(\boldsymbol{v}^{n-1} + \boldsymbol{v}^n),$$

for the first-order backward difference and the mid-point value, respectively. Let $\mathcal{D}$ be an open polygonal convex domain of $\mathbb{R}^3$ and $\mathcal{T}_h(\mathcal{D})$ a triangulation of $\mathcal{D}$ with characteristic size h. We consider the following standard continuous Lagrange finite element spaces of degree k:

$$\begin{aligned} \boldsymbol{X}_h^k(\mathcal{D}) &\overset{\text{def}}{=} \left\{ \boldsymbol{v} \in \boldsymbol{H}^1(\mathcal{D}) \ : \ \boldsymbol{v}|_K \in [\mathbb{P}_k(K)]^3, \quad \forall K \in \mathcal{T}_h(\mathcal{D}) \right\}, \\ Q_h^k(\mathcal{D}) &\overset{\text{def}}{=} \left\{ v \in H^1(\mathcal{D}) \ : \ v|_K \in \mathbb{P}_k(K), \quad \forall K \in \mathcal{T}_h(\mathcal{D}) \right\}. \end{aligned} \tag{2.3.1}$$

We then introduce the finite element spaces $\boldsymbol{V}_h \overset{\text{def}}{=} \boldsymbol{X}_h^1(\Omega) \cap \boldsymbol{V}$ and $Q_h \overset{\text{def}}{=} Q_h^1(\Omega) \cap Q$ for the approximation of the fluid velocity $\boldsymbol{u}$ and pressure p, respectively, while for the solid displacement $\boldsymbol{r}$ and rotation $\boldsymbol{\theta}$ their approximations will be looked for into $\boldsymbol{Y}_H \overset{\text{def}}{=} \boldsymbol{X}_H^1(0, L) \cap \boldsymbol{Y}$. Here, h and H respectively denote the characteristic sizes of the fluid and solid (centerline) meshes.

2.3.1 Discrete formulation of the coupled model with reduced order interface conditions

For the time discretization of (2.2.27), we consider a semi-implicit scheme in which the geometrical coupling is treated in a explicit manner, as follows:

$$\boldsymbol{\phi}_H^n = (\boldsymbol{I}_3 \cdot \boldsymbol{e}_z)\boldsymbol{e}_z + \overline{\boldsymbol{r}_H^{n-1}} + \overline{\boldsymbol{\Lambda}_H^{n-1}}\big(\boldsymbol{I}_3 - (\boldsymbol{I}_3 \cdot \boldsymbol{e}_z)\boldsymbol{e}_z\big) \quad \text{in} \quad \widehat{\omega}^\varepsilon, \quad \Sigma^{\varepsilon,n} = \boldsymbol{\phi}_H^n(\widehat{\Sigma}^\varepsilon).$$

We also introduce the discrete Lagrange multiplier space $\boldsymbol{F}_{N,H}^n$, discrete counterpart of $\boldsymbol{F}_N(t)$, as

$$\begin{aligned} \boldsymbol{F}_{N,H}^n \overset{\text{def}}{=} \Bigg\{ & \widehat{\boldsymbol{v}}_H \circ (\boldsymbol{\phi}_H^n)^{-1} \in \boldsymbol{L}^2(\Sigma^{\varepsilon,n}) \ : \ \widehat{\boldsymbol{v}}_H(s,\nu) = \boldsymbol{a}_{0,H}(s) \\ & + \sum_{k=1}^{N} \big(\boldsymbol{a}_{k,H}(s)\cos(k\nu) + \boldsymbol{b}_{k,H}(s)\sin(k\nu) \big), \quad \boldsymbol{a}_{k,H}, \boldsymbol{b}_{k,H} \in \boldsymbol{Y}_H \Bigg\} \end{aligned} \tag{2.3.2}$$

which simply amounts to replace $\boldsymbol{L}^2(0, L)$ by $\boldsymbol{Y}_H$ in (2.2.26). Note that here a unique approximation space $\boldsymbol{Y}_H$ is involved in the approximation of the beam unknowns and of

the Lagrange multiplier, but this is not mandatory. We consider a backward-Euler semi-implicit time-discretization for the fluid sub-problem (2.2.21) and a mid-point scheme for the solid sub-problem (2.2.4). The remaining kinematic and dynamic conditions in (2.2.27) are discretized with an implicit scheme. The resulting solution procedure is of strongly coupled nature (see, e.g., [Fernández and Gerbeau, 2009]). By gathering all the above mentioned ingredients, the proposed numerical approximation of (2.2.4), (2.2.21), (2.2.27) is detailed in Algorithm 1. In the step (2.3.4) of Algorithm 1, the discrete fluid

Algorithm 1 Discrete formulation of the reduced coupled model (2.2.4), (2.2.21), (2.2.27).

For $n \geqslant 1$,

Step 1: Update interface position:

$$\boldsymbol{\phi}_H^n = (\boldsymbol{I}_3 \cdot \boldsymbol{e}_z)\boldsymbol{e}_z + \overline{\boldsymbol{r}_H^{n-1}} + \overline{\boldsymbol{\Lambda}_H^{n-1}}\big(\boldsymbol{I}_3 - (\boldsymbol{I}_3 \cdot \boldsymbol{e}_z)\boldsymbol{e}_z\big) \quad \text{in} \quad \widehat{\omega}^\varepsilon, \quad \Sigma^{\varepsilon,n} = \boldsymbol{\phi}_H^n(\widehat{\Sigma}^\varepsilon), \tag{2.3.3}$$

where $\boldsymbol{\Lambda}_H^{n-1}$ is obtained from $\boldsymbol{\theta}_H^{n-1}$ using nonlinear formula (2.2.3).

Step 2: Find $(\boldsymbol{u}_h^n, p_h^n, \boldsymbol{\lambda}_{N,H}^n, \boldsymbol{r}_H^n, \boldsymbol{\theta}_H^n) \in \boldsymbol{V}_h \times Q_h \times \boldsymbol{F}_{N,H} \times \boldsymbol{Y}_H \times \boldsymbol{Y}_H$ with $\dot{\boldsymbol{r}}_H^{n-\frac{1}{2}} = \partial_\tau \boldsymbol{r}_H^n$ and $\dot{\boldsymbol{\theta}}_H^{n-\frac{1}{2}} = \partial_\tau \boldsymbol{\theta}_H^n$ such that

$$\begin{cases} \rho_{\mathrm{f}}(\partial_\tau \boldsymbol{u}_h^n, \boldsymbol{v}_h)_\Omega + a_{\Omega,h}^{\mathrm{f}}\big(\boldsymbol{u}_h^{n-1}; (\boldsymbol{u}_h^n, p_h^n), (\boldsymbol{v}_h, q_h)\big) \\ \quad + \rho_{\mathrm{b}}(\boldsymbol{A}\partial_\tau \dot{\boldsymbol{r}}_H^n, \delta\boldsymbol{r}_H)_{(0,L)} + \rho_{\mathrm{b}}\big(\boldsymbol{I}\partial_\tau \dot{\boldsymbol{\theta}}_H^n, \delta\boldsymbol{\theta}_H\big)_{(0,L)} \\ \quad + a_H^{\mathrm{b}}\big((\boldsymbol{r}_H^{n-\frac{1}{2}}, \boldsymbol{\theta}_H^{n-\frac{1}{2}}), (\delta\boldsymbol{r}_H, \delta\boldsymbol{\theta}_H)\big) \\ \quad - \big(\boldsymbol{\lambda}_H^n, \boldsymbol{v}_h - \overline{\delta\boldsymbol{r}_H} \circ (\boldsymbol{\phi}_H^n)^{-1} - \overline{\delta\boldsymbol{\theta}_H} \circ (\boldsymbol{\phi}_H^n)^{-1} \wedge (\boldsymbol{I}_3 - \overline{\boldsymbol{r}_H^{n-1}} \circ (\boldsymbol{\phi}_H^n)^{-1} - ((\boldsymbol{\phi}_H^n)^{-1} \cdot \boldsymbol{e}_z)\boldsymbol{e}_z)\big)_{\varepsilon,n} \\ \quad + \big(\boldsymbol{\mu}_N, \boldsymbol{u}_h^n - \partial_\tau \boldsymbol{\phi}_H^{n+1} \circ (\boldsymbol{\phi}_H^n)^{-1}\big)_{\varepsilon,n} = 0 \end{cases} \tag{2.3.4}$$

for all $(\boldsymbol{v}_h, q_h, \boldsymbol{\mu}_{N,H}, \delta\boldsymbol{r}_H, \boldsymbol{\theta}_H) \in \boldsymbol{V}_h \times Q_h \times \boldsymbol{F}_{N,H} \times \boldsymbol{Y}_H \times \boldsymbol{Y}_H$.

tri-linear form is given by

$$\begin{aligned} a_{\Omega,h}^{\mathrm{f}}\big(\boldsymbol{z}_h; (\boldsymbol{u}_h, p_h), (\boldsymbol{v}_h, q_h)\big) &\stackrel{\text{def}}{=} c_h^n\big(\boldsymbol{z}_h; (\boldsymbol{u}_h, \boldsymbol{v}_h)\big) + a_\Omega\big((\boldsymbol{u}_h, p_h), (\boldsymbol{v}_h, q_h)\big) \\ &\quad + s_{\Omega,h}\big(\boldsymbol{z}_h; (\boldsymbol{u}_h, p_h), (\boldsymbol{v}_h, q_h)\big), \\ c_h^n(\boldsymbol{z}; \boldsymbol{u}_h, \boldsymbol{v}_h) &\stackrel{\text{def}}{=} c_\Omega(\boldsymbol{z}_h; \boldsymbol{u}_h, \boldsymbol{v}_h) + \frac{\rho_{\mathrm{f}}}{2}\big((\nabla \cdot \boldsymbol{z}_h)\boldsymbol{u}_h, \boldsymbol{v}_h\big)_\Omega, \\ s_{\Omega,h}\big(\boldsymbol{z}_h; (\boldsymbol{u}_h, p_h), (\boldsymbol{v}_h, q_h)\big) &\stackrel{\text{def}}{=} \\ &\sum_{K \in \mathcal{T}_h(\Omega)} \int_K \delta_h\big(\rho_{\mathrm{f}}(\boldsymbol{z}_h \cdot \nabla)\boldsymbol{u}_h + \nabla p_h\big) \cdot \big(\rho_{\mathrm{f}}(\boldsymbol{z}_h \cdot \nabla)\boldsymbol{v}_h + \nabla q_h\big), \\ \delta_h &\stackrel{\text{def}}{=} \gamma_{\mathrm{S}}\left(\rho_{\mathrm{f}}\sqrt{\frac{4}{\tau^2} + \frac{16\mu^2}{h^4(\rho_{\mathrm{f}})^2} + \frac{4|\boldsymbol{z}_h|^2}{h^2}}\right)^{-1}, \end{aligned} \tag{2.3.5}$$

where $s_{\Omega,h}$ corresponds to the SUPG/PSPG stabilization (see, e.g., [Tezduyar, 1991]) and $\gamma_{\mathrm{S}} > 0$ is a user-defined parameter. For the discrete beam bi-linear form, we consider the locking-free formulation introduced in [Chapelle, 1997], viz.,

$$a_H^{\mathrm{b}}\big((\boldsymbol{r}_H,\boldsymbol{\theta}_H),(\boldsymbol{r}_H,\delta\boldsymbol{r}_H)\big) \overset{\text{def}}{=} \big(\boldsymbol{\partial}_s\boldsymbol{\theta}_H,\partial_s\delta\boldsymbol{\theta}_H\big)_{(0,L)} + \big(\boldsymbol{G}\widehat{\Pi}_H^0(\partial_s\boldsymbol{r}_H^n-\boldsymbol{\theta}_H^n\wedge\boldsymbol{e}_z),\partial_s\delta\boldsymbol{r}_h-\delta\boldsymbol{\theta}\wedge\boldsymbol{e}_z\big)_{(0,L)}, \quad (2.3.6)$$

where $\widehat{\boldsymbol{\Pi}}_H^0$ denotes the L^2 projection onto $\boldsymbol{X}_H^0(0,L)$.

2.3.1 Energy estimate (small rotational velocity) In the spirit of Section 2.2.3.4, we provide an energy estimate for Algorithm 1 under a small rotational velocity framework of (2.2.33). In this context, Algorithm 1 reduces to the following discrete coupled problem: find $(\boldsymbol{u}_h^n,p_h^n,\boldsymbol{\lambda}_{N,H}^n,\boldsymbol{r}_H^n,\boldsymbol{\theta}_H^n)\in\boldsymbol{V}_h\times Q_h\times\boldsymbol{F}_{N,H}^n\times\boldsymbol{Y}_H\times\boldsymbol{Y}_H$ with $\dot{\boldsymbol{r}}_H^{n-\frac{1}{2}}=\partial_\tau\boldsymbol{r}_H^n$ and $\dot{\boldsymbol{\theta}}_H^{n-\frac{1}{2}}=\partial_\tau\boldsymbol{\theta}_H^n$ such that

$$\begin{cases}
\boldsymbol{\phi}_H^n=(\boldsymbol{I}_3\cdot\boldsymbol{e}_z)\boldsymbol{e}_z+\overline{\boldsymbol{r}_H^{n-1}}+\overline{\boldsymbol{\Lambda}_h^{n-1}}\big(\boldsymbol{I}_3-(\boldsymbol{I}_3\cdot\boldsymbol{e}_z)\boldsymbol{e}_z\big) \quad \text{in} \quad \widehat{\omega}^\varepsilon\\
\rho_{\mathrm{f}}(\partial_\tau\boldsymbol{u}_h^n,\boldsymbol{v}_h)_\Omega+a_{\Omega,h}^{\mathrm{f}}\big(\boldsymbol{u}_h^{n-1};(\boldsymbol{u}_h^n,p_h^n),(\boldsymbol{v}_h,q_h)\big)\\
+\rho_{\mathrm{b}}\big(\boldsymbol{A}\partial_\tau\dot{\boldsymbol{r}}_H^n,\delta\boldsymbol{r}_H\big)_{(0,L)}+\rho_{\mathrm{b}}\big(\boldsymbol{I}\partial_\tau\dot{\boldsymbol{\theta}}_H^n,\delta\boldsymbol{\theta}_H\big)_{(0,L)}\\
+a_H^{\mathrm{b}}\big((\boldsymbol{r}_H^{n-\frac{1}{2}},\boldsymbol{\theta}_H^{n-\frac{1}{2}}),(\delta\boldsymbol{r}_H,\delta\boldsymbol{\theta}_H)\big)-\big(\boldsymbol{\lambda}_{N,H}^n,\boldsymbol{v}_h\big)_{\varepsilon,n}+\big(\boldsymbol{\mu}_{N,H},\boldsymbol{u}_h^n\big)_{\varepsilon,n}\\
-\big(\boldsymbol{\lambda}_{N,H}^n,\overline{\delta\boldsymbol{r}_H}\circ(\boldsymbol{\phi}_H^n)^{-1}\big)_{\varepsilon,n}-\big(\boldsymbol{\mu}_{N,H},\overline{\dot{\boldsymbol{r}}_H^{n-\frac{1}{2}}}\circ(\boldsymbol{\phi}_H^n)^{-1}\big)_{\varepsilon,n}\\
-\big(\boldsymbol{\lambda}_{N,H}^n,\overline{\delta\boldsymbol{\theta}_H}\circ(\boldsymbol{\phi}_H^n)^{-1}\wedge(\boldsymbol{I}_3-\overline{\boldsymbol{r}_H^{n-1}}\circ(\boldsymbol{\phi}_H^n)^{-1}-((\boldsymbol{\phi}_H^n)^{-1}\cdot\boldsymbol{e}_z)\boldsymbol{e}_z)\big)_{\varepsilon,n}\\
-\big(\boldsymbol{\mu}_{N,H},\overline{\dot{\boldsymbol{\theta}}_H^{n-\frac{1}{2}}}\circ(\boldsymbol{\phi}_H^n)^{-1}\wedge(\boldsymbol{I}_3-\overline{\boldsymbol{r}_H^{n-1}}\circ(\boldsymbol{\phi}_H^n)^{-1}-((\boldsymbol{\phi}_H^n)^{-1}\cdot\boldsymbol{e}_z)\boldsymbol{e}_z)\big)_{\varepsilon,n}=0.
\end{cases} \quad (2.3.7)$$

for all $(\boldsymbol{v}_h,q_h,\boldsymbol{\mu}_{N,H},\delta\boldsymbol{r}_H,\boldsymbol{\theta}_H)\in\boldsymbol{V}_h\times Q_h\times\boldsymbol{F}_{N,H}^n\times\boldsymbol{Y}_H\times\boldsymbol{Y}_H$. The energy stability of this method is stated in the following result.

Theorem 2.3.1. *Let* $\big\{(\boldsymbol{u}_h^n,p_h^n,\boldsymbol{\lambda}_{N,H}^n,\boldsymbol{r}_H^n,\boldsymbol{\theta}_H^n)\big\}_{n\geqslant1}\subset\boldsymbol{V}_h\times Q_h\times\boldsymbol{F}_{N,H}^n\times\boldsymbol{Y}_H\times\boldsymbol{Y}_H$ *be given by problem* (2.3.7)*. There holds*

$$\mathfrak{E}^n\leqslant\mathfrak{E}^0,\quad\forall n\geqslant0 \quad (2.3.8)$$

where the discrete mechanical energy $\mathfrak{E}^n$ *of the system is defined by*

$$\mathfrak{E}^n\overset{\text{def}}{=}\frac{\rho_{\mathrm{f}}}{2}\|\boldsymbol{u}_h^n\|_{0,\Omega}^2+\frac{\rho_{\mathrm{b}}}{2}\|\dot{\boldsymbol{r}}_H^n\|_{\mathbf{A},(0,L)}^2+\frac{\rho_{\mathrm{b}}}{2}\|\dot{\boldsymbol{\theta}}_H^n\|_{\mathbf{I},(0,L)}^2+\frac{1}{2}\big\|(\boldsymbol{r}_H^n,\boldsymbol{\theta}_H^n)\big\|_{\mathrm{b},H}^2,$$

with

$$\|(\cdot,\cdot)\|_{\mathrm{b},H}=\sqrt{a_H^{\mathrm{b}}\big((\cdot,\cdot),(\cdot,\cdot)\big)}.$$

Proof. By testing (2.3.7) with

$$(\boldsymbol{v}_h, q_h, \boldsymbol{\mu}_{N,H}, \delta\boldsymbol{r}_H, \delta\boldsymbol{\theta}_H) = (\boldsymbol{u}_h^n, p_h, \boldsymbol{\lambda}_{N,H}^n, \overline{\dot{\boldsymbol{r}}_H^{n-\frac{1}{2}}}, \overline{\dot{\boldsymbol{\theta}}_H^{n-\frac{1}{2}}})$$

we get

$$\begin{aligned}\rho_{\mathrm{f}}(\partial_\tau \boldsymbol{u}_h^n, \boldsymbol{u}_h^n)_\Omega + \rho_{\mathrm{b}}(\boldsymbol{A}\partial_\tau \dot{\boldsymbol{r}}_H^n, \dot{\boldsymbol{r}}_H^{n-\frac{1}{2}})_{(0,L)} + \rho_{\mathrm{b}}(\boldsymbol{I}\partial_\tau \dot{\boldsymbol{\theta}}_H^n, \dot{\boldsymbol{\theta}}_H^{n-\frac{1}{2}})_{(0,L)} \\ + a_{\Omega,h}^{\mathrm{f}}\big(\boldsymbol{u}_h^{n-1}; (\boldsymbol{u}_h^n, p_h^n), (\boldsymbol{u}_h^n, p_h^n)\big) + a_H^{\mathrm{b}}\big((\boldsymbol{r}_H^{n-\frac{1}{2}}, \boldsymbol{\theta}_H^{n-\frac{1}{2}}), (\dot{\boldsymbol{r}}_H^{n-\frac{1}{2}}, \dot{\boldsymbol{\theta}}_H^{n-\frac{1}{2}})\big) = 0.\end{aligned} \tag{2.3.9}$$

Using integration by parts and the boundary conditions of $\boldsymbol{u}_h^{n-1}$, $\boldsymbol{u}_h^n$, we have

$$a_{\Omega,h}^{\mathrm{f}}(\boldsymbol{u}_h^{n-1}; (\boldsymbol{u}_h^n, p_h), (\boldsymbol{u}_h^n, p_h)) \geqslant 2\mu_{\mathrm{f}}\|\varepsilon(\boldsymbol{u}_h^n)\|_\Omega^2.$$

Moreover for any quantities $\boldsymbol{v}^n, \boldsymbol{v}^{n-1}$ and inner product $(\cdot,\cdot)$, it holds

$$\begin{cases}(\boldsymbol{v}^n - \boldsymbol{v}^{n-1}, \boldsymbol{v}^n) = \dfrac{1}{2}(\|\boldsymbol{v}^n\|^2 - \|\boldsymbol{v}^{n-1}\|^2 + \|\boldsymbol{v}^n - \boldsymbol{v}^{n-1}\|^2) \geqslant \dfrac{1}{2}\partial_\tau\|\boldsymbol{v}^n\|^2, \\ (\boldsymbol{v}^n - \boldsymbol{v}^{n-1}, \dfrac{\boldsymbol{v}^n + \boldsymbol{v}^{n-1}}{2}) = \dfrac{1}{2}\partial_\tau\|\boldsymbol{v}^n\|^2\end{cases}$$

where $\|\cdot\| \overset{\text{def}}{=} \sqrt{(\cdot,\cdot)}$. We deduce that

$$\partial_\tau\left(\frac{\rho_{\mathrm{f}}}{2}\|\boldsymbol{u}_h^n\|_\Omega^2 + \frac{\rho_{\mathrm{b}}}{2}\|\dot{\boldsymbol{r}}_H^n\|_{\boldsymbol{A},(0,L)}^2 + \frac{\rho_{\mathrm{b}}}{2}\|\dot{\boldsymbol{\theta}}_H^n\|_{\boldsymbol{I},(0,L)}^2 + \frac{1}{2}\|\boldsymbol{r}_H^n, \boldsymbol{\theta}_H^n\|_{\mathrm{b},H}^2\right) \leqslant 0.$$

The estimate (2.3.8) then follows by summing over $\{0 \dots n\}$, which completes the proof. □

Remark 3. Once again, to obtain the energy estimate and because we consider a linear Timoshenko beam formulation, we have to assume small rotational velocity which induces a mismatch between the structure velocity at the boundary and the velocity associated to the domain motion. It is nevertheless not an issue to derive the stability of the scheme due to the fictitious domain approach. It is not the case for the discrete counterpart of the ALE formulation where the velocities should match at the interface and where one should either consider a linear reconstruction of the geometry or a non linear beam equation.

2.3.2 Inf-sup stability A crucial point when dealing with Lagrange multipliers is to ensure that the inf-sup condition associated to the bilinear form $(\boldsymbol{\lambda}_{N,H}^n, \boldsymbol{v}_h)_\varepsilon$ is satisfied on $\boldsymbol{F}_{N,H}^n \times \boldsymbol{V}_h$. In [Kuchta et al., 2020], the authors establish the inf-sup condition for the case $N = 0$ under some conditions on the triangulations of Ω, $(0, L)$ and $\widehat{\Sigma}^\varepsilon$. To deal with general meshes, they propose a discretization of $(0, L)$ depending on the intersection of

the fluid elements and the beam centerline. With the the addition of a stabilization term, they established the inf-sup condition on $\boldsymbol{F}_{0,H}^n \times \boldsymbol{V}_h$ where the coefficients $\boldsymbol{a}_{k,H}$, $\boldsymbol{b}_{k,H}$ introduced in (2.3.2) and defining the space $\boldsymbol{F}_{0,H}^n$ belong to $\boldsymbol{X}_h^0(0,L)$ instead of $\boldsymbol{X}_h^1(0,L)$. For $N > 0$, we consider in Chapter 3 a two-dimensional problem and prove a stability result on $\boldsymbol{F}_{N,H}^n \times (\boldsymbol{X}_h^k(\Omega) \cap \boldsymbol{V})$, provided $N \leqslant k$. In the same framework, we also introduce a general stabilization term, which in 3D would take the form (see also [Barrenechea and González, 2018])

$$s_h^\lambda(\boldsymbol{\mu}_{N,H}, \boldsymbol{\lambda}_{N,H}^n) = \gamma \varepsilon^{-1} \left(\frac{h}{\varepsilon}\right) (\boldsymbol{\mu}_{N,H}, \boldsymbol{\lambda}_{N,H}^n)_{\varepsilon,n},$$

and proved unconditional stability for any pair $(\boldsymbol{\lambda}_{N,H}^n, \boldsymbol{v}_h) \in \boldsymbol{F}_{N,H}^n \times (\boldsymbol{X}_h^k(\Omega) \cap \boldsymbol{V})$ (i. e. with any restriction on N). However, no stability proof has been provided in the specific case addressed here. Nevertheless, as we encountered no issues during the numerical simulations, we chose not to include any stabilization term in our numerical study.

2.3.3 Evaluation of the coupling terms In this section, we provide details on the computation of the coupling terms involved in step (2.3.4) of Algorithm 1. For the sake of conciseness, we only give the expressions of the algebraic counterparts of the bilinear form $(\boldsymbol{\lambda}_{N,H}^n, \boldsymbol{v}_h)_{\varepsilon,n}$. The evaluation of the remaining coupling terms follow similarly. Let $\{\boldsymbol{\psi}_i^{\mathrm{f}}\}_{1 \leqslant i \leqslant N_h}$ and $\{\boldsymbol{\psi}_j^{\mathrm{b}}\}_{1 \leqslant j \leqslant N_H}$ be the basis functions of $\boldsymbol{V}_h$ and $\boldsymbol{Y}_H$, respectively, and let $\{\boldsymbol{x}_i\}_{1 \leqslant i \leqslant N_h}$ and $\{s_j\}_{1 \leqslant j \leqslant N_H}$ be the corresponding nodes. We have

$$(\boldsymbol{\lambda}_{N,H}^n, \boldsymbol{v}_h)_\varepsilon = \sum_{i=1}^{N_h} \boldsymbol{v}_h(\boldsymbol{x}_i) (\boldsymbol{\lambda}_{N,H}^n, \boldsymbol{\psi}_i^{\mathrm{f}})_{\varepsilon,n}.$$

Using the definition of $\boldsymbol{F}_{N,H}^n$ given in (2.3.2) with tensorized notations, we have

$$(\boldsymbol{\lambda}_{N,H}^n, \boldsymbol{v}_h)_{\varepsilon,n} = \sum_{i=1}^{N_h} \boldsymbol{v}_h(\boldsymbol{x}_i) \left(\left(\overline{\boldsymbol{a}_{0,H}} + \sum_{k=0}^{N} (\boldsymbol{a}_{k,H} \otimes c_k + \boldsymbol{b}_{k,H} \otimes s_k) \right) \circ (\boldsymbol{\phi}_H^n)^{-1}, \boldsymbol{\psi}_i^{\mathrm{f}} \right)_{\varepsilon,n},$$

with $c_k(\nu) \overset{\text{def}}{=} \cos(k\nu)$ and $s_k(\nu) \overset{\text{def}}{=} \sin(k\nu)$ for $k \in \{0, \dots, N\}$. Now, by expressing $\boldsymbol{a}_{k,H}, \boldsymbol{b}_{k,H}$ in terms of their basis functions $\boldsymbol{\psi}_j^{\mathrm{b}}$, we get

$$\begin{aligned}(\boldsymbol{\lambda}_{N,H}^n, \boldsymbol{v}_h)_{\varepsilon,n} = \sum_{i=1}^{N_h} \boldsymbol{v}_h(\boldsymbol{x}_i) \sum_{k=0}^{N} \sum_{j=1}^{N_H} \big[&\boldsymbol{a}_{0,H}(s_j) (\overline{\boldsymbol{\psi}_j^{\mathrm{b}}} \circ (\boldsymbol{\phi}_H^n)^{-1}, \boldsymbol{\psi}_i^{\mathrm{f}})_{\varepsilon,n} \\ &+ \boldsymbol{a}_{k,H}(s_j) ((\boldsymbol{\psi}_j^{\mathrm{b}} \otimes c_k) \circ (\boldsymbol{\phi}_H^n)^{-1}, \boldsymbol{\psi}_i^{\mathrm{f}})_{\varepsilon,n} + \boldsymbol{b}_{k,H}(s_j) ((\boldsymbol{\psi}_j^{\mathrm{b}} \otimes s_k) \circ (\boldsymbol{\phi}_H^n)^{-1}, \boldsymbol{\psi}_i^{\mathrm{f}})_{\varepsilon,n} \big].\end{aligned}$$

Let $(\boldsymbol{b}_N)^{\mathrm{T}} \in \mathbb{R}^{N_H(2N+1)\times N_h}$ denote the algebraic counterpart of the bilinar term $(\boldsymbol{\lambda}^n_{N,H} \circ (\boldsymbol{\phi}^n_H)^{-1}, \boldsymbol{v}_h)_{\varepsilon,n}$, we obtain

$$(\boldsymbol{b}_N)_{il} = \begin{cases} (\overline{\boldsymbol{\psi}^{\mathrm{b}}_j} \circ (\boldsymbol{\phi}^n_H)^{-1}, \boldsymbol{\psi}^{\mathrm{f}}_i)_{\varepsilon,n}, & l = j\cdot(2N+1), \\ ((\boldsymbol{\psi}^{\mathrm{b}}_j \otimes c_k) \circ (\boldsymbol{\phi}^n_H)^{-1}, \boldsymbol{\psi}^{\mathrm{f}}_i)_{\varepsilon,n}, & l = j\cdot(2N+1)+2k+1, \\ ((\boldsymbol{\psi}^{\mathrm{b}}_j \otimes s_k) \circ (\boldsymbol{\phi}^n_H)^{-1}, \boldsymbol{\psi}^{\mathrm{f}}_i)_{\varepsilon,n}, & l = j\cdot(2N+1)+2k+2. \end{cases} \tag{2.3.10}$$

for all $k \in \{0 \dots N\}$. In order to evaluate the coefficients (2.3.10), we need to evaluate the tensorized basis functions $(\boldsymbol{\psi}^{\mathrm{b}}_j \otimes c_k) \circ (\boldsymbol{\phi}^n_h)^{-1}$, $(\boldsymbol{\psi}^{\mathrm{b}}_j \otimes s_k) \circ (\boldsymbol{\phi}^n_h)^{-1}$ on $\Sigma^{\varepsilon,n}$. To do so, we first mesh $\widehat{\Sigma}^{\varepsilon}$ and evaluate them at the mesh points. We then transport the values to the current configuration via the deformation map $\boldsymbol{\phi}^n_h$. Integration is achieved through $\mathbb{P}_1$-interpolation in the deformed mesh by localizing the quadrature points in the fluid mesh. Note that we choose a mesh of $\widehat{\Sigma}^{\varepsilon}$ fine enough so that the error due to the $\mathbb{P}_1$-interpolation is negligible compared to the numerical approximation error of the PDE.

2.3.4 Matrix formulation We consider a partitioned solution procedure for the numerical resolution of problem (2.3.4) based on [Fernández and Moubachir, 2005b]. To this purpose, we introduce $\boldsymbol{U}^n$, $\boldsymbol{P}^n$, $\boldsymbol{L}^n$, $\boldsymbol{R}^n$ and $\boldsymbol{T}^n$ as the arrays of degrees of freedom associated with $\boldsymbol{u}^n_h$, p^n_h, $\boldsymbol{\lambda}^n_{N,H}$, $\boldsymbol{r}^n_H$ and $\boldsymbol{\theta}^n_H$ respectively. Taking $(\delta\boldsymbol{r}_H, \delta\boldsymbol{\theta}_H) = (\boldsymbol{0}, \boldsymbol{0})$ in (2.3.4), we recover the Navier-Stokes equations with Dirichlet boundary condition on $\widehat{\Sigma}^{\varepsilon}$. This problem can be expressed in matrix form as follows:

$$\begin{bmatrix} \boldsymbol{A}_{\mathrm{f}} & \boldsymbol{C}^{\mathrm{T}} & -(\boldsymbol{b}_N)^{\mathrm{T}} \\ -\boldsymbol{C} & \boldsymbol{S} & 0 \\ \boldsymbol{b}_N & 0 & 0 \end{bmatrix} \begin{bmatrix} \boldsymbol{U}^n \\ \boldsymbol{P}^n \\ \boldsymbol{L}^n \end{bmatrix} = \begin{bmatrix} \boldsymbol{b}^{n-1} \\ 0 \\ \boldsymbol{b}_N \boldsymbol{U}_{\mathrm{b}}(\boldsymbol{R}^n, \boldsymbol{T}^n) \end{bmatrix}, \tag{2.3.11}$$

with

$$\boldsymbol{A}_{\mathrm{f}} \overset{\mathrm{def}}{=} \frac{\rho_{\mathrm{f}}}{\tau}\boldsymbol{M}^{\mathrm{f}} + \boldsymbol{K}^{\mathrm{f}}, \quad \boldsymbol{b}^{n-1} \overset{\mathrm{def}}{=} \frac{\rho_{\mathrm{f}}}{\tau}\boldsymbol{M}^{\mathrm{f}}\boldsymbol{U}^{n-1},$$
$$\boldsymbol{U}_{\mathrm{b}}(\boldsymbol{R}, \boldsymbol{T}) \overset{\mathrm{def}}{=} \frac{1}{\tau}\big(\boldsymbol{\Phi}(\boldsymbol{R}, \boldsymbol{T}) - \boldsymbol{\Phi}(\boldsymbol{R}^{n-1}, \boldsymbol{T}^{n-1})\big).$$

Here, the matrices $\boldsymbol{M}^{\mathrm{f}}$, $\begin{bmatrix} \boldsymbol{K}^{\mathrm{f}} & \boldsymbol{C}^{\mathrm{T}} \\ -\boldsymbol{C} & \boldsymbol{S} \end{bmatrix}$ and $\boldsymbol{b}_N$ stand for the algebraic counterpart of

$$(\boldsymbol{u}^n_h, \boldsymbol{v}_h)_{\Omega}, \quad a^{\mathrm{f}}_{\Omega,h}\big(\boldsymbol{u}^{n-1}_h; (\boldsymbol{u}^n_h, p^n_h), (\boldsymbol{v}_h, q_h)\big), \quad (\boldsymbol{\lambda}^n_{N,H}, \boldsymbol{v})_{\varepsilon,n}.$$

With a slight abuse of notation, the operator $\boldsymbol{\Phi}$ allows us to compute the beam deformation given the displacement $\boldsymbol{R}^n$ of the centerline of the beam and its rotation vector $\boldsymbol{T}^n$. To the

matrix system (2.3.11), we can associate the fluid solver operator $\mathcal{F}^n : \mathbb{R}^{N^{\mathrm{b}}} \to \mathbb{R}^{N^{\mathrm{f}}}$ given by

$$\mathcal{F}^n\left(\begin{bmatrix}\boldsymbol{R}^n\\ \boldsymbol{T}^n\end{bmatrix}\right) = \boldsymbol{L}^n.$$

In a similar manner, testing (2.3.4) with $(\boldsymbol{v}_h, q_h, \boldsymbol{\mu}_{N,H}) = (\boldsymbol{0}, 0, \boldsymbol{0})$ yields the linear Timoshenko sub-problem with fluid source terms. The equivalent matrix system writes as follows:

$$\boldsymbol{A}_{\mathrm{b}}\begin{bmatrix}\boldsymbol{R}^{n-\frac{1}{2}}\\ \boldsymbol{T}^{n-\frac{1}{2}}\end{bmatrix} = \boldsymbol{J}^{n-1} + \begin{bmatrix}\boldsymbol{F}^n\\ \boldsymbol{M}^n\end{bmatrix} \tag{2.3.12}$$

with $\boldsymbol{R}^n = 2\boldsymbol{R}^{n-\frac{1}{2}} - \boldsymbol{R}^{n-1}$, $\boldsymbol{T}^n = 2\boldsymbol{T}^{n-\frac{1}{2}} - \boldsymbol{T}^{n-1}$ and where

$$\begin{aligned}
&\boldsymbol{A}_{\mathrm{b}} \overset{\text{def}}{=} \frac{4\rho_{\mathrm{b}}}{\tau^2}\boldsymbol{M}_{\mathrm{b}} + \boldsymbol{K}_{\mathrm{b}},\ \boldsymbol{J}^{n-1} \overset{\text{def}}{=} \frac{\rho_{\mathrm{b}}}{\tau^2}\boldsymbol{M}_{\mathrm{b}}\left(4\begin{bmatrix}\boldsymbol{R}^{n-1}\\ \boldsymbol{T}^{n-1}\end{bmatrix} + 2\tau\begin{bmatrix}\dot{\boldsymbol{R}}^{n-1}\\ \dot{\boldsymbol{T}}^{n-1}\end{bmatrix}\right),\\
&\boldsymbol{F}^n = (\boldsymbol{E}_N^f)^{\mathrm{T}}\boldsymbol{L}^n, \quad \boldsymbol{M}^n = (\boldsymbol{E}_N^m)^{\mathrm{T}}\boldsymbol{L}^n,\\
&\dot{\boldsymbol{R}}^{n-\frac{1}{2}} = \frac{1}{\tau}(\boldsymbol{R}^n - \boldsymbol{R}^{n-1}), \quad \dot{\boldsymbol{T}}^{n-\frac{1}{2}} = \frac{1}{\tau}(\boldsymbol{T}^n - \boldsymbol{T}^{n-1}).
\end{aligned}$$

Here, the matrices $\boldsymbol{M}_{\mathrm{b}}$, $\boldsymbol{K}_{\mathrm{b}}$, $\boldsymbol{E}_N^f$, $\boldsymbol{E}_N^m$ stand for the algebraic counterpart of the bilinear forms

$$(\boldsymbol{A}\boldsymbol{r}_H^n, \delta\boldsymbol{r}_H)_{(0,L)} + (\boldsymbol{I}\boldsymbol{\theta}_H^n, \delta\boldsymbol{\theta}_H)_{(0,L)}, \quad a_H^{\mathrm{b}}\big((\boldsymbol{r}_H^n, \boldsymbol{\theta}_H^n), (\delta\boldsymbol{r}_H, \delta\boldsymbol{\theta}_H)\big), \quad (\boldsymbol{\lambda}_{N,H}^n, \overline{\delta\boldsymbol{r}} \circ (\boldsymbol{\phi}_H^n)^{-1})_{\varepsilon,n},$$
$$(\boldsymbol{\lambda}_{N,H}^n, \overline{\delta\boldsymbol{\theta}} \circ (\boldsymbol{\phi}_H^n)^{-1} \wedge \big(\boldsymbol{I}_3 - \overline{\boldsymbol{r}_H^{n-1}} \circ (\boldsymbol{\phi}_H^n)^{-1} - ((\boldsymbol{\phi}_H^n)^{-1} \cdot \boldsymbol{e}_z)\boldsymbol{e}_z\big))_{\varepsilon,n}.$$

The corresponding solid solution operator $\mathcal{S}^n : \mathbb{R}^{N^{\mathrm{f}}} \to \mathbb{R}^{N^{\mathrm{b}}}$ is defined as

$$\mathcal{S}^n\left(\begin{bmatrix}\boldsymbol{U}^n\\ \boldsymbol{P}^n\\ \boldsymbol{L}^n\end{bmatrix}\right) = \begin{bmatrix}\boldsymbol{R}^n\\ \boldsymbol{T}^n\end{bmatrix}.$$

By composition, solving the coupled problem (2.3.4) is equivalent to compute the roots of the following system

$$\mathcal{R}^n\left(\begin{bmatrix}\boldsymbol{R}^n\\ \boldsymbol{T}^n\end{bmatrix}\right) \overset{\text{def}}{=} \begin{bmatrix}\boldsymbol{R}^n\\ \boldsymbol{T}^n\end{bmatrix} - \mathcal{S}^n \circ \mathcal{F}^n\left(\begin{bmatrix}\boldsymbol{R}^n\\ \boldsymbol{T}^n\end{bmatrix}\right) = \boldsymbol{0}, \tag{2.3.13}$$

which can be iteratively approximated using Newton's method below, where $\mathcal{J}^n$ denotes the Jacobian of the residual operator $\mathcal{R}^n$. As in [Fernández and Moubachir, 2005b], the tangent system (2.3.14) can be solved in a matrix-free fashion via GMRES iterations,

which only invoke the action of the operator $\mathcal{J}^n$ along given directions. Note that the resulting solution procedure is fully partitioned, in the sense that only the fluid and solid operators, and their tangent counterparts, are involved in the numerical resolution of (2.3.4).

Newton algorithm applied to (2.3.13)

Choose $\begin{bmatrix} \boldsymbol{R}^n \\ \boldsymbol{T}^n \end{bmatrix} \in \mathbb{R}^{N^{\mathrm{b}}}$

while $\left\| \mathcal{R}^n \left(\begin{bmatrix} \boldsymbol{R}^n \\ \boldsymbol{T}^n \end{bmatrix} \right) \right\| \geqslant \mathrm{tol}$ **do**

Evaluate the fluid operator $\begin{bmatrix} \boldsymbol{U}^n \\ \boldsymbol{P}^n \end{bmatrix} = \mathcal{F}^n \left(\begin{bmatrix} \boldsymbol{R}^n \\ \boldsymbol{T}^n \end{bmatrix} \right)$

Evaluate the solid operator $\begin{bmatrix} \hat{\boldsymbol{R}}^n \\ \hat{\boldsymbol{T}}^n \end{bmatrix} = \mathcal{S}^n \left(\begin{bmatrix} \boldsymbol{U}^n \\ \boldsymbol{P}^n \end{bmatrix} \right)$

Evaluate the residual $\mathcal{R}^n \left(\begin{bmatrix} \boldsymbol{R}^n \\ \boldsymbol{T}^n \end{bmatrix} \right) = \begin{bmatrix} \boldsymbol{R}^n \\ \boldsymbol{T}^n \end{bmatrix} - \begin{bmatrix} \hat{\boldsymbol{R}}^n \\ \hat{\boldsymbol{T}}^n \end{bmatrix}$

Solve tangent problem

$$\mathcal{J}^n \left(\begin{bmatrix} \boldsymbol{R}^n \\ \boldsymbol{T}^n \end{bmatrix} \right) \begin{bmatrix} \delta\boldsymbol{R} \\ \delta\boldsymbol{T} \end{bmatrix} = -\mathcal{R}^n \left(\begin{bmatrix} \boldsymbol{R}^n \\ \boldsymbol{T}^n \end{bmatrix} \right) \tag{2.3.14}$$

Update $\begin{bmatrix} \boldsymbol{R}^n \\ \boldsymbol{T}^n \end{bmatrix} = \begin{bmatrix} \boldsymbol{R}^n \\ \boldsymbol{T}^n \end{bmatrix} + \begin{bmatrix} \delta\boldsymbol{R} \\ \delta\boldsymbol{T} \end{bmatrix}$

end while

2.3.2 Comparison with other discrete formulations

For the sake of completeness, in this section we provide the discrete formulations of the coupled problems (2.2.4), (2.2.9), (2.2.23) and (2.2.4), (2.2.16), (2.2.25) introduced above. These numerical methods will be used in the numerical experiments of Section 2.3 for comparison purposes.

2.3.1 Coupled problem with ALE formalism in the fluid Since for the the coupled problem (2.2.4), (2.2.9), (2.2.23) the kinematic coupling is enforced in a strong fashion, we consider a triangulation of the reference fluid domain $\widehat{\Omega}_{\mathrm{f}}^{\varepsilon}$ which is fitted to the triangulation of the interface $\widehat{\Sigma}^{\varepsilon}$. We set $\boldsymbol{X}_h^1(\widehat{\Sigma}^{\varepsilon})$ as the trace space of $\boldsymbol{X}_h^1(\widehat{\Omega}_{\mathrm{f}}^{\varepsilon})$ and $\boldsymbol{\Pi}_{\mathrm{b},h}^1$ the corresponding Lagrange interpolation operator onto $\boldsymbol{X}_h^1(\widehat{\Sigma}^{\varepsilon})$. The geometric coupling condition $(2.2.23)_1$ is treated explicitly. For a given displacement $\boldsymbol{r}_H^{n-1} \in \boldsymbol{Y}_H$ and rotation vector $\boldsymbol{\theta}_H^{n-1} \in \boldsymbol{Y}_H$

at time step $n-1$, we define the ALE map $\boldsymbol{\mathcal{A}}_h^n$ as

$$\boldsymbol{\phi}_H^n = (\boldsymbol{I}_3 \cdot \boldsymbol{e}_z)\boldsymbol{e}_z + \overline{\boldsymbol{r}_H^{n-1}} + \overline{\boldsymbol{\Lambda}_h^{n-1}}\big(\boldsymbol{I}_3 - (\boldsymbol{I}_3 \cdot \boldsymbol{e}_z)\boldsymbol{e}_z\big) \text{ in } \widehat{\omega}^\varepsilon, \quad \boldsymbol{\mathcal{A}}_h^n = \boldsymbol{\mathcal{L}}_h\big(\boldsymbol{\Pi}_{\mathrm{b},h}^1 \boldsymbol{\phi}_H^n\big),$$

with $\boldsymbol{\Lambda}_h^{n-1}$ given from $\boldsymbol{\theta}_H^{n-1}$, using (2.2.3), and where $\boldsymbol{\mathcal{L}}_h$ denotes a given discrete lifting operator (e.g., an harmonic extension operator). The one-to-one mapping $\boldsymbol{\mathcal{A}}_h^n$ allows us to consider as fluid unknowns

$$\widehat{\boldsymbol{u}}_h^n \overset{\text{def}}{=} \boldsymbol{u}_h^n \circ \boldsymbol{\mathcal{A}}_{\boldsymbol{h}}^{\boldsymbol{n}}, \quad \widehat{p}_h^n \overset{\text{def}}{=} p_h^n \circ \boldsymbol{\mathcal{A}}_{\boldsymbol{h}}^{\boldsymbol{n}}$$

instead of $\boldsymbol{u}_h^n = \widehat{\boldsymbol{u}}_h^n \circ (\boldsymbol{\phi}_H^n)^{-1}$ and $p_h^n = \widehat{p}_h^n \circ (\boldsymbol{\phi}_H^n)^{-1}$. We then introduce the following finite element space $\boldsymbol{V}_h^{\mathrm{f}} \overset{\text{def}}{=} \boldsymbol{X}_h^1(\widehat{\Omega}_{\mathrm{f}}^\varepsilon) \cap \boldsymbol{H}_{\partial\Omega}^1(\widehat{\Omega}_{\mathrm{f}}^\varepsilon)$ and $Q_h^{\mathrm{f}} \overset{\text{def}}{=} Q_h^1(\widehat{\Omega}_{\mathrm{f}}^\varepsilon) \cap L^2(\widehat{\Omega}_{\mathrm{f}}^\varepsilon)$ for the approximation of the fluid unknowns. We write the fluid and structure equations in weak form and apply a finite element discretization with an implicit treatment of the coupling conditions. The resulting discrete formulation is given in Algorithm 2. One limitation of

Algorithm 2 Discrete formulation of the coupled problem (2.2.4), (2.2.9), (2.2.23).

For $n \geqslant 1$,

Step 1: Update of the beam deformation and of the fluid domain

$$\begin{cases} \boldsymbol{\phi}_H^n = (\boldsymbol{I}_3 \cdot \boldsymbol{e}_z)\boldsymbol{e}_z + \overline{\boldsymbol{r}_H^{n-1}} + \overline{\boldsymbol{\Lambda}_h^{n-1}}\big(\boldsymbol{I}_3 - (\boldsymbol{I}_3 \cdot \boldsymbol{e}_z)\boldsymbol{e}_z\big) \quad \text{in} \quad \widehat{\omega}^\varepsilon, \\ \boldsymbol{\mathcal{A}}_h^n = \boldsymbol{\mathcal{L}}_h\big(\boldsymbol{\Pi}_{\mathrm{b},h}^1 \boldsymbol{\phi}_H^n\big), \quad \Omega_{\mathrm{f}}^{\varepsilon,n} = \boldsymbol{\mathcal{A}}_h^n(\widehat{\Omega}_{\mathrm{f}}^\varepsilon), \quad \widehat{\boldsymbol{w}}_{\mathrm{f},H}^n = \partial_\tau \boldsymbol{\mathcal{A}}_h^n, \end{cases}$$

with $\boldsymbol{\Lambda}_h^{n-1}$ given from $\boldsymbol{\theta}_H^{n-1}$ using (2.2.3).

Step 2: Find $(\widehat{\boldsymbol{u}}_h^n, \widehat{p}_h^n, \boldsymbol{r}_H^n, \boldsymbol{\theta}_H^n) \in \boldsymbol{V}_h^{\mathrm{f}} \times Q_h^{\mathrm{f}} \times \boldsymbol{Y}_H \times \boldsymbol{Y}_H$ with $\dot{\boldsymbol{r}}_H^{n-\frac{1}{2}} = \partial_\tau \boldsymbol{r}_H^n$, $\dot{\boldsymbol{\theta}}_H^{n-\frac{1}{2}} = \partial_\tau \boldsymbol{\theta}_H^n$ and such that

$$\begin{cases} \widehat{\boldsymbol{u}}_h^n = \boldsymbol{\Pi}_{\mathrm{b},h}^1 \partial_\tau \boldsymbol{\phi}_H^n \quad \text{on} \quad \widehat{\Sigma}^\varepsilon, \\ \dfrac{\rho_{\mathrm{f}}}{\tau}\Big[(\boldsymbol{u}_h^n, \boldsymbol{v}_h)_{\Omega_{\mathrm{f}}^{\varepsilon,n}} - (\boldsymbol{u}_h^{n-1}, \boldsymbol{v}_h)_{\Omega_{\mathrm{f}}^{\varepsilon,n-1}}\Big] - \rho_{\mathrm{f}}((\nabla \cdot \boldsymbol{w}_{\mathrm{f},H}^n)\boldsymbol{u}_h^n, \boldsymbol{v}_h)_{\Omega_{\mathrm{f}}^{\varepsilon,n}} \\ + a_{\Omega_{\mathrm{f}}^{\varepsilon,n},h}^{\mathrm{f}}\big(\boldsymbol{u}_h^{n-1} - \boldsymbol{w}_{\mathrm{f},h}^n; (\boldsymbol{u}_h^n, p_h^n), (\boldsymbol{v}_h, q_h)\big) + \rho_{\mathrm{b}}(\boldsymbol{A}\partial_\tau \dot{\boldsymbol{r}}_H^n, \delta\boldsymbol{r}_H)_{(0,L)} \\ + \rho_{\mathrm{b}}\big(\boldsymbol{I}\partial_\tau \dot{\boldsymbol{\theta}}_H^n, \delta\boldsymbol{\theta}_H\big)_{(0,L)} + a_H^{\mathrm{b}}\big((\boldsymbol{r}_H^{n-\frac{1}{2}}, \boldsymbol{\theta}_H^{n-\frac{1}{2}}), (\delta\boldsymbol{r}_H, \delta\boldsymbol{\theta}_H)\big) = 0 \end{cases} \tag{2.3.15}$$

for all $(\widehat{\boldsymbol{v}}_h, \widehat{q}_h, \delta\boldsymbol{r}_H, \boldsymbol{\delta}\theta_H) \in \boldsymbol{V}_h^{\mathrm{f}} \times Q_h^{\mathrm{f}} \times \boldsymbol{Y}_H \times \boldsymbol{Y}_H$ with

$$\widehat{\boldsymbol{v}}_h = \boldsymbol{\Pi}_{\mathrm{b},h}^1\big(\overline{\delta\boldsymbol{r}_H} + \overline{\delta\boldsymbol{\theta}_H} \wedge (\boldsymbol{\phi}_H^n - \overline{\boldsymbol{r}_H^{n-1}} - (\boldsymbol{I}_3 \cdot \boldsymbol{e}_z)\boldsymbol{e}_z)\big) \quad \text{on} \quad \widehat{\Sigma}^\varepsilon.$$

Algorithm 2 lies in the capability of the discrete lifting operator $\boldsymbol{\mathcal{L}}_h$ to guarantee mesh quality when dealing with large interface deflections. This problem is even more pronounced in the context of multiple slender structures immersed in a fluid and that can get into contact. Algorithm 1 overcomes this issue by working with a fixed mesh, but it requires the localization of the interfacial mesh within the fluid mesh and the evaluation of the corresponding coupling terms.

2.3.2 Coupled problem with coupling conditions on the centerline We present in this section the discrete formulation for the coupled problem (2.2.4), (2.2.16),(2.2.25). As in the previous discrete formulations, the geometrical coupling is treated in an explicit fashion as follows:

$$\boldsymbol{\phi}_H^n = \boldsymbol{r}_H^{n-1} \quad \text{on} \quad \{0\}\times\{0\}\times(0,L), \qquad mcB^n = \boldsymbol{\phi}_H^n\big(\{0\}\times\{0\}\times(0,L)\big).$$

Then the discrete problem is similar to the one given in Algorithm 1 but with the Lagrange multipliers belonging to $\boldsymbol{Y}_H^n \overset{\text{def}}{=} \boldsymbol{X}_H^1(\boldsymbol{\mathcal{B}^n})$ instead of $\boldsymbol{F}_{N,H}^n$ and the integrals over $\Sigma^{\varepsilon,n}$ replaced with integrals over $\mathcal{B}^n$. The details of this formulation can be found in Algorithm 3. Compared to Algorithm 1, Algorithm 3 involves the localization of the beam centerline

Algorithm 3 Discrete formulation of the coupled problem (2.2.4), (2.2.16),(2.2.25)

.

For $n \geqslant 1$,

Step 1: Update of the beam centerline location:

$$\boldsymbol{\phi}_H^n = \boldsymbol{I}_3 + \boldsymbol{r}_H^{n-1} \quad \text{in} \quad \{0\}\times\{0\}\times(0,L), \quad \mathcal{B}^n = \boldsymbol{\phi}_H^n(\{0\}\times\{0\}\times(0,L)).$$

Step 2: Find $(\boldsymbol{u}_h^n, p_h^n, \boldsymbol{\lambda}_H^n, \boldsymbol{r}_H^n, \boldsymbol{\theta}_H^n) \in \boldsymbol{V}_h \times Q_h \times \boldsymbol{Y}_H^n \times \boldsymbol{Y}_H \times \boldsymbol{Y}_H$, with $\dot{\boldsymbol{r}}_H^{n-\frac{1}{2}} = \partial_\tau \boldsymbol{r}_H^n$ and $\dot{\boldsymbol{\theta}}_H^{n-\frac{1}{2}} = \partial_\tau \boldsymbol{\theta}_H^n$, such that

$$\begin{aligned}
&\rho_{\mathrm{f}}(\partial_\tau \boldsymbol{u}_h^n, \boldsymbol{v}_h)_\Omega + a_{\Omega,h}^{\mathrm{f}}\big(\boldsymbol{u}_h^{n-1}; (\boldsymbol{u}_h^n, p_h^n), (\boldsymbol{v}_h, q_h)\big) \\
&+ \rho_{\mathrm{b}}(\boldsymbol{A}\partial_\tau \dot{\boldsymbol{r}}_H^n, \delta\boldsymbol{r}_H)_{(0,L)} + \rho_{\mathrm{b}}(\boldsymbol{I}\partial_\tau \dot{\boldsymbol{\theta}}_H^n, \delta\boldsymbol{\theta}_H)_{(0,L)} \\
&+ a_H^{\mathrm{b}}\big((\boldsymbol{r}_H^{n-\frac{1}{2}}, \boldsymbol{\theta}_H^{n-\frac{1}{2}}), (\delta\boldsymbol{r}_H, \delta\boldsymbol{\theta}_H)\big) \\
&- (\boldsymbol{\lambda}_H^n, \boldsymbol{v}_h - \delta\boldsymbol{r}_H \circ (\boldsymbol{\phi}_H^n)^{-1})_{\mathcal{B}^n} + (\boldsymbol{\mu}_H, \boldsymbol{u}_h^n - \partial_\tau \boldsymbol{r}_H^n \circ (\boldsymbol{\phi}_H^n)^{-1})_{\mathcal{B}^n}
\end{aligned} \tag{2.3.16}$$

for all $(\boldsymbol{v}_h, q_h, \boldsymbol{\mu}_H, \delta\boldsymbol{r}_H, \delta\boldsymbol{\theta}_H) \in \boldsymbol{V}_h \times Q_h \times \boldsymbol{Y}_H^n \times \boldsymbol{Y}_H \times \boldsymbol{Y}_H$.

mesh wihtin the fluid mesh, instead of the interfacial mesh, making the assembly of the matrix $\boldsymbol{b}_N$, introduced in (2.3.10), faster. Furthermore, the matrix sparsity is slightly better for the Algorithm 3 as the number of fluid elements intersected by the 1D beam centerline is inherently smaller than when dealing with the 2D interface. For $N = 0$, passing from one reduced-order model to the other basically consists in computing the average value of the fluid velocity on each cross section instead of taking it at their center, then the number of degrees of freedom for the Lagrange multipliers space remains unchanged, and consequently, the size of the system matrix is the same.

2.4 Numerical experiments

In this section, we illustrate the accuracy of Algorithm 1 by comparing its numerical solution with those provided by Algorithms 2 and 3. The results provided by Algorithm 2 are taken as the reference solution (full order model). We first consider the case of a single beam and investigate the influence of several parameters, such as the mesh size h, the

beam thickness ε, the number of Fourier modes N and the Reynolds number Re. In our context, the Reynolds number is given by $Re \stackrel{\text{def}}{=} 2u_{\text{ref}}\rho_{\text{f}}\varepsilon/\mu_{\text{f}}$ where u_{ref} is a reference velocity whose value will be specified for each test case. To illustrate the robustness of the proposed modeling approach, we also consider the case of large displacements using a non-linear beam model, with multiple beams that can be in contact. All the numerical simulations have been performed with the `FELiScE` finite element library [mathematics for bio-medical applications, 2023].

2.4.1 Single beam immersed in a Stokesian flow

In the first numerical example, we consider the mechanical interaction between an incompressible viscous fluid and a single beam in a rectangular domain of dimensions $3 \times 1 \times 1$ centered at $(0.5, 0.5, 0)$. We assume that the fluid is described by Stokes equations, so that the inertia terms in (2.2.6) are neglected. Homogeneous Neumann boundary conditions are enforced at the outlet Γ_{out}, homogeneous Dirichlet condition on the lower face ($z = 0$) of the domain, and the perfect slip conditions on the other three lateral faces, as illustrated in Figure 2.3.

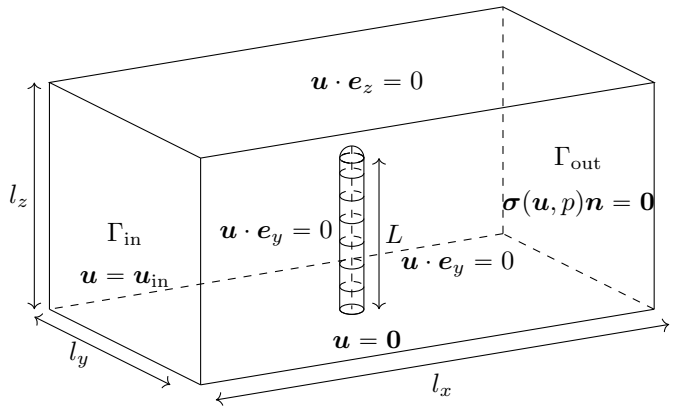

Figure 2.3: *Geometrical setting for the single beam immersed in a rectangular fluid domain.*

The following parabolic velocity profile is enforced at the inlet boundary Γ_{in}:

$$\boldsymbol{u}_{\text{in}}(\boldsymbol{x}, t) \stackrel{\text{def}}{=} u_{\text{ref}} \left(1 + \cos\left(\frac{2\pi t}{T}\right)\right)\big(1 - (z-1)(z+1)\big)\boldsymbol{e}_x, \tag{2.4.1}$$

with final time $T = 0.06$. The following beam parameters are considered: Young's modulus $E = 10^7$, radius $\varepsilon = 0.06$ and density $\rho_{\text{b}} = 1$. For the fluid, we take a density $\rho_{\text{f}} = 1$. We run simulations for different values of h/ε, representing the resolution of the beam interface by the fluid mesh. Specifically, we consider two types of fluid meshes, see Figure 2.4. The first one is refined in a region near the beam interface, with $h/\varepsilon = 1/4$, and

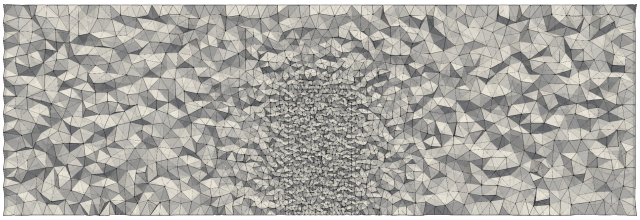

(a) *Refined fluid mesh - Algorithms 1 and 3*

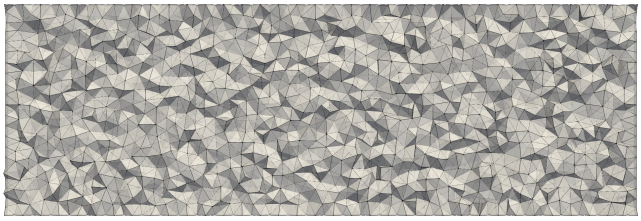

(b) *Uniform fluid mesh - Algorithms 1 and 3*

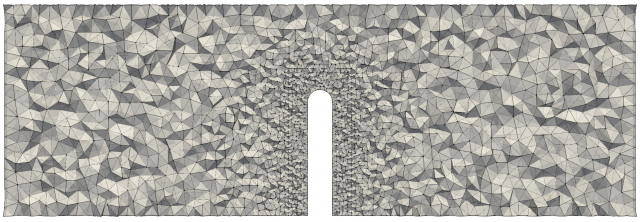

(c) *Refined fluid mesh - Algorithm 2*

Figure 2.4: *Cut plane of the fluid mesh for different resolutions of the beam interface and* $\varepsilon = 0.06$.

we have $h = 0.05$ on the faces of the rectangular domain. The second type correspond to a uniform mesh in the whole fluid domain, with $h = 0.05$. Note that for Algorithm 2, which serves as reference in the comparisons, we only consider the refined fluid mesh fitted to the interface. For the beam and the Lagrange multiplier space, we discretize the interval

$(0, L)$ with a uniform mesh such that $H = 0.05$. The behavior of the coupled system is studied over the time interval $[0, 0.06]$ with a time-step length of $\tau = 5 \cdot 10^{-3}$.

2.4.1.1 Impact of fluid mesh refinement

2.4.1 Case $h/\varepsilon \ll 1$ We consider here the refined fluid mesh. In Figure 2.5, we report the time history of the displacement of the last cross-section of the beam obtained with Algorithms 1, 2 and 3 for different values of viscosity μ_{f} and of the reference velocity u_{ref}, deliberately calibrated to keep comparable displacement amplitudes across the different test cases. In Table 2.1, we also provide the relative error in the L^∞ norm with respect to the solution provided by Algorithm 2. Lastly in Figure 2.6, we present snapshots of the fluid velocity magnitude and pressure fields at the final time $t = 0.06$.

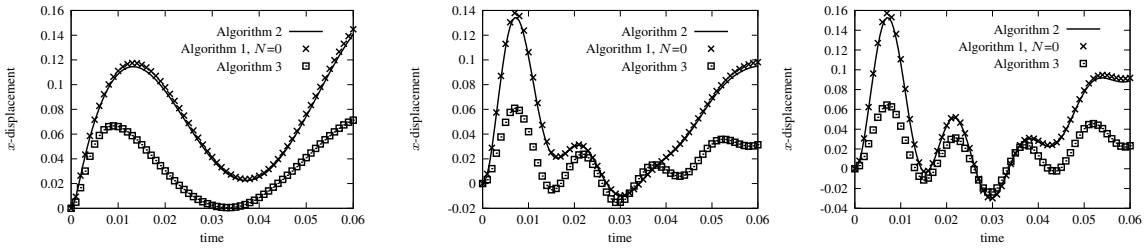

(a) $\mu_{\mathrm{f}} = 1$, $u_{\mathrm{ref}} = 10$. **(b)** $\mu_{\mathrm{f}} = 0.1$, $u_{\mathrm{ref}} = 50$. **(c)** $\mu_{\mathrm{f}} = 0.05$, $u_{\mathrm{ref}} = 100$.

Figure 2.5: *Time history of the displacement of the last cross-section of the beam along the x-axis for several fluid viscosities μ_{f} and reference inlet velocities u_{ref}, with $h/\varepsilon \ll 1$.*

	$\mu_{\mathrm{f}} = 1$, $u_{\mathrm{ref}} = 10.$	$\mu_{\mathrm{f}} = 0.1$, $u_{\mathrm{ref}} = 50.$	$\mu_{\mathrm{f}} = 0.05$, $u_{\mathrm{ref}} = 100.$
Algorithm 1, $N = 0$	$2.84 \cdot 10^{-2}$	$2.88 \cdot 10^{-2}$	$3.01 \cdot 10^{-2}$
Algorithm 3	$4.94 \cdot 10^{-1}$	$5.46 \cdot 10^{-1}$	$5.78 \cdot 10^{-1}$

Table 2.1: *Relative error $\|\big(\boldsymbol{r}(L,\cdot) - \boldsymbol{r}^{\mathrm{ref}}(L,\cdot)\big) \cdot \boldsymbol{e}_x\|_\infty / \|\boldsymbol{r}^{\mathrm{ref}}(L,\cdot) \cdot \boldsymbol{e}_x\|_\infty$ where $\boldsymbol{r}^{\mathrm{ref}}(L,\cdot)$ is the displacement of the last cross-section of the beam computed with Algorithm 2, with $h/\varepsilon \ll 1$.*

We can observe that the displacement, velocity and pressure fields obtained with Algorithm 1 provide a very good approximation of the reference given by Algorithm 2. In this context, taking $N = 0$ seems to be sufficient for accurately capturing both the beam and fluid dynamics. This can be attributed to the fact that the numerical solution of Algorithm 2 presents a symmetric flow pattern around the beam, which results in a small torque acting onto beam and a subsequent low angular velocity. Additionally, the force transmitted to the beam and the subsequent beam displacement velocity for Algorithm 2 belongs to the functional space F_0. In contrast, Algorithm 3 does not provide a satisfactory numerical solution. The area of influence of the beam on the fluid appears considerably smaller compared to Algorithm 2. The lower magnitude of the velocity and pressure is no-

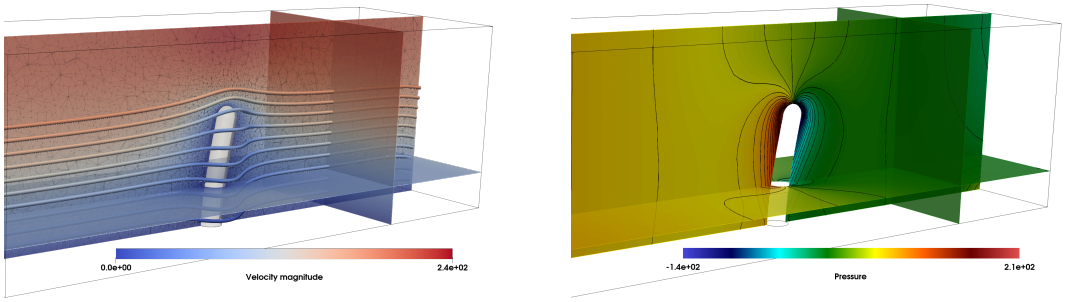

(a) *Algorithm 2 - Reference Solution.*

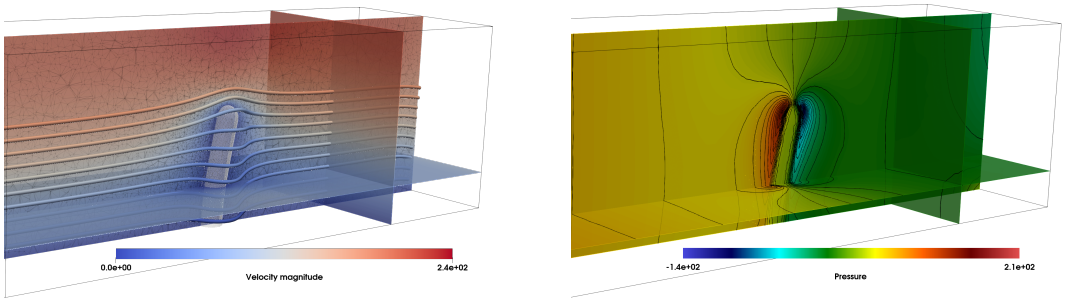

(b) *Algorithm 1,* $N = 0$.

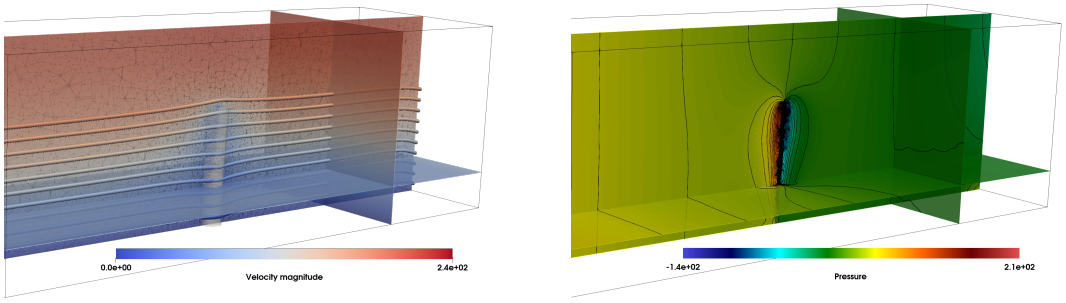

(c) *Algorithm 3.*

Figure 2.6: *Snapshots of the fluid velocity magnitude (left) and pressure (right) at time* $t = 0.06$ *obtained with Algorithms 1–3, with* $h/\varepsilon \ll 1$.

ticeable in Figure 2.6, which is also consistent with differences in displacement observed in Figure 2.5 and Table 2.1. As discussed in [Hagmeyer et al., 2022], the extent of the influence of the beam on the surrounding fluid for Algorithm 3 is determined by the size of the fluid elements. When $h/\varepsilon \ll 1$, this difference becomes important and then leads to a considerable deviation from the reference solution.

2.4.2 Case $h/\varepsilon \approx 1$ We now consider the uniform fluid mesh. In this configuration, the thickness of the beam ($\varepsilon = 0.06$) is roughly equal to the size of the fluid elements. As

indicated above, we keep a refined mesh for Algorithm 2, which serves as reference solution.

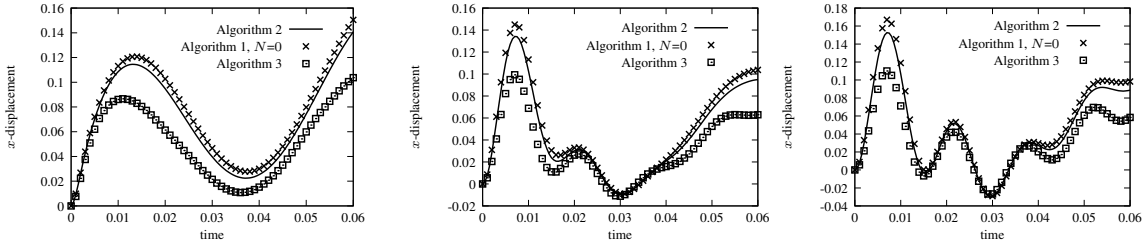

(a) $\mu_{\mathrm{f}} = 1$, $u_{\mathrm{ref}} = 10$. **(b)** $\mu_{\mathrm{f}} = 0.1$, $u_{\mathrm{ref}} = 50$. **(c)** $\mu_{\mathrm{f}} = 0.05$, $u_{\mathrm{ref}} = 100$.

Figure 2.7: *Time history of the displacement of the last cross-section of the beam along the x-axis for various fluid viscosity μ_{f} and reference inlet velocity u_{ref}, with $h/\varepsilon \approx 1$.*

	$\mu_{\mathrm{f}} = 1$, $u_{\mathrm{ref}} = 10$.	$\mu_{\mathrm{f}} = 0.1$, $u_{\mathrm{ref}} = 50$.	$\mu_{\mathrm{f}} = 0.05$, $u_{\mathrm{ref}} = 100$.
Algorithm 1, $N = 0$	$6.88 \cdot 10^{-2}$	$8.14 \cdot 10^{-2}$	$9.39 \cdot 10^{-2}$
Algorithm 3	$2.63 \cdot 10^{-1}$	$2.71 \cdot 10^{-1}$	$2.85 \cdot 10^{-1}$

Table 2.2: *Relative error $\|\big(\boldsymbol{r}(L,\cdot) - \boldsymbol{r}^{\mathrm{ref}}(L,\cdot)\big) \cdot \boldsymbol{e}_x\|_\infty / \|\boldsymbol{r}^{\mathrm{ref}}(L,\cdot) \cdot \boldsymbol{e}_x\|_\infty$ where $\boldsymbol{r}^{\mathrm{ref}}(L,\cdot)$ is the displacement of the last cross-section of the beam computed with Algorithm 2, with $h/\varepsilon \approx 1$.*

The results for the displacement of the last beam cross-section are given in Figure 2.7, relative error in L^∞ norm with respect to the reference solution are presented in Table 2.2 and snapshots of the velocity magnitude and pressure at time $t = 0.06$ are provided in Figure 2.8. We can observe that Algorithm 1 is able to capture the dynamics of the beam displacement and the main fluid velocity/pressure patterns. However, the comparison with Algorithm 2 degrades a bit with respect to the previous case ($h/\varepsilon \ll 1$). This is visible in the slight deviations observed in the displacement history and in the pressure pattern. As regards Algorithm 3, provides a better approximation of the beam displacement than in the scenario $h/\varepsilon \ll 1$. However, the solution is still less accurate than the one obtained with Algorithm 1. Furthermore, although an improvement can be seen in the solution for beam displacement, Figure 2.7 shows that the solution for fluid velocity suffers from the same limitations as in the case $h/\varepsilon \ll 1$. In general, with a coarser mesh, we observe, however, that the pressure jump for both Algorithm 1 and 3 is smaller than the one obtained with Algorithm 2. This can be attributed to the singularity in the pressure, whose approximation using continuous piece-wise affine functions requires a fine mesh to be captured accurately.

2.4.3 Case $h/\varepsilon \gg 1$ Here, we still consider the uniform mesh. However, we decrease the value of ε, in particular, we consider $\varepsilon \in \{0.06, 0.04, 0.02\}$. In Algorithm 2, as before, the mesh is refined around the beam to ensure that $h/\varepsilon = 1/4$, which resolves the interface

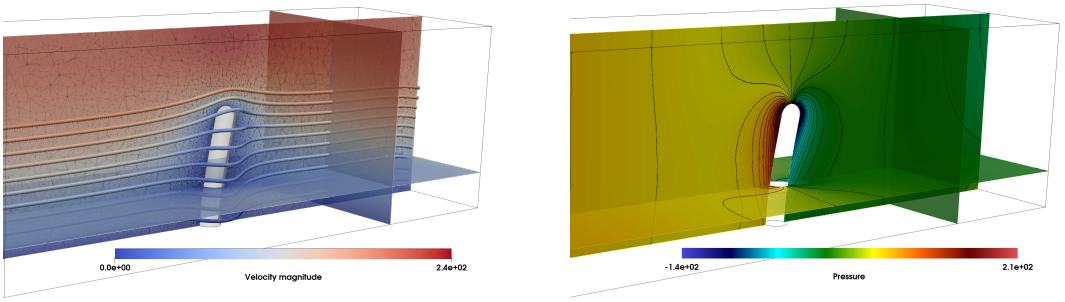

(a) *Algorithm 2 - Reference solution.*

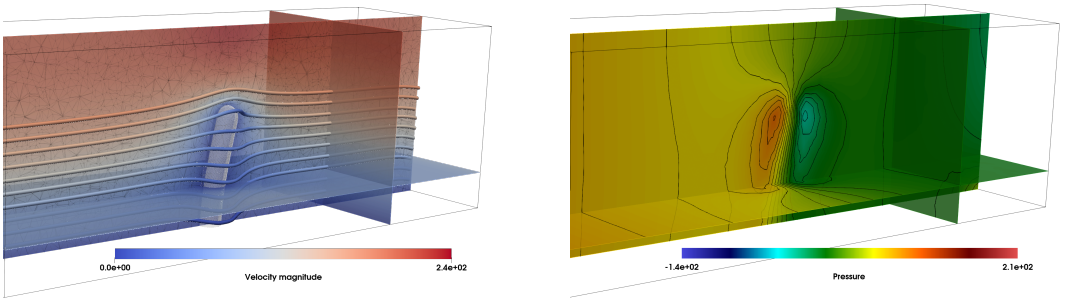

(b) *Algorithm 1 with* $N = 0$.

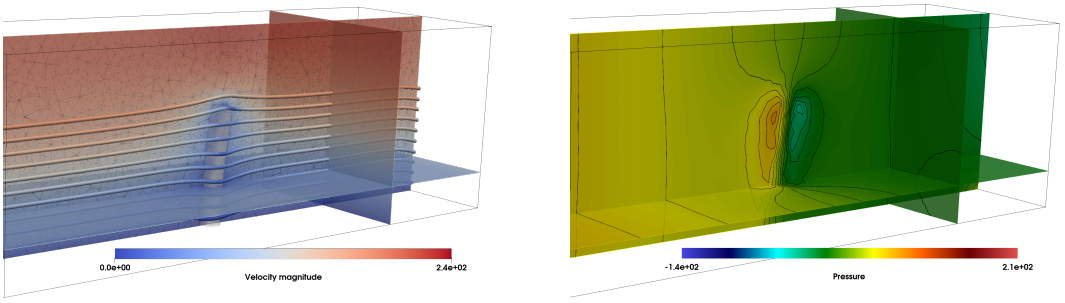

(c) *Algorithm 3.*

Figure 2.8: *Snapshots of the fluid velocity magnitude (left) and pressure (right) at time* $t = 0.06$ *obtained with Algorithms 1–3, with* $h/\varepsilon \approx 1$.

regardless of the beam thickness ε.

	$\varepsilon = 0.06$, $E = 10^7$.	$\varepsilon = 0.04$, $E = 4 \cdot 10^7$.	$\varepsilon = 0.02$, $E = 4 \cdot 10^8$.
Algorithm 1, $N = 0$	$9.39 \cdot 10^{-2}$	$1.13 \cdot 10^{-1}$	$2.20 \cdot 10^{-1}$
Algorithm 3	$2.85 \cdot 10^{-1}$	$1.45 \cdot 10^{-1}$	$2.03 \cdot 10^{-1}$

Table 2.3: *Relative error* $\|\big(\boldsymbol{r}(L,\cdot) - \boldsymbol{r}^{\mathrm{ref}}(L,\cdot)\big) \cdot \boldsymbol{e}_x\|_\infty / \|\boldsymbol{r}^{\mathrm{ref}}(L,\cdot) \cdot \boldsymbol{e}_x\|_\infty$ *where* $\boldsymbol{r}^{\mathrm{ref}}(L,\cdot)$ *is the displacement of the last cross-section of the beam computed with Algorithm 2, with* $h/\varepsilon \gg 1$.

To keep comparable amplitudes for the beam displacement independently of the beam

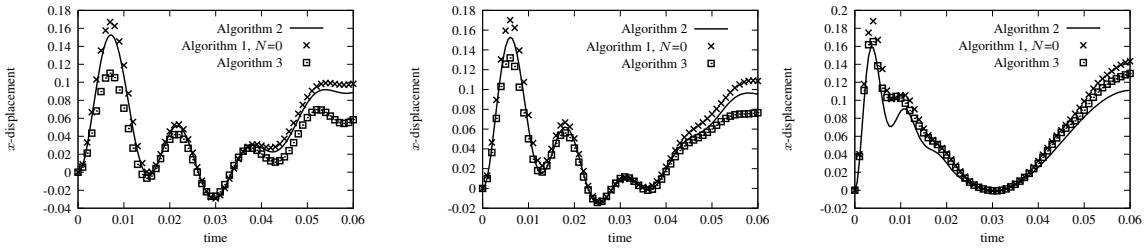

(a) $\varepsilon = 0.06$, $E = 10^7$. **(b)** $\varepsilon = 0.04$, $E = 4 \cdot 10^7$. **(c)** $\varepsilon = 0.02$, $E = 4 \cdot 10^8$.

Figure 2.9: *Time history of the displacement of the last cross-section of the beam along the x-axis for various thickness ε and Young's modulus E - $h/\varepsilon \gg 1$.*

thickness, the Young's modulus of the beam is modified accordingly with values $E \in \{10^7, 4 \cdot 10^7, 4 \cdot 10^8\}$. We fix $\mu_{\mathrm{f}} = 0.05$ and $u_{\mathrm{ref}} = 100$. The results obtained are reported in Figure 2.9 for the beam displacement, in Table 2.3 for the relative error in L^∞ norm and in Figure 2.10 for the velocity and pressure fields. We can clearly observe that by reducing ε, the numerical approximations of the beam displacement, the fluid velocity and the fluid pressure provided by Algorithms 1 and 3 get closer. The price to pay is a significant degradation of the accuracy of Algorithm 1 with respect to the previous cases.

In conclusion, as the ratio h/ε increases, the resolution of the mesh becomes insufficient to accurately capture the fluid-solid interface. In this context, the numerical comparisons indicate that imposing the coupling conditions on the centerline delivers similar accuracy to enforcing them on the interface. However, given the relatively large mesh size compared to the beam thickness, delivering an accurate solution for the fluid pressure and velocity on the interface becomes challenging. The primary advantage of the Algorithm 1 lies in its ability to capture the dynamics of the problem effectively with a reasonably refined fluid mesh near the interface, while maintaining reduced order interface conditions in the spirit of Algorithm 2.

2.4.1.2 Influence of the number of Fourier modes

In this section, we consider a variant of the previous numerical example in which the beam is immersed in a shear flow, with the purpose of inducing torsional effects on the beam and illustrate the importance, in this new context, of considering enough modes ($N \geqslant 1$) in Algorithm 1. We consider homogeneous Neumann boundary conditions on Γ_{in} and Γ_{out}, homogeneous Dirichlet boundary conditions on the lower face of the domain, and

$$\boldsymbol{u} = u_{\mathrm{ref}}(y - 0.5)(1 - (x - 1)(x + 1))\boldsymbol{e}_x$$

on the three other lateral faces, with $u_{\mathrm{ref}} = 40$. In order to further induce torsional effects in the beam, we consider elliptical cross-sections with an aspect ratio $a = 2$ and a small axis $\varepsilon = 0.04$. The physical parameters are $\mu_{\mathrm{f}} = 1$, $E = 4 \cdot 10^5$ and $\rho_{\mathrm{b}} = 1$.

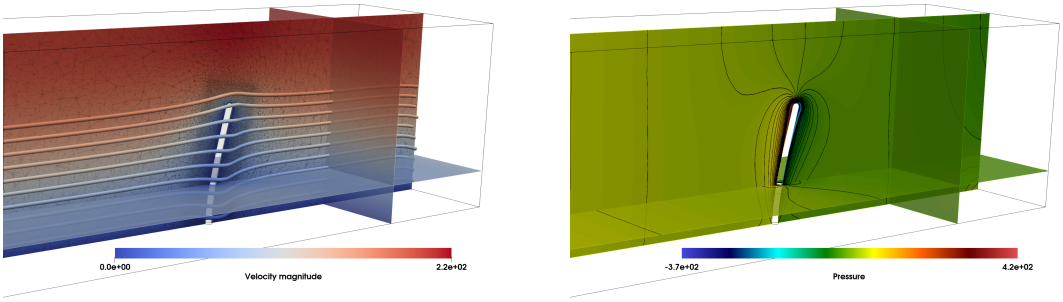

(a) *Algorithm 2, reference solution.*

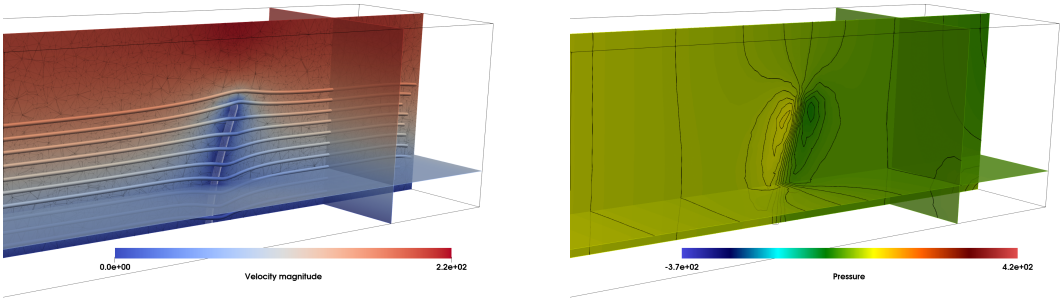

(b) *Algorithm 1 with* $N = 0$.

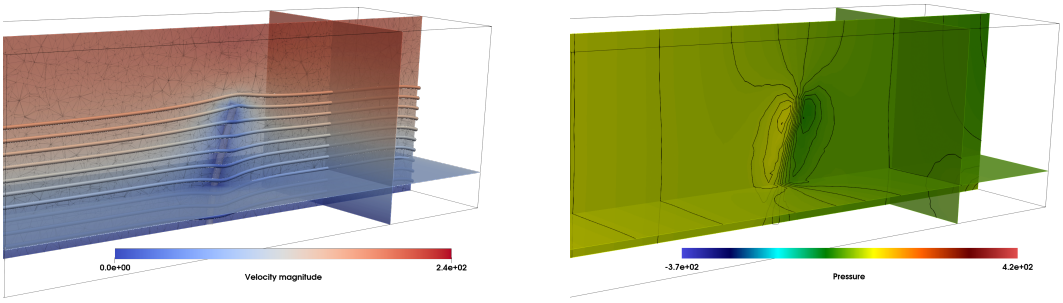

(c) *Algorithm 3.*

Figure 2.10: *Snapshots of the fluid velocity magnitude (left) and pressure (right) at time* $t = 0.06$ *obtained with Algorithms 1–3, with* $h/\varepsilon \gg 1$.

In Algorithms 1 and 2, we consider the same type of fluid meshes, refined around the beam ($h/\varepsilon = 1/4$) and uniform on the faces of the rectangular domain ($h = 0.05$). We compare the approximations provided by Algorithm 1 and Algorithm 2 with $N = 0, 1$. In Figure 2.11, we report the time history of the rotation of the last cross-section around the z axis over the time interval $[0, 0.06]$. In Figure 2.12, we provide some snapshots of the beam deformed configuration at time $t \in \{0, 0.02, 0.04, 0.06\}$. We can clearly observe that Algorithm 1 with $N = 0$ cannot capture the torsion induced by the shear fluid flow on the beam. Indeed, since the Lagrange multiplier is constant on each cross-section, no torque

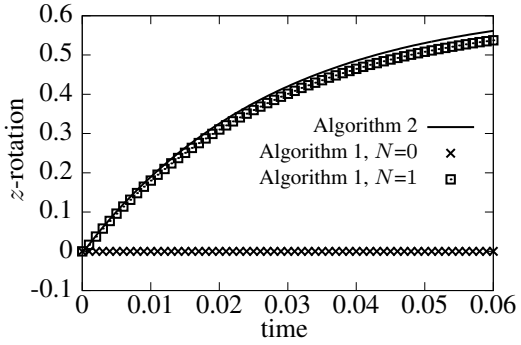

Figure 2.11: *Rotation of the last cross-section along the z-axis of the beam immersed in a shear flow.*

is transmitted to the beam. As a result, since the beam is initially at rest, it remains steady throughout the simulation. In contrast, Algorithm 1 with $N = 1$ is able to reproduce the rotational motion around the z-axis obtained with Algorithm 2. Similarly, the velocity of the beam interface, mainly determined by its torsion velocity around the z-axis, is well captured, as shown in Figure 2.12. In terms of displacement, this favorable outcome comes from the fact that the moment transmitted to the structure, as well as the rotation velocity of the beam interface, given in equations (2.2.23), belong to the space F_1.

2.4.2 Single beam immersed in a Navier-Stokes flow

In this section, we keep the geometric configuration considered in Section 2.4.1, but now with a beam immersed in a Navier-Stokes flow, so that the Reynolds number is not zero anymore. The fluid velocity is initialized with the solution of the Stokes equations, in which the velocity on the beam is set to zero. We consider a fluid density $\rho_{\mathrm{f}} = 1$ and a beam density $\rho_{\mathrm{b}} = 1$. The thickness of the beam cross-section is set to $\varepsilon = 0.06$ and the Reynolds number $Re \in \{2.4, 120, 480\}$, with $\mu_{\mathrm{f}} \in \{1, 0.1, 0.05\}$ and $u_{\mathrm{ref}} \in \{10, 50, 100\}$, respectively. To keep similar displacement amplitudes when varying the Reynolds number, the Young modulus of the beam is chosen as $E \in \{10^7, 1.6 \cdot 10^8, 3 \cdot 10^8\}$. We use a mesh that accurately resolves the beam interface such that $h/\varepsilon = 1/4$ in a region near the beam and $h = 0.05$ on the faces of the rectangular domain.

2.4.1 Impact of the Reynolds number We first investigate the influence of the Reynolds number on the accuracy of Algorithm 1. In Figure 2.13, we report the time history of the displacement of the lass cross-section of the beam with $Re \in \{2.4, 120, 480\}$ and $E \in \{4 \cdot 10^7, 4 \cdot 10^7, 4 \cdot 10^8\}$, and in Table 2.4 the L^∞ relative error with respect to Algorithm 2. Note that in Figure 2.13, we introduced an additional algorithm, referred to as Algorithm 2-Ω in in which the fluid is solved in the whole domain Ω. The motivation of this algorithm will be discussed in the next paragraph. We observe that the higher the

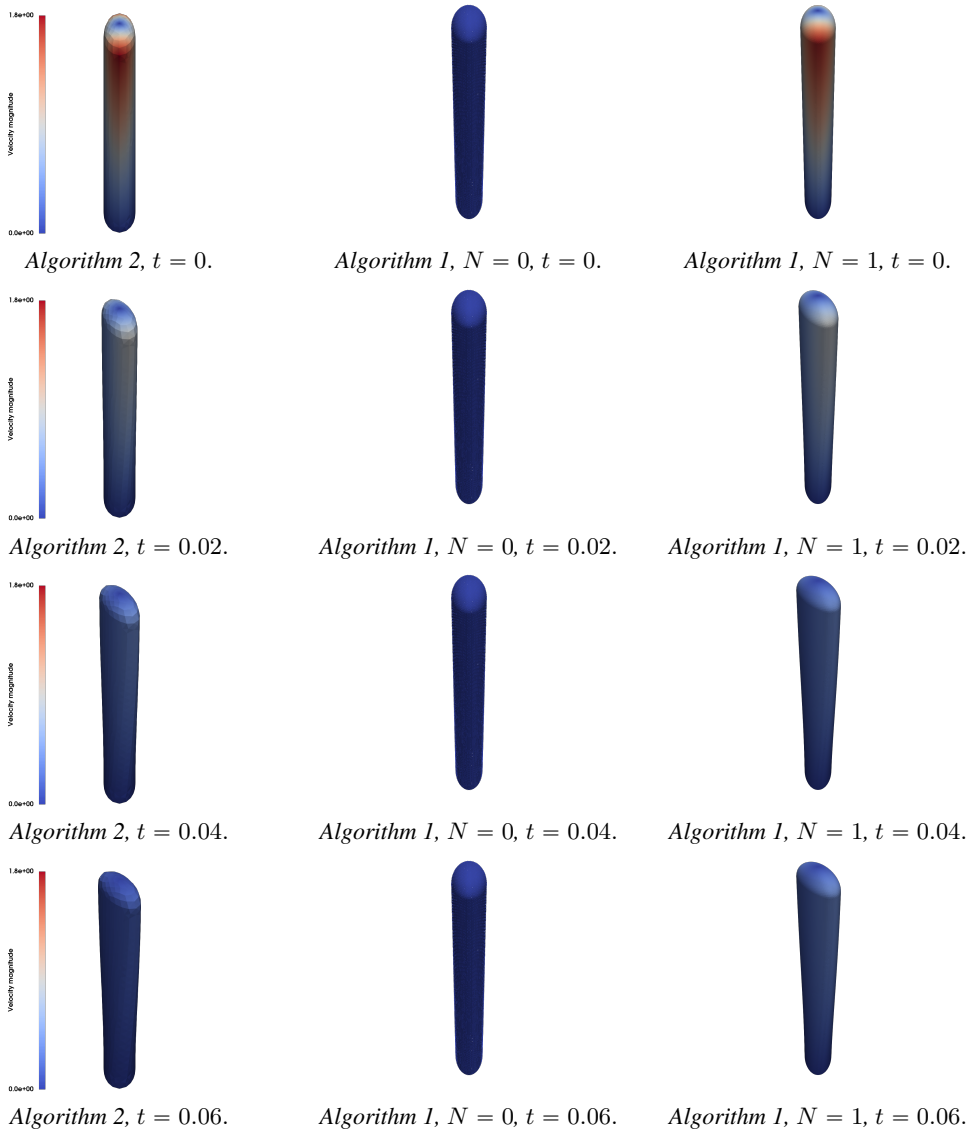

Algorithm 2, $t = 0$. *Algorithm 1*, $N = 0$, $t = 0$. *Algorithm 1*, $N = 1$, $t = 0$.

Algorithm 2, $t = 0.02$. *Algorithm 1*, $N = 0$, $t = 0.02$. *Algorithm 1*, $N = 1$, $t = 0.02$.

Algorithm 2, $t = 0.04$. *Algorithm 1*, $N = 0$, $t = 0.04$. *Algorithm 1*, $N = 1$, $t = 0.04$.

Algorithm 2, $t = 0.06$. *Algorithm 1*, $N = 0$, $t = 0.06$. *Algorithm 1*, $N = 1$, $t = 0.06$.

Figure 2.12: *Snapshots of the beam deformation and the velocity magnitude induced by a shear flow, at time* $t \in \{0, 0.02, 0.04, 0.06\}$ *(from top to bottom).*

Reynolds number the less accurately the displacement of the beam is captured by Algorithm 1. On the contrary, the accuracy of the results is improved by increasing the number of Fourier modes N. In particular, the numerical solution appears to converge when N increases. Indeed, the accuracy gap between $N = 0$ and $N = 1$ is quite significant, but decreases significantly between $N = 1$ and $N = 2$. However, the numerical results indi-

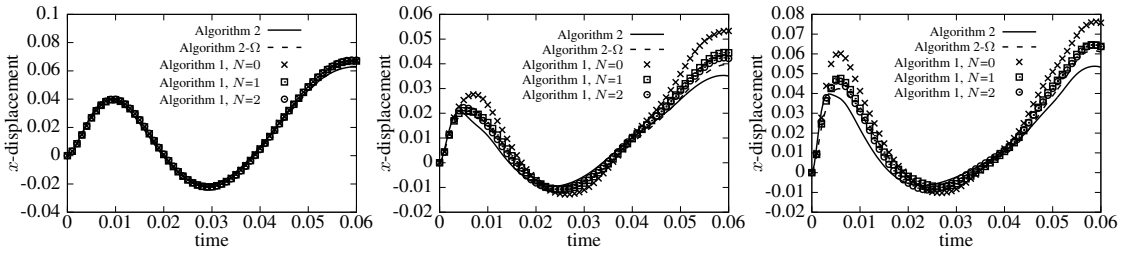

(a) $Re = 2.4$, $E = 4 \cdot 10^7$. **(b)** $Re = 120$, $E = 1.6 \cdot 10^8$. **(c)** $Re = 480$, $E = 3 \cdot 10^8$.

Figure 2.13: *Time history of the displacement of the last cross-section of the beam along the x-axis for various Reynolds number Re and Young's modulus E.*

	$Re = 2.4$, $E = 4 \cdot 10^7$.		$Re = 120$, $E = 1.6 \cdot 10^8$.		$Re = 480$, $E = 3 \cdot 10^8$.	
	Algorithm 2	Algorithm 2-Ω	Algorithm 2	Algorithm 2-Ω	Algorithm 2	Algorithm 2-Ω
Algorithm 1, $N = 0$	$7.05 \cdot 10^{-2}$	$6.49 \cdot 10^{-2}$	$5.17 \cdot 10^{-1}$	$3.41 \cdot 10^{-1}$	$4.31 \cdot 10^{-1}$	$2.90 \cdot 10^{-1}$
Algorithm 1, $N = 1$	$6.95 \cdot 10^{-2}$	$6.38 \cdot 10^{-2}$	$2.67 \cdot 10^{-1}$	$1.27 \cdot 10^{-1}$	$2.06 \cdot 10^{-1}$	$8.75 \cdot 10^{-2}$
Algorithm 1, $N = 2$	$7.89 \cdot 10^{-2}$	$7.30 \cdot 10^{-2}$	$2.02 \cdot 10^{-1}$	$7.66 \cdot 10^{-2}$	$2.00 \cdot 10^{-1}$	$8.43 \cdot 10^{-2}$

Table 2.4: *Relative error $\|\big(\boldsymbol{r}(L,\cdot) - \boldsymbol{r}^{\mathrm{ref}}(L,\cdot)\big) \cdot \boldsymbol{e}_x\|_\infty / \|\boldsymbol{r}^{\mathrm{ref}}(L,\cdot) \cdot \boldsymbol{e}_x\|_\infty$ where $\boldsymbol{r}^{\mathrm{ref}}(L,\cdot)$ is the displacement of the last cross-section of the beam computed with Algorithm 2 or Algorithm 2-Ω.*

cate that the limit differs from the numerical solution provided by Algorithm 2, notably as the Reynolds number increases. One possible explanation of this mismatchis that, in the fictitious domain approach, the fluid equations are solved in the entire domain Ω, which introduces a non-physical flow in the part occupied by the beam with the subsequent additional artificial stress on the interface. It is worth noting that, in the case of a Stokes flow, the numerical results of Section 2.4.1 indicate that the impact of such spurious stress on the accuracy of Algorithm 1 is rather limited.

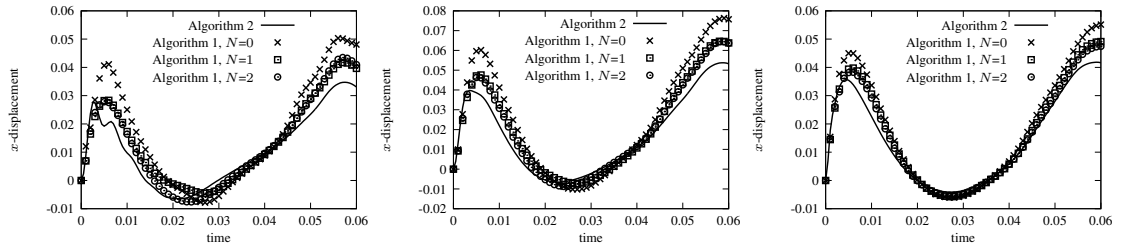

(a) $Re = 800$, $\varepsilon = 0.1$, $E = 10^8$. **(b)** $Re = 480$, $\varepsilon = 0.06$, $E = 3 \cdot 10^8$. **(c)** $Re = 160$, $\varepsilon = 0.02$, $E = 1.2 \cdot 10^{10}$.

Figure 2.14: *Time history of the displacement of the last cross-section of the beam along the x-axis for various beam thickness ε.*

	$Re = 800$, $\varepsilon = 0.1$, $E = 10^8$.	$Re = 480$, $\varepsilon = 0.06$, $E = 1.2 \cdot 10^9$.	$Re = 160$, $\varepsilon = 0.02$, $E = 1.2 \cdot 10^{10}$.
Algorithm 1, $N = 0$	$6.22 \cdot 10^{-1}$	$4.31 \cdot 10^{-1}$	$3.23 \cdot 10^{-1}$
Algorithm 1, $N = 1$	$2.61 \cdot 10^{-1}$	$2.06 \cdot 10^{-1}$	$1.96 \cdot 10^{-1}$
Algorithm 1, $N = 2$	$2.54 \cdot 10^{-1}$	$2.00 \cdot 10^{-1}$	$1.63 \cdot 10^{-1}$

Table 2.5: *Relative error* $\|\big(\boldsymbol{r}(L,\cdot) - \boldsymbol{r}^{\mathrm{ref}}(L,\cdot)\big) \cdot \boldsymbol{e}_x\|_\infty / \|\boldsymbol{r}^{\mathrm{ref}}(L,\cdot) \cdot \boldsymbol{e}_x\|_\infty$ *where* $\boldsymbol{r}^{\mathrm{ref}}(L,\cdot)$ *is the displacement of the last cross-section of the beam computed with Algorithm 2.*

2.4.2 Impact of the fictitious domain method In order to investigate the impact of the spurious internal fluid on the accuracy of Algorithm 1, we consider a variant of Algorithm 2 in which the fluid is solved in the whole domain Ω, so that the portion of the domain occupied by the beam is also filled with the fluid. This variant will be termed Algorithm 2-Ω. Figure 2.13 and Table 2.4 indicate that the displacement of the last cross-section of the beam obtained with Algorithm 1, with $N \in \{1, 2\}$, is close to the one provided by Algorithm 2-Ω. Since the volume of the region occupied by the beam is proportional to ε^2, one would expect that the perturbation induced by the artificial fluid decreases as ε tends to zero. We propose to exhibit this phenomenon by gradually decreasing the thickness of the beam, by taking $\varepsilon \in \{0.1, 0.04, 0.02\}$ while keeping the same fluid parameters as in the case with $Re = 480$ and $\varepsilon = 0.06$. To keep similar amplitudes of the beam deflection, we take the Young's modulus $E \in \{10^8, 1.2 \cdot 10^9, 1.2 \cdot 10^{10}\}$. In Figure 2.14 we report the time history of the displacement of the last cross-section of the beam and in Table 2.5 the L^∞ relative error with respect to Algorithm 2. We observe that the displacement of the last beam cross-section approaches the reference solution as the thickness decreases. Another difficulty of standard fictitious domain methods is the approximation of the pressure jump across the beam interface via continuous functions. In Figure 2.15, we provide snapshots of the magnitude of the velocity and the pressure fields obtained with $Re = 480$ and a constant velocity inlet $\boldsymbol{u}_{\mathrm{in}} = 2u_{\mathrm{ref}}\boldsymbol{e}_x$. We can clearly observe that the pressure jump provided by Algorithm 2-Ω is smaller than the one obtained with Algorithm 2. We can also notice that the continuous pressure approximation does not ensure mass conservation across the interface, as a spurious flow is generated inside the region occupied by the beam. As a result, the vortices that form behind the beam are also much weaker. Although increasing the number of modes in Algorithm 1 significantly reduces the amount of spurious fluid, notably for $N = 2$, the obtained numerical solutions is much closer to the one provided by Algorithm 2-Ω than by Algorithm 2.

Some solutions exist to circumvent these issues. In order to correctly evaluate the fluid stress at the interface, one can force the fluid velocity inside the fictitious region to be equal to the solid velocity using, for instance, distributed Lagrange multipliers [Girault and Glowinski, 1995, Boffi and Gastaldi, 2015]. However, this approach often requires the introduction of 3D corrections, which jeopardize the reduced nature of the present methodology. Thus, we have chosen to not include them into the present study.

In order to mitigate the impact of the spurious stress across the interface, we consider

the approach which consists in introducing a scalar Lagrange multiplier to guarantee mass conservation within the domain $\Omega_{\mathrm{f}}^{\varepsilon}(t)$ (see [Corti et al., 2023, Ohmori and Saito, 2007]), viz.,

$$\int_{\partial\Omega_{\mathrm{f}}^{\varepsilon}(t)} \boldsymbol{u}\cdot\boldsymbol{n}^{+} = 0.$$

We denote by Algorithm 1 - MC the solution procedure obtained by combining Algorithm 1 with this approach. Figure 2.15 reports the snapshots of the fluid velocity magnitude and pressure obtained with Algorithms 1 and 2, Algorithm 2-Ω and Algorithm 1-MC at time $t = 0.06$. We can observe that the introduction of the scalar mass conservation constraint noticeably reduces the fluid flow both inside and across the beam. Furthermore, the pressure and field around the beam are rendered with greater fidelity, particularly near the beam interface, where we observe an increased upward velocity along the interface, together with vortices forming much closer to the beam.

2.4.3 Multiple-beams immersed in incompressible viscous flow

In order to further assess the robustness of the proposed approach, we consider a more complex scenario involving a swarm of beams made of 75 circular beams, arranged with 5 along the y-axis and 15 along the x-axis. The beams have a radius $\varepsilon = 0.05$ and are spaced 0.05 apart from each other. The boundary conditions are similar to the one described in the previous section with a time dependent inlet velocity (2.4.1). The beam is modeled by a non-linear co-rotational formulation that allows for large deformations (see [Krenk, 2009, Chapter 5]). In this formulation, the total motion of the beam is divided between the motion of the element-based local co-rotating frame of reference and the deformation of the element within this local frame. For the element's deformation within this local frame, the generalized Timoshenko linear beam theory is used as described in Section 2.2.1. Given the proximity of the beams, they are likely to come in contact. To address this issue, we have incorporated a penalty contact algorithm using a raytracing projection on the 2D beam interface described in Section 2.A.1 of the Appendix. All the beams have the same Young's modulus and density, $E = 10^8$ and $\rho_{\mathrm{b}} = 1$, respectively.

We first consider a Stokes flow with viscosity $\mu_{\mathrm{f}} = 1$ and reference inlet velocity $u_{\mathrm{ref}} = 10$. The size of the mesh is uniform throughout the fluid domain, with $h = 0.05$. In Figure 2.16, we provide snapshots of the fluid velocity magnitude computed with Algorithm 1 at times $t \in \{0.05, 0.1, 0.2, 0.3, 0.45, 0.6\}$. We observe a collective behavior of the beams oscillating from left to right. In particular, they do not get into contact. We then consider a Navier-Stokes flow, with Reynolds number $Re = 480$, computed with $\mu_{\mathrm{f}} = 0.05$, $u_{\mathrm{ref}} = 100$ and $\rho_{\mathrm{f}} = 1$. The fluid mesh is kept uniform with a smaller mesh size $h = 0.035$. Snapshots of the fluid velocity magnitude calculated with Algorithm 1 with $N = 2$ are provided in Figure 2.17. We observe a significant reduction in fluid velocity due to the presence of beams. Additionally, a distinct wave flow pattern appears in

the upper region. We also observe orthogonal waves to the inlet flow pushing the beams outward, thereby increasing the fluid velocity within these regions of the domain.

2.5 Conclusion

In this chapter, we have proposed a new approach for the modeling and simulation of slender structures immersed in a 3D flow. A salient feature of the proposed methodology is that the 3D fluid model and the reduced 1D solid model are coupled via well-posed trace operators of co-dimension two, based on a suitable Fourier projection of the kinematic constraint on the 2D interface. The method has been extensively compared with a full order (ALE based) approach and an alternative reduced based method. Numerical evidence indicates that, at low Reynolds numbers, the method is accurate regardless of the ratio between the background mesh size and the radius of the beam. For moderate Reynolds numbers, accurately capturing the fluid flow around the two-dimensional beam interface requires both mesh refinement and a higher number of Fourier modes.

The numerical comparisons also indicated that, for high Reynolds numbers, most of the numerical errors arise from the fictitious domain method. As a result, we have proposed strategies to address these issues without resorting to 3D techniques, to guarantee consistency with the underlying reduced nature of the method. Furthermore, numerical evidence has been provided on the fact that the choice of the approximated Fourier space can have a significant influence on the dynamic of the beams, including whether it is possible to capture the rotation of the cross-sections.

Finally, to assert the robustness of the method and its potential integration with more general computational frameworks for fluids and solids, we have tested it considering a significant number of beams that can get into contact.

In Chapter 5, we propose a stable and accurate loosely coupled schemes allowing to strike a balance between computational efficiency and accuracy.

2.A Appendix

2.A.1 Contact algorithm

To address contact interactions, we integrate a contact term into Algorithm 1. This contact term is based on a ray-tracing strategy with penalization on the reconstructed interface of the beams following the method presented for example in [Chouly et al., 2023, Chapter 11]. Since the balance equations are defined on the beam centerline, the penalization term is then integrated on each cross section to obtain a one-dimensional force.

To define the contact term, we consider two distinct beams $\widehat{\omega}_1^\varepsilon$ and $\widehat{\omega}_2^\varepsilon$ such that $\widehat{\Sigma}_1^\varepsilon \stackrel{\text{def}}{=} \partial\widehat{\omega}_1^\varepsilon \backslash \partial\Omega$ is the master surface and $\widehat{\Sigma}_2^\varepsilon \stackrel{\text{def}}{=} \partial\widehat{\omega}_2^\varepsilon \backslash \partial\Omega$ is the slave surface. For all $\boldsymbol{x} \in \Sigma_2^{\varepsilon,n} \stackrel{\text{def}}{=}$

$\boldsymbol{\phi}^n(\widehat{\Sigma}_2^\varepsilon)$, denoting by $\boldsymbol{n}_x$ the outer normal of the surface $\Sigma_2^{\varepsilon,n} \overset{\text{def}}{=} \boldsymbol{\phi}^n(\widehat{\Sigma}_2^\varepsilon)$ at point $\boldsymbol{x}$, we denote by $\boldsymbol{\Pi}_{\mathrm{R}}(\boldsymbol{x})$ the closest intersection of the master surface $\Sigma_1^{\varepsilon,n}$ with the line passing through $\boldsymbol{x}$ and having direction $\boldsymbol{n}_x$. This strategy can be referred to as ray-tracing (see Figure 2.18). We then introduce a gap function denoted by g which satisfies

$$g(\boldsymbol{x}) = (\boldsymbol{\Pi}_{\mathrm{R}}(\boldsymbol{x}) - \boldsymbol{x}) \cdot \boldsymbol{n}_x = (\boldsymbol{\Pi}_{\mathrm{R}}(\boldsymbol{\phi}_H^n(\widehat{\boldsymbol{x}})) - \boldsymbol{\phi}_H^n(\widehat{\boldsymbol{x}})) \cdot \boldsymbol{n}_x$$

where $\widehat{\boldsymbol{x}} \overset{\text{def}}{=} (\boldsymbol{\phi}_H^n)^{-1}(\boldsymbol{x})$. The non-penetration conditions writes $g \geqslant 0$ and is enforced through penalization. The contact term for the beam $\widehat{\omega}_1^\varepsilon$ is then given by

$$\frac{\gamma}{2h^2} \int_{\widehat{\Sigma}_2^\varepsilon} [(\boldsymbol{\Pi}_{\mathrm{R}}(\boldsymbol{\phi}_H^n(\widehat{\boldsymbol{x}})) - \boldsymbol{\phi}_H^n(\widehat{\boldsymbol{x}})) \cdot \boldsymbol{n}_x]_+ (\overline{\delta \boldsymbol{r}_H}(\widehat{\boldsymbol{x}}) - \overline{\delta \boldsymbol{r}_H}(\widehat{\boldsymbol{y}})) \cdot \boldsymbol{n}_x, \quad \forall\, \delta \boldsymbol{r}_H \in \boldsymbol{Y}_H,$$

where $\gamma > 0$ is user- defined parameter and the function $[\cdot]_+$ is the positive part operator given by

$$[x]_+ = \begin{cases} x & \text{if} \quad x \geqslant 0, \\ 0 & \text{if} \quad x < 0. \end{cases} \quad \forall x \in \mathbb{R}.$$

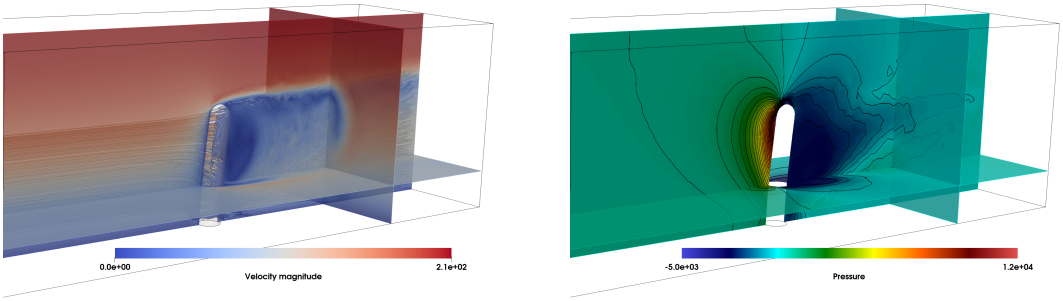

(a) *Algorithm 2.*

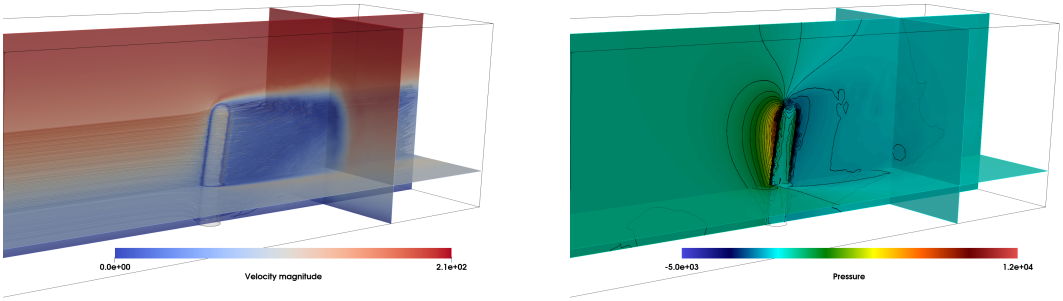

(b) *Algorithm 2-*Ω.

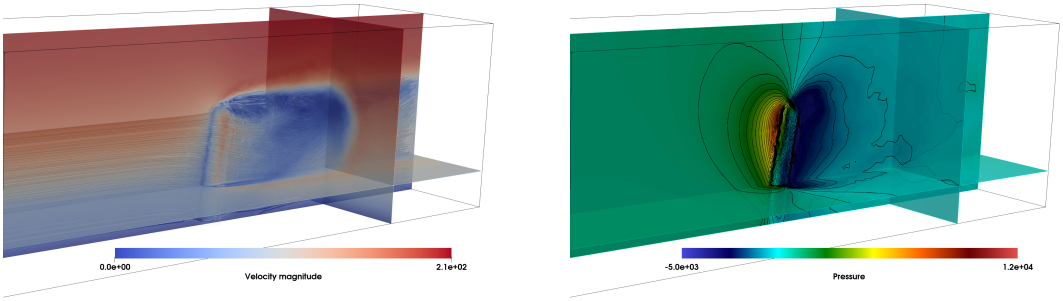

(c) *Algorithm 1,* $N = 0$.

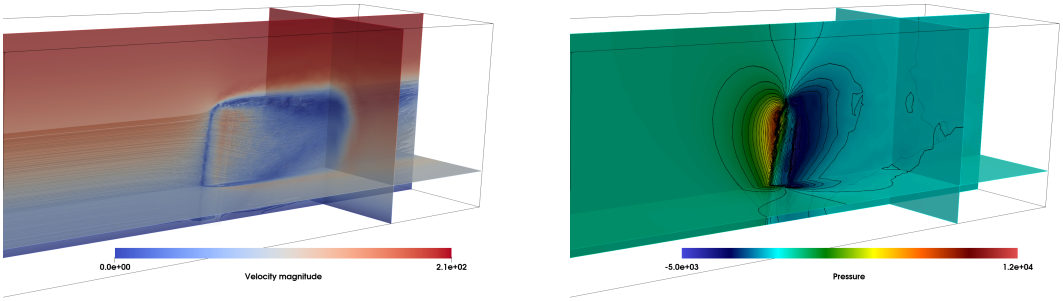

(d) *Algorithm 1,* $N = 1$.

Figure 2.15: *Snapshots of the fluid velocity magnitude (left) and pressure (right) at time* $t = 0.06$ *with Algorithm 2, Algorithm 2-*Ω*, Algorithm 1 and Algorithm 1-MC, with* $Re = 480$.

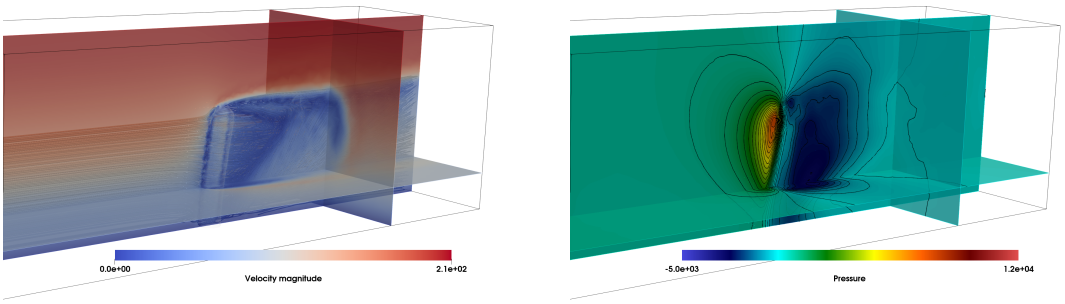

(e) *Algorithm 1,* $N = 2$.

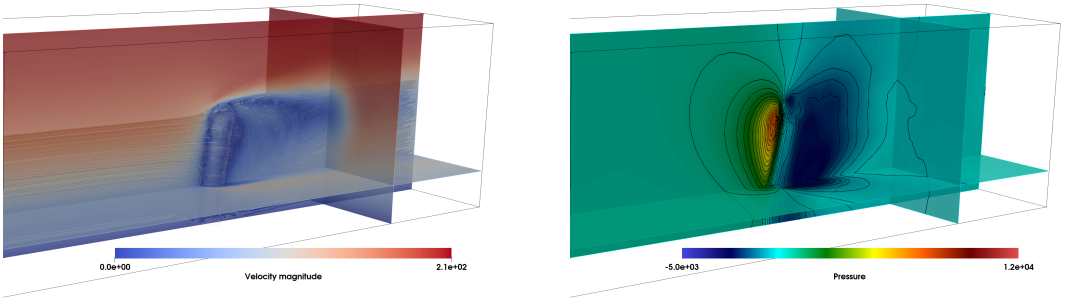

(f) *Algorithm 1-MC,* $N = 2$.

Figure 2.15: *Snapshots of the fluid velocity magnitude (left) and pressure (right) at time* $t = 0.06$ *with Algorithm 2, Algorithm 2-*Ω*, Algorithm 1 and Algorithm 1-MC, with* $Re = 480$*. (cont.)*

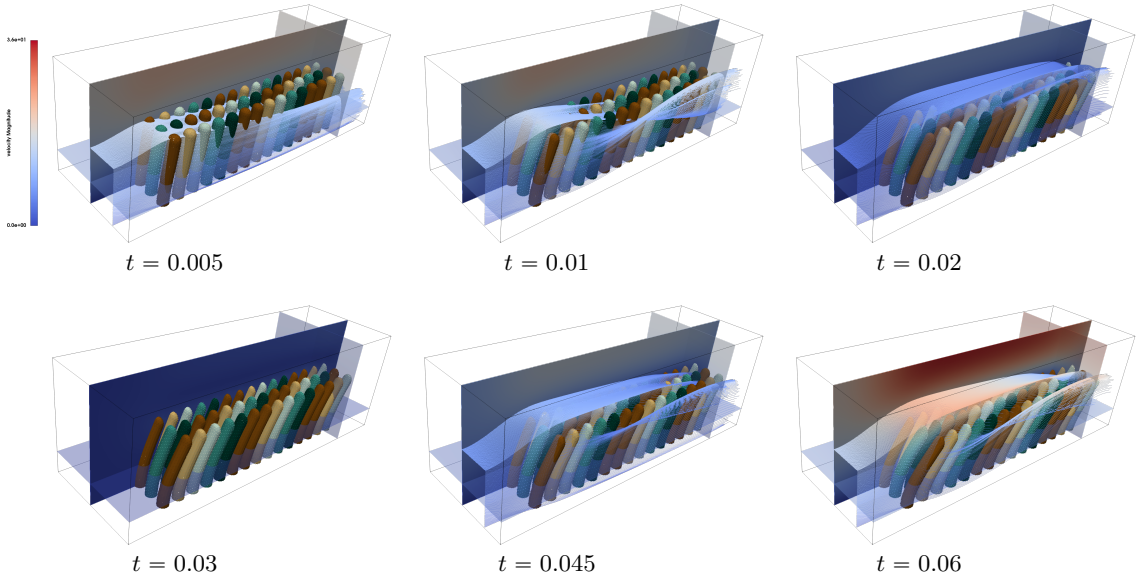

Figure 2.16: *Snapshots of the fluid velocity magnitude for multiple beams immersed in a Stokes flow with Algorithm 1 and* $N = 0$ *at time* $t \in \{0.005, 0.01, 0.02, 0.03, 0.045, 0.06\}$ *(note that at time* $t = 0.03$*, the inlet velocity is null).*

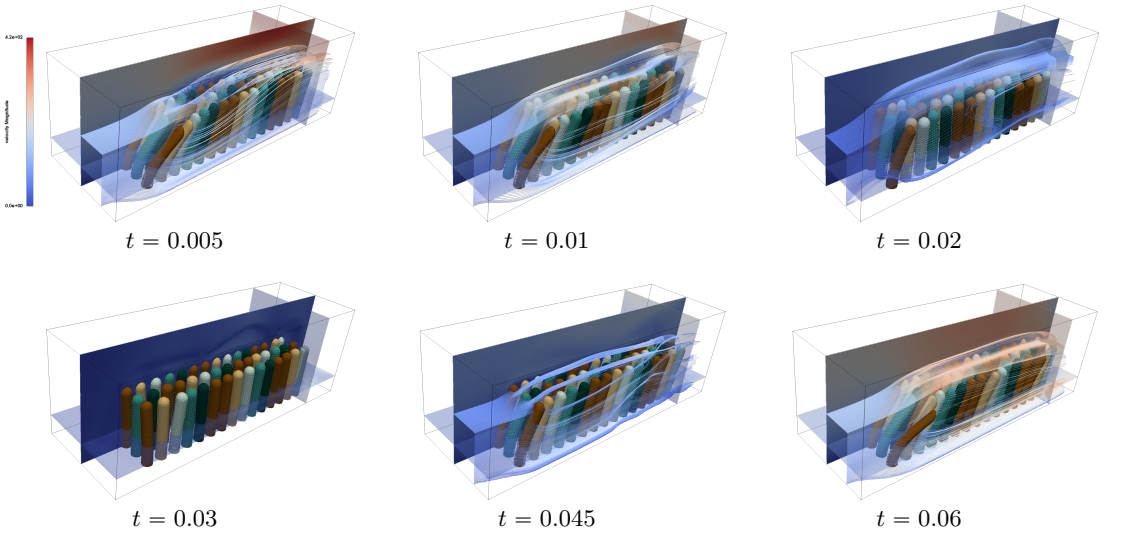

Figure 2.17: *Snapshots of the fluid magnitude fluid for multiple beams immersed in a Navier-Stokes flow with Algorithm 1 and* $N = 2$ *at time* $t \in \{0.005, 0.01, 0.02, 0.03, 0.045, 0.06\}$ *(note that at time* $t = 0.03$*, the inlet velocity is null).*

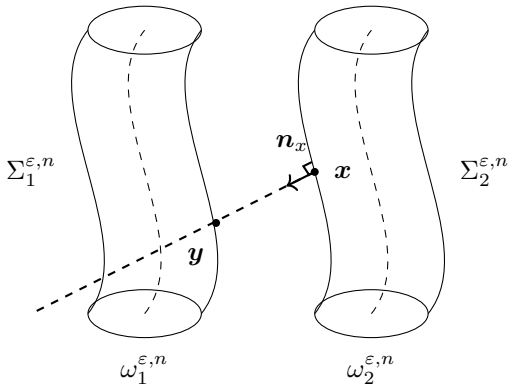

Figure 2.18: *Ray-tracing strategy*

CHAPTER 3

Mathematical and numerical analysis of reduced order interface conditions and augmented finite element method for mixed-dimensional problems

Corresponding to the preprint [Boulakia et al., 2023].

3.1 Introduction

In this chapter, we provide a rigorous analysis of the two-dimensional problem that arises by studying a transversal section of (2.2.21). Instead of dealing with a two-way interaction, we focus on the obstacle fluid sub-problem where the interface kinematic coupling conditions are substituted with non-homogeneous Dirichlet condition on a fixed circular internal boundary. We also make a drastic simplification of the fluid model, stepping back to the scalar Poisson equation. However, as we will see, this study already contains the main difficulties of the more general mathematical model introduced in Chapter 2. The extension to the Stokes problem is presented in Chapter 4.

Consistent notations are used with respect to Chapter 2. Specifically, the symbol Ω denotes a fixed smooth bounded domain of $\mathbb{R}^2$ including its origin $\mathbf{0}$ (note that in this chapter, the obstacle is assumed to be of circular shape and not elliptical). The obstacle

is represented by an inclusion ω^ε of size ε defined by $\omega^\varepsilon \overset{\text{def}}{=} \varepsilon\omega$, where $\omega \overset{\text{def}}{=} B(\mathbf{0}, 1)$ is the open ball of center $\mathbf{0}$ and radius 1. In all the chapter, we assume that ε belongs to an admissible set $(0, \varepsilon_{\max})$ where $\varepsilon_{max} \overset{\text{def}}{=} \sup\{\varepsilon > 0 \ : \ \overline{\omega^\varepsilon} \subset \Omega\}$ and we denote by Ω^ε the complementary of $\overline{\omega^\varepsilon}$ in Ω. The transition from the three-dimensional (3D) to the two-dimensional (2D) geometrical setting is illustrated in Figure 3.1. In this new setting,

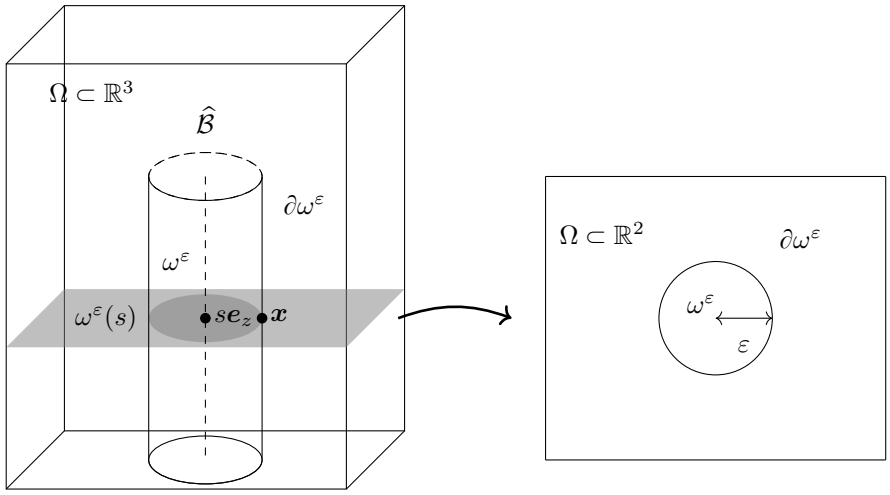

Figure 3.1: *Transition from 3D to 2D geometrical setting.*

we conserve a mixed-dimentional formulation by projecting the Dirichlet boundary conditions on a finite-dimensional space F_N. To give a rigorous definition of F_N, as done in Section 2.2.2.5, we introduce a local coordinate θ on the obstacle such that any point $\boldsymbol{x}$ on $\partial\omega^\varepsilon$ can be parametrized as

$$\boldsymbol{x} = \varepsilon(\cos(\theta)\boldsymbol{e}_x + \sin(\theta)\boldsymbol{e}_y).$$

We also introduce the function $v(\varepsilon) : (0, 2\pi) \to \mathbb{R}$ defined for any function $v : \partial\omega^\varepsilon \to \mathbb{R}$ by the relation

$$v(\varepsilon)(\theta) \overset{\text{def}}{=} v(\varepsilon(\cos(\theta)\boldsymbol{e}_x + \sin(\theta)\boldsymbol{e}_y)) \quad \forall\theta \in (0, 2\pi) \quad \forall\varepsilon > 0. \tag{3.1.1}$$

The space F_N is then given by

$$F_N \overset{\text{def}}{=} \{v \in L^2(\partial\omega^\varepsilon) \ : \ v(\varepsilon)(\theta) = a_0 + \sum_{k=1}^{N}(a_k\cos(k\theta) + b_k\sin(k\theta)), \quad a_k, b_k \in \mathbb{R}\}. \tag{3.1.2}$$

Note that F_N can also be interpreted as the restriction to one cross-section of the space introduced in (2.2.26) for circular shapes=. The reduced order problem considered in this

chapter is formulated as follows: find $u_N^\varepsilon \in H_0^1(\Omega)$ and $\lambda_N^\varepsilon \in F_N$ such that

$$\begin{cases} (\nabla u_N^\varepsilon, \nabla v)_\Omega - (\lambda_N^\varepsilon, v)_\varepsilon = (f, v)_\Omega & \forall v \in H_0^1(\Omega), \\ (\mu_N, u_N^\varepsilon)_\varepsilon = (\mu_N, u_{\mathrm{b}})_\varepsilon & \forall \mu_N \in F_N, \end{cases} \tag{3.1.3}$$

where $u_{\mathrm{b}} \in H^{\frac{1}{2}}(\partial\omega^\varepsilon)$ and $f \in L^2(\Omega)$ are given and the re-scaled inner product $(\cdot,\cdot)_\varepsilon$ is defined by

$$(u, v)_\varepsilon = \big(u(\varepsilon), v(\varepsilon)\big)_{(0,2\pi)}.$$

The choice of a re-scaled inner product is motivated by the analysis of (3.1.3) provided in Section 3.3 where it enables to obtain uniform estimates on the solution (Theorem 3.3.1).

We finally assume that f is such that $\mathbf{0} \notin \mathrm{supp}(f)$. This hypothesis is used as well in Section 3.3 for the asymptotic analysis of (3.1.3) as $\varepsilon \to 0$. Indeed, a salient result of this chapter is the convergence when $\varepsilon \to 0$ of the solution of Problem (3.1.3) to the one of the corresponding full order Poisson problem (Theorem 3.3.4): find $(u^\varepsilon, \lambda^\varepsilon) \in H_0^1(\Omega)) \times H^{-\frac{1}{2}}(\partial\omega^\varepsilon)$ such that

$$\begin{cases} (\nabla u^\varepsilon, \nabla v)_\Omega - \langle \lambda^\varepsilon, v\rangle_{-\frac{1}{2},\partial\omega^\varepsilon} = (f, v)_\Omega & \forall v \in H_0^1(\Omega), \\ \langle \mu, u^\varepsilon\rangle_{-\frac{1}{2},\partial\omega^\varepsilon} = \langle \mu, u_{\mathrm{b}}\rangle_{-\frac{1}{2},\partial\omega^\varepsilon} & \forall \mu \in H^{\frac{1}{2}}(\partial\omega^\varepsilon). \end{cases} \tag{3.1.4}$$

Note that, in this context, Problem (3.1.4) can be considered as the counterpart of Problem (2.2.9) in the simplified setting we consider in this chapter. For standard Dirichlet boundary conditions, the asymptotic analysis of Problem (3.1.4) can be found in many works, we refer the reader to [Maz'ya et al., 1984, Maz'ya and Nazarov, 1987, Maz'Ya et al., 2000,Nazarov, 1999,Nazarov and Sokołowski, 2003,Bonnaillie-Noël and Dambrine, 2013, Bonnaillie-Noël et al., 2007] for a non-exhaustive review. The available results will be adapted below to the case of the dimensional mismatch at the internal boundary. Our approximation results highlight that the reduced order model proposed in (3.1.3) is a consistent and reliable approximation (3.1.4). To be more specific, we will state that the accuracy of the approximation is of order ε^{N+1} (Theorem 3.3.4). This implies that, for a given ε, by increasing the number of Fourier modes, we can increase the accuracy with respect to the full order model.

Then at the discrete level, to be consistent with the 3D case, we will analyse the *fictitious domain* methods [Glowinski et al., 1994], where a Lagrange multiplier is applied to impose the Dirichlet boundary conditions on the hole, while using a regular unfitted grid for the finite element discretization of the problem. In particular, the mesh will not be fitted to the internal boundary. In this framework, we saw in the numerical results presented in Section 2.4 that the standard finite element method presents decreasing performances when $\varepsilon \to 0$, unless restrictions on the computational mesh step-size are enforced. Note that to avoid this phenomena on general unfitted computational meshes, alternative methods such as the boundary element method [Antoine et al., 2012] can be employed. Analyzing the

2D problem at hand enables the obtain estimate on the dependence of the numerical error to the parameter ε and to propose strategies to reduce its negative impact on the numerical approximation error. We will focus on a strategy consisting in taking advantage of the asymptotic development of the solution combined with an augmented Galerkin approach to obtain a convergence of arbitrary order with respect to the mesh size (see [Claeys and Collino, 2010, Bonnaillie-Noël and Dambrine, 2013, Chesnel and Claeys, 2016]). More precisely, our approximation result (Theorem 3.4.6) states that the discretization error is of order h^k where h is the mesh size and k is the polynomial order of the finite element space. The case when the number of Fourier modes is given by $N = 0$ (which consists in only enforcing the mean value on the interface) with homogeneous Dirichlet boundary conditions on the hole (namely $u_{\mathrm{b}} = 0$ in (3.1.4)) has been treated in [Claeys and Collino, 2010] for the Helmholtz equations and obstacles of arbitrary shape. Besides the error estimates of the solution, we provide error estimates of the Lagrange multiplier that depend explicitly on the parameters N and h. This study is particularly important in view of better understanding the limitations of the 3D problem introduced in Chapter 2, since the Lagrange multiplier is related to the forces that are exchanged at the interface.

Overall, this chapter covers two main original topics, the asymptotic analysis of the 2D reduced order model toward the full order one and the numerical approximation of it with a thorough analysis of the stability and convergence properties of different variants of the method. The chapter is organized as follows. In Section 3.2, we address the asymptotic properties of Problem (3.1.3) when the hole becomes arbitrarily small and we use it to motivate the derivation of our reduced order model. In Section 3.3, we perform the well-posedness and asymptotic analysis of the reduced model. The analysis of the fully discrete version of the reduced order model is addressed in Section 3.4, the results of which are supported by the numerical experiments of Section 3.5.

Note that most of the results proved in this chapter for Problem (3.1.3) can be derived from classical properties inherent to elliptic problems. Our attention will then focus on the dependence of the various results on the parameters h, ε and N. In particular, in what follows, the notation $a \lesssim b$ is equivalent to $a \leqslant Cb$ where C will denote the constant of a generic upper bound assumed to be uniformly independent of the variables of the inequality and of the mesh size h, the size of the hole ε and the dimension of the projection space F_N defined in (3.1.2).

Remark 4. In a fluid-solid interaction context, the internal Dirichlet boundary condition would be equal to the velocity of the inclusion, typically we would have $u_{\mathrm{b}} = \boldsymbol{v}_{\mathrm{b}} + \varepsilon w_{\mathrm{b}} \boldsymbol{e}_\theta$ where $\boldsymbol{e}_\theta = (-\sin(\theta), \cos(\theta))$ with $\boldsymbol{v}_{\mathrm{b}} \in \mathbb{R}^3$, $w_{\mathrm{b}} \in \mathbb{R}$. This case will be treated in Chapter 4.

Remark 5. We consider in this paper a circular obstacle centered in $\mathbf{0}$ but all the results can be generalized to an obstacle centered in $\boldsymbol{r}$ with $\boldsymbol{r} \in \Omega$. This construction is also easily generalized to multiple obstacles, provided that they do not intersect each other and do not

intersect with the support of f.

Remark 6. In our study, we consider Dirichlet homogeneous boundary conditions on the external boundary $\partial\Omega$. However, our work can be extended without difficulty to non-homogeneous Dirichlet boundary conditions.

3.2 Preliminary results

3.2.1 Limit of the Poisson problem with small holes

In this section, we provide some results on the asymptotic behavior of (3.1.4) as a motivation for the derivation of (3.1.3). The Lax-Milgram theorem allows to prove that the problem: find $u^0 \in H^1_0(\Omega)$ such that

$$(\nabla u^0, \nabla v)_{\Omega^\varepsilon} = (f, v)_{\Omega^\varepsilon} \quad \forall v \in H^1_0(\Omega) \tag{3.2.1}$$

is well-posed and that the solution u^0 satisfies the following standard energy bound:

$$\|u^0\|_{1,\Omega} \lesssim \|f\|_\Omega.$$

Moreovever, if $u_\mathrm{b} = 0$, then problem (3.2.1) represents the limit case of problem (3.1.4) when $\varepsilon \to 0$. More specifically, u^ε satisfies

$$\|u^\varepsilon - u^0\|_{1,\Omega^\varepsilon} \lesssim |\log(\varepsilon)|^{-\frac{1}{2}} \|f\|_\Omega. \tag{3.2.2}$$

This estimate is a classical result which can be seen as a consequence of the fact that the H^1-capacity of ω^ε tends to 0 as $|\log(\varepsilon)|^{-1}$, see for instance [Henrot and Pierre, 2006] for a discussion about capacity. Thus, in the particular case of homogeneous boundary conditions on $\partial\omega^\varepsilon$, the solution of the problem (3.1.4) tends to the solution of the problem (3.2.1) when $\varepsilon \to 0$ and, to approximate the problem (3.1.4), one may consider the limit problem without obstacle. In other words, one could just ignore the presence of the obstacle. However, inequality (3.2.2) also shows that the convergence is very slow with respect to the size of the inclusion. To give an idea, $|\log(\varepsilon)|^{-\frac{1}{2}} \approx 0.201$ for $\varepsilon = 10^{-10}$. For this reason, we it seems necessary to introduce reduced order problems whose solutions can approximate u^ε better than u^0.

3.2.2 Notations and some results on Fourier analysis

In this section, we introduce some notations and classical properties on Fourier analysis, useful in the subsequent analysis of Problem 3.1.3. We refer for example to [Zygmund, 2002] for more in-depth exploration of this topic. First we denote by $\Pi^\varepsilon_N : L^2(\partial\omega^\varepsilon) \to F_N$ the L^2 projection on F_N associated to the inner product $(\cdot,\cdot)_\varepsilon$. Setting $c_k(\theta) \overset{\text{def}}{=} \cos(k\theta)$

and $s_k(\theta) = \sin(k\theta)$, the operator Π_N^ε satisfies

$$(\Pi_N^\varepsilon v)(\varepsilon)(\theta) = \mathscr{F}_0^{\mathrm{c}} v(\varepsilon) + \sum_{k=1}^{N} \left(\mathscr{F}_k^{\mathrm{c}} v(\varepsilon) \cos(k\theta) + \mathscr{F}_k^{\mathrm{s}} v(\varepsilon) \sin(k\theta) \right) \quad \forall v \in L^2(\partial\omega^\varepsilon),$$

where the operators $\mathscr{F}_k^{\mathrm{c}} : L^2(0, 2\pi) \to \mathbb{R}$ and $\mathscr{F}_k^{\mathrm{s}} : L^2(0, 2\pi) \to \mathbb{R}$ are given by

$$\mathscr{F}_0^{\mathrm{c}} v = \frac{1}{2\pi}(v, 1)_{(0,2\pi)}, \quad \mathscr{F}_k^{\mathrm{c}} v = \frac{1}{\pi}(v, c_k)_{(0,2\pi)}, \quad \mathscr{F}_k^{\mathrm{s}} v = \frac{1}{\pi}(v, s_k)_{(0,2\pi)} \tag{3.2.3}$$

for all $k \geqslant 1$ and $v \in L^2(0, 2\pi)$. This expression is called the Fourier series decomposition of v at order N and the k^{th} Fourier modes of v are defined as the pair $(\mathscr{F}_k^{\mathrm{c}} v\, c_k, \mathscr{F}_k^{\mathrm{s}} v\, s_k)$. Noting that for $v \in L^2(\partial\omega^\varepsilon)$, $\|v\|_\varepsilon = \|v(\varepsilon)\|_{(0,2\pi)}$, classical results on Fourier series in $L^2(0, 2\pi)$ imply for $v \in L^2(\partial\omega^\varepsilon)$,

$$\|\Pi_N^\varepsilon v - v\|_\varepsilon \to 0, \quad N \to \infty,$$

and as a result, by defining $a_k \overset{\text{def}}{=} \mathscr{F}_k^{\mathrm{c}} v(\varepsilon)$ and $b_k \overset{\text{def}}{=} \mathscr{F}_k^{\mathrm{s}} v(\varepsilon)$, we have

$$\begin{aligned} \|\Pi_N^\varepsilon v\|_\varepsilon^2 = 2\pi \left(a_0^2 + \sum_{k=1}^{N} \left(\frac{a_k^2}{2} + \frac{b_k^2}{2} \right) \right) &\leqslant 2\pi \left(a_0^2 + \sum_{k=1}^{\infty} \left(\frac{a_k^2}{2} + \frac{b_k^2}{2} \right) \right) \\ &= \|v\|_\varepsilon^2, \end{aligned}$$

In particular, Π_N^ε is continuous on $(L^2(\partial\omega^\varepsilon), \|\cdot\|_\varepsilon)$ with an operator norm uniformly independent of ε. In the problem at hand, F_N stands for an approximation of $H^{\frac{1}{2}}(\partial\omega^\varepsilon)$. Since $H^{\frac{1}{2}}(\partial\omega^\varepsilon) \subset L^2(\partial\omega^\varepsilon)$, the elements of $H^{\frac{1}{2}}(\partial\omega^\varepsilon)$ also admit a Fourier series decomposition and we can introduce an auxiliary norm $\|\cdot\|_{\frac{1}{2}}^{\mathscr{F}}$ on $H^{\frac{1}{2}}(\partial\omega^\varepsilon)$ depending on the Fourier coefficients and defined for $v \in H^{\frac{1}{2}}(\partial\omega^\varepsilon)$ by

$$\|v\|_{\frac{1}{2},\varepsilon}^{\mathscr{F}} \overset{\text{def}}{=} \left((\mathscr{F}_0^{\mathrm{c}} v(\varepsilon))^2 + \sum_{k=1}^{\infty} (1+k) \left((\mathscr{F}_k^{\mathrm{c}} v(\varepsilon))^2 + (\mathscr{F}_k^{\mathrm{s}} v(\varepsilon))^2 \right) \right)^{\frac{1}{2}}.$$

The norm $\|\cdot\|_{\frac{1}{2},\varepsilon}^{\mathscr{F}}$ is well defined on $H^{\frac{1}{2}}(\partial\omega^\varepsilon)$ and is equivalent to the norm $\|\cdot\|_{\frac{1}{2},\varepsilon}$ defined by

$$\|v\|_{\frac{1}{2},\varepsilon} \overset{\text{def}}{=} \|v(\varepsilon)\|_{\frac{1}{2},(0,2\pi)} \quad \forall v \in H^{\frac{1}{2}}(\partial\omega^\varepsilon),$$

(see, e.g., [Hsiao and Wendland, 2008, Lemma 2.4.5]) . Moreover, since the norms $\|\cdot\|_{\frac{1}{2},\varepsilon}$ and $\|\cdot\|_{\frac{1}{2},\varepsilon}^{\mathscr{F}}$ are re-scaled with respect to ε, the constants appearing in the norm equivalence are uniformly independent of ε. We then deduce

$$\|\Pi_N^\varepsilon v\|_{\frac{1}{2},\varepsilon}^{\mathscr{F}} \leqslant \|v\|_{\frac{1}{2},\varepsilon}^{\mathscr{F}}, \quad \|\Pi_N^\varepsilon v\|_{\frac{1}{2},\varepsilon} \lesssim \|v\|_{\frac{1}{2},\varepsilon} \quad \forall v \in H^{\frac{1}{2}}(\partial\omega^\varepsilon).$$

In particular, Π_N^ε is continuous on $(H^{\frac{1}{2}}(\partial\omega^\varepsilon),\ \|\cdot\|_{\frac{1}{2},\varepsilon})$ with an operator norm uniformly independent of ε. To conclude this part, we notice that $H^{-\frac{1}{2}}(\partial\omega^\varepsilon)$ can be equipped with the duality product $\langle\cdot,\cdot\rangle_{-\frac{1}{2},\varepsilon}$ and the norm $\|\cdot\|_{-\frac{1}{2},\varepsilon}$ defined for $\lambda \in H^{\frac{1}{2}}(\partial\omega^\varepsilon)$ and $\mu \in H^{-\frac{1}{2}}(\partial\omega^\varepsilon)$ by

$$\langle\lambda,\mu\rangle_{-\frac{1}{2},\varepsilon} \stackrel{\text{def}}{=} \varepsilon^{-1}\langle\lambda,\mu\rangle_{-\frac{1}{2},\partial\omega^\varepsilon}, \quad \|\lambda\|_{-\frac{1}{2},\varepsilon} \stackrel{\text{def}}{=} \sup_{\mu\in H^{\frac{1}{2}}(\partial\omega^\varepsilon)} \frac{\langle\lambda,\mu\rangle_{-\frac{1}{2},\varepsilon}}{\|\mu\|_{\frac{1}{2},\varepsilon}}. \tag{3.2.4}$$

Note that the duality product $\langle\cdot,\cdot\rangle_{-\frac{1}{2},\varepsilon}$ satisfies in particular

$$\langle\lambda,\mu\rangle_{-\frac{1}{2},\varepsilon} = \varepsilon^{-1}(\lambda,\mu)_{\partial\omega^\varepsilon} = (\lambda,\mu)_\varepsilon \quad \forall\lambda\in L^2(\partial\omega^\varepsilon) \quad \forall\mu\in H^{\frac{1}{2}}(\partial\omega^\varepsilon). \tag{3.2.5}$$

3.3 Analysis of the two-dimensional reduced order model

3.3.1 Well-posedness

In this section, we study the well-posedness of Problem (3.1.3) and establish the following theorem.

Theorem 3.3.1. *Problem* (3.1.3) *admits a unique solution* $(u_N^\varepsilon,\lambda_N^\varepsilon)$ *in* $H_0^1(\Omega)\times F_N$. *Moreover, this solution satisfies the following energy bound:*

$$\|u_N^\varepsilon\|_{1,\Omega} + \|\lambda_N^\varepsilon\|_{-\frac{1}{2},\varepsilon} \lesssim \|u_{\mathrm{b}}\|_{\frac{1}{2},\varepsilon} + \|f\|_\Omega. \tag{3.3.1}$$

This result states that the solution of the reduced order problem continuously depends on the data and the continuity constant does not dependent on ε and N. For the proof of Theorem 3.3.1, we need the introduction of two preliminaries lemmas, their proof are reported in the Sections 3.A.2 and 3.A.3 of the Appendix, respectively. The first lemma gives an estimate of the trace operator on $\partial\omega^\varepsilon$ of a H^1 function defined in Ω.

Lemma 3.3.2. *For all* $v\in H^1(\Omega)$,

$$\|v\|_{\frac{1}{2},\varepsilon} \lesssim |\log(\varepsilon)|^{\frac{1}{2}}\|v\|_{1,\Omega}.$$

The second lemma introduces a continuous lifting in the whole domain Ω of functions given in $H^{\frac{1}{2}}(\partial\omega^\varepsilon)$.

Lemma 3.3.3. *Let* $\eta\in H^{\frac{1}{2}}(\partial\omega^\varepsilon)$ *be given, there exists* $v_\eta^\varepsilon\in H_0^1(\Omega)$ *solution of*

$$\begin{cases} -\Delta v_\eta^\varepsilon = 0 & \text{in} \quad \Omega^\varepsilon\cup\omega^\varepsilon, \\ v_\eta^\varepsilon = \eta & \text{on} \quad \partial\omega^\varepsilon. \end{cases} \tag{3.3.2}$$

Moreover, v_η^ε satisfies the following energy bound:

$$\|v_\eta^\varepsilon\|_{1,\Omega} \lesssim \|\eta\|_{\frac{1}{2},\varepsilon}. \tag{3.3.3}$$

Proof of Theorem 3.3.1. Let us introduce some notations. We notice that Problem (3.1.3) can be written under the form: find $(u_N^\varepsilon, \lambda_N^\varepsilon) \in H_0^1(\Omega) \times F_N$ such that

$$\begin{cases} a(u_N^\varepsilon, v) - b(\lambda_N^\varepsilon, v) = (f, v)_\Omega & \forall v \in H_0^1(\Omega), \\ b(\mu, u_N^\varepsilon) = c(\mu) & \forall \mu \in F_N, \end{cases} \tag{3.3.4}$$

where the bilinear forms $a : H_0^1(\Omega) \times H_0^1(\Omega) \to \mathbb{R}$, $b : F_N \times H_0^1(\Omega) \to \mathbb{R}$ and the linear form $c : F_N \to \mathbb{R}$ are given by

$$a(u, v) = (\nabla u, \nabla v)_\Omega, \quad b(\mu, u) = (\mu, u)_\varepsilon, \quad c(\mu) = (\mu, \varphi)_\varepsilon. \tag{3.3.5}$$

To prove our result, we will apply to Problem (3.3.4) the BNB theorem for saddle point problems (we refer to [Brezzi, 1974] or to [Ern and Guermond, 2004, Theorem 2.34]). First, using Poincaré inequality and Cauchy-Schwarz inequality, we have that the bilinear form a is continuous and coercive, with a norm $\|a\|$ and a positive coercivity constant α bounded independently of N and ε. As well, using Cauchy-Schwarz inequality and Lemma 3.3.2, we can derive the following inequality for b:

$$|b(\mu_N, v)| \leqslant \|\mu_N\|_{-\frac{1}{2},\varepsilon} \|v\|_{\frac{1}{2},\varepsilon} \lesssim |\log(\varepsilon)|^{\frac{1}{2}} \|\mu_N\|_{-\frac{1}{2},\varepsilon} \|v\|_{1,\Omega} \quad \forall (\mu_N, v) \in F_N \times H_0^1(\Omega).$$

Consequently, the bilinear form b is continuous and we have

$$\|b\| \lesssim |\log(\varepsilon)|^{\frac{1}{2}}. \tag{3.3.6}$$

Lastly, we have

$$|c(\mu_N)| \lesssim \|\mu_N\|_{-\frac{1}{2},\varepsilon} \|u_{\mathrm{b}}\|_{\frac{1}{2},\varepsilon} \quad \forall \mu_N \in F_N, \tag{3.3.7}$$

proving the continuity of the linear form c. We can also deduce from (3.3.7) that the norm of c, denoted by $\|c\|$, is bounded, up to a multiplicative constant uniformly independent of N and ε, by $\|u_{\mathrm{b}}\|_{\frac{1}{2},\varepsilon}$. Now, we prove the inf-sup condition by establishing the existence of $\beta > 0$, uniformly independent of N and ε, satisfying

$$\sup_{v \in H_0^1(\Omega)} \frac{(\mu_N, v)_\varepsilon}{\|v\|_{1,\Omega}} \geqslant \beta \|\mu_N\|_{-\frac{1}{2},\varepsilon} \quad \forall \mu_N \in F_N. \tag{3.3.8}$$

Let $\eta \in H^{\frac{1}{2}}(\partial\omega^\varepsilon)$, according to Lemma 3.3.3, there exists $v_\eta^\varepsilon \in H_0^1(\Omega)$ such that $v_\eta^\varepsilon = \eta$ on $\partial\omega^\varepsilon$ and

$$\|v_\eta^\varepsilon\|_{1,\Omega} \leqslant \beta \|\eta\|_{\frac{1}{2},\varepsilon},$$

with $\beta > 0$ uniformly independent of N and ε. We deduce that

$$\|\mu_N\|_{-\frac{1}{2},\varepsilon} = \sup_{\eta \in H^{\frac{1}{2}}(\partial\omega^\varepsilon)} \frac{(\mu_N,\eta)_\varepsilon}{\|\eta\|_{\frac{1}{2},\varepsilon}} \leqslant \beta^{-1} \sup_{v \in H^1_0(\Omega)} \frac{(\mu_N,v)_\varepsilon}{\|v\|_{1,\Omega}} \quad \forall \mu_N \in F_N,$$

Thus we get (3.3.8). By applying BNB theorem, we deduce that (3.3.4) admits a unique solution $(u_N^\varepsilon, \lambda_\varepsilon^N) \in H(\Omega) \times F_N$. Moreover, according to [Ern and Guermond, 2004, Theorem 2.34], this solution satisfies

$$\|u_N^\varepsilon\|_{1,\Omega} \leqslant \frac{1}{\beta}(1+\frac{\|a\|}{\alpha})\|u_{\rm b}\|_{\frac{1}{2},\varepsilon} + \frac{1}{\|a\|}\|f\|_\Omega \lesssim \|u_{\rm b}\|_{\frac{1}{2},\varepsilon} + \|f\|_\Omega,$$
$$\|\lambda_N^\varepsilon\|_{-\frac{1}{2},\varepsilon} \leqslant \frac{\|a\|}{\beta^2}(1+\frac{\|a\|}{\alpha})\|u_{\rm b}\|_{\frac{1}{2},\varepsilon} + \frac{1}{\beta}(1+\frac{\|a\|}{\alpha})\|f\|_\Omega \lesssim \|u_{\rm b}\|_{\frac{1}{2},\varepsilon} + \|f\|_\Omega.$$

which can be written equivalently as (3.3.1). □

3.3.2 Convergence to the full order model

In the previous results, the domain of validity for the ε parameter only depended on the Ω domain. From now on, some results will also depend on an additional parameter ρ defined as the maximum value such that $f = 0$ in ω^ρ and $\omega^\rho \subset \Omega$, which is equivalent to

$$\rho \stackrel{\text{def}}{=} \min\big(d(\{\mathbf{0}\}, \text{supp }(f)), d(\{\mathbf{0}\}, \partial\Omega)\big), \tag{3.3.9}$$

where $d(\cdot,\cdot)$ is the Euclidean distance of two sets. Note that we have in particular $\rho \leqslant \varepsilon_{\max}$. In this subsection, we will study the convergence when ε tends to 0 of the solution of the reduced order problem (3.1.3) to the solution of the full order problem (3.1.4) and prove the following theorem.

Theorem 3.3.4. *Let* $(u^\varepsilon, \lambda^\varepsilon) \in H^1_0(\Omega) \times H^{-\frac{1}{2}}(\partial\omega^\varepsilon)$ *be solution of* (3.1.4) *and* $(u_N^\varepsilon, \lambda_N^\varepsilon) \in H^1_0(\Omega) \times F_N$ *solution of* (3.1.3)*, with* $u_{\rm b} \in F_N$*, we have*

$$\|u_N^\varepsilon - u^\varepsilon\|_{1,\Omega^\varepsilon} + \varepsilon\|\varepsilon^{-1}\lambda_N^\varepsilon - \lambda^\varepsilon\|_{-\frac{1}{2},\varepsilon} \lesssim \left(\frac{\varepsilon}{\rho}\right)^{N+1} (\|u_{\rm b}\|_{\frac{1}{2},\varepsilon} + \|f\|_\Omega) \tag{3.3.10}$$

Thanks to this result, we see that the convergence in ε of $u_N^\varepsilon - u^\varepsilon$ behaves like ε^{N+1} where N is the degree of the trigonometric polynomials of the approximation space F_N. In particular, this result can be used to adjust N to reach a certain accuracy, ε being fixed. For $N = 0$, the error estimate (3.3.10) does not give the convergence of $\varepsilon^{-1}\lambda_N^\varepsilon - \lambda^\varepsilon$ in the $H^{-\frac{1}{2}}$ re-scaled norm $\|\cdot\|_{-\frac{1}{2},\varepsilon}$. Instead, if we use the definition (3.2.4) of the $H^{-\frac{1}{2}}$ re-scaled norm, we can prove that

$$\|\mu\|_{-\frac{1}{2},\partial\omega^\varepsilon} \lesssim \varepsilon^{\frac{1}{2}}\|\mu\|_{-\frac{1}{2},\varepsilon},$$

so, if we consider the standard norm $\|\cdot\|_{-\frac{1}{2},\partial\omega^\varepsilon}$, we obtain

$$\|\varepsilon^{-1}\lambda_N^\varepsilon - \lambda^\varepsilon\|_{-\frac{1}{2},\partial\omega^\varepsilon} \lesssim \left(\frac{\varepsilon}{\rho}\right)^{N+\frac{1}{2}} \left(\|u_{\mathrm{b}}\|_{\frac{1}{2},\varepsilon} + \|f\|_\Omega\right).$$

For the proof of Theorem 3.3.4, we introduce two preliminaries lemmas. The first lemma is a classical result of fictitious domain method, giving an expression of λ_ε^N in relation to the gradient jump of u_N^ε accross $\partial\omega^\varepsilon$.

Lemma 3.3.5. *Let $(u_N^\varepsilon, \lambda_N^\varepsilon) \in H_0^1(\Omega) \times F_N$ be the solution of Problem* (3.1.3)*. Then, we have*

$$\lambda_N^\varepsilon = \varepsilon\big((\nabla u_N^\varepsilon)^+ \cdot \boldsymbol{n}^+ - (\nabla u_N^\varepsilon)^- \cdot \boldsymbol{n}^+\big) \quad \textit{in} \quad H^{-\frac{1}{2}}(\partial\omega^\varepsilon). \tag{3.3.11}$$

where $\boldsymbol{n}^+$ is the exterior normal to $\partial\Omega^\varepsilon$, $(\nabla u_N^\varepsilon)^+$ is the restriction of ∇u_N^ε to Ω^ε and $(\nabla u_N^\varepsilon)^-$ is the restriction of ∇u_N^ε to ω^ε.

The proof of this lemma is given in Section 3.A.4 of the Appendix. The second lemma describes the behavior of the Fourier modes of $u_N^\varepsilon(\varepsilon)$.

Lemma 3.3.6. *Consider $u_{\mathrm{b}} \in F_N$ be given. There exist $(a_k^\varepsilon)_{k\geqslant N+1}$ and $(b_k^\varepsilon)_{k\geqslant N+1}$ such that for $\varepsilon \in (0,\rho)$,*

$$u(\varepsilon)(\theta) - u_{\mathrm{b}}(\theta) = \sum_{k=N+1}^{\infty} \left(\frac{\varepsilon}{\rho}\right)^k (a_k^\varepsilon \cos(k\theta) + b_k^\varepsilon \sin(k\theta)) \quad \forall\theta \in (0,2\pi).$$

Moreover,

$$\left(\sum_{k=N+1}^{\infty} (1+k)\left(|a_k^\varepsilon|^2 + |b_k^\varepsilon|^2\right)\right)^{\frac{1}{2}} \lesssim \|u_{\mathrm{b}}\|_{\frac{1}{2},\varepsilon} + \|f\|_\Omega.$$

Proof of Lemma 3.3.6. First of all, we introduce polar coordinates such for any real function v defined in Ω, we write

$$v(r,\theta) \overset{\text{def}}{=} v(r(\cos(\theta)\boldsymbol{e}_x + \sin(\theta)\boldsymbol{e}_y)) \quad \forall(r,\theta) \in [0,\varepsilon_{\max}] \times (0,2\pi).$$

We now consider a fixed $0 < \varepsilon < \rho$. Using seperation of variable, a general formulation for harmonic solutions is given by

$$\phi_0(r) + \sum_{k=1}^{\infty} r^k(\phi_k^{\mathrm{c}}(r)\cos(k\theta) + \phi_k^{\mathrm{s}}(r)\sin(k\theta)) \quad \forall(r,\theta) \in \mathbb{R}^+ \times (0,2\pi), \tag{3.3.12}$$

with

$$\phi_0 \in \mathrm{span}\{1, \log(r)\}, \quad \phi_k^{\mathrm{c}},\ \phi_k^{\mathrm{s}} \in \mathrm{span}\{r^{-k}, r^k\}.$$

We refer to [Kounchev, 2001] for the derivation of (3.3.12). Since the solution u_N^ε is harmonic in both the sub-domains ω^ε and $\omega^\rho \backslash \omega^\varepsilon$, and belongs to $H^1(\Omega)$, we can infer the following expression for u_N^ε in ω^ρ:

$$u_N^\varepsilon(r,\theta) = c_{1,0}^{\ominus} + \sum_{k=1}^{\infty} r^k \left(c_{1,k}^{\ominus} \cos(k\theta) + s_{1,k}^{\ominus} \sin(k\theta) \right) \tag{3.3.13}$$

for all $(r,\theta) \in [0,\varepsilon] \times (0,2\pi)$, and

$$\begin{aligned} u_N^\varepsilon(r,\theta) = c_{1,0}^{\oplus} + c_{2,0}^{\oplus} \log(r) \\ + \sum_{k=1}^{\infty} (c_{1,k}^{\oplus} r^k + c_{2,k}^{\oplus} r^{-k}) \cos(k\theta) + (s_{1,k}^{\oplus} r^k + s_{2,k}^{\oplus} r^{-k}) \sin(k\theta), \end{aligned} \tag{3.3.14}$$

for all $(r,\theta) \in [\varepsilon,\rho] \times (0,2\pi)$. We begin by examining the boundary conditions on $\partial\omega^\varepsilon$ and $\partial\omega^\rho$. On one hand, the condition

$$(\mu_N, u_N^\varepsilon)_\varepsilon = (\mu_N, u_{\mathrm{b}})_\varepsilon \quad \forall \mu_N \in F_N,$$

applied to (3.3.13), implies

$$c_{1,0}^{\ominus} = \mathscr{F}_0^{\mathrm{c}} u_{\mathrm{b}}(\varepsilon), \quad c_{1,k}^{\ominus} \varepsilon^k = \mathscr{F}_k^{\mathrm{c}} u_{\mathrm{b}}(\varepsilon), \quad s_{1,k}^{\ominus} \varepsilon^k = \mathscr{F}_k^{\mathrm{s}} u_{\mathrm{b}}(\varepsilon) \quad \forall k \geqslant 1. \tag{3.3.15}$$

On the other hand, evaluating (3.3.14) for $r = \rho$ and projecting the resulting expression on the various Fourier modes, we obtain

$$\begin{aligned} &c_{1,0}^{\oplus} + c_{1,0}^{\oplus} \log(\rho) = \mathscr{F}_0^{\mathrm{c}} u_N^\varepsilon(\rho), \\ &c_{1,k}^{\oplus} \rho^k + c_{2,k}^{\oplus} \rho^{-k} = \mathscr{F}_k^{\mathrm{c}} u_N^\varepsilon(\rho), \quad s_{1,k}^{\oplus} \rho^k + s_{2,k}^{\oplus} \rho^{-k} = \mathscr{F}_k^{\mathrm{s}} u_N^\varepsilon(\rho) \quad \forall k \geqslant 1. \end{aligned} \tag{3.3.16}$$

We now consider the k^{th} Fourier modes of u_N^ε on $\partial\omega^\varepsilon$. Specifically, by taking $r = \varepsilon$ both in (3.3.13) and (3.3.14), we derive

$$c_{1,k}^{\ominus} \varepsilon^k = c_{1,k}^{\oplus} \varepsilon^k + c_{2,k}^{\oplus} \varepsilon^{-k}, \quad s_{1,k}^{\ominus} \varepsilon^k = s_{1,k}^{\oplus} \varepsilon^k + s_{2,k}^{\oplus} \varepsilon^{-k} \quad \forall k \geqslant N+1. \tag{3.3.17}$$

Eventually, we use result of Lemma 3.3.5. From expressions (3.3.13) and (3.3.14), we deduce the following expressions in $H^{-\frac{1}{2}}(\partial\omega^\varepsilon)$:

$$\left((\nabla u_N^\varepsilon)^+ \cdot \boldsymbol{n}^+ \right)(\varepsilon)(\theta) = -\left(\frac{\partial u_N^\varepsilon}{\partial r} \right)^+ (\varepsilon)(\theta) = -\sum_{k=1}^{\infty} k\varepsilon^{k-1} (c_{1,k}^{\ominus} \cos(k\theta) + s_{1,k}^{\ominus} \sin(k\theta))$$

for all $\theta \in (0, 2\pi)$, and

$$\big((\nabla u_N^\varepsilon)^- \cdot \boldsymbol{n}^+\big)(\varepsilon)(\theta) = -\left(\frac{\partial u_N^\varepsilon}{\partial r}\right)^- (\varepsilon)(\theta) = \\ -\frac{c_{2,0}^\oplus}{r} - \sum_{k=1}^{\infty} \big(k(c_{1,k}^\oplus \varepsilon^{k-1} - c_{2,k}^\oplus \varepsilon^{-k-1})\cos(k\theta) \\ + k(s_{1,k}^\oplus \varepsilon^{k-1} - s_{2,k}^\oplus \varepsilon^{-k-1})\sin(k\theta)\big)$$

for all $\theta \in (0, 2\pi)$. Then, by projecting equation (3.3.11) on the Fourier modes greater than $N+1$, we obtain

$$c_{1,k}^\ominus \varepsilon^k = c_{1,k}^\oplus \varepsilon^k - c_{2,k}^\oplus \varepsilon^{-k}, \quad s_{1,k}^\ominus \varepsilon^k = s_{1,k}^\oplus \varepsilon^k - s_{2,k}^\oplus \varepsilon^{-k} \quad \forall k \geqslant N+1. \tag{3.3.18}$$

Gathering equations (3.3.15), (3.3.16) and (3.3.18), we get

$$c_{1,k}^\ominus = \rho^{-k} \mathscr{F}_k^{\mathrm{c}} u_{\mathrm{b}}(\rho), \quad s_{1,k}^\ominus = \rho^{-k} \mathscr{F}_k^{\mathrm{s}} u_{\mathrm{b}}(\rho) \quad \forall k \geqslant N+1. \tag{3.3.19}$$

Now setting $a_k^\varepsilon = \mathscr{F}_k^{\mathrm{c}} u_{\mathrm{b}}(\rho)$ and $b_k^\varepsilon = \mathscr{F}_k^{\mathrm{s}} u_{\mathrm{b}}(\rho)$, we deduce from (3.3.15) and (3.3.19),

$$u_N^\varepsilon(\varepsilon)(\theta) = u_{\mathrm{b}}(\varepsilon)(\theta) + \sum_{k=N+1}^{\infty} \left(\frac{\varepsilon}{\rho}\right)^k (a_k^\varepsilon \cos(k\theta) + b_k^\varepsilon \sin(k\theta)) \quad \forall \theta \in (0, 2\pi).$$

We can conclude the proof using successively the equivalence of the norm $\|\cdot\|_{\frac{1}{2},\rho}^{\mathscr{F}}$ and $\|\cdot\|_{\frac{1}{2},\rho}$, Theorem 3.3.2 with $\varepsilon = \rho$ and Theorem 3.3.1,

$$\left(\sum_{k=N+1}^{\infty} (1+k)\big(|a_k^\varepsilon|^2 + |b_k^\varepsilon|^2\big)\right)^{\frac{1}{2}} = \|u_N^\varepsilon\|_{\frac{1}{2},\rho}^{\mathscr{F}} \lesssim \|u_N^\varepsilon\|_{\frac{1}{2},\rho} \lesssim \|u_N^\varepsilon\|_{1,\Omega} \\ \lesssim \|u_{\mathrm{b}}\|_{\frac{1}{2},\varepsilon} + \|f\|_\Omega.$$

□

Let us notice that, following the computations made in this proof, we can obtain an expression of u_N^ε in ω^ρ with respect to the Fourier coefficients $\mathscr{F}_k^{\mathrm{c}} u_N^\varepsilon(\rho)$ and $\mathscr{F}_k^{\mathrm{c}} u_N^\varepsilon(\rho)$ for $k \geqslant N+1$, and the first N+1 Fourier coefficients of $u_{\mathrm{b}}(\varepsilon)$. This expression will be useful in the next section for the analysis of the numerical approximation but we state it at this

stage. We have

$$
\begin{aligned}
u_N^\varepsilon(r,\theta) = &\left(\mathscr{F}_0^{\mathrm{c}} u_N^\varepsilon(\rho) \frac{\log(r/\varepsilon)}{\log(\rho/\varepsilon)} + \mathscr{F}_0^{\mathrm{c}} u_{\mathrm{b}}(\varepsilon) \frac{\log(r/\rho)}{\log(\varepsilon/\rho)} \right. \\
&+ \sum_{k=1}^{N} \Big(\mathscr{F}_k^{\mathrm{c}} u_N^\varepsilon(\rho) \frac{(r/\varepsilon)^k - (\varepsilon/r)^k}{(\rho/\varepsilon)^k - (\varepsilon/\rho)^k} \cos(k\theta) + \mathscr{F}_k^{\mathrm{s}} u_N^\varepsilon(\rho) \frac{(r/\varepsilon)^k - (\varepsilon/r)^k}{(\rho/\varepsilon)^k - (\varepsilon/\rho)^k} \sin(k\theta) \\
&\left. + \sum_{k=1}^{N} \mathscr{F}_k^{\mathrm{c}} u_{\mathrm{b}}(\varepsilon) \frac{(r/\rho)^k - (\rho/r)^k}{(\varepsilon/\rho)^k - (\rho/\varepsilon)^k} \cos(k\theta) + \mathscr{F}_k^{\mathrm{s}} u_{\mathrm{b}}(\varepsilon) \frac{(r/\rho)^k - (\rho/r)^k}{(\varepsilon/\rho)^k - (\rho/\varepsilon)^k} \sin(k\theta) \right) \mathbb{1}_{r \geqslant \varepsilon} \\
&+ \left(\mathscr{F}_0^{\mathrm{c}} u_{\mathrm{b}}(\varepsilon) + \sum_{k=1}^{N} \left(\frac{r}{\varepsilon} \right)^k \left(\mathscr{F}_k^{\mathrm{c}} u_{\mathrm{b}}(\varepsilon) \cos(k\theta) + \mathscr{F}_k^{\mathrm{s}} u_{\mathrm{b}}(\varepsilon) \sin(k\theta) \right) \right) \mathbb{1}_{r < \varepsilon} \\
&+ \sum_{k=N+1}^{\infty} \left(\frac{r}{\rho} \right)^k \left(\mathscr{F}_k^{\mathrm{c}} u_N^\varepsilon(\rho) \cos(k\theta) + \mathscr{F}_k^{\mathrm{s}} u_N^\varepsilon(\rho) \sin(k\theta) \right)
\end{aligned}
\tag{3.3.20}
$$

for all $(r,\theta) \in [0,\rho] \times (0,2\pi)$. Let us note that expression (3.3.20) is valid for any $u_{\mathrm{b}} \in H^{\frac{1}{2}}(\partial\omega^\varepsilon)$. We are now ready to prove Theorem 3.3.4.

Proof of Theorem 3.3.4. We consider a fixed $0 < \varepsilon < \rho$. Let us first note that $u_N^\varepsilon - u^\varepsilon$ satisfies (3.3.2) in Ω^ε with $\eta = u_N^\varepsilon - u_{\mathrm{b}}$ and so, using Lemma 3.3.3 and the ε-equivalence of the norm $\|\cdot\|_{\frac{1}{2},\varepsilon}$ and $\|\cdot\|^{\mathscr{F}}_{\frac{1}{2},\varepsilon}$, we get

$$
\|u_N^\varepsilon - u^\varepsilon\|_{1,\Omega^\varepsilon} \lesssim \|u_N^\varepsilon - u_{\mathrm{b}}\|_{\frac{1}{2},\varepsilon} \lesssim \|u_N^\varepsilon - u_{\mathrm{b}}\|^{\mathscr{F}}_{\frac{1}{2},\varepsilon}. \tag{3.3.21}
$$

Then, according to Lemma 3.3.6,

$$
u_N^\varepsilon(\varepsilon)(\theta) - u_{\mathrm{b}}(\varepsilon)(\theta) = \sum_{k=N+1}^{+\infty} \left(\frac{\varepsilon}{\rho} \right)^k (a_k^\varepsilon \cos(k\theta) + b_k^\varepsilon \sin(k\theta)) \quad \forall \theta \in (0,2\pi),
$$

with

$$
\left(\sum_{k=N+1}^{+\infty} (1+k)(|a_k^\varepsilon|^2 + |b_k^\varepsilon|^2) \right)^{\frac{1}{2}} \lesssim \|u_{\mathrm{b}}\|_{\frac{1}{2},\varepsilon} + \|f\|_\Omega.
$$

So by definition of the norm $\|\cdot\|^{\mathscr{F}}_{\frac{1}{2},\varepsilon}$

$$\begin{aligned}\|u^\varepsilon_N - u_{\rm b}\|^{\mathscr{F}}_{\frac{1}{2},\varepsilon} &= \left(\frac{\varepsilon}{\rho}\right)^{N+1}\left(\sum_{n=N+1}^{+\infty}(1+k)\left(\frac{\varepsilon}{\rho}\right)^{2(n-N-1)}(|a^\varepsilon_k|^2+|b^\varepsilon_k|^2)\right)^{\frac{1}{2}}\\ &\leqslant \left(\frac{\varepsilon}{\rho}\right)^{N+1}\left(\sum_{n=N+1}^{+\infty}(1+k)(|a^\varepsilon_k|^2+|b^\varepsilon_k|^2)\right)^{\frac{1}{2}}\\ &\lesssim \left(\frac{\varepsilon}{\rho}\right)^{N+1}(\|u_{\rm b}\|_{\frac{1}{2},\varepsilon}+\|f\|_\Omega).\end{aligned}$$

Using this inequality in (3.3.21) gives (3.3.10) for $(u^\varepsilon_N - u^\varepsilon)$. Now, for proving on the Lagrange multipliers, we notice that $(u^\varepsilon_N - u^\varepsilon, \varepsilon^{-1}\lambda^\varepsilon_N - \lambda^\varepsilon)$ satisfies

$$(\nabla(u^\varepsilon_N - u^\varepsilon), \nabla v)_\Omega - \varepsilon\langle\varepsilon^{-1}\lambda^\varepsilon_N - \lambda^\varepsilon, v\rangle_{-\frac{1}{2},\varepsilon} = 0 \quad \forall v \in H^1_0(\Omega).$$

By definition of the norm $\|\cdot\|_{-\frac{1}{2},\varepsilon}$

$$\|\varepsilon^{-1}\lambda^\varepsilon_N - \lambda^\varepsilon\|_{-\frac{1}{2},\varepsilon} = \sup_{\eta\in H^{\frac{1}{2}}(\partial\omega^\varepsilon)}\frac{\langle\varepsilon^{-1}\lambda^\varepsilon_N - \lambda^\varepsilon, \eta\rangle_{-\frac{1}{2},\varepsilon}}{\|\eta\|_{\frac{1}{2},\varepsilon}}.$$

Moreover for $\eta \in H^{\frac{1}{2}}(\partial\omega^\varepsilon)$, if we take $v = v^\varepsilon_\eta \in H^1_0(\Omega)$ with v^ε_η solution of (3.3.2), according Lemma 3.3.3, we have

$$\|\varepsilon^{-1}\lambda^\varepsilon_N - \lambda^\varepsilon\|_{-\frac{1}{2},\varepsilon} \lesssim \sup_{v\in H^1_0(\Omega)}\frac{\langle\varepsilon^{-1}\lambda^\varepsilon_N - \lambda^\varepsilon, v\rangle_{-\frac{1}{2},\varepsilon}}{\|v\|_{1,\Omega}}.$$

We deduce that

$$\|\varepsilon^{-1}\lambda^\varepsilon_N - \lambda^\varepsilon\|_{-\frac{1}{2},\varepsilon} \lesssim \frac{1}{\varepsilon}\sup_{v\in H^1_{\partial\Omega}(\Omega^\varepsilon)}\frac{(\nabla(u^\varepsilon_N - u^\varepsilon), \nabla v)}{\|v\|_{1,\Omega^\varepsilon}} \lesssim \frac{1}{\varepsilon}\|u^\varepsilon_N - u^\varepsilon\|_{1,\Omega^\varepsilon},$$

and conclude that (3.3.10) holds. □

Remark 7. To simplify the presentation, in this subsection, we assumed that $u_{\rm b}$ belongs to F_N. This assumption is satisfied for example for $N \geqslant 1$ if $u_{\rm b}$ is the velocity of a rigid solid in 2D as described in Remark 4. In the general case one has to take into account the error $\|u_{\rm b} - \Pi^\varepsilon_N u_{\rm b}\|_{\frac{1}{2},\varepsilon}$ between $u_{\rm b}$ and its projection and the convergence properties given by Theorem 3.3.4 remain valid if, for instance,

$$\|u_{\rm b} - \Pi^\varepsilon_N u_{\rm b}\|_{\frac{1}{2},\varepsilon} \lesssim \varepsilon^{N+1}.$$

Remark 8. As introduced in Chapter 2, for the numerical implementation of iterative methods, the quantity of interest which corresponds to the force exerted by the fluid is $(\nabla u_N^\varepsilon)^+ \cdot \boldsymbol{n}^+$ which does not coincide with the Lagrange multiplier λ_N^ε. Nevertheless we can notice that this quantity can be computed from λ_N^ε using Lemma 3.3.5 and the explicit expression of $(\nabla u_N^\varepsilon)^- \cdot \boldsymbol{n}^+$ provided by formula (3.3.20). More precisely, we have in $H^{-\frac{1}{2}}(\partial\omega^\varepsilon)$

$$(\nabla u_N^\varepsilon)^+ \cdot \boldsymbol{n}^+ = -\frac{1}{\varepsilon}\lambda_N^\varepsilon - \frac{1}{\varepsilon}\sum_{k=1}^{N} k(\mathscr{F}_k^{\mathrm{c}} u_{\mathrm{b}}(\varepsilon)\cos(k\theta) + \mathscr{F}_k^{\mathrm{s}} u_{\mathrm{b}}(\varepsilon)\sin(k\theta)) - R_N \quad (3.3.22)$$

where

$$R_N \overset{\text{def}}{=} \frac{1}{\varepsilon}\sum_{k=N+1}^{\infty} k\varepsilon^{k-1}(a_k^\varepsilon \cos(k\theta) + b_k^\varepsilon \sin(k\theta))$$

and the coefficients $a_k^\varepsilon \overset{\text{def}}{=} \mathscr{F}_k^{\mathrm{c}} u_N^\varepsilon(\rho)$ and $b_k^\varepsilon \overset{\text{def}}{=} \mathscr{F}_k^{\mathrm{s}} u_N^\varepsilon(\rho)$ satisfy

$$\sum_{k=N+1}^{\infty}(1+k)\left(|a_k^\varepsilon|^2 + |b_k^\varepsilon|^2\right) \lesssim \|u_{\mathrm{b}}\|^2_{\frac{1}{2},\varepsilon} + \|f\|^2_\Omega.$$

This inequality implies that

$$\|R_N\|_{-\frac{1}{2},\varepsilon} \lesssim \varepsilon^N(\|u_{\mathrm{b}}\|_{\frac{1}{2},\varepsilon} + \|f\|_\Omega).$$

Thus, to compute $(\nabla u_N^\varepsilon)^+ \cdot \boldsymbol{n}^+$ with an accuracy of ε^N it is enough to compute the first two terms of (3.3.22).

Remark 9. The parameter ρ plays an important role in the extension of the method to several obstacles. In that case, ρ also depends on the distances between inclusions, and so we see that, when the inclusions get closer from each others, the estimate of $u_N^\varepsilon - u^\varepsilon$ deteriorates. The advantage of our approach is that, in that case, the loss of precision can be compensated for by increasing N the number of modes.

3.3.3 Regularity of the solution

By rewriting the Problem (3.1.3) in strong form and considering λ_N^ε as a given data of the problem, we get that $u_N^\varepsilon \in H_0^1(\Omega)$ satisfies

$$-\Delta u_N^\varepsilon = f + \lambda_N^\varepsilon \delta_\varepsilon \quad \text{in} \quad \Omega, \quad (3.3.23)$$

where the distribution $v\delta_\varepsilon$ is such that for all $\psi \in \mathcal{C}_0^\infty(\Omega)$, $\langle v\delta_\varepsilon, \psi\rangle_\Omega = \langle v, \psi\rangle_{-\frac{1}{2},\varepsilon}$. Due to the presence of the Dirac source $\lambda_N^\varepsilon\delta_\varepsilon$ in Problem (3.3.23), it is well known that the global H^2 regularity for u_N^ε cannot be reached. However, we can prove that the solution u_N^ε is more regular than H^1.

Theorem 3.3.7. *Let $0 < \eta < \frac{1}{2}$ be given. Then, if $u_{\mathrm{b}} \in H^1(\partial\omega^\varepsilon)$, the solution of Problem* (3.1.3) *satisfies the additional regularity $u_N^\varepsilon \in H^{\frac{3}{2}-\eta}(\Omega)$ and the following estimate holds:*

$$\|u_N^\varepsilon\|_{\frac{3}{2}-\eta,\Omega} \lesssim (\|f\|_\Omega + \varepsilon^{-1}\|u_{\mathrm{b}}\|_{1,\varepsilon})\|\mathscr{T}_{\frac{1}{2}+\eta,0}(\Omega,\partial\omega^\varepsilon)\|, \tag{3.3.24}$$

where

$$\|v\|_{1,\varepsilon} \overset{\text{def}}{=} \|v(\varepsilon)\|_{1,(0,2\pi)} \quad \forall v \in H^1(\partial\omega^\varepsilon),$$

and $\mathscr{T}_{\frac{1}{2}+\eta,0}(\Omega,\partial\omega^\varepsilon)$ is the trace operator from $(H^{\frac{1}{2}+\eta}(\Omega),\ \|\cdot\|_{\frac{1}{2}+\eta,\Omega})$ to $(L^2(\partial\omega^\varepsilon),\ \|\cdot\|_\varepsilon)$.

To prove Theorem 3.3.7, we will need an auxiliary lemma presented in [Gong et al., 2014].

Lemma 3.3.8. *Let $\mathcal{D}$ be a bounded, convex domain in $\mathbb{R}^2$. Let $\gamma \subset \mathcal{D}$ be a $\mathcal{C}^2$-surface such that the distance between γ and $\partial\mathcal{D}$ is positive. We consider the following problem*

$$\begin{cases} -\Delta y = \zeta\delta_\gamma & \text{in} \quad \mathcal{D}, \\ y = 0 & \text{on} \quad \partial\mathcal{D}, \end{cases} \tag{3.3.25}$$

where $\zeta \in L^2(\gamma)$. Then problem (3.3.25) *admits a unique solution y which belongs to $H^{\frac{3}{2}-\eta}(\mathcal{D})$ for any $\eta > 0$. Furthermore there exists a constant C such that*

$$\|y\|_{\frac{3}{2}-\eta,\mathcal{D}} \leqslant C\|\zeta\delta_\gamma\|_{-\frac{1}{2}-\eta,\mathcal{D}}$$

where C is uniformly independent ofζ and γ.

Proof of Theorem 3.3.7. Since $\lambda_N^\varepsilon\delta_\varepsilon \in L^2(\partial\omega^\varepsilon)$, the application of Lemma 3.3.8 immediately yields $u_N^\varepsilon \in H^{\frac{3}{2}-\eta}(\Omega)$. To show the bound (3.3.24), we start observing that Lemma 3.3.8 also gives us

$$\|u_N^\varepsilon\|_{\frac{3}{2}-\eta,\Omega} \lesssim \|\lambda_N^\varepsilon\delta_\varepsilon\|_{-\frac{1}{2}-\eta,\Omega}. \tag{3.3.26}$$

The $H^{-\frac{1}{2}-\eta}$ norm is defined as

$$\|\lambda_N^\varepsilon\delta_\varepsilon\|_{-\frac{1}{2}-\eta,\Omega} = \sup_{v\in H_0^{\frac{1}{2}+\eta}(\Omega)} \frac{(\lambda_N^\varepsilon, v)_\varepsilon}{\|v\|_{\frac{1}{2}+\eta,\Omega}}. \tag{3.3.27}$$

By applying Cauchy-Schwarz inequality to (3.3.27), we get

$$(\lambda_N^\varepsilon, v)_\varepsilon \leqslant \|\lambda_N^\varepsilon\|_\varepsilon\|v\|_\varepsilon \quad \forall v \in H^{\frac{3}{2}+\eta}(\Omega). \tag{3.3.28}$$

Next, employing the trace theorem in (3.3.28), we derive

$$(\lambda_N^\varepsilon, v)_\varepsilon \lesssim \|\lambda_N^\varepsilon\|_\varepsilon\|\mathscr{T}_{\frac{1}{2}+\eta,0}(\Omega,\partial\omega^\varepsilon)\|\|v\|_{\frac{1}{2}+\eta,\Omega} \quad \forall v \in H^{\frac{3}{2}+\eta}(\Omega),$$

Now substituting this last expression into (3.3.27), we obtain

$$\|\lambda_N^\varepsilon \delta_\varepsilon\|_{-\frac{1}{2}-\eta,\Omega} \lesssim \|\lambda_N^\varepsilon\|_\varepsilon \|\mathscr{T}_{\frac{1}{2}+\eta,0}(\Omega, \partial\omega^\varepsilon)\|. \tag{3.3.29}$$

Thanks to equality (3.3.11) as well as expression (3.3.20), we can have an explicit expression of λ_N^ε on $\partial\omega^\varepsilon$ according to the first $N+1$ Fourier modes of $u_N^\varepsilon(\rho)$ and $u_{\rm b}(\varepsilon)$. In particular, after some manipulations, we can prove that

$$\|\lambda_N^\varepsilon\|_\varepsilon \lesssim \|u_N^\varepsilon\|_{1,\rho} + \varepsilon^{-1}\|u_{\rm b}\|_{1,\varepsilon}. \tag{3.3.30}$$

Using successively trace inequality and the regularizing property of elliptic problems for u_N^ε on the domain $\Omega\backslash\omega^\rho$, we also have

$$\|u_N^\varepsilon\|_{1,\rho} \lesssim \|u_N^\varepsilon\|_{2,\Omega\backslash\omega^\rho} \lesssim \|u_N^\varepsilon\|_{\Omega\backslash\omega^\rho} + \|f\|_\Omega \lesssim \|u_{\rm b}\|_{\frac{1}{2},\varepsilon} + \|f\|_\Omega \tag{3.3.31}$$

Gathering (3.3.30) and (3.3.31), we deduce that

$$\|\lambda_N^\varepsilon\|_\varepsilon \lesssim \|u_{\rm b}\|_{\frac{1}{2},\varepsilon} + \varepsilon^{-1}\|u_{\rm b}\|_{1,\varepsilon} + \|f\|_\Omega \lesssim \|f\|_\Omega + \varepsilon^{-1}\|u_{\rm b}\|_{1,\varepsilon}$$

Coming back to (3.3.26) and (3.3.29), we obtain inequality (3.3.24). □

Please note that we have used a general expression for the trace norm as we were unable to derive its dependence with respect to the parameter ε.

3.4 Discrete approximation

For the discrete approximation of (3.1.3), we consider the same framework as in Chapter 2. In particular, we set for $k \geqslant 1$,

$$X_h^k(\Omega) \stackrel{\rm def}{=} \{v_h \in H^1(\Omega) \ : \ v_h|_K \in \mathbb{P}_k, \ \forall K \in \mathcal{T}_h(\Omega)\},$$

where $\mathbb{P}_k$ is the vector space of polynomials of degree less than or equal to k, and $\mathcal{T}_h(\mathcal{D})$ a triangulation of $\mathcal{D}$ with characteristic size h. We introduce the finite element space $V_h^k \stackrel{\rm def}{=} X_h^k(\Omega) \cap H_0^1(\Omega)$ for the approximation of the solution u_N^ε. Interestingly, we just need to discretize the space $H_0^1(\Omega)$ as the space F_N is already of finite dimension.

3.4.1 Unstabilized finite element method

The standard discrete version of (3.1.3) writes: find $(u_{N,h}^\varepsilon, \lambda_{N,h}^\varepsilon) \in V_h^k \times F_N$ such that

$$(\nabla u_{N,h}^\varepsilon, \nabla v_h)_\Omega - (\lambda_{N,h}^\varepsilon, v_h)_\varepsilon + (\mu_N, u_{N,h}^\varepsilon - u_{\rm b})_\varepsilon = (f, v_h)_\Omega \tag{3.4.1}$$

for all $(v_h, \mu_N) \in V_h^k \times F_N$. Problem (3.4.1) is a saddle point problem that will be analyzed in the framework of the available general theory, see for example [Boffi et al., 2013],[[Ern and Guermond, 2004], Lemma 2.44]. In particular, the central property is the inf-sup stability of the form $(\lambda, v_h)_\varepsilon$ that will be discussed in Section 3.4.1.2.

3.4.1.1 Approximability

Problem (3.4.1) is a saddle point problem that will be analyzed in the framework of the available general theory, see for example [Boffi et al., 2013, Ern and Guermond, 2004]. In particular, a key property is the inf-sup stability of the bilinear form $(\lambda_N, v_h)_\varepsilon$ that will be discussed in the next section. For the approximation of Problem (3.4.1), we start by introduce the Scott-Zhang operator $\Pi_h^{\mathrm{Z},k} : H_0^1(\Omega) \to V_h^k$, defined in [Scott and Zhang, 1990]. It satisfies the following approximation properties.

Proposition 3.4.1. *The Scott-Zhang operator is continuous and consistant, that is*

$$\|\Pi_h^{\mathrm{Z},k} v\|_{1,\Omega} \lesssim \|v\|_{1,\Omega}, \quad \Pi_h^{\mathrm{Z},k} v = v \quad \forall v \in H_0^1(\Omega).$$

Let $k, s \geqslant 1$, for $K \in \mathcal{T}_h(\Omega)$ and $v \in H^s(S_K)$, then

$$h^{-\frac{1}{2}} \|\Pi_h^{\mathrm{Z},k} v - v\|_K + h^{\frac{1}{2}} \|\nabla \Pi_h^{\mathrm{Z},k} v - v\|_K \lesssim h^{l+\frac{1}{2}} |v|_{s,S_K} \quad l = \min\{k, s-1\}, \tag{3.4.2}$$

where S_K is a domain made of the elements neighboring K. Moreover, we have

$$\|v - \Pi_h^{\mathrm{Z},k} v\|_{1,\Omega} \lesssim h^l |v|_{s,\Omega} \quad l = \min\{k, s-1\} \quad \forall v \in H_0^s(\Omega). \tag{3.4.3}$$

3.4.1.2 Inf-Sup Stability

The aim of this section is to discuss the discrete counterpart of the inf-sup condition for problem (3.4.1). We prove below that it is satisfied under the assumption that $k \geqslant N$ which corresponds to the case where the polynomial degree in the discrete space V_h^k is larger than or equal to the degree of the trigonometric polynomials in the reduced space F_N. We start by constructing an adequate Fortin operator that will be used to establish the inf-sup condition.

Lemma 3.4.1. *We assume $k \geqslant N$ and $\mu \in H^{\frac{1}{2}}(\partial\omega^\varepsilon)$ be given. Then, there exists $v_{\mu,h}^\varepsilon \in V_h^k$ such that*

$$(\lambda_N, v_{\mu,h}^\varepsilon)_\varepsilon = (\lambda_N, \mu)_\varepsilon \quad \forall \lambda_N \in F_N, \tag{3.4.4}$$

$$\|v_{\mu,h}^\varepsilon\| \lesssim (1 + \frac{h}{\varepsilon})^N \|\mu\|_{\frac{1}{2},\partial\omega^\varepsilon}. \tag{3.4.5}$$

Proof of Proposition 3.4.1. Let $\mu \in H^{\frac{1}{2}}(\partial\omega^\varepsilon)$ be a given function and $k \geqslant N$. We set

$$a_j^\varepsilon \overset{\text{def}}{=} \mathscr{F}_j^{\mathrm{c}} \mu(\varepsilon), \quad b_j^\varepsilon \overset{\text{def}}{=} \mathscr{F}_j^{\mathrm{s}} \mu(\varepsilon) \quad \forall j \geqslant 0,$$

and $v_\mu^\varepsilon \in H_0^1(\Omega)$ such that inside $\omega^{\varepsilon+h}$, v_μ^ε is given by

$$v_\mu^\varepsilon(r,\theta) \stackrel{\text{def}}{=} a_0^\varepsilon + \sum_{j=1}^{N} a_j^\varepsilon \left(\frac{r}{\varepsilon}\right)^j \cos(j\theta) + b_j^\varepsilon \left(\frac{r}{\varepsilon}\right)^j \sin(j\theta)$$
$$\forall (r,\theta) \in [0, \varepsilon+h] \times (0, 2\pi), \quad (3.4.6)$$

and outside $\omega^{\varepsilon+h}$, v_μ^ε is the harmonic lifting of $v_\mu^\varepsilon|_{\partial\omega^{\varepsilon+h}}$ into $H^1_{\partial\Omega}(\Omega^{\varepsilon+h})$. By observing that v_μ^ε is solution of (3.3.2) where $\varepsilon = \varepsilon + h$ and $\eta = \Pi_N^\varepsilon \mu$, as established in Lemma 3.3.3, we deduce that

$$\|v_\mu^\varepsilon\|_{1,\Omega} \lesssim \|v_\mu^\varepsilon\|_{\frac{1}{2},\varepsilon+h}.$$

Furthermore, by setting $r = \varepsilon + h$ in (3.4.6), we obtain the following expression for $v_\mu^\varepsilon(\varepsilon+h)$:

$$v_\mu^\varepsilon(\varepsilon+h)(\theta) = a_0^\varepsilon + \sum_{j=1}^{N} a_j^\varepsilon \left(1+\frac{h}{\varepsilon}\right)^j \cos(j\theta) + b_j^\varepsilon \left(1+\frac{h}{\varepsilon}\right)^j \sin(j\theta) \quad \forall \theta \in (0, 2\pi).$$

By $\varepsilon+h$-equivalence of the norm $\|\cdot\|_{\frac{1}{2},\varepsilon+h}$ and $\|\cdot\|^{\mathscr{F}}_{\frac{1}{2},\varepsilon+h}$, we have

$$\begin{aligned}\|v_\mu^\varepsilon\|_{\frac{1}{2},\varepsilon+h} \lesssim \|v_\mu^\varepsilon\|^{\mathscr{F}}_{\frac{1}{2},\varepsilon+h} &= \left(|a_0^\varepsilon|^2 + \sum_{j=1}^{N}(1+j)\left(1+\frac{h}{\varepsilon}\right)^{2j}\left(|a_j^\varepsilon|^2+|b_j^\varepsilon|^2\right)\right)^{\frac{1}{2}} \\ &\leqslant \left(1+\frac{h}{\varepsilon}\right)^N \left(|a_0^\varepsilon|^2 + \sum_{j=1}^{\infty}(1+j)(|a_j^\varepsilon|^2+|b_j^\varepsilon|^2)\right)^{\frac{1}{2}} \lesssim \left(1+\frac{h}{\varepsilon}\right)^N \|\mu\|_{\frac{1}{2},\varepsilon}.\end{aligned}$$

Note that, using Chebyshev polynomials, we can express the trigonometric polynomials $\left(\frac{r}{\varepsilon}\right)^j \cos(j\theta)$ and $\left(\frac{r}{\varepsilon}\right)^j \sin(j\theta)$ as polynomials in $x \stackrel{\text{def}}{=} r\cos(\theta)$ and $y \stackrel{\text{def}}{=} r\sin(\theta)$ with degrees less than or equal to j:

$$\begin{aligned}\left(\frac{r}{\varepsilon}\right)^j \cos(j\theta) &= \frac{1}{\varepsilon^j} \sum_{0\leqslant 2i\leqslant j} \binom{j}{2i} (-1)^i y^{2i} x^{j-2i}, \\ \left(\frac{r}{\varepsilon}\right)^j \sin(j\theta) &= \frac{1}{\varepsilon^j} \sum_{0\leqslant 2i+1\leqslant j} \binom{j}{2i+1} (-1)^i y^{2i+1} x^{j-2i-1}\end{aligned}$$

with $(x,y) = (r\cos(\theta), r\sin(\theta))$. Since, by assumption, $N \leqslant k$, we deduce that $v_\mu^\varepsilon|_{\omega^{\varepsilon+h}} \in \mathbb{P}_k$. We now set $v_{\mu,h}^\varepsilon = \Pi_h^{Z,k} v_\mu^\varepsilon$. By definition of h, the domain $\omega^{\varepsilon+h}$ contains all the elements $K \in \mathcal{T}_h(\Omega)$ that intersect $\partial\omega^\varepsilon$. Consequently, thanks to the properties of stability

and strong consistency satisfied by $\Pi_h^{\mathrm{Z},k}$, we have

$$\begin{cases} \|v_{\mu,h}^{\varepsilon}\|_{1,\Omega} \lesssim \|v_{\mu}^{\varepsilon}\|_{1,\Omega} \leqslant \beta^{-1}(1+\frac{h}{\varepsilon})^{N}\|\mu\|_{\frac{1}{2},\varepsilon}, \\ v_{\mu,h}^{\varepsilon} = v_{\mu}^{\varepsilon} = \Pi_N^{\varepsilon}\mu \quad \text{on} \quad \partial\omega^{\varepsilon}, \end{cases}$$

where β is a constant uniformly independent of h, N and ε. □

We then deduce the following inf-sup condition for the bilinear form $(\lambda_N, v_h)_{\varepsilon}$.

Lemma 3.4.2. *We assume that $k \geqslant N$. There exists a constant $\beta > 0$ uniformly independent of h, N and ε such that for all $\lambda_N \in F_N$,*

$$\sup_{v_h \in V_h^k} \frac{(\lambda_N, v_h)_{\varepsilon}}{\|v_h\|_{1,\Omega}} \geqslant \beta(1+\frac{h}{\varepsilon})^{-N}\|\lambda_N\|_{-\frac{1}{2},\varepsilon}.$$

Proof of Lemma 3.4.2. Let $\lambda_N \in F_N$ be given. According to Lemma 3.4.1, for all $\mu \in H^{\frac{1}{2}}(\partial\omega^{\varepsilon})$ there exists $v_{\mu,h}^{\varepsilon} \in V_h^k$ such that

$$(\lambda_N, v_{\mu,h}^{\varepsilon})_{\varepsilon} = (\lambda_N, v_{\mu,h}^{\varepsilon})_{\varepsilon}, \quad \|v_{\mu,h}^{\varepsilon}\| \lesssim (1+\frac{h}{\varepsilon})^{N}\|\mu\|_{\frac{1}{2},\partial\omega^{\varepsilon}}.$$

From these two properties on $v_{\mu,h}^{\varepsilon}$, it comes

$$\frac{(\lambda_N, v_{\mu,h}^{\varepsilon})_{\varepsilon}}{\|v_{\mu,h}^{\varepsilon}\|_{1,\Omega}} \geqslant \beta\left(1+\frac{h}{\varepsilon}\right)^{-N}\frac{(\lambda_N,\mu)_{\varepsilon}}{\|\mu\|_{\frac{1}{2},\varepsilon}} = \beta\left(1+\frac{h}{\varepsilon}\right)^{-N}\frac{(\lambda_N,\mu)_{\varepsilon}}{\|\mu\|_{\frac{1}{2},\varepsilon}} \quad \forall \mu \in H^{\frac{1}{2}}(\partial\omega^{\varepsilon}).$$

Taking successively the supremum over $v_h \in V_h^k$ and $\mu \in H^{\frac{1}{2}}(\partial\omega^{\varepsilon})$, we finally obtain

$$\sup_{v_h \in V_h^k} \frac{(\lambda_N, v_h)_{\varepsilon}}{\|v_h\|_{1,\Omega}} \geqslant \beta\left(1+\frac{h}{\varepsilon}\right)^{-N} \sup_{\mu \in H^{\frac{1}{2}}(\partial\omega^{\varepsilon})} \frac{(\lambda_N,\mu)_{\varepsilon}}{\|\mu\|_{\frac{1}{2},\varepsilon}} = \beta\left(1+\frac{h}{\varepsilon}\right)^{-N}\|\lambda_N\|_{-\frac{1}{2},\varepsilon}.$$

This concludes the proof. □

By applying the estimate on discrete saddle point problems given by in [Ern and Guermond, 2004, Lemma 2.44] and by taking into account that the discretization space for the Lagrange multipliers coincides with the continuous one, we have

$$\begin{aligned} \|u_N^{\varepsilon} - u_{N,h}^{\varepsilon}\|_{1,\Omega} &\leqslant \big(1+\frac{\|a\|}{\alpha}\big)\big(1+\frac{\|b\|}{\beta_h}\big)\inf_{v_h \in V_h^k}\|u_N^{\varepsilon} - v_h\|_{1,\Omega}, \\ \|\lambda_N^{\varepsilon} - \lambda_{N,h}^{\varepsilon}\|_{-\frac{1}{2},\varepsilon} &\leqslant \frac{\|a\|}{\beta_h}\big(1+\frac{\|a\|}{\alpha}\big)\big(1+\frac{\|b\|}{\beta_h}\big)\inf_{v_h \in V_h^k}\|u_N^{\varepsilon} - v_h\|_{1,\Omega} \end{aligned} \tag{3.4.7}$$

where β_h is given by $\beta_h = \beta\big(1+\frac{h}{\varepsilon}\big)^{-N}$ according to Lemma 3.4.2. Moreover, the norm $\|a\|$ and the coercivity constant α of a are bounded independently of h, N and ε and the norm of b is bounded by (3.3.6). So we deduce the following general a-priori estimates for the discrete error:

$$\begin{aligned}\|u_N^\varepsilon - u_{N,h}^\varepsilon\|_{1,\Omega} &\lesssim (1+\frac{h}{\varepsilon})^N |\log(\varepsilon)|^{\frac{1}{2}} \inf_{v_h\in V_h^k} \|u_N^\varepsilon - v_h\|_{1,\Omega},\\ \|\lambda_N^\varepsilon - \lambda_{N,h}^\varepsilon\|_{-\frac{1}{2},\varepsilon} &\lesssim (1+\frac{h}{\varepsilon})^{2N} |\log(\varepsilon)|^{\frac{1}{2}} \inf_{v_h\in V_h^k} \|u_N^\varepsilon - v_h\|_{1,\Omega}.\end{aligned} \tag{3.4.8}$$

Estimates (3.4.8) are not fully satisfactory due to the presence of the factor $\big(1+\frac{h}{\varepsilon}\big)^N$ that comes from the inf-sup condition of Lemma 3.4.2. It shows that the scheme (3.4.1) is affected by a loss of stability when $\varepsilon \to 0$ for a fixed computational mesh. This is an example of the well known *locking phenomenon* (see for example [Boffi et al., 2013, Ern and Guermond, 2004]) that appears because the inclusion becomes too small with respect to the mesh size and by consequence the solution $u_{N,h}^\varepsilon$ becomes over-constrained. To overcome the limitations of the scheme (3.4.1) with respect to stability, we propose in the next section a stabilized variant of it.

3.4.2 Stabilized finite element method

We introduce in this section a stabilized formulation based on a penalty method. We look for $u_{N,h}^\varepsilon \in V_h^k$ and $\lambda_{N,h}^\varepsilon \in F_N$ such that

$$\begin{cases} \big(\nabla u_{N,h}^\varepsilon, \nabla v_h\big)_\Omega - \big(\lambda_{N,h}^\varepsilon, v_h\big)_\varepsilon = (f, v_h)_\Omega\,, & \forall v_h \in V_h,\\ \big(\mu_N, u_{N,h}^\varepsilon\big)_\varepsilon + s_h^\lambda(\mu_N, \lambda_{N,h}^\varepsilon) = (\mu_N, u_{\mathrm{b}})_\varepsilon & \forall \mu_N \in F_N, \end{cases} \tag{3.4.9}$$

where $s_h^\lambda(\mu_N,\lambda_N) : F_N \times F_N \to \mathbb{R}$ is a stabilization term defined for all $(\mu_N,\lambda_N) \in F_N \times F_N$ by (see also [Barrenechea and González, 2018])

$$s_h^\lambda(\mu_N,\lambda_N) = \gamma_\lambda \left(\frac{h}{\varepsilon}\right) \varepsilon^{-1}(\mu_N,\lambda_N)_\varepsilon, \tag{3.4.10}$$

where $\gamma_\lambda > 0$ is a user-defined parameter uniformly independent of N, h and ε. We also introduce the following (augmented) bilinear form $B_h : (V_h^k \times F_N) \times (V_h^k \times F_N)$ defined for all $(u_h,\lambda_N),(v_h,\mu_N) \in V_h^k \times F_N$ by

$$B_h((u_h,\lambda_N),(v_h,\mu_N)) = a(u_h,v_h) - b(\lambda_N,v_h) + b(\mu_N,u_h) + s_h^\lambda(\mu_N,\lambda_N).$$

Problem (3.4.9) is equivalent to find $(u_{N,h}^\varepsilon, \lambda_{N,h}^\varepsilon) \in V_h^k \times F_N$ such that

$$B_h((u_{N,h}^\varepsilon,\lambda_{N,h}^\varepsilon),(v_h,\mu_N)) = (f,v_h)_\Omega + (\mu_N,u_{\mathrm{b}})_\varepsilon \quad \forall\,(v_h,\mu_N) \in V_h^k \times F_N\,. \tag{3.4.11}$$

3.4.2.1 Preliminary results

For the analysis of problem (3.4.9) we introduce the following discrete trace lemma (see [Hansbo and Hansbo, 2002]).

Proposition 3.4.2. *Let Γ be an internal smooth boundary dividing Ω into two open sets and $K \in \mathcal{T}_h(\Omega)$. We set $\Gamma_K \overset{\text{def}}{=} \Gamma \cap K$. There exists a constant $C > 0$ depending only on the maximum curvature of Γ such that for*

$$\|v\|^2_{\Gamma_K} \leqslant C(h^{-1}\|v\|^2_K + h\|v\|^2_{1,K}) \quad \forall v \in H^1_0(\Omega). \tag{3.4.12}$$

For the analysis of the augmented bilinear form, we introduce the following norm:

$$\|(v_h, \mu)\|_\varepsilon = \left(\|v_h\|^2_{1,\Omega} + \|\mu\|^2_{-\frac{1}{2},\varepsilon} + \left(\frac{h}{\varepsilon}\right)\varepsilon^{-1}\|\mu\|^2_\varepsilon\right)^{\frac{1}{2}} \quad \forall\, (v_h, \mu) \in V^k_h \times F_N.$$

3.4.2.2 Stability

We start by constructing an adequate Fortin operator that will be used to establish the inf-sup condition.

Lemma 3.4.3. *Let $\lambda_N \in F_N$ be given, there exists $\boldsymbol{v}^\varepsilon_{\lambda_N,h} \in V^k_h$ such that*

$$\frac{3}{4}\|\lambda_N\|^2_{-\frac{1}{2},\varepsilon} \leqslant -(\lambda_N, v^\varepsilon_{\lambda_N,h})_\varepsilon + C\left(\frac{\varepsilon}{h}\right)\varepsilon^{-1}\|\lambda_N\|^2_\varepsilon, \quad \|v^\varepsilon_{\lambda_N,h}\|_{1,\Omega} \lesssim \|\lambda_N\|_{-\frac{1}{2},\varepsilon},$$

with C uniformly independent of h, N and ε.

Proof of Lemma 3.4.3. Let $\lambda_N \in F_N$ be given. Using definition (3.2.4) of the norm $\|\cdot\|_{-\frac{1}{2},\varepsilon}$, since F_N is a closed subspace of $L^2(\partial\omega^\varepsilon)$, there exists $\mu_N \in F_N$ such that $\|\mu_N\|_{\frac{1}{2},\varepsilon} = 1$ and

$$\|\lambda_N\|_{-\frac{1}{2},\varepsilon} = (\lambda_N, \mu_N)_\varepsilon .$$

Taking $\underline{\mu}_N = -\mu_N\|\lambda_N\|_{-\frac{1}{2},\varepsilon}$, we have $\|\underline{\mu}_N\|_{\frac{1}{2},\varepsilon} = \|\lambda_N\|_{-\frac{1}{2},\varepsilon}$ and

$$-\left(\lambda_N, \underline{\mu}_N\right)_\varepsilon = \|\lambda_N\|^2_{-\frac{1}{2},\varepsilon}.$$

According to Lemma 3.3.3, there exists $v^\varepsilon_{\underline{\mu}_N} \in H^1_0(\Omega)$ such that $v^\varepsilon_{\underline{\mu}_N} = \underline{\mu}_N$ on $\partial\omega^\varepsilon$ and

$$\|v^\varepsilon_{\underline{\mu}_N}\|_{1,\Omega} \lesssim \|\underline{\mu}_N\|_{\frac{1}{2},\varepsilon} = \|\lambda_N\|_{-\frac{1}{2},\varepsilon}. \tag{3.4.13}$$

Applying Proprosition 3.4.1 to the re-scaled function $v^{\varepsilon}_{\underline{\mu}_N}(\varepsilon)$, we have, for all $K \in \mathcal{T}_h(\Omega)$ such that $K \cap \partial\omega^{\varepsilon} \neq \varnothing$,

$$\begin{aligned}\|\Pi_h^{\mathrm{Z},k} v^{\varepsilon}_{\underline{\mu}_N}(\varepsilon) - v^{\varepsilon}_{\underline{\mu}_N}(\varepsilon)\|^2_{\frac{K}{\varepsilon}\cap\partial\omega} \lesssim \left(\frac{h}{\varepsilon}\right)^{-1} \|\Pi_h^{\mathrm{Z}k} v^{\varepsilon}_{\underline{\mu}_N}(\varepsilon) - v^{\varepsilon}_{\underline{\mu}_N}(\varepsilon)\|^2_{0,\frac{K}{\varepsilon}} \\ + \left(\frac{h}{\varepsilon}\right) \|\nabla\big(\Pi_h^{\mathrm{Z},k} v^{\varepsilon}_{\underline{\mu}_N}(\varepsilon) - v^{\varepsilon}_{\underline{\mu}_N}(\varepsilon)\big)\|^2_{0,\frac{K}{\varepsilon}}.\end{aligned}$$

Using the approximation property of $\Pi_h^{\mathrm{Z},k}$ given in (3.4.2), we obtain that

$$\|\Pi_h^{\mathrm{Z},k} v^{\varepsilon}_{\underline{\mu}_N}(\varepsilon) - v^{\varepsilon}_{\underline{\mu}_N}(\varepsilon)\|^2_{\frac{K}{\varepsilon}\cap\partial\omega} \lesssim \left(\frac{h}{\varepsilon}\right) \|\nabla v_{\underline{\mu}_N}(\varepsilon)\|^2_{\frac{S_K}{\varepsilon}}.$$

A scaling argument then leads to

$$\|\Pi_h^{\mathrm{Z},k} v^{\varepsilon}_{\underline{\mu}_N} - v^{\varepsilon}_{\underline{\mu}_N}\|^2_{K\cap\partial\omega^{\varepsilon}} \lesssim \left(\frac{h}{\varepsilon}\right) \|\nabla v^{\varepsilon}_{\underline{\mu}_N}\|^2_{S_K}.$$

Summing over all tiles K intersecting $\partial\omega^{\varepsilon}$, we get, according to (3.4.13),

$$\|\Pi_h^{\mathrm{Z},k} v^{\varepsilon}_{\underline{\mu}_N} - v^{\varepsilon}_{\underline{\mu}_N}\|^2_{\partial\omega^{\varepsilon}} \lesssim \left(\frac{h}{\varepsilon}\right) \|v^{\varepsilon}_{\underline{\mu}_N}\|^2_{1,\Omega} \lesssim \left(\frac{h}{\varepsilon}\right) \|\lambda_N\|^2_{-\frac{1}{2},\varepsilon}.$$

Then using Cauchy-Schwarz inequality and the scaling between the norms $\|\cdot\|_{\varepsilon}$ and $\|\cdot\|_{\partial\omega^{\varepsilon}}$ deduced from (3.2.5), we get

$$\begin{aligned}|\left(\lambda_N, \Pi_h^{\mathrm{Z},k} v^{\varepsilon}_{\underline{\mu}_N} - v^{\varepsilon}_{\underline{\mu}_N}\right)_{\varepsilon}| &\lesssim C \left(\frac{h}{\varepsilon}\right)^{\frac{1}{2}} \varepsilon^{-\frac{1}{2}} \|\lambda_N\|_{\varepsilon} \|\lambda_N\|_{-\frac{1}{2},\varepsilon}, \\ &\leqslant \frac{1}{4}\|\lambda_N\|^2_{-\frac{1}{2},\varepsilon} + C\left(\frac{h}{\varepsilon}\right)\varepsilon^{-1}\|\lambda_N\|^2_{\varepsilon},\end{aligned}$$

with C uniformly independent of N, h and ε. Setting $v^{\varepsilon}_{\lambda_N,h} = \Pi_h^{\mathrm{Z},k} v^{\varepsilon}_{\underline{\mu}_N}$, we obtain

$$\begin{aligned}\|\lambda_N\|^2_{-\frac{1}{2},\varepsilon} + (\lambda_N, \underline{\mu}_N)_{\varepsilon} &= -(\lambda_N, v_{\underline{\mu}_N} - \Pi_h^{\mathrm{Z},k} v_{\underline{\mu}_N})_{\varepsilon}, \\ &\leqslant \frac{1}{4}\|\lambda_N\|^2_{\varepsilon} + C\left(\frac{h}{\varepsilon}\right)\varepsilon^{-1}\|\lambda_N\|^2_{\varepsilon}.\end{aligned}$$

Furthermore, using the continuity of the Scott-Zhang interpolator and inequality (3.4.13), we have

$$\|v^{\varepsilon}_{\lambda_N,h}\|_{1,\Omega} \lesssim \|v^{\varepsilon}_{\underline{\mu}_N}\|_{1,\Omega} \lesssim \|\lambda_N\|_{-\frac{1}{2},\varepsilon}.$$

This concludes the proof. □

The stability of the stabilized problem (3.4.9) is addressed in the following lemma.

Lemma 3.4.4. *There exists a constant $\beta > 0$ uniformly independent of h, N and ε such that*

$$\inf_{(u_h,\lambda_N)\in V_h^k\times F_N}\ \sup_{(v_h,\mu_N)\in V_h^k\times F_N}\frac{B_h((u_h,\lambda_N),(v_h,\mu_N))}{\|(u_h,\lambda_N)\|_\varepsilon\|(v_h,\mu_N)\|_\varepsilon}\geqslant\beta.$$

Proof. Let (u_h,λ_N) be given in $V_h^k\times F_N$. First, taking $(v_h,\mu_N)=(u_h,\lambda_N)$ in the definition of B_h, we observe that

$$B_h\left((u_h,\lambda_N),(u_h,\lambda_N)\right)=\|\nabla u_h\|_\Omega^2+\gamma_\lambda\left(\frac{h}{\varepsilon}\right)\varepsilon^{-1}\|\lambda_N\|_\varepsilon^2. \tag{3.4.14}$$

Furthermore, according to Lemma 3.4.3, there exists $v^\varepsilon_{\lambda_N,h}\in V_h^k$ and $C_1>0$ uniformly independent of h, N and ε such that

$$\frac{3}{4}\|\lambda_N\|^2_{-\frac{1}{2},\varepsilon}\leqslant-(\lambda_N,v^\varepsilon_{\lambda_N,h})_\varepsilon+C_1\left(\frac{\varepsilon}{h}\right)\varepsilon^{-1}\|\lambda_N\|_\varepsilon^2, \tag{3.4.15}$$

$$\|v^\varepsilon_{\lambda_N,h}\|_{1,\Omega}\lesssim\|\lambda_N\|_{-\frac{1}{2},\varepsilon}. \tag{3.4.16}$$

We will prove that, for $\alpha>0$ small enough, there exists $C_m>0$ such that

$$B_h\big((u_h,\lambda_N),(u_h+\alpha_\lambda v^\varepsilon_{\lambda_N,h},\lambda_N)\big)\geqslant C_m\|(u_h,\lambda_N)\|_\varepsilon^2. \tag{3.4.17}$$

From (3.4.16), there exists $C_2>0$ uniformly independent of N, h and ε such that

$$|\left(\nabla u_h,\nabla v^\varepsilon_{\lambda_N,h}\right)_\Omega|\lesssim\|\nabla u_h\|_\Omega\|\lambda_N\|_{-\frac{1}{2},\varepsilon}\leqslant C_2\|u_h\|^2_{1,\Omega}+\frac{1}{4}\|\lambda_N\|^2_{-\frac{1}{2},\varepsilon}. \tag{3.4.18}$$

Combining (3.4.15) and (3.4.18), and by taking $(v_h,\mu_N)=(v^\varepsilon_{\lambda_N,h},0)$ in the definition of B_h, we have

$$\begin{aligned}B_h((u_h,\lambda_N),(v^\varepsilon_{\lambda_N,h},0))&=(\nabla u_h,\nabla v^\varepsilon_{\lambda_N,h})-(\lambda_N,v^\varepsilon_{\lambda_N,h})_\varepsilon,\\&\geqslant-C_2\|u_h\|^2_{1,\Omega}+\frac{1}{2}\|\lambda_N\|^2_{-\frac{1}{2},\varepsilon}-C_1\left(\frac{h}{\varepsilon}\right)\varepsilon^{-1}\|\lambda_N\|_\varepsilon^2.\end{aligned}$$

Gathering finally this inequality and (3.4.14), we get

$$\begin{aligned}&B_h\left((u_h,\lambda_N),(u_h+\alpha_\lambda v^\varepsilon_{\lambda_N,h},\lambda)\right)\geqslant\\&\alpha\|u_h\|^2_{1,\Omega}+\gamma_\lambda\varepsilon^{-1}\left(\frac{h}{\varepsilon}\right)\|\lambda_N\|_\varepsilon^2+\frac{\alpha_\lambda}{2}\|\lambda_N\|^2_{-\frac{1}{2},\varepsilon}+\alpha_\lambda(-C_2\|u_h\|^2_{1,\Omega}-C_1\left(\frac{h}{\varepsilon}\right)\varepsilon^{-1}\|\lambda_N\|_\varepsilon^2),\end{aligned}$$

with α the positive coercivity constant of a. This leads to (3.4.17) if we take $\alpha_\lambda > 0$ small enough with

$$C_m = \min\left(\alpha - \alpha_\lambda C_2, \frac{1}{2}\alpha_\lambda, \gamma_\lambda - \alpha_\lambda C_1\right).$$

To end the proof, we notice that, from the triangle inequality, the continuity of $\Pi_h^{\mathrm{Z},k}$ and the inequality (3.4.16), we have

$$\|(u_h + \alpha_\lambda v^\varepsilon_{\lambda_N,h}, \lambda_N)\|_\varepsilon \leqslant \|(u_h,\lambda_N)\|_\varepsilon + \alpha_\lambda C \|\lambda_N\|_{-\frac{1}{2},\varepsilon} \leqslant C_M \|(u_h,\lambda_N)\|_\varepsilon, \qquad (3.4.19)$$

where

$$C_M = 1 + \alpha_\lambda C.$$

Thus, dividing (3.4.17) by (3.4.19), we get, with $v_h = u_h + \alpha_\lambda v^\varepsilon_{\lambda_N,h}$ and $\mu_N = \lambda_N$,

$$\frac{B_h((u_h,\lambda),(v_h,\mu))}{\|(v_h,\mu_N)\|_\varepsilon} \geqslant \frac{C_m}{C_M}\|(u_h,\lambda_N)\|_\varepsilon,$$

which implies that

$$\sup_{(v_h,\mu_N)\in V_h^k\times F_N} \frac{B_h((u_h,\lambda_N),(v_h,\mu_N))}{\|(v_h,\mu_N)\|_\varepsilon} \geqslant \frac{C_m}{C_M}\|(u_h,\lambda_N)\|_\varepsilon \quad \forall (u_h,\lambda_N)\in V_h^k\times F_N,$$

leading to the desired result. □

To conclude the analysis of the stabilized formulation, we address the consistency of the method. Since $\lambda^\varepsilon_{N,h} - \lambda^\varepsilon_N \in F_N$, we can apply Lemma 3.4.4 to have an estimate of $(u^\varepsilon_{N,h} - \Pi_h^{\mathrm{Z},k} u^\varepsilon_N, \lambda^\varepsilon_{N,h} - \lambda^\varepsilon_N)$. Precisely, we have,

$$\|(u^\varepsilon_{N,h} - \Pi_h^{\mathrm{Z},k} u^\varepsilon_N, \lambda^\varepsilon_{N,h} - \lambda^\varepsilon_N)\|_\varepsilon \lesssim \sup_{(v_h,\mu_N)\in V_h^k\times F_N} \frac{B_h((u^\varepsilon_{N,h} - \Pi_h^{\mathrm{Z},k} u^\varepsilon_N, \lambda^\varepsilon_{N,h} - \lambda^\varepsilon_N),(v_h,\mu_N))}{\|(v_h,\mu_N)\|_\varepsilon}.$$

By combining the equations of the continuous problem (3.3.4) and the discrete problem (3.4.11), the following holds for all $(v_h,\mu_N)\in V_h^k\times F_N$:

$$B_h((u^\varepsilon_{N,h} - \Pi_h^{\mathrm{Z},k} u^\varepsilon_N, \lambda^\varepsilon_{N,h} - \lambda^\varepsilon_N),(v_h,\mu_N)) = a(u^\varepsilon_N - \Pi_h^{\mathrm{Z},k} u^\varepsilon_N, v_h) + b(\mu_N, u^\varepsilon_N - \Pi_h^{\mathrm{Z},k} u^\varepsilon_N) + s_h(\mu_N,\lambda^\varepsilon_N)$$

Using the continuity of the bilinear forms a, b (with the norm estimated by (3.3.6)) and s_h, we can establish that:

$$|a(u^\varepsilon_N - \Pi_h^{\mathrm{Z},k} u^\varepsilon_N, v_h) + b(\mu, u^\varepsilon_N - \Pi_h^{\mathrm{Z},k} u^\varepsilon_N) + s_h(\mu_N,\lambda^\varepsilon_N)| \lesssim \left(|\log(\varepsilon)|^{\frac{1}{2}}\|u^\varepsilon_N - \Pi_h^{\mathrm{Z},k} u^\varepsilon_N\|_{1,\Omega} + \frac{h^{\frac{1}{2}}}{\varepsilon}\|\lambda^\varepsilon_N\|_\varepsilon\right)\|(v_h,\mu_N)\|_\varepsilon.$$

Gathering these estimates and using the triangle inequality, we derive the following a-priori estimate in terms of the approximation error of the Scott-Zhang interpolation operator:

$$\begin{aligned}\|(u_N^\varepsilon - u_{N,h}^\varepsilon, \lambda_N^\varepsilon - \lambda_{N,h}^\varepsilon)\|_\varepsilon &\lesssim \|(u_N^\varepsilon - \Pi_h^{\mathrm{Z},k} u_N^\varepsilon, 0)\|_\varepsilon + \|(\Pi_h^{\mathrm{Z},k} u_N^\varepsilon - u_{N,h}^\varepsilon, \lambda_N^\varepsilon - \lambda_{N,h}^\varepsilon)\|_\varepsilon, \\ &\lesssim |\log(\varepsilon)|^{\frac{1}{2}} \|u_N^\varepsilon - \Pi_h^{\mathrm{Z},k} u_N^\varepsilon\|_{1,\Omega} + \varepsilon^{-\frac{1}{2}} \left(\frac{h}{\varepsilon}\right)^{\frac{1}{2}} \|\lambda_N^\varepsilon\|_\varepsilon. \quad (3.4.20)\end{aligned}$$

If we compare this estimate with the corresponding estimates (3.4.8) obtained for the non stabilized scheme, we remark that the estimation of the approximation error (3.4.20) is not affected by any restriction on N. However, it shows that the stabilized scheme converges at a sub-optimal rate $h^{\frac{1}{2}}$ independently of the FE polynomial order $k > 0$. Then, if low-order convergence is acceptable, one should look at the stabilized scheme with low order finite element approximation ($k = 1$). Otherwise, if a sufficiently refined resolution of the inclusions is affordable, namely $h \simeq \varepsilon$ and if the constraint $k \geqslant N$ can be satisfied, the estimate results (3.4.8) seem more attractive, provided that the finite element space suitably approximates the solution of the problem. This is another difficulty of this problem (see, for example, Remark 10) that will be discussed and resolved in the next two sections.

3.4.2.3 Approximation properties and convergence

Because of the limited regularity of the solution, the approximation properties of the finite element method are not optimal. In particular, due to the approximation properties (3.4.3) satisfied by the Scott-Zhang interpolation operator, since $u_N^\varepsilon \in H_0^s(\Omega)$ with $s = \frac{3}{2} - \eta$, we have the following interpolation error estimate

$$\|u_N^\varepsilon - \Pi_h^{\mathrm{Z},k} u_N^\varepsilon\|_\Omega + h\|\nabla(u_N^\varepsilon - \Pi_h^{\mathrm{Z},k} u_N^\varepsilon)\|_\Omega \lesssim h^{\frac{1}{2}-\eta} \|u_N^\varepsilon\|_{\frac{3}{2}-\eta,\Omega} \quad \forall k > 0. \quad (3.4.21)$$

Thus, for the discrete problem without stabilization studied in Section 3.4.1.2, if we combine (3.4.21) with the a-priori error estimate (3.4.8) we obtain that, under the assumption that $k \geqslant N$,

$$\|u_N^\varepsilon - u_{N,h}^\varepsilon\|_{1,\Omega} \lesssim (1 + \frac{h}{\varepsilon})^N h^{\frac{1}{2}-\eta} \|u_N^\varepsilon\|_{\frac{3}{2}-\eta,\Omega}, \quad (3.4.22)$$

$$\|\lambda_N^\varepsilon - \lambda_{N,h}^\varepsilon\|_{-\frac{1}{2},\varepsilon} \lesssim (1 + \frac{h}{\varepsilon})^{2N} h^{\frac{1}{2}-\eta} \|u_N^\varepsilon\|_{\frac{3}{2}-\eta,\Omega}. \quad (3.4.23)$$

On the other hand, for the stabilized method studied in Section 3.4.2, adopting a similar approach, we have for any $k > 0$ the following result

$$\|(u_N^\varepsilon - u_{N,h}^\varepsilon, \lambda_N^\varepsilon - \lambda_{N,h}^\varepsilon)\|_\varepsilon \leqslant |\log(\varepsilon)|^{\frac{1}{2}} h^{\frac{1}{2}-\eta} \|u_N^\varepsilon\|_{\frac{3}{2}-\eta,\Omega} + \varepsilon^{-1} h^{\frac{1}{2}} \|\lambda_N^\varepsilon\|_\varepsilon. \quad (3.4.24)$$

The previous inequalities show that with respect to the approximation properties, the numerical schemes with or without stabilization are equivalent and both are sub-optimal. We also observe that there is no advantage in using high-order finite elements. As a consequence, since we are limited to the case $k = 1$, the restriction $k \geqslant N$ for the scheme without stabilization entails that we can not exploit the additional accuracy provided by high-order Fourier modes. In this respect, the stabilized scheme guarantees more flexibility.

Remark 10. In the limit when $\varepsilon \to 0$, the regularity of the continuous problem further decreases. In particular, the H^s-norm of u_N^ε for $s \geqslant 1$, which pop out in (3.4.22)-(3.4.23) and (3.4.24) may tend to infinity when $\varepsilon \to 0$. This can be illustrated by the very simple exterior problem

$$\begin{cases} -\Delta v^\varepsilon(\varepsilon) = 0 & \text{in} \quad \omega^\rho \backslash \omega^\varepsilon, \\ \widehat{v}_\varepsilon = 0 & \text{on} \quad \partial\omega^\rho, \\ \widehat{v}_\varepsilon = L & \text{on} \quad \partial\omega^\varepsilon, \end{cases}$$

that features the following analytical solution

$$v^\varepsilon(\varepsilon)(|x|) = L\frac{\log(|x|/\rho)}{\log(\varepsilon/\rho)}.$$

Thus, we obtain, for $s \geqslant 1$,

$$\|v^\varepsilon(\varepsilon)\|_{s,\Omega} \sim \frac{1}{\varepsilon^{s-1}} \text{ when } \varepsilon \to 0.$$

These considerations show that for small inclusions it is particularly difficult to achieve a desired accuracy with a standard approximation method.

Remark 11. Under some additional assumptions on the mesh, we can prove convergence results better than those stated in (3.4.22)-(3.4.23) and (3.4.24). Let $\mathcal{T}_h(\Omega)$ be a δ-resolving mesh with respect to the interface, that is the edges of $\mathcal{T}_h(\Omega)$ have a maximum distance of δ to $\partial\omega^\varepsilon$. This condition is in particular fulfilled with $\delta = \mathcal{O}(h^2)$ when the nodes of the mesh $\mathcal{T}_h(\Omega)$ fall on the interface $\partial\omega^\varepsilon$. With a little abuse of notation, we call this case the *conforming mesh* configuration. In this case, following the approach of Theorem 5.2 in [Köppl et al., 2018], under the restriction that $k = 1 \geqslant N$, we obtain the following quasi-optimal convergence results for the numerical scheme without stabilization,

$$\|u_N^\varepsilon - u_{N,h}^\varepsilon\|_{1,\Omega} \lesssim (1 + \frac{h}{\varepsilon})^N h \left(\|u_N^\varepsilon\|_{2,\Omega^\varepsilon} + \|u_N^\varepsilon\|_{2,\omega^\varepsilon}\right),$$
$$\|\lambda_N^\varepsilon - \lambda_{N,h}^\varepsilon\|_{-\frac{1}{2},\varepsilon} \lesssim (1 + \frac{h}{\varepsilon})^{2N} h \left(\|u_N^\varepsilon\|_{2,\Omega^\varepsilon} + \|u_N^\varepsilon\|_{2,\omega^\varepsilon}\right).$$

We note that for δ-meshes, the stabilized scheme remains sub-optimal because the consistency error, of order $h^{\frac{1}{2}}$, dominates over the approximation error.

Overall, the approximation properties of the proposed (original and stabilized) schemes are not satisfactory, in particular because quadratic convergence rates or higher are prevented. To overcome this limitation, we propose an improvement of the approximation method in the next section.

3.4.3 Augmented finite element method

As pointed out in the previous section, the standard finite element method may suffer from numerical locking when $\varepsilon/h \to 0$. The other limitation of the standard finite element method is the sub-optimality of the convergence in h for continuous finite elements when the mesh does not conform to the $\partial\omega^\varepsilon$ interface. This is a classical limitation of fictitious domain problems and can be attributed to the poor estimation of the gradient jump by $\mathcal{C}^1$ functions across the interface. In this section, we will introduce an augmented finite element method which allows us to obtain an numerical approximation error uniformly independent of ε and of arbitrary order in h.

3.4.3.1 Definition of the augmented finite element space

In order to overcome the limitations described above, we propose to enrich the finite element space by adding well-chosen functions that allow to better approximate the singular behaviour of u_N^ε when ε tends to 0 and the jump at the interface $\partial\omega^\varepsilon$. The design of these functions directly comes from the expression of the solution u_N^ε in ω^ρ with respect to its Fourier modes on $\partial\omega^\rho$ and $\partial\omega^\varepsilon$ given by equation (3.3.20). In what follows, we assume that $\varepsilon > 0$ is small enough to have $2\varepsilon < \rho$ where the parameter ρ is given in (3.3.9). We first define χ a radial cut-off $\mathcal{C}^\infty$ function satisfying

$$\chi(r) = \begin{cases} 1 & \forall r \leqslant \dfrac{1}{2}\rho, \\ 0 & \forall r > \dfrac{3}{4}\rho. \end{cases}$$

We then set for $j \in \{1, \dots, N\}$,

$$\begin{cases} \phi_0^{\varepsilon,\mathrm{c}}(r,\theta) \overset{\text{def}}{=} \chi(r)\dfrac{\log(r/\rho)}{\log(\varepsilon/\rho)}\mathbb{1}_{r\geqslant\varepsilon} + \mathbb{1}_{r<\varepsilon}, \\ \phi_j^{\varepsilon,\mathrm{c}}(r,\theta) \overset{\text{def}}{=} \chi(r)\left(\dfrac{(\rho/r)^j - (r/\rho)^j}{(\rho/\varepsilon)^j - (\varepsilon/\rho)^j}\right)\cos(j\theta)\mathbb{1}_{r\geqslant\varepsilon} + \left(\dfrac{r}{\varepsilon}\right)^j\cos(j\theta)\mathbb{1}_{r<\varepsilon}, \\ \phi_j^{\varepsilon,\mathrm{s}}(r,\theta) \overset{\text{def}}{=} \chi(r)\left(\dfrac{(\rho/r)^j - (r/\rho)^j}{(\rho/\varepsilon)^j - (\varepsilon/\rho)^j}\right)\sin(j\theta)\mathbb{1}_{r\geqslant\varepsilon} + \left(\dfrac{r}{\varepsilon}\right)^j\sin(j\theta)\mathbb{1}_{r<\varepsilon} \end{cases}$$

for all $(r,\theta) \in \mathbb{R}^+ \times (0, 2\pi)$. We consider the augmented finite element space $V_{N,h}^k$ given by

$$V_{N,h}^k \overset{\text{def}}{=} X_h^k(\Omega) \bigcup \operatorname{span}\{\phi_0^{\varepsilon,\mathrm{c}},\, \phi_j^{\varepsilon,l}, \quad 1 \leqslant j \leqslant N, \quad l \in \{\mathrm{c},\mathrm{s}\}\}.$$

In particular, we notice that the number of additional functions is equal to $2N+1$, that is the dimension of F_N. Indeed, as we will see in the proof of Theorem 3.4.6, adding a Lagrange multiplier allows to better solve the condition at the interface but also adds a term in the singular part when $\varepsilon \to 0$ and in the gradient jump at the $\partial\omega^\varepsilon$ interface. We can now introduce the discrete formulation: find $(\tilde{u}^\varepsilon_{N,h}, \tilde{\lambda}^\varepsilon_{N,h}) \in V^k_{N,h} \times F_N$ such that

$$\begin{cases} (\nabla \tilde{u}^\varepsilon_{N,h}, \nabla v_h)_\Omega - (\tilde{\lambda}^\varepsilon_{N,h}, v_h)_\varepsilon = (f, v_h)_\Omega \quad \forall v_h \in V^k_{N,h}, \\ (\mu_N, \tilde{u}^\varepsilon_{N,h})_\varepsilon = (\mu_N, u_{\mathrm{b}})_\varepsilon \quad \forall \mu_N \in F_N. \end{cases} \tag{3.4.25}$$

3.4.3.2 Inf-sup stability

In the augmented finite element space, we are able to derive an inf-sup condition uniformly independent of h, N and ε.

Lemma 3.4.5. *There exists $\mathbb{R} \ni \beta > 0$ uniformly independent of h, N and ε such that for all $\lambda_N \in F_N$,*

$$\sup_{v_h \in V^k_{N,h}} \frac{(\lambda_N, v_h)_\varepsilon}{\|v_h\|_{1,\Omega}} \geqslant \beta \|\lambda_N\|_{-\frac{1}{2},\varepsilon}.$$

Proof. We introduce the functions $\tilde{\phi}^{\varepsilon,l}_j$ solutions of Problem (3.3.2) with

$$\eta(\varepsilon)(\theta) = \cos(j\theta) \quad l = \mathrm{c}, \quad \eta(\varepsilon)(\theta) = \sin(j\theta) \quad l = \mathrm{s}.$$

These functions satisfy in particular $\phi^{\varepsilon,l}_j = \chi(r)\tilde{\phi}^{\varepsilon,l}_j$. Using definition (3.2.4) of the norm $\|\cdot\|_{-\frac{1}{2},\varepsilon}$, we have

$$\|\lambda_N\|_{-\frac{1}{2},\varepsilon} = \sup_{\mu \in H^{\frac{1}{2}}(\partial\omega^\varepsilon)} \frac{(\lambda_N, \mu)_\varepsilon}{\|\mu\|_{\frac{1}{2},\varepsilon}} \quad \forall \lambda_N \in F_N.$$

For a given $\mu \in H^{\frac{1}{2}}(\partial\omega^\varepsilon)$, we define $\tilde{v}^\varepsilon_{N,\mu} \in H^1_0(\Omega)$ and $v^\varepsilon_{N,\mu} \in V^k_{N,h}$ by

$$\tilde{v}^\varepsilon_{N,\mu} \overset{\text{def}}{=} \mathscr{F}^{\mathrm{c}}_0 \mu(\varepsilon)\tilde{\phi}^{\varepsilon,\mathrm{c}}_0 + \sum_{j=1}^{N} \mathscr{F}^{\mathrm{c}}_j \mu(\varepsilon)\tilde{\phi}^{\varepsilon,\mathrm{c}}_j + \mathscr{F}^{\mathrm{s}}_j \mu(\varepsilon)\tilde{\phi}^{\varepsilon,\mathrm{s}}_j, \quad v^\varepsilon_{N,\mu} \overset{\text{def}}{=} \chi(r)\tilde{v}^\varepsilon_{N,\mu}.$$

By linearity, $\tilde{v}^\varepsilon_{N,\mu}$ is solution of Problem (3.3.2) with $\eta = \Pi^\varepsilon_N \mu$, so according to Lemma 3.3.3 and by continuity of Π^ε_N on $(H^{\frac{1}{2}}(\partial\omega^\varepsilon), \|\cdot\|_{\frac{1}{2},\varepsilon})$, we have

$$\|\tilde{v}^\varepsilon_{N,\mu}\|_{1,\Omega} \lesssim \|\Pi^\varepsilon_N \mu\|_{\frac{1}{2},\varepsilon} \lesssim \|\mu\|_{\frac{1}{2},\varepsilon}.$$

Consequently, we also have $v^\varepsilon_{N,\mu} = \tilde{v}^\varepsilon_{N,\mu} = \Pi^\varepsilon_N(\mu)$ on $\partial\omega^\varepsilon$ and

$$\|v^\varepsilon_{N,\mu}\|_{1,\Omega} \lesssim \|\tilde{v}^\varepsilon_{N,\mu}\|_{1,\Omega} \leqslant \beta \|\mu\|_{\frac{1}{2},\varepsilon}.$$

with $\beta > 0$ uniformly independent of N, ε and h. Finally, we obtain

$$\frac{(\lambda,\mu)_\varepsilon}{\|\mu\|_{\frac{1}{2},\varepsilon}} = \frac{(\lambda,\Pi_\varepsilon^N\mu)_\varepsilon}{\|\mu\|_{\frac{1}{2},\varepsilon}} \leqslant \beta^{-1}\frac{(\lambda,v_{N,\mu}^\varepsilon)_\varepsilon}{\|v_{N,\mu}^\varepsilon\|_{1,\Omega}} \leqslant \beta^{-1}\sup_{v_h\in V_{N,h}^k}\frac{(\lambda,v_h)_\varepsilon}{\|v_h\|_{1,\Omega}} \quad \forall \mu \in H^{\frac{1}{2}}(\partial\omega^\varepsilon).$$

Taking the supremum over $\mu \in H^{\frac{1}{2}}(\partial\omega^\varepsilon)$ gives the result. □

3.4.3.3 Approximation properties and convergence

To conclude this section, we give an estimate of the approximation error for the augmented finite element method.

Theorem 3.4.6. *Let $k \in \mathbb{N}^*$. We assume that f belongs to $H^{k-1}(\Omega)$. Let $(u_N^\varepsilon, \lambda_N^\varepsilon)$ be the solution of problem* (3.1.3) *and $(\tilde{u}_{N,h}^\varepsilon, \tilde{\lambda}_{N,h}^\varepsilon)$ be the solution of problem* (3.4.25)*. Then, we have*

$$\|u_N^\varepsilon - \tilde{u}_{N,h}^\varepsilon\|_{1,\Omega} + \|\lambda_N^\varepsilon - \tilde{\lambda}_{N,h}^\varepsilon\|_{-\frac{1}{2},\varepsilon} \lesssim |\log(\varepsilon)|^{\frac{1}{2}} h^k \left(\|f\|_{k-1,\Omega} + \|u_{\mathrm{b}}\|_{\frac{1}{2},\varepsilon}\right). \tag{3.4.26}$$

If we compare the result given by our theorem to the approximation properties of the original and stabilized schemes presented in Section 3.4.2.3, we see that the augmented finite element method overcomes the previous limitations of sub-optimal convergence. In addition, if we gather the estimate (3.3.10) of the error $u^\varepsilon - u_N^\varepsilon$ coming from the model reduction and the estimate (3.4.26) of the error $u_N^\varepsilon - \tilde{u}_{N,h}^\varepsilon$ coming from the numerical approximation, we get this estimate for the global error:

$$\|u^\varepsilon - \tilde{u}_{N,h}^\varepsilon\|_{1,\Omega} + \varepsilon\|\lambda^\varepsilon - \varepsilon^{-1}\lambda_{N,h}^\varepsilon\|_{-\frac{1}{2},\varepsilon} \lesssim \left(\varepsilon^{N+1} + |\log(\varepsilon)|^{\frac{1}{2}}h^k\right)\left(\|f\|_{k-1,\Omega} + \|u_{\mathrm{b}}\|_{\frac{1}{2},\varepsilon}\right).$$

This estimate shows that, h and ε being fixed, it is possible to reach a given convergence order by adjusting the parameters of the method k and N.

Proof of Theorem 3.4.6. Since, for all $j \geqslant 0$ and $l \in \{\mathrm{c},\mathrm{s}\}$, $\phi_j^{\varepsilon,l}$ belongs to $H_0^1(\Omega)$, the enrichment of the space V_h^k preserves the coercivity condition. Moreover, according to Lemma 3.4.5, the inf-sup condition is satisfied for the spaces $V_{N,h}^k$ and F_N. So, applying the general theory on discrete saddle point problem presented in (3.4.7) we have

$$\|u_N^\varepsilon - \tilde{u}_{N,h}^\varepsilon\|_{1,\Omega} + \|\lambda_N^\varepsilon - \tilde{\lambda}_{N,h}^\varepsilon\|_{-\frac{1}{2},\varepsilon} \lesssim |\log(\varepsilon)|^{\frac{1}{2}} \inf_{w_h\in V_{N,h}^k}\|u_N^\varepsilon - w_h\|_{1,\Omega}. \tag{3.4.27}$$

As mentioned previously, the enrichment of the standard finite element space V_h^k by $V_{N,h}^k$ will allow to get a better approximation of u_N^ε by providing a better estimate of the singular

part of u_N^ε. To highlight this feature, we use (3.3.20) and write u_N^ε as the sum of a regular part $u_{N,\mathrm{R}}^\varepsilon$ and a singular part $u_{N,\mathrm{S}}^\varepsilon$ defined respectively by:

$$u_{N,\mathrm{R}}^\varepsilon(r,\theta) \stackrel{\text{def}}{=} \mathscr{F}_0^{\mathrm{c}} u_N^\varepsilon(\rho) + \sum_{j=1}^{\infty} \left(\frac{r}{\rho}\right)^j \left(\mathscr{F}_j^{\mathrm{c}} u_N^\varepsilon(\rho)\cos(j\theta) + \mathscr{F}_j^{\mathrm{s}} u_N^\varepsilon(\rho)\sin(j\theta)\right)$$

for all $(r,\theta) \in [0,\rho] \times (0,2\pi)$ and

$$\begin{aligned}
u_{N,\mathrm{S}}^\varepsilon(r,\theta) \stackrel{\text{def}}{=} \Bigg(& - \mathscr{F}_0^{\mathrm{c}} u_N^\varepsilon(\rho) \frac{\log(r/\rho)}{\log(\varepsilon/\rho)} + \mathscr{F}_0^{\mathrm{c}} u_{\mathrm{b}}(\varepsilon) \frac{\log(r/\rho)}{\log(\varepsilon/\rho)} \\
& - \sum_{j=1}^{N} \left(\frac{\varepsilon}{\rho}\right)^j \frac{(r/\rho)^j - (\rho/r)^j}{(\varepsilon/\rho)^j - (\rho/\varepsilon)^j} \left(\mathscr{F}_j^{\mathrm{c}} u_N^\varepsilon(\rho)\cos(j\theta) + \mathscr{F}_j^{\mathrm{s}} u_N^\varepsilon(\rho)\sin(j\theta)\right) \\
& + \sum_{j=1}^{N} \frac{(r/\rho)^j - (\rho/r)^j}{(\varepsilon/\rho)^j - (\rho/\varepsilon)^j} \left(\mathscr{F}_j^{\mathrm{c}} u_{\mathrm{b}}(\varepsilon)\cos(j\theta) + \mathscr{F}_j^{\mathrm{s}} u_{\mathrm{b}}(\varepsilon)\sin(j\theta)\right) \Bigg) \mathbb{1}_{r \geqslant \varepsilon} \\
& + \Bigg(- \mathscr{F}_0^{\mathrm{c}} u_N^\varepsilon(\rho) - \sum_{j=1}^{N} \left(\frac{r}{\rho}\right)^j \left(\mathscr{F}_j^{\mathrm{c}} u_N^\varepsilon(\rho)\cos(j\theta) + \mathscr{F}_j^{\mathrm{s}} u_N^\varepsilon(\rho)\sin(j\theta)\right) \\
& + \mathscr{F}_0^{\mathrm{c}} u_{\mathrm{b}}(\varepsilon) + \sum_{j=1}^{N} \left(\frac{r}{\varepsilon}\right)^j \left(\mathscr{F}_j^{\mathrm{c}} u_{\mathrm{b}}(\varepsilon)\cos(j\theta) + \mathscr{F}_j^{\mathrm{s}} u_{\mathrm{b}}(\varepsilon)\sin(j\theta)\right) \Bigg) \mathbb{1}_{r < \varepsilon}
\end{aligned}$$

for all $(r,\theta) \in [0,\rho] \times (0,2\pi)$. The functions $u_{N,\mathrm{R}}^\varepsilon$ and $u_{N,\mathrm{S}}^\varepsilon$ belong to $H^1(\Omega)$ and, according to (3.3.20), we have $u_N^\varepsilon = u_{N,\mathrm{R}}^\varepsilon + u_{N,\mathrm{S}}^\varepsilon$ in ω_ρ, which leads in particular to

$$\chi u_N^\varepsilon = \chi u_{N,\mathrm{R}}^\varepsilon + \chi u_{N,\mathrm{S}}^\varepsilon \quad \text{in} \quad \Omega.$$

Let us now prove that the truncated singular part belongs to the approximation space, that

is that $\chi u^\varepsilon_{N,\mathrm{S}}$ belongs to $V^k_{N,h}$. First, we notice that, by definition of the $\phi^{\varepsilon,l}_j$, we have

$$\begin{aligned}
&\chi(r)\big(-\mathscr{F}^{\mathrm{c}}_0 u^\varepsilon_N(\rho)+\mathscr{F}^{\mathrm{c}}_0 u_{\mathrm{b}}(\varepsilon)\big)\left(\frac{\log(r/\rho)}{\log(\varepsilon/\rho)}\mathbb{1}_{r\geqslant\varepsilon}+\mathbb{1}_{r<\varepsilon}\right)=\\
&\qquad\qquad\big(-\mathscr{F}^{\mathrm{c}}_0 u^\varepsilon_N(\rho)+\mathscr{F}^{\mathrm{c}}_0 u_{\mathrm{b}}(\varepsilon)\big)\phi^{\varepsilon,\mathrm{c}}_0(r,\theta),\\
&\chi(r)\left(-\mathscr{F}^{\mathrm{c}}_0 u^\varepsilon_N(\rho)\left(\frac{\varepsilon}{\rho}\right)^j+\mathscr{F}^{\mathrm{c}}_j u_{\mathrm{b}}(\varepsilon)\right)\\
&\qquad\left(\frac{(r/\rho)^j-(\rho/r)^j}{(\varepsilon/\rho)^j-(\rho/\varepsilon)^j}\mathbb{1}_{r\geqslant\varepsilon}+\left(\frac{r}{\varepsilon}\right)^j\mathbb{1}_{r<\varepsilon}\right)\cos(j\theta)\\
&\qquad\qquad=\left(-\mathscr{F}^{\mathrm{c}}_0 u^\varepsilon_N(\rho)\left(\frac{\varepsilon}{\rho}\right)^j+\mathscr{F}^{\mathrm{c}}_j u_{\mathrm{b}}(\varepsilon)\right)\phi^{\varepsilon,\mathrm{c}}_j,\\
&\chi(r)\left(-\mathscr{F}^{\mathrm{s}}_0 u^\varepsilon_N(\rho)\left(\frac{\varepsilon}{\rho}\right)^j+\mathscr{F}^{\mathrm{s}}_j u_{\mathrm{b}}(\varepsilon)\right)\\
&\qquad\left(\frac{(r/\rho)^j-(\rho/r)^j}{(\varepsilon/\rho)^j-(\rho/\varepsilon)^j}\mathbb{1}_{r\geqslant\varepsilon}+\left(\frac{r}{\varepsilon}\right)^j\mathbb{1}_{r<\varepsilon}\right)\sin(j\theta)\\
&\qquad\qquad=\left(-\mathscr{F}^{\mathrm{s}}_0 u^\varepsilon_N(\rho)\left(\frac{\varepsilon}{\rho}\right)^j+\mathscr{F}^{\mathrm{s}}_j u_{\mathrm{b}}(\varepsilon)\right)\phi^{\varepsilon,\mathrm{s}}_j.
\end{aligned}$$

We deduce that

$$\begin{aligned}
\chi(r)u^\varepsilon_{N,\mathrm{S}}(r,\theta)=&(-\mathscr{F}^{\mathrm{c}}_0 u^\varepsilon_N(\rho)+\mathscr{F}^{\mathrm{c}}_0 u_{\mathrm{b}}(\varepsilon))\phi^{\varepsilon,\mathrm{c}}_0(r,\theta)\\
&+\sum_{j=1}^N\big(-\mathscr{F}^{\mathrm{c}}_j u^\varepsilon_N(\rho)\left(\frac{\varepsilon}{\rho}\right)^j+\mathscr{F}^{\mathrm{c}}_j u_{\mathrm{b}}(\varepsilon)\big)\phi^{\varepsilon,\mathrm{c}}_j(r,\theta)\\
&+\sum_{j=1}^N\big(-\mathscr{F}^{\mathrm{s}}_j u^\varepsilon_N(\rho)\left(\frac{\varepsilon}{\rho}\right)^j+\mathscr{F}^{\mathrm{s}}_j u_{\mathrm{b}}(\varepsilon)\big)\phi^{\varepsilon,\mathrm{s}}_j(r,\theta)
\end{aligned}$$

for all $(r,\theta)\in\mathbb{R}^+\times(0,2\pi)$, and thus we get that $\chi u^\varepsilon_{N,\mathrm{S}}\in X^k_{N,h}(\Omega)$. Therefore, for the right hand side of (3.4.27), we have in particular

$$\inf_{w_h\in V^k_{N,h}}\|u^\varepsilon_N-w_h\|_{1,\Omega}\leqslant\inf_{v_h\in V^k_h}\|u^\varepsilon_N-\chi u^\varepsilon_{N,\mathrm{S}}-v_h\|_{1,\Omega}.$$

Moreover, writing $u^\varepsilon_N=\chi u^\varepsilon_N+(1-\chi)u^\varepsilon_N$, it comes

$$u^\varepsilon_N-\chi u^\varepsilon_{N,\mathrm{S}}=\chi u^\varepsilon_{N,\mathrm{R}}+(1-\chi)u^\varepsilon_N,$$

so that estimate (3.4.27) becomes

$$\|u_N^\varepsilon - \tilde{u}_{N,h}^\varepsilon\|_{1,\Omega} + \|\lambda_N^\varepsilon - \tilde{\lambda}_{N,h}^\varepsilon\|_{-\frac{1}{2},\varepsilon} \lesssim |\log(\varepsilon)|^{\frac{1}{2}} \inf_{v_h \in V_h^k} \|\chi u_{N,\mathrm{R}}^\varepsilon + (1-\chi)u_N^\varepsilon - v_h\|_{1,\Omega}. \quad (3.4.28)$$

It is now sufficient to prove that the function $\chi u_{N,\mathrm{R}}^\varepsilon + (1-\chi)u_N^\varepsilon$ is well estimated by the elements of V_h^k. To do this, we will prove that this function belongs to $H^{k+1}(\Omega)$. First, since $u_{N,\mathrm{R}}^\varepsilon$ is an harmonic function, thanks to the interior regularizing property of elliptic operators (we refer to [Evans, 1998]), we have

$$\begin{aligned}\|u_{N,\mathrm{R}}^\varepsilon\|_{k+1,\omega^{3\rho/4}}^2 &\lesssim \|u_{N,\mathrm{R}}^\varepsilon\|_{\omega^\rho}^2 \lesssim |\mathscr{F}_0^{\mathrm{c}} u_N^\varepsilon(\rho)|^2 + \sum_{j=1}^{\infty} |\mathscr{F}_j^{\mathrm{c}} u_N^\varepsilon(\rho)|^2 + |\mathscr{F}_j^{\mathrm{s}} u_N^\varepsilon(\rho)|^2 \\ &\lesssim \|u_N^\varepsilon\|_{\omega^\rho}^2 \lesssim \|u_{\mathrm{b}}\|_{\frac{1}{2},\varepsilon}^2 + \|f\|_\Omega^2\end{aligned}$$

thanks to Theorem 3.3.1. Thus, by definition of χ, we get that $\chi u_{N,\mathrm{R}}^\varepsilon$ belongs to $H^{k+1}(\Omega)$ and we have

$$\|\chi u_{N,\mathrm{R}}^\varepsilon\|_{k+1,\Omega} \lesssim \|u_{\mathrm{b}}\|_{\frac{1}{2},\varepsilon} + \|f\|_\Omega.$$

Moreover, since u_N^ε satisfies $-\Delta u_N^\varepsilon = f$ in Ω^ε and $u_N^\varepsilon = 0$ on $\partial\Omega$ and since $\Omega\backslash\omega^{\rho/2}$ is relatively compact in $\Omega^\varepsilon \cup \partial\Omega$, the regularizing property of elliptic problems (we also refer to [Evans, 1998] for this result) implies that u_N^ε belongs to $H^{k+1}(\Omega\backslash\omega_{\rho/2})$ and we have

$$\|u_N^\varepsilon\|_{k+1,\Omega\backslash\omega_{\rho/2}} \lesssim \|u_N^\varepsilon\|_{\Omega\backslash\omega_{\rho/2}} + \|f\|_{k-1,\Omega} \lesssim \|u_{\mathrm{b}}\|_{\frac{1}{2},\varepsilon} + \|f\|_{k-1,\Omega}$$

This implies that $(1-\chi)u_N^\varepsilon$ belongs to $H^{k+1}(\Omega)$ and we have

$$\|(1-\chi)u_N^\varepsilon\|_{k+1,\Omega} \lesssim \|u_{\mathrm{b}}\|_{\frac{1}{2},\varepsilon} + \|f\|_{k-1,\Omega}.$$

Gathering these results, we deduce that $\chi u_{N,\mathrm{R}}^\varepsilon + (1-\chi)u_N^\varepsilon$ belongs to $H^{k+1}(\Omega)$ and

$$\|\chi u_{N,\mathrm{R}}^\varepsilon + (1-\chi)u_N^\varepsilon\|_{k+1,\Omega} \lesssim \|u_{\mathrm{b}}\|_{\frac{1}{2},\varepsilon} + \|f\|_{k-1,\Omega}.$$

By this way, using interpolation estimates for the finite element space V_h^k in $H^{k+1}(\Omega)$, (3.4.28) becomes

$$\|u_N^\varepsilon - \tilde{u}_{N,h}^\varepsilon\|_{1,\Omega} + \|\lambda_N^\varepsilon - \tilde{\lambda}_{N,h}^\varepsilon\|_{-\frac{1}{2},\varepsilon} \lesssim |\log(\varepsilon)|^{\frac{1}{2}} h^k \|\chi u_{N,\mathrm{R}}^\varepsilon + (1-\chi)u_N^\varepsilon\|_{k+1,\Omega}$$

and thus we get (3.4.26). □

Remark 12. Let us notice that the use of an enriched finite element space enables to significantly mitigates the adverse effects stemming from small values of ε and to reach any order of convergence in h. This is first made possible by getting an inf-sup condition uniformly independent of ε and h, but also by the fact that the singular part of the solution

u_N^ε is only in the first Fourier modes, and is therefore well captured by the enrichment functions. Eventually, we see that the estimate of Theorem 3.3.1 requires only a regularity in $H^{\frac{1}{2}}(\partial\omega^\varepsilon)$ for u_{b}. This assumption, which may seem rather weak, is due to the fact that thanks to the enrichment of the finite element space the convergence analysis of the scheme only relies on the regularity of the solution away from the inclusion.

3.5 Numerical experiments

Following the main results of this work, we divide this section in two parts. First, we analyze the behavior of the error due to the reduced order boundary conditions, referring to this part as the convergence in ε. We perform numerical tests to illustrate that the properties stated in Theorem 3.3.4 are actually observed in practice. Second, we analyze the approximation properties of the reduced order problem discretized by the finite element method, using both the standard formulation and the augmented formulation. The numerical tests shown in the second section address the error analysis with respect to the space discretization parameter h and complement the analysis shown in Section 3.4.

3.5.1 Convergence in ε

In this section we first analyze the case of a single inclusion, for which a rigorous analysis has been presented here. However, as mentioned in the introduction, the proposed approach can be easily extended to several obstacles of different sizes. The behavior of our method in this case is addressed in the second paragraph of this section. Finally, in the third part of this section, for the case of multiple inclusions, we analyze the effect of the distance between inclusions, an essential consideration across various applications.

3.5.1.1 Single inclusion

We consider a square domain $\Omega = (-0.5, 0.5) \times (-0.5, 0.5)$ with an inclusion located at $(0.2, 0.1)$ and we make ε vary in the set $\{0.05, 0.04, 0.03, 0.02, 0.01\}$. On the external boundary $\partial\Omega$, we impose non homogeneous Dirichlet boundary conditions presented in Figure 3.2. Although our mathematical study focus on homogeneous Dirichlet boundary conditions, the results of the previous sections remain valid in this more general case. As for the inclusion, we set $u_{\mathrm{b}} = 0$. To illustrate Theorem 3.3.4, we compute the convergence rate with respect to ε of the reduced order problem towards the full order problem for increasing values of N in the definition of F_N. In the general case, the continuous solutions are not known a priori. Therefore, we compute the linear finite element approximation of the reduced and full order problems for a conforming mesh (defined as δ-resolving mesh in Remark 11) with h small enough ($h \approx 10^{-3}$) in order to have a negligible discretization error in comparison with the model reduction error. The convergence curves are given in Figure 3.3. They represent the H^1-norms of the difference $e_{N,h}^\varepsilon \overset{\text{def}}{=} u_{N,h}^\varepsilon - u_h^\varepsilon$ between

the discrete solutions of the full order problem and the reduced order problem for $N = 0$, 1 and 2 modes. If we compare the slopes of the error curves with the expected slopes (represented by the black lines), we notice that the match between theory and observations is very satisfactory. The numerical solution of the reduced order problem and the magnitude of the errors $e^{\varepsilon}_{0,h}$, $e^{\varepsilon}_{1,h}$ and $e^{\varepsilon}_{2,h}$ for $\varepsilon = 0.05$ are reported in Figure 3.4.

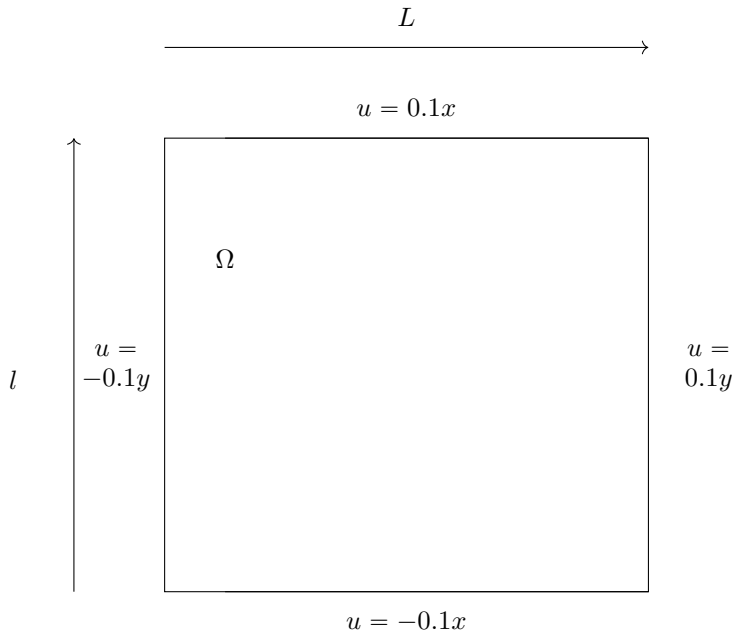

Figure 3.2: *Boundary conditions for the square domain.*

3.5.1.2 Multiple inclusions

We consider a square domain $\Omega = (-0.5, 0.5) \times (-0.5, 0.5)$ with four inclusions positioned respectively in $(0.2, 0.1)$, $(-0.3, 0.1)$, $(-0.2, 0.2)$, $(0.1, -0.2)$ and of sizes 0.05, 0.04, 0.06 and 0.03. As in the previous tests, the boundary conditions on $\partial\Omega$ are described by Figure 3.2 and $u_{\mathrm{b}} = 0$ on the inclusions. The results obtained for $N = 0$, 1 and 2 are reported in Figure 3.5. There, the parameter ε corresponds to the size of the first inclusion and all the other inclusions are scaled proportionally. Again, we can notice that the convergence rates coincide with the expected ones. The numerical solution of the reduced order problem and the errors $e^{\varepsilon}_{0,h}$, $e^{\varepsilon}_{1,h}$ and $e^{\varepsilon}_{2,h}$ are reported in Figure 3.6.

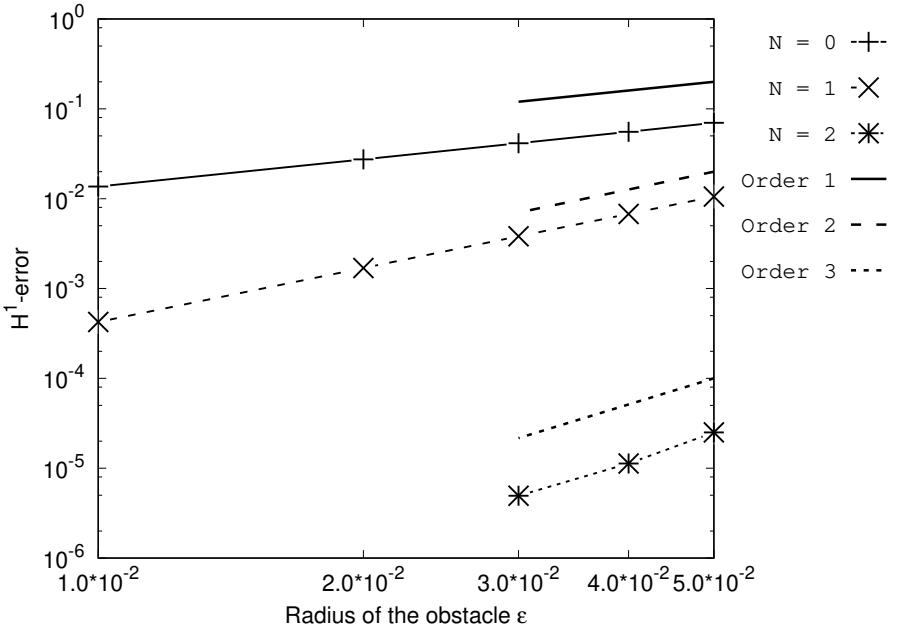

Figure 3.3: *Modelling error with respect to the radius ε for different values of modes N in the case of a single inclusion.*

3.5.1.3 Behavior of the model error for close obstacles

We consider here a test case to illustrate the behavior of the method when obstacles are close to each other. The domain is the same as in the previous sections and we consider uniform Dirichlet boundary conditions equal to 1 and two inclusions of radius 0.05 initially centered in $(-0.1, 0)$ and $(0.1, 0)$. The boundary values imposed on each inclusion are respectively 0.5 and 1.5 and are enforced with $N \in \{0, 1, 2\}$ modes. The numerical solution of such problem is given in Figure 3.7 panel (a). Then, the distance between the two inclusions is gradually reduced. The numerical solution with inclusions separated by a distance of 0.01 is shown in panel (b). The comparison of the two top panels shows that the solution in the circle deviates from the constant as the two inclusions get closer. More quantitative results are given in Figure 3.7 panel (c). We see that the model error increases as the distance between the two obstacles decreases, as expected with the inverse dependence on ρ in the estimate presented in Theorem 3.3.4. We also notice that this effect becomes more pronounced as the number of modes increases.

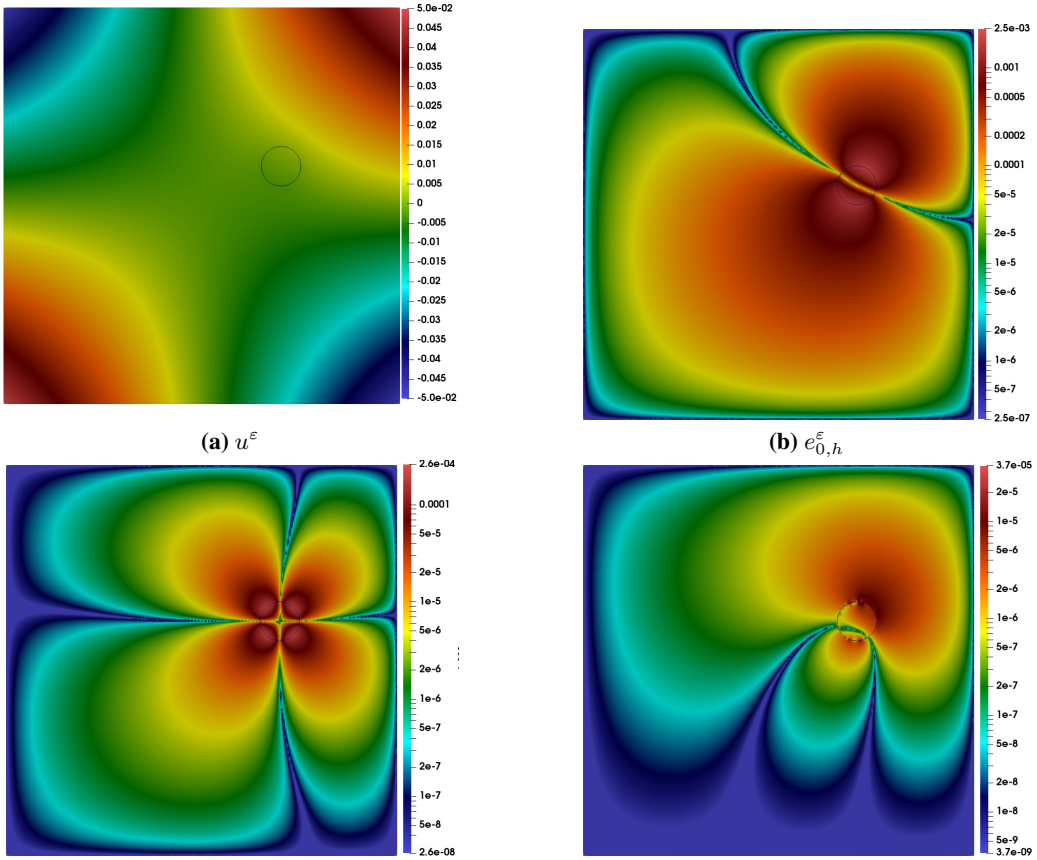

(a) u^ε **(b)** $e^\varepsilon_{0,h}$

(c) $e^\varepsilon_{1,h}$ **(d)** $e^\varepsilon_{2,h}$

Figure 3.4: *Contour plots of the solution u^ε and the magnitude of the discrete model errors $e^\varepsilon_{0,h}$, $e^\varepsilon_{1,h}$ and $e^\varepsilon_{2,h}$ on a log-scale axis for an inclusion of radius $\varepsilon = 0.05$.*

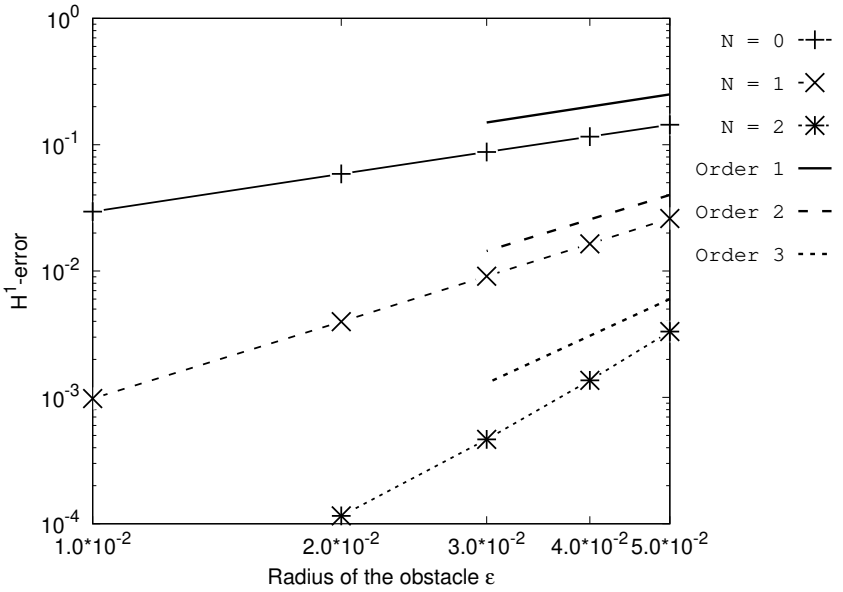

Figure 3.5: *The modelling error with respect to the radius of four inclusions for different values of N.*

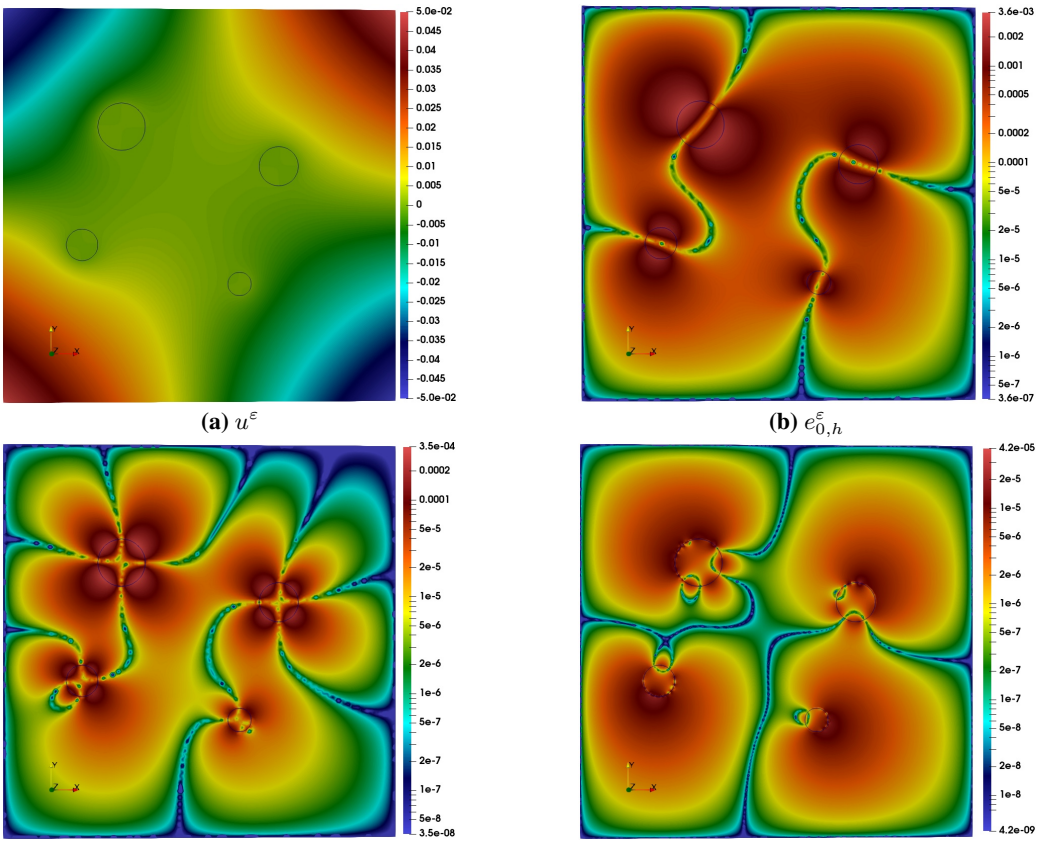

(a) u^ε **(b)** $e^\varepsilon_{0,h}$

(c) $e^\varepsilon_{1,h}$ **(d)** $e^\varepsilon_{2,h}$

Figure 3.6: *Contour plots of the solution u^ε and of the discrete model errors $e^\varepsilon_{0,h}$, $e^\varepsilon_{1,h}$ and $e^\varepsilon_{2,h}$ on a log-scale axis for multiple obstacles of radius $\varepsilon = 0.05$.*

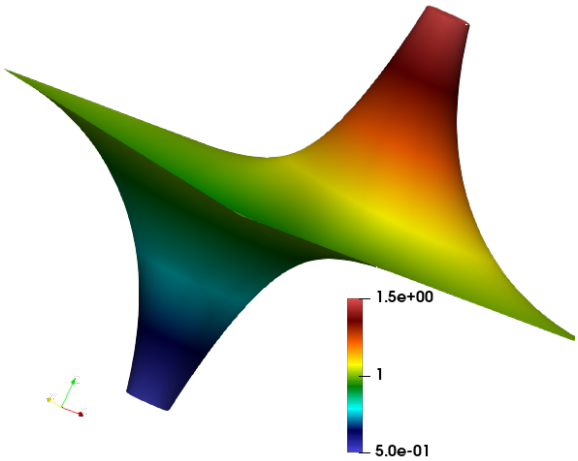

(a) *Distance between the obstacles equal to 0.2.*

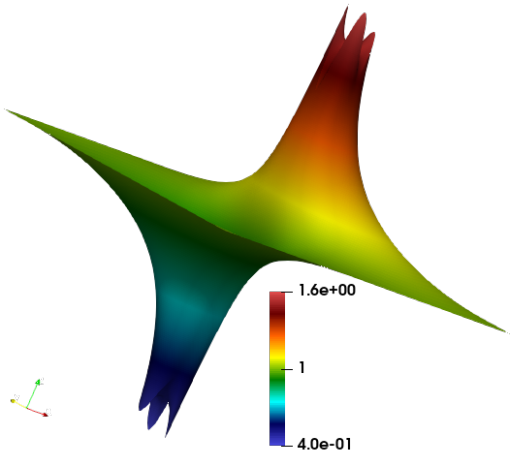

(b) *Distance between the obstacles equal to 0.12.*

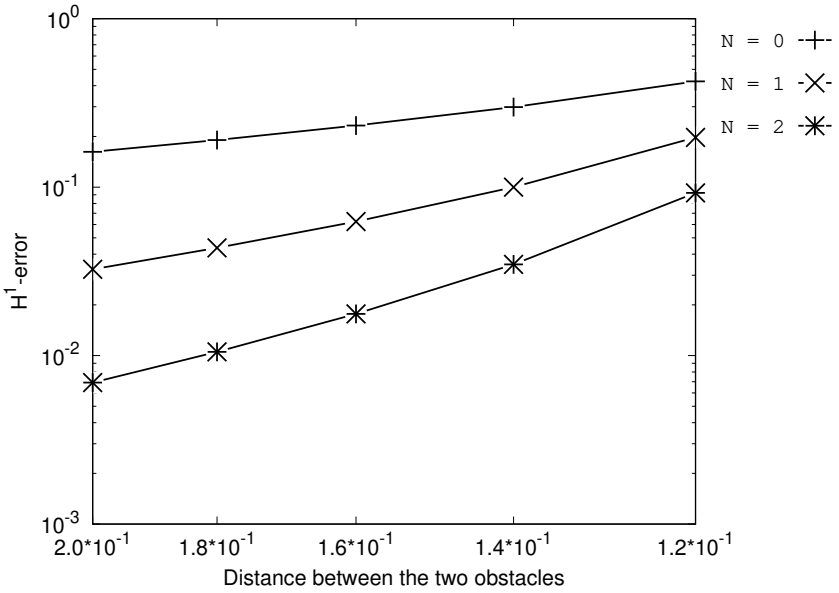

(c) *Evolution of the error with respect to the distance between the obstacles.*

Figure 3.7: *Effect of the inter-inclusions distance on the model error. By comparing panels (a) and (b) we see that the approximation of the solution at the interior boundary worsens when the centers of the inclusions approach. In panel (c) we see the variation of the model error when the distance between the inclusions progressively changes.*

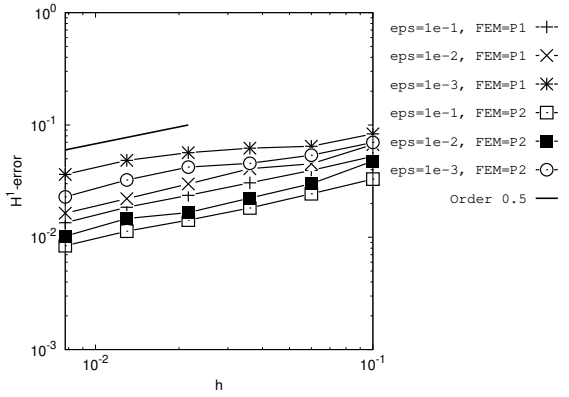

(a) H^1 *rel. err.* $u^{\varepsilon}_{N,h}$, $N = 0$, *non-augmented FEM.*

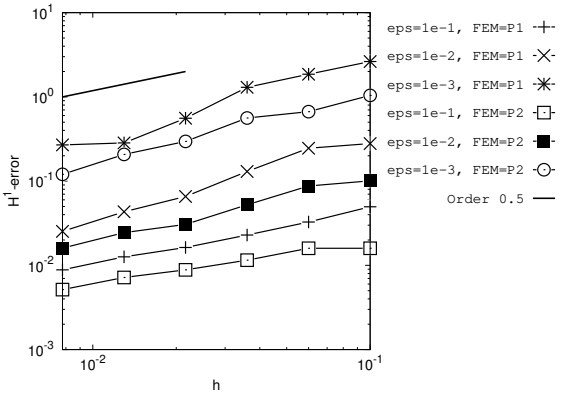

(b) H^1 *rel. err.* $u^{\varepsilon}_{N,h}$, $N = 1$, *non-augmented FEM.*

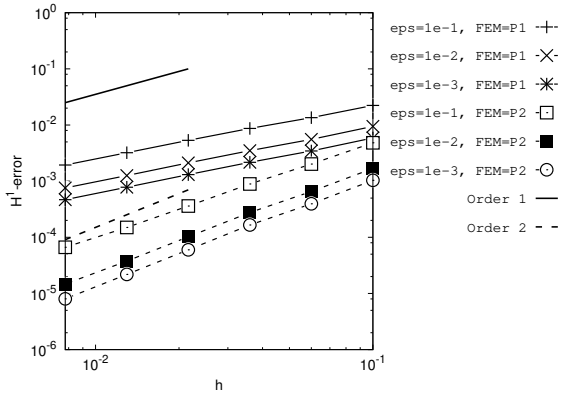

(c) H^1 *rel. err.* $u^{\varepsilon}_{N,h}$, $N = 0$, *augmented FEM.*

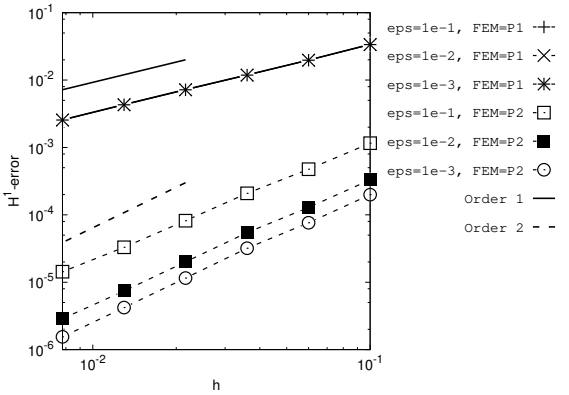

(d) H^1 *rel. err.* $u^{\varepsilon}_{N,h}$, $N = 1$, *augmented FEM.*

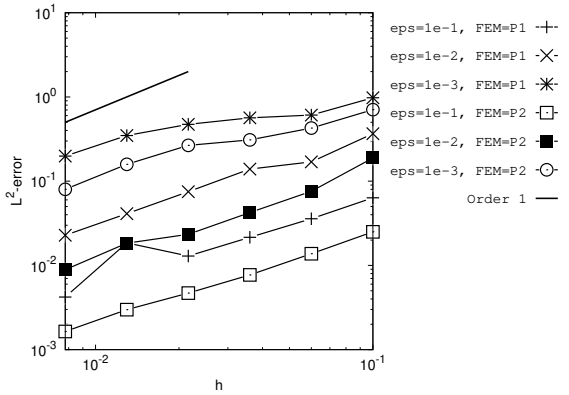

(e) L^2 *rel. err.* $\lambda^{\varepsilon}_{N,h}$, $N = 0$, *non-augmented FEM.*

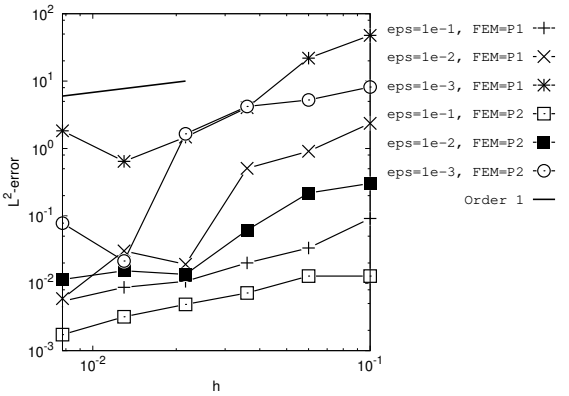

(f) L^2 *rel. err.* $\lambda^{\varepsilon}_{N,h}$, $N = 1$, *non-augmented FEM.*

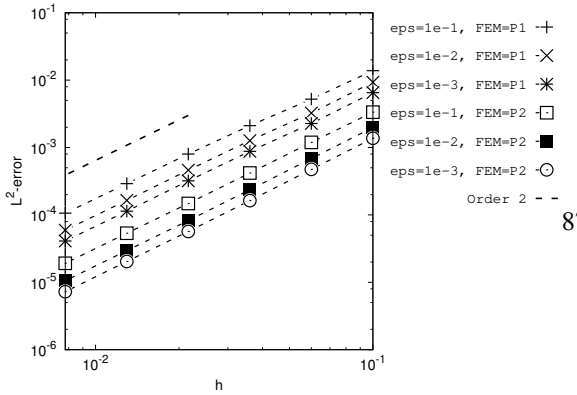

(g) L^2 *rel. err.* $\lambda^{\varepsilon}_{N,h}$, $N = 0$, *augmented FEM.*

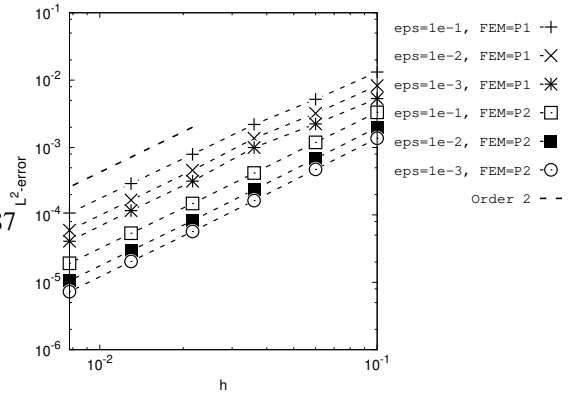

(h) L^2 *rel. err.* $\lambda^{\varepsilon}_{N,h}$, $N = 1$, *augmented FEM.*

Figure 3.8: *Comparison of the numerical error for the finite element method without and with enrichment.*

3.5.2 Convergence in h

In this section, we illustrate the convergence results presented in (3.4.22) and (3.4.23) for the standard finite element method without stabilization and by Theorem 3.4.6 for the augmented finite element method. We consider a domain $\Omega = (-1.5, 1.5) \times (1.5, 1.5)$ and a single inclusion localized at $(0, 0)$, of radius $\varepsilon \in \{0.1, 0.01, 0.001\}$. Non homogeneous boundary conditions are applied on $\partial\omega^\varepsilon$. Specifically, referring to the continuous solution as u^e_ε, we consider

$$(\mu_N, u^e_\varepsilon)_\varepsilon = (\mu_N, u_{\mathrm{b}})_\varepsilon \quad \forall \mu_N \in F_N, \quad u_{\mathrm{b}} = 1 + \cos(\theta) + \sin(\theta).$$

By setting the appropriate Dirichlet boundary conditions, the continuous solution writes for $N = 0$,

$$\begin{cases} u^e_\varepsilon &= \begin{cases} 1 + \left(\dfrac{r}{\rho}\right)\cos(\theta) + \left(\dfrac{r}{\rho}\right)\sin(\theta) & r \leqslant \varepsilon, \\ \dfrac{\log(r/\rho)}{\log(\varepsilon/\rho)} + \left(\dfrac{r}{\rho}\right)\cos(\theta) + \left(\dfrac{r}{\rho}\right)\sin(\theta) & r > \varepsilon, \end{cases} \\ \lambda^e_\varepsilon &= \dfrac{1}{\varepsilon\log(\varepsilon/\rho)}, \end{cases}$$

and for $N = 1$,

$$u^\varepsilon_{\mathrm{e}} = \begin{cases} 1 + \left(\dfrac{r}{\varepsilon}\right)\cos(\theta) + \left(\dfrac{r}{\varepsilon}\right)\sin(\theta) + (\dfrac{r}{\rho})^2\cos(2\theta) + (\dfrac{r}{\rho})^2\sin(2\theta) & r \leqslant \varepsilon, \\ \dfrac{\log(r/\rho)}{\log(\varepsilon/\rho)} + \dfrac{(r/\rho) - (\rho/r)}{(\varepsilon/\rho) - (\rho/\varepsilon)}\cos(\theta) + \dfrac{(r/\rho) - (\rho/r)}{(\varepsilon/\rho) - (\rho/\varepsilon)}\sin(\theta) & \\ \qquad + \left(\dfrac{r}{\rho}\right)^2\cos(2\theta) + \left(\dfrac{r}{\rho}\right)^2\sin(2\theta) & r > \varepsilon, \end{cases}$$

$$\lambda^e_\varepsilon = \frac{1}{\varepsilon\log(\varepsilon/\rho)} + \left(\frac{(1/\rho) - (\rho/\varepsilon^2)}{(\varepsilon/\rho) - (\rho/\varepsilon)} - \frac{1}{\varepsilon}\right)\cos(\theta) + \left(\frac{(1/\rho) - (\rho/\varepsilon^2)}{(\varepsilon/\rho) - (\rho/\varepsilon)} - \frac{1}{\varepsilon}\right)\sin(\theta),$$

with $\rho = 0.4$. In what follows we analyze the relative error for the solution $u^\varepsilon_{N,h}$ in the H^1 and L^2 norms and for the Lagrange multiplier $\lambda^\varepsilon_{N,h}$ in the L^2 norm, namely

$$\frac{\|u^\varepsilon_N - u^\varepsilon_{N,h}\|_{H^1(\Omega)}}{\|u^\varepsilon_N\|_{H^1(\Omega)}}, \quad \frac{\|u^\varepsilon_N - u^\varepsilon_{N,h}\|_{L^2(\Omega)}}{\|u^\varepsilon_N\|_{L^2(\Omega)}}, \quad \frac{\|\lambda^\varepsilon_N - \lambda^\varepsilon_{N,h}\|_{L^2(\partial\omega^\varepsilon)}}{\|\lambda^\varepsilon_N\|_{L^2(\partial\omega^\varepsilon)}}.$$

The numerical results for the h-convergence of the reduced order method computed with the standard or augmented finite element method are compared in Figure 3.8. We focus our attention on two items: the convergence rate with respect to h and the influence of ε on the numerical error. For the first item, we test the two methods for linear (FEM-P1) and

quadratic (FEM-P2) finite elements, which correspond to different markers in each plot. For the second item, we use the parametrization of the exact solutions in ε to compute several numerical errors for $\varepsilon \in \{10^{-1}, 10^{-2}, 10^{-3}\}$. Again, each test is identified by a different marker in the plots. Also, in both cases we perform the error analysis for $N = 0$ (on the left column) and $N = 1$ (on the right column).

For the standard finite element formulation, we observe that independently of the choice of finite elements order, linear or quadratic, the convergence rate in the H^1-norm is limited to 0.5, due to the low regularity of the solution on the whole domain. We also observe that the scatter of the error curves with respect to ε is stronger in the case $N = 1$, as expected from estimate (3.4.22). Still in agreement with this estimate, we also observe that the numerical error increases when decreasing ε for a fixed value of h.

For the augmented finite element method, the situation changes completely, as predicted by (3.4.26), the optimal order of convergence is observed in all the numerical tests. For the H^1-norm of the solution, the theoretical order of convergence is almost exactly verified in the experiments. For the Lagrange multipliers, super-convergence is clearly observed for linear finite elements, but the theoretical rate is respected by the quadratic ones. . Finally, we observe that for the augmented finite element method the convergence error of the solution and of the Lagrange multipliers is not negatively affected by the size of the inclusion, namely ε. Quite the contrary, unlike what suggests estimate (3.4.26), we observe that the numerical error decreases with ε.

Conclusions

In this chapter, we considered a Poisson problem defined on a domain with small circular holes, subject to reduced order non homogeneous Dirichlet boundary conditions. This problem can be seen as a prototype problem for better understanding the application of mixed-dimensional coupling conditions in fluid-structure interaction applications (but also other applications involving domain with high dimensional gap such as fiber-reinforced materials [Khristenko et al., 2021]) where the small inclusions represent either particles (as in Chapter 4) or slender structures immersed into a fluid (as in Chapter 2). To address these challenging applications using computational models, a thorough mathematical understanding of the fundamental mathematical aspects of the problem is extremely useful. As highlighted in [Babuška et al., 2017], a mathematically-informed approach is a prerequisite for safe and reliable computations.

For these reasons, we focused on the fundamental aspects of the approximation of the problem. On one hand, we analysed the continuous problem built on the approximation of the Dirichlet boundary conditions on the inclusion by means of averaged operators (projection operators onto a Fourier-based finite-dimensional space). On the other hand, we studied the properties of the finite element method used for the approximation of the reduced order model.

By means of suitable a-priori estimates of the model error and of the finite element approximation error, we provided guidelines to optimally balance the approximation parameters of the proposed simplified modeling approach. In particular a crucial issue was to provide a good approximation strategy of the Lagrange multiplier so that these theoretical results could be useful for fluid-structure interaction problems.

3.A Appendix

3.A.1 Preliminary lemmas

In this section, we state several results that will be used in the next sections of the appendix for the proof of some lemmas used in this chapter. We recall that $\varepsilon \in (0, \varepsilon_{\max})$ where $\varepsilon_{\max}$ is the fixed parameter defined by $\varepsilon_{\max} = \sup\{\varepsilon > 0 \mid \overline{\omega^\varepsilon} \subset \Omega\}$. The first two Lemmas and their proof are drawn from [Caubet et al., 2016, Lemma C.1, Lemma C.3] for the Stokes equations, themselves based on the results presented in [Sid Idris, 2001, Chapter 3].

Lemma 3.A.1. *For $\varphi \in H^{\frac{1}{2}}(\partial\Omega)$, the following problem*

$$\begin{cases} -\Delta v^\varepsilon = 0 & \text{in} \quad \Omega^\varepsilon, \\ v^\varepsilon = \varphi & \text{on} \quad \partial\Omega, \\ v^\varepsilon = 0 & \text{on} \quad \partial\omega^\varepsilon, \end{cases} \tag{3.A.1}$$

admits a unique weak solution in $H^1(\Omega^\varepsilon)$. Moreover,

$$\|v^\varepsilon\|_{1,\Omega^\varepsilon} \lesssim \|\varphi\|_{\frac{1}{2},\partial\Omega}.$$

Proof of Lemma 3.A.1. We consider $v^{\varepsilon_{\max}}$ the solution of (3.A.1) for $\varepsilon = \varepsilon_{\max}$. It satisfies

$$|v^{\varepsilon_{\max}}|_{1,\Omega^{\varepsilon_{\max}}} = \left(\int_{\Omega^{\varepsilon_{\max}}} |\nabla v^{\varepsilon_{\max}}|^2\right)^{\frac{1}{2}} \lesssim \|\varphi\|_{\frac{1}{2},\partial\Omega}. \tag{3.A.2}$$

Now consider $\tilde{v}^{\varepsilon_{\max}} \in H^1(\Omega)$ the extension by 0 of $v^{\varepsilon_{\max}}$ to all Ω. Notice that since $\varepsilon < \varepsilon_{\max}$, $\omega^\varepsilon \subset \omega^{\varepsilon_{max}}$ and $\Omega^{\varepsilon_{\max}} \subset \Omega^\varepsilon$, so, by minimization of energy, we have

$$|v^\varepsilon|_{1,\Omega^\varepsilon} \leqslant |\tilde{v}^{\varepsilon_{\max}}|_{1,\Omega^\varepsilon} = |v^{\varepsilon_{\max}}|_{1,\Omega^{\varepsilon_{\max}}},$$

and thanks to equation (3.A.2),

$$|v^\varepsilon|_{1,\Omega^\varepsilon} \lesssim \|\varphi\|_{\frac{1}{2},\partial\Omega}. \tag{3.A.3}$$

Let u^0 be the solution of the problem (3.2.1). Denoting by $\tilde{v}^\varepsilon$ the extension of v^ε to all Ω, since $\tilde{v}^\varepsilon - u^0 \in H_0^1(\Omega)$, we can apply the Poincaré inequality to get

$$\|v^\varepsilon\|_{\Omega^\varepsilon} = \|\tilde{v}^\varepsilon\|_\Omega \leqslant \|\tilde{v}^\varepsilon - u^0\|_\Omega + \|u^0\|_\Omega \lesssim (|v^\varepsilon|_{1,\Omega^\varepsilon} + |u^0|_{1,\Omega}) + \|u^0\|_\Omega.$$

The well-posedness of the problem (3.2.1) also gives

$$\|u^0\|_{1,\Omega} \lesssim \|\varphi\|_{\frac{1}{2},\partial\Omega}. \tag{3.A.4}$$

Combining equations (3.A.3) and (3.A.4) finally gives us

$$\|v^\varepsilon\|_{\Omega^\varepsilon} \lesssim \|\varphi\|_{\frac{1}{2},\partial\Omega}.$$

This concludes the proof of the lemma. □

Lemma 3.A.2. *For any $L \in \mathbb{R}$, the problem*

$$\begin{cases} -\Delta v^\varepsilon = 0 & \textit{in} \quad \Omega^\varepsilon, \\ v^\varepsilon = 0 & \textit{on} \quad \partial\Omega, \\ v^\varepsilon = L & \textit{on} \quad \partial\omega^\varepsilon, \end{cases}$$

admits a unique weak solution in $H^1(\Omega^\varepsilon)$. Morevover,

$$\|v^\varepsilon\|_{1,\Omega^\varepsilon} \lesssim |\log(\varepsilon)|^{-\frac{1}{2}}|L|.$$

Proof of the Lemma 3.A.2. Let us define w^ε the unique solution of the system

$$\begin{cases} -\Delta w^\varepsilon = 0 & \text{in} \quad \omega^{\varepsilon_{\max}/\varepsilon}\backslash\bar{\omega}, \\ w^\varepsilon = 0 & \text{on} \quad \partial\omega^{\varepsilon_{\max}/\varepsilon}, \\ w^\varepsilon = L & \text{on} \quad \partial\omega. \end{cases}$$

We also consider the function $v^\varepsilon(\varepsilon)$ defined on $\dfrac{\Omega}{\varepsilon}\backslash\bar{\omega}$ by $v^\varepsilon(\varepsilon)(\boldsymbol{x}) = v^\varepsilon(\varepsilon\boldsymbol{x})$ for all $\boldsymbol{x} \in \frac{\Omega}{\varepsilon}\backslash\bar{\omega}$. The function $v^\varepsilon(\varepsilon)$ satisfies

$$\begin{cases} -\Delta v^\varepsilon(\varepsilon) = 0 & \text{in } \frac{\Omega}{\varepsilon}\backslash\bar{\omega}, \\ v^\varepsilon(\varepsilon) = 0 & \text{on } \frac{1}{\varepsilon}\partial\Omega, \\ v^\varepsilon(\varepsilon) = L & \text{on } \partial\omega. \end{cases} \tag{3.A.5}$$

Notice that we have $\bar{\omega} \subset \omega^{\varepsilon_{\max}/\varepsilon} \subset \frac{\Omega}{\varepsilon}$. Now we consider $\tilde{w}_\varepsilon$ the extension of w^ε to $\frac{\Omega}{\varepsilon}\backslash\bar{\omega}$ by zero in the outer part of the extended domain. Therefore, by the principle of minimization of energy, we have

$$|v^\varepsilon|_{1,\Omega^\varepsilon} = |v^\varepsilon(\varepsilon)|_{1,\frac{\Omega}{\varepsilon}\backslash\bar{\omega}} \leqslant |\tilde{w}_\varepsilon|_{1,\frac{\Omega}{\varepsilon}\backslash\bar{\omega}} = |w^\varepsilon|_{1,\omega^{\varepsilon_{\max}/\varepsilon}\backslash\bar{\omega}}. \tag{3.A.6}$$

A computation provides for all $\boldsymbol{x} \in \omega_{\varepsilon_{\max}/\varepsilon}\backslash\bar{\omega}$,

$$w^\varepsilon(\boldsymbol{x}) = L\frac{\log(\varepsilon_{\max}/\varepsilon) - \log(|\boldsymbol{x}|)}{\log(\varepsilon_{\max}/\varepsilon)}$$

and

$$|w^\varepsilon|_{1,\omega^\varepsilon \max/\varepsilon \setminus \bar{\omega}} \lesssim |\log(\varepsilon)|^{-\frac{1}{2}} |L|.$$

So we get

$$|v^\varepsilon|_{1,\Omega^\varepsilon} \lesssim |\log(\varepsilon)|^{-\frac{1}{2}} |L|. \tag{3.A.7}$$

Finally, we consider $\tilde{v}_\varepsilon$ the extension of v^ε to Ω by L. Since this extension is in $H_0^1(\Omega)$, we can use the Poincaré inequality to obtain

$$\|v^\varepsilon\|_{\Omega^\varepsilon} \leqslant \|\tilde{v}^\varepsilon\|_\Omega \lesssim |\tilde{v}^\varepsilon|_{1,\Omega} \lesssim |v^\varepsilon|_{1,\Omega^\varepsilon}.$$

Using inequality (3.A.7), we get the result. □

Once again, the following Lemma and its proof are drawn from [Caubet et al., 2016, Lemma B.2, Lemma 4.2] for the Stokes equations, themselves based on the results presented in [Sid Idris, 2001, Chapter 3].

Lemma 3.A.3. *For any $u_\mathrm{b} \in H^{\frac{1}{2}}(\partial\omega^\varepsilon)$, the problem*

$$\begin{cases} -\Delta v^\varepsilon = 0 & \text{in } \Omega^\varepsilon, \\ v^\varepsilon = 0 & \text{on } \partial\Omega, \\ v^\varepsilon = u_\mathrm{b} & \text{on } \partial\omega^\varepsilon, \end{cases}$$

admits a unique weak solution in $H^1(\Omega^\varepsilon)$. Moreover,

$$\|v^\varepsilon\|_{1,\Omega^\varepsilon} \lesssim \|u_\mathrm{b}(\varepsilon)\|_{\frac{1}{2},\partial\omega}.$$

Proof. Lax-Milgram theorem allows to prove that the problem

$$\begin{cases} -\Delta V = 0 & \text{in } \mathbb{R}^2 \setminus \bar{\omega}, \\ V = u_\mathrm{b}(\varepsilon) & \text{in } \partial\omega, \end{cases} \tag{3.A.8}$$

is well posed and has a unique solution in

$$W_0^{1,2}(\mathbb{R}^2\setminus\bar{\omega}) = \{u \in \mathcal{D}'(\mathbb{R}^2\setminus\bar{\omega}) \mid \log(\rho)^{-1} u \in L^2_{-1}(\mathbb{R}^2\setminus\bar{\omega}), \nabla u \in L^2(\mathbb{R}^2\setminus\bar{\omega})\}$$

where

$$\rho(\boldsymbol{x}) = (1 + |\boldsymbol{x}|^2)^{\frac{1}{2}}$$

and

$$L^2_{-1}(\mathbb{R}^2\setminus\bar{\omega}) = \{u \in \mathcal{D}'(\mathbb{R}^2\setminus\bar{\omega}) \mid \rho^{-1} u \in L^2(\mathbb{R}^2\setminus\bar{\omega})\},$$

(see [Giroire, 1987] for example). We will try to give an explicit representation of V. By setting $-\Delta V = 0$ in ω, the problem (3.A.8) has a unique solution in $\mathbb{R}^2$ and we have that

$$-\Delta V = \nabla V \cdot \boldsymbol{n}^+ \, \delta_{\partial\omega}$$

in $\mathcal{D}'(\mathbb{R}^2)$ where $\boldsymbol{n}^+$ is the exterior normal on $\partial\Omega^\varepsilon$. Now let us define

$$W = E * \left(\nabla V \cdot \boldsymbol{n}^+ \, \delta_{\partial\omega}\right)$$

where E is the fundamental solution of the Laplace equation given for $\boldsymbol{x} \in \mathbb{R}^2 \backslash \{\mathbf{0}\}$ by

$$E(\boldsymbol{x}) = -\frac{\log(|\boldsymbol{x}|)}{2\pi},$$

and * is the convolution product. We have

$$-\Delta W = \nabla V \cdot \boldsymbol{n}^+ \, \delta_{\partial\omega}$$

in $\mathcal{D}'(\mathbb{R}^2)$. Then $V - W$ is a harmonic tempered distribution. A classical result of Fourier analysis states that harmonic tempered distribution are polynomials (see [Dautray and Lions, 1985] for example). Then $V = L + W$ with L a polynomial and for $\boldsymbol{y} \in \mathbb{R}^2 \backslash \omega$,

$$W(\boldsymbol{y}) = \int_{\partial\omega} t(\boldsymbol{x}) E(\boldsymbol{y} - \boldsymbol{x}) \mathrm{d}s(\boldsymbol{x}),$$

with $t(\boldsymbol{x}) = \nabla V \cdot \boldsymbol{n}^+$. Using a Taylor development for E, we get

$$E(\boldsymbol{y} - \boldsymbol{x}) = E(\boldsymbol{y}) - \nabla E(\boldsymbol{y} - \alpha\boldsymbol{x}) \cdot \boldsymbol{x}$$

for some $\alpha \in (0, 1)$. We then have

$$W(\boldsymbol{y}) = E(\boldsymbol{y}) \int_{\partial\omega} t(\boldsymbol{x}) \mathrm{d}s(\boldsymbol{x}) - \int_{\partial\omega} t(\boldsymbol{x}) \nabla E(\boldsymbol{y} - \alpha\boldsymbol{x}) \cdot \boldsymbol{x} \mathrm{d}s(\boldsymbol{x}).$$

Let us denote

$$U(\boldsymbol{y}) = \int_{\partial\omega} t(\boldsymbol{x}) \nabla E(\boldsymbol{y} - \alpha\boldsymbol{x}) \cdot \boldsymbol{x} \mathrm{d}s(\boldsymbol{x}).$$

By computation, we get that $U(\boldsymbol{y}) = o(1/|\boldsymbol{y}|)$ when $|\boldsymbol{y}| \to \infty$ so $(\log(\rho))^{-1} U \in L^2_{-1}(\mathbb{R}^2 \backslash \bar{\omega})$. As $(\log(\rho))^{-1} V \in L^2_{-1}(\mathbb{R}^2 \backslash \bar{\omega})$ and $(\log(\rho))^{-1} \notin L^2_{-1}(\mathbb{R}^2 \backslash \bar{\omega})$, we necessarily have that

$$\int_{\partial\omega} t(\boldsymbol{x}) \mathrm{d}s(\boldsymbol{x}) = 0$$

and that L is a constant. By computation, we have that for $|\boldsymbol{y}|$ sufficiently large,

$$|W(\boldsymbol{y})| \lesssim \|u_{\mathrm{b}}(\varepsilon)\|_{\frac{1}{2},\partial\omega} \frac{1}{|\boldsymbol{y}|} \text{ and } |\nabla W(\boldsymbol{y})| \lesssim \|u_{\mathrm{b}}(\varepsilon)\|_{\frac{1}{2},\partial\omega} \frac{1}{|\boldsymbol{y}|^2}.$$

Let $A > 0$ such that the previous inequality is satisfied for $|\boldsymbol{y}| > A$. We have for $\|\boldsymbol{y}\| > A$,

$$|L| \lesssim |V(\boldsymbol{y})| + \|u_{\mathrm{b}}(\varepsilon)\|_{\frac{1}{2},\partial\omega} \frac{1}{|\boldsymbol{y}|}.$$

Integrating for $|\boldsymbol{y}| > A$, we get

$$|L| \left(\int_{|\boldsymbol{y}|>A} \frac{1}{\log(|\boldsymbol{y}|)^2 |\boldsymbol{y}|^2} \right)^{\frac{1}{2}} \lesssim \left(\int_{|\boldsymbol{y}|>A} \frac{|V(\boldsymbol{y})|^2}{\log(|\boldsymbol{y}|)^2 |\boldsymbol{y}|^2} \right)^{\frac{1}{2}} + \|u_{\mathrm{b}}(\varepsilon)\|_{\frac{1}{2},\partial\omega} \left(\int_{|\boldsymbol{y}|>A} \frac{1}{\log(|\boldsymbol{y}|)^2 |\boldsymbol{y}|^4} \right)^{\frac{1}{2}}.$$

The fact that A is uniformly independent ofu_{b} and the well-posedness of the problem (3.A.8) give

$$|L| \lesssim \|u_{\mathrm{b}}(\varepsilon)\|_{\frac{1}{2},\partial\omega}.$$

Using similar computations as in [[Guillaume and Idris, 2002], Lemma 7.1], we also have

$$\|W(\frac{\boldsymbol{x}}{\varepsilon})\|_{1,\Omega^\varepsilon} \lesssim \varepsilon \|u_{\mathrm{b}}(\varepsilon)\|_{\frac{1}{2},\partial\omega}.$$

We then define $z^\varepsilon := v^\varepsilon - W(\frac{\boldsymbol{x}}{\varepsilon})$, z^ε satisfies

$$\begin{cases} -\Delta z^\varepsilon = 0 & \text{in } \Omega^\varepsilon, \\ z^\varepsilon = -W(\frac{\boldsymbol{x}}{\varepsilon}) & \text{on } \partial\Omega, \\ z^\varepsilon = L & \text{on } \partial\omega^\varepsilon. \end{cases}$$

Using Lemma 3.A.1 and Lemma 3.A.2 we get that

$$\begin{aligned} \|z^\varepsilon\|_{1,\Omega^\varepsilon} &\lesssim \|W\left(\frac{\boldsymbol{x}}{\varepsilon}\right)\|_{\frac{1}{2},\partial\Omega} + |\log(\varepsilon)|^{-\frac{1}{2}} |L|, \\ &\lesssim \varepsilon \|u_{\mathrm{b}}(\varepsilon)\|_{\frac{1}{2},\partial\omega} + |\log(\varepsilon)|^{-\frac{1}{2}} \|u_{\mathrm{b}}(\varepsilon)\|_{\frac{1}{2},\partial\omega}. \end{aligned}$$

So finally, we get

$$\begin{aligned} \|v^\varepsilon\|_{1,\Omega^\varepsilon} &\lesssim \|z^\varepsilon\|_{1,\Omega^\varepsilon} + \|W(\frac{\boldsymbol{x}}{\varepsilon})\|_{1,\Omega^\varepsilon}, \\ &\lesssim \varepsilon \|u_{\mathrm{b}}(\varepsilon)\|_{\frac{1}{2},\partial\omega} + |\log(\varepsilon)|^{-\frac{1}{2}} \|u_{\mathrm{b}}(\varepsilon)\|_{\frac{1}{2},\partial\omega} + \|u_{\mathrm{b}}(\varepsilon)\|_{\frac{1}{2},\partial\omega}, \\ \|v^\varepsilon\|_{1,\Omega^\varepsilon} &\lesssim \|u_{\mathrm{b}}(\varepsilon)\|_{\frac{1}{2},\partial\omega}. \end{aligned}$$

□

3.A.2 Proof of Lemma 3.3.2

Restated Lemma 3.3.2. *For all* $v \in H^1(\Omega)$,

$$\|v\|_{\frac{1}{2},\varepsilon} \lesssim |\log(\varepsilon)|^{\frac{1}{2}} \|v\|_{1,\Omega}.$$

Proof of Lemma 3.3.2. According to [Maz'ya and Poborchi, 1998, Section 4.1.3], the norm

$$\langle u \rangle_{\frac{1}{2},\partial\omega^\varepsilon} = \inf_{v \in H^1(\Omega^\varepsilon),\, v|_{\partial\omega^\varepsilon} = u} \|v\|_{1,\Omega^\varepsilon} \quad \forall u \in H^{\frac{1}{2}}(\partial\omega^\varepsilon), \tag{3.A.9}$$

is equivalent, uniformly in ε, to the norm

$$|\log(\varepsilon)|^{-\frac{1}{2}} \| \cdot \|_\varepsilon + | \cdot |_{\frac{1}{2},\varepsilon}.$$

By definition of the norm $\langle \cdot \rangle_{\frac{1}{2},\partial\omega^\varepsilon}$, we have

$$\langle v \rangle_{\frac{1}{2},\partial\omega^\varepsilon} \leqslant \|v\|_{1,\Omega^\varepsilon} \quad \forall v \in H^1(\Omega^\varepsilon),$$

and consequently

$$|\log(\varepsilon)|^{-\frac{1}{2}} \|v\|_\varepsilon + |v|_{\frac{1}{2},\varepsilon} \lesssim \|v\|_{1,\Omega^\varepsilon} \quad \forall v \in H^1(\Omega^\varepsilon).$$

Eventually, by definition of the norm $\| \cdot \|_{\frac{1}{2},\varepsilon}$ we can conclude

$$\begin{aligned} \|v\|_{\frac{1}{2},\varepsilon} = \|v\|_\varepsilon + |v|_{\frac{1}{2},\varepsilon} \lesssim & |\log(\varepsilon)|^{\frac{1}{2}} (|\log(\varepsilon)|^{-\frac{1}{2}} \|v\|_\varepsilon + |v|_{\frac{1}{2},\varepsilon}) \\ \lesssim & |\log(\varepsilon)|^{\frac{1}{2}} \|v\|_{1,\Omega^\varepsilon} \lesssim |\log(\varepsilon)|^{\frac{1}{2}} \|v\|_{1,\Omega} \quad \forall v \in H^1(\Omega). \end{aligned}$$

□

3.A.3 Proof of Lemma 3.3.3

Restated Lemma 3.3.3. *Let* $\eta \in H^{\frac{1}{2}}(\partial\omega^\varepsilon)$ *be given, there exists* $v_\eta^\varepsilon \in H_0^1(\Omega)$ *solution of*

$$\begin{cases} -\Delta v_\eta^\varepsilon = 0 \quad \textit{in} \quad \Omega^\varepsilon \cup \omega^\varepsilon, \\ \quad v_\eta^\varepsilon = \eta \quad \textit{on} \quad \partial\omega^\varepsilon. \end{cases} \tag{3.A.10}$$

Moreover, v_η^ε *satisfies the following energy bound:*

$$\|v_\eta^\varepsilon\|_{1,\Omega} \lesssim \|\eta\|_{\frac{1}{2},\varepsilon}. \tag{3.A.11}$$

Proof of Lemma 3.3.3. Consider $\eta \in H^{\frac{1}{2}}(\partial\omega^\varepsilon)$. Classical results on elliptic regularity ensures the existence of $v_\eta^\varepsilon \in H_0^1(\Omega)$ satisfying (3.3.2). Now, we would like to prove the bound (3.3.3). On one hand, according to Lemma 3.A.3,

$$\|v_\eta^\varepsilon\|_{1,\Omega^\varepsilon} \lesssim \|\eta\|_{\frac{1}{2},\varepsilon}. \tag{3.A.12}$$

On the other hand, setting $v_\eta^\varepsilon(\varepsilon)$ defined on ω such that $v_\eta^\varepsilon(\varepsilon)(\boldsymbol{x}) = v_\eta^\varepsilon(\varepsilon\boldsymbol{x})$ for all $\boldsymbol{x} \in \omega$, we have that $v_\eta^\varepsilon(\varepsilon)$ satisfies

$$\begin{cases} -\Delta v_\eta^\varepsilon(\varepsilon) = 0 & \text{in} \quad \omega, \\ v_\eta^\varepsilon(\varepsilon) = \eta(\varepsilon) & \text{on} \quad \partial\omega. \end{cases}$$

We deduce that

$$\|v_\eta^\varepsilon(\varepsilon)\|_{1,\omega} \lesssim \|\eta(\varepsilon)\|_{\frac{1}{2},\partial\omega}.$$

By re-scaling, we have that

$$\varepsilon^{-2}\|v_\eta^\varepsilon\|_{\omega^\varepsilon}^2 + \|\nabla v_\eta^\varepsilon\|_{\omega^\varepsilon}^2 \lesssim \|\eta\|_{\frac{1}{2},\varepsilon}^2$$

and

$$\|v_\eta^\varepsilon\|_{1,\omega^\varepsilon} \lesssim \|\eta\|_{\frac{1}{2},\varepsilon}. \tag{3.A.13}$$

Gathering (3.A.12) and (3.A.13), we obtain inequality (3.3.3). □

3.A.4 Proof of Lemma 3.3.5

Restated Lemma 3.3.5. *Let $(u_N^\varepsilon, \lambda_N^\varepsilon) \in H_0^1(\Omega) \times F_N$ be the solution of Problem* (3.1.3)*. Then, we have*

$$\lambda_N^\varepsilon = \varepsilon\big((\nabla u_N^\varepsilon)^+ \cdot \boldsymbol{n}^+) - (\nabla u_N^\varepsilon)^- \cdot \boldsymbol{n}^+\big) \quad \textit{in} \quad H^{-\frac{1}{2}}(\partial\omega^\varepsilon). \tag{3.A.14}$$

where $\boldsymbol{n}^+$ is the exterior normal to $\partial\Omega^\varepsilon$, $(\nabla u_N^\varepsilon)^+$ is the restriction of ∇u_N^ε to Ω^ε and $(\nabla u_N^\varepsilon)^-$ is the restriction of ∇u_N^ε to ω^ε.

Proof of Lemma 3.3.5. On one hand, we have, for all $\phi \in H_0^1(\Omega)$

$$\begin{aligned} \int_\Omega \nabla u_N^\varepsilon \nabla\phi &= \int_{\Omega^\varepsilon} \nabla u_N^\varepsilon \nabla\phi + \int_{\omega^\varepsilon} \nabla u_N^\varepsilon \nabla\phi \\ &= -\int_{\Omega^\varepsilon} \Delta u_N^\varepsilon \phi - \int_{\omega^\varepsilon} \Delta u_N^\varepsilon \phi + \langle (\nabla u_N^\varepsilon)^+ \boldsymbol{n}^+ - (\nabla u_N^\varepsilon)^- \boldsymbol{n}^+, \phi\rangle_{-\frac{1}{2},\partial\omega^\varepsilon}, \end{aligned}$$

and since $-\Delta u_N^\varepsilon = f$ in Ω^ε and $-\Delta u_N^\varepsilon = 0$ in ω^ε, we obtain the equality

$$\int_\Omega \nabla u_N^\varepsilon \nabla\phi = \langle (\nabla u_N^\varepsilon)^+ \boldsymbol{n}^+ - (\nabla u_N^\varepsilon)^- \boldsymbol{n}^+, \phi\rangle_{-\frac{1}{2},\partial\omega^\varepsilon} + \int_\Omega f\phi.$$

On the other hand, we have

$$\int_\Omega \nabla u_N^\varepsilon \nabla\phi = (\lambda_N^\varepsilon, \phi)_\varepsilon + \int_\Omega f\phi.$$

Identifying these two relations, we get

$$(\lambda_N^\varepsilon, \phi)_\varepsilon = \varepsilon^{-1}(\lambda_N^\varepsilon, \phi)_{\partial\omega^\varepsilon} = \langle (\nabla u_\varepsilon^N)^+ \boldsymbol{n}^+ - (\nabla u_\varepsilon^N)^- \boldsymbol{n}^+, \phi \rangle_{-\frac{1}{2}, \partial\omega^\varepsilon}$$

for all $\phi \in H_0^1(\Omega)$. Thus, since the trace operator from $H_0^1(\Omega)$ on $H^{\frac{1}{2}}(\partial\omega^\varepsilon)$ is surjective, we get (3.3.11). □

CHAPTER 4

A new computational approach for the simulation of small particles in a two-dimensional Stokesian flow: formulation and error analysis

4.1 Introduction

This chapter is made up of two parts. In a first part, we extend the analysis presented in Chapter 3 to the case of the Stokes problem with obstacle. As in the previous chapter, the fundamental idea consists in projecting the Dirichlet boundary conditions onto a Fourier-based finite-dimensional space $\boldsymbol{F}_N$ of dimension N. In Section 4.2.1, we first establish the well-posedness of the reduced order problem and provide uniform a priori estimates on the solutions with respect to the obstacle size (Theorem 4.2.1). We also present a convergence result towards the solution of the full order Stokes problem where standard Dirichlet boundary conditions on the obstacle are considered (Theorem 4.2.5). Finally, as in Chapter 3, we propose two discretization methods based on the fictitious domain approach. The first method introduced in Section 4.3.1 is a low-order finite element method with stabilization, while the second method, presented in Section 4.3.2, is an augmented finite element method, which enables the use of high-order finite elements and partly addresses the limitations of the fictitious domain method due to the low regularity of the solutions of the continuous problem.

In the second part, we extend this method to a fluid-structure interaction framework for rigid particles immersed in a Stokes fluid. Simulating small particles suspended in a Stokes fluid (or Navier-Stokes) finds numerous applications: we can mention the case of aerosols the respiratory system [Kleinstreuer and Zhang, 2003, Kleinstreuer and Zhang, 2010, Tu et al., 2012], the modeling of red blood cells in blood flow [Polwaththe Gallage et al., 2012, Ye et al., 2016] and the modeling of concretes [Roussel et al., 2007] or reinforced plastics [Yashiro et al., 2011], among others. Several numerical approaches have been reported in the literature, using either fitted or unfitted mesh. In the fitted mesh framework, typically based on an ALE formalism of the fluid, we can cite [Takashi and Hughes, 1992, Sarrate et al., 2001] for Stokes equations with inertial term or automatic mesh moving method [Hu et al., 1992, Feng et al., 1994a, Feng et al., 1994b, Johnson and Tezduyar, 1997]. However, as already discussed, these methods can be cumbersome in the presence of large displacements and rotations of the rigid structures. To overcome this difficulty, many immersed type of methods have been developed. We can cite the immersed boundary method [Feng and Michaelides, 2004, Uhlmann, 2005, Kallemov et al., 2016, Abdol Azis et al., 2019], the immersed finite element method [Zhang et al., 2004, Liu et al., 2007], the fictitious domain method [Glowinski et al., 1999b, Glowinski et al., 2001, Veeramani et al., 2007], the extended finite method [Wagner et al., 2001, Wagner et al., 2003], penalization-based methods [Angot et al., 1999, Janela et al., 2005], lattice-Boltzmann methods [Ladd, 1994a, Ladd, 1994b, Ladd and Verberg, 2001]. In the case of small particles and a Stokesian fluid, similarly to the slender body theory developed in 3D, methods based on Stokeslets can also hold significance. These methods rely on a truncated multipole expansion solution of the Stokes equations [Weinbaum et al., 1990, Yeo and Maxey, 2010]. In the spirit of the previous chapters, we present in Section 4.4 a discrete reduced order approach for simulation of rigid elliptical particles immersed in a two-dimensional Stokesian flow using the low-order stabilized fictitious domain method introduced in Section 4.3.1 and a semi-implicit coupling scheme for time-discretization. In the numerical Section 4.5, we illustrate the theoretical results obtained in the first part and give numerical evidence of the accuracy of the reduced order model with respect to a fully two-dimensional one computed either with an ALE/automatic mesh moving method or a fictitious domain method with Lagrange multipliers.

4.2 Analysis of the Stokes problem with reduced order boundary conditions

In this section, we adapt the analysis provided in Chapter 3 for the Poisson problem to the case of Stokes equations. We consider the same geometric setting and notation: the symbol Ω denotes a fixed bounded smooth domain of $\mathbb{R}^2$, ω^ε is a circular obstacle of size ε such that $\overline{\omega^\varepsilon} \subset \Omega$ and Ω^ε are complementary to $\overline{\omega}^\varepsilon$ in Ω. Using the same notation as in (3.1.1) adapted to the polar coordinates, we denote, for all functions $\boldsymbol{v} : \partial\omega^\varepsilon \to \mathbb{R}^2$, by

$\boldsymbol{v}(\varepsilon)$ the re-scaled function $\boldsymbol{v}(\varepsilon) : (0, 2\pi) \to \mathbb{R}^2$ defined by

$$\boldsymbol{v}(\varepsilon)(\theta) \stackrel{\text{def}}{=} \boldsymbol{v}(\varepsilon(\cos(\theta)\boldsymbol{e}_x + \sin(\theta)\boldsymbol{e}_y) \quad \forall \theta \in (0, 2\pi).$$

We then set $(\cdot,\cdot)_\varepsilon$, $\langle\cdot,\cdot\rangle_{-\frac{1}{2},\varepsilon}$, $\|\cdot\|_\varepsilon$, $\|\cdot\|_{-\frac{1}{2},\varepsilon}$ and $\|\cdot\|_{\frac{1}{2},\varepsilon}$ as the vector counterparts of the functions introduced in Section 3.2.2. Following the reduced order modeling approach introduced in Chapters 2 and 3, we denote by $\boldsymbol{F}_N$ a finite-dimensional space that approximates the Lagrange multiplier space $\boldsymbol{H}^{-\frac{1}{2}}(\partial\omega^\varepsilon)$. In this section, we consider a constrained space of the N first Fourier modes satisfying no net flow across the interface (see Remark 13 below). In particular, we set

$$\boldsymbol{F}_N \stackrel{\text{def}}{=} \left\{ \boldsymbol{v} \in \boldsymbol{L}^2_{0,\boldsymbol{n}}(\partial\omega^\varepsilon) \ : \boldsymbol{v}(\varepsilon)(\theta) = \boldsymbol{a}_0 + \sum_{k=1}^{N} (\boldsymbol{a}_k \cos(k\theta) + \boldsymbol{b}_k \sin(k\theta)), \quad \boldsymbol{a}_k,\, \boldsymbol{b}_k \in \mathbb{R}^2 \right\}$$

where

$$\boldsymbol{L}^2_{0,\boldsymbol{n}}(\partial\omega^\varepsilon) \stackrel{\text{def}}{=} \left\{ \boldsymbol{v} \in \boldsymbol{L}^2(\partial\omega^\varepsilon) \ : \ \int_{\partial\omega^\varepsilon} \boldsymbol{v}\cdot\boldsymbol{n}^- = 0 \right\}.$$

and $\boldsymbol{n}^-$ is the exterior normal to $\partial\omega^\varepsilon$. Note that $\boldsymbol{F}_N$ is equal to

$$\begin{aligned} \boldsymbol{F}_N = \big\{ \boldsymbol{v} \in \boldsymbol{L}^2_{0,\boldsymbol{n}}(\partial\omega^\varepsilon) \ : \ \boldsymbol{v}(\varepsilon)(\theta) = \boldsymbol{a}_0 + \sum_{i=1}^{3} a_i \boldsymbol{g}_i(\theta) \\ + \sum_{k=2}^{N} (\boldsymbol{a}_k \cos(k\theta) + \boldsymbol{b}_k \sin(k\theta)), \quad a_i \in \mathbb{R},\ \boldsymbol{a}_k,\, \boldsymbol{b}_k \in \mathbb{R}^2 \big\} \end{aligned} \tag{4.2.1}$$

where

$$\boldsymbol{g}_1(\theta) \stackrel{\text{def}}{=} \sin(\theta)\boldsymbol{e}_x + \cos(\theta)\boldsymbol{e}_y,\ \boldsymbol{g}_2(\theta) = \cos(\theta)\boldsymbol{e}_x - \sin(\theta)\boldsymbol{e}_y,\ \boldsymbol{g}_3(\theta) = \sin(\theta)\boldsymbol{e}_x - \cos(\theta)\boldsymbol{e}_y$$

for all $\theta \in (0, 2\pi)$. Similarly to Section 3.2.2, we introduce a Fourier norm $\|\cdot\|^{\mathscr{F}}_{\frac{1}{2},\varepsilon}$ on $\boldsymbol{H}^{\frac{1}{2}}(\partial\omega^\varepsilon)$ such that for $\boldsymbol{v} \in \boldsymbol{H}^{\frac{1}{2}}(\partial\omega^\varepsilon)$,

$$\|\boldsymbol{v}\|^{\mathscr{F}}_{\frac{1}{2},\varepsilon} \stackrel{\text{def}}{=} \left(\big(|\xi^{\varepsilon,\mathrm{c}}_{0,r}|^2 + |\xi^{\varepsilon,\mathrm{c}}_{0,\theta}|^2\big) + \sum_{k=1}^{\infty} (1+k)\big(|\xi^{\varepsilon,\mathrm{c}}_{k,r}|^2 + |\xi^{\varepsilon,\mathrm{c}}_{k,\theta}| + |\xi^{\varepsilon,\mathrm{s}}_{k,r}| + |\xi^{\varepsilon,\mathrm{s}}_{k,\theta}|^2\big) \right)^{\frac{1}{2}}. \tag{4.2.2}$$

where

$$\begin{cases} \xi^{\varepsilon,j}_{k,r} \stackrel{\text{def}}{=} \mathscr{F}^j_k(\boldsymbol{v}(\varepsilon)\cdot\boldsymbol{e}_r), \quad \xi^{\varepsilon,j}_{k,\theta} \stackrel{\text{def}}{=} \mathscr{F}^j_k(\boldsymbol{v}(\varepsilon)\cdot\boldsymbol{e}_\theta) \quad \forall (k,j) \in \{0,\dots,N\} \times \{\mathrm{c},\mathrm{s}\}, \\ \boldsymbol{e}_r \stackrel{\text{def}}{=} \cos(\theta)\boldsymbol{e}_x + \sin(\theta)\boldsymbol{e}_y, \quad \boldsymbol{e}_\theta \stackrel{\text{def}}{=} -\sin(\theta)\boldsymbol{e}_x + \cos(\theta)\boldsymbol{e}_y, \end{cases} \tag{4.2.3}$$

with the operators $\mathscr{F}_k^j : L^2(\partial\omega^\varepsilon) \to \mathbb{R}$ introduced in (3.2.3). Following the same steps as in Section 3.2.2, we can prove that the norms $\|\cdot\|_{\frac{1}{2},\varepsilon}^{\mathscr{F}}$ and $\|\cdot\|_{\frac{1}{2},\varepsilon}$ are equivalent with constants uniformly independent of ε. Furthermore, denoting by $\boldsymbol{\Pi}_N^\varepsilon : \boldsymbol{L}^2(\partial\omega^\varepsilon) \mapsto \boldsymbol{F}_N$ the L^2 projector on $\boldsymbol{F}_N$ for the inner-product $(\cdot,\cdot)_\varepsilon$, we have

$$\|\boldsymbol{\Pi}_N^\varepsilon \boldsymbol{v}\|_{\frac{1}{2},\varepsilon}^{\mathscr{F}} \leqslant \|\boldsymbol{v}\|_{\frac{1}{2},\varepsilon}^{\mathscr{F}}, \quad \|\boldsymbol{\Pi}_N^\varepsilon \boldsymbol{v}\|_{\frac{1}{2},\varepsilon} \lesssim \|\boldsymbol{v}\|_{\frac{1}{2},\varepsilon} \quad \forall \boldsymbol{v} \in \boldsymbol{H}^{\frac{1}{2}}(\partial\omega^\varepsilon). \tag{4.2.4}$$

With respect to the reduced order Poisson problem introduced in (2.2.33), we also make two additional assumptions. Firstly, for the sake of simplicity, we consider an homogeneous right hand side $\boldsymbol{f} = \boldsymbol{0}$. Note, nonetheless, that all the results presented in this chapter can be easily extended to the case $\boldsymbol{f} \in L^2(\Omega)$ and $\operatorname{supp} \boldsymbol{f} \cap \omega^\varepsilon = \varnothing$. Secondly, as a premise to the fluid-particles coupled problem introduced in Section 4.4, we assume that the Dirichlet boundary conditions on $\partial\omega^\varepsilon$ write

$$\boldsymbol{u}_{\mathrm{b}} = \boldsymbol{v}_{\mathrm{b}} + \varepsilon w_b \boldsymbol{e}_\theta \quad \text{on} \quad \partial\omega^\varepsilon, \quad \boldsymbol{v}_{\mathrm{b}} \in \mathbb{R}^2, w_{\mathrm{b}} \in \mathbb{R}. \tag{4.2.5}$$

Let

$$\boldsymbol{V} \overset{\text{def}}{=} \boldsymbol{H}_0^1(\Omega), \quad Q \overset{\text{def}}{=} \{q \in L^2(\Omega) \mid q|_{\omega^\varepsilon} \in L_0^2(\omega^\varepsilon), \quad q|_{\Omega^\varepsilon} \in L_0^2(\Omega^\varepsilon)\},$$

be the functional space for the velocity and pressure, respectively, the considered reduced order Stokes problem is formulated as follows: find $(\boldsymbol{u}_N^\varepsilon, p_N^\varepsilon, \boldsymbol{\lambda}_N^\varepsilon) \in \boldsymbol{V} \times Q \times \boldsymbol{F}_N$ such that

$$\begin{cases} 2(\boldsymbol{\varepsilon}(\boldsymbol{u}_N^\varepsilon), \boldsymbol{\varepsilon}(\boldsymbol{v}))_\Omega - (p_N^\varepsilon, \operatorname{div} \boldsymbol{v})_\Omega - (\boldsymbol{\lambda}_N^\varepsilon, \boldsymbol{v})_\varepsilon = 0 & \forall \boldsymbol{v} \in \boldsymbol{V}, \\ (q, \operatorname{div} \boldsymbol{u}_N^\varepsilon)_\Omega = 0 & \forall q \in Q, \\ (\boldsymbol{\mu}_N, \boldsymbol{v})_\varepsilon = (\boldsymbol{\mu}_N, \boldsymbol{v}_{\mathrm{b}} + \varepsilon w_b \boldsymbol{e}_\theta)_\varepsilon & \forall \boldsymbol{\mu}_N \in \boldsymbol{F}_N. \end{cases} \tag{4.2.6}$$

Here $\boldsymbol{\varepsilon}(\boldsymbol{u}) \overset{\text{def}}{=} \frac{1}{2}\big(\boldsymbol{\nabla}\boldsymbol{u} + (\boldsymbol{\nabla}\boldsymbol{u})^{\mathrm{T}}\big)$ is the strain tensor introduced in (2.2.7). In what follows, we also make use of the Cauchy stress tensor, also introduced in (2.2.7), defined by $\boldsymbol{\sigma}(\boldsymbol{u}, p) \overset{\text{def}}{=} 2\mu_{\mathrm{f}}\boldsymbol{\varepsilon}(\boldsymbol{u}) - p\boldsymbol{I}_3$.

Remark 13. The choices above for $\boldsymbol{F}_N$ and Q as admissible spaces for the Lagrangian multipliers and the pressure are justified as follows. The strong formulation of the associated full order problem is given by

$$\begin{cases} -\Delta \boldsymbol{u}_N^\varepsilon + \nabla p_N^\varepsilon = 0 & \text{in} \quad \Omega^\varepsilon \cup \omega^\varepsilon, \\ \operatorname{div} \boldsymbol{u}_N^\varepsilon = 0 & \text{in} \quad \Omega, \\ \boldsymbol{u}_N^\varepsilon = \boldsymbol{v}_{\mathrm{b}} + \varepsilon w_b \boldsymbol{e}_\theta & \text{on} \quad \partial\omega^\varepsilon, \\ \boldsymbol{\lambda}_N^\varepsilon = \big(\boldsymbol{\sigma}(\boldsymbol{u}_N^\varepsilon, p_N^\varepsilon)^+ \boldsymbol{n}^+ - \boldsymbol{\sigma}(\boldsymbol{u}_N^\varepsilon, p_N^\varepsilon)^- \boldsymbol{n}^+\big) & \text{on} \quad \partial\omega^\varepsilon. \end{cases} \tag{4.2.7}$$

where the last equation is proved in Lemma 4.2.22. The pressure can be decomposed as $p_N^\varepsilon = \hat{p}_N^\varepsilon + \bar{p}^\varepsilon$, with $\hat{p}_N^\varepsilon \in Q$ and $\bar{p}_N^\varepsilon$ constant (not necessarily the same value) in Ω^ε and

ω^ε. By inserting this relation into (4.2.7) we get the following expression for $\boldsymbol{u}_N^\varepsilon$ and $\hat{p}_N^\varepsilon$

$$\begin{cases} -\Delta \boldsymbol{u}_N^\varepsilon + \nabla \hat{p}_N^\varepsilon = 0 & \text{in} \quad \Omega^\varepsilon \cup \omega^\varepsilon, \\ \text{div } \boldsymbol{u}_N^\varepsilon = 0 & \text{in} \quad \Omega, \\ \boldsymbol{u}_N^\varepsilon = \boldsymbol{v}_\text{b} + \varepsilon w_b \boldsymbol{e}_\theta & \text{on} \quad \partial\omega^\varepsilon \end{cases}$$

On the other hand, for the Lagrange multiplier we get

$$\boldsymbol{\lambda}_N^\varepsilon = \left(\boldsymbol{\sigma}(\boldsymbol{u}_N^\varepsilon, \hat{p}_N^\varepsilon)^+ \boldsymbol{n}^+ - \boldsymbol{\sigma}(\boldsymbol{u}_N^\varepsilon, \hat{p}_N^\varepsilon)^- \boldsymbol{n}^+\right) - c\boldsymbol{n}^+ \quad \text{on} \quad \partial\omega^\varepsilon,$$

with $c = (\bar{p}^\varepsilon)^+ - (\bar{p}^\varepsilon)^-$. The undetermination of $\boldsymbol{\lambda}^\varepsilon$ with respect to the constant c is then removed by taking it in $\boldsymbol{L}^2_{0,\boldsymbol{n}}(\partial\omega^\varepsilon)$.

4.2.1 Well-posedness

In this section, we study the well-posedness of Problem (4.2.6) and establish the following theorem.

Theorem 4.2.1. *Problem* (4.2.6) *admits a unique solution* $(\boldsymbol{u}_N^\varepsilon, p_N^\varepsilon, \boldsymbol{\lambda}_N^\varepsilon)$ *in* $\boldsymbol{V} \times Q \times \boldsymbol{F}_N$. *Moreover, the following a priori estimate holds:*

$$\|\boldsymbol{u}_N^\varepsilon\|_{1,\Omega} + |\log(\varepsilon)|^{-\frac{1}{2}} \|p_N^\varepsilon\|_\Omega + \|\boldsymbol{\lambda}_N^\varepsilon\|_{-\frac{1}{2},\varepsilon} \lesssim |\boldsymbol{v}_\text{b}| + \varepsilon |w_\text{b}|. \tag{4.2.8}$$

Similarly to the results obtained for the reduced order Poisson problem presented in Theorem 3.3.1, this result states that the velocity and the Lagrange multiplier depend continuously on the data with a constant uniformly independent of N and ε. On the other hand, we observe on the pressure norm a dependence in $|\log(\varepsilon)|^{\frac{1}{2}}$ as $\varepsilon \to 0$. This behavior is a consequence of Lemma 4.2.3 which itself derives from the asymptotic properties of the trace operator given by Lemma 3.3.2.

For the proof of Theorem 4.2.1, we need the introduction of two preliminary lemmas whose proofs are given in the appendix of this chapter (Sections 4.A.2 and 4.A.3, respectively). The first lemma introduces a divergence free continuous lifting in the whole domain Ω of functions defined in $\boldsymbol{H}^{\frac{1}{2}}(\partial\omega^\varepsilon) \cap \boldsymbol{L}^2_{0,\boldsymbol{n}}(\partial\omega^\varepsilon)$. It can be seen as the Stokesian counterpart of Lemma 3.3.3.

Lemma 4.2.2. *Let* $\boldsymbol{\eta} \in \boldsymbol{H}^{\frac{1}{2}}(\partial\omega^\varepsilon) \cap \boldsymbol{L}^2_{0,\boldsymbol{n}}(\partial\omega^\varepsilon)$ *be given, there exists* $(\boldsymbol{v}_{\boldsymbol{\eta}}^\varepsilon, q_{\boldsymbol{\eta}}^\varepsilon) \in \boldsymbol{V} \times Q$ *such that*

$$\begin{cases} -\Delta \boldsymbol{v}_{\boldsymbol{\eta}}^\varepsilon + \nabla q_{\boldsymbol{\eta}}^\varepsilon = 0 & \textit{in} \quad \Omega^\varepsilon \cup \omega^\varepsilon, \\ \text{div } \boldsymbol{v}_{\boldsymbol{\eta}}^\varepsilon = 0 & \textit{in} \quad \Omega, \\ \boldsymbol{v}_{\boldsymbol{\eta}}^\varepsilon = \boldsymbol{\eta} & \textit{on} \quad \partial\omega^\varepsilon. \end{cases}$$

Moreover, the following a priori estimate holds:

$$\|\boldsymbol{v}_{\boldsymbol{\eta}}^{\varepsilon}\|_{1,\Omega} \lesssim \|\boldsymbol{\eta}\|_{\frac{1}{2},\varepsilon}. \tag{4.2.9}$$

The second lemma is a variant of the surjectivity theorem for the divergence operator.

Lemma 4.2.3. *Let $q \in Q$ be given, there exists $\boldsymbol{w}_q^{\varepsilon} \in \boldsymbol{V}$ such that*

$$\begin{cases} \operatorname{div} \boldsymbol{w}_q^{\varepsilon} = q & \textit{in} \quad \Omega, \\ \boldsymbol{w}_q^{\varepsilon} = 0 & \textit{on} \quad \partial\omega^{\varepsilon}, \end{cases}$$

and

$$\|\boldsymbol{w}_q^{\varepsilon}\|_{1,\Omega} \lesssim |\log(\varepsilon)|^{\frac{1}{2}} \|q\|_{\Omega}.$$

To prove Theorem 4.2.1, we use a variation of the BNB (see [Brezzi, 1974] or [Ern and Guermond, 2004, Theorem 2.34]) specifically designed for twofold saddle point problems.

Theorem 4.2.4. *Let Q_1 and Q_2 be two reflexive Banach spaces, $a : X \times X \to \mathbb{R}$, $b_1 : Q_1 \times X \to \mathbb{R}$, $b_2 : Q_2 \times X \to \mathbb{R}$ three continuous bilinear forms, $c_1 : Q_1 \to \mathbb{R}$, $c_2 : Q_2 \to \mathbb{R}$, $d : X \to \mathbb{R}$ three continuous linear forms, we consider the twofold saddle point problem: find $(u, \lambda_1, \lambda_2) \in X \times Q_1 \times Q_2$ such that*

$$\begin{cases} a(u,v) - b_1(\lambda_1, v) - b_2(\lambda_2, v) = d(v), & \forall v \in X, \\ b_1(\mu_1, u) = c_1(\mu_1), & \forall \mu_1 \in Q_1, \\ b_2(\mu_2, u) = c_2(\mu_2), & \forall \mu_2 \in Q_2. \end{cases} \tag{4.2.10}$$

Let

$$Z_{b_i} \overset{\text{def}}{=} \{v \in X | b_i(\mu_i, v) = 0 \ \forall \mu_i \in Q_i\} \subset X \ i = 1, 2. \tag{4.2.11}$$

We suppose that there exists $\beta_1,\ \beta_2 > 0$ such that

$$\sup_{v \in Z_{b_2}} \frac{b_1(\lambda_1, v)}{\|v\|_X} \geqslant \beta_1 \|\lambda_1\|_{Q_1} \quad \forall \lambda_1 \in Q_1,$$
$$\sup_{v \in Z_{b_1}} \frac{b_2(\lambda_2, v)}{\|v\|_X} \geqslant \beta_2 \|\lambda_2\|_{Q_2} \quad \forall \lambda_2 \in Q_2,$$

and that there exists $\alpha > 0$

$$a(v,v) \geqslant \alpha \|v\|_X \quad \forall v \in X. \tag{4.2.12}$$

Then the Problem (4.2.10) *is well posed and we have the following estimates on* u*,* λ_1 *and* λ_2*:*

$$\|u\|_X \leqslant \alpha^{-1}\|d\| + \beta_1^{-1}(1+\alpha^{-1}\|a\|)\|c_1\| + \beta_2^{-1}(1+\alpha^{-1}\|a\|)\|c_2\|, \tag{4.2.13}$$

and

$$\|\lambda_1\|_{Q_1} \leqslant \beta_1^{-1}(\|d\| + \|a\|\|u\|_X), \quad \|\lambda_2\|_{Q_2} \leqslant \beta_2^{-1}(\|d\| + \|a\|\|u\|_X).$$

The proof of this theorem is given in Section 4.A.4 of the Appendix.

Proof. To prove this result, we will apply Theorem 4.2.4 to Problem (4.2.6). Let us introduce some notations. We notice that Problem (4.2.6) can be written in the following form: find $(\boldsymbol{u}_N^\varepsilon, p_N^\varepsilon, \boldsymbol{\lambda}_N^\varepsilon) \in \boldsymbol{V} \times Q \times \boldsymbol{F}_N$ such that

$$\begin{aligned} a(\boldsymbol{u}_N^\varepsilon, \boldsymbol{v}) - b_1(p_N^\varepsilon, \boldsymbol{v}) - b_2(\boldsymbol{\lambda}_N^\varepsilon, \boldsymbol{v}) &= 0 \quad \forall \boldsymbol{v} \in \boldsymbol{V}, \\ b_1(q, \boldsymbol{u}_N^\varepsilon) &= 0 \quad \forall q \in Q, \\ b_2(\boldsymbol{\mu}_N, \boldsymbol{u}_N^\varepsilon) &= c(\boldsymbol{\mu}_N) \quad \forall \boldsymbol{\mu}_N \in \boldsymbol{F}_N, \end{aligned} \tag{4.2.14}$$

where the bilinear forms $a : \boldsymbol{V} \times \boldsymbol{V} \to \mathbb{R}$, $b_1 : Q \times \boldsymbol{V} \to \mathbb{R}$, $b_2 : \boldsymbol{F}_N \times \boldsymbol{V} \to \mathbb{R}$ and the linear form $c : \boldsymbol{F}_N \to \mathbb{R}$ are given by

$$\begin{aligned} &a(\boldsymbol{u}, \boldsymbol{v}) = 2(\boldsymbol{\varepsilon}(\boldsymbol{u}), \boldsymbol{\varepsilon}(\boldsymbol{v}))_\Omega, \quad b_1(q, \boldsymbol{v}) = (q, \operatorname{div} \boldsymbol{v})_\Omega, \quad b_2(\boldsymbol{\mu}_N, \boldsymbol{v}) = (\boldsymbol{\mu}_N, \boldsymbol{v})_\varepsilon \\ &c(\boldsymbol{\mu}_N) = (\boldsymbol{\mu}_N, \boldsymbol{v}_\mathrm{b} + \varepsilon w_\mathrm{b} \boldsymbol{e}_\theta)_\varepsilon. \end{aligned} \tag{4.2.15}$$

First, using Korn inequality and Cauchy-Schwarz inequality, we have that the bilinear form a is continuous and coercive, with norm $\|a\|$ and coercivity constant α bounded independently of N and ε. Similarly, using Cauchy-Schwarz inequality and Lemma 3.3.2, we can derive the following inequalities for b_1 and b_2:

$$\begin{cases} |b_1(p, \boldsymbol{v})| \leqslant \|p\|_\Omega \|\operatorname{div} \boldsymbol{v}\|_\Omega \leqslant \|p\|_\Omega \|\boldsymbol{v}\|_{1,\Omega}, \\ |b_2(\boldsymbol{\mu}_N, \boldsymbol{v})| \leqslant \|\boldsymbol{\mu}_N\|_{-\frac{1}{2},\varepsilon} \|\boldsymbol{v}\|_{\frac{1}{2},\varepsilon} \lesssim |\log(\varepsilon)|^{\frac{1}{2}} \|\boldsymbol{\mu}_N\|_{-\frac{1}{2},\varepsilon} \|\boldsymbol{v}\|_{1,\Omega} \end{cases} \tag{4.2.16}$$

for all $(p, \boldsymbol{\mu}_N, \boldsymbol{v}) \in Q \times \boldsymbol{F}_N \times \boldsymbol{V}$. This implies that the bilinear forms b_1 and b_2 are continuous and

$$\|b_1\| \lesssim 1, \quad \|b_2\| \lesssim |\log(\varepsilon)|^{\frac{1}{2}}. \tag{4.2.17}$$

Furthermore, we have

$$\begin{aligned} |c_2(\boldsymbol{\mu}_N)| &\lesssim \|\boldsymbol{\mu}_N\|_{-\frac{1}{2},\varepsilon} \|\boldsymbol{u}_\mathrm{b}\|_{\frac{1}{2},\varepsilon} \\ &\lesssim \|\boldsymbol{\mu}_N\|_{-\frac{1}{2},\varepsilon} (|\boldsymbol{v}_\mathrm{b}| + \varepsilon |w_\mathrm{b}|) \quad \forall \boldsymbol{\mu}_N \in \boldsymbol{F}_N, \end{aligned} \tag{4.2.18}$$

which gives the continuity of the linear form c_2. We also deduce from (4.2.18) that the norm $\|c_2\|$ of c_2 is bounded by $|\boldsymbol{v}_{\rm b}| + \varepsilon|w_{\rm b}|$ up to multiplicative constant uniformly independent of N and ε. Let us now prove the inf-sup conditions by establishing the existence of β_1, $\beta_2 > 0$ uniformly independent of N and ε satisfying

$$\left\{\begin{array}{l} \displaystyle\sup_{\boldsymbol{v}\in\boldsymbol{V},\,\boldsymbol{\Pi}_\varepsilon^N(\boldsymbol{v})=\boldsymbol{0}} \frac{b_1(q,\boldsymbol{v})}{\|\boldsymbol{v}\|_{1,\Omega}} \geqslant \beta_1|\log(\varepsilon)|^{-\frac{1}{2}}\|q\|_\Omega \quad \forall q\in Q, \\ \displaystyle\sup_{\boldsymbol{v}\in\boldsymbol{H}_0^1(\Omega),\,\mathrm{div}\,\boldsymbol{v}=0} \frac{b_2(\boldsymbol{\mu}_N,\boldsymbol{v})}{\|\boldsymbol{v}\|_{1,\Omega}} \geqslant \beta_2\|\boldsymbol{\mu}_N\|_{-\frac{1}{2},\varepsilon} \quad \forall \boldsymbol{\mu}_N\in\boldsymbol{F}_N. \end{array}\right. \tag{4.2.19}$$

Let $q \in Q$ be given. According to Lemma 4.2.3, there exists $\boldsymbol{w}_q^\varepsilon \in \boldsymbol{H}_0^1(\Omega)$ such that

$$\mathrm{div}\,\boldsymbol{w}_q^\varepsilon = q \quad \text{in} \quad \Omega, \quad \boldsymbol{w}_q^\varepsilon = \boldsymbol{0} \quad \text{on} \quad \partial\omega^\varepsilon, \quad \|\boldsymbol{w}_q^\varepsilon\|_{1,\Omega} \leqslant \beta_1|\log(\varepsilon)|^{\frac{1}{2}}\|q\|_\Omega,$$

with β_1 uniformly independent of N and ε. We deduce that

$$\begin{aligned} \|q\|_\Omega = \frac{(q,\mathrm{div}\,\boldsymbol{w}_q^\varepsilon)_\Omega}{\|q\|_\Omega} &\leqslant \beta_1^{-1}|\log(\varepsilon)|^{\frac{1}{2}}\frac{(q,\mathrm{div}\,\boldsymbol{w}_q^\varepsilon)_\Omega}{\|\boldsymbol{w}_q^\varepsilon\|_{1,\Omega}} \\ &\leqslant \beta_1^{-1}|\log(\varepsilon)|^{\frac{1}{2}} \sup_{\boldsymbol{v}\in\boldsymbol{H}_0^1(\Omega),\,\boldsymbol{\Pi}_N^\varepsilon(\boldsymbol{v})=\boldsymbol{0}} \frac{b_1(q,\boldsymbol{v})}{\|\boldsymbol{v}\|_{1,\Omega}}, \end{aligned}$$

Let $\boldsymbol{\mu}_N \in \boldsymbol{F}_N$ be given. For all $\boldsymbol{\eta} \in \boldsymbol{H}^{\frac{1}{2}}(\partial\omega^\varepsilon)$, $\boldsymbol{\Pi}_N(\boldsymbol{\eta}) \in \boldsymbol{H}^{\frac{1}{2}}(\partial\omega^\varepsilon) \cap \boldsymbol{L}^2_{0,\boldsymbol{n}}(\partial\omega^\varepsilon)$, so according to Lemma 4.2.2, there exists $\boldsymbol{v}_{\boldsymbol{\eta}}^\varepsilon \in \boldsymbol{H}_0^1(\Omega)$ such that

$$\boldsymbol{v}_{\boldsymbol{\eta}}^\varepsilon = \boldsymbol{\Pi}_N(\boldsymbol{\eta}) \quad \text{on} \quad \partial\omega^\varepsilon, \quad \mathrm{div}\,\boldsymbol{v}_{\boldsymbol{\eta}}^\varepsilon = 0 \quad \text{in} \quad \Omega, \quad \|\boldsymbol{v}_{\boldsymbol{\eta}}^\varepsilon\|_{1,\Omega} \lesssim \|\boldsymbol{\Pi}_N^\varepsilon(\boldsymbol{\eta})\|_{\frac{1}{2},\varepsilon} \leqslant \beta_2\|\boldsymbol{\eta}\|_{\frac{1}{2},\varepsilon},$$

with β_2 uniformly independent of N and ε. We deduce that

$$\frac{(\boldsymbol{\mu}_N,\boldsymbol{\eta})_{-\frac{1}{2},\varepsilon}}{\|\boldsymbol{\eta}\|_{\frac{1}{2},\varepsilon}} = \frac{(\boldsymbol{\mu}_N,\boldsymbol{v}_{\boldsymbol{\eta}}^\varepsilon)_\varepsilon}{\|\boldsymbol{\mu}_N\|_{\frac{1}{2},\varepsilon}} \leqslant \beta_2^{-1}\frac{(\boldsymbol{\mu}_N,\boldsymbol{v}_{\boldsymbol{\eta}}^\varepsilon)_\varepsilon}{\|\boldsymbol{v}_{\boldsymbol{\eta}}^\varepsilon\|_{1,\Omega}} \leqslant \beta_2^{-1} \sup_{\boldsymbol{v}\in\boldsymbol{H}_0^1(\Omega),\,\mathrm{div}\,\boldsymbol{v}=0} \frac{(\boldsymbol{\mu}_N,\boldsymbol{v})_\varepsilon}{\|\boldsymbol{v}\|_{1,\Omega}}.$$

We conclude by taking the supremum over $\boldsymbol{\eta} \in \boldsymbol{H}^{\frac{1}{2}}(\partial\omega^\varepsilon)$. By Theorem 4.2.4, we deduce that Problem (4.2.6) is well-posed and that the solution satisfies

$$\begin{aligned} &\|\boldsymbol{u}_N^\varepsilon\|_{1,\Omega} \lesssim \beta_2^{-1}(1+\alpha^{-1}\|a\|)(|\boldsymbol{v}_{\rm b}| + \varepsilon|w_{\rm b}|) \lesssim |\boldsymbol{v}_{\rm b}| + \varepsilon|w_{\rm b}| \\ &\|p_N^\varepsilon\|_\Omega \lesssim \beta_1^{-1}|\log(\varepsilon)|^{\frac{1}{2}}(\|a\|\|\boldsymbol{u}_N^\varepsilon\|_{1,\Omega}) \lesssim |\log(\varepsilon)|^{\frac{1}{2}}(|\boldsymbol{v}_{\rm b}| + \varepsilon|w_{\rm b}|), \\ &\|\boldsymbol{\lambda}_N^\varepsilon\|_{-\frac{1}{2},\varepsilon} \lesssim \beta_2^{-1}\|a\|\|\boldsymbol{u}_N^\varepsilon\|_{1,\Omega} \lesssim |\boldsymbol{v}_{\rm b}| + \varepsilon|w_{\rm b}|, \end{aligned}$$

which can be written equivalently as (4.2.1). □

4.2.2 Convergence to the full order model

The objective of this section is to study the behavior of the solution of Problem (4.2.14) as $\varepsilon \to 0$. Specifically, similarly to the convergence result given in Theorem 3.3.4 relative to the reduced order Poisson problem, we aim to analyze its asymptotic behavior with respect to the solution of the following full order Stokes problem: find $(\boldsymbol{u}^\varepsilon, p^\varepsilon, \boldsymbol{\lambda}^\varepsilon) \in \boldsymbol{V} \times Q \times \boldsymbol{H}_\star^{-\frac{1}{2}}(\partial\omega^\varepsilon)$ such that

$$\begin{cases} 2(\boldsymbol{\varepsilon}(\boldsymbol{u}^\varepsilon), \boldsymbol{\varepsilon}(\boldsymbol{v}))_\Omega - (p^\varepsilon, \operatorname{div} \boldsymbol{v})_\Omega - \langle \boldsymbol{\lambda}^\varepsilon, \boldsymbol{v} \rangle_{-\frac{1}{2},\partial\omega^\varepsilon} = 0 \quad \forall \boldsymbol{v} \in \boldsymbol{V}, \\ (q, \operatorname{div} \boldsymbol{u}^\varepsilon)_\Omega = 0 \quad \forall q \in Q, \\ \langle \boldsymbol{\mu}, \boldsymbol{u}^\varepsilon \rangle_{-\frac{1}{2},\partial\omega^\varepsilon} = \langle \boldsymbol{\mu}, \boldsymbol{v}_{\mathrm{b}} + w_b \boldsymbol{e}_\theta \rangle_{-\frac{1}{2},\partial\omega^\varepsilon} \quad \forall \boldsymbol{\mu} \in \boldsymbol{H}_\star^{-\frac{1}{2}}(\partial\omega^\varepsilon), \end{cases} \tag{4.2.20}$$

where $\boldsymbol{H}_\star^{-\frac{1}{2}}(\partial\omega^\varepsilon)$ is the dual space of $\boldsymbol{H}^{\frac{1}{2}}(\partial\omega^\varepsilon) \cap \boldsymbol{L}^2_{0,\boldsymbol{n}}(\partial\omega^\varepsilon)$ equipped with the following norm:

$$\|\boldsymbol{\lambda}\|^\star_{-\frac{1}{2},\varepsilon} = \sup_{\boldsymbol{\mu} \in \boldsymbol{H}^{\frac{1}{2}}(\partial\omega^\varepsilon) \cap \boldsymbol{L}^2_{0,\boldsymbol{n}}(\partial\omega^\varepsilon)} \frac{\langle \boldsymbol{\lambda}, \boldsymbol{\mu} \rangle_{-\frac{1}{2},\varepsilon}}{\|\boldsymbol{\mu}\|_{\frac{1}{2},\varepsilon}} \quad \forall \boldsymbol{\lambda} \in \boldsymbol{H}_\star^{-\frac{1}{2}}(\partial\omega^\varepsilon).$$

The convergence result regarding Problem (4.2.14) is given in Theorem 4.2.5. Since in this chapter, we take $\boldsymbol{f} = \boldsymbol{0}$, the parameter ρ is defined by $\rho \overset{\text{def}}{=} d(\{\boldsymbol{0}\}, \partial\Omega)$ where as in Chapter 3, $d(\cdot,\cdot)$ is the Euclidean distance of two sets.

Theorem 4.2.5. *Let $(\boldsymbol{u}^\varepsilon, p^\varepsilon, \boldsymbol{\lambda}^\varepsilon) \in \boldsymbol{V} \times Q \times \boldsymbol{H}_\star^{-\frac{1}{2}}(\partial\omega^\varepsilon)$ and let $(\boldsymbol{u}_N^\varepsilon, p_N^\varepsilon, \boldsymbol{\lambda}_N^\varepsilon) \in \boldsymbol{V} \times Q \times \boldsymbol{F}_N$ be the solution of* (4.2.14) *and* (4.2.20)*, respectively. There exists $0 < \tilde{\rho} < \rho$ such that for all $\varepsilon \in (0, \tilde{\rho})$, we have*

$$\|\boldsymbol{u}_N^\varepsilon - \boldsymbol{u}^\varepsilon\|_{1,\Omega} + \varepsilon \|\varepsilon^{-1}\boldsymbol{\lambda}_N^\varepsilon - \boldsymbol{\lambda}^\varepsilon\|^\star_{-\frac{1}{2},\varepsilon} + |\log(\varepsilon)|^{-\frac{1}{2}} \|p_N^\varepsilon - p^\varepsilon\|_\Omega \lesssim (1+N) \left(\frac{\varepsilon}{\rho}\right)^{N+1} (|\boldsymbol{v}_{\mathrm{b}}| + \varepsilon |w_{\mathrm{b}}|). \tag{4.2.21}$$

In the same way as for the proof of the convergence of the Poisson problem we need two preliminary lemmas. The first lemma is a standard result which gives an expression of $\boldsymbol{\lambda}_N^\varepsilon$ in terms of the stress jump across $\partial\omega^\varepsilon$. It is the counterpart of Lemma 3.3.5 adapted to the Stokes equations.

Lemma 4.2.6. *Let $(\boldsymbol{u}_N^\varepsilon, p_N^\varepsilon, \boldsymbol{\lambda}_N^\varepsilon) \in \boldsymbol{V} \times Q \times \boldsymbol{F}_N$ be the solution of Problem* (4.2.14)*. We have in $\boldsymbol{H}^{-\frac{1}{2}}(\partial\omega^\varepsilon)$*

$$\boldsymbol{\lambda}_N^\varepsilon = \varepsilon \big(\boldsymbol{\sigma}(\boldsymbol{u}_N^\varepsilon, p_N^\varepsilon)^+ \boldsymbol{n}^+ - \boldsymbol{\sigma}(\boldsymbol{u}_N^\varepsilon, p_N^\varepsilon)^- \boldsymbol{n}^+ \big), \tag{4.2.22}$$

where $\boldsymbol{n}^+$ is the exterior normal vector to $\partial\Omega^\varepsilon$, and $\boldsymbol{\sigma}(\boldsymbol{u}_N^\varepsilon, p_N^\varepsilon)^+$ and $\boldsymbol{\sigma}(\boldsymbol{u}_N^\varepsilon, p_N^\varepsilon)^-$ are the restrictions of $\boldsymbol{\sigma}(\boldsymbol{u}_N^\varepsilon, p_N^\varepsilon)$ to Ω^ε and ω^ε, respectively.

The proof of this lemma is given in Section 4.A.5 of the Appendix. The second lemma describes the behaviour of the Fourier modes of $\boldsymbol{u}_N^\varepsilon$ on $\partial\omega^\varepsilon$. As for the previous Lemma, it can be seen as the adaption of Lemma 3.3.6 to the Stokes equations.

Lemma 4.2.7. *Let $\boldsymbol{u}_N^\varepsilon \in \boldsymbol{V}$ be the solution of Problem* (4.2.14) *and let $\boldsymbol{u}_\mathrm{b}$ be given by* (4.2.5)*. There exists $a_{k,r}^\varepsilon$, $a_{k,\theta}^\varepsilon$, $b_{k,r}^\varepsilon$, $b_{k,\theta}^\varepsilon \in \mathbb{R}$ such that for $\varepsilon \in (0,\rho)$,*

$$\begin{aligned}(\boldsymbol{u}_N^\varepsilon(\varepsilon)(\theta) - \boldsymbol{u}_\mathrm{b}(\varepsilon)(\theta)) \cdot \boldsymbol{e}_r &= \left(\frac{\varepsilon}{\rho}\right)^{N+1} \sum_{k=N}^{\infty} \big(a_{k,r}^\varepsilon \cos(k\theta) + b_{k,r}^\varepsilon \sin(k\theta)\big),\\ (\boldsymbol{u}_N^\varepsilon(\varepsilon)(\theta) - \boldsymbol{u}_\mathrm{b}(\varepsilon)(\theta)) \cdot \boldsymbol{e}_\theta &= \left(\frac{\varepsilon}{\rho}\right)^{N+1} \sum_{k=N}^{\infty} \big(a_{k,\theta}^\varepsilon \cos(k\theta) + b_{k,\theta}^\varepsilon \sin(k\theta)\big),\end{aligned} \tag{4.2.23}$$

Moreover, there exists $0 < \tilde\rho < \rho$ such that for $\varepsilon \in (0,\tilde\rho)$, the following estimate holds:

$$\left(\sum_{k=N}^{\infty} (1+k)\big(|a_{k,r}^\varepsilon|^2 + |a_{k,\theta}^\varepsilon|^2 + |b_{k,r}^\varepsilon|^2 + |b_{k,\theta}^\varepsilon|^2\big)\right)^{\frac12} \lesssim (1+N)\,(|\boldsymbol{v}_\mathrm{b}| + \varepsilon|w_\mathrm{b}|).$$

For clarity, its proof is given in the Section 4.A.6 of the Appendix.

Proof of Theorem 4.2.5. We consider a fixed $\varepsilon \in (0,\tilde\rho)$. Let us note that $\boldsymbol{u}_N^\varepsilon - \boldsymbol{u}^\varepsilon$ satisfies (4.2.2) in Ω with $\boldsymbol{\eta} = \boldsymbol{u}_N^\varepsilon - \boldsymbol{u}_\mathrm{b}$. Therefore, using Lemma 4.2.2 and the ε-equivalence of the norms $\|\cdot\|_{\frac12,\varepsilon}$ and $\|\cdot\|_{\frac12,\varepsilon}^{\mathscr{F}}$, we get

$$\|\boldsymbol{u}_N^\varepsilon - \boldsymbol{u}^\varepsilon\|_{1,\Omega} \lesssim \|\boldsymbol{u}_N^\varepsilon - \boldsymbol{u}_\mathrm{b}\|_{\frac12,\varepsilon} \lesssim \|\boldsymbol{u}_N^\varepsilon - \boldsymbol{u}_\mathrm{b}\|_{\frac12,\varepsilon}^{\mathscr{F}}.$$

Thus, using Lemma 4.2.7 and the definition of the norm $\|\cdot\|_{\frac12,\varepsilon}^{\mathscr{F}}$, we have that there exists $\tilde\rho > 0$ such that for $\varepsilon \in (0,\tilde\rho)$,

$$\|\boldsymbol{u}_N^\varepsilon - \boldsymbol{u}^\varepsilon\|_{1,\Omega} \lesssim (1+N)\left(\frac{\varepsilon}{\rho}\right)^{N+1} (|\boldsymbol{v}_\mathrm{b}| + \varepsilon|w_\mathrm{b}|). \tag{4.2.24}$$

To obtain an estimate for $\|\varepsilon^{-1}\boldsymbol{\lambda}_N - \boldsymbol{\lambda}^\varepsilon\|_{-\frac12,\varepsilon}^\star$, we notice from the formulation (4.2.14) and (4.2.20) that $(\boldsymbol{u}_N^\varepsilon - \boldsymbol{u}^\varepsilon, p_N^\varepsilon - p^\varepsilon, \varepsilon^{-1}\boldsymbol{\lambda}_N^\varepsilon - \boldsymbol{\lambda}^\varepsilon)$ satisfies

$$2(\boldsymbol{\varepsilon}(\boldsymbol{u}_N^\varepsilon - \boldsymbol{u}^\varepsilon), \boldsymbol{\varepsilon}(\boldsymbol{v}))_\Omega - (p_N^\varepsilon - p^\varepsilon, \operatorname{div}\boldsymbol{v})_\Omega - \langle \varepsilon^{-1}\boldsymbol{\lambda}_N^\varepsilon - \boldsymbol{\lambda}^\varepsilon, \boldsymbol{v}\rangle_{-\frac12,\varepsilon} = 0 \quad \forall \boldsymbol{v} \in \boldsymbol{H}_0^1(\Omega).$$

By definition of the $\|\cdot\|_{-\frac12,\varepsilon}^\star$ norm,

$$\|\varepsilon^{-1}\boldsymbol{\lambda}_N^\varepsilon - \boldsymbol{\lambda}^\varepsilon\|_{-\frac12,\varepsilon}^\star = \sup_{\boldsymbol{\eta}\in \boldsymbol{H}^{\frac12}(\partial\omega^\varepsilon)\cap \boldsymbol{L}^2_{0,\boldsymbol{n}}(\partial\omega^\varepsilon)} \frac{\langle \varepsilon^{-1}\boldsymbol{\lambda}_N^\varepsilon - \boldsymbol{\lambda}^\varepsilon, \boldsymbol{\eta}\rangle_{-\frac12,\varepsilon}}{\|\boldsymbol{\eta}\|_{\frac12,\varepsilon}}$$

For all $\boldsymbol{\eta} \in \boldsymbol{H}^{\frac{1}{2}}(\partial\omega^\varepsilon) \cap \boldsymbol{L}^2_{0,\boldsymbol{n}}(\partial\omega^\varepsilon)$, taking $\boldsymbol{v}^\varepsilon_{\boldsymbol{\eta}} \in \boldsymbol{H}^1_0(\Omega)$ as defined in Lemma 4.2.2, we have

$$\begin{aligned}\frac{\langle \varepsilon^{-1}\boldsymbol{\lambda}^\varepsilon_N - \boldsymbol{\lambda}^\varepsilon, \boldsymbol{\eta}\rangle_{-\frac{1}{2},\varepsilon}}{\|\boldsymbol{\eta}\|_{\frac{1}{2},\varepsilon}} &\lesssim \frac{\langle \varepsilon^{-1}\boldsymbol{\lambda}^\varepsilon_N - \boldsymbol{\lambda}^\varepsilon, \boldsymbol{v}^\varepsilon_{\boldsymbol{\eta}}\rangle_{-\frac{1}{2},\varepsilon}}{\|\boldsymbol{v}^\varepsilon_{\boldsymbol{\eta}}\|_{1,\Omega}} \\ &\lesssim \sup_{\boldsymbol{v}\in\boldsymbol{V},\,\mathrm{div}\,\boldsymbol{v}=0} \frac{\langle \varepsilon^{-1}\boldsymbol{\lambda}^\varepsilon_N - \boldsymbol{\lambda}^\varepsilon, \boldsymbol{v}\rangle_{-\frac{1}{2},\varepsilon}}{\|\boldsymbol{v}\|_{1,\Omega}} \\ &\lesssim \varepsilon^{-1} \sup_{\boldsymbol{v}\in\boldsymbol{V},\,\mathrm{div}\,\boldsymbol{v}=0} \frac{2(\boldsymbol{\varepsilon}(\boldsymbol{u}^\varepsilon_N - \boldsymbol{u}^\varepsilon), \boldsymbol{\varepsilon}(\boldsymbol{v}))_\Omega}{\|\boldsymbol{v}\|_{1,\Omega}}\end{aligned}$$

Taking the supremum over $\boldsymbol{\eta} \in \boldsymbol{H}^{\frac{1}{2}}(\partial\omega^\varepsilon) \cap \boldsymbol{L}^2_{0,\boldsymbol{n}}(\partial\omega^\varepsilon)$, we deduce that

$$\|\varepsilon^{-1}\boldsymbol{\lambda}^\varepsilon_N - \boldsymbol{\lambda}^\varepsilon\|^*_{-\frac{1}{2},\varepsilon} \lesssim \varepsilon^{-1}\|\boldsymbol{u}^\varepsilon_N - \boldsymbol{u}^\varepsilon\|_{1,\Omega},$$

Similarly, by taking $\boldsymbol{v}^\varepsilon_{p^\varepsilon - p^\varepsilon_N}$ as defined in Lemma 4.3.9, we also have

$$\|p^\varepsilon_N - p^\varepsilon\|_\Omega \lesssim |\log(\varepsilon)|^{\frac{1}{2}}\|\boldsymbol{u}^\varepsilon_N - \boldsymbol{u}^\varepsilon\|_{1,\Omega}.$$

We conclude thanks to (4.2.24) that (4.2.21) holds. □

Remark 14. Note that, in the fictitious domain method, as expressed in Lemma 4.2.6 for the solution of problem (4.2.14), the force and moment transmitted to the structure include a spurious internal fluid stress. This applies in particular to the solution of (4.2.20). However, since $(\boldsymbol{u}^\varepsilon, p^\varepsilon)$ is solution of the Stokes equation in ω^ε with rigid body motion on $\partial\omega^\varepsilon$, we have

$$\boldsymbol{\sigma}(\boldsymbol{u}^\varepsilon, p^\varepsilon)^-\boldsymbol{n}^+ = p^-\boldsymbol{n}^+ \quad \text{on} \quad \partial\omega^\varepsilon.$$

with p^- constant. We then deduce that

$$\int_{\partial\omega^\varepsilon} \boldsymbol{\sigma}(\boldsymbol{u}^\varepsilon, p^\varepsilon)^-\boldsymbol{n}^+ = \boldsymbol{0}, \quad \int_{\partial\omega^\varepsilon} \boldsymbol{e}_\theta \cdot \boldsymbol{\sigma}(\boldsymbol{u}^\varepsilon, p^\varepsilon)^-\boldsymbol{n}^+ = 0.$$

such that there is no furious force contributions. In particular for all $\delta\boldsymbol{r} \in \mathbb{R}^2$,

$$\begin{aligned}&|(\varepsilon^{-1}\boldsymbol{\lambda}^\varepsilon_N - \boldsymbol{\sigma}(\boldsymbol{u}^\varepsilon, p^\varepsilon)^+\boldsymbol{n}^+, \delta\boldsymbol{r})_{\partial\omega^\varepsilon}| = |\varepsilon(\varepsilon^{-1}\boldsymbol{\lambda}^\varepsilon_N - \boldsymbol{\lambda}^\varepsilon, \delta\boldsymbol{r})_\varepsilon| \\ &\lesssim \varepsilon\|\varepsilon^{-1}\boldsymbol{\lambda}^\varepsilon_N - \boldsymbol{\lambda}^\varepsilon\|^*_{-\frac{1}{2},\varepsilon}\|\delta\boldsymbol{r}\|_{\frac{1}{2},\varepsilon} \lesssim (1+N)\left(\frac{\varepsilon}{\rho}\right)^{N+1}(|\boldsymbol{v}_\mathrm{b}| + \varepsilon|w_\mathrm{b}|)|\delta\boldsymbol{r}|,\end{aligned}$$

and for all $\delta\theta \in \mathbb{R}$,

$$\begin{aligned}&|(\varepsilon^{-1}\boldsymbol{\lambda}^\varepsilon_N - \boldsymbol{\sigma}(\boldsymbol{u}^\varepsilon, p^\varepsilon)^+\boldsymbol{n}^+, \varepsilon\delta\theta\boldsymbol{e}_\theta)_{\partial\omega^\varepsilon}| = |\varepsilon(\varepsilon^{-1}\boldsymbol{\lambda}^\varepsilon_N - \boldsymbol{\lambda}^\varepsilon, \varepsilon\delta\theta\boldsymbol{e}_\theta)_\varepsilon| \\ &\lesssim \varepsilon\|\varepsilon^{-1}\boldsymbol{\lambda}^\varepsilon_N - \boldsymbol{\lambda}^\varepsilon\|^*_{-\frac{1}{2},\varepsilon}\|\delta\theta\boldsymbol{e}_\theta\|_{\frac{1}{2},\varepsilon} \lesssim \left(\frac{\varepsilon}{\rho}\right)^{N+1}(|\boldsymbol{v}_\mathrm{b}| + \varepsilon|w_\mathrm{b}|)|\delta\theta|,\end{aligned}$$

such that the resultant force and moment applied on $\partial\omega^\varepsilon$ are well approximated by $\varepsilon^{-1}\boldsymbol{\lambda}^\varepsilon_N$ as $\varepsilon \to 0$.

4.3 Numerical approximation

This section is devoted to the discretization of Problem (4.2.6). Similarly to the reduced order Poisson problem introduced in Chapter 3, the reduced order Dirichlet boundary conditions on $\partial\omega^\varepsilon$ do not prevent potential discontinuities of the pressure or the velocity gradient. More precisely, we cannot reach the traditional $H^1(\Omega)$ and $\boldsymbol{H}^2(\Omega)$ regularity for the pressure and velocity. In particular, proceeding similarly to Section 3.3.3, we could prove that the maximum regularity for u_N^ε and p_N^ε is $\boldsymbol{H}^{\frac{3}{2}-\eta}$ and $H^{\frac{1}{2}-\eta}$, respectively, for $\eta > 0$. Consequently, in Section 4.3.1, we introduce a low-order fictitious domain stabilized finite element method based on continuous piecewise affine approximations, which is the adaptation of the discrete Problem (3.4.1) to the Stokes equations. Following that, to address the issue posed by the low regularity of the reduced order Stokes solution, in a similar manner to what done in Section 3.4.3 for the reduced order Poisson problem, we present in Section 4.3.2 an augmented high-order divergence-free conforming finite element method. This method is based on the inclusion of additional velocity and pressure singular functions in the finite element space designed to capture the singularities of the continuous solution.

4.3.1 Low-order stabilized finite element method scheme

In this section, we propose and analyze the stability of a low-order stabilized finite element method for discretizing Problem (4.2.6). We recall here the definition of the standard spaces of continuous piecewise affine functions given in the previous chapters:

$$\boldsymbol{X}_h^1(\Omega) \stackrel{\text{def}}{=} \left\{\boldsymbol{v} \in \boldsymbol{H}^1(\Omega) \mid \boldsymbol{v}|_K \in [\mathbb{P}_1(K)]^3, \quad \forall K \in \mathcal{T}_h(\Omega)\right\},$$
$$X_h^1(\Omega) \stackrel{\text{def}}{=} \left\{v \in H^1(\Omega) \mid v|_K \in \mathbb{P}_1(K), \quad \forall K \in \mathcal{T}_h(\Omega)\right\}.$$

We then introduce the discrete spaces $\boldsymbol{V}_h$ and Q_h for the approximation of the fluid velocity $\boldsymbol{u}_N^\varepsilon$ and the fluid pressure p_N^ε as follows:

$$\boldsymbol{V}_h \stackrel{\text{def}}{=} \boldsymbol{X}_h^1(\Omega) \cap \boldsymbol{V}, \quad Q_h \stackrel{\text{def}}{=} X_h^1(\Omega) \cap Q.$$

The Lagrange multiplier space remains unchanged and is still equal to $\boldsymbol{F}_N$. In order to overcome the instability of the saddle point problem due to the choice of the Lagrange multiplier space $\boldsymbol{F}_N$, we introduce the following stabilization term (see also [Barrenechea and González, 2018]):

$$s_h^\lambda(\boldsymbol{\mu}_N, \boldsymbol{\lambda}_N) \stackrel{\text{def}}{=} \gamma_\lambda \left(\frac{h}{\varepsilon}\right) \varepsilon^{-1}(\boldsymbol{\mu}_N, \boldsymbol{\lambda}_N)_\varepsilon, \quad \forall (\boldsymbol{\mu}_N, \boldsymbol{\lambda}_N) \in \boldsymbol{F}_N \times \boldsymbol{F}_N,$$

where $\gamma_\lambda > 0$ is a user-defined dimensionless parameter uniformly independent of h, N and ε. Furthermore, the following Brezzi-Pitkaranta stabilization [Brezzi and Pitkäranta,

1984] is considered to overcome the lack of inf-sup compatibility between the velocity and pressure spaces $\boldsymbol{V}_h$ and Q_h:

$$s_h^p(q_h, p_h) \stackrel{\text{def}}{=} \gamma_p |\log(\varepsilon)| h^2 (\nabla q_h, \nabla p_h)_\Omega, \quad \forall (q_h, p_h) \in Q_h,$$

where $\gamma_p > 0$ is a user-defined dimensionless parameter uniformly independent of h, N and ε. The proposed stabilized finite element approximation of Problem (4.4.3) reads as follows: find $(\boldsymbol{u}_{N,h}^\varepsilon, p_{N,h}^\varepsilon, \boldsymbol{\lambda}_{N,h}^\varepsilon) \in \boldsymbol{V}_h \times Q_h \times \boldsymbol{F}_N$ such that

$$\begin{aligned} a(\boldsymbol{u}_{N,h}^\varepsilon, \boldsymbol{v}_h) - b_1(p_{N,h}^\varepsilon, \boldsymbol{v}_h) - b_2(\boldsymbol{\lambda}_{N,h}^\varepsilon, \boldsymbol{v}_h) = 0 \quad & \forall \boldsymbol{v}_h \in \boldsymbol{V}_h, \\ b_2(q_h, p_h) + s_h^p(q_h, p_{N,h}^\varepsilon) = 0 \quad & \forall q_h \in Q_h \\ b_1(\boldsymbol{\mu}_N, \boldsymbol{u}_{N,h}^\varepsilon) + s_h^\lambda(\boldsymbol{\mu}_N, \boldsymbol{\lambda}_{N,h}^\varepsilon) = (\boldsymbol{\mu}_N, \boldsymbol{v}_{\mathrm{b}} + w_{\mathrm{b}} \boldsymbol{e}_\theta)_\varepsilon \quad & \forall \boldsymbol{\mu}_N \in \boldsymbol{F}_N \end{aligned} \tag{4.3.1}$$

where the bilinear forms a, b_1 and b_2 are given in (4.2.15).

4.3.1.1 Interpolation operators

The minimum regularity required for the Scott-Zhang operator introduced in Proposition 3.4.1 is $H^{\frac{1}{2}}(\Omega)$. However, due to the potential discontinuity at the interface $\partial\omega^\varepsilon$, the maximum regularity of the pressure is $H^{\frac{1}{2}-\eta}(\Omega)$. Consequently, we consider quasi-interpolation operators designed for the approximation of non smooth functions, (see e.g. [Ern and Guermond, 2021, Chapitre 22]). Let $\tilde{\Pi}_h : H^{\frac{1}{2}-\eta}(\Omega) \to X_h^1(\Omega)$ be a given quasi-interpolation operator, it satisfies

$$\|q - \tilde{\Pi}_h q\|_\Omega \lesssim h^{\frac{1}{2}-\eta} \|q\|_{\frac{1}{2}-\eta,\Omega}, \quad h\|\nabla(\tilde{\Pi}_h q)\|_\Omega \lesssim h^{\frac{1}{2}-\eta} \|q\|_{\frac{1}{2}-\eta,\Omega}. \tag{4.3.2}$$

The first estimate is a consequence of the approximation properties of quasi-interpolators (see, e.g., [Ern and Guermond, 2021, Theorem 22.6]) while the second is a consequence of an inverse inequality (see, e.g, [Corti et al., 2023, Lemma 4.3]). However, the extension of $\tilde{\Pi}_h$ to a quasi-interpolator $\overline{\Pi}_h$ with value in Q_h is a bit technical due to the use of unfitted meshes. Hence, we make the assumption without proof that there exists $\overline{\Pi}_h : Q \to Q_h$ satisfying (4.3.2).

4.3.1.2 Preliminary results

We start by introducing a well-designed interpolation operator that will be used to establish the inf-sup condition, see [Corti et al., 2023, Proposition 4.5].

Proposition 4.3.1. *There exists a linear operator $\boldsymbol{\Pi}_h^0 : \boldsymbol{V} \to \boldsymbol{V}_h$ such that for every $\boldsymbol{v} \in \boldsymbol{V}$, we have*

$$\boldsymbol{\Pi}_h^0(\boldsymbol{v}) = \boldsymbol{0} \quad \textit{on} \quad \partial\omega^\varepsilon, \tag{4.3.3}$$

$$\boldsymbol{\Pi}_h^0(\boldsymbol{v}) = \boldsymbol{0} \quad \textit{if} \quad \boldsymbol{v} = \boldsymbol{0} \quad \textit{on} \quad \partial\Omega. \tag{4.3.4}$$

Moreover, for each $\boldsymbol{v} \in \boldsymbol{V}$ such that $\boldsymbol{v} = \boldsymbol{0}$ on $\partial\omega^\varepsilon$, it holds

$$\|\boldsymbol{v} - \boldsymbol{\Pi}_h^0 \boldsymbol{v}\|_{1,\Omega} \lesssim h\|\boldsymbol{v}\|_{1,\Omega}, \tag{4.3.5}$$

$$\|\boldsymbol{\Pi}_h^0 \boldsymbol{v}\|_{1,\Omega} \lesssim \|\boldsymbol{v}\|_{1,\Omega}. \tag{4.3.6}$$

We now introduce two preliminary lemmas corresponding to the discrete counterpart of Lemma 4.2.2 and Lemma 4.2.3 respectively.

Lemma 4.3.1. *Consider $\boldsymbol{\lambda}_N \in \boldsymbol{F}_N$ be given. There exists $\boldsymbol{v}^\varepsilon_{\boldsymbol{\lambda}_N,h} \in \boldsymbol{V}_h$ such that*

$$\frac{3}{4}\|\boldsymbol{\lambda}_N\|^2_{-\frac{1}{2},\varepsilon} \leqslant -(\boldsymbol{\lambda}_N, \boldsymbol{v}^\varepsilon_{\boldsymbol{\lambda}_N,h})_\varepsilon + C\left(\frac{h}{\varepsilon}\right)\varepsilon^{-1}\|\boldsymbol{\lambda}_N\|^2_\varepsilon, \quad \|\boldsymbol{v}^\varepsilon_{\boldsymbol{\lambda}_N,h}\|_{1,\Omega} \lesssim \|\boldsymbol{\lambda}_N\|_{-\frac{1}{2},\varepsilon},$$

with C uniformly independent of h, N and ε. Moreover, the following estimate holds:

$$|(q_h, \operatorname{div} \boldsymbol{v}^\varepsilon_{\boldsymbol{\lambda}_N,h})_\Omega| \lesssim h|\log(\varepsilon)|^{\frac{1}{2}}\|\nabla q_h\|_\Omega \|\boldsymbol{\lambda}_N\|_{-\frac{1}{2},\varepsilon} \quad \forall q_h \in Q_h.$$

Proof of Lemma 4.3.1. Let $\boldsymbol{\lambda}_N \in \boldsymbol{F}_N$ be given. According to Lemma 3.4.3, there exists $\boldsymbol{\mathring{v}}^\varepsilon_{\boldsymbol{\lambda}_N,h}$ such that

$$\frac{3}{4}\|\boldsymbol{\lambda}_N\|^2_{-\frac{1}{2},\varepsilon} \leqslant -(\boldsymbol{\lambda}_N, \boldsymbol{\mathring{v}}^\varepsilon_{\boldsymbol{\lambda}_N,h})_\varepsilon + C\left(\frac{h}{\varepsilon}\right)\varepsilon^{-1}\|\boldsymbol{\lambda}_N\|^2_\varepsilon, \tag{4.3.7}$$

$$\|\boldsymbol{\mathring{v}}^\varepsilon_{\boldsymbol{\lambda}_N,h}\|_{1,\Omega} \lesssim \|\boldsymbol{\lambda}_N\|_{-\frac{1}{2},\varepsilon}. \tag{4.3.8}$$

with C uniformly independent of h, N and ε. Furthermore, according to Lemma 4.A.2, there exists $\boldsymbol{\mathring{w}}^\varepsilon_{\boldsymbol{\lambda}_N} \in \boldsymbol{H}^1_0(\Omega)$ such that

$$\operatorname{div} \boldsymbol{\mathring{w}}^\varepsilon_{\boldsymbol{\lambda}_N} = \operatorname{div} \boldsymbol{\mathring{v}}_{\boldsymbol{\lambda}_N,h} \quad \text{in} \quad \Omega, \tag{4.3.9}$$

$$\boldsymbol{\mathring{w}}^\varepsilon_{\boldsymbol{\lambda}_N} = \boldsymbol{0} \quad \text{on} \quad \partial\omega^\varepsilon, \tag{4.3.10}$$

$$\|\boldsymbol{\mathring{w}}^\varepsilon_{\boldsymbol{\lambda}_N}\|_{1,\Omega} \lesssim |\log(\varepsilon)|^{\frac{1}{2}}\|\operatorname{div} \boldsymbol{\mathring{v}}^\varepsilon_{\boldsymbol{\lambda}_N,h}\|_\Omega. \tag{4.3.11}$$

By combining (4.3.8) and (4.3.11), we derive

$$\begin{aligned}\|\boldsymbol{\mathring{w}}^\varepsilon_{\boldsymbol{\lambda}_N}\|_{1,\Omega} \lesssim |\log(\varepsilon)|^{\frac{1}{2}}\|\operatorname{div} \boldsymbol{\mathring{v}}^\varepsilon_{\boldsymbol{\lambda}_N,h}\|_\Omega &\lesssim |\log(\varepsilon)|^{\frac{1}{2}}\|\boldsymbol{\mathring{v}}^\varepsilon_{\boldsymbol{\lambda}_N,h}\|_{1,\Omega}, \\ &\lesssim |\log(\varepsilon)|^{\frac{1}{2}}\|\boldsymbol{\lambda}_N\|_{-\frac{1}{2},\varepsilon}.\end{aligned} \tag{4.3.12}$$

Subsequently, we set $\boldsymbol{v}^\varepsilon_{\boldsymbol{\lambda}_N,h} \overset{\text{def}}{=} \boldsymbol{\mathring{v}}^\varepsilon_{\boldsymbol{\lambda}_N,h} - \boldsymbol{\Pi}_h^0 \boldsymbol{\mathring{w}}^\varepsilon_{\lambda_N}$. Considering (4.3.3) and (4.3.10), it holds

$$\boldsymbol{v}^\varepsilon_{\boldsymbol{\lambda}_N,h} = \boldsymbol{\mathring{v}}^\varepsilon_{\boldsymbol{\lambda}_N,h} \quad \text{on} \quad \partial\omega^\varepsilon.$$

Moreover, based on (4.3.6), (4.3.8) and (4.3.12), we have

$$\begin{aligned}\|\boldsymbol{v}^{\varepsilon}_{\boldsymbol{\lambda}_N,h}\|_{1,\Omega} \lesssim \|\boldsymbol{\mathring{v}}^{\varepsilon}_{\boldsymbol{\lambda}_N,h}\|_{1,\Omega} + \|\boldsymbol{\Pi}^0_h \boldsymbol{\mathring{w}}^{\varepsilon}_{\boldsymbol{\lambda}_N,h}\| &\lesssim \|\boldsymbol{\lambda}_N\|_{-\frac{1}{2},\varepsilon} + |\log(\varepsilon)|^{\frac{1}{2}}\|\boldsymbol{\lambda}_N\|_{-\frac{1}{2},\varepsilon},\\ &\lesssim |\log(\varepsilon)|^{\frac{1}{2}}\|\boldsymbol{\lambda}_N\|_{-\frac{1}{2},\varepsilon}.\end{aligned}$$

Finally, by using successively (4.3.9), the properties of $\boldsymbol{\Pi}^0_h$ (Lemma 4.3.1) and estimate (4.3.12), for $q_h \in Q_h$,

$$\begin{aligned}&(q_h, \text{div } \boldsymbol{v}^{\varepsilon}_{\boldsymbol{\lambda}_N,h})_\Omega = (q_h, \text{div } (\boldsymbol{\mathring{v}}^{\varepsilon}_{\boldsymbol{\lambda}_N,h} - \boldsymbol{\Pi}^0_h \boldsymbol{\mathring{w}}^{\varepsilon}_{\boldsymbol{\lambda}_N,h}))_\Omega,\\ &= (q_h, \text{div } (\boldsymbol{\mathring{w}}^{\varepsilon}_{\boldsymbol{\lambda}_N,h} - \boldsymbol{\Pi}^0_h \boldsymbol{\mathring{w}}^{\varepsilon}_{\boldsymbol{\lambda}_N,h}))_\Omega = -(\nabla q_h, \boldsymbol{\mathring{w}}^{\varepsilon}_{\boldsymbol{\lambda}_N,h} - \boldsymbol{\Pi}^0_h \boldsymbol{\mathring{w}}^{\varepsilon}_{\boldsymbol{\lambda}_N,h})_\Omega,\\ &\lesssim h\|\nabla q_h\|_\Omega \|\boldsymbol{w}^{\varepsilon}_{\boldsymbol{\lambda}_N,h}\|_\Omega \lesssim h|\log(\varepsilon)|^{\frac{1}{2}}\|\nabla q_h\|_\Omega \|\boldsymbol{\lambda}_N\|_{-\frac{1}{2},\varepsilon}.\end{aligned}$$

This concludes the proof. □

Lemma 4.3.2. *Let $q_h \in Q_h$ be given. There exists $\boldsymbol{w}^{\varepsilon}_{q_h,h}$ such that*

$$\frac{3}{4}\|q_h\|^2_\Omega \leqslant -(q_h, \text{div } \boldsymbol{w}^{\varepsilon}_{q_h,h})_\Omega + Ch^2|\log(\varepsilon)|\|\nabla q_h\|^2_\Omega, \quad (\boldsymbol{\mu}_N, \boldsymbol{w}^{\varepsilon}_{q_h,h})_\varepsilon = 0 \quad \forall \boldsymbol{\mu}_N \in \boldsymbol{F}_N,$$

with C uniformly independent of h, N and ε. Moreover, the following estimate holds:

$$\|\boldsymbol{w}^{\varepsilon}_{q_h,h}\|_{1,\Omega} \lesssim |\log(\varepsilon)|^{\frac{1}{2}}\|q_h\|_\Omega.$$

Proof of Lemma 4.3.2. Let $q_h \in Q_h$ be given, since $q_h \in Q$, according to Lemma 4.2.3 there exists $\boldsymbol{w}^{\varepsilon}_{q_h} \neq 0 \in \boldsymbol{H}^1_0(\Omega)$ such that

$$\begin{aligned}&\text{div } \boldsymbol{w}^{\varepsilon}_{q_h} = -q_h \quad \text{in} \quad \Omega, \quad \boldsymbol{w}^{\varepsilon}_{q_h} = \boldsymbol{0} \quad \text{on} \quad \partial\omega^{\varepsilon},\\ &\|\boldsymbol{w}^{\varepsilon}_{q_h}\|_{1,\Omega} \lesssim |\log(\varepsilon)|^{\frac{1}{2}}\|q_h\|_\Omega.\end{aligned}$$

By using the properties of $\boldsymbol{\Pi}^0_h$ (see Lemma 4.3.1) and the previous estimates,

$$\begin{aligned}&\|q_h\|^2_\Omega + (q_h, \text{div } (\boldsymbol{\Pi}^0_h \boldsymbol{w}^{\varepsilon}_{q_h}))_\Omega = -(q_h, \text{div}(\boldsymbol{w}^{\varepsilon}_{q_h} - \boldsymbol{\Pi}^0_h \boldsymbol{w}^{\varepsilon}_{q_h}))_\Omega = (\nabla q_h, \boldsymbol{w}^{\varepsilon}_{q_h} - \boldsymbol{\Pi}^0_h \boldsymbol{w}^{\varepsilon}_{q_h})_\Omega\\ &\lesssim h\|\nabla q_h\|_\Omega \|\boldsymbol{w}^{\varepsilon}_{q_h}\|_{1,\Omega} \lesssim h|\log(\varepsilon)|^{\frac{1}{2}}\|\nabla q_h\|_\Omega \|q_h\|_\Omega \leqslant \frac{1}{4}\|q_h\|^2_\Omega + Ch^2|\log(\varepsilon)|\|\nabla q_h\|^2_\Omega.\end{aligned}$$

with C uniformly independent of h, N and ε. Setting $\boldsymbol{w}^{\varepsilon}_{q_h,h} = \boldsymbol{\Pi}^0_h \boldsymbol{w}^{\varepsilon}_{q_h}$ concludes the proof. □

4.3.1.3 Stability

To analyse the stability of Problem (4.3.1), we introduce the following (augmented) bilinear form $B_h : (\boldsymbol{V}_h \times Q_h \times \boldsymbol{F}_N) \times (\boldsymbol{V}_h \times Q_h \times \boldsymbol{F}_N)$ defined for all $(\boldsymbol{u}_h, p_h, \boldsymbol{\lambda}_N), (\boldsymbol{v}_h, q_h, \boldsymbol{\mu}_N) \in \boldsymbol{V}_h \times Q_h \times \boldsymbol{F}_N$ by

$$B_h((\boldsymbol{u}_h, p_h, \boldsymbol{\lambda}_N), (\boldsymbol{v}_h, q_h, \boldsymbol{\mu}_N)) = a(\boldsymbol{u}_h, \boldsymbol{v}_h) - b_1(\boldsymbol{\lambda}_N, \boldsymbol{v}_h) - b_2(p_h, \boldsymbol{v}_h) + b_1(\boldsymbol{\mu}_N, \boldsymbol{u}_h) + b_2(q_h, \boldsymbol{u}_h) + s_h^{\lambda}(\boldsymbol{\mu}_N, \boldsymbol{\lambda}_N) + s_h^{p}(p_h, q_h). \quad (4.3.13)$$

Problem (4.3.1) is equivalent to find $(\boldsymbol{u}_{N,h}^{\varepsilon}, p_{N,h}^{\varepsilon}, \boldsymbol{\lambda}_{N,h}^{\varepsilon}) \in \boldsymbol{V}_h \times Q_h \times \boldsymbol{F}_N$ such that

$$B_h((\boldsymbol{u}_{N,h}^{\varepsilon}, p_{h,N}^{\varepsilon}, \boldsymbol{\lambda}_{N,h}^{\varepsilon}), (\boldsymbol{v}_h, q_h, \boldsymbol{\mu}_N)) = (\boldsymbol{\mu}_N, \boldsymbol{v}_{\mathrm{b}} + \varepsilon w_{\mathrm{b}} \boldsymbol{e}_{\theta})_{\varepsilon}$$

for all $(\boldsymbol{v}_h, q_h, \boldsymbol{\mu}_N) \in \boldsymbol{V}_h \times Q_h \times \boldsymbol{F}_N$. For the analysis of the augmented bilinear form, we introduce the following norm:

$$\|(\boldsymbol{v}_h, q_h, \boldsymbol{\mu}_N)\|_{\varepsilon} \stackrel{\text{def}}{=} \left(\|\boldsymbol{v}_h\|_{1,\Omega}^2 + |\log(\varepsilon)|^{-1}\|p_h\|_{\Omega}^2 + \|\boldsymbol{\mu}_N\|_{-\frac{1}{2},\varepsilon}^2 + h^2|\log(\varepsilon)|\|\nabla p_h\|_{\Omega}^2 + \left(\frac{h}{\varepsilon}\right)\varepsilon^{-1}\|\boldsymbol{\mu}_N\|_{\varepsilon}^2\right)^{\frac{1}{2}}$$

for all $(\boldsymbol{v}_h, q_h, \boldsymbol{\mu}_N) \in \boldsymbol{V}_h \times Q_h \times \boldsymbol{F}_N$. The stability of the stabilized problem is addressed in the following lemma.

Lemma 4.3.3. *There exists a constant $\beta > 0$ uniformly independent of h, N and ε such that*

$$\sup_{(\boldsymbol{v}_h, q_h, \boldsymbol{\mu}_N) \in \boldsymbol{V}_h \times Q_h \times \boldsymbol{F}_N} \frac{B_h((\boldsymbol{u}_h, p_h, \boldsymbol{\lambda}_N), (\boldsymbol{v}_h, q_h, \boldsymbol{\mu}_N))}{\|(\boldsymbol{u}_h, p_h, \boldsymbol{\lambda}_N)\|_{\varepsilon}\|(\boldsymbol{v}_h, q_h, \boldsymbol{\mu}_N)\|_{\varepsilon}} \geqslant \beta$$

for all $(\boldsymbol{u}_h, p_h, \boldsymbol{\lambda}_N) \in \boldsymbol{V}_h \times Q_h \times \boldsymbol{F}_N$.

Proof of Lemma 4.3.3. Consider $(\boldsymbol{u}_h, p_h, \boldsymbol{\lambda}_N) \in \boldsymbol{V}_h \times Q_h \times \boldsymbol{F}_N$ be given. First, taking $(\boldsymbol{v}_h, q_h, \boldsymbol{\mu}_N) = (\boldsymbol{u}_h, q_h, \boldsymbol{\lambda}_N)$ in the definition of B_h, we observe that

$$B_h\left((\boldsymbol{u}_h, p_h, \boldsymbol{\lambda}_N), (\boldsymbol{u}_h, p_h, \boldsymbol{\lambda}_N)\right) = 2\|\boldsymbol{\varepsilon}(\boldsymbol{u}_h)\|_{\Omega}^2 + \gamma_p|\log(\varepsilon)|h^2\|\nabla p_h\|_{\Omega}^2 + \gamma_{\lambda}\left(\frac{h}{\varepsilon}\right)\varepsilon^{-1}\|\lambda_N\|_{\varepsilon}^2. \quad (4.3.14)$$

According to Lemma 4.3.1, there exists $\boldsymbol{v}_{\boldsymbol{\lambda}_N,h}^{\varepsilon}$, and $C_1, D_1 > 0$ uniformly independent of h, N and ε such that

$$\frac{3}{4}\|\boldsymbol{\lambda}_N\|_{-\frac{1}{2},\varepsilon}^2 \leqslant -(\boldsymbol{\lambda}_N, \boldsymbol{v}_{\boldsymbol{\lambda}_N,h}^{\varepsilon})_{\varepsilon} + C_1\left(\frac{h}{\varepsilon}\right)\varepsilon^{-1}\|\boldsymbol{\lambda}_N\|_{\varepsilon}^2, \quad (4.3.15)$$

$$|(p_h, \operatorname{div} \boldsymbol{v}_{\boldsymbol{\lambda}_N,h}^{\varepsilon})_{\Omega}| \leqslant D_1 h^2|\log(\varepsilon)|\|\nabla p_h\|_{\Omega}^2 + \frac{1}{4}\|\boldsymbol{\lambda}_N\|^2, \quad (4.3.16)$$

$$\|\boldsymbol{v}_{\boldsymbol{\lambda}_N,h}^{\varepsilon}\|_{1,\Omega} \lesssim \|\boldsymbol{\lambda}_N\|_{-\frac{1}{2},\varepsilon}. \quad (4.3.17)$$

From (4.3.17), we deduce that there exists $B_1 > 0$ uniformly independent of h, N and ε such that

$$2\left(\boldsymbol{\varepsilon}(\boldsymbol{u}_h), \boldsymbol{\varepsilon}(\boldsymbol{v}^{\varepsilon}_{\boldsymbol{\lambda}_N,h})\right)_\Omega \leqslant B_1\|\boldsymbol{u}_h\|^2_{1,\Omega} + \frac{1}{4}\|\boldsymbol{\lambda}\|^2_{-\frac{1}{2},\varepsilon}. \tag{4.3.18}$$

Combining (4.3.15), (4.3.16) and (4.3.18), and taking $(\boldsymbol{v}_h, q_h, \boldsymbol{\mu}_N) = (\boldsymbol{v}^{\varepsilon}_{\boldsymbol{\lambda}_N,h}, 0, \mathbf{0})$ in the definition of B_h, we get

$$\begin{aligned} B_h((\boldsymbol{u}_h, p_h, \boldsymbol{\lambda}_N), (\boldsymbol{v}^{\varepsilon}_{\boldsymbol{\lambda}_N,h}, 0, \mathbf{0})) \geqslant \\ \frac{1}{4}\|\boldsymbol{\lambda}_N\|^2_{-\frac{1}{2},\varepsilon} - B_1\|\boldsymbol{u}_h\|^2_{1,\Omega} - C_1(\frac{h}{\varepsilon})\varepsilon^{-1}\|\boldsymbol{\lambda}_N\|^2_{-\frac{1}{2},\varepsilon} - D_1h^2|\log(\varepsilon)|\|\nabla p_h\|^2_\Omega. \end{aligned} \tag{4.3.19}$$

Similarly, according to Lemma 4.3.2, there exists $\boldsymbol{w}^{\varepsilon}_{p_h,h}$ and $D_2 > 0$ uniformly independent of h, N and ε such that

$$\frac{3}{4}\|p_h\|^2_\Omega \leqslant -(p_h, \operatorname{div} \boldsymbol{w}^{\varepsilon}_{p_h,h})_\Omega + D_2h^2|\log(\varepsilon)|\|\nabla p_h\|^2_\Omega, \tag{4.3.20}$$

$$(\boldsymbol{\mu}_N, \boldsymbol{w}^{\varepsilon}_{p_h,h})_\varepsilon = 0 \quad \forall \boldsymbol{\mu}_N \in \boldsymbol{F}_N, \tag{4.3.21}$$

$$\|\boldsymbol{w}^{\varepsilon}_{p_h,h}\|_{1,\Omega} \lesssim |\log(\varepsilon)|^{\frac{1}{2}}\|p_h\|_\Omega. \tag{4.3.22}$$

From (4.3.22), we deduce that there exists $B_2 > 0$ uniformly independent of h, N and ε such that

$$2\left(\boldsymbol{\varepsilon}(\boldsymbol{u}_h), \boldsymbol{\varepsilon}(\boldsymbol{w}^{\varepsilon}_{p_h,h})\right)_\Omega \leqslant B_2|\log(\varepsilon)|\|\boldsymbol{u}_h\|^2_{1,\Omega} + \frac{1}{4}\|p_h\|^2_\Omega. \tag{4.3.23}$$

Combining (4.3.20), (4.3.21) and (4.3.23), and taking $(\boldsymbol{v}_h, q_h, \boldsymbol{\mu}_N) = (\boldsymbol{w}^{\varepsilon}_{p_h,h}, 0, \mathbf{0})$ in the definition of B_h, we get

$$\begin{aligned} B((\boldsymbol{u}_h, p_h, \boldsymbol{\lambda}_N), (\boldsymbol{w}^{\varepsilon}_{p_h,h}, 0, \mathbf{0})) \geqslant \\ \frac{1}{2}\|p_h\|^2_\Omega - B_2|\log(\varepsilon)|\|\boldsymbol{u}_h\|^2_{1,\Omega} - D_2h^2|\log(\varepsilon)|\|\nabla p\|^2_\Omega. \end{aligned} \tag{4.3.24}$$

Taking finally $(\boldsymbol{v}_h, q_h, \boldsymbol{\mu}_N) = (\boldsymbol{u}_h + \alpha_\lambda \boldsymbol{v}^{\varepsilon}_{\boldsymbol{\lambda}_N,h} + |\log(\varepsilon)|^{-1}\alpha_p \boldsymbol{w}^{\varepsilon}_{p_h,h}, p_h, \boldsymbol{\lambda}_N)$ as tests functions in B_h, by gathering (4.3.14), (4.3.19) and (4.3.24), we obtain

$$\begin{aligned} B((\boldsymbol{u}_h, p_h, \boldsymbol{\lambda}_N), (\boldsymbol{u}_h + \alpha_\lambda \boldsymbol{v}^{\varepsilon}_{\boldsymbol{\lambda}_N,h} + |\log(\varepsilon)|^{-1}\alpha_p \boldsymbol{w}^{\varepsilon}_{p_h,h}, p_h, \boldsymbol{\lambda}_N) \geqslant (\alpha - \alpha_\lambda B_1 - \alpha_p B_2)\|\boldsymbol{u}_h\|^2_{1,\Omega} \\ + |\log(\varepsilon)|^{-1}\frac{\alpha_p}{2}\|p_h\|^2_\Omega + \frac{\alpha_\lambda}{4}\|\boldsymbol{\lambda}_N\|^2_{-\frac{1}{2},\varepsilon} + (\gamma_\lambda - \alpha_\lambda C_1)\left(\frac{h}{\varepsilon}\right)\varepsilon^{-1}\|\boldsymbol{\lambda}_N\|^2_\varepsilon \\ + (\gamma_p - \alpha_\lambda D_1 - |\log(\varepsilon)|^{-1}\alpha_p D_2)|\log(\varepsilon)|h^2\|\nabla p_h\|^2_\Omega. \end{aligned} \tag{4.3.25}$$

where α is the positive coercivity constant of the bilinear form a. Choosing α_p and α_λ appropriately such that the following inequalities hold true

$$\alpha - \alpha_\lambda B_1 - \alpha_p B_2 > 0,\ \gamma_\lambda - \alpha_\lambda C_1 > 0,\ \gamma_p - \alpha_\lambda D_1 - |\log(\varepsilon_{\max})|^{-1}\alpha_p D_2 > 0,$$

we get the desired result. Finally, using the triangle inequality and the a priori estimates for $\boldsymbol{v}^{\varepsilon}_{\boldsymbol{\lambda}_N,h}$ and $\boldsymbol{w}^{\varepsilon}_{p_h,h}$ given in (4.3.17) and (4.3.22), respectively, we obtain

$$\begin{aligned}
&\|(\boldsymbol{u}_h + \alpha_\lambda \boldsymbol{v}^{\varepsilon}_{\boldsymbol{\lambda}_N,h} + |\log(\varepsilon)|^{-1}\alpha_p \boldsymbol{w}^{\varepsilon}_{p_h,h}, p_h, \boldsymbol{\lambda}_N)\|_\varepsilon \\
&\leqslant \|(\boldsymbol{u}_h, p_h, \boldsymbol{\lambda}_N)\|_\varepsilon + \alpha_\lambda C_3 \|\boldsymbol{\lambda}_N\|_{-\frac{1}{2},\varepsilon} + |\log(\varepsilon)|^{-\frac{1}{2}}\alpha_p D_3 \|p_h\|_\Omega \\
&\leqslant C_M \|(\boldsymbol{u}_h, p_h, \boldsymbol{\lambda}_N)\|_\varepsilon
\end{aligned} \tag{4.3.26}$$

where $C_3, D_3 > 0$ are constant uniformly independent of h, N and ε and

$$C_M \overset{\text{def}}{=} 1 + \alpha_\lambda C_3 + \alpha_p D_3.$$

Thus dividing (4.3.26) by (4.3.25), we get, with $\boldsymbol{v}_h = \boldsymbol{u}_h + \alpha_\lambda \boldsymbol{w}^{\varepsilon}_{\boldsymbol{\lambda}_N,h} + |\log(\varepsilon)|^{-1}\alpha_p \boldsymbol{w}^{\varepsilon}_{q_h,h}$, $q_h = p_h$ and $\boldsymbol{\mu}_N = \boldsymbol{\lambda}_N$,

$$\frac{B_h((\boldsymbol{u}_h, p_h, \boldsymbol{\lambda}_N), (\boldsymbol{v}_h, q_h, \boldsymbol{\mu}_N))}{\|(\boldsymbol{v}_h, q_h, \boldsymbol{\mu}_N)\|_\varepsilon} \geqslant \frac{C_m}{C_M}\|(\boldsymbol{u}_h, p_h, \boldsymbol{\lambda}_N)\|_\varepsilon,$$

which implies that

$$\sup_{(\boldsymbol{v}_h, q_h, \boldsymbol{\mu}) \in \boldsymbol{V}_h \times Q_h \times \boldsymbol{F}_N} \frac{B_h((\boldsymbol{u}_h, p_h, \boldsymbol{\lambda}_N), (\boldsymbol{v}_h, q_h, \boldsymbol{\mu}_N))}{\|(\boldsymbol{v}_h, q_h, \boldsymbol{\mu}_N)\|_\varepsilon} \geqslant \frac{C_m}{C_M}\|(\boldsymbol{u}_h, p_h, \boldsymbol{\lambda}_N)\|_\varepsilon$$

for all $(\boldsymbol{u}_h, p_h, \boldsymbol{\lambda}_N) \in \boldsymbol{V}_h \times Q_h \times \boldsymbol{F}_N$, leading to the desired result. □

4.3.1.4 Consistency and convergence

To conclude the analysis of the stabilized formulation, we address the consistency of the method. Since $\boldsymbol{\lambda}^{\varepsilon}_{N,h} - \boldsymbol{\lambda}^{\varepsilon}_N \in \boldsymbol{F}_N$, we can apply Lemma 4.3.3 to have an estimate of $(\boldsymbol{u}^{\varepsilon}_{N,h} - \boldsymbol{\Pi}^{\mathrm{Z},1}_h(\boldsymbol{u}^{\varepsilon}_N), p^{\varepsilon}_{N,h} - \overline{\Pi}_h(p^{\varepsilon}_N), \boldsymbol{\lambda}^{\varepsilon}_{N,h} - \boldsymbol{\lambda}^{\varepsilon}_N)$. Precisely, we have

$$\begin{aligned}
&\|(\boldsymbol{u}^{\varepsilon}_{N,h} - \boldsymbol{\Pi}^{\mathrm{Z},1}_h(\boldsymbol{u}^{\varepsilon}_N), p^{\varepsilon}_{N,h} - \overline{\Pi}_h(p^{\varepsilon}_N), \boldsymbol{\lambda}^{\varepsilon}_{N,h} - \boldsymbol{\lambda}^{\varepsilon}_N)\|_\varepsilon \lesssim \\
&\sup_{(\boldsymbol{v}_h, q_h, \boldsymbol{\mu}_N) \in \boldsymbol{V}_h \times Q_h \times \boldsymbol{F}_N} \frac{B_h((\boldsymbol{u}^{\varepsilon}_{N,h} - \boldsymbol{\Pi}^{\mathrm{Z},1}_h(\boldsymbol{u}^{\varepsilon}_N), p^{\varepsilon}_{N,h} - \overline{\Pi}_h(p^{\varepsilon}_{N,h}), \boldsymbol{\lambda}^{\varepsilon}_{N,h} - \boldsymbol{\lambda}^{\varepsilon}_N), (\boldsymbol{v}_h, q_h, \boldsymbol{\mu}_N))}{\|(\boldsymbol{v}_h, q_h, \boldsymbol{\mu}_N)\|_\varepsilon}.
\end{aligned}$$

Let us introduce the approximation errors $e_p \overset{\text{def}}{=} p^{\varepsilon}_N - \overline{\Pi}_h p^{\varepsilon}_N$ and $\boldsymbol{e}_u = \boldsymbol{u}^{\varepsilon}_N - \boldsymbol{\Pi}^{\mathrm{Z},1}_h \boldsymbol{u}^{\varepsilon}_N$. By combining the equations of the continuous problem (4.2.14) and the discrete problem (4.3.1), the following relation holds:

$$\begin{aligned}
&B_h((\boldsymbol{u}^{\varepsilon}_{N,h} - \boldsymbol{\Pi}^{\mathrm{Z},1}_h(\boldsymbol{u}^{\varepsilon}_N), p^{\varepsilon}_{N,h} - \overline{\Pi}_h(p^{\varepsilon}_N), \boldsymbol{\lambda}^{\varepsilon}_{N,h} - \boldsymbol{\lambda}^{\varepsilon}_N), (\boldsymbol{v}_h, q_h, \boldsymbol{\mu}_N)) = a(\boldsymbol{e}_u, \boldsymbol{v}_h) \\
&- b_1(e_p, \boldsymbol{v}_h) + b_1(q_h, \boldsymbol{e}_u) - s^p_h(q_h, \overline{\Pi}_h(p^{\varepsilon}_N)) + b_2(\boldsymbol{\mu}_N, \boldsymbol{e}_u) - s^{\lambda}_h(\boldsymbol{\mu}_N, \boldsymbol{\lambda}^{\varepsilon}_{N,h})
\end{aligned}$$

for all $(\boldsymbol{v}_h, q_h, \boldsymbol{\mu}_N) \in \boldsymbol{V}_h \times Q_h \times \boldsymbol{F}_N$. By using the continuity of the bilinear forms a, b_1, b_2 (with the norm established in (4.2.17)), s_h^λ and s_h^p, we can further establish:

$$\begin{aligned}\frac{|a(\boldsymbol{e}_u, \boldsymbol{v}_h) - b_1(e_p, \boldsymbol{v}_h) + b_1(q_h, \boldsymbol{e}_u) + b_2(\boldsymbol{\mu}_N, \boldsymbol{e}_u) - s_h^p(q_h, \overline{\Pi}_h(p_N^\varepsilon)) - s_h^\lambda(\boldsymbol{\mu}_N, \boldsymbol{\lambda}_{N,h}^\varepsilon)|}{\|(\boldsymbol{v}_h, q_h, \boldsymbol{\mu}_N)\|_\varepsilon} \\ \lesssim |\log(\varepsilon)|^{\frac{1}{2}} \|\boldsymbol{e}_u\|_{1,\Omega} + \|e_p\|_\Omega + |\log(\varepsilon)|^{\frac{1}{2}} h \|\nabla \overline{\Pi}_h(p_N^\varepsilon)\|_\Omega + \varepsilon^{-\frac{1}{2}} \left(\frac{h}{\varepsilon}\right)^{\frac{1}{2}} \|\boldsymbol{\lambda}_N^\varepsilon\|_\varepsilon,\end{aligned}$$

for all $(\boldsymbol{v}_h, q_h, \boldsymbol{\mu}_N) \in \boldsymbol{V}_h \times Q_h \times \boldsymbol{F}_N$. Using the classical error decomposition, we finally derive

$$\begin{aligned}&\|(\boldsymbol{u}_N^\varepsilon - \boldsymbol{u}_{N,h}^\varepsilon, p_N^\varepsilon - p_{N,h}^\varepsilon, \boldsymbol{\lambda}_N^\varepsilon - \boldsymbol{\lambda}_{N,h}^\varepsilon)\|_\varepsilon \\ &\lesssim \|\boldsymbol{e}_u, e_p, 0\|_\varepsilon + \|(\boldsymbol{u}_{N,h}^\varepsilon - \boldsymbol{\Pi}_h^{\mathrm{Z},1}(\boldsymbol{u}_N^\varepsilon), p_{N,h}^\varepsilon - \overline{\Pi}_h(p_N^\varepsilon), \boldsymbol{\lambda}_{N,h}^\varepsilon - \boldsymbol{\lambda}_N^\varepsilon)\|_\varepsilon \\ &\lesssim |\log(\varepsilon)|^{\frac{1}{2}} \|\boldsymbol{e}_u^\varepsilon\|_{1,\Omega} + \|e_p^\varepsilon\|_{1,\Omega} + |\log(\varepsilon)|^{\frac{1}{2}} h \|\nabla \overline{\Pi}_h(p_N^\varepsilon)\|_\Omega + \varepsilon^{-\frac{1}{2}} \left(\frac{h}{\varepsilon}\right)^{\frac{1}{2}} \|\boldsymbol{\lambda}_N^\varepsilon\|_\varepsilon.\end{aligned} \tag{4.3.27}$$

In conclusion, according to Proposition 3.4.1 and the assumption (4.3.2) made on the quasi-interpolation operator $\overline{\Pi}_h$, the following a priori convergence estimates hold:

$$\begin{aligned}&\|(\boldsymbol{u}_N^\varepsilon - \boldsymbol{u}_{N,h}^\varepsilon, p_N^\varepsilon - p_{N,h}^\varepsilon, \boldsymbol{\lambda}_N^\varepsilon - \boldsymbol{\lambda}_{N,h}^\varepsilon)\|_\varepsilon \\ &\lesssim |\log(\varepsilon)|^{\frac{1}{2}} h^{\frac{1}{2}-\eta} \|\boldsymbol{u}_N^\varepsilon\|_{\frac{3}{2}-\eta,\Omega} + |\log(\varepsilon)|^{\frac{1}{2}} h^{\frac{1}{2}-\eta} \|p_N^\varepsilon\|_{\frac{1}{2}-\eta,\Omega} + \varepsilon^{-\frac{1}{2}} \left(\frac{h}{\varepsilon}\right)^{\frac{1}{2}} \|\boldsymbol{\lambda}_N^\varepsilon\|_\varepsilon.\end{aligned} \tag{4.3.28}$$

Let us observe that similarly to the stabilized fictitious domain finite element method introduced for the Poisson case in Section 3.4.2, the stability of Problem 4.3.1 is independent of the ratio h/ε and this way does not suffer from any restriction when ε is small with respect to h. On the other hand, proceeding in a similar way as in Remark 10, we can show that, at least for some specific boundary conditions on $\partial\omega^\varepsilon$ and exterior domain Ω^ε, we have

$$\|\boldsymbol{u}_N^\varepsilon\|_{\frac{3}{2}-\eta,\Omega} \sim \frac{1}{\varepsilon^{\eta-\frac{1}{2}}}, \quad \|p_N^\varepsilon\|_{\frac{1}{2}-\eta,\Omega} \sim \frac{1}{\varepsilon^{\eta-\frac{1}{2}}}.$$

Consequently, the convergence error (4.3.28) behaves as h/ε which can be can an issue for small obstacles. To overcome the limitations of the low-order stabilized finite element method, we propose an improvement of the approximation method in the next section.

4.3.2 Augmented finite element method

The previous section highlights that the numerical error of classical stabilized low-order finite elements behaves as h/ε and subsequently this error can be large for a small ratio between the size of the obstacle and the size of the mesh. Additionally, as expected, the

a priori estimate (4.3.28) is sub-optimal due to the discontinuity of the velocity gradient and pressure fields across the immersed interface. In this section, we will follow a similar approach as in Section 3.4.3 for the Poisson case. We propose and analyze an augmented finite element method that aims at reducing the negative impact of small obstacle size on numerical error. The key ingredient of our method is the incorporation of singular functions into the finite element basis for the velocity and pressure approximation.

4.3.2.1 Definition of the augmented finite element space

One important aspect of the augmented finite element method we propose in this section is to properly manage the interaction between the basis functions of the polynomial space and the singular enrichment functions. In particular, for standard spaces of continuous piecewise polynomial functions, the divergence-free condition is generally fulfilled only in a weak sense, formally, the discrete velocity $\boldsymbol{u}_h$ satisfy

$$(q_h, \operatorname{div} \boldsymbol{u}_h) = 0$$

for all q_h in the discrete approximation space, which does not guarantee that this condition would still hold for q_h a non-polynomial function. Subsequently, to avoid perturbing the inf-sup conditions on the polynomial approximation spaces, instead of considering the Lagrange finite element method for the approximation of the velocity and pressure space, We consider an inf sup stable conforming element pair that satisfies $\boldsymbol{V}_h^k \subset \boldsymbol{V}$, $Q_h^{k-1} \subset Q$ and $\operatorname{div} \boldsymbol{V}_h^k \subset Q_h^{k-1}$. In particular if $(q_h, \operatorname{div} \boldsymbol{u}_h) = 0 \ \forall q_h \in Q_h^{k-1}$ then $\operatorname{div} \boldsymbol{u}_h = 0$. We also assume that for $(\boldsymbol{u}, p) \in \boldsymbol{H}^k(\Omega) \cap \boldsymbol{V} \times H^{k-1}(\Omega) \cap Q$ the following estimates hold:

$$\inf_{q_h \in Q_h^{k-1}} \|q - q_h\|_\Omega \lesssim h^{k-1} \|q\|_{k,\Omega}, \qquad \inf_{\boldsymbol{u}_h \in \boldsymbol{V}_h^k} \|\boldsymbol{u} - \boldsymbol{u}_h\|_{1,\Omega} \lesssim h^k \|\boldsymbol{u}\|_{k+1,\Omega}. \tag{4.3.29}$$

See for example [Guzmán and Neilan, 2014] for the construction of a finite element pair $\boldsymbol{V}_h^k \times Q_h^{k-1}$ satisfying such assumptions with $k = 2$, $\boldsymbol{V} = \boldsymbol{H}_0^1(\Omega)$ and $Q = L_0^2(\Omega)$. Note that due to time constraints, this method has not been tested in the numerical section, but we hope to provide numerical results shortly.

In contrast to the Poisson case described in Section 3.4.3, the low regularity of the solution is also due to the discontinuity of the pressure across $\partial\omega^\varepsilon$. Consequently, we need to enrich both discrete spaces $\boldsymbol{V}_h^k$ and Q_h^{k-1} to reach the optimal convergence of the finite element method. Moreover, due to the pressures added in the approximation space Q_h^{k-1}, it also comes necessary to enrich the velocity space with functions called *supremizers*, as they make possible the satisfaction of the inf-sup condition. From the results of Section 4.2.2, we can write an explicit solution of $\boldsymbol{u}_N^\varepsilon$ as follows:

$$\boldsymbol{u}_N^\varepsilon = \boldsymbol{u}_{N,\mathrm{S}}^\varepsilon + \boldsymbol{u}_{N,\mathrm{R}}^{\varepsilon,1} + \boldsymbol{u}_{N,\mathrm{R}}^{\varepsilon,2} \tag{4.3.30}$$

with

$$\boldsymbol{u}_{N,\mathrm{S}}^{\varepsilon} = \sum_{j=0}^{N}\sum_{l=1}^{2} a_{l,j}^{u}\boldsymbol{\phi}_{l,j}^{\varepsilon,\mathrm{c}} + b_{l,j}^{u}\boldsymbol{\phi}_{l,j}^{\varepsilon,\mathrm{s}}, \quad \boldsymbol{u}_{N,\mathrm{R}}^{\varepsilon} = \boldsymbol{u}_{N,\mathrm{R}}^{\varepsilon,1} + \boldsymbol{u}_{N,\mathrm{R}}^{\varepsilon,2}, \tag{4.3.31}$$

where the expressions of the coefficients $a_{l,j}^{u}$, $b_{l,j}^{u}$, the singular functions $\boldsymbol{\phi}_{l,j}^{\varepsilon,\mathrm{c}}$, $\boldsymbol{\phi}_{l,j}^{\varepsilon,\mathrm{s}}$ and the regular function $\boldsymbol{u}_{N,\mathrm{R}}^{\varepsilon,1}$ are given in Section 4.A.7.1. Similarly,

$$p_{N}^{\varepsilon} = p_{N,\mathrm{S}}^{\varepsilon} + p_{N,\mathrm{R}}^{\varepsilon,1} + p_{N,\mathrm{R}}^{\varepsilon,2} \tag{4.3.32}$$

with

$$p_{N,\mathrm{S}}^{\varepsilon} = \sum_{j=0}^{N} a_{j}^{p}\varphi_{j}^{\varepsilon,\mathrm{c}} + b_{j}^{p}\varphi_{j}^{\varepsilon,\mathrm{s}}, \quad p_{N,\mathrm{R}}^{\varepsilon} = p_{N,\mathrm{R}}^{\varepsilon,1} + p_{N,\mathrm{R}}^{\varepsilon,2},$$

where the expressions of the coefficients a_{j}^{p}, b_{j}^{p}, the singular functions $\varphi_{j}^{\varepsilon,\mathrm{c}}$, $\varphi_{j}^{\varepsilon,\mathrm{s}}$ and the regular functions $p_{N,\mathrm{R}}^{\varepsilon,1}$ are given in Section 4.A.7.2. As for the pair $(\boldsymbol{u}_{N,R}^{2,\varepsilon}, p_{N,R}^{2,\varepsilon})$, it is the unique solution of the Stokes equation in ω^{ρ} with boundary condition

$$\boldsymbol{u}_{N,R}^{2,\varepsilon} = \boldsymbol{u}_{N}^{\varepsilon} - \Pi_{N+1}^{\rho}(\boldsymbol{u}_{N}^{\varepsilon}\cdot\boldsymbol{e}_{\theta})\boldsymbol{e}_{\theta} - \Pi_{N+1}^{\rho}(\boldsymbol{u}_{N}^{\varepsilon}\cdot\boldsymbol{e}_{r})\boldsymbol{e}_{r} \quad \text{on} \quad \partial\omega^{\rho},$$

where for $N \geqslant 0$, Π_{N}^{ρ} is the counterpart of Π_{N}^{ε} for $\varepsilon = \rho$. We now introduce χ a radial cut-off $\mathcal{C}^{\infty}$ function satisfying

$$\chi(r) \overset{\text{def}}{=} \begin{cases} 1 & \forall r \leqslant \dfrac{1}{2}\rho, \\ 0 & \forall r > \dfrac{3}{4}\rho. \end{cases}$$

A natural choice for enrichment functions would be to take $\chi\boldsymbol{\phi}_{l,j}^{\varepsilon,m}$. However, as for the polynomial approximation space, to prove the inf-sup condition of the discrete formulation, it is convenient to have divergence-free enrichment functions. To this purpose, we introduce the stream functions associated with $\boldsymbol{\phi}_{l,j}^{\varepsilon,m}$ denoted by $\psi_{l,j}^{\varepsilon,m}$ such that $\psi_{l,j}^{\varepsilon,m} \in H^{2}(\Omega)\cap L_{0}^{2}(\Omega)$, see Section 4.A.8. We then take as enrichment functions for the velocity approximation space $\tilde{\boldsymbol{\phi}}_{l,j}^{\varepsilon,m} = \mathbf{curl}\ (\chi\psi_{l,j}^{\varepsilon,m})$. For pressure, we consider the functions $\tilde{\varphi}_{l,j}^{\varepsilon,m} = \chi\varphi_{l,j}^{\varepsilon,m}$. Furthermore, to derive a uniformly independent inf-sup condition in h, N and ε, we also introduce some *supremizers* for the added pressures. To this purpose, we consider the following problem for a given pressure $\tilde{\varphi}_{j}^{\varepsilon,m} \in L^{2}(\Omega)$: find $(\tilde{\boldsymbol{\varsigma}}_{j}^{\varepsilon,m}, \tilde{\gamma}_{j}^{\varepsilon,m}) \in \boldsymbol{V}\times Q$ such that

$$\begin{cases} -\Delta\tilde{\boldsymbol{\varsigma}}_{j}^{\varepsilon,m} + \nabla\tilde{\gamma}_{j}^{\varepsilon,m} = \mathbf{0} & \text{in} \quad \Omega^{\varepsilon}, \\ -\Delta\tilde{\boldsymbol{\varsigma}}_{j}^{\varepsilon,m} + \nabla\tilde{\gamma}_{j}^{\varepsilon,m} = \mathbf{0} & \text{in} \quad \omega^{\varepsilon}, \\ \operatorname{div}\tilde{\boldsymbol{\varsigma}}_{j}^{\varepsilon,m} = \tilde{\varphi}_{j}^{\varepsilon,m} & \text{in} \quad \Omega^{\varepsilon}, \\ \tilde{\boldsymbol{\varsigma}}_{j}^{\varepsilon,m} = \mathbf{0} & \text{on} \quad \partial\omega^{\varepsilon}. \end{cases} \tag{4.3.33}$$

We then consider the augmented finite element space $\boldsymbol{V}_{N,h}^k$ and $Q_{N,h}^k$ defined by

$$\begin{cases} \boldsymbol{V}_{N,h}^k = \boldsymbol{V}_h^k \cup \text{span}\,\{\tilde{\boldsymbol{\phi}}_{l,j}^{\varepsilon,m}, \tilde{\boldsymbol{\varsigma}}_j^{\varepsilon,m}\}, \\ Q_{N,h}^{k-1} = Q_h^{k-1} \cup \text{span}\,\{\tilde{\varphi}_j^{\varepsilon,m}\}. \end{cases}$$

The discrete formulation of the augmented finite element method writes: find $(\tilde{\boldsymbol{u}}_{N,h}^{\varepsilon}, \tilde{p}_{N,h}^{\varepsilon}, \tilde{\boldsymbol{\lambda}}_{N,h}^{\varepsilon}) \in \boldsymbol{F}_N \in \boldsymbol{V}_{N,h}^k \times Q_{N,h}^{k-1}$

$$\begin{aligned} a(\tilde{\boldsymbol{u}}_{N,h}^{\varepsilon}, \tilde{\boldsymbol{v}}_h) - b_1(\tilde{p}_{N,h}^{\varepsilon}, \tilde{\boldsymbol{v}}_h) - b_2(\tilde{\boldsymbol{\lambda}}_{N,h}^{\varepsilon}, \tilde{\boldsymbol{v}}_h) = 0 \quad & \forall \tilde{\boldsymbol{v}}_h \in \boldsymbol{V}_{N,h}^k \\ b_1(\tilde{q}_h, \tilde{\boldsymbol{u}}_{N,h}^{\varepsilon}) = 0 \quad & \forall \tilde{q}_h \in Q_{N,h}^{k-1} \\ b_2(\boldsymbol{\mu}_N, \tilde{\boldsymbol{u}}_{N,h}^{\varepsilon}) = c(\boldsymbol{\mu}_N) \quad & \forall \boldsymbol{\mu}_N \in \boldsymbol{F}_N \end{aligned} \tag{4.3.34}$$

where the definition of the bilinear and linear forms a, b_1, b_2 and c are given in (4.2.15).

4.3.2.2 Inf-Sup stability

In this subsection, we deal with the inf-sup condition for the augmented finite element space. As in the case of the continuous case, we consider a variant of the BNB theorem specifically designed for twofold saddle point problems.

Theorem 4.3.4. *Let X_h be a subspace of X, $Q_{h,1}$ a subspace of Q_1 and $Q_{h,2}$ a subspace of Q_2. Assume that $Q_{h,1}$ and $Q_{h,2}$ are finite dimensional and consider the approximate problem: find $(u_h, \lambda_{h,1}, \lambda_{h,2}) \in X_h \times Q_{h,1} \times Q_{h,2}$ such that*

$$\begin{aligned} a(u_h, v_h) - b_1(\lambda_{h,1}, v_h) - b_2(\lambda_{h,2}, v_h) = d(v) \quad & \forall v_h \in X_h, \\ b_1(\mu_{h,1}, u_h) = c_1(\mu_{h,1}) \quad & \forall \mu_{h,1} \in Q_{h,1}, \\ b_2(\mu_{h,2}, u_h) = c_2(\mu_{h,2}) \quad & \forall \mu_{h,2} \in Q_{h,2}. \end{aligned} \tag{4.3.35}$$

Let

$$Z_{h,b_i} \overset{\text{def}}{=} \{v \in X_h \mid b_i(\mu_{h,i}, v_h) = 0 \quad \forall \mu_{h,i}\} \subset X_h \quad i = 1, 2.$$

We suppose that there exists $\beta_{h,1} > 0$ such that for all $\lambda_{h,1} \in Q_{h,1}$,

$$\sup_{v_h \in Z_{h,b_2}} \frac{b_1(\lambda_{h,1}, v_h)}{\|v_h\|_X} \geqslant \beta_{h,1} \|\lambda_{h,1}\|_{Q_1}$$

and that there exists $\beta_{h,2} > 0$ such that for all $\lambda_{h,2} \in Q_{h,2}$,

$$\sup_{v_h \in Z_{h,b_1}} \frac{b_2(\lambda_{h,2}, v_h)}{\|v_h\|_X} \geqslant \beta_{h,2} \|\lambda_{h,2}\|_{Q_2}.$$

Then the Problem (4.3.35) *is well posed and satisfies the estimates*

$$\begin{aligned}
\|u-u_h\|_X \leqslant & a_{1h} \inf_{v_h\in X_h} \|u-v_h\|_X \\
& + a_{2h} \inf_{\mu_{h,1}\in Q_{h,1}} \|\lambda_1-\mu_{h,1}\|_{Q_1} + a_{3h} \inf_{\mu_{h,2}\in Q_{h,2}} \|\lambda_2-\mu_{h,2}\|_{Q_2}. \\
\|\lambda_1-\lambda_{h,1}\|_{Q_1} \leqslant & b_{1h} \inf_{v_h\in X_h} \|u-v_h\|_X \\
& + b_{2h} \inf_{\mu_{h,1}\in Q_{h,1}} \|\lambda_1-\mu_{h,1}\|_{Q_1} + b_{3h} \inf_{\mu_{h,2}\in Q_{h,2}} \|\lambda_2-\mu_{h,2}\|_{Q_2}. \\
\|\lambda_2-\lambda_{h,2}\|_{Q_1} \leqslant & c_{1h} \inf_{v_h\in X_h} \|u-v_h\|_X + \\
& c_{2h} \inf_{\mu_{h,1}\in Q_{h,1}} \|\lambda_1-\mu_{h,1}\|_{Q_1} + c_{3h} \inf_{\mu_{h,2}\in Q_{h,2}} \|\lambda_2-\mu_{h,2}\|_{Q_2}.
\end{aligned}$$

with $a_{1h} = \left(1+\dfrac{\|a\|}{\alpha}\right)\left(1+\dfrac{\|b_1\|}{\beta_{1,h}}+\dfrac{\|b_2\|}{\beta_{2,h}}\right)$, $a_{2h} = \dfrac{\|b_1\|}{\alpha}$ *if* $Z_{h,b_1} \nsubseteq Z_{b_1}$, $a_{2h} = 0$ *otherwise,* $a_{3h} = \dfrac{\|b_2\|}{\alpha}$ *if* $Z_{h,b_2} \nsubseteq Z_{b_2}$, $a_{3h} = 0$ *otherwise,* $b_{1h} = a_{1h}\dfrac{\|a\|}{\beta_{h,1}}$, $b_{2h} = 1+\dfrac{\|b_1\|}{\beta_{h,1}} + a_{2h}\dfrac{\|a\|}{\beta_{h,1}}$, $b_{3h} = a_{3h}\dfrac{\|a\|}{\beta_{h,1}}$, $c_{1h} = a_{1h}\dfrac{\|a\|}{\beta_{h,2}}$, $c_{2h} = a_{2h}\dfrac{\|a\|}{\beta_{h,2}}$, $c_{3h} = 1+\dfrac{\|b_2\|}{\beta_{h,2}} + a_{3h}\dfrac{\|a\|}{\beta_{h,2}}$.

The proof of this theorem is given in Section 4.A.9. We now introduce two preliminary lemmas corresponding to the discrete counterpart of Lemma 4.2.2 and Lemma 4.2.3 for the augmented finite element method. Their proofs are given in Sections 4.A.10 and 4.A.11 of the appendix, respectively.

Lemma 4.3.5. *Let* $\boldsymbol{\eta} \in \boldsymbol{H}^{\frac{1}{2}}(\partial\omega^\varepsilon)$ *be given, there exists* $\tilde{\boldsymbol{v}}^\varepsilon_{\boldsymbol{\eta}} \in \boldsymbol{V}^k_{N,h}$ *and* $0 < \tilde{\rho} < \rho$ *such that for* $\varepsilon \in (0,\tilde{\rho})$,

$$(\boldsymbol{\mu}_N, \tilde{\boldsymbol{v}}^\varepsilon_{\boldsymbol{\eta}})_\varepsilon = (\boldsymbol{\mu}_N, \boldsymbol{\eta})_\varepsilon \quad \forall \boldsymbol{\mu}_N \in \boldsymbol{F}_N, \quad \|\tilde{\boldsymbol{v}}^\varepsilon_{\boldsymbol{\eta}}\|_{1,\Omega} \lesssim \|\boldsymbol{\eta}\|_{\frac{1}{2},\varepsilon}.$$

Moreover, for any $\tilde{q}_h \in Q^{k-1}_{N,h}$,

$$(\tilde{q}_h, \operatorname{div} \tilde{\boldsymbol{v}}^\varepsilon_{\boldsymbol{\eta}})_\Omega = 0.$$

Lemma 4.3.6. *Let* $\tilde{q}_h \in Q^{k-1}_{N,h}$ *be given, there exists* $\boldsymbol{w}^\varepsilon_{\tilde{q}_h} \in \boldsymbol{V}^k_{N,h}$ *such that*

$$(\tilde{q}_h, \operatorname{div} \tilde{\boldsymbol{w}}^\varepsilon_{\tilde{q}_h})_\Omega = \|\tilde{q}_h\|^2_\Omega, \quad \|\tilde{\boldsymbol{w}}^\varepsilon_{\tilde{q}_h}\|_{1,\Omega} \lesssim |\log(\varepsilon)|^{\frac{1}{2}}\|\tilde{q}_h\|_\Omega.$$

Moreover, for any $\boldsymbol{\mu}_N \in \boldsymbol{F}_N$,

$$(\boldsymbol{\mu}_N, \tilde{\boldsymbol{w}}^\varepsilon_{\tilde{q}_h}) = 0.$$

The inf-sup condition for Problem (4.3.34) is given in the following lemma.

Lemma 4.3.7. *There exists $\beta_1, \beta_2 > 0$ uniformly independent of h, N and ε and $0 < \rho < \tilde{\rho}$ such that for all $\varepsilon \in (0, \tilde{\rho})$,*

$$\sup_{\tilde{\boldsymbol{v}}_h \in \boldsymbol{V}_{N,h}^k,\, b_2(\boldsymbol{\mu}_N, \tilde{\boldsymbol{v}}_h)=0} \frac{b_1(\tilde{p}_h, \tilde{\boldsymbol{v}}_h)}{\|\tilde{\boldsymbol{v}}_h\|_{1,\Omega}} \geqslant \beta_1 |\log(\varepsilon)|^{-\frac{1}{2}} \|\tilde{p}_h\|_\Omega \quad \forall \tilde{p}_h \in Q_{N,h}^k,$$

$$\sup_{\tilde{\boldsymbol{v}}_h \in \boldsymbol{V}_{N,h}^k,\, b_1(\tilde{q}_h, \tilde{\boldsymbol{v}}_h)=0} \frac{b_2(\boldsymbol{\lambda}_N, \tilde{\boldsymbol{v}}_h)}{\|\tilde{\boldsymbol{v}}_h\|_{1,\Omega}} \geqslant \beta_2 \|\boldsymbol{\lambda}_N\|_{-\frac{1}{2},\varepsilon} \quad \forall \boldsymbol{\lambda}_N \in \boldsymbol{F}_N.$$

Proof of Lemma 4.3.7. We consider $\tilde{q}_h \in Q_{N,h}^{k-1}$ be given. According to Lemma 4.3.6, there exists $\tilde{\boldsymbol{w}}_{\tilde{q}_h}^\varepsilon \in \boldsymbol{V}_{N,h}^k$ and $\beta_1 > 0$ uniformly independent of h, N and ε such that

$$(\tilde{q}_h, \operatorname{div} \tilde{\boldsymbol{w}}_{\tilde{q}_h}^\varepsilon) = \|\tilde{q}_h\|_\Omega^2, \quad \|\tilde{\boldsymbol{w}}_{\tilde{q}_h}^\varepsilon\|_{1,\Omega} \leqslant \beta_1 |\log(\varepsilon)|^{\frac{1}{2}} \|\tilde{q}_h\|_\Omega,$$

and

$$(\boldsymbol{\mu}_N, \tilde{\boldsymbol{w}}_{\tilde{q}_h}) = \boldsymbol{0} \quad \forall \boldsymbol{\mu}_N \in \boldsymbol{F}_N.$$

We deduce that

$$\begin{aligned}\|\tilde{q}_h\|_\Omega = \frac{(\tilde{q}_h, \operatorname{div} \tilde{\boldsymbol{w}}_{\tilde{q}_h})_\Omega}{\|\tilde{q}_h\|_\Omega} &\leqslant \beta_1^{-1} |\log(\varepsilon)|^{\frac{1}{2}} \frac{(\tilde{q}_h, \operatorname{div} \tilde{\boldsymbol{w}}_{\tilde{q}_h})}{\|\tilde{\boldsymbol{w}}_{\tilde{q}_h}\|_\Omega} \\ &\leqslant \beta_1^{-1} |\log(\varepsilon)|^{\frac{1}{2}} \sup_{\tilde{\boldsymbol{v}}_h \in \boldsymbol{V}_{N,h}^k,\, b_2(\boldsymbol{\mu}_N, \tilde{\boldsymbol{v}}_h)_\varepsilon = 0} \frac{b_1(\tilde{q}_h, \operatorname{div} \tilde{\boldsymbol{v}}_h)}{\|\tilde{\boldsymbol{v}}_h\|_{1,\Omega}}\end{aligned}$$

We consider $\boldsymbol{\lambda}_N \in \boldsymbol{F}_N$ be given. According to Lemma 4.3.5, for any $\boldsymbol{\eta} \in \boldsymbol{H}^{\frac{1}{2}}(\partial\omega^\varepsilon)$, there exists $\tilde{\boldsymbol{v}}_{\boldsymbol{\eta}}^\varepsilon \in \boldsymbol{V}_{N,h}^k$ and $\beta_2 > 0$ uniformly independent of h, N and ε such that

$$(\boldsymbol{\lambda}_N, \tilde{\boldsymbol{v}}_{\boldsymbol{\eta}}^\varepsilon)_\varepsilon = (\boldsymbol{\lambda}_N, \boldsymbol{\eta})_\varepsilon, \quad \|\tilde{\boldsymbol{v}}_{\boldsymbol{\eta}}^\varepsilon\|_{1,\Omega} \leqslant \beta_2 \|\boldsymbol{\eta}\|_{\frac{1}{2},\varepsilon},$$

and

$$(\tilde{q}_h, \operatorname{div} \tilde{\boldsymbol{v}}_{\boldsymbol{\eta}}^\varepsilon)_\Omega = 0 \quad \forall \tilde{q}_h \in Q_{N,h}^{k-1}.$$

We deduce that for any $\boldsymbol{\eta} \in \boldsymbol{H}^{\frac{1}{2}}(\partial\omega^\varepsilon)$,

$$\frac{(\boldsymbol{\lambda}_N, \boldsymbol{\eta})_\varepsilon}{\|\boldsymbol{\eta}\|_{\frac{1}{2},\varepsilon}} = \frac{(\boldsymbol{\lambda}_N, \tilde{\boldsymbol{v}}_{\boldsymbol{\eta}}^\varepsilon)_\varepsilon}{\|\boldsymbol{\eta}\|_{\frac{1}{2},\varepsilon}} \lesssim \beta_2 \frac{(\boldsymbol{\lambda}_N, \tilde{\boldsymbol{v}}_{\boldsymbol{\eta}}^\varepsilon)_\varepsilon}{\|\tilde{\boldsymbol{v}}_{\boldsymbol{\eta}}^\varepsilon\|_{\frac{1}{2},\varepsilon}} \lesssim \beta_2^{-1} \sup_{\tilde{\boldsymbol{v}}_h \in \boldsymbol{V}_{N,h}^k,\, b_1(\tilde{q}_h, \tilde{\boldsymbol{v}}_h)=0} \frac{b_2(\boldsymbol{\lambda}_N, \tilde{\boldsymbol{v}}_h)}{\|\tilde{\boldsymbol{v}}_h\|_{1,\Omega}}$$

We conclude taking the supremum over $\boldsymbol{\eta} \in \boldsymbol{H}^{\frac{1}{2}}(\partial\omega^\varepsilon)$. This concludes the proof. □

4.3.2.3 Approximation properties and convergence

To conclude this section, we give an estimate for the approximation error for the augmented finite element method.

Theorem 4.3.8. *Let $k \geqslant 1$. Let $(\boldsymbol{u}_N^\varepsilon, p_N^\varepsilon, \boldsymbol{\lambda}_N^\varepsilon)$ be solution of Problem* (4.4.3) *and $(\tilde{\boldsymbol{u}}_{N,h}^\varepsilon, \tilde{p}_{N,h}^\varepsilon, \tilde{\boldsymbol{\lambda}}_{N,h}^\varepsilon)$ be solution of Problem* (4.3.1). *There exists $0 < \tilde{\rho} < \rho$ such that for $\varepsilon \in (0, \tilde{\rho})$,*

$$\|\boldsymbol{u}_N^\varepsilon - \tilde{\boldsymbol{u}}_{N,h}^\varepsilon\|_{1,\Omega} + |\log(\varepsilon)|^{-\frac{1}{2}}\|p_N^\varepsilon - \tilde{p}_{N,h}^\varepsilon\|_\Omega + \|\tilde{\boldsymbol{\lambda}}_{N,h}^\varepsilon - \boldsymbol{\lambda}_N^\varepsilon\|_{-\frac{1}{2},\varepsilon} \lesssim |\log(\varepsilon)|^{\frac{1}{2}} h^k(|\boldsymbol{v}_\mathrm{b}| + \varepsilon|w_\mathrm{b}|)$$

We introduce a preliminary lemma providing an a priori estimate of the trace of $\boldsymbol{u}_{N,\mathrm{S}}^\varepsilon$ on $\partial\omega^\rho$ in terms of $\boldsymbol{v}_\mathrm{b}$ and w_b. The proof of this Lemma is given in the Section 4.A.12 of the Appendix.

Lemma 4.3.9. *Let $\boldsymbol{u}_{N,\mathrm{S}}^\varepsilon$ defined by* (4.3.31)*, there exists $0 < \tilde{\rho} < \rho$ such that for all $\varepsilon \in (0, \tilde{\rho})$,*

$$\|\boldsymbol{u}_{N,\mathrm{S}}^\varepsilon\|_{\frac{1}{2},\partial\omega^\rho} \lesssim |\boldsymbol{v}_\mathrm{b}| + \varepsilon|w_\mathrm{b}|.$$

Proof of Theorem 4.3.8. Since for all $j \geqslant 0$, $l \in \{1,2\}$ and $m \in \{\mathrm{c},\mathrm{s}\}$, $\tilde{\boldsymbol{\phi}}_{j,l}^{\varepsilon,m} \in \boldsymbol{H}_0^1(\Omega)$, the enrichment of the space $\boldsymbol{V}_{N,h}^k$ preserves the coercivity condition. Moreover, according to Lemma 4.3.7, the inf-sup conditions of Theorem 4.3.4 is satisfied for the spaces $\boldsymbol{V}_{N,h}^k/Q_{N,h}^{k-1}$ and $\boldsymbol{V}_{N,h}^k/\boldsymbol{F}_N$ with $\beta_{1,h} = |\log(\varepsilon)|^{-\frac{1}{2}}\beta_1$ and $\beta_{2,h} = \beta_2$. Moreover, the norm $\|a\|$ and the coercivity constant α of a are bounded independently of h, N and ε, and the norm of b_1 and b_2 are bounded by (4.2.17). So, appyling Theorem 4.3.4, we deduce that there exists $\tilde{\rho}_1 > 0$ such that for $\varepsilon \in (0, \tilde{\rho}_1)$,

$$\begin{aligned}&\|\boldsymbol{u}_N^\varepsilon - \tilde{\boldsymbol{u}}_{N,h}^\varepsilon\|_{1,\Omega} + |\log(\varepsilon)|^{-\frac{1}{2}}\|p_N^\varepsilon - \tilde{p}_{N,h}^\varepsilon\|_\Omega + \|\boldsymbol{\lambda}_N^\varepsilon - \tilde{\boldsymbol{\lambda}}_{N,h}^\varepsilon\|_{-\frac{1}{2},\varepsilon}\\ &\lesssim |\log(\varepsilon)|^{\frac{1}{2}}\left(\inf_{\tilde{\boldsymbol{v}}_h \in \boldsymbol{V}_{N,h}^k}\|\boldsymbol{u}_N^\varepsilon - \tilde{\boldsymbol{v}}_h\|_{1,\Omega} + \inf_{\tilde{q}_h \in Q_{N,h}^{k-1}}\|p_N^\varepsilon - \tilde{q}_h\|_\Omega\right)\end{aligned}$$

As previously mentioned, enriching the product space $\boldsymbol{V}_h^k \times Q_h^{k-1}$ with $\boldsymbol{V}_{N,h}^k \times Q_{N,h}^{k-1}$ aims to improve the approximation of $\boldsymbol{u}_N^\varepsilon$ and p_N^ε by providing a more accurate representation of their singular parts. To achieve this, let us examine the decomposition introduced in (4.3.30)-(4.3.32) of $\boldsymbol{u}_N^\varepsilon$ and p_N^ε between a singular and a regular part. We have

$$\chi\boldsymbol{u}_N^\varepsilon = \chi\boldsymbol{u}_{N,\mathrm{S}}^\varepsilon + \chi\boldsymbol{u}_{N,\mathrm{R}}^\varepsilon, \quad \chi p_N^\varepsilon = \chi p_{N,\mathrm{S}}^\varepsilon + \chi p_{N,\mathrm{R}}^\varepsilon.$$

By definition of the enrichment functions and using the product rule for differentiation, we have

$$\tilde{\boldsymbol{\phi}}_{l,j}^{\varepsilon,m} = \mathbf{curl}\,(\chi\psi_{l,j}^{\varepsilon,m}) = \psi_{l,j}^{\varepsilon,m}\mathbf{curl}\,\chi + \chi\boldsymbol{\phi}_{l,j}^{\varepsilon,m}.$$

In particular, setting

$$\overset{\star}{\psi}{}_{N,\mathrm{S}}^{\varepsilon} \overset{\mathrm{def}}{=} \sum_{j=0}^{N}\sum_{l=1}^{2} a_{l,j}^{u}\psi_{l,j}^{\varepsilon,\mathrm{c}} + b_{l,j}^{u}\psi_{l,j}^{\varepsilon,\mathrm{s}},$$

the following equality holds

$$\overset{\star}{\psi}{}_{N,\mathrm{S}}^{\varepsilon}\mathbf{curl}\,\chi + \chi\boldsymbol{u}_{N,\mathrm{S}}^{\varepsilon} = \sum_{j=0}^{N}\sum_{l=1}^{2} a_{l,j}^{u}\tilde{\boldsymbol{\phi}}_{l,j}^{\varepsilon,\mathrm{c}} + b_{l,j}^{u}\tilde{\boldsymbol{\phi}}_{l,j}^{\varepsilon,\mathrm{s}} \in \boldsymbol{V}_{N,h}^{k}. \tag{4.3.36}$$

Similarly, we can prove that $\chi p_{N,\mathrm{S}}^{\varepsilon} \in Q_{N,h}^{k-1}$. Therefore, we have for $\varepsilon \in (0,\tilde{\rho}_1)$,

$$\begin{aligned}
&\|\boldsymbol{u}_N^{\varepsilon} - \tilde{\boldsymbol{u}}_{N,h}^{\varepsilon}\|_{1,\Omega} + |\log(\varepsilon)|^{-\frac{1}{2}}\|p_N^{\varepsilon} - \tilde{p}_{N,h}^{\varepsilon}\|_{\Omega} + \|\boldsymbol{\lambda}_N^{\varepsilon} - \tilde{\boldsymbol{\lambda}}_{N,h}^{\varepsilon}\|_{-\frac{1}{2},\varepsilon} \\
&\lesssim |\log(\varepsilon)|^{\frac{1}{2}}\Big(\inf_{\boldsymbol{v}_h\in\boldsymbol{V}_h^k}\|\boldsymbol{u}_N^{\varepsilon} - \chi\boldsymbol{u}_{N,\mathrm{S}}^{\varepsilon} - \overset{\star}{\psi}{}_{N,\mathrm{S}}^{\varepsilon}\mathbf{curl}\,\chi - \boldsymbol{v}_h\|_{1,\Omega} \\
&+ \inf_{q_h\in Q_h^{k-1}}\|p_N^{\varepsilon} - \chi p_{N,\mathrm{S}}^{\varepsilon} - q_h\|_{\Omega}\Big)
\end{aligned} \tag{4.3.37}$$

Furthermore, by writing $\boldsymbol{u}_N^{\varepsilon} = \chi\boldsymbol{u}_N^{\varepsilon} + (1-\chi)\boldsymbol{u}_N^{\varepsilon}$ and $p_N^{\varepsilon} = \chi p_N^{\varepsilon} + (1-\chi)p_N^{\varepsilon}$, it comes

$$\begin{aligned}
\boldsymbol{u}_N^{\varepsilon} - \chi\boldsymbol{u}_{N,\mathrm{S}}^{\varepsilon} &= \chi(\boldsymbol{u}_{N,R}^{1,\varepsilon} + \boldsymbol{u}_{N,R}^{2,\varepsilon}) + (1-\chi)\boldsymbol{u}_N^{\varepsilon}, \\
p_N^{\varepsilon} - \chi p_{N,\mathrm{S}}^{\varepsilon} &= \chi(p_{N,\mathrm{R}}^{1,\varepsilon} + p_{N,\mathrm{R}}^{2,\varepsilon}) + (1-\chi)p_N^{\varepsilon},
\end{aligned}$$

so that estimate (4.3.37) becomes

$$\begin{cases}
\|\boldsymbol{u}_N^{\varepsilon} - \tilde{\boldsymbol{u}}_{N,h}^{\varepsilon}\|_{1,\Omega} + |\log(\varepsilon)|^{-\frac{1}{2}}\|p_N^{\varepsilon} - \tilde{p}_{N,h}^{\varepsilon}\|_{\Omega} + \|\boldsymbol{\lambda}_N^{\varepsilon} - \tilde{\boldsymbol{\lambda}}_{N,h}^{\varepsilon}\|_{-\frac{1}{2},\varepsilon} \\
\quad\lesssim |\log(\varepsilon)|^{\frac{1}{2}}\Big(\inf_{\boldsymbol{v}_h\in\boldsymbol{V}_h^k}\|\chi(\boldsymbol{u}_{N,R}^{1,\varepsilon} + \boldsymbol{u}_{N,R}^{2,\varepsilon}) + (1-\chi)\boldsymbol{u}_N^{\varepsilon} - \overset{\star}{\psi}{}_{N,\mathrm{S}}^{\varepsilon}\mathbf{curl}\,\chi - \boldsymbol{v}_h\|_{1,\Omega} \\
\qquad + \inf_{q_h\in Q_h^{k-1}}\|\chi(p_{N,\mathrm{R}}^{1,\varepsilon} + p_{N,\mathrm{R}}^{2,\varepsilon}) + (1-\chi)p_N^{\varepsilon} - q_h\|_{\Omega}\Big)
\end{cases}$$

It is now sufficient to prove that the functions

$$\chi(\boldsymbol{u}_{N,R}^{1,\varepsilon} + \boldsymbol{u}_{N,R}^{2,\varepsilon}) + (1-\chi)\boldsymbol{u}_{N,\mathrm{S}}^{\varepsilon} - \overset{\star}{\psi}{}_{N,\mathrm{S}}^{\varepsilon}\mathbf{curl}\,\chi, \quad \chi(p_{N,\mathrm{R}}^{1,\varepsilon} + p_{N,\mathrm{R}}^{2,\varepsilon}) + (1-\chi)p_{N,\mathrm{S}}^{\varepsilon},$$

are well estimated by the elements of $\boldsymbol{V}_h^k$ and Q_h^{k-1}, respectively. To to so, we will prove that they belong to $\boldsymbol{H}^{k+1}(\Omega)$ and $H^k(\Omega)$, respectively. In what follows, we provide successively a priori estimates for $(\boldsymbol{u}_{N,\mathrm{R}}^{1,\varepsilon}, p_{N,\mathrm{R}}^{1,\varepsilon})$, $(\boldsymbol{u}_{N,\mathrm{R}}^{2,\varepsilon}, p_{N,\mathrm{R}}^{2,\varepsilon})$, $\overset{\star}{\psi}{}_{N,\mathrm{S}}^{\varepsilon}$ and $((1-\chi)\boldsymbol{u}_N^{\varepsilon}, (1-\chi)p_N^{\varepsilon})$.

• First note that $(\boldsymbol{u}_{N,\mathrm{R}}^{1,\varepsilon}, p_{N,\mathrm{R}}^{1,\varepsilon})$ is solution of the Stokes equation in ω^ρ, so thanks to the interior regularizing property of the Stokes operator we have

$$\begin{aligned}\|\boldsymbol{u}_{N,\mathrm{R}}^{1,\varepsilon}\|_{k+1,\omega^{3\rho/4}} + |\log(\varepsilon)|^{-\frac{1}{2}}\|p_{N,\mathrm{R}}^{1,\varepsilon}\|_{k,\omega^{3\rho/4}} &\lesssim \|\boldsymbol{u}_{N,\mathrm{R}}^{1,\varepsilon}\|_{1,\omega^\rho} + |\log(\varepsilon)|^{-\frac{1}{2}}\|p_{N,\mathrm{R}}^{1,\varepsilon}\|_{\omega^\rho}\\ &\lesssim \|\boldsymbol{u}_{N,\mathrm{R}}^{1,\varepsilon}\|_{\frac{1}{2},\partial\omega^\rho}.\end{aligned}$$

Furthermore,

$$\boldsymbol{u}_{N,\mathrm{R}}^{1,\varepsilon} + \boldsymbol{u}_{N,\mathrm{S}}^{\varepsilon} = \Pi_{N+1}^{\rho}(\boldsymbol{u}_N^{\varepsilon}\cdot\boldsymbol{e}_\theta)\boldsymbol{e}_\theta + \Pi_{N+1}^{\rho}(\boldsymbol{u}_N^{\varepsilon}\cdot\boldsymbol{e}_r)\boldsymbol{e}_r \quad \text{on} \quad \partial\omega^\rho,$$

so by continuity of the L^2 projector Π_N^ρ on $(H^{\frac{1}{2}}(\partial\omega^\rho), \|\cdot\|_{\frac{1}{2},\partial\rho})$, we have

$$\|\boldsymbol{u}_{N,\mathrm{R}}^{1,\varepsilon}\|_{\frac{1}{2},\partial\omega^\rho} \lesssim \|\boldsymbol{u}_N^{\varepsilon}\|_{\frac{1}{2},\partial\omega^\rho} + \|\boldsymbol{u}_{N,\mathrm{S}}^{\varepsilon}\|_{\frac{1}{2},\partial\omega^\rho}$$

Gathering this equation, Lemma 4.3.9, the standard trace theorem from $\boldsymbol{H}^{\frac{1}{2}}(\partial\omega^\rho)$ to $\boldsymbol{H}^1(\Omega)$ and Theorem 4.2.1, we deduce that there exists $0 < \tilde{\rho}_2 < \rho$ such that for $\varepsilon \in (0, \tilde{\rho}_2)$,

$$\begin{aligned}\|\boldsymbol{u}_{N,\mathrm{R}}^{1,\varepsilon}\|_{\frac{1}{2},\partial\omega^\rho} &\lesssim \|\boldsymbol{u}_N^{\varepsilon}\|_{\frac{1}{2},\partial\omega^\rho} + |\boldsymbol{v}_{\mathrm{b}}| + \varepsilon|w_{\mathrm{b}}| \lesssim \|\boldsymbol{u}_N^{\varepsilon}\|_{1,\Omega} + |\boldsymbol{v}_{\mathrm{b}}| + \varepsilon|w_{\mathrm{b}}|,\\ &\lesssim |\boldsymbol{v}_{\mathrm{b}}| + \varepsilon|w_{\mathrm{b}}|.\end{aligned}$$

• Similarly, $(\boldsymbol{u}_{N,R}^{\varepsilon,2}, p_{N,R}^{\varepsilon,2})$ is solution of the Stokes equation in ω^ρ with boundary conditions

$$\boldsymbol{u}_{N,\mathrm{R}}^{\varepsilon,2} = \boldsymbol{u}_N^{\varepsilon} - \Pi_{N+1}^{\rho}(\boldsymbol{u}_N^{\varepsilon}\cdot\boldsymbol{e}_\theta)\boldsymbol{e}_\theta - \Pi_{N+1}^{\rho}(\boldsymbol{u}_N^{\varepsilon}\cdot\boldsymbol{e}_r)\boldsymbol{e}_r \quad \text{on} \quad \partial\omega^\rho.$$

Using again the interior regularizing property of the Stokes operator, the continuity of the L^2 projector Π_N^ρ on $(H^{\frac{1}{2}}(\partial\omega^\rho), \|\cdot\|_{\frac{1}{2},\partial\rho})$ and Theorem 4.2.1, we get

$$\begin{aligned}\|\boldsymbol{u}_{N,\mathrm{R}}^{\varepsilon,2}\|_{k+1,\omega^{3\rho/4}} + |\log(\varepsilon)|^{-\frac{1}{2}}&\|p_{N,\mathrm{R}}^{2,\varepsilon}\|_{k,\omega^{3\rho/4}}\\ &\lesssim \|\boldsymbol{u}_{N,\mathrm{R}}^{2,\varepsilon}\|_{1,\omega^\rho} + |\log(\varepsilon)|^{-\frac{1}{2}}\|p_{N,\mathrm{R}}^{2,\varepsilon}\|_{\omega^\rho}\\ &\lesssim \|\boldsymbol{u}_{N,\mathrm{R}}^{2,\varepsilon}\|_{\frac{1}{2},\partial\omega^\rho} \lesssim \|\boldsymbol{u}_N^{\varepsilon}\|_{\frac{1}{2},\partial\omega^\rho} \lesssim |\boldsymbol{v}_{\mathrm{b}}| + \varepsilon|w_{\mathrm{b}}|.\end{aligned}$$

• Now since $\overset{\star}{\psi}{}_{N,\mathrm{S}}^{\varepsilon}$ is a stream function associated to $\boldsymbol{u}_{N,\mathrm{S}}^{\varepsilon}$, $\overset{\star}{\psi}{}_{N,\mathrm{S}}^{\varepsilon}$ satisfy a biharmonic equation. We deduce from the regularizing effect of the biharmonic equation, the Poincaré-Wirtinger inequality in $H^2(\omega^\rho) \cap L_0^2(\omega^\rho)$ and Lemma 4.3.9, that for $\varepsilon \in (0, \tilde{\rho}_2)$,

$$\begin{aligned}\|\overset{\star}{\psi}{}_{N,\mathrm{S}}^{\varepsilon}\|_{k+1,\omega^{3\rho/4}} &\lesssim \|\overset{\star}{\psi}{}_{N,\mathrm{S}}^{\varepsilon}\|_{1,\omega^\rho}\\ &\lesssim \|\boldsymbol{u}_{N,\mathrm{S}}^{\varepsilon}\|_{\omega^\rho} \lesssim \|\boldsymbol{u}_{N,\mathrm{S}}^{\varepsilon}\|_{\frac{1}{2},\partial\omega^\rho} \lesssim \|\boldsymbol{u}_N^{\varepsilon}\|_{1,\Omega} \lesssim |\boldsymbol{v}_{\mathrm{b}}| + \varepsilon|w_{\mathrm{b}}|.\end{aligned}$$

• Finally, since $(\boldsymbol{u}_N^\varepsilon, p_N^\varepsilon)$ satisfy the Stokes equations and $\boldsymbol{u}_N^\varepsilon = 0$ on $\partial\Omega$ and since $\Omega\backslash\omega^{\rho/2}$ is relatively compact in $\Omega^\varepsilon \cup \partial\Omega$, the regularizing properties of the Stokes equations imply that $(\boldsymbol{u}_N^\varepsilon, p_N^\varepsilon) \in \boldsymbol{H}^{k+1}(\Omega\backslash\omega^{\rho/2}) \times H^k(\Omega\backslash\omega^{\rho/2})$ and we have

$$\begin{aligned}\|\boldsymbol{u}_N^\varepsilon\|_{k+1,\Omega\backslash\omega^{\rho/2}} + |\log(\varepsilon)|^{-\frac{1}{2}}\|p_N^\varepsilon\|_{k,\Omega\backslash\omega^{\rho/2}} &\lesssim \|\boldsymbol{u}_N^\varepsilon\|_{1,\Omega\backslash\omega^{\rho/2}} + |\log(\varepsilon)|^{-\frac{1}{2}}\|p_N^\varepsilon\|_{\Omega\backslash\omega^{\rho/2}} \\ &\lesssim |\boldsymbol{v}_{\rm b}| + \varepsilon|w_{\rm b}|.\end{aligned}$$

This implies that $((1-\chi)\boldsymbol{u}_N^\varepsilon, (1-\chi)p_N^\varepsilon) \in \boldsymbol{H}^{k+1}(\Omega) \times H^k(\Omega)$ and

$$\|(1-\chi)\boldsymbol{u}_N^\varepsilon\|_{k+1,\Omega} + |\log(\varepsilon)|^{-\frac{1}{2}}\|(1-\chi)p_N^\varepsilon\|_{k,\Omega} \lesssim |\boldsymbol{v}_{\rm b}| + \varepsilon|w_{\rm b}|.$$

Gathering these results, we deduce that

$$\begin{aligned}&\chi(\boldsymbol{u}_{N,\rm R}^{1,\varepsilon} + \boldsymbol{u}_{N,\rm R}^{2,\varepsilon}) + (1-\chi)\boldsymbol{u}_N^\varepsilon - \overset{\star}{\psi}{}_{N,S}^\varepsilon \mathbf{curl}\,\chi \in \boldsymbol{H}^{k+1}(\Omega), \\ &\chi(p_{N,\rm R}^{1,\varepsilon} + p_{N,\rm R}^{2,\varepsilon}) + (1-\chi)p_N^\varepsilon \in H^k(\Omega),\end{aligned}$$

and for $\varepsilon \in (0, \tilde{\rho}_2)$,

$$\begin{aligned}\|\chi(\boldsymbol{u}_{N,\rm R}^{1,\varepsilon} + \boldsymbol{u}_{N,\rm R}^{2,\varepsilon}) + (1-\chi)\boldsymbol{u}_N^\varepsilon - \overset{\star}{\psi}{}_{N,S}^\varepsilon \mathbf{curl}\,\chi\|_{k+1,\Omega} \\ + \|\chi(p_{N,\rm R}^{1,\varepsilon} + p_{N,\rm R}^{2,\varepsilon}) + (1-\chi)p_N^\varepsilon\|_{k,\Omega} \lesssim (|\boldsymbol{v}_{\rm b}| + \varepsilon|w_{\rm b}|).\end{aligned}$$

Setting $\tilde{\rho} = \min(\tilde{\rho}_1, \tilde{\rho}_2)$ and applying (4.3.29) concludes the proof of the Theorem. □

As a conclusion of this section, gathering Theorem 4.2.5 on the model approximation error and Theorem 4.3.8 on the numerical approximation error, we get for the global error:

$$\begin{aligned}\|\boldsymbol{u}^\varepsilon - \tilde{\boldsymbol{u}}_{N,h}^\varepsilon\|_{1,\Omega} + |\log(\varepsilon)|^{-\frac{1}{2}}\|p^\varepsilon - \tilde{p}_{N,h}^\varepsilon\|_\Omega + \varepsilon\|\boldsymbol{\lambda}^\varepsilon - \varepsilon^{-1}\tilde{\boldsymbol{\lambda}}_{N,h}^\varepsilon\|_{-\frac{1}{2},\varepsilon} \\ \lesssim (\varepsilon^{N+1} + |\log(\varepsilon)|^{\frac{1}{2}}h^k)(|\boldsymbol{v}_{\rm b}| + \varepsilon|w_{\rm b}|)\end{aligned}$$

As for the Poisson case, this shows that, h and ε being fixed, it is possible to reach a given convergence order by adjusting the parameters of the method k and N.

4.4 A Reduced order coupled model for small particles immersed in a Stokesian flow

In this section we extend Problem (4.2.6) to the case of small particles and a Stokesian flow.

4.4.1 Particle model

Using notations consistent with Chapter 2, the particle is assumed to be shaped as an ellipse, centered at the origin $\mathbf{0}$, and denoted as $\widehat{\omega}^\varepsilon \overset{\text{def}}{=} \varepsilon\mathcal{E}(a,1)$, where $\mathcal{E}(a,1)$ stands for an elliptical region in the (xOy) plane with the major axis a and the minor axis 1. The current position $\omega^\varepsilon(t)$ of the particle is then given by the image of the deformation map $\boldsymbol{\phi} : \widehat{\omega}^\varepsilon \times \mathbb{R}^+ \to \mathbb{R}^2$ defined by

$$\boldsymbol{\phi}(\widehat{\boldsymbol{x}}, t) = \boldsymbol{r}(t) + \boldsymbol{\Lambda}(t)\widehat{\boldsymbol{x}} \quad \forall (\widehat{\boldsymbol{x}}, t) \in \widehat{\omega}^\varepsilon \times \mathbb{R}^+, \tag{4.4.1}$$

where $\boldsymbol{r} : \mathbb{R}^+ \to \mathbb{R}^2$ stands for the displacement of the center of the ellipse and $\boldsymbol{\Lambda} : \mathbb{R}^+ \to SO(2)$ describes the rotation of the ellipse. Here, $SO(2)$ is the two-dimensional counterpart of $SO(3)$ introduced in (2.2.2). In 2D, the rotation matrix $\boldsymbol{\Lambda}$ is expressed in terms of a scalar function $\theta : \mathbb{R}^+ \to \mathbb{R}$ by the relation

$$\boldsymbol{\Lambda} \overset{\text{def}}{=} \begin{bmatrix} \cos(\theta) & -\sin(\theta) \\ \sin(\theta) & \cos(\theta) \end{bmatrix}. \tag{4.4.2}$$

In this formulation, θ represents the rotation angle with respect to $\boldsymbol{e}_x$ (see Figure 4.1). We assume that the dynamics of the particle are governed by the following equations of conservation of linear and angular momentum:

$$\begin{cases} \rho_{\mathrm{b}} A \ddot{\boldsymbol{r}} = \boldsymbol{f}, \\ \rho_{\mathrm{b}} I \ddot{\theta} = m, \end{cases}$$

where ρ_{b} is the density of the particles, A is the area of the particles, I is the moment of inertia, and $\boldsymbol{f}$ and m are, respectively, the resultant force and torque. Following the same

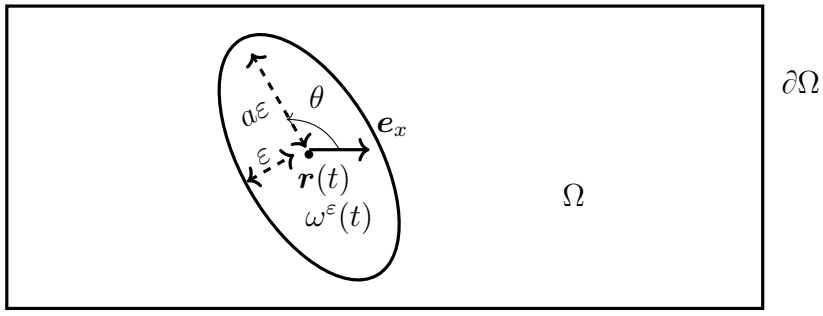

Figure 4.1: *Current configuration of the elliptical particle*

assumptions of Chapter 2, we assume that the particle moves within a smooth bounded domain $\Omega \subset \mathbb{R}^2$.

4.4.2 Reduced order coupled problem

In what follows, for the sake of simplicity, we reuse the same notations as the previous sections adapted the case of moving elliptical particles. We assume that the fluid satisfies the Stokes equation in the whole domain Ω and reduced order coupling conditions are applied on the particle interface $\partial\omega^\varepsilon(t)$. As the shape of the particle is elliptical, we slightly modify the definition of the finite dimensional space $\boldsymbol{F}_N$ given in (4.2.1). We also extend its definition to moving particles. To this purpose, similarly to Chapter 2, we introduce a local coordinate ν on the boundary of the ellipse in reference configuration such that any point of $\partial\widehat{\omega}^\varepsilon$ can be parametrized by

$$\widehat{\boldsymbol{x}} = \varepsilon(\cos(\nu)\boldsymbol{e}_x + a\sin(\nu)\boldsymbol{e}_y) \quad \forall \nu \in (0, 2\pi).$$

We then introduce the re-scaled function $\widehat{\boldsymbol{v}}(\varepsilon)(\nu) : \boldsymbol{L}^2(\partial\widehat{\omega}^\varepsilon) \to \boldsymbol{L}^2(0, 2\pi)$ defined by

$$\widehat{\boldsymbol{v}}(\varepsilon)(\nu) \stackrel{\text{def}}{=} \widehat{\boldsymbol{v}}(\varepsilon(\cos(\nu)\boldsymbol{e}_x + a\sin(\nu)\boldsymbol{e}_y) \quad \forall \nu \in (0, 2\pi).$$

Finally, the reduced order space $\boldsymbol{F}_N(t)$ is given by

$$\boldsymbol{F}_N(t) \stackrel{\text{def}}{=} \{\widehat{\boldsymbol{v}} \circ \boldsymbol{\phi}_t^{-1} \in \boldsymbol{L}^2_{0,\boldsymbol{n}}(\partial\omega^\varepsilon(t)) : \\ \widehat{\boldsymbol{v}}(\varepsilon)(\nu) = \boldsymbol{a}_0 + \sum_{k=1}^{N} \boldsymbol{a}_k \cos(k\nu) + \boldsymbol{b}_k \sin(k\nu), \quad \boldsymbol{a}_k, \boldsymbol{b}_k \in \mathbb{R}^2\}.$$

We also introduce the explicit expression of the particle velocity $\boldsymbol{u}_{\mathrm{b}} \stackrel{\text{def}}{=} \partial_t\boldsymbol{\phi} \circ \boldsymbol{\phi}_t^{-1}$ in terms of the solid unknowns $\boldsymbol{r}$ and θ:

$$\boldsymbol{u}_{\mathrm{b}}(\boldsymbol{x}, t) = \dot{\boldsymbol{r}} + \dot{\theta}(\boldsymbol{x} - \boldsymbol{r})^\perp \quad \forall (\boldsymbol{x}, t) \in \omega^\varepsilon(t) \times \mathbb{R}^+,$$

where for $\boldsymbol{x} = (x_1,\, x_2)$, we have denoted by $\boldsymbol{x}^\perp$ the vector $(-x_2, x_1)$. Let $\boldsymbol{V} \stackrel{\text{def}}{=} \boldsymbol{H}^1_0(\Omega)$ and

$$Q(t) \stackrel{\text{def}}{=} \left\{q \in L^2(\Omega) \ : \ q|_{\omega^\varepsilon(t)} \in L^2_0(\omega^\varepsilon(t)) \quad q|_{\Omega^\varepsilon(t)} \in L^2_0(\Omega^\varepsilon(t))\right\}$$

be the function space for the velocity and pressure, the reduced order coupled problem reads: we look for $(\boldsymbol{u}_N^\varepsilon, p_N^\varepsilon, \boldsymbol{\lambda}_N^\varepsilon, \boldsymbol{r}, \theta)$ such that $(\boldsymbol{u}_N^\varepsilon(t), p_N^\varepsilon(t), \boldsymbol{\lambda}_N^\varepsilon(t), \boldsymbol{r}(t), \theta(t)) \in \boldsymbol{V} \times Q(t) \times \boldsymbol{F}_N(t) \times \mathbb{R}^2 \times \mathbb{R}$ a.e. $t \in \mathbb{R}^+$ and

$$\begin{cases} \boldsymbol{\phi}_t(\widehat{\boldsymbol{x}}) = \boldsymbol{r} + \boldsymbol{\Lambda}\widehat{\boldsymbol{x}} \quad \forall \widehat{\boldsymbol{x}} \in \widehat{\omega}^\varepsilon, \\ a^{\mathrm{f}}_\Omega\big((\boldsymbol{u}_N^\varepsilon, p_N^\varepsilon), (\boldsymbol{v}, q)\big) + \rho_{\mathrm{b}} A\ddot{\boldsymbol{r}} \cdot \delta\boldsymbol{r} + \rho_{\mathrm{b}} I\ddot{\theta}\delta\theta \\ - \big(\boldsymbol{\lambda}_N^\varepsilon, \boldsymbol{v} - \delta\boldsymbol{r} - \delta\theta(\boldsymbol{x} - \boldsymbol{r})^\perp\big)_{\varepsilon,t} \\ + \big(\boldsymbol{\mu}_N, \boldsymbol{u}_N^\varepsilon - \dot{\boldsymbol{r}} - \dot{\theta}(\boldsymbol{x} - \boldsymbol{r})^\perp\big)_{\varepsilon,t} = 0 \end{cases} \tag{4.4.3}$$

for all $(\boldsymbol{v}, q, \boldsymbol{\mu}_N, \delta\boldsymbol{r}, \delta\theta) \in \boldsymbol{V} \times Q(t) \times \boldsymbol{F}_N(t) \times \mathbb{R}^2 \times \mathbb{R}$, where $\boldsymbol{\Lambda}$ is given in terms of θ by (4.4.2), and the inner product $(\cdot,\cdot)_{\varepsilon,t}$ is defined by

$$(\boldsymbol{u}, \boldsymbol{v})_{\varepsilon,t} \stackrel{\text{def}}{=} \int_{\partial\omega^\varepsilon(t)} (\boldsymbol{u}\cdot\boldsymbol{v})\widehat{h}\circ\boldsymbol{\phi}_t^{-1}, \quad \widehat{h}(\varepsilon)(\nu) \stackrel{\text{def}}{=} \left(\varepsilon\sqrt{a^2\cos^2(\nu)+\sin^2(\nu)}\right)^{-1}.$$

Here the bilinear form $a_\Omega^{\mathrm{f}} : (\boldsymbol{V}\times Q(t)) \times (\boldsymbol{V}\times Q(t)) \to \mathbb{R}$ is defined by

$$a_\Omega^{\mathrm{f}}((\boldsymbol{u},p),(\boldsymbol{v},q)) \stackrel{\text{def}}{=} \mu_{\mathrm{f}} a(\boldsymbol{u},\boldsymbol{v}) - b_1(p,\boldsymbol{v}) + b_1(q,\boldsymbol{u})$$

where the definition of the bilinear forms a and b_1 are given in (4.2.15).

4.4.3 Numerical approximation

This section is devoted to the discretization of Problem (4.4.3). For sake of completeness, we also provide the discrete formulation of the two following problems introduced in Chapter 2, adapted to the simulation of an immersed particle in a two dimensional Stokesian flow: the ALE coupled problem (2.2.4),(2.2.9),(2.2.23) and the fictitious domain coupled model (2.2.4), (2.2.10) ,(2.2.24). In Section 4.5, we use the former two models with standard interface coupling conditions to assess the accuracy of the reduced order coupled model.

4.4.4 Discrete formulation of the reduced order coupled problem

We introduce in this section the time and space discretization of Problem 4.4.3. For the time discretization, we use the same notations as the previous chapters. We denote by $\tau > 0$ the time step length and for $n \in \mathbb{N}$, we set $t^n \stackrel{\text{def}}{=} n\tau$. For a given function $\boldsymbol{v}$ depending on t, we set

$$\boldsymbol{v}^n, \quad \partial_\tau \boldsymbol{v}^n \stackrel{\text{def}}{=} \frac{1}{\tau}(\boldsymbol{v}^n - \boldsymbol{v}^{n-1}), \quad \boldsymbol{v}^{n-\frac{1}{2}} \stackrel{\text{def}}{=} \frac{1}{2}(\boldsymbol{v}^{n-1} + \boldsymbol{v}^n)$$

for an approximation of $\boldsymbol{v}(t^n)$, the backward Euler difference and the mid point evaluation, respectively. We then consider a semi-implicit scheme in which the geometrical coupling is treated in an explicit fashion, as follows: for a given displacement $\boldsymbol{r} \in \mathbb{R}^2$ and a given rotation $\theta \in \mathbb{R}$, it reads

$$\boldsymbol{\phi}^n(\widehat{\boldsymbol{x}}) = \boldsymbol{r}^{n-1} + \boldsymbol{\Lambda}^{n-1}\widehat{\boldsymbol{x}} \quad \forall \widehat{\boldsymbol{x}} \in \widehat{\omega}^\varepsilon.$$

where $\boldsymbol{\Lambda}^{n-1}$ is obtained in terms of θ^{n-1} by (4.4.2). For the space discretization, similarly to Section 4.3.1, we consider a low-order stabilized formulation based on piecewise affine approximations. In particular, we set $\boldsymbol{V}_h \stackrel{\text{def}}{=} \boldsymbol{X}_h^1(\Omega) \cap \boldsymbol{V}$ and $Q_h^n \stackrel{\text{def}}{=} X_h^1(\Omega) \cap Q^n$ for the

discretization of the velocity $\boldsymbol{u}_N^\varepsilon$ and pressure p_N^ε. We also introduce the discrete Lagrange multiplier space $\boldsymbol{F}_{N,h}^n$, discrete counterpart of $\boldsymbol{F}_N(t)$, as

$$\boldsymbol{F}_{N,h}^n \stackrel{\text{def}}{=} \Big\{ \widehat{\boldsymbol{v}}_h \circ (\boldsymbol{\phi}^n)^{-1} \in \boldsymbol{L}^2_{0,\boldsymbol{n}}(\partial\omega^{\varepsilon,n}) : \\ \widehat{\boldsymbol{v}}_h(\varepsilon)(\nu) = \boldsymbol{a}_0 + \sum_{k=1}^{N} \boldsymbol{a}_k \cos(k\nu) + \boldsymbol{b}_k \sin(k\nu), \quad \boldsymbol{a}_k, \boldsymbol{b}_k \in \mathbb{R}^2 \Big\}.$$

We then consider a backward Euler scheme for the fluid and solid inertial terms. The remaining kinematic and dynamic conditions of Problem (4.4.3) are discretized with an implicit scheme. The resulting strongly coupled scheme is given in Algorithm 4.

Algorithm 4 Discrete formulation of the reduced order coupled model (4.4.3).

For $n \geqslant 1$,

Step 1: Update interface position:

$$\boldsymbol{\phi}^n(\widehat{\boldsymbol{x}}) = \boldsymbol{r}^{n-1} + \boldsymbol{\Lambda}^{n-1}\widehat{\boldsymbol{x}} \quad \forall \widehat{\boldsymbol{x}} \in \widehat{\omega}^\varepsilon, \quad \omega^{\varepsilon,n} = \boldsymbol{\phi}^n(\widehat{\omega}^\varepsilon),$$

where $\boldsymbol{\Lambda}^{n-1}$ is obtained in terms of θ^{n-1} by (4.4.2).

Step 2: Find $(\boldsymbol{u}_{N,h}^{\varepsilon,n}, p_{N,h}^{\varepsilon,n}, \boldsymbol{\lambda}_{N,h}^{\varepsilon,n}, \boldsymbol{r}^n, \theta^n) \in \boldsymbol{V}_h \times Q_h^n \times \boldsymbol{F}_{N,h}^n \times \mathbb{R}^2 \times \mathbb{R}$ with $\dot{\boldsymbol{r}}^n = \partial_\tau \boldsymbol{r}^n$ and $\dot{\theta}^n = \partial_\tau \theta^n$ such that

$$\begin{cases} a_\Omega^{\mathrm{f}}\big((\boldsymbol{u}_{N,h}^{\varepsilon,n}, p_{N,h}^{\varepsilon,n}), (\boldsymbol{v}_h, q_h)\big) - (1/\mu_{\mathrm{f}}) s_h^p(q_h, p_{N,h}^{\varepsilon,n}) - (1/\mu_{\mathrm{f}}) s_h^\lambda(\boldsymbol{\mu}_N, \boldsymbol{\lambda}_{N,h}^{\varepsilon,n}) \\ + I\partial_\tau\dot{\theta}^n\delta\theta + M\partial_\tau\dot{\boldsymbol{r}}^n \cdot \delta\boldsymbol{r} \\ - \big(\boldsymbol{\lambda}_{N,h}^n, \boldsymbol{v}_h - \delta\boldsymbol{r} - \delta\theta(\boldsymbol{I}_2 - \boldsymbol{r}^{n-1})^\perp\big)_{\varepsilon,n} \\ + \big(\boldsymbol{\mu}_{N,h}, \boldsymbol{u}_{N,h}^{\varepsilon,n} - \dot{\boldsymbol{r}}^{n-1} - \dot{\theta}^{n-1}(\boldsymbol{I}_2 - \boldsymbol{r}^{n-1})^\perp\big)_{\varepsilon,n} = 0 \end{cases} \tag{4.4.4}$$

for all $(\boldsymbol{v}_h, q_h, \boldsymbol{\mu}_N, \delta\boldsymbol{r}, \delta\theta) \in \boldsymbol{V}_h^n \times Q_h^n \times \boldsymbol{F}_{N,h}^n \times \mathbb{R}^2 \times \mathbb{R}$.

4.4.5 Comparison with other discrete formulations

For the sake of completeness, in this section, we provide the space-time fully discrete formulation of an ALE and fictitious domain method with standard coupling conditions on the fluid-structure interface. These numerical methods will be used in the numerical experiments of Section 4.5 for comparison purposes.

4.4.5.1 Coupled problem with ALE formalism

In this section, we present the discrete formulation of the two dimensional counterpart of the coupled problem (2.2.4),(2.2.9),(2.2.23) for small particles immersed in a two dimensional Stokesian flow. Similarly to what has been done for the fluid-structure ALE coupled problem described in Section 2.3.1, we consider a triangulation of the reference

fluid domain which is fitted to the particle boundary $\partial\omega^{\varepsilon,n}$. We set $\boldsymbol{V}_h^{\partial\widehat{\omega}} \overset{\text{def}}{=} \boldsymbol{X}_h^1(\partial\widehat{\omega})$ as the trace space of $\boldsymbol{X}_h^1(\widehat{\Omega}^\varepsilon)$ and $\boldsymbol{\Pi}_{\mathrm{b},h}^1$ the corresponding interpolator onto $\boldsymbol{V}_h^{\partial\widehat{\omega}}$. The geometrical coupling is then treated explicitly. For a given displacement $\boldsymbol{r}^{n-1} \in \mathbb{R}^2$ and a given rotation θ^{n-1}, we define the ALE map as

$$\boldsymbol{\phi}^n(\widehat{\boldsymbol{x}}) = \boldsymbol{r}^{n-1} + \boldsymbol{\Lambda}^{n-1}\widehat{\boldsymbol{x}} \quad \forall \widehat{\boldsymbol{x}} \in \widehat{\omega}^\varepsilon, \quad \boldsymbol{\mathcal{A}}_h^n = \boldsymbol{\mathcal{L}}_h(\boldsymbol{\Pi}_{\mathrm{b},h}^1 \boldsymbol{\phi}^n),$$

where $\boldsymbol{\Lambda}^{n-1}$ given in terms of θ^{n-1} by (4.4.2) and $\boldsymbol{\mathcal{L}}_h$ denotes a given lifting operator (e.g., an harmonic extension operator). The one-to-one mapping $\boldsymbol{\mathcal{A}}_h^n$ allows use to consider as fluid unknowns

$$\widehat{\boldsymbol{u}}_h^{\varepsilon,n} = \boldsymbol{u}_h^{\varepsilon,n} \circ \boldsymbol{\mathcal{A}}_h^n, \quad \widehat{p}_h^{\varepsilon,n} = p_h^{\varepsilon,n} \circ \boldsymbol{\mathcal{A}}_h^n.$$

We then introduce the following finite element space $\boldsymbol{V}_h^{\mathrm{f}} \overset{\text{def}}{=} \boldsymbol{X}_h^1(\widehat{\Omega}^\varepsilon) \cap \boldsymbol{H}_0^1(\widehat{\Omega}^\varepsilon)$ and $Q_h^{\mathrm{f}} = X_h^1(\widehat{\Omega}^\varepsilon) \cap L^2(\widehat{\Omega}^\varepsilon)$ for the approximation of the fluid unknowns. We apply a finite element approximation with an implicit treatment of the coupling conditions. The fully discrete strongly coupled scheme is given in Algorithm 5. One limitation of Algorithm 5 lies in

Algorithm 5 Discrete formulation of the coupled problem with ALE formalism in the fluid

For $n \geqslant 1$,

Step 1: Update of the particle position and of the fluid domain

$$\begin{cases} \boldsymbol{\phi}^n(\widehat{\boldsymbol{x}}) = \boldsymbol{r}^{n-1} + \boldsymbol{\Lambda}^{n-1}\widehat{\boldsymbol{x}} \quad \forall \widehat{\boldsymbol{x}} \in \widehat{\omega}^\varepsilon, \\ \boldsymbol{\mathcal{A}}_h^n = \boldsymbol{\mathcal{L}}_h\big(\boldsymbol{\Pi}_{\mathrm{b},h}^1 \boldsymbol{\phi}^n\big), \quad \Omega_{\mathrm{f}}^{\varepsilon,n} = \boldsymbol{\mathcal{A}}_h^n(\widehat{\Omega}_{\mathrm{f}}^\varepsilon), \end{cases}$$

with $\boldsymbol{\Lambda}^{n-1}$ in terms of θ^{n-1} by (4.4.2).

Step 2: Find $(\widehat{\boldsymbol{u}}_h^{\varepsilon,n}, \widehat{p}_h^{\varepsilon,n}, \boldsymbol{r}^n, \theta^n) \in \boldsymbol{V}_h^{\mathrm{f}} \times Q_h^{\mathrm{f}} \times \mathbb{R}^2 \times \mathbb{R}$ with $\dot{\boldsymbol{r}}^n = \partial_\tau \boldsymbol{r}^n$, $\dot{\theta}^n = \partial_\tau \theta^n$ and such that

$$a_{\Omega_{\mathrm{f}}^{\varepsilon,n}}^{\mathrm{f}}\big((\boldsymbol{u}_h^{\varepsilon,n}, p_h^{\varepsilon,n}), (\boldsymbol{v}_h, q_h)\big) - (1/\mu_{\mathrm{f}}) s_h^p(q_h, p_h^{\varepsilon,n}) + \rho_{\mathrm{b}} A \partial_\tau \dot{\boldsymbol{r}}^n \cdot \delta\boldsymbol{r} + \rho_{\mathrm{b}} I \partial_\tau \dot{\theta}^n \delta\theta = 0 \tag{4.4.5}$$

for all $(\widehat{\boldsymbol{v}}_h, \widehat{q}_h, \delta\boldsymbol{r}, \delta\theta) \in \boldsymbol{V}_h^{\mathrm{f}} \times Q_h^{\mathrm{f}} \times \mathbb{R}^2 \times \mathbb{R}$ with

$$\widehat{\boldsymbol{v}}_h = \boldsymbol{\Pi}_{\mathrm{b},h}^1\big(\delta\boldsymbol{r} + \delta\theta(\boldsymbol{\phi}^n - \boldsymbol{r}^{n-1})^\perp\big) \quad \text{on} \quad \partial\widehat{\omega}^\varepsilon.$$

the capability of the discrete lifting operator $\boldsymbol{\mathcal{L}}_h$ to guarantee mesh quality when dealing with large interface deflections. This problem is even more pronounced in the context of multiple particles immersed in a fluid and that can get into contact. In the next section, we introduce an algorithm, with full order interface condition, that overcomes this issue by working with a fixed mesh.

Remark 15. For the sake of consistency with Chapter 2, we used the denomination ALE for a stationary Stokes fluid, although, due to the absence of inertial terms in the fluid domain, in pratice, the formulation (4.4.5) corresponds to the Stokes equations with moving domain.

4.4.5.2 Coupled problem with fictitious domain method

In this section, we present the discrete formulation of the two dimensional counterpart of the coupled problem (2.2.4), (2.2.10) ,(2.2.24) for small particles immersed in a two dimensional Stokesian flow. We consider $\boldsymbol{V}_h \overset{\text{def}}{=} \boldsymbol{X}_h^1(\Omega) \cap \boldsymbol{V}$, $Q_h^n \overset{\text{def}}{=} X_h^1(\Omega) \cap Q^n$ and $\boldsymbol{L}_H^n = \boldsymbol{X}_H^1(\partial\omega^{\varepsilon,n})$ for the approximation of the velocity, pressure and Lagrange multiplier. Similarly to the stabilized discrete formulation of problem (4.4.3) presented in Section (4.3.1), to overcome the instability of the saddle-point problem due to the choice of the Lagrange multiplier finite element space $\boldsymbol{L}_H^n$, and to avoid any restriction on the ration h/H, we introduce the following stabilization term :

$$s_h^{BH} \overset{\text{def}}{=} \gamma_\lambda h \left(\boldsymbol{\mu}_H, \boldsymbol{\lambda}_H^{\varepsilon,n}\right)_{\partial\omega^{\varepsilon,n}},$$

with $\gamma_\lambda > 0$ a user-defined dimensionless parameter. We apply a finite element approximation on the whole domain Ω with implicit treatment of the coupling conditions. The resulting strongly coupled formulation is given in Algorithm 6.

Algorithm 6 Discrete formulation of the fictitious domain coupled model

For $n \geqslant 1$,
Step 1: Update interface position:

$$\boldsymbol{\phi}^n(\widehat{\boldsymbol{x}}) = \boldsymbol{r}^{n-1} + \boldsymbol{\Lambda}^{n-1}\widehat{\boldsymbol{x}} \quad \forall \widehat{\boldsymbol{x}} \in \widehat{\omega}^\varepsilon, \quad \omega^{\varepsilon,n} = \boldsymbol{\phi}^n(\omega^\varepsilon).$$

where $\boldsymbol{\Lambda}^{n-1}$ is obtained from θ^{n-1} using nonlinear formula (4.4.2).
Step 2: Find $(\boldsymbol{u}_h^{\varepsilon,n}, p_h^{\varepsilon,n}, \boldsymbol{\lambda}_H^{\varepsilon,n}, \boldsymbol{r}^n, \theta^n) \in \boldsymbol{V}_h \times Q_h \times \boldsymbol{L}_H^n \times \mathbb{R}^2 \times \mathbb{R}$ with $\dot{\boldsymbol{r}}^n = \partial_\tau \boldsymbol{r}^n$ and $\dot{\theta}^n = \partial_\tau \theta^n$ such that

$$\begin{cases} a_{\Omega,h}^{\mathrm{f}}\big((\boldsymbol{u}_h^{\varepsilon,n}, p_h^{\varepsilon,n}), (\boldsymbol{v}_h, q_h)\big) + \rho_{\mathrm{b}} A \partial_\tau \dot{\boldsymbol{r}}^n \cdot \delta\boldsymbol{r} + \rho_{\mathrm{b}} I \partial_\tau \dot{\theta}^n \delta\theta \\ - \big(\boldsymbol{\lambda}_H^n, \boldsymbol{v}_h - \delta\boldsymbol{r} - \delta\theta(\boldsymbol{x} - \boldsymbol{r}^{n-1})^\perp\big)_{\partial\omega^{\varepsilon,n}} - (1/\mu_{\mathrm{f}}) s_h^p(q_h, p_h^{\varepsilon,n}) - (1/\mu_{\mathrm{f}}) s_h^{BH}(\boldsymbol{\mu}_H, \boldsymbol{\lambda}_H^{\varepsilon,n}) \\ + \big(\boldsymbol{\mu}_H, \boldsymbol{u}_h^n - \dot{\boldsymbol{r}}^{n-1} - \dot{\theta}^{n-1}(\boldsymbol{x} - \boldsymbol{r}^{n-1})^\perp\big)_{\partial\omega^{\varepsilon,n}} = 0 \end{cases}$$

for all $(\boldsymbol{v}_h, q_h, \boldsymbol{\mu}_H, \delta\boldsymbol{r}, \delta\theta) \in \boldsymbol{V}_h \times Q_h \times \boldsymbol{L}_H^n \times \mathbb{R}^2 \times \mathbb{R}$.

4.5 Numerical experiments

Following the structure of this chapter, we divide this section into two parts. First, we analyze the modeling error of Problem 4.2.6 with respect to the solution obtained with Problem 4.2.20, referring to this part as the convergence in ε. We conduct the numerical experiments for both a circular inclusion, for which Theorem 4.2.5 applies, and an elliptical inclusion, for which no formal proof has been presented in this chapter. In a second part, we illustrate the accuracy of Algorithm 4 by comparing its solution with those provided by Algorithm 5 and Algorithm 6. In this section, we consider the case of a single

particle and investigate the influence of its size ε and the number of Fourier modes N on the solution of the reduced order coupled model. Note that due to time constraints, we will not present numerical results for the augmented finite element method (4.3.34) at this time. However, we aim to provide them shortly.

4.5.1 Convergence in ε

In this section, in order to illustrate the result of Theorem 4.2.5, we will look at the convergence of the solution of Problem (4.4.3) with respect to the solution of Problem (4.2.20). To this purpose, we consider successively two inclusions, one circular (with an aspect ratio of $a = 1$), and the other elliptical with an aspect ratio of $a = 2$ centered at $(0.1, 0.2)$, and varying in size with $\varepsilon \in \{0.1, 0.08, 0.06, 0.04, 0.02\}$. The fluid domain is taken as the unit square with the following boundary conditions

$$\begin{cases} \boldsymbol{u}_N^\varepsilon = \mathbf{0} & y \in \{-0.5, 0.5\}, \\ p_N^\varepsilon = 0 & x = -0.5, \\ p_N^\varepsilon = 10 & x = 0.5. \end{cases}$$

The number of modes is chosen such that $N \in \{0, 1\}$. To solve this problem, we use a conforming mesh with respect to the inclusion with the mesh size h sufficiently small such that the numerical error due to the discrete approximation of both the reduced order and full order solutions can be neglected with respect to the error of the model. The H^1-error is reported in Figure 4.2. As proven in Section 4.2.2, the convergence velocity of the two solutions behaves as ε^{N+1} for the circle. Although no theoretical proof has been given, we observe a similar behavior for the elliptical inclusion.

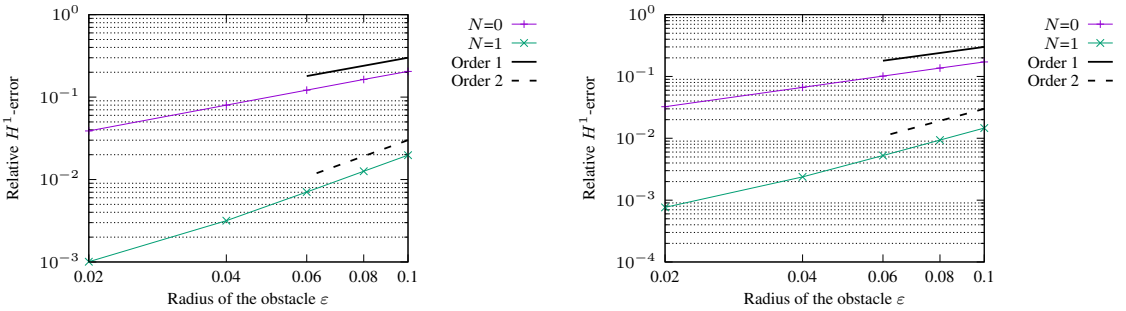

(a) *Circular inclusion (a =1)* **(b)** *Elliptical inclusion (a = 2)*

Figure 4.2: *Relative H^1-error for decreasing values of ε for a single inclusion.*

4.5.2 Oscillations of an elastically supported particle immersed in a Stokesian flow

As the first example of fluid-structure interaction, we consider the mechanical interaction between a viscous fluid and an elastically supported circular particle in a rectangular domain $\Omega = (-1.5, 1.5) \times (-0.5, 0.5)$. The fluid satisfies the Stokes equations and the boundary conditions for the fluid are similar to the previous test case (see Figure 4.3):

$$\begin{cases} \boldsymbol{u}_N^\varepsilon = \mathbf{0} & y \in \{-0.5, 0.5\}, \\ p_N^\varepsilon = 0 & x = -1.5, \\ p_N^\varepsilon = 10 & x = 1.5. \end{cases}$$

We assume that the solid is elastically supported and its displacement is constrained along the $\boldsymbol{e}_x$ direction. The following parameters for the particle model are considered: size

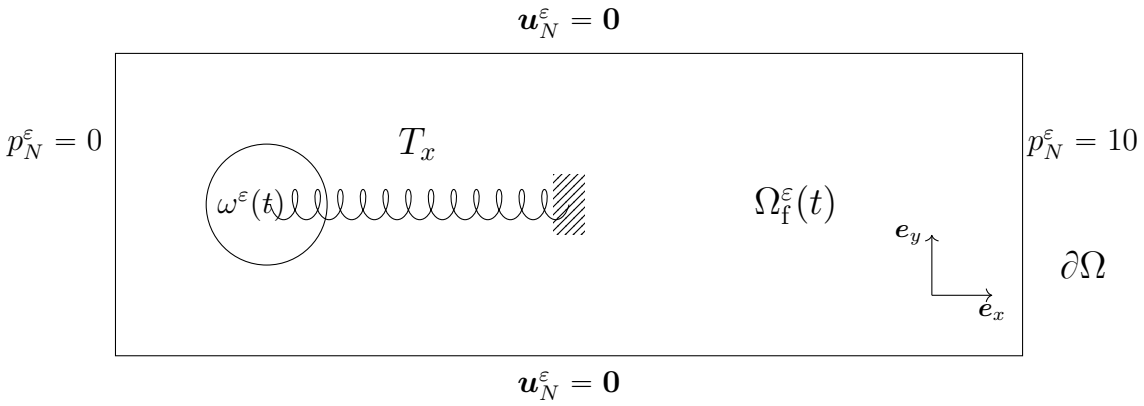

Figure 4.3: *Elastically supported particle immersed in a Stokesian flow*

$\varepsilon \in \{0.06, 0.04, 0.02\}$, density $\rho_{\mathrm{b}} = 1$ and string's tension $T_x = 10$. The particle is supposed to be initially at rest. For the fluid, we take a viscosity $\mu_{\mathrm{f}} = 1$. We run the simulations over the time interval $[0, 0.1]$ with a time step $\tau = 5 \cdot 10^{-4}$ and a uniform mesh satisfying $h/\varepsilon = 1/4$. In Figure 4.4, we plot the displacement of the particle along the x-axis obtained with Algorithm 4 and Algorithm 5. For Algorithm 4, the number of Fourier modes is taken $N = 0$. We observe that taking $N = 0$ appears to be sufficient to accurately approximate the displacement of the particle, even for relatively large radius. In Figure 4.5, snapshots of the fluid velocity and pressure are provided at times $t = 0.03$ for $\varepsilon = 0.06$. We observe as well that the pressure and velocity of the fluid are well reproduced, at least qualitatively, by the reduced order model with $N = 0$.

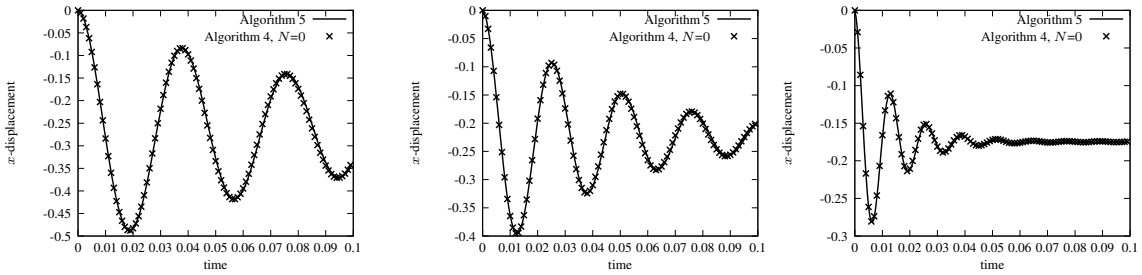

(a) $\varepsilon = 0.06$ **(b)** $\varepsilon = 0.04$ **(c)** $\varepsilon = 0.02$

Figure 4.4: *Time history of the displacement along the x-axis of an elastically supported particle immersed in a Stokesian flow.*

4.5.3 Jeffery orbits

We now consider an ellipse of aspect ratio $a = 2$ centered at the origin $\mathbf{0}$ in a rectangular domain $\Omega = (-1.5, 1.5) \times (-0.5, 0.5)$. The Stokesian flow is assumed to be driven by the following linear shear flow with shear rate $G = 1$ (see Figure 4.6):

$$\begin{cases} \boldsymbol{u}_N^\varepsilon = (G, 0) & y = 0.5, \\ \boldsymbol{u}_N^\varepsilon = (-G, 0) & y = -0.5, \\ \boldsymbol{u}_N^\varepsilon \cdot \boldsymbol{e}_y = 0, \quad (\boldsymbol{\sigma}(\boldsymbol{u}_N^\varepsilon, p_N^\varepsilon) \cdot \boldsymbol{e}_x) \cdot \boldsymbol{e}_x = 0 & x \in \{-1.5, 1.5\}. \end{cases}$$

The physical parameters of the fluid and the solid are given by $\mu_{\mathrm{f}} = 1$ and $\rho_{\mathrm{b}} = 1$. The mesh size is such that $h/\varepsilon = 1/4$. The behaviour of the coupled system is studied over the time interval $[0, 30]$ with time-step $\tau = 10^{-2}$. We consider the approximation provided by Algorithm 4 with $N \in \{0, 1\}$ and decreasing size $\varepsilon \in \{0.1, 0.05, 0.02\}$. We compare this approximation with the exact solution reported in [Gay, 1968] for $L = \infty$:

$$\begin{cases} \theta(t) = \tan^{-1}\left(a \tan\left(\dfrac{aGt}{a^2+1}\right)\right), \\ \dot{\theta}(t) = \dfrac{G}{a^2+1}(a^2\cos^2(\theta(t)) + \sin^2(\theta(t))) \end{cases} \tag{4.5.1}$$

for all $t \in \mathbb{R}^+$. In Figure 4.7, we plot the time history of the rotation of the ellipse. We can clearly observe that when $N = 0$, Algorithm 4 fails to accurately capture the rotational effects induced by the shear flow on the ellipse. On the contrary by adding the first Fourier mode ($N = 1$), Algorithm 4 is able to capture the rotation, particularly when the size ε of the ellipse is small.

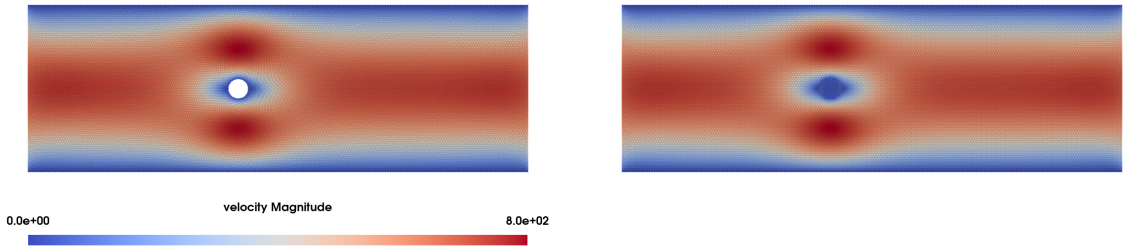

(a) *Algorithm 5, velocity snapshots*

(b) *Algorithm 4 with* $N = 0$*, velocity snapshots*

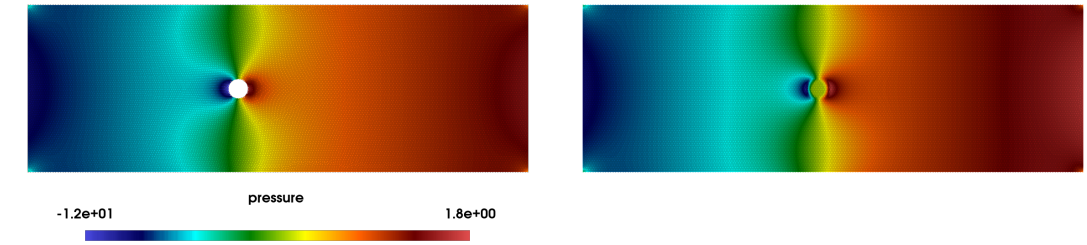

(c) *Algorithm 5, pressure snaphots*

(d) *Algorithm 4 with* $N = 0$*, pressure snaphots*

Figure 4.5: *Snapshots of the fluid velocity magnitude (up) and pressure (down) at times* $t = 0.03$ *for an elastically supported particle obtained with Algorithm 4–5 for* $\varepsilon = 0.06$*.*

4.5.4 Free fall of an elliptical particle immersed in a Stokesian flow

At last example, we study the free fall motion of an elliptical particle immersed in a Stokesian flow, with size $\varepsilon = 0.1$ and aspect ratio $a = 2$, subjected to a constant gravitational force $\boldsymbol{g} = -\boldsymbol{e}_y$. The elliptical particle is initially at rest. The fluid domain is rectangular with $\Omega = (-0.5, 0.5) \times (-1.5, 1.5)$. We assume the following boundary conditions for the fluid equations (see Figure 4.8):

$$\begin{cases} \boldsymbol{u}_N^\varepsilon = \boldsymbol{0} & x \in \{-0.5, 0.5\}, \\ \boldsymbol{u}_N^\varepsilon = \boldsymbol{0} & y = 1.5, \\ \boldsymbol{\sigma}(\boldsymbol{u}_N^\varepsilon, p_N^\varepsilon)\boldsymbol{e}_y = \boldsymbol{0} & y = -1.5. \end{cases}$$

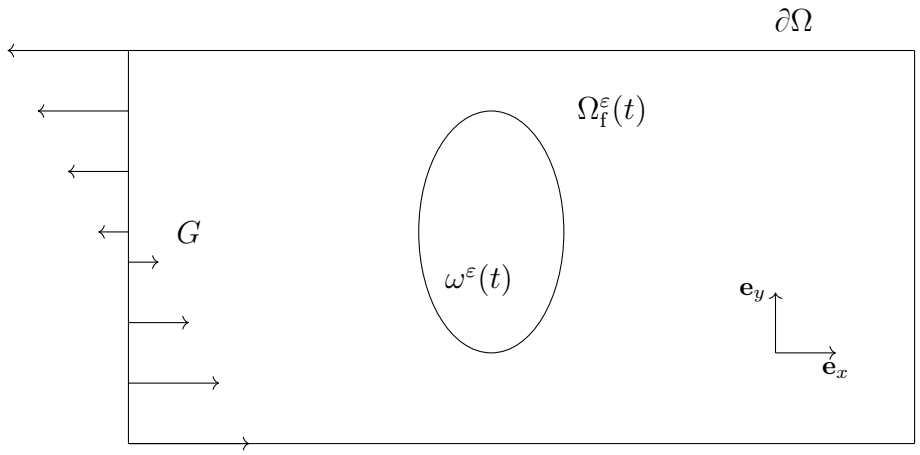

Figure 4.6: *Geometrical setting for the Jeffery orbits test case.*

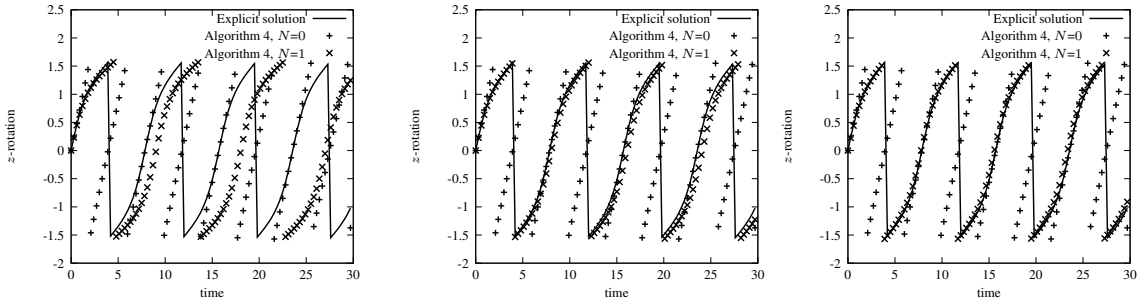

(a) $\varepsilon = 0.1$ **(b)** $\varepsilon = 0.05$ **(c)** $\varepsilon = 0.02$

Figure 4.7: *Time history of the rotation of an elliptical particle immersed in a shear flow for different sizes ε and number of Fourier modes $N \in \{0, 1\}$.*

The physical parameters of the fluid and solid are given by $\mu_{\mathrm{f}} = 1$ and $\rho_{\mathrm{b}} = 2 \cdot 10^{-2}$. The coupled system is simulated over the time interval $[0, 4000]$ with time-step $\tau = 1$, and an uniform mesh of size $h = 0.025$. To investigate the impact of the number of Fourier modes on Algoritm 4, we consider three different truncation levels $N \in \{0, 1, 2\}$. We compare these approximations with the solution given by Algorithm 6 for a similar time-step $\tau = 1$, a uniform fluid mesh of size $h = 0.01$ and a discretization step for the Lagrange multiplier space of size $H = 0.01$. In Figure 4.9, we plot the displacement of the elliptical particle along the x- and y-axis, and its rotation. For the case $N = 0$, the ellipse exits the domain at $t = 1674$, which explains why no displacement and rotation are given for the following time steps. Regardless of the number of Fourier modes chosen, we observe that the displacement of the ellipse along the y-axis is accurately captured by Algorithm 4.

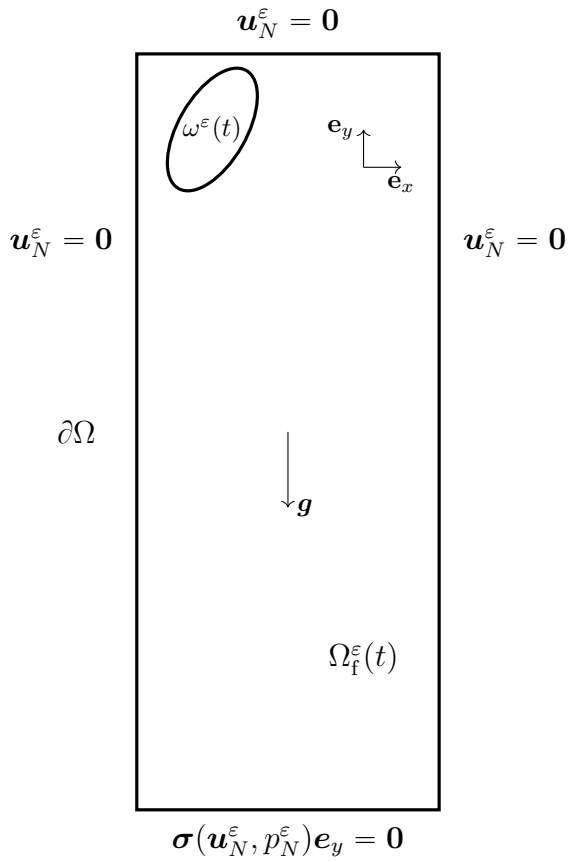

Figure 4.8: *Free fall of an elliptical particle in a Stokesian flow.*

This observation aligns with the conclusion drawn in Section 4.5.2, suggesting that a single mode ($N = 0$) is sufficient to capture the translational motion of the particle. Moreover, as discussed in Section 4.5.3, our analysis indicates that at least one additional mode ($N = 1$) is necessary for an accurate representation of the rotational dynamics. Introducing a third mode ($N = 2$) further improves the approximation of the rotation and, in a more indirect manner, also improves the representation of the translational motion along the x-axis. In Figure 4.10, we provide snapshots of the fluid velocity magnitude at times $\{0, 500, 1000, 2000, 4000\}$. In addition to the previous observations, we can cleary see the improved capturing of the fluid dynamics when passing from the mode $N = 1$ to the mode $N = 2$, particularly noticeable at times $t = 2000$ and $t = 4000$.

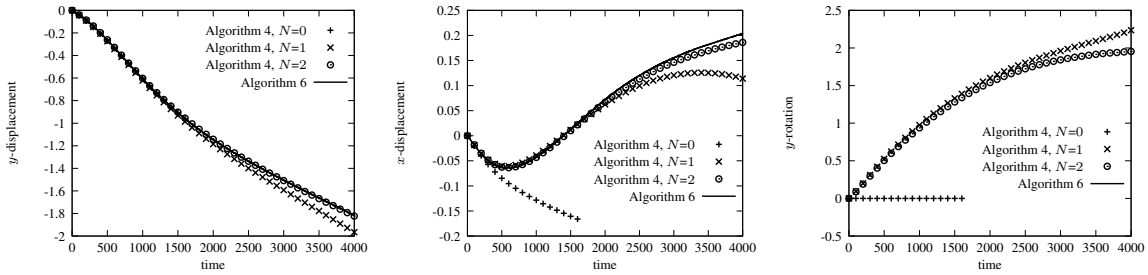

(a) *Displacement along the y-axis* **(b)** *Displacement along the x-axis* **(c)** *Rotation of the ellipse*

Figure 4.9: *Time history of the rotation and displacement of a falling ellipse in a Stokesian flow.*

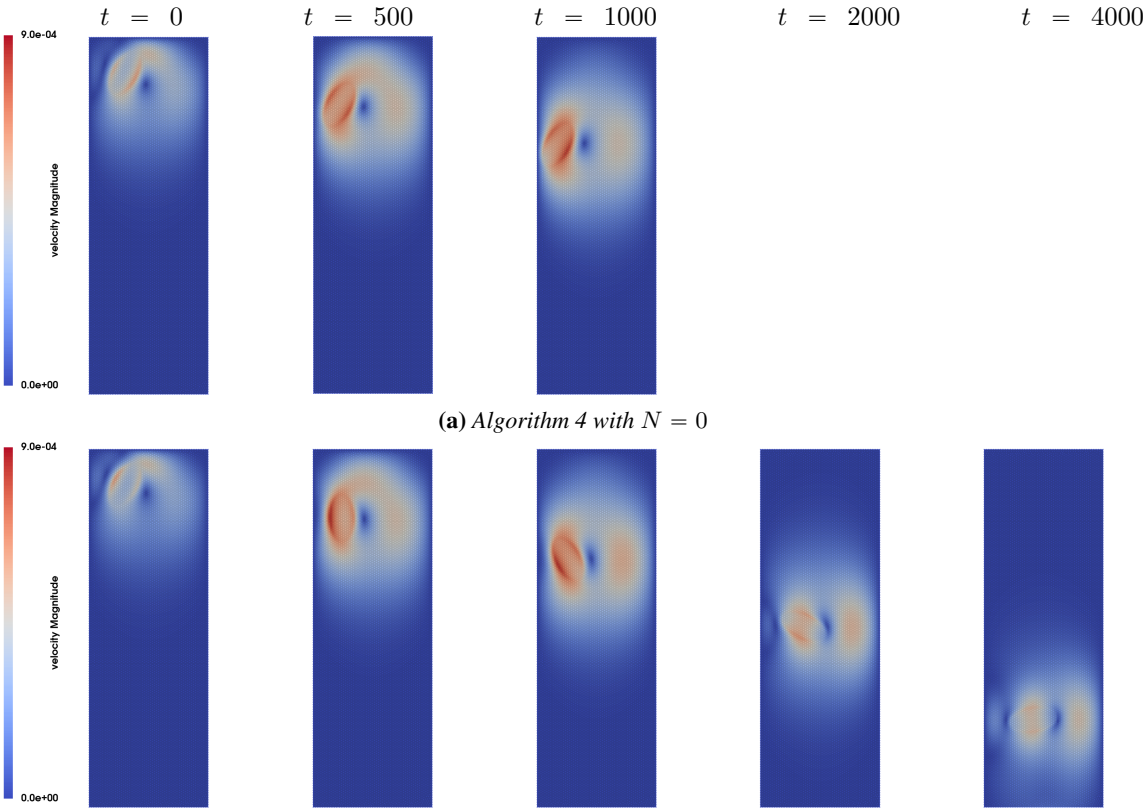

(a) *Algorithm 4 with $N = 0$*

(b) *Algorithm 4 with $N = 1$*

Figure 4.10: *Snaphots of the fluid velocity magnitude at time $t \in \{0, 500, 1000, 2000, 4000\}$ for a falling elliptical particle in a Stokesian flow with Algorithm 4, $N = 1$ and Algorithm 6*

Conclusion

In the first part of this chapter, we extended the analysis provided in Chapter 3 to Stokes equations with non-homogeneous Dirichlet boundary conditions, where the space of La-

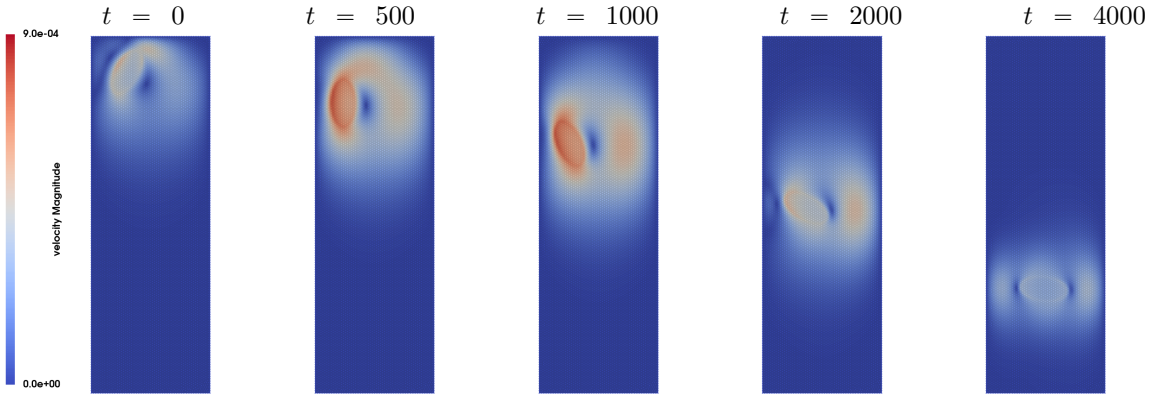

(c) *Algorithm 4 with* $N = 1$

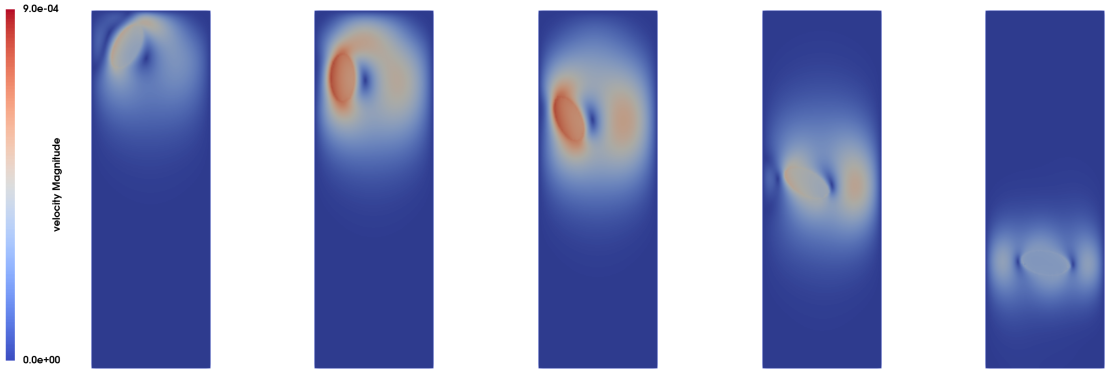

(d) *Algorithm 6*

Figure 4.10: *Snaphots of the fluid velocity magnitude at time* $t \in \{0, 500, 1000, 2000, 4000\}$ *for a falling elliptical particle in a Stokesian flow with Algorithm 4,* $N = 1$ *and Algorithm 6 (cont.)*

grange multipliers considered is an extension to the vector case of the space of the first N Fourier modes. We proved that similar properties to the Poisson case were satisfied: the problem is well-posed and converges when $\varepsilon \to 0$ towards the problem with standard Dirichlet boundary conditions. We also establish, similarly to the Poisson case, that the low-order stabilized finite element discretization provides sub-optimal order of convergence, due on one hand to the discontinuity of pressure and velocity gradient across the immersed interface and on the other hand to the singular behavior of the continuous solutions for $\varepsilon \to 0$. Therefore, we proposed an augmented finite element method with stable velocity-pressure conforming finite element pairs and additional singular functions designed to better capture the discontinuities and asymptotic singularities of the solution. We proved that we could restore the optimal order of convergence and significantly reduce the dependence in ε of the convergence constant in the numerical approximation error. In the second part, we adapted the finite element method to the fluid-structure interaction

problem of small particles immersed in a Stokes fluid. Through several numerical experiments, we illustrated the theoretical results obtained for the obstacle problem and gave numerical evidence of the accuracy of the reduced order fluid-structure coupled model.

4.A Appendix

4.A.1 Preliminary lemmas

In this section of the appendix, we state several results that will be used in the next sections of the appendix for the proof of some lemmas used in this chapter. We recall that $\varepsilon \in (0, \varepsilon_{\max})$ where $\varepsilon_{\max}$ is the fixed parameter defined by $\varepsilon_{\max} \overset{\text{def}}{=} \sup\{\varepsilon > 0 \mid \overline{\omega^\varepsilon} \subset \Omega\}$. The first three Lemmas and their proof are drawn from in [Caubet et al., 2016, Lemma C.1, Lemma C.2, Lemma C.3], themselves based on results presented in [Sid Idris, 2001, Chapter 3]

Lemma 4.A.1. *For $\boldsymbol{\varphi} \in \boldsymbol{H}^{\frac{1}{2}}(\partial\Omega) \cap \boldsymbol{L}^2_{0,\boldsymbol{n}}(\partial\Omega)$, the following problem*

$$\begin{cases} -\Delta \boldsymbol{v}^\varepsilon + \nabla q^\varepsilon = \boldsymbol{0} & \text{in} \quad \Omega^\varepsilon, \\ \operatorname{div} \boldsymbol{v}^\varepsilon = 0 & \text{in} \quad \Omega^\varepsilon, \\ \boldsymbol{v}^\varepsilon = \boldsymbol{\varphi} & \text{on} \quad \partial\Omega, \\ \boldsymbol{v}^\varepsilon = \boldsymbol{0} & \text{on} \quad \partial\omega^\varepsilon, \end{cases} \tag{4.A.1}$$

admits a unique weak solution in $\boldsymbol{H}^1(\Omega^\varepsilon) \times L^2_0(\Omega^\varepsilon)$. Moreover,

$$\|\boldsymbol{v}^\varepsilon\|_{1,\Omega^\varepsilon} \lesssim \|\boldsymbol{\varphi}\|_{\frac{1}{2},\partial\Omega}.$$

Proof of Lemma 4.A.1. We consider $\boldsymbol{v}^{\varepsilon_{\max}}$ the solution of (4.A.1) for $\varepsilon = \varepsilon_{\max}$. It satisfies

$$|\boldsymbol{v}^{\varepsilon_{\max}}|_{1,\Omega^{\varepsilon_{\max}}} = \left(\int_{\Omega^{\varepsilon_{\max}}} |\nabla \boldsymbol{v}^{\varepsilon_{\max}}|^2 \right)^{\frac{1}{2}} \lesssim \|\boldsymbol{\varphi}\|_{\frac{1}{2},\partial\Omega}. \tag{4.A.2}$$

Now consider $\tilde{\boldsymbol{v}}^{\varepsilon_{\max}} \in \boldsymbol{H}^1_0(\Omega)$ the extension by 0 of $\boldsymbol{v}^{\varepsilon_{\max}}$ to all Ω. Notice that since $\varepsilon < \varepsilon_{\max}$, $\omega^\varepsilon \subset \omega^{\varepsilon_{\max}}$ and $\Omega^{\varepsilon_{\max}} \subset \Omega^\varepsilon$, so, by minimization of energy, we have

$$|\boldsymbol{v}^\varepsilon|_{1,\Omega^\varepsilon} \leqslant |\tilde{\boldsymbol{v}}^{\varepsilon_{\max}}|_{1,\Omega^\varepsilon} = |\boldsymbol{v}^{\varepsilon_{\max}}|_{1,\Omega^{\varepsilon_{\max}}},$$

and thanks to equation (4.A.2),

$$|\boldsymbol{v}^\varepsilon|_{1,\Omega^\varepsilon} \lesssim \|\boldsymbol{\varphi}\|_{\frac{1}{2},\partial\Omega}. \tag{4.A.3}$$

Now consider $(\boldsymbol{v}^0, l^0) \in \boldsymbol{H}^1(\Omega) \times L^2_0(\Omega)$ the solution of the system

$$\begin{cases} -\Delta \boldsymbol{v}^0 + \nabla l^0 = \boldsymbol{0} & \text{in} \quad \Omega, \\ \text{div } \boldsymbol{v}^0 = 0 & \text{in} \quad \Omega, \\ \boldsymbol{v}^0 = \boldsymbol{\varphi} & \text{on} \quad \partial\Omega. \end{cases}$$

The well-posedness of this problem gives

$$\|\boldsymbol{v}^0\|_{1,\Omega} \lesssim \|\boldsymbol{\varphi}\|_{\frac{1}{2},\partial\Omega}. \tag{4.A.4}$$

Denoting by $\tilde{\boldsymbol{v}}^\varepsilon$ the extension by zero of $\boldsymbol{v}^\varepsilon$ to all Ω, since $\tilde{\boldsymbol{v}}^\varepsilon - \boldsymbol{v}^0 \in H^1_0(\Omega)$, we can apply the Poincaré inequality to get

$$\|\boldsymbol{v}^\varepsilon\|_{\Omega^\varepsilon} = \|\tilde{\boldsymbol{v}}^\varepsilon\|_\Omega \leqslant \|\tilde{\boldsymbol{v}}^\varepsilon - \boldsymbol{v}^0\|_\Omega + \|\boldsymbol{v}^0\|_\Omega \lesssim (|\boldsymbol{v}^\varepsilon|_{1,\Omega^\varepsilon} + |\boldsymbol{v}^0|_{1,\Omega}) + \|\boldsymbol{v}^0\|_\Omega.$$

Combining this inequality with (4.A.3) and (4.A.4), we deduce that

$$\|\boldsymbol{v}^\varepsilon\|_{\Omega^\varepsilon} \lesssim \|\boldsymbol{\varphi}\|_{\frac{1}{2},\partial\Omega}$$

which concludes the proof of the lemma. □

From the previous Lemma, we get the following one:

Lemma 4.A.2. *Let $\boldsymbol{\varphi} \in \boldsymbol{H}^1(\Omega)$ be such that* div $\boldsymbol{\varphi} = 0$ *in* Ω. *We denote by $(\boldsymbol{v}^\varepsilon, q^\varepsilon) \in \boldsymbol{H}^1(\omega^\varepsilon) \times L^2_0(\Omega^\varepsilon)$ the solution of the Stokes problem*

$$\begin{cases} -\Delta \boldsymbol{v}_\varepsilon + \nabla q^\varepsilon = \boldsymbol{0} & \textit{in} \quad \Omega^\varepsilon, \\ \text{div } \boldsymbol{v}^\varepsilon = 0 & \textit{in} \quad \Omega^\varepsilon, \\ \boldsymbol{v}^\varepsilon = \boldsymbol{0} & \textit{on} \quad \partial\Omega, \\ \boldsymbol{v}^\varepsilon = \boldsymbol{\varphi} & \textit{on} \quad \partial\omega^\varepsilon. \end{cases}$$

If there exists $q \in L^2_0(\Omega)$ such that $-\Delta\boldsymbol{\varphi} + \nabla q = 0$ in Ω, then

$$\|\boldsymbol{v}^\varepsilon\|_{1,\Omega^\varepsilon} \lesssim \|\boldsymbol{\varphi}\|_{\frac{1}{2},\Omega}.$$

Proof of Lemma 4.A.2. We consider the pair $(\boldsymbol{w}^\varepsilon \overset{\text{def}}{=} \boldsymbol{v}^\varepsilon - \boldsymbol{\varphi},\ l^\varepsilon \overset{\text{def}}{=} q^\varepsilon - q)$. It satisfies

$$\begin{cases} -\Delta \boldsymbol{w}^\varepsilon + \nabla l^\varepsilon = \boldsymbol{0} & \text{in} \quad \Omega^\varepsilon, \\ \text{div } \boldsymbol{w}^\varepsilon = 0 & \text{in} \quad \Omega^\varepsilon, \\ \boldsymbol{w}^\varepsilon = -\boldsymbol{\varphi} & \text{on} \quad \partial\Omega, \\ \boldsymbol{w}^\varepsilon = \boldsymbol{0} & \text{on} \quad \partial\omega^\varepsilon, \end{cases}$$

By the previous lemma

$$\|\boldsymbol{w}^\varepsilon\|_{1,\Omega^\varepsilon} \lesssim \|\boldsymbol{\varphi}\|_{\frac{1}{2},\partial\Omega}.$$

Noticing that $\boldsymbol{\varphi}$ is defined in the whole domain and is solution of the Stokes equations, we have:

$$\|\boldsymbol{\varphi}\|_{1,\Omega^\varepsilon} \leqslant \|\boldsymbol{\varphi}\|_{1,\Omega} \lesssim \|\boldsymbol{\varphi}\|_{\frac{1}{2},\partial\Omega}.$$

Therefore, we finally get

$$\|\boldsymbol{v}^\varepsilon\|_{1,\omega^\varepsilon} \leqslant \|\boldsymbol{w}^\varepsilon\|_{1,\Omega^\varepsilon} + \|\boldsymbol{\varphi}\|_{1,\Omega^\varepsilon} \lesssim \|\boldsymbol{\varphi}\|_{\frac{1}{2},\partial\Omega}.$$

□

Lemma 4.A.3. *For any $\boldsymbol{L} \in \mathbb{R}^2$, the problem*

$$\begin{cases} -\Delta \boldsymbol{v}^\varepsilon + \nabla q^\varepsilon = \boldsymbol{0} & \textit{in} \quad \Omega^\varepsilon, \\ \operatorname{div} \boldsymbol{v}^\varepsilon = 0 & \textit{in} \quad \Omega^\varepsilon, \\ \boldsymbol{v}^\varepsilon = \boldsymbol{0} & \textit{on} \quad \partial\Omega, \\ \boldsymbol{v}^\varepsilon = \boldsymbol{L} & \textit{on} \quad \partial\omega^\varepsilon, \end{cases}$$

admits a unique weak solution in $\boldsymbol{H}^1(\Omega^\varepsilon) \times L^2_0(\Omega^\varepsilon)$. Morevover,

$$\|\boldsymbol{v}^\varepsilon\|_{1,\Omega^\varepsilon} \lesssim |\log(\varepsilon)|^{-\frac{1}{2}} |\boldsymbol{L}|.$$

Proof of Lemma 4.A.3. Let us define by $(\boldsymbol{w}^\varepsilon(\varepsilon), l^\varepsilon(\varepsilon))$ the unique solution of the system

$$\begin{cases} -\Delta \boldsymbol{w}^\varepsilon(\varepsilon) + \nabla l^\varepsilon(\varepsilon) = \boldsymbol{0} & \text{in} \quad \omega^{\varepsilon_{\max}/\varepsilon} \backslash \overline{\omega}, \\ \operatorname{div} \boldsymbol{w}^\varepsilon(\varepsilon) = 0 & \text{in} \quad \omega^{\varepsilon_{\max}/\varepsilon} \backslash \overline{\omega}, \\ \boldsymbol{w}^\varepsilon(\varepsilon) = \boldsymbol{0} & \text{on} \quad \partial\omega^{\varepsilon_{\max}/\varepsilon}, \\ \boldsymbol{w}^\varepsilon(\varepsilon) = \boldsymbol{L} & \text{on} \quad \partial\omega. \end{cases}$$

We also consider the pair $(\boldsymbol{v}^\varepsilon(\varepsilon), q^\varepsilon(\varepsilon))$ which satisfies

$$\begin{cases} -\Delta \boldsymbol{v}^\varepsilon(\varepsilon) + \nabla q^\varepsilon(\varepsilon) = \boldsymbol{0} & \text{in} \quad \dfrac{\Omega}{\varepsilon} \backslash \overline{\omega}, \\ \operatorname{div} \boldsymbol{v}^\varepsilon(\varepsilon) = 0 & \text{in} \quad \dfrac{\Omega}{\varepsilon}, \\ \boldsymbol{v}^\varepsilon(\varepsilon) = \boldsymbol{0} & \text{on} \quad \dfrac{1}{\varepsilon}\partial\Omega, \\ \boldsymbol{v}^\varepsilon(\varepsilon) = \boldsymbol{L} & \text{on} \quad \partial\omega. \end{cases}$$

Notice that we have $\omega \subset \omega^{\varepsilon_{\max}/\varepsilon} \subset \frac{\Omega}{\varepsilon}$. Now we consider $\tilde{\boldsymbol{w}}^\varepsilon(\varepsilon)$ the extension of $\boldsymbol{w}^\varepsilon(\varepsilon)$ to $\frac{\Omega}{\varepsilon}\backslash\overline{\omega}$ by zero in the outer part of the extended domain and $\boldsymbol{L}$ in the inner part of the extended domain. Therefore, by the principle of minimization of energy, we have

$$|\boldsymbol{v}^\varepsilon|_{1,\Omega^\varepsilon} = |\boldsymbol{v}^\varepsilon(\varepsilon)|_{1,\frac{\Omega}{\varepsilon}\backslash\overline{\omega}} \leqslant |\tilde{\boldsymbol{w}}^\varepsilon(\varepsilon)|_{1,\frac{\Omega}{\varepsilon}\backslash\overline{\omega}} = |\boldsymbol{w}^\varepsilon(\varepsilon)|_{1,\omega^{\varepsilon_{\max}/\varepsilon}\backslash\overline{\omega}}. \tag{4.A.5}$$

Let $\boldsymbol{\psi}(\varepsilon) \overset{\text{def}}{=} \boldsymbol{L} + 4\pi\boldsymbol{E}\dfrac{\boldsymbol{L}}{\log(\varepsilon_{\max}/\varepsilon)}$ and $q(\varepsilon) \overset{\text{def}}{=} 4\pi\mu\boldsymbol{P}\cdot\dfrac{\boldsymbol{L}}{\log(\varepsilon_m/\varepsilon)}$ where $(\boldsymbol{E},\boldsymbol{P})$ is the fundamental solution of Stokes equations in $\mathbb{R}^2$ given by

$$\boldsymbol{E}(\boldsymbol{x}) \overset{\text{def}}{=} \frac{1}{4\pi\mu}(-\log(|\boldsymbol{x}|)\boldsymbol{I}_2 + \boldsymbol{e}_r\boldsymbol{e}_r^{\mathrm{T}}), \quad \boldsymbol{P}(\boldsymbol{x}) \overset{\text{def}}{=} \frac{\boldsymbol{x}}{2\pi|\boldsymbol{x}|^2}. \tag{4.A.6}$$

We have

$$\begin{cases} -\mu\Delta\boldsymbol{\psi}(\varepsilon) + \nabla q(\varepsilon) = \boldsymbol{0} & \text{in} \quad \omega^{\varepsilon_{\max}/\varepsilon}\backslash\overline{\omega}, \\ \operatorname{div}\boldsymbol{\psi}(\varepsilon) = 0 & \text{in} \quad \omega^{\varepsilon_{\max}/\varepsilon}\backslash\overline{\omega}, \\ \boldsymbol{\psi}(\varepsilon) = \dfrac{\boldsymbol{e}_r\boldsymbol{e}_r^{\mathrm{T}}\boldsymbol{L}}{\log(\varepsilon_{\max}/\varepsilon)} & \text{on} \quad \partial\omega^{\varepsilon_{\max}/\varepsilon}, \\ \boldsymbol{\psi}(\varepsilon) = \boldsymbol{L} + \dfrac{\boldsymbol{e}_r\boldsymbol{e}_r^{\mathrm{T}}\boldsymbol{L}}{\log(\varepsilon_{\max}/\varepsilon)} & \text{on} \quad \partial\omega, \end{cases}$$

and a computation provides:

$$|\boldsymbol{\psi}(\varepsilon)|_{1,\omega^{\varepsilon_{\max}/\varepsilon}\backslash\overline{\omega}} \lesssim |\boldsymbol{L}||\log(\varepsilon)|^{-\frac{1}{2}}.$$

Now, notice that the pair $(\boldsymbol{w}^\varepsilon(\varepsilon) - \boldsymbol{\psi}(\varepsilon),\, l^\varepsilon(\varepsilon) - q^\varepsilon(\varepsilon))$ is solution of the Stokes equations with boundary conditions $-\dfrac{\boldsymbol{e}_r\boldsymbol{e}_r^{\mathrm{T}}\boldsymbol{L}}{\log(\varepsilon_{\max}/\varepsilon)}$ in both borders of the domain. Therefore, using the previous lemmas, we get that:

$$|\boldsymbol{w}^\varepsilon(\varepsilon) - \boldsymbol{\psi}(\varepsilon)|_{1,\omega^{\varepsilon_{\max}/\varepsilon}\backslash\overline{\omega}} \lesssim |\log(\varepsilon)|^{-\frac{1}{2}}\|\boldsymbol{e}_r\boldsymbol{e}_r^{\mathrm{T}}\boldsymbol{L}\|_{\frac{1}{2},\partial\omega^{\varepsilon_{\max}}} \lesssim |\log(\varepsilon)|^{-\frac{1}{2}}|\boldsymbol{L}|.$$

So, we get:

$$\begin{aligned} |\boldsymbol{v}^\varepsilon|_{1,\Omega^\varepsilon} \leqslant |\boldsymbol{w}^\varepsilon(\varepsilon)|_{1,\omega^{\varepsilon_{\max}}\backslash\overline{\omega^\varepsilon}} &\leqslant |\boldsymbol{w}^\varepsilon(\varepsilon) - \boldsymbol{\psi}(\varepsilon)|_{1,\omega^{\varepsilon_{\max}/\varepsilon}\backslash\overline{\omega}} + |\boldsymbol{\psi}(\varepsilon)|_{1,\omega^{\varepsilon_{\max}/\varepsilon}\backslash\overline{\omega}}, \\ &\lesssim |\log(\varepsilon)|^{-\frac{1}{2}}|\boldsymbol{L}|. \end{aligned}$$

Finally, we consider $\tilde{\boldsymbol{v}}^\varepsilon$ the extension of $\boldsymbol{v}^\varepsilon$ to Ω by $\boldsymbol{L}$. Since this extension is in $\boldsymbol{H}_0^1(\Omega)$, we can use the Poincaré inequality to obtain

$$\|\boldsymbol{v}^\varepsilon\|_{\Omega^\varepsilon} \leqslant \|\tilde{\boldsymbol{v}}^\varepsilon\|_\Omega \lesssim |\tilde{\boldsymbol{v}}^\varepsilon|_{1,\Omega} \lesssim |\boldsymbol{v}^\varepsilon|_{1,\Omega^\varepsilon}.$$

Using equation (3.A.7), we get the result. □

Once again, the following Lemma and its proof are drawn from [Caubet et al., 2016, Lemma B.2, Lemma 4.2], themselves based on results presented in [Sid Idris, 2001, Chapter 3].

Lemma 4.A.4. *For any $\boldsymbol{u}_{\mathrm{b}} \in \boldsymbol{H}^{\frac{1}{2}}(\partial\omega^\varepsilon) \cap \boldsymbol{L}^2_{0,\boldsymbol{n}}$, the problem*

$$\begin{cases} -\Delta \boldsymbol{v}^\varepsilon + \nabla q^\varepsilon = 0 & \textit{in} \quad \Omega^\varepsilon, \\ \operatorname{div} \boldsymbol{v}^\varepsilon = 0 & \textit{in} \quad \Omega^\varepsilon, \\ \boldsymbol{v}^\varepsilon = \boldsymbol{0} & \textit{on} \quad \partial\Omega, \\ \boldsymbol{v}^\varepsilon = \boldsymbol{u}_{\mathrm{b}} & \textit{on} \quad \partial\omega^\varepsilon, \end{cases}$$

admits a unique weak solution in $\boldsymbol{H}^1(\Omega^\varepsilon)$. Moreover,

$$\|\boldsymbol{v}^\varepsilon\|_{1,\Omega^\varepsilon} \lesssim \|\boldsymbol{u}_{\mathrm{b}}(\varepsilon)\|_{\frac{1}{2},\omega} = \|\boldsymbol{u}_{\mathrm{b}}\|_{\frac{1}{2},\varepsilon}.$$

Proof. Let us first consider the following system:

$$\begin{cases} -\Delta \boldsymbol{u} + \nabla p = \boldsymbol{0} & \text{in} \quad \mathbb{R}^2\backslash\overline{\omega}, \\ \operatorname{div} \boldsymbol{u} = 0 & \text{in} \quad \mathbb{R}^2\backslash\overline{\omega}, \\ \boldsymbol{u} = \boldsymbol{u}_{\mathrm{b}}(\varepsilon) & \text{on} \quad \partial\omega. \end{cases} \tag{4.A.7}$$

According to Lax-Milgram theorem, this problem is well posed and has a unique solution in

$$\boldsymbol{W}^{1,2}_0(\mathbb{R}^2\backslash\overline{\omega}) = \{\boldsymbol{u} \in \mathcal{D}'(\mathbb{R}^2\backslash\overline{\omega}) \mid \log(\rho)^{-1}\boldsymbol{u} \in L^2_{-1}(\mathbb{R}^2\backslash\overline{\omega}),\ \nabla\boldsymbol{u} \in L^2(\mathbb{R}^2\backslash\overline{\omega}),\ \operatorname{div}\boldsymbol{u} = \boldsymbol{0}\}$$

where

$$\rho(\boldsymbol{x}) = (1 + |\boldsymbol{x}|^2)^{\frac{1}{2}}$$

and

$$\boldsymbol{L}^2_{-1}(\mathbb{R}^2\backslash\overline{\omega}) = \{\boldsymbol{u} \in \mathcal{D}'(\mathbb{R}^2\backslash\overline{\omega}) \mid \rho^{-1}\boldsymbol{u} \in L^2(\mathbb{R}^2\backslash\overline{\omega})\},$$

(see [Giroire, 1987] for example). By setting $-\Delta\boldsymbol{u} + \nabla p = 0$ in ω, the problem (4.A.7) has a unique solution in $\mathbb{R}^2$ and we have that

$$-\Delta\boldsymbol{u} + \nabla p = [\boldsymbol{\sigma}(\boldsymbol{u}, p)\boldsymbol{n}^+]\delta_{\partial\omega} \overset{\text{def}}{=} \boldsymbol{T} \quad \text{in} \quad \boldsymbol{\mathcal{D}}'(\mathbb{R}^2),$$

where $\boldsymbol{n}^+$ is the exterior normal of $\partial\Omega^\varepsilon$. Now let us define

$$\boldsymbol{v} \overset{\text{def}}{=} \boldsymbol{E} * \boldsymbol{T}, \quad q \overset{\text{def}}{=} \boldsymbol{P} * \boldsymbol{T}$$

where $(\boldsymbol{E}, \boldsymbol{P})$ is the fundamental solution of the Stokes equation given by (4.A.6) and $\star$ is the convolution product. Then,

$$-\Delta\boldsymbol{v} + \nabla q = \boldsymbol{T} \quad \text{in} \quad \boldsymbol{\mathcal{D}}'(\mathbb{R}^2).$$

Therefore $(\boldsymbol{u}-\boldsymbol{v}, p-q)$ solves Stokes equations in $\mathbb{R}^2$ and this solution is given by polynomials (see [Dautray and Lions, 1985] for example). Thus, we can write that

$$\boldsymbol{u}(\boldsymbol{y}) = \boldsymbol{E} * \boldsymbol{T}(\boldsymbol{y}) + \boldsymbol{u}_1(\boldsymbol{y}) = \int_{\partial\omega} \boldsymbol{E}(\boldsymbol{y}-\boldsymbol{x})\boldsymbol{t}(\boldsymbol{x})\mathrm{d}s(\boldsymbol{x}) + \boldsymbol{u}_1(\boldsymbol{y}),$$
$$p(\boldsymbol{y}) = \boldsymbol{P} * \boldsymbol{T}(\boldsymbol{y}) + P_1(\boldsymbol{y}) = \int_{\partial\omega} \boldsymbol{P}(\boldsymbol{y}-\boldsymbol{x})\cdot\boldsymbol{t}(\boldsymbol{x})\mathrm{d}s(\boldsymbol{x}) + P_1(\boldsymbol{y}),$$

where $\boldsymbol{u}_1$ and P_1 are polynomials and $\boldsymbol{t} = \boldsymbol{\sigma}(\boldsymbol{u}, p)\boldsymbol{n}^+$. Using a first order Taylor expansion of $\boldsymbol{E}$:

$$\boldsymbol{E}(\boldsymbol{y}-\boldsymbol{x}) = \boldsymbol{E}(\boldsymbol{y})\int_{\partial\omega}\boldsymbol{t}(\boldsymbol{x})\mathrm{d}s(\boldsymbol{x}) + \boldsymbol{V}(\boldsymbol{y}).$$

with $\boldsymbol{V}(\boldsymbol{y}) = o(1/|\boldsymbol{y}|)$ when $|\boldsymbol{y}| \to \infty$ and uniformly independent of $\boldsymbol{x}$. In particular$(\log(\rho))^{-1}\boldsymbol{V} \in \boldsymbol{L}^2_{-1}(\mathbb{R}^2\backslash\bar{\omega})$. As $(\log(\rho))^{-1}\boldsymbol{u} \in \boldsymbol{L}^2_{-1}(\mathbb{R}^2\backslash\bar{\omega})$ and $(\log(\rho))^{-1} \notin \boldsymbol{L}^2_{-1}(\mathbb{R}^2\backslash\bar{\omega})$, we necessarily have that

$$\int_{\partial\omega}\boldsymbol{t}(\boldsymbol{x})\mathrm{d}s(\boldsymbol{x}) = \boldsymbol{0}.$$

We deduce that $\boldsymbol{u}_1 \in \boldsymbol{L}^2_{-1}(\mathbb{R}^2\backslash\bar{\omega})$, so that we must have $\boldsymbol{u}_1 = \boldsymbol{L}$, where $\boldsymbol{L}$ is constant. Consequently, $\boldsymbol{u} = \boldsymbol{W} + \boldsymbol{L}$. By computation, we have that there exists A uniformly independent of $\boldsymbol{u}_\mathrm{b}$, such that for all $\boldsymbol{y}$ satisfying $|\boldsymbol{y}| > A$,

$$|\boldsymbol{W}(\boldsymbol{y})| \lesssim \|\boldsymbol{u}_\mathrm{b}(\varepsilon)\|_{\frac{1}{2},\partial\omega}\frac{1}{|\boldsymbol{y}|}, \quad |\boldsymbol{\nabla}\boldsymbol{W}(\boldsymbol{y})| \lesssim \|\boldsymbol{u}_\mathrm{b}(\varepsilon)\|_{\frac{1}{2},\partial\omega}\frac{1}{|\boldsymbol{y}|^2}.$$

By this way, we have for all $\|\boldsymbol{y}\| > A$,

$$|\boldsymbol{L}| \lesssim |\boldsymbol{u}(\boldsymbol{y})| + \|\boldsymbol{u}_\mathrm{b}(\varepsilon)\|_{\frac{1}{2},\partial\omega}\frac{1}{|\boldsymbol{y}|}.$$

We get that, for all $|\boldsymbol{y}| > A$

$$|\boldsymbol{L}|\left(\int_{|\boldsymbol{y}|>A}\frac{1}{\log(|\boldsymbol{y}|)^2|\boldsymbol{y}|^2}\right)^{\frac{1}{2}} \lesssim \left(\int_{|\boldsymbol{y}|>A}\frac{|\boldsymbol{u}(\boldsymbol{y})|^2}{\log(|\boldsymbol{y}|)^2|\boldsymbol{y}|^2}\right)^{\frac{1}{2}} + \|\boldsymbol{u}_\mathrm{b}(\varepsilon)\|_{\frac{1}{2},\partial\omega}\left(\int_{|\boldsymbol{y}|>A}\frac{1}{\log(|\boldsymbol{y}|)^2|\boldsymbol{y}|^4}\right)^{\frac{1}{2}}.$$

The fact that A is uniformly independent of $\boldsymbol{u}_\mathrm{b}$ and the well-posedness of the problem (4.A.7) give

$$|\boldsymbol{L}| \lesssim \|\boldsymbol{u}_\mathrm{b}(\varepsilon)\|_{\frac{1}{2},\partial\omega}.$$

Using similar computations as in [Caubet et al., 2016, Lemma B.3], we also have

$$\|\boldsymbol{W}(\frac{\boldsymbol{x}}{\varepsilon})\|_{1,\Omega^\varepsilon} \lesssim \varepsilon \|\boldsymbol{u}_{\mathrm{b}}(\varepsilon)\|_{\frac{1}{2},\partial\omega}.$$

We then define $\boldsymbol{z}^\varepsilon \overset{\text{def}}{=} \boldsymbol{v}^\varepsilon - \boldsymbol{W}(\frac{\boldsymbol{x}}{\varepsilon})$ and $p_{\boldsymbol{z}^\varepsilon} \overset{\text{def}}{=} q^\varepsilon - \varepsilon^{-1} P_{\boldsymbol{W}}(\frac{\boldsymbol{x}}{\varepsilon})$. Notice that the couple $(\boldsymbol{z}^\varepsilon, p_{\boldsymbol{z}^\varepsilon})$ satisfies

$$\begin{cases} -\Delta \boldsymbol{z}^\varepsilon + \nabla p_{\boldsymbol{z}^\varepsilon} = \boldsymbol{0} & \text{in} \quad \Omega^\varepsilon, \\ \qquad \operatorname{div} \boldsymbol{z}^\varepsilon = 0 & \text{in} \quad \Omega^\varepsilon, \\ \boldsymbol{z}^\varepsilon = -\boldsymbol{W}(\frac{\boldsymbol{x}}{\varepsilon}) & \text{on} \quad \partial\Omega, \\ \qquad \boldsymbol{z}^\varepsilon = \boldsymbol{L} & \text{on} \quad \partial\omega^\varepsilon. \end{cases}$$

Using Lemma 4.A.1 and Lemma 4.A.3, we get that

$$\begin{aligned} \|\boldsymbol{z}^\varepsilon\|_{1,\Omega^\varepsilon} &\lesssim \|\boldsymbol{W}(\frac{\boldsymbol{x}}{\varepsilon})\|_{\frac{1}{2},\partial\Omega} + |\log(\varepsilon)|^{-\frac{1}{2}} |\boldsymbol{L}|, \\ &\lesssim \varepsilon \|\boldsymbol{u}_{\mathrm{b}}(\varepsilon)\|_{\frac{1}{2},\partial\omega} + |\log(\varepsilon)|^{-\frac{1}{2}} \|\boldsymbol{u}_{\mathrm{b}}(\varepsilon)\|_{\frac{1}{2},\partial\omega}. \end{aligned}$$

So finally, we get

$$\begin{aligned} \|\boldsymbol{v}^\varepsilon\|_{1,\Omega^\varepsilon} &\lesssim \|\boldsymbol{z}^\varepsilon\|_{1,\Omega^\varepsilon} + \|\boldsymbol{W}(\frac{\boldsymbol{x}}{\varepsilon})\|_{1,\Omega^\varepsilon}, \\ &\lesssim \varepsilon \|\boldsymbol{u}_{\mathrm{b}}(\varepsilon)\|_{\frac{1}{2},\partial\omega} + |\log(\varepsilon)|^{-\frac{1}{2}} \|\boldsymbol{u}_{\mathrm{b}}(\varepsilon)\|_{\frac{1}{2},\partial\omega} + \|\boldsymbol{u}_{\mathrm{b}}(\varepsilon)\|_{\frac{1}{2},\partial\omega} \lesssim \|\boldsymbol{u}_{\mathrm{b}}(\varepsilon)\|_{\frac{1}{2},\partial\omega}. \end{aligned}$$

□

4.A.2 Proof of Lemma 4.2.2

Restated Lemma 4.2.2. *Let $\boldsymbol{\eta} \in \boldsymbol{H}^{\frac{1}{2}}(\partial\omega^\varepsilon) \cap \boldsymbol{L}^2_{0,\boldsymbol{n}}(\partial\omega^\varepsilon)$ be given, there exists $(\boldsymbol{v}^\varepsilon_{\boldsymbol{\eta}}, l^\varepsilon_{\boldsymbol{\eta}}) \in \boldsymbol{V} \times Q$ such that*

$$\begin{cases} -\Delta \boldsymbol{v}^\varepsilon_{\boldsymbol{\eta}} + \nabla l^\varepsilon_{\boldsymbol{\eta}} = 0 & \textit{in} \quad \Omega^\varepsilon \cup \omega^\varepsilon, \\ \qquad \operatorname{div} \boldsymbol{v}^\varepsilon_{\boldsymbol{\eta}} = 0 & \textit{in} \quad \Omega, \\ \boldsymbol{v}^\varepsilon_{\boldsymbol{\eta}} = \boldsymbol{\eta} & \textit{on} \quad \partial\omega^\varepsilon, \end{cases} \tag{4.A.8}$$

and

$$\|\boldsymbol{v}^\varepsilon_{\boldsymbol{\eta}}\|_{1,\Omega} \lesssim \|\boldsymbol{\eta}\|_{\frac{1}{2},\varepsilon}. \tag{4.A.9}$$

Proof of Lemma 4.2.2. Classical results on Stokes equations ensure the existence of $(\boldsymbol{v}^\varepsilon_{\boldsymbol{\eta}}, l^\varepsilon_{\boldsymbol{\eta}})$ in $\boldsymbol{V} \times Q$ satisfying (4.A.8). Now, we would like to prove the a priori estimate (4.A.9). On one hand, according to Lemma 4.A.4,

$$\|\boldsymbol{v}^\varepsilon_{\boldsymbol{\eta}}\|_{1,\Omega^\varepsilon} \lesssim \|\boldsymbol{\eta}\|_{\frac{1}{2},\varepsilon}. \tag{4.A.10}$$

On the other hand, by setting $(v^\varepsilon_{\boldsymbol{\eta}}(\varepsilon), l^\varepsilon_{\boldsymbol{\eta}}(\varepsilon))$ defined on ω such that $(v^\varepsilon_{\boldsymbol{\eta}}(\varepsilon)(\boldsymbol{x}), l^\varepsilon_{\boldsymbol{\eta}}(\varepsilon)(\boldsymbol{x})) = (v^\varepsilon_{\boldsymbol{\eta}}(\varepsilon\boldsymbol{x}), l^\varepsilon_{\boldsymbol{\eta}}(\varepsilon\boldsymbol{x}))$ for all $\boldsymbol{x} \in \omega$, the pair $(\boldsymbol{v}^\varepsilon_{\boldsymbol{\eta}}(\varepsilon), l^\varepsilon_{\boldsymbol{\eta}}(\varepsilon))$ satisfies

$$\begin{cases} -\Delta \boldsymbol{v}^\varepsilon_{\boldsymbol{\eta}}(\varepsilon) + \nabla l_{\boldsymbol{\eta}}(\varepsilon) = 0 \quad \text{in} \quad \omega, \\ \qquad\qquad \text{div } \boldsymbol{v}^\varepsilon_{\boldsymbol{\eta}}(\varepsilon) = 0 \quad \text{in} \quad \omega, \\ \qquad\qquad \boldsymbol{v}^\varepsilon_{\boldsymbol{\eta}}(\varepsilon) = \boldsymbol{\eta}(\varepsilon) \quad \text{on} \quad \partial\omega. \end{cases}$$

We deduce that

$$\|\boldsymbol{v}^\varepsilon_{\boldsymbol{\eta}}(\varepsilon)\|_{1,\omega} \lesssim \|\boldsymbol{\eta}(\varepsilon)\|_{\frac{1}{2},\partial\omega}.$$

By re-scaling we have

$$\varepsilon^{-2}\|\boldsymbol{v}^\varepsilon_{\boldsymbol{\eta}}\|^2_{\omega^\varepsilon} + \|\nabla \boldsymbol{v}^\varepsilon_{\boldsymbol{\eta}}\|^2_{\omega^\varepsilon} \lesssim \|\boldsymbol{\eta}(\varepsilon)\|^2_{\frac{1}{2},\partial\omega}.$$

and

$$\|\boldsymbol{v}^\varepsilon_{\boldsymbol{\eta}}\|_{1,\omega^\varepsilon} \lesssim \|\boldsymbol{\eta}\|_{\frac{1}{2},\varepsilon}. \tag{4.A.11}$$

Gathering (4.A.10) and (4.A.11), we obtain inequality (4.A.9). □

4.A.3 Proof of Lemma 4.2.3

Restated Lemma 4.2.3. *Let $q \in Q$ be given, there exists $\boldsymbol{w}^\varepsilon_q \in \boldsymbol{H}^1_0(\Omega)$ such that*

$$\begin{cases} \text{div } \boldsymbol{w}^\varepsilon_q = q \quad \textit{in} \quad \Omega, \\ \qquad \boldsymbol{w}^\varepsilon_q = 0 \quad \textit{on} \quad \partial\omega^\varepsilon, \end{cases}$$

and

$$\|\boldsymbol{w}^\varepsilon_q\|_{1,\Omega} \lesssim |\log(\varepsilon)|^{\frac{1}{2}}\|q\|_\Omega.$$

Proof of Lemma 4.2.3. Consider $q \in Q$ be given. We first define $(\boldsymbol{v}^\varepsilon_q, l^\varepsilon_q) \in \boldsymbol{H}^1_0(\Omega) \times L^2_0(\Omega)$ the unique solution of the system

$$\begin{cases} -\Delta \boldsymbol{v}^\varepsilon_q + \nabla l^\varepsilon_q = 0 \quad \text{in} \quad \Omega, \\ \qquad\quad \text{div } \boldsymbol{v}^\varepsilon_q = q \quad \text{in} \quad \Omega. \end{cases}$$

It satisfies

$$\|\boldsymbol{v}^\varepsilon_q\|_{1,\Omega} \lesssim \|q\|_\Omega. \tag{4.A.12}$$

Next, we consider $(\tilde{\boldsymbol{v}}^\varepsilon_q, \tilde{l}^\varepsilon_q) \in \boldsymbol{H}^1(\Omega) \times L^2_0(\Omega)$ solution of

$$\begin{cases} -\Delta \tilde{\boldsymbol{v}}_q + \nabla \tilde{l}^\varepsilon_q = 0 \quad \text{in} \quad \Omega, \\ \qquad\quad \text{div } \tilde{\boldsymbol{v}}^\varepsilon_q = 0 \quad \text{in} \quad \Omega, \\ \qquad\quad \tilde{\boldsymbol{v}}^\varepsilon_q = -\boldsymbol{v}^\varepsilon_q \quad \text{on} \quad \partial\Omega, \\ \qquad\quad \tilde{\boldsymbol{v}}^\varepsilon_q = -\boldsymbol{v}^\varepsilon_q \quad \text{on} \quad \partial\omega^\varepsilon. \end{cases}$$

Since $q \in Q$, $\int_{\partial\omega^\varepsilon} \boldsymbol{v}_q^\varepsilon \cdot \boldsymbol{n}^- = \int_{\partial\Omega} \boldsymbol{v}_q^\varepsilon \cdot \boldsymbol{n}^+ = 0$, so according to Lemma 4.A.1 and Lemma 4.A.4, by linearity, we have

$$\|\tilde{\boldsymbol{v}}_q^\varepsilon\|_{1,\Omega} \lesssim \|\boldsymbol{v}_q^\varepsilon\|_{\frac{1}{2},\partial\Omega} + \|\boldsymbol{v}_q^\varepsilon\|_{\frac{1}{2},\varepsilon}.$$

Consequently, using succesively (4.A.12), the standard trace inequality from $\boldsymbol{H}^{\frac{1}{2}}(\partial\Omega)$ to $\boldsymbol{H}^1(\Omega)$, and Lemma 3.3.2 for the estimate of the trace theorem on the boundary $\partial\omega^\varepsilon$, we obtain

$$\|\tilde{\boldsymbol{v}}_q^\varepsilon\|_{1,\Omega} \lesssim |\log(\varepsilon)|^{\frac{1}{2}} \|q\|_\Omega.$$

Eventually, if we set $\boldsymbol{w}_q^\varepsilon \overset{\text{def}}{=} \boldsymbol{v}_q^\varepsilon + \tilde{\boldsymbol{v}}_q^\varepsilon \in \boldsymbol{H}_0^1(\Omega)$, we see that it satisfies the desired properties. □

4.A.4 Proof of Theorem 4.2.4

Restated Theorem 4.2.4. *Let Q_1 and Q_2 be two reflexive Banach spaces, $a : X \times X \to \mathbb{R}$, $b_1 : Q_1 \times X \to \mathbb{R}$, $b_2 : Q_2 \times X \to \mathbb{R}$ three continuous bilinear forms, $c_1 : Q_1 \to \mathbb{R}$, $c_2 : Q_2 \to \mathbb{R}$, $d : X \to \mathbb{R}$ three continuous linear forms, we consider the twofold saddle point problem: find $(u, \lambda_1, \lambda_2) \in X \times Q_1 \times Q_2$ such that*

$$\begin{cases} a(u,v) - b_1(\lambda_1, v) - b_2(\lambda_2, v) = d(v), & \forall v \in X, \\ b_1(\mu_1, u) = c_1(\mu_1), & \forall \mu_1 \in Q_1, \\ b_2(\mu_2, u) = c_2(\mu_2), & \forall \mu_2 \in Q_2. \end{cases} \tag{4.A.13}$$

Let

$$Z_{b_i} \overset{\text{def}}{=} \{v \in X | b_i(\mu_i, v) = 0 \ \forall \mu_i \in Q_i\} \subset X \ i = 1, 2. \tag{4.A.14}$$

We suppose that there exists $\beta_1 > 0$, $\beta_2 > 0$ such that

$$\sup_{v \in Z_{b_2}} \frac{b_1(\lambda_1, v)}{\|v\|_X} \geqslant \beta_1 \|\lambda_1\|_{Q_1} \quad \forall \lambda_1 \in Q_1, \tag{4.A.15}$$

$$\sup_{v \in Z_{b_1}} \frac{b_2(\lambda_2, v)}{\|v\|_X} \geqslant \beta_2 \|\lambda_2\|_{Q_2} \quad \forall \lambda_2 \in Q_2. \tag{4.A.16}$$

and that there exists $\alpha > 0$

$$a(v,v) \geqslant \alpha \|v\|_X^2 \quad \forall v \in X. \tag{4.A.17}$$

Then the Problem (4.A.13) *is well posed and we have the following estimates on u, λ_1 and λ_2:*

$$\|u\|_X \leqslant \alpha^{-1}\|d\| + \beta_1^{-1}(1 + \alpha^{-1}\|a\|)\|c_1\| + \beta_2^{-1}(1 + \alpha^{-1}\|a\|)\|c_2\|, \tag{4.A.18}$$

and

$$\|\lambda_1\|_{Q_1} \leqslant \beta_1^{-1}(\|d\| + \|a\|\|u\|_X), \quad \|\lambda_2\|_{Q_2} \leqslant \beta_2^{-1}(\|d\| + \|a\|\|u\|_X).$$

Proof of Theorem 4.2.4. We begin by noticing that conditions (4.A.15) and (4.A.16) imply that there exists $w_1 \in Z_{b_2}$ and $w_2 \in Z_{b_1}$ such that

$$\begin{aligned} b_1(\mu_1, w_1) &= c_1(\mu_1) \quad \forall \mu_1 \in Q_1, \quad \|w_1\|_X \leqslant \beta_1^{-1}\|c_1\|, \\ b_2(\mu_2, w_2) &= c_2(\mu_2) \quad \forall \mu_2 \in Q_2, \quad \|w_2\|_X \leqslant \beta_2^{-1}\|c_2\|. \end{aligned}$$

Setting now

$$\kappa = u - w \tag{4.A.19}$$

with $w = w_1 + w_2$, we have for all $\mu_1 \in Q_1$, $\mu_2 \in Q_2$,

$$\begin{aligned} b_1(\mu_1, \kappa) &= b_1(\mu_1, w_1) + b_1(\mu_1, w_2) - b_1(\mu_1, u) = c_1(\mu_1) - c_1(\mu_1) = 0, \\ b_2(\mu_2, \kappa) &= b_2(\mu_2, w_1) + b_2(\mu_2, w_2) - b_2(\mu_2, u) = c_2(\mu_2) - c_2(\mu_2) = 0. \end{aligned}$$

We deduce then that $\kappa \in Z_{b_1} \cap Z_{b_2}$. Besides we have for all $v \in Z_{b_1} \cap Z_{b_2}$,

$$a(\kappa, v) = a(u, v) - a(w, v) = d(v) - a(w, v).$$

The continuity assumption on a and d, as well as the coercivity assumption (4.A.17) on a, imply

$$\alpha\|\kappa\|_X \leqslant \frac{a(\kappa, \kappa)}{\|\kappa\|_X} = \frac{d(\kappa) - a(w, \kappa)}{\|\kappa\|_X} \leqslant \|d\| + \|a\|\|w\|_X.$$

So, we get

$$\|\kappa\|_X \leqslant \alpha^{-1}(\|d\| + \|a\|\|w\|_X).$$

Applying triangular inequality to equation (4.A.19), we obtain

$$\|u\|_X \leqslant \|\kappa\|_X + \|w\|_X \leqslant \alpha^{-1}\|d\| + \beta_1^{-1}(\alpha^{-1}\|a\| + 1)\|c_1\| + \beta_2^{-1}(\alpha^{-1}\|a\| + 1)\|c_2\|.$$

which corresponds to (4.A.18). Taking $v \in Z_{b_1}$ in the first equation of system (4.A.13), we have

$$b_2(\lambda_2, v) = d(v) - a(u, v).$$

By continuity of a and d and the inf-sup condition (4.A.16) on b_2, we get

$$\beta_2\|\lambda_2\|_{Q_2} \leqslant \sup_{v \in Z_{b_1}, v \neq 0} \frac{b_2(\lambda_2, v)}{\|v\|_X} = \sup_{v \in Z_{b_1}, v \neq 0} \frac{d(v) - a(u, v)}{\|v\|_X} \leqslant \|d\| + \|a\|\|u\|_X.$$

We thus obtain

$$\|\lambda_2\|_{Q_2} \leqslant \beta_2^{-1}(\|d\| + \|a\|\|u\|_X).$$

Finally, we have in a similar way

$$\|\lambda_1\|_{Q_1} \leqslant \beta_1^{-1}(\|d\| + \|a\|\|u\|_X).$$

□

4.A.5 Proof of Lemma 4.2.6

Lemma 4.A.5. *Let $(\boldsymbol{u}_N^\varepsilon, p_N^\varepsilon, \boldsymbol{\lambda}_N^\varepsilon) \in \boldsymbol{V} \times Q \times \boldsymbol{F}_N$ be the solution of Problem* (4.2.14)*. We have in $\boldsymbol{H}^{-\frac{1}{2}}(\partial\omega^\varepsilon)$*

$$\boldsymbol{\lambda}_N^\varepsilon = \varepsilon\big(\boldsymbol{\sigma}(\boldsymbol{u}_N^\varepsilon, p_N^\varepsilon)^+\boldsymbol{n}^+ - \boldsymbol{\sigma}(\boldsymbol{u}_N^\varepsilon, p_N^\varepsilon)^-\boldsymbol{n}^+\big), \tag{4.A.20}$$

where $\boldsymbol{n}^+$ is the exterior normal vector to $\partial\Omega^\varepsilon$, and $\boldsymbol{\sigma}(\boldsymbol{u}_N^\varepsilon, p_N^\varepsilon)^+$ and $\boldsymbol{\sigma}(\boldsymbol{u}_N^\varepsilon, p_N^\varepsilon)^-$ are the restrictions of $\boldsymbol{\sigma}(\boldsymbol{u}_N^\varepsilon, p_N^\varepsilon)$ to Ω^ε and ω^ε, respectively.

Proof of Lemma 4.2.6. On one hand, we have, for $\boldsymbol{\phi} \in \boldsymbol{H}_0^1(\Omega)$,

$$\begin{aligned}
&2\int_\Omega \boldsymbol{\varepsilon}(\boldsymbol{u}_N^\varepsilon) : \boldsymbol{\varepsilon}(\boldsymbol{\phi}) - \int_\Omega p_N^\varepsilon \mathrm{div}\ \boldsymbol{\phi} \\
&= 2\int_{\Omega^\varepsilon} \boldsymbol{\varepsilon}(\boldsymbol{u}_N^\varepsilon) : \boldsymbol{\varepsilon}(\boldsymbol{\phi}) + 2\int_{\omega^\varepsilon} \boldsymbol{\varepsilon}(\boldsymbol{u}_N^\varepsilon) : \boldsymbol{\varepsilon}(\boldsymbol{\phi}) - \int_{\Omega^\varepsilon} p_N^\varepsilon \mathrm{div}\ \boldsymbol{\phi} - \int_{\omega^\varepsilon} p_N^\varepsilon \mathrm{div}\ \boldsymbol{\phi}, \\
&= -\int_{\Omega^\varepsilon} \boldsymbol{\Delta}\boldsymbol{u}_N^\varepsilon \cdot \boldsymbol{\phi} - \int_{\omega^\varepsilon} \boldsymbol{\Delta}\boldsymbol{u}_N^\varepsilon \cdot \boldsymbol{\phi} + \int_{\Omega^\varepsilon} \nabla p^\varepsilon \cdot \phi + \int_{\omega^\varepsilon} \nabla p^\varepsilon \cdot \phi \\
&+ \big\langle (\boldsymbol{\sigma}(\boldsymbol{u}_N^\varepsilon, p_N^\varepsilon)^+\boldsymbol{n}^+ - \boldsymbol{\sigma}(\boldsymbol{u}_N^\varepsilon, p_N^\varepsilon)^-\boldsymbol{n}^+, \boldsymbol{\phi}\big\rangle_{-\frac{1}{2},\partial\omega^\varepsilon},
\end{aligned}$$

and since $-\Delta\boldsymbol{u}_N^\varepsilon + \nabla p^\varepsilon = \boldsymbol{0}$ in Ω^ε and $-\Delta\boldsymbol{u}_N^\varepsilon + \nabla p^\varepsilon = \boldsymbol{0}$ in ω^ε,

$$2\int_\Omega \boldsymbol{\varepsilon}(\boldsymbol{u}_N^\varepsilon) : \boldsymbol{\varepsilon}(\boldsymbol{\phi}) - \int_\Omega p_N^\varepsilon \mathrm{div}\ \boldsymbol{\phi} = \big\langle \boldsymbol{\sigma}(\boldsymbol{u}_N^\varepsilon, p_N^\varepsilon)^+\boldsymbol{n}^+ - \boldsymbol{\sigma}(\boldsymbol{u}_N^\varepsilon, p_N^\varepsilon)^-\boldsymbol{n}^+, \boldsymbol{\phi}\big\rangle_{-\frac{1}{2},\partial\omega^\varepsilon}$$

On the other hand, we have

$$2\int_\Omega \boldsymbol{\varepsilon}(\boldsymbol{u}_N^\varepsilon) : \boldsymbol{\varepsilon}(\boldsymbol{\phi}) - \int_\Omega p_N^\varepsilon \mathrm{div}\ \boldsymbol{\phi} = (\boldsymbol{\lambda}_N^\varepsilon, \boldsymbol{\phi})_\varepsilon \quad \forall \boldsymbol{\phi} \in \boldsymbol{H}_0^1(\Omega).$$

Identifying these two relations, we obtain

$$\begin{aligned}
(\boldsymbol{\lambda}_N^\varepsilon, \boldsymbol{\phi})_\varepsilon &= \varepsilon^{-1}(\boldsymbol{\lambda}_N^\varepsilon, \boldsymbol{\phi})_{\partial\omega^\varepsilon} \\
&= \big\langle \boldsymbol{\sigma}(\boldsymbol{u}_N^\varepsilon, p_N^\varepsilon)^+\boldsymbol{n}^+ - \boldsymbol{\sigma}(\boldsymbol{u}_N^\varepsilon, p_N^\varepsilon)^-\boldsymbol{n}^+, \boldsymbol{\phi}\big\rangle_{-\frac{1}{2},\partial\omega^\varepsilon}
\end{aligned}$$

for all $\boldsymbol{\phi} \in \boldsymbol{H}_0^1(\Omega)$. Thus, since the trace operator from $\boldsymbol{H}_0^1(\Omega)$ on $\boldsymbol{H}^{\frac{1}{2}}(\partial\omega^\varepsilon)$ is surjective, we get (4.A.20). □

4.A.6 Proof of Lemma 4.2.7

Restated Lemma 4.2.7. *Let $\boldsymbol{u}_N^\varepsilon \in \boldsymbol{V}$ be the solution of Problem* (4.2.14) *and let $\boldsymbol{u}_\mathrm{b}$ be given by* (4.2.5)*. There exists $a_{k,r}^\varepsilon$, $a_{k,\theta}^\varepsilon$, $b_{k,r}^\varepsilon$, $b_{k,\theta}^\varepsilon \in \mathbb{R}$ such that for $\varepsilon \in (0,\rho)$,*

$$\begin{aligned}(\boldsymbol{u}_N^\varepsilon(\varepsilon)(\theta) - \boldsymbol{u}_\mathrm{b}(\varepsilon)(\theta)) \cdot \boldsymbol{e}_r &= \left(\frac{\varepsilon}{\rho}\right)^{N+1} \sum_{k=N}^{\infty} \big(a_{k,r}^\varepsilon \cos(k\theta) + b_{k,r}^\varepsilon \sin(k\theta)\big),\\ (\boldsymbol{u}_N^\varepsilon(\varepsilon)(\theta) - \boldsymbol{u}_\mathrm{b}(\varepsilon)(\theta)) \cdot \boldsymbol{e}_\theta &= \left(\frac{\varepsilon}{\rho}\right)^{N+1} \sum_{k=N}^{\infty} \big(a_{k,\theta}^\varepsilon \cos(k\theta) + b_{k,\theta}^\varepsilon \sin(k\theta)\big),\end{aligned} \tag{4.A.21}$$

Moreover, there exists $0 < \tilde{\rho} < \rho$ such that for $\varepsilon \in (0,\tilde{\rho})$, the following estimate holds:

$$\left(\sum_{k=N}^{\infty} (1+k)\big(|a_{k,r}^\varepsilon|^2 + |a_{k,\theta}^\varepsilon|^2 + |b_{k,r}^\varepsilon|^2 + |b_{k,\theta}^\varepsilon|^2\big)\right)^{\frac{1}{2}} \lesssim (1+N)\,(|\boldsymbol{v}_\mathrm{b}| + \varepsilon|w_\mathrm{b}|).$$

Proof of Lemma 4.2.7. Since $\operatorname{div} \boldsymbol{u}_N^\varepsilon = 0$ in Ω, there exists a scalar function ψ_N^ε called stream function satisfying

$$\boldsymbol{u}_N^\varepsilon \cdot \boldsymbol{e}_r = \frac{1}{r}\partial_\theta \psi_N^\varepsilon, \quad \boldsymbol{u}_N^\varepsilon \cdot \boldsymbol{e}_\theta = -\partial_r \psi_N^\varepsilon. \tag{4.A.22}$$

Moreover, since $\boldsymbol{u}_N^\varepsilon$ satisfies the homogeneous Stokes equations in each subdomain $\omega^\rho\backslash\overline{\omega^\varepsilon}$ and ω^ε, ψ_N^ε satisfies the following biharmonic equation

$$-\Delta^2 \psi_N^\varepsilon = 0 \quad \text{in} \quad \omega^\rho\backslash\overline{\omega^\varepsilon}, \quad -\Delta^2 \psi_N^\varepsilon = 0 \quad \text{in} \quad \omega^\varepsilon.$$

Using separation of variables method and the polar coordinates $(r,\theta) \in \mathbb{R}^2 \times (0,2\pi)$ such that

$$\boldsymbol{v}(r,\theta) \overset{\text{def}}{=} \boldsymbol{v}(r(\cos(\theta)\boldsymbol{e}_x + \sin(\theta)\boldsymbol{e}_y)),$$

we can derive a general form for ψ_N^ε given by

$$\psi_N^\varepsilon(r,\theta) = \Phi_0(r) + \sum_{k=1}^{\infty} \Phi_k^c(r)\cos(k\theta) + \Phi_k^s(r)\sin(k\theta) \tag{4.A.23}$$

for all $(r,\theta) \in [0,\varepsilon^{\max}] \times (0,2\pi)$, where the radial functions Φ_k^c and Φ_k^s depend on the subdomains ω^ε and $\omega^\rho\backslash\overline{\omega^\varepsilon}$ and satisfy

$$\begin{cases} \Phi_0 \in \operatorname{span}\{r^2,\, \log(r),\, 1,\, r^2\log(r)\}, \quad \Phi_1^\mathrm{c}, \Phi_1^\mathrm{s} \in \operatorname{span}\{r^3,\, r,\, r\log(r),\, r^{-1}\},\\ \Phi_k^\mathrm{c}, \Phi_k^\mathrm{s} \in \operatorname{span}\{r^{k+2},\, r^k,\, r^{-k+2},\, r^{-k}\} \quad \forall k \geqslant 2. \end{cases}$$

We refer to [Kounchev, 2001] for the derivation of (4.A.23). From (4.A.22) and (4.A.23), we can infer the following expression for $\boldsymbol{u}_N^\varepsilon$ in ω^ε and $\omega^\rho \backslash \overline{\omega^\varepsilon}$:

$$\begin{aligned}\boldsymbol{u}_N^\varepsilon(r,\theta)\cdot\boldsymbol{e}_r &= -(c_{1,1}^{\ominus} r^2 + c_{2,1}^{\ominus})\sin(\theta) + (s_{1,1}^{\ominus} r^2 + s_{2,1}^{\ominus})\cos(\theta) \\ &+ \sum_{k=2}^{\infty} -k(c_{1,k}^{\ominus} r^{k+1} + c_{2,k}^{\ominus} r^{k-1})\sin(k\theta) + \sum_{k=2}^{\infty} \quad k(s_{1,k}^{\ominus} r^{k+1} + s_{2,k}^{\ominus} r^{k-1})\cos(k\theta)\end{aligned} \tag{4.A.24}$$

$$\begin{aligned}\boldsymbol{u}_N^\varepsilon(r,\theta)\cdot\boldsymbol{e}_\theta =& -2c_{1,0}^{\ominus} r - (3c_{1,1}^{\ominus} r^2 + c_{2,1}^{\ominus})\cos(\theta) - (3s_{1,1}^{\ominus} r^2 + s_{2,1}^{\ominus})\sin(\theta) \\ &- \sum_{k=2}^{\infty} \left((k+2)c_{1,k}^{\ominus} r^{k+1} + k c_{2,k}^{\ominus} r^{k-1}\right)\cos(k\theta) \\ &- \sum_{k=2}^{\infty} \left((k+2)s_{1,k}^{\ominus} r^{k+1} + k s_{2,k}^{\ominus} r^{k-1}\right)\sin(k\theta)\end{aligned} \tag{4.A.25}$$

for all $(r,\theta) \in [0,\varepsilon] \times (0, 2\pi)$ and

$$\begin{aligned}\boldsymbol{u}_N^\varepsilon(r,\theta)\cdot\boldsymbol{e}_r =& -(c_{1,1}^{\oplus} r^2 + c_{2,1}^{\oplus} + c_{3,1}^{\oplus}\log(r) + c_{4,1}^{\oplus} r^{-2})\sin(\theta) \\ &+ (s_{1,1}^{\oplus} r^2 + s_{2,1}^{\oplus} + s_{3,1}^{\oplus}\log(r) + s_{4,1}^{\oplus} r^{-2})\cos(\theta) \\ &- \sum_{k=2}^{\infty} k(c_{1,k}^{\oplus} r^{k+1} + c_{2,k}^{\oplus} r^{k-1} + c_{3,k}^{\oplus} r^{-k+1} + c_{4,k}^{\oplus} r^{-k-1})\sin(k\theta) \\ &+ \sum_{k=2}^{\infty} k(s_{1,k}^{\oplus} r^{k+1} + s_{2,k}^{\oplus} r^{k-1} + s_{3,k}^{\oplus} r^{-k+1} + s_{4,k}^{\oplus} r^{-k-1})\cos(k\theta),\end{aligned} \tag{4.A.26}$$

$$\begin{aligned}\boldsymbol{u}_N^\varepsilon(r,\theta)\cdot\boldsymbol{e}_\theta =& -(2c_{1,0}^{\oplus} r + c_{2,0}^{\oplus} r^{-1}) \\ &- (3c_{1,1}^{\oplus} r^2 + c_{2,1}^{\oplus} + c_{3,1}^{\oplus}(\log(r)+1) - c_{4,1}^{\oplus} r^{-2})\cos(\theta) \\ &- (3s_{1,1}^{\oplus} r^2 + s_{2,1}^{\oplus} + s_{3,1}^{\oplus}(\log(r)+1) - s_{4,1}^{\oplus} r^{-2})\sin(\theta) \\ &- \sum_{k=2}^{\infty} \quad ((k+2)c_{1,k}^{\oplus} r^{k+1} \quad + k c_{2,k}^{\oplus} r^{k-1})\cos(k\theta) \\ &- \sum_{k=2}^{\infty} ((-k+2)c_{3,k}^{\oplus} r^{-k+1} - k c_{4,k}^{\oplus} r^{-k-1})\cos(k\theta) \\ &- \sum_{k=2}^{\infty} \quad ((k+2)s_{1,k}^{\oplus} r^{k+1} \quad + k s_{2,k}^{\oplus} r^{k-1})\sin(k\theta) \\ &- \sum_{k=2}^{\infty} ((-k+2)s_{3,k}^{\oplus} r^{-k+1} - k s_{4,k}^{\oplus} r^{-k-1})\sin(k\theta)\end{aligned} \tag{4.A.27}$$

for all $(r,\theta) \in [\varepsilon,\rho] \times (0,2\pi)$. The rest of the proof is structured as follows. First, we will derive a series of equations for the coefficients $c^{\ominus}_{j,k}, c^{\oplus}_{j,k}$ and $s^{\ominus}_{j,k}, s^{\oplus}_{j,k}$ from which will deduce their expressions in terms of the boundary conditions on $\partial\omega^{\varepsilon}$ and the value of $\boldsymbol{u}^{\varepsilon}_N$ on $\partial\omega^{\rho}$. More precisely, the coefficients will be expressed in terms of $\boldsymbol{v}_{\rm b}$, $w_{\rm b}$ and the following quantities:

$$\xi^{\varepsilon,j}_{k,r} \stackrel{\rm def}{=} \mathscr{F}^j_k(\boldsymbol{u}^{\varepsilon}_N(\rho)\cdot\boldsymbol{e}_r), \quad \xi^{\varepsilon,j}_{k,\theta} \stackrel{\rm def}{=} \mathscr{F}^j_k(\boldsymbol{u}^{\varepsilon}_N(\rho)\cdot\boldsymbol{e}_\theta) \tag{4.A.28}$$

for all $(k,j) \in \{0,\dots,N\}\times\{\mathrm{c},\mathrm{s}\}$, where the operated $\mathscr{F}^j_k : (0,L) \to \mathbb{R}$ are defined in (3.2.3). In a second step, we will use the a priori estimate on $\boldsymbol{u}^{\varepsilon}_N$ given by Theorem 4.2.1 to establish the desired a priori bounds only in terms of the data $\boldsymbol{v}_{\rm b}$ and $w_{\rm b}$. We only consider the coefficients $c^{\ominus}_{j,k}, c^{\oplus}_{j,k}$, as the coefficients $s^{\ominus}_{j,k}, s^{\oplus}_{j,k}$ play a symmetric role. Let us start by writing the reduced order boundary conditions on ω^{ε}. These conditions read

$$(\boldsymbol{\mu}_N, \boldsymbol{u}^{\varepsilon}_N)_{\varepsilon} = \big(\boldsymbol{\mu}_N, \boldsymbol{v}_{\rm b} + \varepsilon w_{\rm b}\boldsymbol{e}_\theta\big)_{\varepsilon} \quad \forall \boldsymbol{\mu}_N \in \boldsymbol{F}_N, \tag{4.A.29}$$

By writing this condition again each basis element of the finite-dimension space $\boldsymbol{F}_N$ introduced in (4.2.1), we get the following set of equations:

$$\begin{cases} (\boldsymbol{e}_x, \boldsymbol{u}^{\varepsilon}_N)_{\varepsilon} = \boldsymbol{v}_{\rm b}\cdot\boldsymbol{e}_x, \\ (\boldsymbol{e}_y, \boldsymbol{u}^{\varepsilon}_N)_{\varepsilon} = \boldsymbol{v}_{\rm b}\cdot\boldsymbol{e}_y, \\ (\sin(\theta)\boldsymbol{e}_x + \cos(\theta)\boldsymbol{e}_y, \boldsymbol{u}^{\varepsilon}_N)_{\varepsilon} = 0, \\ (\sin(\theta)\boldsymbol{e}_x - \cos(\theta)\boldsymbol{e}_y, \boldsymbol{u}^{\varepsilon}_N)_{\varepsilon} = -w_{\rm b} \\ (\cos(\theta)\boldsymbol{e}_x - \sin(\theta)\boldsymbol{e}_y, \boldsymbol{u}^{\varepsilon}_N)_{\varepsilon} = 0, \end{cases} \quad \begin{cases} (\cos(k\theta)\boldsymbol{e}_x, \boldsymbol{u}^{\varepsilon}_N)_{\varepsilon} = 0, \\ (\cos(k\theta)\boldsymbol{e}_y, \boldsymbol{u}^{\varepsilon}_N)_{\varepsilon} = 0, \\ (\sin(k\theta)\boldsymbol{e}_x, \boldsymbol{u}^{\varepsilon}_N)_{\varepsilon} = 0, \\ (\sin(k\theta)\boldsymbol{e}_y, \boldsymbol{u}^{\varepsilon}_N)_{\varepsilon} = 0, \end{cases} \tag{4.A.30}$$

for all $k \in \{2,\dots,N\}$. Since the expressions (4.A.24)-(4.A.25) and (4.A.26)-(4.A.27) of $\boldsymbol{u}^{\varepsilon}_N$ are given in a polar frame, we would like to reformulate the system (4.A.30) in polar coordinates. To do so, we notice that for $k \in \{2,\dots,N\}$, the system (4.A.30) is equivalent to

$$\begin{cases} (\cos(k\theta)\boldsymbol{e}_x + \sin(k\theta)\boldsymbol{e}_y, \boldsymbol{u}^{\varepsilon}_N)_{\varepsilon} = 0, \\ (\sin(k\theta)\boldsymbol{e}_x + \cos(k\theta)\boldsymbol{e}_y, \boldsymbol{u}^{\varepsilon}_N)_{\varepsilon} = 0, \\ (\sin(k\theta)\boldsymbol{e}_x - \cos(k\theta)\boldsymbol{e}_y, \boldsymbol{u}^{\varepsilon}_N)_{\varepsilon} = 0, \\ (\cos(k\theta)\boldsymbol{e}_x - \sin(k\theta)\boldsymbol{e}_y, \boldsymbol{u}^{\varepsilon}_N)_{\varepsilon} = 0, \end{cases} \tag{4.A.31}$$

such that the kinematic coupling condition (4.A.29) writes equivalently in polar coordi-

nates

$$\begin{cases} (\cos(\theta)\boldsymbol{e}_r - \sin(\theta)\boldsymbol{e}_\theta, \boldsymbol{u}_N^\varepsilon)_\varepsilon = \boldsymbol{v}_{\rm b}\cdot\boldsymbol{e}_x, \\ (\sin(\theta)\boldsymbol{e}_r + \cos(\theta)\boldsymbol{e}_\theta, \boldsymbol{u}_N^\varepsilon)_\varepsilon = \boldsymbol{v}_{\rm b}\cdot\boldsymbol{e}_y, \\ (\sin(2\theta)\boldsymbol{e}_r + \cos(2\theta)\boldsymbol{e}_\theta, \boldsymbol{u}_N^\varepsilon)_\varepsilon = 0, \\ (-\boldsymbol{e}_\theta, \boldsymbol{u}_N^\varepsilon)_\varepsilon = -w_{\rm b}, \\ (\cos(2\theta)\boldsymbol{e}_r - \sin(2\theta)\boldsymbol{e}_\theta, \boldsymbol{u}_N^\varepsilon)_\varepsilon = 0, \\ (\cos((k-1)\theta)\boldsymbol{e}_r + \sin((k-1)\theta)\boldsymbol{e}_\theta, \boldsymbol{u}_N^\varepsilon)_\varepsilon = 0, \\ (\sin((k+1)\theta)\boldsymbol{e}_r + \cos((k+1)\theta)\boldsymbol{e}_\theta, \boldsymbol{u}_N^\varepsilon)_\varepsilon = 0, \\ (\sin((k-1)\theta)\boldsymbol{e}_r - \cos((k-1)\theta)\boldsymbol{e}_\theta, \boldsymbol{u}_N^\varepsilon)_\varepsilon = 0, \\ (\cos((k+1)\theta)\boldsymbol{e}_r - \sin((k+1)\theta)\boldsymbol{e}_\theta, \boldsymbol{u}_N^\varepsilon)_\varepsilon = 0 \end{cases} \tag{4.A.32}$$

for all $k \in \{2, \dots, N\}$. Applying (4.A.32) to (4.A.24)-(4.A.25) yields the following conditions on the $c_{j,k}^{\ominus}$:

- $N = 0$: $\quad 2\varepsilon^2 c_{1,1}^{\ominus} - c_{2,1}^{\ominus} = \boldsymbol{v}_{\rm b}\cdot\boldsymbol{e}_y,$ (4.A.33)
- $N = 1$: $\quad -2c_{1,0}^{\ominus} = w_{\rm b}, \quad 2\varepsilon^2 c_{1,1}^{\ominus} - c_{2,1}^{\ominus} = \boldsymbol{v}_{\rm b}\cdot\boldsymbol{e}_y,$ (4.A.34)
- $N \geqslant 2$: $\begin{cases} -2c_{1,0}^{\ominus} = w_{\rm b}, \quad c_{1,1}^{\ominus} = 0, \quad -c_{2,1}^{\ominus} = \boldsymbol{v}_{\rm b}\cdot\boldsymbol{e}_y, \\ k \in \{2, \dots, N-1\} : c_{1,k}^{\ominus} = c_{2,k}^{\ominus} = 0, \\ \quad k \in \{N,\, N+1\} : -(k+1)\varepsilon^2 c_{1,k}^{\ominus} - k c_{2,k}^{\ominus} = 0. \end{cases}$ (4.A.35)

We proceed by expressing the boundary conditions on $\partial\omega^\rho$. By evaluating equations (4.A.26)-(4.A.27) for $r = \rho$ and subsequently projecting the resulting expressions onto the different Fourier modes, we obtain

- ⋆ $k = 0 : -(2c_{1,0}^{\oplus}\rho + c_{2,0}^{\oplus}\rho^{-1}) = \xi_{0,\theta}^{\varepsilon,\mathrm{c}},$ (4.A.36)
- ⋆ $k = 1 : \begin{cases} -(c_{1,1}^{\oplus}\rho^2 + c_{2,1}^{\oplus} + c_{3,1}^{\oplus}\log(\rho) + c_{4,1}^{\oplus}\rho^{-2}) = \xi_{1,r}^{\varepsilon,\mathrm{s}}, \\ -(3c_{1,1}^{\oplus}\rho^2 + c_{2,1}^{\oplus} + c_{3,1}^{\oplus}(\log(\rho)+1) - c_{4,1}^{\oplus}\rho^{-2}) = \xi_{1,\theta}^{\varepsilon,\mathrm{c}}, \end{cases}$ (4.A.37)
- ⋆ $k \geqslant 2 : \begin{cases} -k(\rho^{k+1}c_{1,k}^{\oplus} + \rho^{k-1}c_{2,k}^{\oplus}) \\ \qquad\qquad - k(\rho^{-k+1}c_{3,k}^{\oplus} + \rho^{-k-1}c_{4,k}^{\oplus}) = \xi_{k,r}^{\varepsilon,\mathrm{s}}, \\ -\big((k+2)\rho^{k+1}c_{1,k}^{\oplus} + k\rho^{k-1}c_{2,k}^{\oplus}\big) \\ \qquad\qquad - \big((-k+2)\rho^{-k+1}c_{3,k}^{\oplus} - k\rho^{-k-1}c_{4,k}^{\oplus}\big) = \xi_{k,\theta}^{\varepsilon,\mathrm{c}}. \end{cases}$ (4.A.38)

We now look at the k^{th} Fourier modes of $\boldsymbol{u}_N^\varepsilon$ on $\partial\omega^\varepsilon$. Namely, taking $r = \varepsilon$ both in

(4.A.24)-(4.A.25) and (4.A.26)-(4.A.27) we get

$$\star \quad k=0: -(2\varepsilon c_{1,0}^{\oplus}+\varepsilon^{-1}c_{2,0}^{\oplus}) = -2\varepsilon c_{1,0}^{\ominus}, \tag{4.A.39}$$

$$\star \quad k=1: \begin{cases} -(\varepsilon^2 c_{1,1}^{\oplus}+c_{2,1}^{\oplus}+\log(\varepsilon)c_{3,1}^{\oplus}+\varepsilon^{-2}c_{4,1}^{\oplus}) = \\ \qquad\qquad -(\varepsilon^2 c_{1,1}^{\ominus}+c_{2,1}^{\ominus}), \\ -(3\varepsilon^2 c_{1,1}^{\oplus}+c_{2,1}^{\oplus}+(\log(\varepsilon)+1)c_{3,1}^{\oplus}-\varepsilon^{-2}c_{4,1}^{\oplus}) = \\ \qquad\qquad -(3\varepsilon^2 c_{1,1}^{\ominus}+c_{2,1}^{\ominus}), \end{cases} \tag{4.A.40}$$

$$\star \quad k\geqslant 2: \begin{cases} -k(\varepsilon^{k+1}c_{1,k}^{\oplus}+\varepsilon^{k-1}c_{2,k}^{\oplus}) \\ \qquad -k(\varepsilon^{-k+1}c_{3,k}^{\oplus}+\varepsilon^{-k-1}c_{4,k}^{\oplus}) = \\ \qquad\qquad -k(\varepsilon^{k+1}c_{1,k}^{\ominus}+\varepsilon^{k-1}c_{2,k}^{\ominus}), \\ -((k+2)\varepsilon^{k+1}c_{1,k}^{\oplus}+k\varepsilon^{k-1}c_{2,k}^{\oplus}) \\ \qquad -((-k+2)\varepsilon^{-k}c_{3,k}^{\oplus}-k\varepsilon^{-k-1}c_{4,k}^{\oplus}) = \\ \qquad\qquad -((k+2)\varepsilon^{k+1}c_{1,k}^{\ominus}+k\varepsilon^{k-1}c_{2,k}^{\ominus}). \end{cases} \tag{4.A.41}$$

Finally, we apply the result of Lemma 4.2.6 to close the system of equations. To do so, we need an expression of p_N^{ε} in terms of the coefficients $c_{k,j}^{\ominus}, c_{k,j}^{\oplus}$ and $s_{k,j}^{\ominus}, s_{k,j}^{\oplus}$. We have that p_N^{ε} is harmonic in ω^{ε} and $\omega^{\rho}\backslash\overline{\omega^{\varepsilon}}$, so from the method of separation of variables, we can derive a general form of p_N^{ε} in ω^{ε},

$$p_N^{\varepsilon}(r,\theta) = \sum_{k=1}^{\infty} \gamma_{1,k}^{\ominus} r^k \cos(k\theta) + \sigma_{1,k}^{\ominus} r^k \sin(k\theta) \quad \forall (r,\theta)\in[0,\varepsilon)\times(0,2\pi), \tag{4.A.42}$$

and in $\omega^{\rho}\backslash\overline{\omega^{\varepsilon}}$,

$$p_N^{\varepsilon}(r,\theta) = \sum_{k=1}^{\infty} (\gamma_{1,k}^{\oplus} r^k + \gamma_{2,k}^{\oplus} r^{-k})\cos(k\theta) + (\sigma_{1,k}^{\oplus} r^k + \sigma_{2,k}^{\oplus} r^{-k})\sin(k\theta), \tag{4.A.43}$$

for all $(r,\theta)\in(\varepsilon,\rho]\times(0,2\pi)$. Since $(\boldsymbol{u}_N^{\varepsilon}, p_N^{\varepsilon})$ solves the Stokes equations in $\widehat{\omega}^{\rho}\backslash\overline{\omega^{\varepsilon}}$ and in ω^{ε}, we have

$$\Delta \boldsymbol{u}_N^{\varepsilon} = \nabla p_N \quad \text{in} \quad \omega^{\rho}\backslash\overline{\omega^{\varepsilon}}, \quad \Delta \boldsymbol{u}_N^{\varepsilon} = \nabla p_N \quad \text{in} \quad \omega^{\varepsilon}. \tag{4.A.44}$$

From (4.A.44), we deduce an expression of the coefficients $\sigma_{j,k}^{\ominus}$ (resp. $\sigma_{j,k}^{\oplus}$) in terms of the coefficients $c_{j,k}^{\ominus}$ (resp. $c_{j,k}^{\oplus}$) as follows:

$$\begin{aligned} &\sigma_{1,1}^{\ominus} = -8c_{1,1}^{\ominus}, \quad \sigma_{1,1}^{\oplus} = -8c_{1,1}^{\oplus}, \quad \sigma_{2,1}^{\oplus} = 2c_{3,1}^{\oplus}, \\ &\sigma_{1,k}^{\ominus} = -4(k+1)c_{1,k}^{\ominus}, \quad \sigma_{1,k}^{\oplus} = -4(k+1)c_{1,k}^{\oplus}, \quad \sigma_{2,k}^{\oplus} = -4(k-1)c_{3,k}^{\oplus} \end{aligned} \tag{4.A.45}$$

for all $k \geqslant 2$. By substituting (4.A.45) into (4.A.42) and (4.A.43), we derive an expression for the pressure jump across the interface, $\partial\omega^\varepsilon$, in terms of the coefficients $c^{\ominus}_{j,k}$ and $c^{\oplus}_{j,k}$. Similarly, differentiating (4.A.24) and (4.A.26) yields an expression for the gradient jump across the interface, again in terms of the coefficients $c^{\ominus}_{j,k}$ and $c^{\oplus}_{j,k}$. Consequently, we can deduce an expression for the stress jump accross $\partial\omega^\varepsilon$. Using the result from Lemma 4.2.6, we obtain

- $\{N \in \{0,1\},\, k=1\}$:

$$10\varepsilon^2 c^{\ominus}_{1,1} = 10\varepsilon^2 c^{\oplus}_{1,1} - 3c^{\oplus}_{3,1} + 6\varepsilon^{-2}c^{\oplus}_{4,1}, \tag{4.A.46}$$

- $\{N=1,\, k=0\}$:

$$c^{\ominus}_{1,0} = c^{\oplus}_{1,0}, \tag{4.A.47}$$

- $\{N \geqslant 1,\, k \geqslant 2 \cap k \in \{N,\, N+1\}\}$:

$$\begin{aligned}(k+1)(k+4)\varepsilon^{k+1}c^{\oplus}_{1,k}\varepsilon^{k+1} + k(k-1)\varepsilon^{k-1}c^{\oplus}_{2,k}\\ + (3k^2+k-4)\varepsilon^{-k+1}c^{\oplus}_{3,k} + 3k(k+1)\varepsilon^{-k-1}c^{\oplus}_{4,k}\\ = (k+1)(k+4)\varepsilon^{k+1}c^{\ominus}_{1,k} + k(k-1)\varepsilon^{k-1}c^{\ominus}_{2,k}.\end{aligned} \tag{4.A.48}$$

- $\{N \geqslant 0,\, k \geqslant N+2\}$:

$$\begin{cases}(k+1)(k-4)\varepsilon^{k+1}c^{\oplus}_{1,k} + k(k-1)\varepsilon^{k-1}c^{\oplus}_{2,k}\\ \qquad - (k+4)(k-1)c^{\oplus}_{3,k}\varepsilon^{-k+1} - k(k+1)c^{\oplus}_{4,k}\varepsilon^{-k-1}\\ \qquad = (k+1)(k-4)\varepsilon^{k+1}c^{\ominus}_{1,k} + k(k-1)\varepsilon^{k-1}c^{\ominus}_{2,k}\\ k(k+1)\varepsilon^{k+1}c^{\oplus}_{1,k} + k(k-1)\varepsilon^{k-1}c^{\oplus}_{2,k}\\ \qquad + k(k-1)c^{\oplus}_{3,k}\varepsilon^{-k+1} + k(k+1)c^{\oplus}_{4,k}\varepsilon^{-k-1}\\ \qquad = k(k+1)\varepsilon^{k+1}c^{\ominus}_{1,k} + k(k-1)\varepsilon^{k-1}c^{\ominus}_{2,k}\end{cases} \tag{4.A.49}$$

Thanks to the system of equations obtained above, we can express the coefficients $c^{\ominus}_{k,j}$, $c^{\oplus}_{k,j}$ in terms of $\xi^{\varepsilon,j}_{k,r}, \xi^{\varepsilon,j}_{k,\theta}$ defined in (4.A.28). In details, setting $\tilde{\varepsilon} = \varepsilon/\rho$ we have

- $\{N=0,\, k=0\}$, from (4.A.36), (4.A.39) and (4.A.47),

$$c^{\oplus}_{1,0} = -\frac{\xi^{\varepsilon,s}_{0,\theta}}{2\rho}, \quad c^{\oplus}_{2,0} = 0, \quad c^{\ominus}_{1,0} = c^{\oplus}_{1,0}. \tag{4.A.50}$$

- $\{N \geqslant 1,\, k=0\}$, from (4.A.34), (4.A.35)$_1$, (4.A.36) and (4.A.39),

$$c^{\oplus}_{1,0} = -\frac{\varepsilon^2 w_{\mathrm{b}} - \rho\xi^{\varepsilon,c}_{0,\theta}}{2(\varepsilon^2-\rho^2)}, \quad c^{\ominus}_{1,0} = -\frac{\mathrm{d}_t\theta}{2}, \quad c^{\oplus}_{2,0} = -\varepsilon^2 w_{\mathrm{b}} - 2c^{\oplus}_{1,0}\varepsilon^2.$$

- $\{N \in \{0,1\},\, k=1\}$, from (4.A.33), (4.A.37), (4.A.40) and (4.A.46),

$$
\begin{aligned}
c_{1,1}^{\oplus} &= \frac{A_1^\varepsilon \xi_{1,r}^{\varepsilon,\mathrm{s}} + B_1^\varepsilon \xi_{1,\theta}^{\varepsilon,\mathrm{c}} + C_1^\varepsilon \boldsymbol{v}_\mathrm{b}\cdot\boldsymbol{e}_y}{D_1^\varepsilon}, & c_{2,1}^{\oplus} &= \frac{E_1^\varepsilon \xi_{1,r}^{\varepsilon,\mathrm{s}} + F_1^\varepsilon \xi_{1,\theta}^{\varepsilon,\mathrm{c}} + G_1^\varepsilon \boldsymbol{v}_\mathrm{b}\cdot\boldsymbol{e}_y}{D_1^\varepsilon}\\
c_{1,1}^{\ominus} &= c_{1,1}^{\oplus}, & c_{2,1}^{\ominus} &= -2\varepsilon^2 c_{1,1}^{\oplus} - \boldsymbol{v}_\mathrm{b}\cdot\boldsymbol{e}_y,\\
c_{3,1}^{\oplus} &= -2\frac{2\varepsilon^2 c_{1,1}^{\oplus} + c_{2,1}^{\oplus} + \boldsymbol{v}_\mathrm{b}\cdot\boldsymbol{e}_y}{2\log(\varepsilon)+1}, & c_{4,1}^{\oplus} &= -\varepsilon^2\frac{2\varepsilon^2 c_{1,1}^{\oplus} + c_{2,1}^{\oplus} + \boldsymbol{v}_\mathrm{b}\cdot\boldsymbol{e}_y}{2\log(\varepsilon)+1}.
\end{aligned}
$$

with

$$
\begin{cases}
A_1^\varepsilon = \rho^2(2\log(\tilde\varepsilon) + (\tilde\varepsilon-1)(\tilde\varepsilon+1)),\\
B_1^\varepsilon = \rho^2(-2\log(\tilde\varepsilon) + (\tilde\varepsilon-1)(\tilde\varepsilon+1)),\\
C_1^\varepsilon = 2\rho(1-\tilde\varepsilon)(1+\tilde\varepsilon),\\
E_1^\varepsilon = -\rho^4(6\log(\tilde\varepsilon) + (6\log(\rho)+3) + 4\tilde\varepsilon^2(\log(\rho)+1) - 2\tilde\varepsilon^4),\\
F_1^\varepsilon = \rho^4(2\log(\tilde\varepsilon) + (2\log(\rho)+1) - 4\tilde\varepsilon^2\log(\rho) - 2\tilde\varepsilon^4),\\
G_1^\varepsilon = 2\rho^4((2\log(\rho)-1) + 2\tilde\varepsilon^2),\\
D_1^\varepsilon = 4\rho^4((\log(\tilde\varepsilon)+1) - 2\tilde\varepsilon^2 + \tilde\varepsilon^4).
\end{cases}
\tag{4.A.51}
$$

- $\{N \geqslant 2,\, k=1\}$, from (4.A.35)$_1$, (4.A.37) and (4.A.40),

$$
\begin{aligned}
c_{1,1}^{\oplus} &= \frac{A_1^\varepsilon \xi_{1,r}^{\varepsilon,\mathrm{s}} + B_1^\varepsilon \xi_{1,\theta}^{\varepsilon,\mathrm{c}}}{D_1^\varepsilon}, & c_{2,1}^{\oplus} &= \frac{E_1^\varepsilon \xi_{1,r}^{\varepsilon,\mathrm{s}} + F_1^\varepsilon \xi_{1,\theta}^{\varepsilon,\mathrm{c}}}{D_1^\varepsilon},\\
c_{1,1}^{\ominus} &= 0, \quad c_{2,1}^{\ominus} = -\mathrm{d}_t\boldsymbol{r}\cdot\boldsymbol{e}_y, & c_{3,1}^{\oplus} &= -2\frac{2c_{1,1}^{\oplus}\varepsilon^2 + c_{2,1}^{\oplus} + \boldsymbol{v}_\mathrm{b}\cdot\boldsymbol{e}_y}{2\log(\varepsilon)+1},\\
c_{4,1}^{\oplus} &= \varepsilon^2\frac{\varepsilon^2 c_{1,1}^{\oplus}(2\log(\varepsilon)-1) - c_{2,1}^{\oplus} - \mathrm{d}_t\boldsymbol{r}\cdot\boldsymbol{e}_y}{2\log(\varepsilon)+1},
\end{aligned}
$$

with

$$
\begin{cases}
A_1^\varepsilon = \rho^2(2\log(\tilde\varepsilon) - 1 + \tilde\varepsilon^2),\\
B_1^\varepsilon = \rho^2(-2\log(\tilde\varepsilon) - 1 + \tilde\varepsilon^2),\\
E_1^\varepsilon = \rho^4(-6\log(\tilde\varepsilon) + 3(2\log(\rho)-1) + 4\tilde\varepsilon^2(\log(\rho)+1) - \tilde\varepsilon^4),\\
F_1^\varepsilon = \rho^4(\log(\tilde\varepsilon) + \log(\rho) + 1 - 4\tilde\varepsilon^2\log(\rho) - \tilde\varepsilon^4),\\
D_1^\varepsilon = \rho^2(4(\log(\tilde\varepsilon)+1) + \tilde\varepsilon^2(\log(\tilde\varepsilon)-1)).
\end{cases}
$$

- $\{N \geqslant 2,\ k \in \{2, \dots, N-1\}\}$, from $(4.A.35)_2$, (4.A.38) and (4.A.41),

$$
\begin{aligned}
&c_{1,k}^{\oplus} = \frac{A_k^{\varepsilon}\xi_{k,r}^{\varepsilon,\mathrm{s}} + B_k^{\varepsilon}\xi_{k,\theta}^{\varepsilon,\mathrm{c}}}{D_k^{\varepsilon}}, \quad c_{2,k}^{\oplus} = \frac{E_k^{\varepsilon}\xi_{k,r}^{\varepsilon,\mathrm{s}} + F_k^{\varepsilon}\xi_{k,\theta}^{\varepsilon,\mathrm{c}}}{kD_k^{\varepsilon}} \\
&c_{1,k}^{\ominus} = 0, \quad c_{2,k}^{\ominus} = 0, \qquad c_{3,k}^{\oplus} = -\varepsilon^{2(k-1)}\big((k+1)\varepsilon^2 c_{1,k}^{\oplus} + k c_{2,k}^{\oplus}\big), \\
&c_{4,k}^{\oplus} = \varepsilon^{2k}\big(k\varepsilon^2 c_{1,k}^{\oplus} + (k-1)c_{2,k}^{\oplus}\big).
\end{aligned}
$$

with

$$
\begin{cases}
A_k^{\varepsilon} = \rho^{3k-1}(1 + (k-2)\tilde{\varepsilon}^{2(k-1)} - (k-1)\tilde{\varepsilon}^{2k}), \\
B_k^{\varepsilon} = -\rho^{3k-1}(1 - k\tilde{\varepsilon}^{2(k-1)} + (k-1)\tilde{\varepsilon}^{2k}), \\
E_k^{\varepsilon} = \rho^{3k+1}((k+2) + (k+1)(k-2)\tilde{\varepsilon}^{2k} - k^2\tilde{\varepsilon}^{2(k+1)}), \\
F_k^{\varepsilon} = -k\rho^{3k+1}(1 - (k+1)\tilde{\varepsilon}^{2k} + k\tilde{\varepsilon}^{2(k+1)}), \\
D_k^{\varepsilon} = 2\rho^{4k}(1 - k^2\tilde{\varepsilon}^{2(k-1)} + 2(k^2-1)\tilde{\varepsilon}^{2k} - k^2\tilde{\varepsilon}^{2(k+1)} + \tilde{\varepsilon}^{4k}).
\end{cases}
\tag{4.A.52}
$$

- $\{k \geqslant 2,\ k \in \{N, N+1\}\}$, from $(4.A.35)_3$, (4.A.38), (4.A.41) and (4.A.48)

$$
\begin{aligned}
&c_{1,k}^{\oplus} = \frac{A_k^{\varepsilon}\xi_{k,r}^{\varepsilon,\mathrm{s}} + B_k^{\varepsilon}\xi_{k,\theta}^{\varepsilon,\mathrm{c}}}{D_k^{\varepsilon}}, \quad c_{2,k}^{\oplus} = \frac{E_k^{\varepsilon}\xi_{k,r}^{\varepsilon,\mathrm{s}} + F_k^{\varepsilon}\xi_{k,\theta}^{\varepsilon,\mathrm{c}}}{kD_k^{\varepsilon}}, \\
&c_{1,k}^{\ominus} = c_{1,k}^{\oplus}, \qquad\qquad c_{2,k}^{\ominus} = -\frac{k+1}{k}\varepsilon^2 c_{1,k}^{\oplus}, \\
&c_{3,k}^{\oplus} = -\varepsilon^{2(k-1)}((k+1)\varepsilon^2 c_{1,k}^{\oplus} + k c_{2,k}^{\oplus}), \\
&c_{4,k}^{\oplus} = \varepsilon^{2k}\frac{k-1}{k}((k+1)\varepsilon^2 c_{1,k}^{\oplus} + k c_{2,k}^{\oplus}).
\end{aligned}
$$

with

$$
\begin{cases}
A_k^{\varepsilon} = -\rho^{k+1}(1 + (k-2)\tilde{\varepsilon}^{2(k-1)} - (k-1)\tilde{\varepsilon}^{2k}), \\
B_k^{\varepsilon} = \rho^{k+1}(1 - k\tilde{\varepsilon}^{2(k-1)} + (k-1)\tilde{\varepsilon}^{2k}), \\
E_k^{\varepsilon} = \rho^{k+3}((k+2) + (k-2)(k+1)\tilde{\varepsilon}^{2k} - (k^2-1)\tilde{\varepsilon}^{2(k+1)}), \\
F_k^{\varepsilon} = -\rho^{k+3}(k - k(k+1)\tilde{\varepsilon}^{2k} - (k^2-1)\tilde{\varepsilon}^{2(k+1)}), \\
D_k^{\varepsilon} = -2\rho^{2(k+1)}(1 - k^2\tilde{\varepsilon}^{2(k-1)} + 2(k^2-1)\tilde{\varepsilon}^{2k} - (k^2-1)\tilde{\varepsilon}^{2(k+1)}).
\end{cases}
\tag{4.A.53}
$$

- $\{N = 0,\ k \geqslant 2\} \bigcup \{k \geqslant N+2\}$, from (4.A.38), (4.A.41) and (4.A.49)

$$
\begin{aligned}
&c_{1,k}^{\oplus} = \frac{\xi_{k,r}^{\varepsilon,\mathrm{s}} - \xi_{k,\theta}^{\varepsilon,\mathrm{c}}}{2\rho^{k+1}}, \qquad c_{2,k}^{\oplus} = -\frac{(k+2)\xi_{k,r}^{\varepsilon,\mathrm{s}} - \xi_{k,\theta}^{\varepsilon,\mathrm{c}}}{2k\rho^{k-1}}, \\
&c_{1,k}^{\ominus} = c_{1,k}^{\oplus}, \quad c_{2,k}^{\ominus} = c_{2,k}^{\oplus}, \quad c_{3,k}^{\oplus} = c_{4,k}^{\oplus} = 0.
\end{aligned}
$$

We deduce that $\boldsymbol{u}_N^\varepsilon - \boldsymbol{u}_{\mathrm{b}}$ satisfies (4.2.23) with

- $N = 0$
  - $\star$ $k = 0$: $\quad a_{\theta,0}^\varepsilon = \xi_{0,\theta}^{\varepsilon,\mathrm{c}}$
  - $\star$ $k = 1$: $\quad b_{r,1}^\varepsilon = \tilde{\varepsilon}\rho^2 c_{1,1}^\oplus, \quad a_{\theta,1}^\varepsilon = -\tilde{\varepsilon}\rho^2 c_{1,1}^\oplus,$
  - $\star$ $k \geqslant 2$:

$$\begin{cases} b_{r,k}^\varepsilon = -k\dfrac{\xi_{k,r}^{\varepsilon,\mathrm{s}} - \xi_{k,\theta}^{\varepsilon,\mathrm{c}}}{2}\tilde{\varepsilon}^{k-N} + \dfrac{(k+2)\xi_{k,r}^{\varepsilon,\mathrm{s}} - k\xi_{k,\theta}^{\varepsilon,\mathrm{c}}}{2}\tilde{\varepsilon}^{k-N-2}, \\ a_{\theta,k}^\varepsilon = -(k+2)\dfrac{\xi_{k,r}^{\varepsilon,\mathrm{s}} - \xi_{k,\theta}^{\varepsilon,\mathrm{c}}}{2}\tilde{\varepsilon}^{k-N} + \dfrac{(k+2)\xi_{k,r}^{\varepsilon,\mathrm{s}} - k\xi_{k,\theta}^{\varepsilon,\mathrm{c}}}{2}\tilde{\varepsilon}^{k-N-2}. \end{cases}$$

- $N \geqslant 1$,
  - $\star$ $k \in \{N, N+1\}$:

$$b_{r,k}^\varepsilon = \tilde{\varepsilon}^{k-N}\rho^{k+1}c_{1,k}^\oplus, \quad a_{\theta,k}^\varepsilon = -\tilde{\varepsilon}^{k-N}\rho^{k+1}c_{1,k}^\oplus$$

  - $\star$ $k \geqslant N+2$:

$$\begin{cases} b_{r,k}^\varepsilon = -k\dfrac{\xi_{k,r}^{\varepsilon,\mathrm{s}} - \xi_{k,\theta}^{\varepsilon,\mathrm{c}}}{2}\tilde{\varepsilon}^{k-N} + \dfrac{(k+2)\xi_{k,r}^{\varepsilon,\mathrm{s}} - k\xi_{k,\theta}^{\varepsilon,\mathrm{c}}}{2}\tilde{\varepsilon}^{k-N-2}, \\ a_{\theta,k}^\varepsilon = -(k+2)\dfrac{\xi_{k,r}^{\varepsilon,\mathrm{s}} - \xi_{k,\theta}^{\varepsilon,\mathrm{c}}}{2}\tilde{\varepsilon}^{k-N} + \dfrac{(k+2)\xi_{k,r}^{\varepsilon,\mathrm{s}} - k\xi_{k,\theta}^{\varepsilon,\mathrm{c}}}{2}\tilde{\varepsilon}^{k-N-2}. \end{cases}$$

In conclusion, we provide estimates on $c_{1,k}^\oplus$ for $k \in \{N, N+1\}$. In particular, we derive estimates up to a multiplicative constant uniformly independent of k. To denote this, we introduce a subscript k to $\lesssim$, indicated as $\lesssim_k$. In what follows, we will extensively make use of the following estimation:

$$|P(k)| \lesssim_k (1+k)^{\deg(P)}, \quad \forall k \in \mathbb{N}, \tag{4.A.54}$$

where P is a polynomial function of degree $\deg(P) \in \mathbb{R}$.

- $k = 1$

$$c_{1,1}^\oplus = \frac{A_1^\varepsilon \xi_{1,r}^{\varepsilon,\mathrm{s}} + B_1^\varepsilon \xi_{1,\theta}^{\varepsilon,\mathrm{c}} + C_1^\varepsilon \boldsymbol{v}_{\mathrm{b}} \cdot \boldsymbol{e}_y}{D_1^\varepsilon}$$

  with A_1^ε, B_1^ε, C_1^ε and D_1^ε given in (4.A.54). We deduce that

$$\rho^2 c_{1,1}^\oplus \xrightarrow[\tilde{\varepsilon}\to 0]{} \frac{1}{2}\xi_{1,r}^{\varepsilon,\mathrm{s}} - \frac{1}{2}\xi_{1,\theta}^{\varepsilon,\mathrm{c}}.$$

  Hence, there exists $\rho_1 > 0$ such that for $\varepsilon \in (0, \rho_1)$,

$$\rho^2 |c_{1,1}^\oplus| \lesssim |\xi_{1,r}^{\varepsilon,\mathrm{s}}| + |\xi_{1,\theta}^{\varepsilon,\mathrm{c}}|.$$

- $k \geqslant 2 \cap k \in \{N, N+1\}$,

$$c_{1,k}^{\oplus} = \frac{A_k^{\varepsilon}\xi_{k,r}^{\varepsilon,\mathrm{s}} + B_k^{\varepsilon}\xi_{k,\theta}^{\varepsilon,\mathrm{c}}}{D_k^{\varepsilon}},$$

with A_k, B_k given in (4.A.53). We begin by providing upper bounds for $|A_k^{\varepsilon}|$ and $|B_k^{\varepsilon}|$. Taking $\tilde{\varepsilon} \in (0, 1/4)$, we have

$$\begin{aligned}
|A_k^{\varepsilon}| &\lesssim_k \rho^{k+1}\left(1 + (1+k)(1/4)^{2(k-1)} + (1+k)(1/4)^{2(k+1)}\right), \\
|B_k^{\varepsilon}| &\lesssim_k \rho^{k+1}\left(1 + (1+k)\,(1/4)^{2(k-1)} + (1+k)(1/4)^{2(k+1)}\right)
\end{aligned}$$

Since the sequences $(1+k)(1/4)^{2(k-1)}$ and $(1+k)(1/4)^{2(k+1)}$ are bounded independently of k, we deduce that for $\varepsilon \in (0, \rho/4)$,

$$|A_k^{\varepsilon}| \lesssim_k \rho^{k+1}, \quad |B_k^{\varepsilon}| \lesssim_k \rho^{k+1}.$$

Similarly for D_k^{ε}, considering $\tilde{\varepsilon} \in (0, 1/4)$, we have

$$D_k^{\varepsilon} \lesssim_k -\rho^{2(k+1)}(1 - k^2(1/4)^{2(k-1)} - (k-1)(k+1)(1/4)^{2(k+1)})$$

Since the sequences $k^2\left(\frac{1}{4}\right)^{2(k-1)}$ and $(k-1)(k+1)\left(\frac{1}{4}\right)^{2(k+1)}$ are decreasing for $k \geqslant 2$, we deduce that

$$D_k^{\varepsilon} \lesssim_k -\rho^{2(k+1)}(1 - 4(1/4)^2 - 3(1/4)^4) \lesssim_k -\rho^{2(k+1)}$$

Therefore, for $k \geqslant 2 \cap k \in \{N, N+1\}$ and $\varepsilon \in (0, \rho/4)$,

$$\rho^{k+1}|c_{1,k}^{\oplus}| \lesssim_k |\xi_{k,r}^{\varepsilon,\mathrm{s}}| + |\xi_{k,\theta}^{\varepsilon,\mathrm{c}}|.$$

- $k \geqslant N+2$

$$|b_{r,k}^{\varepsilon}|^2 + |a_{\theta,k}^{\varepsilon}|^2 \lesssim_k (1+k)^2\tilde{\varepsilon}^{2(N-k-2)}$$

Finally, by taking $\tilde{\rho} = \min(\rho_1, \rho/4)$ and setting

$$\xi_k \overset{\mathrm{def}}{=} (|\xi_{k,r}^{\varepsilon,\mathrm{s}}|^2 + |\xi_{k,\theta}^{\varepsilon,\mathrm{c}}|^2 + |\xi_{k,\theta}^{\varepsilon,\mathrm{s}}|^2 + |\xi_{k,r}^{\varepsilon,\mathrm{c}}|^2)^{\frac{1}{2}} \tag{4.A.55}$$

we deduce that, for all $\varepsilon \in (0, \tilde{\rho})$,

$$\star \quad k \in \{N, N+1\} : |b_{r,k}^{\varepsilon}|^2 + |a_{\theta,k}|^2 \lesssim_k \left(\frac{\varepsilon}{\rho}\right)^{2(N-k)} \xi_k^2,$$

$$\star \quad k \geqslant N+2 : |b_{r,k}^{\varepsilon}|^2 + |a_{\theta,k}^{\varepsilon}|^2 \lesssim_k (1+k)^2\left(\frac{\varepsilon}{\rho}\right)^{2(N-k-2)} \xi_k^2.$$

We can proceed in a similar way to obtain a priori estimates for $b^{\varepsilon}_{\theta,k}$ and $a^{\varepsilon}_{r,k}$. We then get that, for all $\varepsilon \in (0, \tilde{\rho})$,

$$\begin{aligned}
&\sum_{k=N}^{\infty}(1+k)\big(|a^{\varepsilon}_{r,k}|^2+|a^{\varepsilon}_{\theta,k}|^2+|b^{\varepsilon}_{r,k}|^2+|b^{\varepsilon}_{\theta,k}|^2\big)\\
&=\sum_{k=N}^{N+1}(1+k)\big(|a^{\varepsilon}_{r,k}|^2+|a^{\varepsilon}_{\theta,k}|^2+|b^{\varepsilon}_{r,k}|^2+|b^{\varepsilon}_{\theta,k}|^2\big)\\
&+\sum_{k=N+2}^{\infty}(1+k)\big(|a^{\varepsilon}_{r,k}|^2+|a^{\varepsilon}_{\theta,k}|^2+|b^{\varepsilon}_{r,k}|^2+|b^{\varepsilon}_{\theta,k}|^2\big),\\
&\lesssim\sum_{k=N}^{N+1}(1+k)\xi_k^2+(1+N)^2\sum_{k=0}^{\infty}\left(\frac{\tilde{\rho}}{\rho}\right)^{2k}(1+k)^2(1+k+N+2)\xi^2_{k+N+2}
\end{aligned}$$

where the last inequality comes from $(1+k+N+2)^2 \lesssim_k (1+k)^2(1+N)^2$. Since the sequence $\left(\frac{\tilde{\rho}}{\rho}\right)^{2k}(1+k)^2$ is bounded, using successively the equivalence between the norm $\|\cdot\|^{\mathscr{F}}_{\frac{1}{2},\rho}$ and $\|\cdot\|_{\frac{1}{2},\rho}$, the standard trace theorem from $\boldsymbol{H}^{\frac{1}{2}}(\partial\omega^{\rho})$ to $\boldsymbol{H}^1(\Omega)$ and Theorem 4.2.1, we finally have

$$\begin{aligned}
&\sum_{k=N}^{\infty}(1+k)\big(|a^{\varepsilon}_{r,k}|^2+|a^{\varepsilon}_{\theta,k}|^2+|b^{\varepsilon}_{r,k}|^2+|b^{\varepsilon}_{\theta,k}|^2\big)\lesssim(1+N)^2\sum_{k=0}^{\infty}(1+k)\xi_k^2\\
&\lesssim(1+N)^2\|\boldsymbol{u}^{\varepsilon}_N\|^{\mathscr{F}}_{\frac{1}{2},\rho}\lesssim(1+N)^2\|\boldsymbol{u}^{\varepsilon}_N\|_{1,\Omega}\lesssim(1+N)^2\big(|\boldsymbol{v}_{\mathrm{b}}|+\varepsilon|w_{\mathrm{b}}|\big).
\end{aligned}\tag{4.A.56}$$

This concludes the proof. □

4.A.7 Decomposition of the solution of (4.4.3) into a regular and singular part

4.A.7.1 Coefficients and singular functions for the velocity decomposition

In this section, we provide the expression of the coefficients $a^u_{l,j}/b^u_{l,j}$ and singular functions $\boldsymbol{\phi}^{\varepsilon,\mathrm{c}}_{l,j}/\boldsymbol{\phi}^{\varepsilon,\mathrm{s}}_{l,j}$ for the decomposition of $\boldsymbol{u}^{\varepsilon}_N$ into a regular and singular part, as presented in equation (4.3.30). From one value of N to the following, if nothing is precised for the value of a function or a coefficient previously defined, it means that it remains unchanged from its last definition. For instance, between cases $N=0$ and $N=1$, the values of $a^u_{1,1}$, $b^u_{1,1}$, $\boldsymbol{\phi}^{\varepsilon,\mathrm{c}}_{1,1}$ and $\boldsymbol{\phi}^{\varepsilon,\mathrm{s}}_{1,1}$ remains unchanged. The singular enrichment functions for the velocity space in the augmented finite element method of Section 4.3.2 are given by:

- $N \in \{0,1\}$:

⋆ $j = 1$:

$$a^u_{1,1} \overset{\text{def}}{=} 2\varepsilon^2 c^{\oplus}_{1,1} + c^{\oplus}_{2,1} + \boldsymbol{v}_{\text{b}} \cdot \boldsymbol{e}_y, \quad b^u_{1,1} \overset{\text{def}}{=} 2\varepsilon^2 s^{\oplus}_{1,1} + s^{\oplus}_{2,1} + \boldsymbol{v}_{\text{b}} \cdot \boldsymbol{e}_x,$$

$$\begin{cases} \boldsymbol{\phi}^{\varepsilon,\text{c}}_{1,1}(r,\theta) \cdot \boldsymbol{e}_r \overset{\text{def}}{=} \left(\mathbb{1}_{r \leqslant \varepsilon} + \dfrac{2\log(r) + (\varepsilon/r)^2}{2\log(\varepsilon) + 1} \mathbb{1}_{r > \varepsilon} \right) \sin(\theta), \\ \boldsymbol{\phi}^{\varepsilon,\text{c}}_{1,1}(r,\theta) \cdot \boldsymbol{e}_\theta \overset{\text{def}}{=} \left(\mathbb{1}_{r \leqslant \varepsilon} + \dfrac{2(\log(r) + 1) - (\varepsilon/r)^2}{2\log(\varepsilon) + 1} \mathbb{1}_{r > \varepsilon} \right) \cos(\theta), \\ \boldsymbol{\phi}^{\varepsilon,\text{s}}_{1,1}(r,\theta) \cdot \boldsymbol{e}_r \overset{\text{def}}{=} -\left(\mathbb{1}_{r \leqslant \varepsilon} + \dfrac{2\log(r) + (r/\varepsilon)^2}{2\log(\varepsilon) + 1} \mathbb{1}_{r > \varepsilon} \right) \cos(\theta), \\ \boldsymbol{\phi}^{\varepsilon,\text{s}}_{1,1}(r,\theta) \cdot \boldsymbol{e}_\theta \overset{\text{def}}{=} \left(\mathbb{1}_{r \leqslant \varepsilon} + \dfrac{2(\log(r) + 1) - (r/\varepsilon)^2}{2\log(\varepsilon) + 1} \mathbb{1}_{r > \varepsilon} \right) \sin(\theta), \end{cases}$$

⋆ $j = 0$:

$$a^u_{1,0} \overset{\text{def}}{=} \varepsilon(w_{\text{b}} + 2c^{\oplus}_{1,0}), \quad b^u_{1,0} = 0,$$

$$\begin{cases} \boldsymbol{\phi}^{\varepsilon,\text{c}}_{1,0} \cdot \boldsymbol{e}_r \overset{\text{def}}{=} 0, \\ \boldsymbol{\phi}^{\varepsilon,\text{c}}_{1,0} \cdot \boldsymbol{e}_\theta \overset{\text{def}}{=} \left(\dfrac{r}{\varepsilon} \right) \mathbb{1}_{r \leqslant \varepsilon} + \left(\dfrac{\varepsilon}{r} \right) \mathbb{1}_{r > \varepsilon}, \end{cases}$$

⋆ $j = 2$:

$$a^u_{1,2} \overset{\text{def}}{=} \varepsilon(3c^{\oplus}_{1,2} + 2c^{\oplus}_{2,2}), \quad b^u_{1,2} \overset{\text{def}}{=} \varepsilon(3s^{\oplus}_{1,2} + 2s^{\oplus}_{2,2}),$$

$$\begin{cases} \boldsymbol{\phi}^{\varepsilon,\text{c}}_{1,2} \cdot \boldsymbol{e}_r \overset{\text{def}}{=} \left(\left(\dfrac{r}{\varepsilon} \right) \mathbb{1}_{r \leqslant \varepsilon} + \left(2 \left(\dfrac{\varepsilon}{r} \right) - \left(\dfrac{\varepsilon}{r} \right)^3 \right) \mathbb{1}_{r > \varepsilon} \right) \sin(2\theta), \\ \boldsymbol{\phi}^{\varepsilon,\text{c}}_{1,2} \cdot \boldsymbol{e}_\theta \overset{\text{def}}{=} \left(\left(\dfrac{r}{\varepsilon} \right) \mathbb{1}_{r \leqslant \varepsilon} + \left(\dfrac{\varepsilon}{r} \right)^3 \mathbb{1}_{r > \varepsilon} \right) \cos(2\theta), \\ \boldsymbol{\phi}^{\varepsilon,\text{s}}_{1,2} \cdot \boldsymbol{e}_r \overset{\text{def}}{=} -\left(\left(\dfrac{r}{\varepsilon} \right) \mathbb{1}_{r \leqslant \varepsilon} + \left(2 \left(\dfrac{\varepsilon}{r} \right) - \left(\dfrac{\varepsilon}{r} \right)^3 \right) \mathbb{1}_{r > \varepsilon} \right) \cos(2\theta), \\ \boldsymbol{\phi}^{\varepsilon,\text{s}}_{1,2} \cdot \boldsymbol{e}_\theta \overset{\text{def}}{=} \left(\left(\dfrac{r}{\varepsilon} \right) \mathbb{1}_{r \leqslant \varepsilon} + \left(\dfrac{\varepsilon}{r} \right)^3 \mathbb{1}_{r > \varepsilon} \right) \sin(2\theta), \end{cases}$$

• $\{N \geqslant 2,\, j = 1\}$:

⋆ $l = 1$:

$$a^u_{1,1} \overset{\text{def}}{=} c^{\oplus}_{1,1}\varepsilon^2, \quad b_{1,1} \overset{\text{def}}{=} s^{\oplus}_{1,1}\varepsilon^2,$$

$$\begin{cases} \boldsymbol{\phi}_{1,1}^{\varepsilon,\mathrm{c}} \cdot \boldsymbol{e}_r \overset{\text{def}}{=} \left(\dfrac{r}{\varepsilon}\right)^2 \sin(\theta)\mathbb{1}_{r\leqslant\varepsilon} \\ \qquad\qquad + \left(\dfrac{4\log(r)}{2\log(\varepsilon)+1} - \dfrac{2\log(\varepsilon)-1}{2\log(\varepsilon)+1}\left(\dfrac{\varepsilon}{r}\right)^2\right)\sin(\theta)\mathbb{1}_{r>\varepsilon}, \\ \boldsymbol{\phi}_{1,1}^{\varepsilon,\mathrm{c}} \cdot \boldsymbol{e}_\theta \overset{\text{def}}{=} 3\left(\dfrac{r}{\varepsilon}\right)^2 \cos(\theta)\mathbb{1}_{r\leqslant\varepsilon} \\ \qquad\qquad + \left(\dfrac{4(\log(r)+1)}{2\log(\varepsilon)+1} + \dfrac{2\log(\varepsilon)-1}{2\log(\varepsilon)+1}\left(\dfrac{\varepsilon}{r}\right)^2\right)\cos(\theta)\mathbb{1}_{r>\varepsilon}, \\ \boldsymbol{\phi}_{1,1}^{\varepsilon,\mathrm{s}} \cdot \boldsymbol{e}_r \overset{\text{def}}{=} -\left(\dfrac{r}{\varepsilon}\right)^2 \cos(\theta)\mathbb{1}_{r\leqslant\varepsilon} \\ \qquad\qquad + \left(\dfrac{4\log(r)}{2\log(\varepsilon)+1} - \dfrac{2\log(\varepsilon)-1}{2\log(\varepsilon)+1}\left(\dfrac{\varepsilon}{r}\right)^2\right)\cos(\theta)\mathbb{1}_{r>\varepsilon}, \\ \boldsymbol{\phi}_{1,1}^{\varepsilon,\mathrm{s}} \cdot \boldsymbol{e}_\theta \overset{\text{def}}{=} 3\left(\dfrac{r}{\varepsilon}\right)^2 \sin(\theta)\mathbb{1}_{r\leqslant\varepsilon} \\ \qquad\qquad + \left(\dfrac{4(\log(r)+1)}{2\log(\varepsilon)+1} + \dfrac{2\log(\varepsilon)-1}{2\log(\varepsilon)+1}\left(\dfrac{\varepsilon}{r}\right)^2\right)\sin(\theta)\mathbb{1}_{r>\varepsilon}, \end{cases}$$

⋆ $l = 2$:

$$a_{2,1}^u \overset{\text{def}}{=} (\boldsymbol{v}_\mathrm{b} \cdot \boldsymbol{e}_y + c_{2,1}^{\oplus}), \quad b_{2,1}^u \overset{\text{def}}{=} (\boldsymbol{v}_\mathrm{b} \cdot \boldsymbol{e}_x + s_{2,1}^{\oplus})$$

$$\begin{cases} \boldsymbol{\phi}_{2,1}^{\varepsilon,\mathrm{c}} \cdot \boldsymbol{e}_r \overset{\text{def}}{=} \sin(\theta)\mathbb{1}_{r\leqslant\varepsilon} + \left(\dfrac{2\log(r)}{2\log(\varepsilon)+1} + \dfrac{1}{2\log(\varepsilon)+1}\left(\dfrac{\varepsilon}{r}\right)^2\right)\sin(\theta)\mathbb{1}_{r>\varepsilon}, \\ \boldsymbol{\phi}_{2,1}^{\varepsilon,\mathrm{c}} \cdot \boldsymbol{e}_\theta \overset{\text{def}}{=} \cos(\theta)\mathbb{1}_{r\leqslant\varepsilon} + \left(\dfrac{2(\log(r)+1)}{2\log(\varepsilon)+1} - \dfrac{1}{2\log(\varepsilon)+1}\left(\dfrac{\varepsilon}{r}\right)^2\right)\cos(\theta)\mathbb{1}_{r>\varepsilon}, \\ \boldsymbol{\phi}_{2,1}^{\varepsilon,\mathrm{s}} \cdot \boldsymbol{e}_r \overset{\text{def}}{=} -\cos(\theta)\mathbb{1}_{r\leqslant\varepsilon} + \left(\dfrac{2\log(r)}{2\log(\varepsilon)+1} + \dfrac{1}{2\log(\varepsilon)+1}\left(\dfrac{\varepsilon}{r}\right)^2\right)\cos(\theta)\mathbb{1}_{r>\varepsilon}, \\ \boldsymbol{\phi}_{2,1}^{\varepsilon,\mathrm{s}} \cdot \boldsymbol{e}_\theta \overset{\text{def}}{=} \sin(\theta)\mathbb{1}_{r\leqslant\varepsilon} + \left(\dfrac{2(\log(r)+1)}{2\log(\varepsilon)+1} - \dfrac{1}{2\log(\varepsilon)+1}\left(\dfrac{\varepsilon}{r}\right)^2\right)\sin(\theta)\mathbb{1}_{r>\varepsilon}, \end{cases}$$

• $\{N \geqslant 2,\, j \in \{2, \ldots, N-1\}\}$:

⋆ $l = 1$:

$$a_{1,j}^u \overset{\text{def}}{=} \varepsilon^{j+1} c_{1,j}^{\oplus}, \quad b_{1,j}^u \overset{\text{def}}{=} \varepsilon^{j+1} s_{1,j}^{\oplus}$$

$$\begin{cases} \boldsymbol{\phi}_{1,j}^{\varepsilon,\mathrm{c}} \cdot \boldsymbol{e}_r \overset{\text{def}}{=} j \left(\frac{r}{\varepsilon}\right)^{j+1} \sin(j\theta) \mathbb{1}_{1 \leqslant \varepsilon} \\ \qquad\qquad + j \left((1+j) \left(\frac{\varepsilon}{r}\right)^{j-1} - j \left(\frac{\varepsilon}{r}\right)^{j+1} \right) \sin(j\theta) \mathbb{1}_{r > \varepsilon}, \\ \boldsymbol{\phi}_{1,j}^{\varepsilon,\mathrm{c}} \cdot \boldsymbol{e}_\theta \overset{\text{def}}{=} (j+2) \left(\frac{r}{\varepsilon}\right)^{j+1} \cos(j\theta) \mathbb{1}_{1 \leqslant \varepsilon} \\ \qquad\qquad + \left((1+j)(-j+2) \left(\frac{\varepsilon}{r}\right)^{j-1} + j^2 \left(\frac{\varepsilon}{r}\right)^{j+1} \right) \cos(j\theta) \mathbb{1}_{r > \varepsilon}, \\ \boldsymbol{\phi}_{1,j}^{\varepsilon,\mathrm{s}} \cdot \boldsymbol{e}_r \overset{\text{def}}{=} - j \left(\frac{r}{\varepsilon}\right)^{j+1} \cos(j\theta) \mathbb{1}_{1 \leqslant \varepsilon} \\ \qquad\qquad - j \left((1+j) \left(\frac{\varepsilon}{r}\right)^{j-1} - j \left(\frac{\varepsilon}{r}\right)^{j+1} \right) \cos(j\theta) \mathbb{1}_{r > \varepsilon}, \\ \boldsymbol{\phi}_{1,j}^{\varepsilon,\mathrm{s}} \cdot \boldsymbol{e}_\theta \overset{\text{def}}{=} (j+2) \left(\frac{r}{\varepsilon}\right)^{j+1} \sin(j\theta) \mathbb{1}_{1 \leqslant \varepsilon} \\ \qquad\qquad + \left((1+j)(-j+2) \left(\frac{\varepsilon}{r}\right)^{j-1} + j^2 \left(\frac{\varepsilon}{r}\right)^{j+1} \right) \sin(j\theta) \mathbb{1}_{r > \varepsilon}, \end{cases}$$

$\star$ $l = 2$:

$$a_{2,j}^u \overset{\text{def}}{=} \varepsilon^{j-1} c_{2,j}^{\oplus}, \quad b_{2,j}^u \overset{\text{def}}{=} \varepsilon^{j-1} s_{2,j}^{\oplus}.$$

$$\begin{cases} \boldsymbol{\phi}_{2,j}^{\varepsilon,\mathrm{c}} \cdot \boldsymbol{e}_r \overset{\text{def}}{=} j \left(\frac{r}{\varepsilon}\right)^{j-1} \sin(j\theta) \mathbb{1}_{1 \leqslant \varepsilon} \\ \qquad\qquad + j \left(j \left(\frac{\varepsilon}{r}\right)^{j-1} - (j-1) \left(\frac{\varepsilon}{r}\right)^{j+1} \right) \sin(j\theta) \mathbb{1}_{r > \varepsilon}, \\ \boldsymbol{\phi}_{2,j}^{\varepsilon,\mathrm{c}} \cdot \boldsymbol{e}_\theta \overset{\text{def}}{=} j \left(\frac{r}{\varepsilon}\right)^{j-1} \cos(j\theta) \mathbb{1}_{1 \leqslant \varepsilon} \\ \qquad\qquad + j \left((-j+2) \left(\frac{\varepsilon}{r}\right)^{j-1} + (j-1) \left(\frac{\varepsilon}{r}\right)^{j+1} \right) \cos(j\theta) \mathbb{1}_{r > \varepsilon}, \\ \boldsymbol{\phi}_{2,j}^{\varepsilon,\mathrm{s}} \cdot \boldsymbol{e}_r \overset{\text{def}}{=} - j \left(\frac{r}{\varepsilon}\right)^{j-1} \cos(j\theta) \mathbb{1}_{1 \leqslant \varepsilon} \\ \qquad\qquad - j \left(j \left(\frac{\varepsilon}{r}\right)^{j-1} - (j-1) \left(\frac{\varepsilon}{r}\right)^{j+1} \right) \cos(j\theta) \mathbb{1}_{r > \varepsilon}, \\ \boldsymbol{\phi}_{2,j}^{\varepsilon,\mathrm{s}} \cdot \boldsymbol{e}_\theta \overset{\text{def}}{=} j \left(\frac{r}{\varepsilon}\right)^{j-1} \sin(j\theta) \mathbb{1}_{1 \leqslant \varepsilon} \\ \qquad\qquad + j \left((-j+2) \left(\frac{\varepsilon}{r}\right)^{j-1} + (j-1) \left(\frac{\varepsilon}{r}\right)^{j+1} \right) \sin(j\theta) \mathbb{1}_{r > \varepsilon}. \end{cases}$$

- $\{j \geqslant 2,\, j \in \{N, N+1\}$:

$$
\begin{aligned}
&a^u_{1,j} = 0, \quad b^u_{1,j} = 0,\\
&a^u_{2,j} \overset{\text{def}}{=} \varepsilon^{j-1}((1+j)\varepsilon^2 c^{\oplus}_{1,j} + j c^{\oplus}_{2,j}), \quad b^u_{2,j} \overset{\text{def}}{=} \varepsilon^{j-1}((1+j)\varepsilon^2 s^{\oplus}_{1,j} + j s^{\oplus}_{2,j})
\end{aligned}
$$

$$
\begin{cases}
\boldsymbol{\phi}^{\varepsilon,\mathrm{c}}_{2,j} \cdot \boldsymbol{e}_r \overset{\text{def}}{=} \left(\dfrac{r}{\varepsilon}\right)^{j-1} \sin(j\theta)\mathbb{1}_{r\leqslant\varepsilon} \\
\qquad\qquad + \left(j\left(\dfrac{r}{\varepsilon}\right)^{j-1} - (j-1)\left(\dfrac{r}{\varepsilon}\right)^{j+1}\right)\sin(j\theta)\mathbb{1}_{r>\varepsilon}, \\
\boldsymbol{\phi}^{\varepsilon,\mathrm{c}}_{2,j} \cdot \boldsymbol{e}_\theta \overset{\text{def}}{=} \left(\dfrac{r}{\varepsilon}\right)^{j-1} \cos(j\theta)\mathbb{1}_{r\leqslant\varepsilon} \\
\qquad\qquad + \left((-j+2)\left(\dfrac{r}{\varepsilon}\right)^{j-1} + (j-1)\left(\dfrac{r}{\varepsilon}\right)^{j+1}\right)\cos(j\theta)\mathbb{1}_{r>\varepsilon}, \\
\boldsymbol{\phi}^{\varepsilon,\mathrm{s}}_{2,j} \cdot \boldsymbol{e}_r \overset{\text{def}}{=} -\left(\dfrac{r}{\varepsilon}\right)^{j-1} \cos(j\theta)\mathbb{1}_{r\leqslant\varepsilon} \\
\qquad\qquad + \left(j\left(\dfrac{r}{\varepsilon}\right)^{j-1} - (j-1)\left(\dfrac{r}{\varepsilon}\right)^{j+1}\right)\cos(j\theta)\mathbb{1}_{r>\varepsilon}, \\
\boldsymbol{\phi}^{\varepsilon,\mathrm{s}}_{2,j} \cdot \boldsymbol{e}_\theta \overset{\text{def}}{=} \left(\dfrac{r}{\varepsilon}\right)^{j-1} \sin(j\theta)\mathbb{1}_{r\leqslant\varepsilon} \\
\qquad\qquad + \left((-j+2)\left(\dfrac{r}{\varepsilon}\right)^{j-1} + (j-1)\left(\dfrac{r}{\varepsilon}\right)^{j+1}\right)\sin(j\theta)\mathbb{1}_{r>\varepsilon}.
\end{cases}
$$

4.A.7.2 Coefficients and singular functions for the pressure decomposition

In this section, we provide the expression of the coefficients a^p_j, b^p_j and singular functions $\varphi^{\varepsilon,\mathrm{c}}_j, \varphi^{\varepsilon,\mathrm{s}}_j$ for the decomposition of p^ε_N into a regular and singular part, as given in equation (4.3.31). Note that, as done for the velocity decomposition given in the previous section, from one case to another, if nothing is precised for the value of a function or a coefficient previously defined, it indicates that it remains unchanged from its previus definition. The enrichment functions for the pressure space in the augmented finite element method of Section 4.3.2 are given by:

- $N = 0$:

$$
a^p_1 = 4\frac{2\varepsilon^2 c^{\oplus}_{1,1} + c^{\oplus}_{2,1} + \boldsymbol{v}_{\mathrm{b}} \cdot \boldsymbol{e}_y}{2\log(\varepsilon) + 1}, \quad b^p_1 = -4\frac{2\varepsilon^2 s^{\oplus}_{1,1} + s^{\oplus}_{2,1} + \boldsymbol{v}_{\mathrm{b}} \cdot \boldsymbol{e}_x}{2\log(\varepsilon) + 1}
$$

$$
\varphi^{\varepsilon,\mathrm{c}}_1 \overset{\text{def}}{=} \left(\frac{1}{r}\right)\sin(\theta)\mathbb{1}_{r>\varepsilon}, \quad \varphi^{\varepsilon,\mathrm{s}}_1 \overset{\text{def}}{=} \left(\frac{1}{r}\right)\cos(\theta)\mathbb{1}_{r>\varepsilon}.
$$

- $N = 1$:

$$a_2^p \overset{\text{def}}{=} 4\varepsilon(3\varepsilon^2 c_{1,2}^{\oplus} + 2c_{2,2}^{\oplus}), \quad b_2^p \overset{\text{def}}{=} -4\varepsilon(3\varepsilon^2 s_{1,2}^{\oplus} + 2s_{2,2}^{\oplus})$$

$$\varphi_2^{\varepsilon,\mathrm{c}} = \left(\frac{1}{r}\right)^2 \sin(2\theta)\mathbb{1}_{r>\varepsilon}, \quad \varphi_2^{\varepsilon,\mathrm{s}} = \left(\frac{1}{r}\right)^2 \cos(2\theta)\mathbb{1}_{r>\varepsilon}$$

- $\{N \geqslant 2 \cap j \geqslant 3\}$:

$$a_j^p \overset{\text{def}}{=} 4\varepsilon^{j-1}(j-1)((1+j)\varepsilon^2 c_{1,j}^{\oplus} + jc_{2,j}^{\oplus}),$$
$$b_j^p \overset{\text{def}}{=} -4\varepsilon^{j-1}(j-1)((1+j)\varepsilon^2 s_{1,j}^{\oplus} + js_{2,j}^{\oplus}).$$

$$\varphi_j^{\varepsilon,\mathrm{c}} = \left(\frac{1}{r}\right)^j \sin(j\theta)\mathbb{1}_{r>\varepsilon}, \quad \varphi_j^{\varepsilon,\mathrm{s}} = \left(\frac{1}{r}\right)^j \cos(j\theta)\mathbb{1}_{r>\varepsilon}$$

4.A.8 Stream functions associated to the enrichment velocities of the augmented finite element method

The additive divergence free functions corresponding to the enrichement velocities defined in Section 4.3.2 are given by:

- $N \in \{0, 1\}$:

$$\begin{cases} \psi_{1,1}^{\varepsilon,\mathrm{c}} \overset{\text{def}}{=} -\varepsilon\left(\frac{r}{\varepsilon}\right)\cos(\theta)\mathbb{1}_{r\leqslant\varepsilon} \\ \qquad\qquad -\varepsilon\left(\frac{2\log(r)}{2\log(\varepsilon)+1}\left(\frac{r}{\varepsilon}\right) + \frac{1}{2\log(\varepsilon)+1}\left(\frac{\varepsilon}{r}\right)\right)\cos(\theta)\mathbb{1}_{r>\varepsilon}, \\ \psi_{1,1}^{\varepsilon,\mathrm{s}} \overset{\text{def}}{=} \varepsilon\left(\frac{r}{\varepsilon}\right)\sin(\theta)\mathbb{1}_{r\leqslant\varepsilon} \\ \qquad +\varepsilon\left(\frac{2}{2\log(\varepsilon)+1}\left(\frac{r}{\varepsilon}\right)\log(r) + \frac{1}{2\log(\varepsilon)+1}\left(\frac{\varepsilon}{r}\right)\right)\sin(\theta)\mathbb{1}_{r>\varepsilon}, \end{cases}$$

- $N = 1$:

$$\begin{cases} \tilde{\psi}_0^{\varepsilon,\mathrm{c}} \overset{\text{def}}{=} -\frac{\varepsilon}{2}\left(\left(\frac{r}{\varepsilon}\right)^2 - (2\log\left(\frac{\varepsilon}{\rho}\right)+1)\right)\mathbb{1}_{r\leqslant\varepsilon} + \varepsilon\log(\frac{r}{\rho})\mathbb{1}_{r>\varepsilon}, \\ \psi_0^{\varepsilon,\mathrm{c}} \overset{\text{def}}{=} \tilde{\psi}_0^{\varepsilon,\mathrm{c}} - \int_{\omega^\rho} \tilde{\psi}_0^{\varepsilon,\mathrm{c}}, \\ \psi_{1,2}^{\varepsilon,\mathrm{c}} \overset{\text{def}}{=} -\varepsilon\left(\frac{r}{\varepsilon}\right)^2\cos(2\theta)\mathbb{1}_{r>\varepsilon} + \varepsilon\left(-2 + \left(\frac{\varepsilon}{r}\right)^2\right)\cos(2\theta)\mathbb{1}_{r>\varepsilon} \\ \psi_{1,2}^{\varepsilon,\mathrm{s}} \overset{\text{def}}{=} \varepsilon\left(\frac{r}{\varepsilon}\right)^2\sin(2\theta)\mathbb{1}_{r\leqslant\varepsilon} + \varepsilon(2 - \left(\frac{r}{\varepsilon}\right)^2\sin(2\theta))\mathbb{1}_{r>\varepsilon} \end{cases}$$

- $\{N \geqslant 2,\, j = 0\}$:

$$\begin{cases} \psi_{1,1}^{\varepsilon,\mathrm{c}} \overset{\text{def}}{=} -\varepsilon \left(\frac{r}{\varepsilon}\right)^3 \cos(\theta) \mathbb{1}_{r \leqslant \varepsilon} \\ \qquad -\varepsilon \left(\frac{4\log(r)}{2\log(\varepsilon)+1} \left(\frac{r}{\varepsilon}\right) - \frac{2\log(\varepsilon)-1}{2\log(\varepsilon)+1} \left(\frac{\varepsilon}{r}\right) \right) \cos(\theta) \mathbb{1}_{r > \varepsilon}, \\ \psi_{1,1}^{\varepsilon,\mathrm{s}} \overset{\text{def}}{=} \varepsilon \left(\frac{r}{\varepsilon}\right)^3 \sin(\theta) \mathbb{1}_{r \leqslant \varepsilon} \\ \qquad +\varepsilon \left(\frac{4\log(r)}{2\log(\varepsilon)+1} \left(\frac{r}{\varepsilon}\right) - \frac{2\log(\varepsilon)-1}{2\log(\varepsilon)+1} \left(\frac{\varepsilon}{r}\right) \right) \sin(\theta) \mathbb{1}_{r > \varepsilon}, \\ \psi_{2,1}^{\varepsilon,\mathrm{c}} \overset{\text{def}}{=} -\varepsilon \left(\frac{r}{\varepsilon}\right) \cos(\theta) \mathbb{1}_{r \leqslant \varepsilon} \\ \qquad -\varepsilon \left(\frac{2\log(r)}{2\log(\varepsilon)+1} \left(\frac{r}{\varepsilon}\right) + \frac{1}{2\log(\varepsilon)+1} \left(\frac{\varepsilon}{r}\right) \right) \cos(\theta) \mathbb{1}_{r > \varepsilon}, \\ \psi_{2,1}^{\varepsilon,\mathrm{s}} \overset{\text{def}}{=} \varepsilon \left(\frac{r}{\varepsilon}\right) \sin(\theta) \mathbb{1}_{r \leqslant \varepsilon} \\ \qquad +\varepsilon \left(\frac{2\log(r)}{2\log(\varepsilon)+1} \left(\frac{r}{\varepsilon}\right) + \frac{1}{2\log(\varepsilon)+1} \left(\frac{\varepsilon}{r}\right) \right) \sin(\theta) \mathbb{1}_{r > \varepsilon}, \end{cases}$$

- $\{N \geqslant 2,\, j \geqslant 2\}$:

$$\begin{cases} \psi_{1,j}^{\varepsilon,\mathrm{c}} \overset{\text{def}}{=} -\varepsilon \left(\frac{r}{\varepsilon}\right)^{j+2} \cos(j\theta) \mathbb{1}_{1 \leqslant \varepsilon} \\ \qquad -\varepsilon \left((1+j) \left(\frac{\varepsilon}{r}\right)^{j-2} - j \left(\frac{\varepsilon}{r}\right)^{j} \right) \cos(j\theta) \mathbb{1}_{r > \varepsilon}, \\ \psi_{1,j}^{\varepsilon,\mathrm{s}} \overset{\text{def}}{=} \varepsilon \left(\frac{r}{\varepsilon}\right)^{j+2} \sin(j\theta) \mathbb{1}_{1 \leqslant \varepsilon} \\ \qquad +\varepsilon \left((1+j) \left(\frac{\varepsilon}{r}\right)^{j-2} - j \left(\frac{\varepsilon}{r}\right)^{j} \right) \sin(j\theta) \mathbb{1}_{r > \varepsilon}, \\ \psi_{2,j}^{\varepsilon,\mathrm{c}} \overset{\text{def}}{=} -\varepsilon \left(\frac{r}{\varepsilon}\right)^{j} \cos(j\theta) \mathbb{1}_{1 \leqslant \varepsilon} \\ \qquad -\varepsilon \left(j \left(\frac{\varepsilon}{r}\right)^{j-2} - (j-1) \left(\frac{\varepsilon}{r}\right)^{j} \right) \cos(j\theta) \mathbb{1}_{r > \varepsilon}, \\ \psi_{2,j}^{\varepsilon,\mathrm{s}} \overset{\text{def}}{=} \varepsilon \left(\frac{r}{\varepsilon}\right)^{j} \sin(j\theta) \mathbb{1}_{1 \leqslant \varepsilon} \\ \qquad +\varepsilon \left(j \left(\frac{\varepsilon}{r}\right)^{j-2} - (j-1) \left(\frac{\varepsilon}{r}\right)^{j} \right) \sin(j\theta) \mathbb{1}_{r > \varepsilon}, \end{cases}$$

- $j \in \{N,\, N+1\}$:

$$\begin{cases} \psi_{2,j}^{\varepsilon,\mathrm{c}} \overset{\text{def}}{=} -\varepsilon \left(\dfrac{r}{\varepsilon}\right)^j \cos(j\theta)\mathbb{1}_{1\leqslant\varepsilon} \\ \qquad\qquad -\varepsilon \left(j\left(\dfrac{\varepsilon}{r}\right)^{j-2} - (j-1)\left(\dfrac{\varepsilon}{r}\right)^j\right)\cos(j\theta)\mathbb{1}_{r>\varepsilon}, \\ \psi_{2,j}^{\varepsilon,\mathrm{s}} \overset{\text{def}}{=} \varepsilon \left(\dfrac{r}{\varepsilon}\right)^j \sin(j\theta)\mathbb{1}_{1\leqslant\varepsilon} \\ \qquad +\varepsilon \left(j\left(\dfrac{\varepsilon}{r}\right)^{j-2} - (j-1)\left(\dfrac{\varepsilon}{r}\right)^j\right)\sin(j\theta)\mathbb{1}_{r>\varepsilon}, \end{cases}$$

4.A.9 Proof of Theorem 4.3.4

Restated Theorem 4.3.4. *Let X_h be a subspace of X, $Q_{h,1}$ a subspace of Q_1 and $Q_{h,2}$ a subspace of Q_2. Assume that $Q_{h,1}$ and $Q_{h,2}$ are finite dimensional and consider the approximate problem: find $(u_h, \lambda_{h,1}, \lambda_{h,2}) \in X_h \times Q_{h,1} \times Q_{h,2}$ such that*

$$\begin{aligned} a(u_h, v_h) - b_1(\lambda_{h,1}, v_h) - b_2(\lambda_{h,2}, v_h) &= d(v_h) \quad \forall v_h \in X_h, \\ b_1(\mu_{h,1}, u_h) &= c_1(\mu_{h,1}) \quad \forall \mu_{h,1} \in Q_{h,1}, \\ b_2(\mu_{h,2}, u_h) &= c_2(\mu_{h,2}) \quad \forall \mu_{h,2} \in Q_{h,2}. \end{aligned} \tag{4.A.57}$$

Let

$$Z_{h,b_i} \overset{\text{def}}{=} \{v_h \in X_h \mid b_i(\mu_{h,i}, v_h) = 0 \quad \forall \mu_{h,i}\} \subset X_h \quad i = 1,\, 2.$$

We suppose that there exists $\beta_{h,1} > 0$, $\beta_{h,2} > 0$ such that

$$\sup_{v_h \in Z_{h,b_2}} \frac{b_1(\lambda_{h,1}, v_h)}{\|v_h\|_X} \geqslant \beta_{h,1}\|\lambda_{h,1}\|_{Q_1} \quad \forall \lambda_{h,1} \in Q_{h,1}, \tag{4.A.58}$$

$$\sup_{v_h \in Z_{h,b_1}} \frac{b_2(\lambda_{h,2}, v_h)}{\|v_h\|_X} \geqslant \beta_{h,2}\|\lambda_{h,2}\|_{Q_2} \quad \forall \lambda_{h,2} \in Q_{h,2}.. \tag{4.A.59}$$

and that there exists α such that

$$a(v_h, v_h) \geqslant \alpha \|v_h\|_X^2. \tag{4.A.60}$$

Then Problem (4.A.57) *is well posed and satisfies the estimates*

$$\begin{aligned}
\|u-u_h\|_X &\leqslant a_{1h}\inf_{v_h\in X_h}\|u-v_h\|_X \\
&\quad + a_{2h}\inf_{\mu_{h,1}\in Q_{h,1}}\|\lambda_1-\mu_{h,1}\|_{Q_1} + a_{3h}\inf_{\mu_{h,2}\in Q_{h,2}}\|\lambda_2-\mu_{h,2}\|_{Q_2}.\\
\|\lambda_1-\lambda_{h,1}\|_{Q_1} &\leqslant b_{1h}\inf_{v_h\in X_h}\|u-v_h\|_X \\
&\quad + b_{2h}\inf_{\mu_{h,1}\in Q_{h,1}}\|\lambda_1-\mu_{h,1}\|_{Q_1} + b_{3h}\inf_{\mu_{h,2}\in Q_{h,2}}\|\lambda_2-\mu_{h,2}\|_{Q_2}.\\
\|\lambda_2-\lambda_{h,2}\|_{Q_1} &\leqslant c_{1h}\inf_{v_h\in X_h}\|u-v_h\|_X + \\
&\quad + c_{2h}\inf_{\mu_{h,1}\in Q_{h,1}}\|\lambda_1-\mu_{h,1}\|_{Q_1} + c_{3h}\inf_{\mu_{h,2}\in Q_{h,2}}\|\lambda_2-\mu_{h,2}\|_{Q_2}.
\end{aligned}$$

with

$$\begin{aligned}
a_{1h} &= \left(1+\frac{\|a\|}{\alpha}\right)\left(1+\frac{\|b_1\|}{\beta_{1,h}}+\frac{\|b_2\|}{\beta_{2,h}}\right),\\
a_{2h} &= \begin{cases}\dfrac{\|b_1\|}{\alpha} & \textit{if}\quad Z_{h,b_1}\not\subset Z_{b_1},\\ 0 & \textit{otherwise}\end{cases}\\
a_{3h} &= \begin{cases}\dfrac{\|b_2\|}{\alpha} & \textit{if}\quad Z_{h,b_2}\not\subset Z_{b_2},\\ 0 & \textit{otherwise}\end{cases}\\
b_{1h} &= a_{1h}\frac{\|a\|}{\beta_{h,1}},\quad b_{2h}=1+\frac{\|b_1\|}{\beta_{h,1}}+a_{2h}\frac{\|a\|}{\beta_{h,1}},\quad b_{3h}=a_{3h}\frac{\|a\|}{\beta_{h,1}},\\
c_{1h} &= a_{1h}\frac{\|a\|}{\beta_{h,2}},\quad c_{2h}=a_{2h}\frac{\|a\|}{\beta_{h,2}},\quad c_{3h}=1+\frac{\|b_2\|}{\beta_{h,2}}+a_{3h}\frac{\|a\|}{\beta_{h,2}}.
\end{aligned}$$

Proof of Theorem 4.3.4. First, let us notice that the conditions (4.A.58) and (4.A.59) imply that there exists $w_{h,1}\in Z_{h,b_2}$ and $w_{h,2}\in Z_{h,b_1}$ such that

$$\begin{aligned}
b_1(\mu_{h,1},w_{h,1}) &= b_1(\mu_{h,1},u-v_h)\quad \forall\mu_{h,1}\in Q_{h,1},\quad \beta_{h,1}\|w_{h,1}\|_X\leqslant\|b_1\|\|u-v_h\|_X,\\
b_2(\mu_{h,2},w_{h,2}) &= b_2(\mu_{h,2},u-v_h)\quad \forall\mu_{h,2}\in Q_{h,2},\quad \beta_{h,2}\|w_{h,2}\|_X\leqslant\|b_2\|\|u-v_h\|_X.
\end{aligned}$$

Setting now $\kappa_h=w_{h,1}+w_{h,2}+v_h$, it is clear that

$$\begin{aligned}
b_1(\mu_{h,1},\kappa_h) &= b_1(\mu_{h,1},u)=d_1(\mu_{h,1})=b_1(\mu_{h,1},u_h)\quad\forall\mu_{h,1}\in Q_{h,1},\\
b_2(\mu_{h,2},\kappa_h) &= b_2(\mu_{h,2},u)=d_2(\mu_{h,1})=b_2(\mu_{2,h},u_h)\quad\forall\mu_{h,2}\in Q_{h,2}.
\end{aligned}$$

We deduce then that $y_h\overset{\text{def}}{=}u_h-k_h\in Z_{b_1,h}\cap Z_{b_2,h}$. Besides, the coercivity assumption

(4.A.60) on a implies

$$\begin{aligned}\alpha\|u_h-\kappa_h\|_X &\leqslant \frac{a(u_h-\kappa_h,y_h)}{\|u_h-\kappa_h\|_X} \leqslant \frac{a(u_h-u,y_h)+a(u-\kappa_h,y_h)}{\|y_h\|_X}\\ &\leqslant \frac{b_1(\lambda_1-\lambda_{h,1},y_h)+b_2(\lambda_2-\lambda_{h,2},y_h)+a(u-\kappa_h,y_h)}{\|y_h\|_X}\end{aligned}$$

If $Z_{h,b_1}\subset Z_{b_1}$ and $Z_{h,b_2}\subset Z_{b_2}$ then

$$\alpha\|u_h-k_h\|_X \leqslant \|a\|\|u-w_h\|_X$$

Using the triangle inequality yields

$$\|u-u_h\|_X \leqslant \left(1+\frac{\|a\|}{\alpha}\right)\|u-\kappa_h\|_X.$$

It $Z_{h,b_1}\subset Z_{b_1}$ and $Z_{h,b_2}\nsubseteq Z_{b_2}$ then

$$b_1(\lambda_1-\lambda_{h,1},y_h)=0$$

and

$$b_2(\lambda_{h,2},y_h)=0=b_2(\mu_{h,2},y_h)\quad \forall\mu_{h,2}\in Q_{h,2}.$$

Since $y_h\in Z_{h,b_2}$, it implies

$$\alpha\|u_h-\kappa_h\|_X \leqslant \|a\|\|u-\kappa_h\|_X+\|b_2\|\|\lambda_2-\mu_{h,2}\|_{Q_2}$$

Using the triangle inequalities yields

$$\|u-u_h\|_X \leqslant \left(1+\frac{\|a\|}{\alpha}\right)\|u-\kappa_h\|_X+\frac{\|b_2\|}{\alpha}\|\lambda_2-\mu_{h,2}\|_{Q_2}$$

The estimate on $\|u-u_h\|_X$ then results on from the inequality

$$\|u-\kappa_h\|_X \leqslant \|u-v_h\|_X+\|\kappa_h\|_X \leqslant \left(1+\frac{\|b_1\|}{\beta_{h,1}}+\frac{\|b_2\|}{\beta_{h,2}}\right)\|u-v_h\|_X.$$

Symetrically, if $Z_{h,b_2}\subset Z_{b_2}$ and $Z_{h,b_1}\nsubseteq Z_{b_1}$

$$\|u-u_h\|_X \leqslant \left(1+\frac{\|a\|}{\alpha}\right)\left(1+\frac{\|b_1\|}{\beta_{h,1}}+\frac{\|b_2\|}{\beta_{h,2}}\right)\|u-v_h\|_X+\frac{\|b_1\|}{\alpha}\|\lambda_1-\mu_{h,1}\|_{Q_1}$$

Eventually, doing the same steps as before, if if $Z_{h,b_2}\nsubseteq Z_{b_2}$ and $Z_{h,b_1}\nsubseteq Z_{b_1}$, we have

$$\begin{aligned}\|u-u_h\|_X \leqslant \left(1+\frac{\|a\|}{\alpha}\right)\left(1+\frac{\|b_1\|}{\beta_{h,1}}+\frac{\|b_2\|}{\beta_{h,2}}\right)&\|u-v_h\|_X\\ &+\frac{\|b_1\|}{\alpha}\|\lambda_1-\mu_{h,1}\|_{Q_1}+\frac{\|b_2\|}{\alpha}\|\lambda_2-\mu_{h,2}\|_{Q_2}\end{aligned}$$

Now, to estimate $\|\lambda_1 - \lambda_{h,1}\|_{Q_1}$, we notice that, since for all $v_h \in Z_{h,b_2}$, $b_1(\lambda_1 - \lambda_{h,1}, v_h) = a(u_h - u, v_h)$, we have

$$b_1(v_h, \mu_{h,1} - \lambda_{h,1}) = a(u_h - u, v_h) + b(v_h, \mu_{1,h} - \lambda) \quad \forall (v_h, \mu_{1,h}) \in X_h \times Q_{h,1}.$$

Condition (4.A.58) then implies

$$\beta_{1,h}\|\lambda_{h,1} - \mu_{h,1}\|_{Q_1} \leqslant \|a\|\|u - u_h\| + \|b_1\|\|\lambda_1 - \mu_{h,1}\| \quad \forall \mu_{h,1} \in Q_{h,1}.$$

The final result follows by triangle inequalities. The same arguments apply to estimate $\|\lambda_2 - \lambda_{h,2}\|$. □

4.A.10 Proof of Lemma 4.3.5

Restated Lemma 4.3.5. *Let $\boldsymbol{\eta} \in \boldsymbol{H}^{\frac{1}{2}}(\partial\omega^\varepsilon)$ be given, there exists $\tilde{\boldsymbol{v}}_{\boldsymbol{\eta}}^\varepsilon \in \boldsymbol{V}_{N,h}^k$ and $\tilde{\rho} > 0$ such that that for $\varepsilon \in (0, \tilde{\rho})$,*

$$(\boldsymbol{\mu}_N, \tilde{\boldsymbol{v}}_{\boldsymbol{\eta}}^\varepsilon)_\varepsilon = (\boldsymbol{\mu}_N, \boldsymbol{\eta})_\varepsilon \quad \forall \boldsymbol{\mu}_N \in \boldsymbol{F}_N, \quad \|\tilde{\boldsymbol{v}}_{\boldsymbol{\eta}}^\varepsilon\|_{1,\Omega} \lesssim \|\boldsymbol{\eta}\|_{\frac{1}{2},\varepsilon}.$$

Moreover, for any $\tilde{q}_h \in Q_{N,h}^{k-1}$,

$$(\tilde{q}_h, \operatorname{div} \tilde{\boldsymbol{v}}_{\boldsymbol{\eta}}^\varepsilon)_\Omega = 0.$$

Proof of Lemma 4.3.5. By definition of the enrichment functions $\tilde{\boldsymbol{\phi}}_{l,j}^{\varepsilon,m}$ we have

$$\tilde{\boldsymbol{\phi}}_{l,j}^{\varepsilon,m} = \mathbf{curl}\,(\chi\psi_{l,j}^{\varepsilon,m}) = \psi_{l,j}^{\varepsilon,m}\mathbf{curl}\,\chi + \chi\mathbf{curl}\,\psi_{l,j}^{\varepsilon,m} = \psi_{l,j}^{\varepsilon,m}\mathbf{curl}\,\chi + \chi\boldsymbol{\phi}_{l,j}^{\varepsilon,m}.$$

Furthermore, since $\operatorname{supp}\,(\mathbf{curl}\,\chi) \subset \omega^{\frac{3}{4}\rho}\backslash\overline{\omega^{\frac{1}{2}\rho}}$, we deduce in particular that

$$\tilde{\boldsymbol{\phi}}_{l,j}^{\varepsilon,m} = \boldsymbol{\phi}_{j,k}^{\varepsilon,m} \quad \text{on} \quad \partial\omega^\varepsilon.$$

By using the explicit expressions of the $\boldsymbol{\phi}_{l,j}^{\varepsilon,m}$ given in Section 4.A.7.1, we get

- $N = 0$:

$$\begin{cases} \boldsymbol{\phi}_{1,1}^{\varepsilon,\mathrm{c}} = \sin(\theta)\boldsymbol{e}_r + \cos(\theta)\boldsymbol{e}_\theta, \\ \boldsymbol{\phi}_{1,1}^{\varepsilon,\mathrm{s}} = -\cos(\theta)\boldsymbol{e}_r + \sin(\theta)\boldsymbol{e}_\theta, \end{cases}$$

- $\{N \geqslant 1,\ j = 0\}$:

$$\boldsymbol{\phi}_{1,0}^{\varepsilon,\mathrm{c}} = \boldsymbol{e}_\theta,$$

- $\{N \geqslant 1,\, j \in \{1, \dots, N-1\}\}$:

$$\begin{cases} \dfrac{1}{j}\boldsymbol{\phi}^{\varepsilon,\mathrm{c}}_{2,j} = \sin(j\theta)\boldsymbol{e}_r + \cos(j\theta)\boldsymbol{e}_\theta, \\ \dfrac{1}{j}\left((1+j)\boldsymbol{\phi}^{\varepsilon,\mathrm{c}}_{2,j} - \boldsymbol{\phi}^{\varepsilon,\mathrm{c}}_{1,j}\right) = \sin(j\theta)\boldsymbol{e}_r - \cos(j\theta)\boldsymbol{e}_\theta, \\ \dfrac{1}{j}\boldsymbol{\phi}^{\varepsilon,\mathrm{s}}_{2,j} = -\cos(j\theta)\boldsymbol{e}_r + \sin(j\theta)\boldsymbol{e}_\theta, \\ \dfrac{1}{j}(\boldsymbol{\phi}^{\varepsilon,\mathrm{s}}_{1,j} - (1+j)\boldsymbol{\phi}^{\varepsilon,\mathrm{s}}_{2,j}) = \cos(j\theta)\boldsymbol{e}_r + \sin(j\theta)\boldsymbol{e}_\theta. \end{cases}$$

- $\{N \geqslant 1,\, j \in \{N, N+2\}\}$:

$$\begin{cases} \boldsymbol{\phi}^{\varepsilon,\mathrm{c}}_{1,j} = \sin(j\theta)\boldsymbol{e}_r + \cos(j\theta)\boldsymbol{e}_\theta \\ \boldsymbol{\phi}^{\varepsilon,\mathrm{s}}_{1,j} = -\cos(j\theta)\boldsymbol{e}_r + \sin(j\theta)\boldsymbol{e}_\theta \end{cases}$$

We deduce that

$\star$ $j = 0$:

$$\begin{cases} \boldsymbol{\xi}^{\varepsilon,\mathrm{c}}_{x,0} \overset{\text{def}}{=} -\boldsymbol{\phi}^{\varepsilon,\mathrm{s}}_{1,1} = \boldsymbol{e}_x \quad \text{on} \quad \partial\omega^\varepsilon, \\ \boldsymbol{\xi}^{\varepsilon,\mathrm{c}}_{y,0} \overset{\text{def}}{=} \boldsymbol{\phi}^{\varepsilon,\mathrm{c}}_{1,1} = \boldsymbol{e}_y \quad \text{on} \quad \partial\omega^\varepsilon, \end{cases}$$

$\star$ $j = 1$

$$\begin{aligned} &\boldsymbol{\xi}^{\varepsilon,\star}_1 \overset{\text{def}}{=} -\boldsymbol{\phi}^{\varepsilon,\mathrm{s}}_{2,2} = \cos(\theta)\boldsymbol{e}_x - \sin(\theta)\boldsymbol{e}_y, \\ &\boldsymbol{\xi}^{\varepsilon,\mathrm{s}}_{x,1} \overset{\text{def}}{=} \frac{1}{2}\left(\frac{1}{2}\boldsymbol{\phi}^{\varepsilon,\mathrm{c}}_{2,2} - \boldsymbol{\phi}^{\varepsilon,\mathrm{c}}_{1,0}\right) = \sin(\theta)\boldsymbol{e}_x \quad \text{on} \quad \partial\omega^\varepsilon, \\ &\boldsymbol{\xi}^{\varepsilon,\mathrm{c}}_{y,1} \overset{\text{def}}{=} \frac{1}{2}\left(\frac{1}{2}\boldsymbol{\phi}^{\varepsilon,\mathrm{c}}_{2,2} + \boldsymbol{\phi}^{\varepsilon,\mathrm{c}}_{1,0}\right) = \cos(\theta)\boldsymbol{e}_y \quad \text{on} \quad \partial\omega^\varepsilon \end{aligned}$$

$\star$ $j \geqslant 2$

$$\begin{cases} \boldsymbol{\xi}^{\varepsilon,\mathrm{c}}_{x,j} \overset{\text{def}}{=} \dfrac{1}{2}\left(\dfrac{1}{j-1}(\boldsymbol{\phi}^{\varepsilon,\mathrm{s}}_{1,j-1} - j\boldsymbol{\phi}^{\varepsilon,\mathrm{s}}_{2,j-1}) - \dfrac{1}{j+1}\boldsymbol{\phi}^{\varepsilon,\mathrm{s}}_{2,j+1}\right) = \cos(j\theta)\boldsymbol{e}_x, \\ \boldsymbol{\xi}^{\varepsilon,\mathrm{s}}_{y,j} \overset{\text{def}}{=} \dfrac{1}{2}\left(\dfrac{1}{j-1}(\boldsymbol{\phi}^{\varepsilon,\mathrm{s}}_{1,j-1} - j\boldsymbol{\phi}^{\varepsilon,\mathrm{s}}_{2,j-1}) + \dfrac{1}{j+1}\boldsymbol{\phi}^{\varepsilon,\mathrm{s}}_{2,j+1}\right) = \sin(j\theta)\boldsymbol{e}_y, \\ \boldsymbol{\xi}^{\varepsilon,\mathrm{s}}_{x,j} \overset{\text{def}}{=} \dfrac{1}{2}\left(\dfrac{1}{j+1}\boldsymbol{\phi}^{\varepsilon,\mathrm{c}}_{2,j+1} + \dfrac{1}{j-1}\left(j\boldsymbol{\phi}^{\varepsilon,\mathrm{s}}_{2,j-1} - \boldsymbol{\phi}^{\varepsilon,\mathrm{s}}_{1,j-1}\right)\right) = \sin(j\theta)\boldsymbol{e}_x, \\ \boldsymbol{\xi}^{\varepsilon,\mathrm{c}}_{y,j} \overset{\text{def}}{=} \dfrac{1}{2}\left(\dfrac{1}{j+1}\boldsymbol{\phi}^{\varepsilon,\mathrm{c}}_{2,j+1} - \dfrac{1}{j-1}\left(j\boldsymbol{\phi}^{\varepsilon,\mathrm{s}}_{2,j-1} - \boldsymbol{\phi}^{\varepsilon,\mathrm{s}}_{1,j-1}\right)\right) = \cos(j\theta)\boldsymbol{e}_y. \end{cases}$$

Let $\zeta_{x,j}^{\varepsilon,m} \in H^2(\omega^\rho) \cap L_0^2(\omega^\rho)$, resp. $\zeta_{y,j}^{\varepsilon,m} \in H^2(\omega^\rho) \cap L_0^2(\omega^\rho)$, be stream functions associated to the functions $\boldsymbol{\xi}_{x,j}^{\varepsilon,m}$, resp. $\boldsymbol{\xi}_{y,j}^{\varepsilon,m}$, for any $\boldsymbol{\eta} \in \boldsymbol{H}^{\frac{1}{2}}(\partial\omega^\varepsilon)$, we set $\overset{\star}{\psi}{}_{\boldsymbol{\eta}}^{\varepsilon} \in H^2(\omega^\rho) \cap L_0^2(\omega^\rho)$ and $\overset{\star}{\boldsymbol{v}}{}_{\boldsymbol{\eta}}^{\varepsilon}$ such that

$$
\begin{cases}
\overset{\star}{\boldsymbol{v}}{}_{\boldsymbol{\eta}}^{\varepsilon} \overset{\text{def}}{=} \mathscr{F}_0^{\text{c}}(\boldsymbol{\mu}(\varepsilon)\cdot\boldsymbol{e}_*)\boldsymbol{\xi}_1^* \\
\qquad + \mathscr{F}_0^{\text{c}}(\boldsymbol{\mu}(\varepsilon)\cdot\boldsymbol{e}_x)\boldsymbol{\xi}_{x,0}^{\varepsilon,\text{c}} + \displaystyle\sum_{j=1}^{n} \mathscr{F}_j^{\text{c}}(\boldsymbol{\mu}(\varepsilon)\cdot\boldsymbol{e}_x)\boldsymbol{\xi}_{x,j}^{\varepsilon,\text{c}} + \mathscr{F}_j^{\text{s}}(\boldsymbol{\mu}(\varepsilon)\cdot\boldsymbol{e}_x)\boldsymbol{\xi}_{x,j}^{\varepsilon,\text{s}} \\
\qquad + \mathscr{F}_0^{\text{c}}(\boldsymbol{\mu}(\varepsilon)\cdot\boldsymbol{e}_y)\boldsymbol{\xi}_{y,0}^{\varepsilon,\text{c}} + \displaystyle\sum_{j=1}^{n} \mathscr{F}_j^{\text{c}}(\boldsymbol{\mu}(\varepsilon)\cdot\boldsymbol{e}_y)\boldsymbol{\xi}_{y,j}^{\varepsilon,\text{c}} + \mathscr{F}_j^{\text{s}}(\boldsymbol{\mu}(\varepsilon)\cdot\boldsymbol{e}_y)\boldsymbol{\xi}_{y,j}^{\varepsilon,\text{s}} \\
\overset{\star}{\psi}{}_{\boldsymbol{\eta}}^{\varepsilon} \overset{\text{def}}{=} \mathscr{F}_0^{\text{c}}(\boldsymbol{\mu}(\varepsilon)\cdot\boldsymbol{e}_*)\zeta_1^* \\
\qquad + \mathscr{F}_0^{\text{c}}(\boldsymbol{\mu}(\varepsilon)\cdot\boldsymbol{e}_x)\zeta_{x,0}^{\varepsilon,\text{c}} + \displaystyle\sum_{j=1}^{n} \mathscr{F}_j^{\text{c}}(\boldsymbol{\mu}(\varepsilon)\cdot\boldsymbol{e}_x)\zeta_{x,j}^{\varepsilon,\text{c}} + \mathscr{F}_j^{\text{s}}(\boldsymbol{\mu}(\varepsilon)\cdot\boldsymbol{e}_x)\zeta_{x,j}^{\varepsilon,\text{s}} \\
\qquad + \mathscr{F}_0^{\text{c}}(\boldsymbol{\mu}(\varepsilon)\cdot\boldsymbol{e}_y)\zeta_{y,0}^{\varepsilon,\text{c}} + \displaystyle\sum_{j=1}^{n} \mathscr{F}_j^{\text{c}}(\boldsymbol{\mu}(\varepsilon)\cdot\boldsymbol{e}_y)\zeta_{y,j}^{\varepsilon,\text{c}} + \mathscr{F}_j^{\text{s}}(\boldsymbol{\mu}(\varepsilon)\cdot\boldsymbol{e}_y)\zeta_{y,j}^{\varepsilon,\text{s}}
\end{cases}
$$

We then define $\tilde{\boldsymbol{v}}_{\boldsymbol{\eta}}^{\varepsilon} \overset{\text{def}}{=} \textbf{curl}\,(\chi\overset{\star}{\psi}{}_{\boldsymbol{\eta}}^{\varepsilon})$. By construction we have $\boldsymbol{\Pi}_N^{\varepsilon}(\tilde{\boldsymbol{v}}_{\boldsymbol{\eta}}^{\varepsilon}) = \boldsymbol{\Pi}_N^{\varepsilon}(\boldsymbol{\eta})$. Moreover, since $\tilde{\boldsymbol{v}}_{\boldsymbol{\eta}}^{\varepsilon} = \textbf{curl}\,(\chi\overset{\star}{\psi}{}_{\boldsymbol{\eta}}^{\varepsilon}) = \chi\overset{\star}{\boldsymbol{v}}{}_{\boldsymbol{\eta}}^{\varepsilon} + \overset{\star}{\psi}{}_{\boldsymbol{\eta}}^{\varepsilon}\textbf{curl}\,\chi$, we deduced

$$
\|\tilde{\boldsymbol{v}}_{\boldsymbol{\eta}}^{\varepsilon}\|_{1,\Omega} \lesssim \|\overset{\star}{\boldsymbol{v}}{}_{\boldsymbol{\eta}}^{\varepsilon}\|_{\omega^\rho} + \|\overset{\star}{\psi}{}_{\boldsymbol{\eta}}^{\varepsilon}\|_{\omega^\rho}.
$$

On on hand, by construction, $\overset{\star}{\boldsymbol{v}}{}_{\boldsymbol{\eta}}^{\varepsilon}$ is solution of: find $(\overset{\star}{\boldsymbol{v}}{}_{\boldsymbol{\eta}}^{\varepsilon}, \overset{\star}{p}{}_{\boldsymbol{\eta}}^{\varepsilon}) \in \boldsymbol{V} \times Q$ such that

$$
\begin{cases}
-\Delta\overset{\star}{\boldsymbol{v}}{}_{\boldsymbol{\eta}}^{\varepsilon} + \nabla\overset{\star}{p}{}_{\boldsymbol{\eta}}^{\varepsilon} = 0 \quad \text{in} \quad \omega^\rho\backslash\omega^\varepsilon, \\
-\Delta\overset{\star}{\boldsymbol{v}}{}_{\boldsymbol{\eta}}^{\varepsilon} + \nabla\overset{\star}{p}{}_{\boldsymbol{\eta}}^{\varepsilon} = 0 \quad \text{in} \quad \omega^\varepsilon, \\
\qquad \overset{\star}{\boldsymbol{v}}{}_{\boldsymbol{\eta}}^{\varepsilon} = \boldsymbol{\Pi}_N^{\varepsilon}(\boldsymbol{\eta}) \quad \text{on} \quad \partial\omega^\varepsilon, \\
\qquad\qquad \overset{\star}{\boldsymbol{v}}{}_{\boldsymbol{\eta}}^{\varepsilon} = \overset{\star}{\boldsymbol{v}}{}_{\boldsymbol{\eta}}^{\varepsilon} \quad \text{on} \quad \partial\omega^\rho.
\end{cases}
$$

We deduce from Lemma 4.2.2 and Lemma 4.A.1, and the continuity of $\boldsymbol{\Pi}_N^{\varepsilon}$ on $(\boldsymbol{H}^{\frac{1}{2}}(\partial\omega^\varepsilon), \|\cdot\|_{\frac{1}{2},\varepsilon})$ given in (4.2.4),

$$
\|\overset{\star}{\boldsymbol{v}}{}_{\boldsymbol{\eta}}^{\varepsilon}\|_{1,\omega^\rho} \lesssim \|\boldsymbol{\eta}\|_{\frac{1}{2},\varepsilon} + \|\overset{\star}{\boldsymbol{v}}{}_{\boldsymbol{\eta}}^{\varepsilon}\|_{\frac{1}{2},\partial\omega^\rho}.
$$

By triangle inequality

$$\begin{aligned}\|\mathring{\boldsymbol{v}}^{\varepsilon}_{\boldsymbol{\eta}}\|^2_{\frac{1}{2},\partial\omega^\rho} \lesssim & |\mathscr{F}^{\mathrm{c}}_0(\boldsymbol{\mu}(\varepsilon)\cdot\boldsymbol{e}_x)|^2\|\boldsymbol{\xi}^{\varepsilon,\mathrm{c}}_{x,0}\|^2_{\frac{1}{2},\partial\omega^\rho} + |\mathscr{F}^{\mathrm{c}}_0(\boldsymbol{\mu}(\varepsilon)\cdot\boldsymbol{e}_y)|^2\|\boldsymbol{\xi}^{\varepsilon,\mathrm{c}}_{y,0}\|^2_{\frac{1}{2},\partial\omega^\rho}\\ &+\sum_{j=1}^{n}|\mathscr{F}^{\mathrm{c}}_j(\boldsymbol{\mu}(\varepsilon)\cdot\boldsymbol{e}_x)|^2\|\boldsymbol{\xi}^{\varepsilon,\mathrm{c}}_{x,j}\|^2_{\frac{1}{2},\partial\omega^\rho} + |\mathscr{F}^{\mathrm{s}}_j(\boldsymbol{\mu}(\varepsilon)\cdot\boldsymbol{e}_x)|^2\|\boldsymbol{\xi}^{\varepsilon,\mathrm{s}}_{x,j}\|^2_{\frac{1}{2},\partial\omega^\rho}\\ &+\sum_{j=1}^{n}|\mathscr{F}^{\mathrm{c}}_j(\boldsymbol{\mu}(\varepsilon)\cdot\boldsymbol{e}_y)|^2\|\boldsymbol{\xi}^{\varepsilon,\mathrm{c}}_{y,j}\|^2_{\frac{1}{2},\partial\omega^\rho} + |\mathscr{F}^{\mathrm{s}}_j(\boldsymbol{\mu}(\varepsilon)\cdot\boldsymbol{e}_y)|^2\|\boldsymbol{\xi}^{\varepsilon,\mathrm{s}}_{y,j}\|^2_{\frac{1}{2},\partial\omega^\rho}.\\ &+|\mathscr{F}^{\mathrm{c}}_0(\boldsymbol{\mu}(\varepsilon)\cdot\boldsymbol{e}_*)|^2\|\boldsymbol{\xi}^{\varepsilon,\star}_1\|^2_{\frac{1}{2},\partial\omega^\rho}\end{aligned}$$

By definition of the functions $\boldsymbol{\xi}^{\varepsilon,m}_{l,j}$, we have

$$\|\boldsymbol{\xi}^{\varepsilon,m}_{l,j}\|_{\frac{1}{2},\partial\omega^\rho} \lesssim \|\boldsymbol{\phi}^{\varepsilon,m}_{2,j+1}\|_{\frac{1}{2},\partial\omega^\rho} + \|\boldsymbol{\phi}^{\varepsilon,m}_{2,j-1}\|_{\frac{1}{2},\partial\omega^\rho} + \|\boldsymbol{\phi}^{\varepsilon,m}_{1,j-1}\|_{\frac{1}{2},\partial\omega^\rho}.$$

Since the norms $\|\cdot\|_{\frac{1}{2},\partial\omega^\rho}$ and $\|\cdot\|^{\mathscr{F}}_{\frac{1}{2},\rho}$ are equivalent we deduce that

$$\begin{aligned}&\star\quad j=0: \quad \|\phi^{\varepsilon,\mathrm{c}}_{1,0}\|_{\frac{1}{2},\partial\omega^\rho} \lesssim \left(\frac{\varepsilon}{\rho}\right),\\ &\star\quad j=1: \quad \|\phi^{\varepsilon,m}_{l,1}\|_{\frac{1}{2},\partial\omega^\rho} \lesssim \frac{|\log(\rho)|+(\varepsilon/\rho)^2}{|\log(\varepsilon)|},\\ &\star\quad j\geqslant 2: \quad \|\phi^{\varepsilon,m}_{l,j}\|_{\frac{1}{2},\partial\omega^\rho} \lesssim_j (1+j)^{\frac{1}{2}}(1+j)\left(\left(\frac{\varepsilon}{\rho}\right)^{j-1}+\left(\frac{\varepsilon}{\rho}\right)^{j+1}\right)\end{aligned}$$

Now, taking $\varepsilon\in(0,\rho/4)$ and keeping only the lower order term in $(1/4)^j$, the following inequalities hold

$$\begin{aligned}j\in\{0,1\}: \quad &\|\boldsymbol{\xi}^{\varepsilon,m}_{l,j}\|_{\frac{1}{2},\partial\omega^\rho} \lesssim_j (1+j)^{\frac{1}{2}},\\ j\geqslant 2: \quad &\|\boldsymbol{\xi}^{\varepsilon,m}_{l,j}\|_{\frac{1}{2},\partial\omega^\rho} \lesssim_j (1+j)^{\frac{1}{2}}(1+j)(1/4)^{j-2}\end{aligned}$$

We conclude that

$$\begin{aligned}\|\mathring{\boldsymbol{v}}^{\varepsilon}_{\boldsymbol{\eta}}\|^2_{\frac{1}{2},\partial\omega^\rho} \lesssim & \sum_{j\in\{0,1\}}(1+j)(|\mathscr{F}^{\mathrm{c}}_j(\boldsymbol{\mu}(\varepsilon)\cdot\boldsymbol{e}_x)|^2+|\mathscr{F}^{\mathrm{s}}_j(\boldsymbol{\mu}(\varepsilon)\cdot\boldsymbol{e}_x)|^2)\\ &+\sum_{j=2}^{\infty}(1+j)(1+j)^2(1/4)^{2(j-2)}(|\mathscr{F}^{\mathrm{c}}_j(\boldsymbol{\mu}(\varepsilon)\cdot\boldsymbol{e}_x)|^2+|\mathscr{F}^{\mathrm{s}}_j(\boldsymbol{\mu}(\varepsilon)\cdot\boldsymbol{e}_x)|^2)\\ &+\sum_{j\in\{0,1\}}(1+j)(|\mathscr{F}^{\mathrm{c}}_j(\boldsymbol{\mu}(\varepsilon)\cdot\boldsymbol{e}_y)|^2+|\mathscr{F}^{\mathrm{s}}_j(\boldsymbol{\mu}(\varepsilon)\cdot\boldsymbol{e}_y)|^2)\\ &+\sum_{j=2}^{\infty}(1+j)(1+j)^2(1/4)^{2(j-2)}(|\mathscr{F}^{\mathrm{c}}_j(\boldsymbol{\mu}(\varepsilon)\cdot\boldsymbol{e}_y)|^2+|\mathscr{F}^{\mathrm{s}}_j(\boldsymbol{\mu}(\varepsilon)\cdot\boldsymbol{e}_y)|^2).\end{aligned}$$

Since the sequence $(1+j)^2(1/4)^{2(j-2)}$ is bounded, by ε-uniform equivalence between the norms $\|\cdot\|_{\frac{1}{2},\varepsilon}$ and $\|\cdot\|^{\mathscr{F}}_{\frac{1}{2},\varepsilon}$, we have for $\varepsilon \in (0, \rho/4)$,

$$\|\overset{\star}{\boldsymbol{v}}{}^{\varepsilon}_{\boldsymbol{\eta}}\|_{\frac{1}{2},\partial\omega^\rho} \lesssim \|\boldsymbol{\eta}\|^{\mathscr{F}}_{\frac{1}{2},\varepsilon} \lesssim \|\boldsymbol{\eta}\|_{\frac{1}{2},\varepsilon}. \tag{4.A.61}$$

It only remains to bound $\|\overset{\star}{\psi}{}^{\varepsilon}_{\boldsymbol{\eta}}\|_\Omega$. By construction **curl** $(\overset{\star}{\psi}{}^{\varepsilon}_{\boldsymbol{\eta}}) = \overset{\star}{\boldsymbol{v}}{}^{\varepsilon}_{\boldsymbol{\eta}}$ so

$$\|\nabla\overset{\star}{\psi}{}^{\varepsilon}_{\boldsymbol{\eta}}\|_{\omega^\rho} \lesssim \|\overset{\star}{\boldsymbol{v}}{}^{\varepsilon}_{\boldsymbol{\eta}}\|_{\omega^\rho}.$$

Now, since $\overset{\star}{\psi}{}^{\varepsilon}_{\boldsymbol{\eta}} \in \cap H^2(\omega^\rho) \cap L^2_0(\omega^\rho)$, we can apply Poincaré-Wirtinger inequality and (4.A.61) to obtain

$$\|\overset{\star}{\psi}{}^{\varepsilon}_{\boldsymbol{\eta}}\|_{1,\omega^\rho} \lesssim \|\overset{\star}{\boldsymbol{v}}{}^{\varepsilon}_{\boldsymbol{\eta}}\|_{\omega^\rho} \lesssim \|\boldsymbol{\eta}\|_{\frac{1}{2},\varepsilon}.$$

This concludes the proof of the Lemma. □

4.A.11 Proof of Lemma 4.3.6

Restated Lemma 4.3.6. *Let $\tilde{q}_h \in Q^{k-1}_{N,h}$, there exists $\tilde{\boldsymbol{w}}^{\varepsilon}_{\tilde{q}_h} \in \boldsymbol{V}^k_{N,h}$ such that*

$$(\tilde{q}_h, \operatorname{div} \tilde{\boldsymbol{w}}^{\varepsilon}_{\tilde{q}_h})_\Omega = \|\tilde{q}_h\|^2_\Omega, \quad \|\tilde{\boldsymbol{w}}^{\varepsilon}_{\tilde{q}_h}\|_{1,\Omega} \lesssim |\log(\varepsilon)|^{\frac{1}{2}}\|\tilde{q}_h\|_\Omega.$$

Moreover, for any $\boldsymbol{\mu}_N \in \boldsymbol{F}_N$,

$$(\boldsymbol{\mu}_N, \tilde{\boldsymbol{w}}^{\varepsilon}_{\tilde{q}_h}) = 0.$$

Proof of Lemma 4.3.6. Let $\tilde{q}_h \in Q^{k-1}_{N,h}$ be given. By definition of $Q^{k-1}_{N,h}$, there exists $(q_h, \tilde{q}) \in Q^k_h \times \operatorname{span}\{\tilde{\varphi}^{\varepsilon,m}_j\}$ such that $\tilde{q}_h = q_h + \tilde{q}$. Since the pair $\boldsymbol{V}^k_h/Q^{k-1}_h$ is an inf-sup stable conforming pair for the divergence operator, there exists $\overset{\star}{\boldsymbol{w}}_{q_h} \in \boldsymbol{V}^k_h$ such that

$$\operatorname{div} \overset{\star}{\boldsymbol{w}}_{q_h} = q_h, \quad \|\overset{\star}{\boldsymbol{w}}_{q_h}\|_{1,\Omega} \lesssim \|q_h\|_\Omega.$$

Furthermore, according to Lemma 4.3.5 and Lemma 3.3.2, there exists $\tilde{\boldsymbol{v}}^{\varepsilon}_{q_h} \in \tilde{\boldsymbol{V}}^k_{h,N}$

$$(\boldsymbol{\mu}_N, \tilde{\boldsymbol{v}}^{\varepsilon}_{q_h})_\varepsilon = (\boldsymbol{\mu}_N, \overset{\star}{\boldsymbol{w}}_{q_h})_\varepsilon \quad \forall \boldsymbol{\mu}_N \in \boldsymbol{F}_N, \quad \|\tilde{\boldsymbol{v}}^{\varepsilon}_{q_h}\|_{1,\Omega} \lesssim \|\overset{\star}{\boldsymbol{w}}_{q_h}\|_{\frac{1}{2},\varepsilon} \lesssim |\log(\varepsilon)|^{\frac{1}{2}}\|q_h\|_\Omega,$$

and

$$\operatorname{div} \tilde{\boldsymbol{v}}^{\varepsilon}_{q_h} = 0 \quad \text{in} \quad \Omega.$$

Similarly, by construction, there exists $\tilde{\boldsymbol{w}}^{\varepsilon}_{\tilde{q}} \in \operatorname{span}\{\tilde{\boldsymbol{\varsigma}}^{\varepsilon,m}_j\} \subset \boldsymbol{V}^k_{N,h}$ such that

$$\operatorname{div} \tilde{\boldsymbol{w}}^{\varepsilon}_{\tilde{q}} = \tilde{q}, \quad \|\tilde{\boldsymbol{w}}^{\varepsilon}_{\tilde{q}}\|_{1,\Omega} \lesssim |\log(\varepsilon)|^{\frac{1}{2}}\|\tilde{q}\|_\Omega,$$

and

$$(\boldsymbol{\mu}_N, \tilde{\boldsymbol{w}}^{\varepsilon}_{\tilde{q}})_\varepsilon = 0 \quad \forall \boldsymbol{\mu}_N \in \boldsymbol{F}_N.$$

Let us set $\tilde{\boldsymbol{w}}^{\varepsilon}_{\tilde{q}_h} = \overset{\star}{\boldsymbol{w}}^{\varepsilon}_{q_h} - \tilde{\boldsymbol{v}}^{\varepsilon}_{q_h} + \tilde{\boldsymbol{w}}^{\varepsilon}_{\tilde{q}}$, we have

$$\operatorname{div} \tilde{\boldsymbol{w}}^{\varepsilon}_{\tilde{q}_h} = \tilde{q}_h, \quad \|\tilde{\boldsymbol{w}}^{\varepsilon}_{\tilde{q}_h}\|_{1,\Omega} \lesssim |\log(\varepsilon)|^{\frac{1}{2}} \|\tilde{q}_h\|_{\Omega},$$

and

$$(\boldsymbol{\mu}_N, \tilde{\boldsymbol{w}}^{\varepsilon}_{\tilde{q}_h})_{\varepsilon} = \mathbf{0} \quad \forall \boldsymbol{\mu}_N \in \boldsymbol{F}_N.$$

This concludes the proof of the Lemma. □

4.A.12 Proof of Lemma 4.3.9

Restated Lemma 4.3.9. *Let $\boldsymbol{u}^{\varepsilon}_{N,\mathrm{S}}$ defined by* (4.3.31)*, there exists $0 < \tilde{\rho} < \rho$ such that for all $\varepsilon \in (0, \tilde{\rho})$,*

$$\|\boldsymbol{u}^{\varepsilon}_{N,\mathrm{S}}\|_{\frac{1}{2},\partial\omega^{\rho}} \lesssim |\boldsymbol{v}_{\mathrm{b}}| + \varepsilon |w_{\mathrm{b}}|.$$

Proof of Lemma 4.3.9. By definition of $\boldsymbol{u}^{\varepsilon}_{N,\mathrm{S}}$ introduced in (4.3.31), we have

$$\|\boldsymbol{u}^{\varepsilon}_{N,\mathrm{S}}\|_{\frac{1}{2},\partial\omega^{\rho}} \leqslant \sum_{j=0}^{N} \sum_{l=1}^{2} |a^{u}_{l,j}| \|\boldsymbol{\phi}^{\varepsilon,\mathrm{c}}_{l,j}\|_{\frac{1}{2},\partial\omega^{\rho}} + |b^{u}_{l,j}| \|\boldsymbol{\phi}^{\varepsilon,\mathrm{s}}_{l,j}\|_{\frac{1}{2},\partial\omega^{\rho}}$$

Using the exact expression of the coefficients $a^{u}_{l,j}$ provided in Section 4.A.7.1, we get:

- $\{N \geqslant 2,\ j \in \{2, N-1\}$:

  $$a^{u}_{1,j} = \varepsilon^{j+1} c^{\oplus}_{1,j}, \quad a^{u}_{2,j} = \varepsilon^{j-1} c^{\oplus}_{2,j}$$

  with

  $$c^{\oplus}_{1,j} = \frac{A^{\varepsilon}_j \xi^{\varepsilon,\mathrm{s}}_{j,r} + B^{\varepsilon}_j \xi^{\varepsilon,\mathrm{c}}_{j,\theta}}{D^{\varepsilon}_j}, \quad c^{\oplus}_{2,j} = \frac{E^{\varepsilon}_j \xi^{\varepsilon,\mathrm{s}}_{j,r} + F^{\varepsilon}_j \xi^{\varepsilon,\mathrm{c}}_{j,\theta}}{j D^{\varepsilon}_j},$$

  and the coefficients A^{ε}_j, B^{ε}_j, E^{ε}_j, F^{ε}_j and D^{ε}_j are given in (4.A.52). Taking $\tilde{\varepsilon} \in (0, 1/4)$ and using estimate (4.A.54), we derive the following a priori estimates for A^{ε}_j, B^{ε}_j, E^{ε}_j, and F^{ε}_j:

  $$\begin{cases} |A^{\varepsilon}_j| \lesssim_j \rho^{3j-1}(1 + (1+j)(1/4)^{2(j-1)} + (1+j)(1/4)^{2j}), \\ |B^{\varepsilon}_j| \lesssim_j \rho^{3j-1}(1 + (1+j)(1/4)^{2(j-1)} + (1+j)(1/4)^{2j}), \\ |E^{\varepsilon}_j| \lesssim_j (1+j)\rho^{3j+1}(1 + (1+j)(1/4)^{2j} + (1+j)(1/4)^{2(j+1)}), \\ |F^{\varepsilon}_j| \lesssim_j (1+j)\rho^{3j+1}(1 + (1+j)(1/4)^{2j} + (1+j)(1/4)^{2(j+1)}). \end{cases}$$

  Since the sequences $(1+j)(1/4)^{2(j-1)}$, $(1+j)(1/4)^{2j}$, $(1+j)(1/4)^{2(j+1)}$ are bounded, we deduce that

  $$|A^{\varepsilon}_j| \lesssim_j \rho^{3j-1},\ |B^{\varepsilon}_j| \lesssim_j \rho^{3j-1},\ |E^{\varepsilon}_j| \lesssim_j (1+j)\rho^{3j+1},\ |F^{\varepsilon}_j| \lesssim_j (1+j)\rho^{3j+1}.$$

We now establish a lower bound for D_j^ε as follows:

$$D_j^\varepsilon \gtrsim_j 2\rho^{4j}\left(1 - j^2(1/4)^{2(j-1)} - j^2(1/4)^{2(j+1)}\right).$$

Since the sequences $j^2\,(1/4)^{2(j-1)}$ and $j^2(1/4)^{2(j+1)}$ are decreasing, we deduce that

$$D_j^\varepsilon \gtrsim_j \rho^{4j}\overbrace{\left(1 - 4(1/4)^2 - 4(1/4)^6\right)}^{>0} \gtrsim_j \rho^{4j}.$$

We conclude that

$$|a_{1,j}^u| \lesssim_j \left(\frac{\varepsilon}{\rho}\right)^{j+1}\left(|\xi_{j,r}^{\varepsilon,\mathrm{s}}| + |\xi_{j,\theta}^{\varepsilon,\mathrm{c}}|\right), \quad |a_{2,j}^u| \lesssim_j \left(\frac{\varepsilon}{\rho}\right)^{j-1}\left(|\xi_{j,r}^{\varepsilon,\mathrm{s}}| + |\xi_{j,\theta}^{\varepsilon,\mathrm{c}}|\right).$$

- $\{N \geqslant 2, j \in \{0,1\}\}$:

$$a_{1,0}^u \overset{\text{def}}{=} \varepsilon(w_\mathrm{b} + 2c_{1,0}^\oplus), \quad a_{1,1}^u \overset{\text{def}}{=} c_{1,1}^\oplus\varepsilon^2, \quad a_{2,1}^u \overset{\text{def}}{=} \boldsymbol{v}_\mathrm{b}\cdot\boldsymbol{e}_y + c_{2,1}^\oplus$$

with

$$\rho c_{1,0}^\oplus \xrightarrow[\varepsilon\to 0]{} -\frac{\xi_{0,\theta}^{\varepsilon,c}}{2}$$
$$\rho^2 c_{1,1}^\oplus \xrightarrow[\varepsilon\to 0]{} \xi_{1,r}^{\varepsilon,\mathrm{s}} - \xi_{1,\theta}^{\varepsilon,\mathrm{c}}, \quad c_{2,1}^\oplus \xrightarrow[\varepsilon\to 0]{} -\frac{3}{2}\xi_{1,r}^{\varepsilon,s} + \frac{1}{4}\xi_{1,\theta}^{\varepsilon,\mathrm{c}}.$$

We deduce that there exists $\rho_0, \rho_1 > 0$ such that

$$|a_{1,0}^u| \lesssim \left(\frac{\varepsilon}{\rho}\right)\left(|\xi_{0,\theta}^{\varepsilon,\mathrm{c}}| + |w_\mathrm{b}|\right) \quad \forall\varepsilon \in (0,\rho_0)$$
$$|a_{1,1}^u| \lesssim \left(\frac{\varepsilon}{\rho}\right)^2\left(|\xi_{1,r}^{\varepsilon,\mathrm{s}}| + |\xi_{1,\theta}^{\varepsilon,\mathrm{c}}|\right), \quad |a_{2,1}^u| \lesssim |\xi_{1,r}^{\varepsilon,\mathrm{s}}| + |\xi_{1,\theta}^{\varepsilon,\mathrm{c}}| + |\boldsymbol{v}_\mathrm{b}\cdot\boldsymbol{e}_y| \quad \forall\varepsilon \in (0,\rho_1).$$

- $\{j \geqslant 2, j \in \{N, N+1\}\}$:

$$a_{2,j}^u = \varepsilon^{j-1}((1+j)c_{1,j}^\oplus + jc_{2,j}^\oplus),$$

with

$$c_{1,j}^\oplus = \frac{A_j^\varepsilon\xi_{j,r}^{\varepsilon,\mathrm{s}} + B_j^\varepsilon\xi_{j,\theta}^{\varepsilon,\mathrm{c}}}{D_j^\varepsilon}, \quad c_{2,j}^\oplus = \frac{E_j^\varepsilon\xi_{j,r}^{\varepsilon,\mathrm{s}} + F_j^\varepsilon\xi_{j,\theta}^{\varepsilon,\mathrm{c}}}{jD_j^\varepsilon},$$

and the coefficients A_j^ε, B_j^ε, E_j^ε, F_j^ε, F_j^ε are given in (4.A.53). Taking $\tilde{\varepsilon} \in (0, 1/4)$ and using estimate (4.A.54), we derive the following a priori estimates for A_j^ε, B_j^ε, E_j^ε, and F_j^ε:

$$\begin{cases} |A_j^\varepsilon| \lesssim_j \rho^{j+1}(1 + (1+j)(1/4)^{2(j-1)} + (1+j)(1/4)^{2j}), \\ |B_j^\varepsilon| \lesssim_j \rho^{j+1}(1 + (1+j)(1/4)^{2(j-1)} + (1+j)(1/4)^{2j}) \\ |E_j^\varepsilon| \lesssim_j (1+j)\rho^{j+3}(1 + (1+j)(1/4)^{2j} + (1+j)(1/4)^{2(j+1)}), \\ |F_j^\varepsilon| \lesssim_j (1+j)\rho^{j+3}(1 + (1+j)(1/4)^{2j} + (1+j)(1/4)^{2(j+1)}). \end{cases}$$

Since the sequences $(1+j)(1/4)^{2(j-1)}$, $(1+j)(1/4)^{2j}$, $(1+j)(1/4)^{2(j+1)}$ are bounded, we deduce that

$$|A_j^\varepsilon| \lesssim_j \rho^{j+1}, \quad |B_j^\varepsilon| \lesssim_j \rho^{j+1}, \quad |E_j^\varepsilon| \lesssim_j (1+j)\rho^{j+3}, \quad |F_j^\varepsilon| \lesssim_j (1+j)\rho^{j+3}.$$

We establish an upper bound for D_j^ε as follows:

$$D_j^\varepsilon \lesssim_j -2\rho^{2(j+1)}(1 - j^2(1/4)^{2(j-1)} - (j-1)(1+j)(1/4)^{2(j+1)})$$

Since the sequences $j^2(1/4)^{2(j-1)}$ and $(j-1)(1+j)(1/4)^{2(j+1)}$ are deacreasing for $j \geqslant 2$, it holds

$$D_j^\varepsilon \lesssim_j -2\rho^{2(j+1)} \overbrace{(1 - 4(1/4)^2 - 3(1/4)^6)}^{>0} \lesssim_j -\rho^{2(j+1)}.$$

We conclude

$$|a_{2,j}^u| \lesssim_j \left((1+j)\left(\frac{\varepsilon}{\rho}\right)^{j-1} + (1+j)\left(\frac{\varepsilon}{\rho}\right)^{j+1}\right)(|\xi_{j,r}^{\varepsilon,\mathrm{s}}| + |\xi_{j,\theta}^{\varepsilon,\mathrm{c}}|).$$

- $\{N \in \{0,1\},\ j \in \{0,1\}\}$:

$$a_{1,0}^u \overset{\text{def}}{=} \varepsilon(w_\mathrm{b} + 2c_{1,0}^\oplus), \quad a_{1,1}^u \overset{\text{def}}{=} 2\varepsilon^2 c_{1,1}^\oplus + c_{2,1}^\oplus + \boldsymbol{v}_\mathrm{b} \cdot \boldsymbol{e}_y$$

with

$$\rho c_{1,0}^\oplus \xrightarrow[\varepsilon\to 0]{} -\frac{\xi_{0,\theta}^{\varepsilon,c}}{2}$$
$$\rho^2 c_{1,1}^\oplus \xrightarrow[\varepsilon\to 0]{} \frac{1}{2}\xi_{1,r}^{\varepsilon,\mathrm{s}} - \frac{1}{2}\xi_{1,\theta}^{\varepsilon,\mathrm{c}}, \quad c_{2,1}^\oplus \xrightarrow[\varepsilon\to 0]{} -\frac{3}{2}\xi_{1,r}^{\varepsilon,\mathrm{s}} + \frac{1}{2}\xi_{1,\theta}^{\varepsilon,\mathrm{c}}$$

We deduce that there exists $\tilde{\rho}_0, \tilde{\rho}_1 > 0$ such that

$$|a_{1,0}^u| \lesssim |\xi_{0,\theta}^{\varepsilon,\mathrm{c}}| + |w_\mathrm{b}| \quad \forall \varepsilon \in (0, \tilde{\rho}_0)$$
$$|a_{1,1}^u| \lesssim (|\xi_{1,r}^{\varepsilon,\mathrm{s}}| + |\xi_{1,\theta}^{\varepsilon,\mathrm{c}}|)\left(\left(\frac{\varepsilon}{\rho}\right)^2 + 1\right) + |\boldsymbol{v}_\mathrm{b} \cdot \boldsymbol{e}_y| \quad \forall \varepsilon \in (0, \tilde{\rho}_1).$$

Using the estimates on the coefficients $a_{j,l}^u/b_{j,l}^u$ and setting $\tilde{\rho} = \min(\rho_0, \rho_1, \rho/4)$ if $N \in \{0,1\}$ or $\tilde{\rho} = \min(\tilde{\rho}_0, \tilde{\rho}_1, \rho/4)$ if $N \geqslant 2$, since the sequence $(1+j)^2(\tilde{\rho}/\rho)^{2(j-1)}$ is bounded, we obtain for $\varepsilon \in (0, \tilde{\rho})$,

$$\begin{aligned}\|\boldsymbol{u}_{N,\mathrm{S}}^\varepsilon\|_{\frac{1}{2},\partial\omega^\rho} &\lesssim \left(\sum_{j=0}^{N-1}(1+j)|\xi_j|^2 + \sum_{j=N}^{N+1}(1+j)(1+j)^2\left(\frac{\tilde{\rho}}{\rho}\right)^{2(j-1)}|\xi_j|^2\right)^{\frac{1}{2}} + |\boldsymbol{v}_\mathrm{b}| + \varepsilon|w_\mathrm{b}| \\ &\lesssim \|\boldsymbol{u}_N^\varepsilon\|_{\frac{1}{2},\rho}^{\mathscr{F}} + |\boldsymbol{v}_\mathrm{b}| + \varepsilon|w_\mathrm{b}|,\end{aligned}$$

where the definition of $|\xi_j|$ is given in (4.A.55). Using successively the equivalence between the norm $\|\cdot\|^{\mathscr{F}}_{\frac{1}{2},\rho}$ and $\|\cdot\|_{\frac{1}{2},\partial\omega^\rho}$, the standard trace theorem from $\boldsymbol{H}^{\frac{1}{2}}(\partial\omega^\rho)$ to $\boldsymbol{H}^1(\Omega)$ and the a priori estimates on $\boldsymbol{u}^\varepsilon_N$ given by Theorem 4.2.1, we get, for $\varepsilon \in (0, \tilde{\rho})$,

$$\|\boldsymbol{u}^\varepsilon_{N,\mathrm{S}}\|_{\frac{1}{2},\partial\omega^\rho} \lesssim |\boldsymbol{v}_\mathrm{b}| + \varepsilon|w_\mathrm{b}|.$$

This concludes the proof. □

CHAPTER 5

Loosely coupled Robin-Robin scheme for slender bodies immersed in an incompressible flow

5.1 Introduction

One key aspect of the modelling approach proposed in Chapter 2 is to introduce a computational framework which reduces the coupling conditions between a 1D structure and a 3D fluid while maintaining a good balance between accuracy and computational efficiency. In Chapter 2, the time-discretization of the coupling condition is based on a semi-implicit coupling scheme. One of the main advantages of this approach is that it delivers unconditionally energy stability (see Theorem 2.3.1) However, as discussed in Section 2.3.4, to solve the coupled system at each time step following a partitioned procedure, the fluid and structure sub-problems need to be solved iteratively, which can be computationally expensive. On the other hand, the stability of less expensive standard explicit coupling schemes, which enable to compute the solution of the coupled problem in a partitioned fashion by invoking the fluid solver only a few times by time-step, is dictated by the amount of added-mass effect in the system [Causin et al., 2005] [Förster et al., 2007], regardless of the discretization parameters. Particularly, in scenarios with low ratio between the fluid and structure densities, or for slender structures, explicit Dirichlet-Neumann schemes are known to suffer from instability.

The first fully explicit stable scheme was introduced for a problem with an incompressibility constraint in the fluid in [Burman and Fernández, 2009], using the Nitsche method [Hansbo, 2005]. In [Burman and Fernández, 2014], it was observed that the Nitsche coupling method could be transformed into a Robin-based coupling scheme without sacrificing stability. Since then, numerous studies have been conducted on Robin-like loosely coupled schemes for fluid-structure interaction (FSI) problems involving thick-walled solids [Banks et al., 2014, Bukač et al., 2014, Fernández et al., 2015b, Gigante and Vergara, 2021, Burman et al., 2022a, Burman et al., 2023]. In the specific case of the coupling with thin walled structure where the solid is represented by a manifold of co-dimension one with respect to the fluid model, many schemes have been developed and analyzed based on the original work [Guidoboni et al., 2009], for instance [Canic et al., 2012, Bukač et al., 2015, Fernández et al., 2015a, Oyekole et al., 2018]. The key principle for stability lies in implicit integration of the solid's inertial contribution within the fluid, enforced through a Robin-type interface condition (which circumvents the aforementioned added mass issues), and extrapolating the remaining solid contributions for accuracy (see, e.g., [Fernández, 2013]).

In this chapter, we investigate a class of Robin-Robin based loosely coupled schemes for the numerical approximation (2.2.4), (2.2.21), (2.2.27), extending the work of [Burman et al., 2022b, Burman et al., 2022a, Burman et al., 2023] to the case of slender structures with co-dimension 2 with respect to the fluid domain. As a first approach, we adopt a simplified framework wherein the rotation effects in the solid are neglected in the interface coupling conditions. We provide an energy stability analysis which guarantees the unconditional stability of the scheme. We also consider some test cases presented in Chapter 2 for which we compare the solutions obtained with the semi-implicit coupled scheme and the Robin-Robin based loosely coupled scheme.

The extension of the Robin-Robin loosely coupled scheme paradigm introduced in [Burman et al., 2022a] to the mixed dimensional model (2.2.4), (2.2.21), (2.2.27) is not straightforward. Let $\alpha \in \mathbb{R}^+$ be a user-defined parameter, $\boldsymbol{u}^n$, $\boldsymbol{u}_{\mathrm{b}}^n$ the discrete velocities of the fluid and structure, and $\boldsymbol{\lambda}^n$ the Lagrange multiplier associated with the kinematic constraint at the fluid-structure interface $\Sigma_{\tilde{\varepsilon}}^n$ at time t^n, the semi-discrete Robin-type coupling condition formally reads

$$\boldsymbol{\lambda}^n + \alpha \boldsymbol{u}^n = \alpha \boldsymbol{u}_{\mathrm{b}}^{n-1} + \boldsymbol{\lambda}^{n-1} \quad \text{on} \quad \Sigma_{\varepsilon}^n. \tag{5.1.1}$$

In [Burman et al., 2022a], the authors proved that for this relation to hold at the discrete level, a variational consistent discretization of stresses, compatible with the loosely coupled scheme, needed to be used. As further discussed in [Burman et al., 2023], this discretization is mainly dependent on the conformity between the structure mesh and the fluid mesh. For the reduced order approach introduced in Chapter 2, due to the projection of the Lagrange multipliers on a finite-dimensional space, the relation (5.1.1) is not expected to hold. Instead, under some assumptions on the beam velocity interface, we will

put in evidence that, by choosing properly the Lagrange multiplier space, it yields

$$\boldsymbol{\lambda}^n - \boldsymbol{\lambda}^{n-1} = \alpha(\boldsymbol{\Pi}(\boldsymbol{u}^n) - \boldsymbol{u}_{\mathrm{b}}^n), \tag{5.1.2}$$

where $\boldsymbol{\Pi}$ is a L^2 projector defined on the velocity admissible space for the solution of the structure sub-problem. In Section 5.2, we will derive the Robin-Robin conditions in a simplified framework, without the contribution of the solid rotation in the coupling conditions, and establish an equality of the form (5.1.2). In Section 5.2.2, building on this relation between velocity and stress, we establish the unconditional stability of the loosely coupled Robin-Robin scheme. Finally, in Section 5.3, we will propose several numerical examples providing numerical evidence of the stability and accuracy of the loosely coupled scheme. We will also apply this scheme to the test case of Section 2.4.3 with multiple beams immersed in a Navier-Stokes fluid of moderate Reynolds numbers.

5.2 Numerical method: Robin-Robin loosely coupled scheme

In this chapter, we consider the same framework as in Chapter 2. The objective is to propose a stable Robin-based loosely coupled scheme for the time discretization of the mixed-dimensional coupled problem (2.2.4), (2.2.21), (2.2.27) as an alternative to the semi-implicit time discretization described in Algorithm 1. We consider the same space discretization as the one presented in Section 2.3.1. More specifically, we set $\boldsymbol{V}_h \overset{\text{def}}{=} \boldsymbol{X}_h^1(\Omega) \cap \boldsymbol{V}$ and $Q_h \overset{\text{def}}{=} X_h^1(\Omega) \cap Q$ for the approximation of the fluid velocity $\boldsymbol{u}$ and pressure p, respectively, while for the solid displacement $\boldsymbol{r}$ and rotation $\boldsymbol{\theta}$, their approximations will be taken into $\boldsymbol{Y}_H \overset{\text{def}}{=} \boldsymbol{X}_H^1(0,L) \cap \boldsymbol{Y}$. The spaces $\boldsymbol{V} = \boldsymbol{H}_0^1(\Omega)$ and $Q = L_0^2(\Omega)$ are the space of admissible fluid velocity and pressure respectively, and $\boldsymbol{Y} \subset \boldsymbol{H}^1(0,L)$ is the space of admissible displacements and rotations of the beam. The definitions of $\boldsymbol{X}_h^1(\Omega)$, $Q_h^1(\Omega)$ and $\boldsymbol{X}_H^1(\Omega)$ are given in (2.3.1). In order to ease the analysis of the method, we consider the Lagrange multiplier space introduced in (2.3.2) in reference configuration:

$$\widehat{\boldsymbol{F}}_{N,H} \overset{\text{def}}{=} \big\{\widehat{\boldsymbol{v}}_H \mid \widehat{\boldsymbol{v}}_H(s,\nu) \overset{\text{def}}{=} \boldsymbol{a}_{0,H}(s) + \sum_{k=1}^{N} \boldsymbol{a}_{k,H}(s)\cos(k\nu) + \boldsymbol{b}_{k,H}\sin(k\nu),\ \boldsymbol{a}_{k,H}, \boldsymbol{b}_{k,H} \in \boldsymbol{Y}_H\big\}. \tag{5.2.1}$$

Furthermore, as mentioned in the introduction, we consider a simplified framework where the contribution of rotations are neglected in the fluid-structure coupling conditions (see Remark 16 below). Consequently, the kinematic and dynamic coupling conditions (2.2.25)

in a space semi-discrete framework becomes

$$\begin{cases} \boldsymbol{\phi}_H = (\boldsymbol{I}_3 \cdot \boldsymbol{e}_z)\boldsymbol{e}_z + \overline{\boldsymbol{r}_H} + \overline{\boldsymbol{\Lambda}_H}\big(\boldsymbol{I}_3 - (\boldsymbol{I}_3 \cdot \boldsymbol{e}_z)\boldsymbol{e}_z\big) \quad \text{in} \quad \widehat{\omega}^\varepsilon, \\ (\boldsymbol{\mu}_{N,H}, \boldsymbol{u}_h \circ \boldsymbol{\phi}_H)_{\widehat{\varepsilon}} = (\boldsymbol{\mu}_{N,H}, \overline{\partial_t \boldsymbol{r}_H})_{\widehat{\varepsilon}} \quad \forall \boldsymbol{\mu}_{N,H} \in \widehat{\boldsymbol{F}}_{N,H}, \\ (\boldsymbol{f}, \delta\boldsymbol{r}_H)_{(0,L)} = -(\boldsymbol{\lambda}_{N,H}, \overline{\delta\boldsymbol{r}_H})_{\widehat{\varepsilon}} \quad \forall \delta\boldsymbol{r}_H \in \boldsymbol{Y}_H, \end{cases} \tag{5.2.2}$$

where $(\cdot,\cdot)_{\widehat{\varepsilon}}$, similarly to the inner-product $(\cdot,\cdot)_\varepsilon$ introduced in (2.2.20), is the following re-scaled L^2 inner-product on $\widehat{\Sigma}^\varepsilon$:

$$(\widehat{\boldsymbol{u}}, \widehat{\boldsymbol{v}})_{\widehat{\varepsilon}} \stackrel{\text{def}}{=} \int_0^L \int_0^{2\pi} \widehat{\boldsymbol{u}}(s,\nu) \cdot \widehat{\boldsymbol{v}}(s,\nu).$$

Let $\widehat{\boldsymbol{F}}_{N^\star,H}$ be the space defined as

$$\widehat{\boldsymbol{F}}_{N^\star,H} \stackrel{\text{def}}{=} \big\{ \widehat{\boldsymbol{v}}_H \in \boldsymbol{L}^2(\widehat{\Sigma}^\varepsilon) \ : \\ \widehat{\boldsymbol{v}}_H(s,\nu) \stackrel{\text{def}}{=} \sum_{k=1}^{N} \boldsymbol{a}_{k,H}(s)\cos(k\nu) + \boldsymbol{b}_{k,H}(s)\sin(k\nu), \ \boldsymbol{a}_{k,H}, \boldsymbol{b}_{k,H} \in \boldsymbol{Y}_H \big\}.$$

Since $\overline{\delta\boldsymbol{r}_H} \in \widehat{\boldsymbol{F}}_{0,H}$ and $\widehat{\boldsymbol{F}}_{N^\star,H}$ is orthogonal to $\widehat{\boldsymbol{F}}_{0,H}$ for the inner-product $(\cdot,\cdot)_{\widehat{\varepsilon}}$, we have that

$$(\boldsymbol{\mu}_{N^\star,H}, \overline{\delta\boldsymbol{r}_H})_{\widehat{\varepsilon}} = 0 \quad \forall (\boldsymbol{\mu}_{N^\star,H}, \delta\boldsymbol{r}_H) \in \widehat{\boldsymbol{F}}_{N^\star,H} \times \boldsymbol{Y}_H.$$

Consequently, if $\widehat{\boldsymbol{\Pi}}_{0,H}$ and $\widehat{\boldsymbol{\Pi}}_{N^\star,H}$ denotes the L^2 orthogonal projection on $\widehat{\boldsymbol{F}}_{0,H}$ and $\widehat{\boldsymbol{F}}_{N^\star,H}$ for the inner-product $(\cdot,\cdot)_\varepsilon$, respectively, writing $\boldsymbol{\lambda}_{N,H} = \boldsymbol{\lambda}_{0,H} + \boldsymbol{\lambda}_{N^\star,H}$ with $(\boldsymbol{\lambda}_{0,H}, \boldsymbol{\lambda}_{N^\star,H}) = (\widehat{\boldsymbol{\Pi}}_0(\boldsymbol{\lambda}_{N,H}), \widehat{\boldsymbol{\Pi}}_{N^\star,H}(\boldsymbol{\lambda}_{N,H}))$, the kinematics and dynamics coupling conditions (5.2.2) can be written equivalently

$$\begin{cases} (\boldsymbol{\mu}_{0,H}, \boldsymbol{u}_h \circ \boldsymbol{\phi}_H)_{\widehat{\varepsilon}} = (\boldsymbol{\mu}_{0,H}, \overline{\partial_t \boldsymbol{r}_H})_{\widehat{\varepsilon}} \quad \forall \boldsymbol{\mu}_{0,H} \in \widehat{\boldsymbol{F}}_{0,H}, \\ (\boldsymbol{\mu}_{N^\star,H}, \boldsymbol{u}_h \circ \boldsymbol{\phi}_H)_{\widehat{\varepsilon}} = 0 \quad \forall \boldsymbol{\mu}_{N^\star,H} \in \widehat{\boldsymbol{F}}_{N^\star,H}, \\ (\boldsymbol{f}, \delta\boldsymbol{r}_H)_{(0,L)} = -(\boldsymbol{\lambda}_{0,H}, \overline{\delta\boldsymbol{r}_H})_{\widehat{\varepsilon}} \quad \forall \delta\boldsymbol{r}_H \in \boldsymbol{Y}_H, \end{cases} \tag{5.2.3}$$

The space semi-discrete formulation of the coupled problem (2.2.4), (2.2.21), (2.2.27) with Lagrange multiplier space (5.2.1) and simplified coupling conditions (5.2.3) is given by: we look for $(\boldsymbol{u}_h, p_h, \boldsymbol{\lambda}_{N,H}, \boldsymbol{r}_H, \boldsymbol{\theta}_H)$ such that $(\boldsymbol{u}_h(t), p_h(t), \boldsymbol{\lambda}_{N,H}(t), \boldsymbol{r}_H(t), \boldsymbol{\theta}_H(t)) \in$

$\boldsymbol{V}_h \times Q_h \times \widehat{\boldsymbol{F}}_{N,H} \times \boldsymbol{Y}_H \times \boldsymbol{Y}_H$ a.e $t \in \mathbb{R}^+$ and is solution of

$$\boldsymbol{\phi}_H = (\boldsymbol{I}_3 \cdot \boldsymbol{e}_z)\boldsymbol{e}_z + \overline{\boldsymbol{r}_H} + \overline{\boldsymbol{\Lambda}_H}\big(\boldsymbol{I}_3 - (\boldsymbol{I}_3 \cdot \boldsymbol{e}_z)\boldsymbol{e}_z\big) \quad \text{in} \quad \widehat{\omega}^\varepsilon, \tag{5.2.4}$$

$$\begin{cases} \rho_{\mathrm{f}}(\partial_t \boldsymbol{u}_h, \boldsymbol{v}_h)_\Omega + a^{\mathrm{f}}_{\Omega,h}\big(\boldsymbol{u}_h; (\boldsymbol{u}_h, p_h), (\boldsymbol{v}_h, q_h)\big) - (\boldsymbol{\lambda}_{N,H}, \boldsymbol{v}_h \circ \boldsymbol{\phi}^n_H)_{\widehat{\varepsilon}} \\ \quad + (\boldsymbol{\mu}_{0,H}, \boldsymbol{u}_h \circ \boldsymbol{\phi}_H - \overline{\dot{\boldsymbol{r}}_H})_{\widehat{\varepsilon}} + (\boldsymbol{\mu}_{N^\star,H}, \boldsymbol{u}_h \circ \boldsymbol{\phi}_H)_{\widehat{\varepsilon}} = 0 \end{cases} \tag{5.2.5}$$

$$\begin{cases} \rho_{\mathrm{b}}\big(\boldsymbol{A}\partial_t \dot{\boldsymbol{r}}_H, \delta\boldsymbol{r}_H\big)_{(0,L)} + + a^{\mathrm{b}}_H\big((\boldsymbol{r}_H, \boldsymbol{\theta}_H), (\delta\boldsymbol{r}_H, \delta\boldsymbol{\theta}_H)\big) \\ \quad + \alpha(\overline{\dot{\boldsymbol{r}}_H} - \boldsymbol{u}_h \circ \boldsymbol{\phi}_H, \overline{\delta\boldsymbol{r}_H})_{\widehat{\varepsilon}} = -\big(\boldsymbol{\lambda}_{0,H}, \overline{\delta\boldsymbol{r}_H}\big)_{\widehat{\varepsilon}}, \\ \boldsymbol{\lambda}_{0,H} = \widehat{\boldsymbol{\Pi}}_{H,0}(\boldsymbol{\lambda}_{N,H}). \end{cases} \tag{5.2.6}$$

for all $(\boldsymbol{v}_h, q_h, \boldsymbol{\mu}_{N,H}, \delta\boldsymbol{r}_H, \delta\boldsymbol{\theta}_H) \in \boldsymbol{V}_h \times Q_h \times \boldsymbol{Y}_h \times \boldsymbol{Y}_H$ with $(\boldsymbol{\mu}_{0,H}, \boldsymbol{\mu}_{N^\star,H}) = (\widehat{\boldsymbol{\Pi}}_{0,H}(\boldsymbol{\mu}_{N,H}), \widehat{\boldsymbol{\Pi}}_{N^\star,H}(\boldsymbol{\mu}_{N,H}))$. The definition of the discrete forms $a^{\mathrm{f}}_{\Omega,h}$ and a^{b}_H are given in (2.3.5) and (2.3.6), respectively.

Remark 16. The choice of neglecting the rotation contribution in the coupling conditions is justified by the difficulties of treating the geometrical dependence of the rotation in the Robin-Robin coupled scheme. However, if one wanted to include the rotations and guarantee energy stability, a simple option would be to update the fluid domain from a linearized version of the deformation map $\boldsymbol{\phi}_H$ with $\boldsymbol{\Lambda}_H \approx \boldsymbol{I}_3 + \boldsymbol{\Theta}_H$. In this case, the proof for energy stability is similar to the one presented in Lemma 5.2.2.

5.2.1 Derivation of the Robin-Robin coupling conditions

As in the previous chapters, the scalar $\tau > 0$ denotes the time step and $\{t_n \overset{\text{def}}{=} n\tau\}_{n\in\mathbb{N}}$ represents the temporal grid. We also set

$$\boldsymbol{v}^n, \quad \partial_\tau \boldsymbol{v}^n \overset{\text{def}}{=} \frac{1}{\tau}(\boldsymbol{v}^n - \boldsymbol{v}^{n-1}), \quad \boldsymbol{v}^{n-\frac{1}{2}} \overset{\text{def}}{=} \frac{1}{2}(\boldsymbol{v}^{n-1} + \boldsymbol{v}^n),$$

for an approximation of $\boldsymbol{v}(t^n)$, the backward Euler difference and the mid point evaluation, respectively. In the coupled problem (5.2.4) - (5.2.6), we notice that only $\boldsymbol{\lambda}_{0,H}$ contributes to the coupling conditions (5.2.3) while $\boldsymbol{\lambda}_{N^\star,H}$ only intervenes in the fluid sub-problems. Consequently, we only consider $\boldsymbol{\lambda}_{0,H}$ for the derivation of the Robin-Robin loosely reduced order coupling conditions. They read for the structure sub-problem and the fluid sub-problem respectively:

$$\begin{aligned} -(\boldsymbol{\lambda}^n_{0,H}, \overline{\delta\boldsymbol{r}_H})_{\widehat{\varepsilon}} + \alpha(\overline{\dot{\boldsymbol{r}}^{n-\frac{1}{2}}_H}, \overline{\delta\boldsymbol{r}_H})_{\widehat{\varepsilon}} \\ = \alpha(\boldsymbol{u}^{n-1}_h \circ \boldsymbol{\phi}^{n-1}_H, \overline{\delta\boldsymbol{r}_H})_{\widehat{\varepsilon}} - (\boldsymbol{\lambda}^{n-1}_{0,H}, \overline{\delta\boldsymbol{r}_H})_{\widehat{\varepsilon}}, \quad \forall \delta\boldsymbol{r}_H \in \boldsymbol{Y}_h \end{aligned} \tag{5.2.7}$$

and

$$-(\boldsymbol{\mu}_{0,H},\boldsymbol{\lambda}_{0,H}^n)_{\hat{\varepsilon}}+\alpha(\boldsymbol{\mu}_{0,H},\boldsymbol{u}_h^n\circ\boldsymbol{\phi}_H^n)_{\hat{\varepsilon}} = \alpha(\boldsymbol{\mu}_{0,H},\overline{\dot{\boldsymbol{r}}_H^{n-\frac{1}{2}}})_{\hat{\varepsilon}}-(\boldsymbol{\mu}_{0,H},\boldsymbol{\lambda}_{0,H}^{n-1})_{\hat{\varepsilon}},\quad \forall\boldsymbol{\mu}_{0,H}\in\widehat{\boldsymbol{F}}_{0,H} \tag{5.2.8}$$

Applying a backward-Euler semi-implicit time discretization for the fluid-sub problem and a mid-point scheme for the solid sub-problem, we obtain the fully discrete formulation of the Robin-Robin scheme given in Algorithm 7.

Algorithm 7 Fully discrete, Robin-Robin, loosely coupled scheme.

For $n\geqslant 1$:

Step 1: Solid sub-problem (Robin): Find $(\boldsymbol{r}_H^n,\boldsymbol{\theta}_H^n)\in\boldsymbol{Y}_H\times\boldsymbol{Y}_H$ such that $(\dot{\boldsymbol{r}}_H^{n-\frac{1}{2}},\dot{\boldsymbol{\theta}}_H^{n-\frac{1}{2}})=(\partial_\tau\boldsymbol{r}_H^n,\partial_\tau\boldsymbol{\theta}_H^n)$ and

$$\begin{cases}\rho_{\mathrm{b}}\big(\boldsymbol{A}\partial_\tau\dot{\boldsymbol{r}}_H^n,\delta\boldsymbol{r}_H\big)_{(0,L)}+\rho_{\mathrm{b}}\big(\boldsymbol{I}\partial_\tau\dot{\boldsymbol{\theta}}_H^n,\delta\boldsymbol{\theta}_H\big)_{(0,L)}+a_H^{\mathrm{b}}\big((\boldsymbol{r}_H^{n-\frac{1}{2}},\boldsymbol{\theta}_H^{n-\frac{1}{2}}),(\delta\boldsymbol{r}_H,\delta\boldsymbol{\theta}_H)\big)\\ +\alpha(\overline{\dot{\boldsymbol{r}}_H^{n-\frac{1}{2}}}-\boldsymbol{u}_h^{n-1}\circ\boldsymbol{\phi}_H^{n-1},\overline{\delta\boldsymbol{r}_H})_{\hat{\varepsilon}}=-\big(\boldsymbol{\lambda}_{0,H}^{n-1},\overline{\delta\boldsymbol{r}_H}\big)_{\hat{\varepsilon}}\end{cases} \tag{5.2.9}$$

for all $(\delta\boldsymbol{r}_H,\delta\boldsymbol{\theta}_H)\in\boldsymbol{Y}_H\times\boldsymbol{Y}_H$.

Step 2: Update the deformation map:

$$\boldsymbol{\phi}_H^n=(\boldsymbol{I}_3\cdot\boldsymbol{e}_z)\boldsymbol{e}_z+\overline{\boldsymbol{r}_H^n}+\overline{\boldsymbol{\Lambda}_H^n}\big(\boldsymbol{I}_3-(\boldsymbol{I}_3\cdot\boldsymbol{e}_z)\boldsymbol{e}_z\big)\quad\text{in}\quad\widehat{\omega}^\varepsilon. \tag{5.2.10}$$

Step 3: Fluid sub-problem (Robin): Find $(\boldsymbol{u}_h^n,p_h^n,\boldsymbol{\lambda}_{N,H}^n)\in\boldsymbol{V}_h\times Q_h\times\widehat{\boldsymbol{F}}_{N,H}$ such that $\boldsymbol{\lambda}_{N,H}^n=\boldsymbol{\lambda}_{0,H}^n+\boldsymbol{\lambda}_{N^\star,H}^n$ with $(\boldsymbol{\lambda}_{0,H}^n,\boldsymbol{\lambda}_{N^\star,H}^n)\in\widehat{\boldsymbol{F}}_{0,H}\times\widehat{\boldsymbol{F}}_{N^\star,H}$ and

$$\begin{cases}\rho_{\mathrm{f}}(\partial_\tau\boldsymbol{u}_h^n,\boldsymbol{v}_h)_\Omega+a_{\Omega,h}^{\mathrm{f}}\big(\boldsymbol{u}_h^{n-1};(\boldsymbol{u}_h^n,p_h^n),(\boldsymbol{v}_h,q_h)\big)-(\boldsymbol{\lambda}_{N,H}^n,\boldsymbol{v}_h\circ\boldsymbol{\phi}_H^n)_{\hat{\varepsilon}}\\ +\alpha(\boldsymbol{\mu}_{0,H},\boldsymbol{u}_h^n\circ\boldsymbol{\phi}_H^n-\overline{\dot{\boldsymbol{r}}_H^{n-\frac{1}{2}}})_{\hat{\varepsilon}}+(\boldsymbol{\mu}_{0,H},\boldsymbol{\lambda}_{0,H}^n-\boldsymbol{\lambda}_{0,H}^{n-1})_{\hat{\varepsilon}}\\ +(\boldsymbol{\mu}_{N^\star,H},\boldsymbol{u}_h^n\circ\boldsymbol{\phi}_H^n)_{\hat{\varepsilon}}=0\end{cases} \tag{5.2.11}$$

for all $(\boldsymbol{v}_h,q_h,\boldsymbol{\mu}_{N,H})\in\boldsymbol{V}_h\times Q_h\times\widehat{\boldsymbol{F}}_{N,H}$ with $(\boldsymbol{\mu}_{0,H},\boldsymbol{\mu}_{N^\star,H})=(\widehat{\boldsymbol{\Pi}}_{0,H}(\boldsymbol{\mu}_{N,H}),\widehat{\boldsymbol{\Pi}}_{N^\star,H}(\mu_{N,H}))$.

Note that in [Burman et al., 2022a], thanks to the conformity between the structure and fluid meshes, the authors proposed an equivalent formulation of the Robin-Robin loosely coupled scheme where the Lagrange multipliers are not unknowns of the fluid sub-problem but simple additional variables explicitly updated at each time step. A similar procedure can actually be applied for our problem to the Lagrange multiplier $\boldsymbol{\lambda}_{0,H}^{n-1}$. First, let us rewrite (5.2.8) as

$$-\boldsymbol{\lambda}_{0,H}^n=-\boldsymbol{\lambda}_{0,H}^{n-1}+\alpha\big(\widehat{\boldsymbol{\Pi}}_{0,H}(\boldsymbol{u}_h^n\circ\boldsymbol{\phi}_h^n)-\overline{\dot{\boldsymbol{r}}_H^{n-\frac{1}{2}}}\big)\quad\text{in}\quad\widehat{\boldsymbol{F}}_{0,H}. \tag{5.2.12}$$

Thanks to equation (5.2.12), **Step 3** of Algorithm 7 can be reformulated as: find $(\boldsymbol{u}_h^n, p_h^n, \boldsymbol{\lambda}_{N^\star,H}^n) \in \boldsymbol{V}_h \times Q_h \times \widehat{\boldsymbol{F}}_{N^\star,H}$ such that

$$\begin{cases} \rho_{\mathrm{f}}(\partial_\tau \boldsymbol{u}_h^n, \boldsymbol{v}_h)_\Omega + a_{\Omega,h}^{\mathrm{f}}\big(\boldsymbol{u}_h^{n-1}; (\boldsymbol{u}_h^n, p_h^n), (\boldsymbol{v}_h, q_h)\big) - (\boldsymbol{\lambda}_{N^\star,H}^n, \boldsymbol{v}_h \circ \boldsymbol{\phi}_H^n)_{\widehat{\varepsilon}} \\ + \alpha\big(\boldsymbol{u}_H^n \circ \boldsymbol{\phi}_H^n - \overline{\dot{\boldsymbol{r}}_h^{n-\frac{1}{2}}}, \widehat{\boldsymbol{\Pi}}_{0,H}(\boldsymbol{v}_h \circ \boldsymbol{\phi}_H^n)\big)_{(0,L)} - \big(\boldsymbol{\lambda}_{0,H}^{n-1}, \boldsymbol{v}_h \circ \boldsymbol{\phi}_H^n\big)_{\widehat{\varepsilon}} \\ + (\boldsymbol{\mu}_{N^\star,H}, \boldsymbol{u}_h^n \circ \boldsymbol{\phi}_H^n)_{\widehat{\varepsilon}} = 0 \end{cases} \tag{5.2.13}$$

for all $(\boldsymbol{v}_h, q_h, \boldsymbol{\mu}_{N^\star,H}) \in \boldsymbol{V}_h \times Q_h \times \widehat{\boldsymbol{F}}_{N^\star,H}$. We can then update $\boldsymbol{\lambda}_{0,H}^n$ through relation (5.2.12). While formulation (5.2.13) may seem more appealing than formulation (5.2.11) because it allows for the removal of the quantity $\boldsymbol{\lambda}_{0,H}^n$ as unknown of the fluid sub-problem, it nevertheless requires computing the L^2 projection of the entire set of test functions $\boldsymbol{v}_h \circ \boldsymbol{\phi}_H^n$ onto the space $\widehat{\boldsymbol{F}}_{0,H}$, which can be quite tedious. Therefore, from a practical point of view, we opted for the formulation (5.2.11) in the implementation.

5.2.2 Analysis of the energy stability

The energy stability of Algorithm 7 is stated in the following theorem

Theorem 5.2.1. *Let $\{(\boldsymbol{u}_h^n, p_h^n, \boldsymbol{r}_H^n, \boldsymbol{\theta}_H^n)\}$ be given by Algorithm 7. There holds*

$$\mathfrak{E}^n + \sum_{m=1}^{n} \mathfrak{D}^m \leqslant \mathfrak{E}^0 \quad \forall n \geqslant 1. \tag{5.2.14}$$

where the discrete mechanical energy $\mathfrak{E}^n$ of the system and $\mathfrak{D}^n$ are defined by

$$\begin{aligned} \mathfrak{E}^n \overset{\text{def}}{=} & \rho_{\mathrm{f}}\|\boldsymbol{u}_h^n\|_\Omega^2 + \rho_{\mathrm{b}}\|\dot{\boldsymbol{r}}_H^n\|_{\boldsymbol{A},(0,L)}^2 + \rho_{\mathrm{b}}\|\dot{\boldsymbol{\theta}}_H^n\|_{\boldsymbol{I},(0,L)}^2 + \|(\boldsymbol{r}_H^n, \boldsymbol{\theta}_H^n)\|_{\mathrm{b},H}^2 \\ & + \tau\alpha\|\widehat{\boldsymbol{\Pi}}_{0,H}(\boldsymbol{u}_h^n \circ \boldsymbol{\phi}_H^n)\|_{\widehat{\varepsilon}}^2 + \frac{\tau}{\alpha}\|\boldsymbol{\lambda}_{0,H}^n\|_{\widehat{\varepsilon}}^2 \\ \mathfrak{D}^n \overset{\text{def}}{=} & 2\mu\tau\|\varepsilon(\boldsymbol{u}_h^n)\|_\Omega^2 + \rho_{\mathrm{f}}\|\boldsymbol{u}_h^n - \boldsymbol{u}_h^{n-1}\|_\Omega^2 + 2\alpha\tau\|\overline{\dot{\boldsymbol{r}}_H^{n-\frac{1}{2}}} - \widehat{\boldsymbol{\Pi}}_{0,H}(\boldsymbol{u}_h^{n-1} \circ \boldsymbol{\phi}_H^{n-1})\|_{\widehat{\varepsilon}}^2. \end{aligned}$$

with

$$\begin{aligned} & \|\cdot\|_{\boldsymbol{A},(0,L)} \overset{\text{def}}{=} \sqrt{(\boldsymbol{A}\,\cdot,\cdot)_{(0,L)}}, \quad \|\cdot\|_{\boldsymbol{I},(0,L)} \overset{\text{def}}{=} \sqrt{(\boldsymbol{I}\,\cdot,\cdot)_{(0,L)}}, \\ & \|\cdot,\cdot\|_{\mathrm{b},H} \overset{\text{def}}{=} \sqrt{a_H^{\mathrm{b}}\big((\cdot,\cdot),(\cdot,\cdot)\big)}. \end{aligned}$$

Proof. By testing equation (5.2.9) with $(\delta\boldsymbol{r}_H, \delta\boldsymbol{\theta}_H) = \tau(\dot{\boldsymbol{r}}_H^{n-\frac{1}{2}}, \dot{\boldsymbol{\theta}}_H^{n-\frac{1}{2}})$, we get

$$\begin{aligned} & \frac{1}{2}\rho_{\mathrm{b}}\|\dot{\boldsymbol{r}}_H^n\|_{\boldsymbol{A},(0,L)}^2 + \frac{1}{2}\rho_{\mathrm{b}}\|\dot{\boldsymbol{\theta}}_H^n\|_{\boldsymbol{I},(0,L)}^2 + \frac{1}{2}\|(\boldsymbol{r}_H^n, \boldsymbol{\theta}_H^n)\|_{\mathrm{b},H}^2 = \\ & \frac{1}{2}\rho_{\mathrm{b}}\|\dot{\boldsymbol{r}}_H^{n-1}\|_{\boldsymbol{A},(0,L)}^2 + \frac{1}{2}\rho_{\mathrm{b}}\|\dot{\boldsymbol{\theta}}_H^{n-1}\|_{\boldsymbol{I},(0,L)}^2 + \frac{1}{2}\|(\boldsymbol{r}_h^{n-1}, \boldsymbol{\theta}_H^{n-1})\|_{\mathrm{b},H}^2 \\ & + \alpha\tau\big(\boldsymbol{u}_h^{n-1} \circ \boldsymbol{\phi}_H^{n-1} - \overline{\dot{\boldsymbol{r}}_H^{n-\frac{1}{2}}}, \overline{\dot{\boldsymbol{r}}_H^{n-\frac{1}{2}}}\big)_{\widehat{\varepsilon}} - \tau\big(\boldsymbol{\lambda}_{0,H}^{n-1}, \overline{\dot{\boldsymbol{r}}_H^{n-\frac{1}{2}}}\big)_{\widehat{\varepsilon}}. \end{aligned}$$

On the other hand, using integration by parts and the boundary conditions of $\boldsymbol{u}_h^{n-1}$, $\boldsymbol{u}_h^n$, we have

$$a_{\Omega,h}^{\mathrm{f}}(\boldsymbol{u}_h^{n-1};(\boldsymbol{u}_h^n,p_h),(\boldsymbol{u}_h^n,p_h)) \geqslant 2\mu_{\mathrm{f}}\|\varepsilon(\boldsymbol{u}_h^n)\|_\Omega^2.$$

We deduce that by taking $(\boldsymbol{v}_h,q_h,\boldsymbol{\mu}_{N^\star,H}) = (\boldsymbol{u}_h^n,p_h^n,\boldsymbol{\lambda}_{N^\star,H}^n)$ in (5.2.11), we obtain

$$\frac{\rho_{\mathrm{f}}}{2}\|\boldsymbol{u}_h^n\|_\Omega^2 + \frac{\rho_{\mathrm{f}}}{2}\|\boldsymbol{u}_h^n-\boldsymbol{u}_h^{n-1}\|_\Omega^2 + 2\mu_{\mathrm{f}}\tau\|\boldsymbol{\varepsilon}(\boldsymbol{u}_h^n)\|_\Omega^2 \leqslant \frac{\rho_{\mathrm{f}}}{2}\|\boldsymbol{u}_h^{n-1}\|_\Omega^2 + \tau(\boldsymbol{\lambda}_{0,H}^n,\boldsymbol{u}_h^n\circ\boldsymbol{\phi}_H^n)_{\widehat{\varepsilon}}$$

By adding these two previous relations, we get

$$\begin{aligned}
&\frac{\rho_{\mathrm{b}}}{2}\|\dot{\boldsymbol{r}}_H^n\|_{\boldsymbol{A},(0,L)}^2 + \frac{\rho_{\mathrm{b}}}{2}\|\dot{\boldsymbol{\theta}}_H^n\|_{\boldsymbol{I},(0,L)}^2 + \frac{1}{2}\|(\boldsymbol{r}_H^n,\boldsymbol{\theta}_H^n)\|_{\mathrm{b},H}^2\\
&+ \frac{\rho_{\mathrm{f}}}{2}\|\boldsymbol{u}_h^n\|_\Omega^2 + \frac{\rho_{\mathrm{f}}}{2}\|\boldsymbol{u}_h^n-\boldsymbol{u}_h^{n-1}\|_\Omega^2 + 2\mu_{\mathrm{f}}\tau\|\varepsilon(\boldsymbol{u}_h^n)\|_\Omega^2\\
&\leqslant \frac{\rho_{\mathrm{b}}}{2}\|\dot{\boldsymbol{r}}_H^{n-1}\|_{\boldsymbol{A},(0,L)}^2 + \frac{\rho_{\mathrm{b}}}{2}\|\dot{\boldsymbol{\theta}}_H^{n-1}\|_{\boldsymbol{I},(0,L)}^2 + \frac{1}{2}\|(\boldsymbol{r}_h^{n-1},\boldsymbol{\theta}_H^{n-1})\|_{\mathrm{b},H}^2 + \frac{\rho_{\mathrm{f}}}{2}\|\boldsymbol{u}_h^{n-1}\|_\Omega^2 + \tau J
\end{aligned}$$

with

$$J \stackrel{\mathrm{def}}{=} \alpha\big(\boldsymbol{u}_h^{n-1}\circ\boldsymbol{\phi}_H^{n-1} - \overline{\dot{\boldsymbol{r}}_H^{n-\frac{1}{2}}},\overline{\dot{\boldsymbol{r}}_H^{n-\frac{1}{2}}}\big)_{\widehat{\varepsilon}} - \big(\boldsymbol{\lambda}_{0,H}^{n-1},\overline{\dot{\boldsymbol{r}}_H^{n-\frac{1}{2}}}\big)_{\widehat{\varepsilon}} + (\boldsymbol{\lambda}_{0,H}^n,\boldsymbol{u}_h^n\circ\boldsymbol{\phi}_H^n)_{\widehat{\varepsilon}}.$$

By using the operator $\widehat{\boldsymbol{\Pi}}_{0,H}$, we can also write

$$J \stackrel{\mathrm{def}}{=} \alpha\big(\widehat{\boldsymbol{\Pi}}_{0,H}(\boldsymbol{u}_h^{n-1}\circ\boldsymbol{\phi}_H^{n-1}) - \overline{\dot{\boldsymbol{r}}_H^{n-\frac{1}{2}}},\overline{\dot{\boldsymbol{r}}_H^{n-\frac{1}{2}}}\big)_{\widehat{\varepsilon}} - \big(\boldsymbol{\lambda}_{0,H}^{n-1},\overline{\dot{\boldsymbol{r}}_H^{n-\frac{1}{2}}}\big)_{\widehat{\varepsilon}} + (\boldsymbol{\lambda}_{0,H}^n,\boldsymbol{u}_h^n\circ\boldsymbol{\phi}_H^n)_{\widehat{\varepsilon}}.$$

After some manipulations, we derive

$$\begin{aligned}
J =&\big(\widehat{\boldsymbol{\Pi}}_{0,H}(\boldsymbol{u}_h^{n-1}\circ\boldsymbol{\phi}_H^{n-1}) - \widehat{\boldsymbol{\Pi}}_{0,H}(\boldsymbol{u}_h^n\circ\boldsymbol{\phi}_H^n) + \widehat{\boldsymbol{\Pi}}_{0,H}(\boldsymbol{u}_h^n\circ\boldsymbol{\phi}_H^n) - \overline{\dot{\boldsymbol{r}}_H^{n-\frac{1}{2}}},\overline{\dot{\boldsymbol{r}}_H^{n-\frac{1}{2}}}\big)_{\widehat{\varepsilon}}\\
&- \big(\boldsymbol{\lambda}_{0,H}^{n-1},\overline{\dot{\boldsymbol{r}}_H^{n-\frac{1}{2}}}\big)_{\widehat{\varepsilon}} + (\boldsymbol{\lambda}_{0,H}^n,\boldsymbol{u}_h^n\circ\boldsymbol{\phi}_H^n)_{\widehat{\varepsilon}}\\
=&\big(\widehat{\boldsymbol{\Pi}}_{0,H}(\boldsymbol{u}_h^{n-1}\circ\boldsymbol{\phi}_H^{n-1}) - \widehat{\boldsymbol{\Pi}}_{0,H}(\boldsymbol{u}_h^n\circ\boldsymbol{\phi}_H^n),\overline{\dot{\boldsymbol{r}}_H^{n-\frac{1}{2}}}\big)_{\widehat{\varepsilon}} + (\boldsymbol{\lambda}_{0,H}^n,\boldsymbol{u}_h^n\circ\boldsymbol{\phi}_H^n)_{\widehat{\varepsilon}}\\
&+ \big(\widehat{\boldsymbol{\Pi}}_{0,H}(\boldsymbol{u}_h^n\circ\boldsymbol{\phi}_H^n) - \overline{\dot{\boldsymbol{r}}_H^{n-\frac{1}{2}}},\overline{\dot{\boldsymbol{r}}_H^{n-\frac{1}{2}}}\big)_{\widehat{\varepsilon}} - \big(\boldsymbol{\lambda}_{0,H}^{n-1},\overline{\dot{\boldsymbol{r}}_H^{n-\frac{1}{2}}}\big)_{\widehat{\varepsilon}}.
\end{aligned}$$

Finally using (5.2.12) with $\delta\boldsymbol{r}_H = \dot{\boldsymbol{r}}_H^{n-\frac{1}{2}}$ in the last line of the above equation, we obtain the following result,

$$\begin{aligned}
J =&\alpha\big(\widehat{\boldsymbol{\Pi}}_{0,H}(\boldsymbol{u}_h^{n-1}\circ\boldsymbol{\phi}_H^{n-1}) - \widehat{\boldsymbol{\Pi}}_{0,H}(\boldsymbol{u}_h^n\circ\boldsymbol{\phi}_H^n),\overline{\dot{\boldsymbol{r}}_H^{n-\frac{1}{2}}}\big)_{\widehat{\varepsilon}} + \big(\boldsymbol{\lambda}_{0,H}^n,\widehat{\boldsymbol{\Pi}}_{0,H}(\boldsymbol{u}_h\circ\boldsymbol{\phi}_H) - \overline{\dot{\boldsymbol{r}}_H^{n-\frac{1}{2}}}\big)_{\widehat{\varepsilon}},\\
=&\alpha\big(\widehat{\boldsymbol{\Pi}}_{0,H}(\boldsymbol{u}_h^{n-1}\circ\boldsymbol{\phi}_H^{n-1}) - \widehat{\boldsymbol{\Pi}}_{0,H}(\boldsymbol{u}_h^n\circ\boldsymbol{\phi}_H^n),\overline{\dot{\boldsymbol{r}}_H^{n-\frac{1}{2}}}\big)_{\widehat{\varepsilon}} + \frac{1}{\alpha}\big(\boldsymbol{\lambda}_{0,H}^n,\boldsymbol{\lambda}_{0,H}^{n-1}-\boldsymbol{\lambda}_{0,H}^n\big)_{\widehat{\varepsilon}}
\end{aligned}$$

and with the following identity

$$(\boldsymbol{v}-\boldsymbol{w},\boldsymbol{\psi}) = \frac{1}{2}\left(\|\boldsymbol{v}\|^2 - \|\boldsymbol{w}\|^2 + \|\boldsymbol{\psi}-\boldsymbol{w}\|^2 - \|\boldsymbol{\psi}-\boldsymbol{v}\|^2\right),$$

we have

$$\begin{aligned}
\big(\widehat{\boldsymbol{\Pi}}_{0,H}(\boldsymbol{u}_h^{n-1}\circ\boldsymbol{\phi}_H^n) - \widehat{\boldsymbol{\Pi}}_{0,H}(\boldsymbol{u}_h^n\circ\boldsymbol{\phi}_H^n), \overline{\dot{\boldsymbol{r}}_H^{n-\frac{1}{2}}}\big)_{\widehat{\varepsilon}} = \\
\|\widehat{\boldsymbol{\Pi}}_{0,H}(\boldsymbol{u}_h^{n-1}\circ\boldsymbol{\phi}_H^{n-1})\|_{\widehat{\varepsilon}}^2 - \|\widehat{\boldsymbol{\Pi}}_{0,H}(\boldsymbol{u}_h^n\circ\boldsymbol{\phi}_H^n)\|_{\widehat{\varepsilon}}^2 \\
- \|\overline{\dot{\boldsymbol{r}}_H^{n-\frac{1}{2}}} - \widehat{\boldsymbol{\Pi}}_{0,H}(\boldsymbol{u}_h^{n-1}\circ\boldsymbol{\phi}_H^{n-1})\|_{\widehat{\varepsilon}}^2 + \|\overline{\dot{\boldsymbol{r}}_H^{n-\frac{1}{2}}} - \widehat{\boldsymbol{\Pi}}_{0,H}(\boldsymbol{u}_h^n\circ\boldsymbol{\phi}_H^n)\|_{\widehat{\varepsilon}}^2 \\
\big(\boldsymbol{\lambda}_{0,H}^n, \boldsymbol{\lambda}_{0,H}^{n-1} - \boldsymbol{\lambda}_{0,H}^n\big)_{\widehat{\varepsilon}} = \quad \|\boldsymbol{\lambda}_{0,H}^{n-1}\|_{\widehat{\varepsilon}}^2 - \|\boldsymbol{\lambda}_{0,H}^n\|_{\widehat{\varepsilon}}^2 - \|\boldsymbol{\lambda}_{0,H}^n - \boldsymbol{\lambda}_{0,H}^{N,n-1}\|_{\widehat{\varepsilon}}^2.
\end{aligned}$$

Using again (5.2.12), we note that

$$\|\boldsymbol{\lambda}_{0,H}^n - \boldsymbol{\lambda}_{0,H}^{n-1}\|_{\widehat{\varepsilon}}^2 = \alpha^2\|\overline{\dot{\boldsymbol{r}}_H^{n-\frac{1}{2}}} - \widehat{\boldsymbol{\Pi}}_{0,H}(\boldsymbol{u}_h^n\circ\boldsymbol{\phi}_H^n)\|_{\widehat{\varepsilon}}^2.$$

Thus we conclude

$$\begin{aligned}
J =& \frac{\alpha}{2}\big(\|\widehat{\boldsymbol{\Pi}}_{0,H}(\boldsymbol{u}_h^{n-1}\circ\boldsymbol{\phi}_H^{n-1})\|_{\widehat{\varepsilon}}^2 - \|\widehat{\boldsymbol{\Pi}}_{0,H}(\boldsymbol{u}_h^n\circ\boldsymbol{\phi}_H^n)\|_{\widehat{\varepsilon}}^2\big) + \frac{1}{2\alpha}\big(\|\boldsymbol{\lambda}_{0,H}^{n-1}\|_{\widehat{\varepsilon}}^2 - \|\boldsymbol{\lambda}_{0,H}^n\|_{\widehat{\varepsilon}}^2\big) \\
&- \frac{\alpha}{2}\|\overline{\dot{\boldsymbol{r}}_H^{n-\frac{1}{2}}} - \widehat{\boldsymbol{\Pi}}_{0,H}(\boldsymbol{u}_h^{n-1}\circ\boldsymbol{\phi}_H^{n-1})\|_{\widehat{\varepsilon}}^2.
\end{aligned}$$

By replacing the time index by m and by summing over $\{0,\dots,n\}$, we obtain the estimate (5.2.14). □

5.2.3 Iterative partitioned solution of the implicit coupling

Algorithm 7 can be interpreted as a single iteration of a Robin-Robin method for the partitioned solution of Algorithm 1 (where the coupling conditions are written in the reference configuration). The corresponding Robin-Robin iterations are detailed in Algorithm 8.

This kind of iterative solution procedures has already been applied for the partitioned solution of strong coupling in [Badia et al., 2008a, Nobile and Vergara, 2008, Gerardo-Giorda et al., 2010], improving the standard Dirichlet-Neumann procedure.

5.3 Numerical results

In this section, we will compare the results obtained with Algorithm 1 and Algorithm 7 for some test cases introduced in Section 2.4 of Chapter 2. In particular, we will investigate the impact of the parameter α and of correction iterations on the simulations obtained with the Robin-Robin loosely coupled scheme.

Algorithm 8 Partitioned Robin-Robin iterations

Step 1: Initialize $\boldsymbol{r}_0$ and $\boldsymbol{\lambda}_0$

Step 2: For $k = 1, \dots$ until convergence

- **Fluid step:** Find $(\boldsymbol{u}_k, p_k, \boldsymbol{\lambda}_k) \in \boldsymbol{V}_h \times Q_h \times \widehat{\boldsymbol{F}}_{N,H}$ such that $\boldsymbol{\lambda}_k = \boldsymbol{\lambda}_{0,k} + \boldsymbol{\lambda}_{N^\star,k}$ with $(\boldsymbol{\lambda}_{0,k}, \boldsymbol{\lambda}_{N^\star,k}) \in \widehat{\boldsymbol{F}}_{0,H} \times \widehat{\boldsymbol{F}}_{N^\star,H}$ and

$$\begin{cases} \dfrac{\rho_{\mathrm{f}}}{\tau}(\boldsymbol{u}_k - \boldsymbol{u}_h^{n-1}, \boldsymbol{v}_h)_\Omega + a^{\mathrm{f}}_{\Omega,h}\big(\boldsymbol{u}_h^{n-1}; (\boldsymbol{u}_k, p_k), (\boldsymbol{v}_h, q_h)\big) - (\boldsymbol{\lambda}_k, \boldsymbol{v}_h \circ \boldsymbol{\phi}_H^n)_{\hat{\varepsilon}} \\ + \alpha(\boldsymbol{\mu}_{0,H}, \boldsymbol{u}_k \circ \boldsymbol{\phi}_H^n - \overline{\dot{\boldsymbol{r}}_{k-1}})_{\hat{\varepsilon}} + (\boldsymbol{\mu}_{0,H}, \boldsymbol{\lambda}_{0,k} - \boldsymbol{\lambda}_{0,k-1})_{\hat{\varepsilon}} \\ + (\boldsymbol{\mu}_{N^\star,H}, \boldsymbol{u}_k \circ \boldsymbol{\phi}_H^n)_{\hat{\varepsilon}} = 0 \end{cases} \tag{5.2.15}$$

  for all $(\boldsymbol{v}_h, q_h, \boldsymbol{\mu}_{N,H}) \in \boldsymbol{V}_h \times Q_h \times \widehat{\boldsymbol{F}}_{N,H}$ with $(\boldsymbol{\mu}_{0,H}, \boldsymbol{\mu}_{N^\star,H}) = (\widehat{\boldsymbol{\Pi}}_{0,H}(\boldsymbol{\mu}_{N,H}), \widehat{\boldsymbol{\Pi}}_{N^\star,H}(\mu_{N,H}))$.

- **Solide step:** Find $(\boldsymbol{r}_k, \boldsymbol{\theta}_k) \in \boldsymbol{Y}_H \times \boldsymbol{Y}_H$ such that $(\dot{\boldsymbol{r}}_k, \dot{\boldsymbol{\theta}}_k) = \frac{1}{\tau}(\boldsymbol{r}_k - \boldsymbol{r}_H^{n-1}, \boldsymbol{\theta}_k - \boldsymbol{\theta}_H^{n-1})$ and

$$\begin{cases} \dfrac{\rho_{\mathrm{b}}}{\tau}\big(\boldsymbol{A}(\dot{\boldsymbol{r}}_k - \dot{\boldsymbol{r}}_H^{n-1}), \delta\boldsymbol{r}_H\big)_{(0,L)} + \dfrac{\rho_{\mathrm{b}}}{\tau}\big(\boldsymbol{I}(\dot{\boldsymbol{\theta}}_k - \dot{\boldsymbol{\theta}}_H^{n-1}), \delta\boldsymbol{\theta}_H\big)_{(0,L)} \\ + a_H^{\mathrm{b}}\big(((\boldsymbol{r}_k + \boldsymbol{r}_H^{n-1})/2, (\boldsymbol{\theta}_k + \boldsymbol{\theta}_H^{n-1})/2), (\delta\boldsymbol{r}_H, \delta\boldsymbol{\theta}_H)\big) \\ + \alpha(\overline{\dot{\boldsymbol{r}}_k} - \boldsymbol{u}_k \circ \boldsymbol{\phi}_H^n, \overline{\delta\boldsymbol{r}_H})_{\hat{\varepsilon}} = -\big(\boldsymbol{\lambda}_{0,k}, \overline{\delta\boldsymbol{r}_H}\big)_{\hat{\varepsilon}} \end{cases} \tag{5.2.16}$$

  for all $(\delta\boldsymbol{r}_H, \delta\boldsymbol{\theta}_H) \in \boldsymbol{Y}_H \times \boldsymbol{Y}_H$.

5.3.1 Single beam in a Stokesian flow

We consider the same geometric configuration and boundary conditions as in the test case of Section 2.4.1 (see Figure 2.3). More specifically, the following parabolic profile is enforced at the inlet boundary Γ_{in}:

$$\boldsymbol{u}_{\mathrm{in}}(\boldsymbol{x}, t) \overset{\mathrm{def}}{=} u_{\mathrm{ref}}\left(1 + \cos\left(\frac{2\pi t}{T}\right)\right)\big(1 - (z-1)(z+1)\big)\boldsymbol{e}_x. \tag{5.3.1}$$

The fluid satisfies the Stokes equations and the solid the linear Timoshenko beam equations. The fluid and solid parameters are given by $\mu_{\mathrm{f}} = 0.05$, $\varepsilon = 0.06$, $\rho_{\mathrm{b}} = 1$, $E = 10^7$, respectively. The fluid mesh satisfies $h/\varepsilon = 1/4$ in the vicinity of the beam and $h = 0.05$ elsewhere. For the beam and Lagrange multiplier space, we discretize the interval $(0, L)$ with a uniform mesh $H = 0.05$. The behavior of the coupled system is studied over the time interval $[0, 0.06]$ with a time-step length of $\tau = 5 \cdot 10^{-3}$.

We consider several values for the Robin coefficient $\alpha \in \{0.1, 0.5, 1\}$ and different correction iterations. In Figure 5.1, we plot the displacement of the beam last cross-section for both Algorithm 1 and Algorithm 7, with $N = 0$, and with or without the addition of a correction iteration. Without the correction iteration, we observe some fluctuations in the solution with respect to the Robin coefficient, the best approximation being given by

$\alpha = 0.1$ for which the solution computed is close to the one of Algorithm 1. Introducing a correction iteration reduces the variability of the method and all the values of α gives a good approximation of the reference solution.

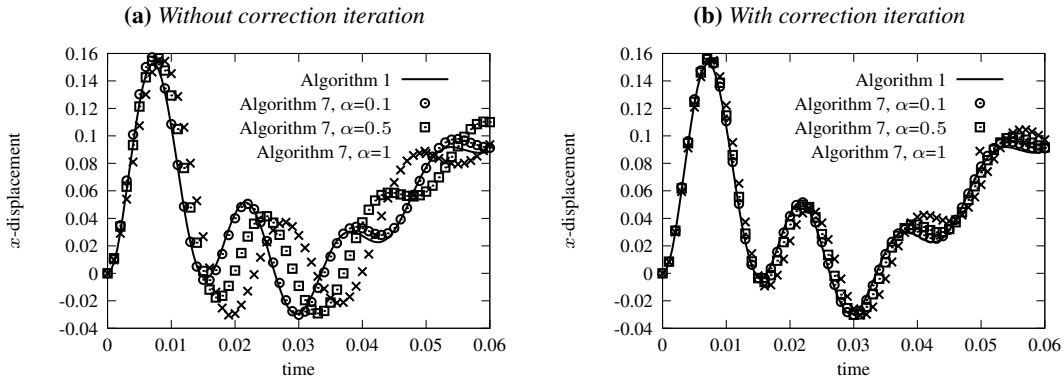

Figure 5.1: *Displacement of the last cross-section of the beam computed with Algorithm 1 and Algorithm 7 with or without correction iteration over the interval* $[0, 0.06]$ *- fluid sub-problem solved with Stokes equations.*

5.3.2 Single beam immersed in a Navier-Stokes flow

We consider the test case Section 2.4.2 for $Re = 480$ and the inlet velocity given in (5.3.1). The fluid and beam parameters are given by $\rho_{\mathrm{b}} = 1$, $\rho_{\mathrm{f}} = 1$, $\mu_{\mathrm{f}} = 0.05$, $E = 3e8$. Similarly to the previous test case, we consider various values for the Robin coefficient $\alpha \in \{0.1, 0.5, 1\}$. We use the same fluid and solid meshes, and time discretization parameters as in the previous section. In Figure 5.2, we plot the displacement of the last cross section of the beam over the time interval $[0, 0.06]$ for Algorithm 1 and Algorithm 7, with $N = 0$, with or without correction. For this test case, the solutions obtained for $\alpha \in \{0.5, 1\}$ without correction are close to the reference solution obtained with Algorithm 1. Adding a correction enables the solution obtained with Algorithm 7 and $\alpha = 0.1$ to approach the reference solution, although it seems that a second correction iteration would be necessary to achieve a more satisfactory solution. Note in that in general, there is not a priori optimal values for the coefficient α , however some works on the error analysis of the loosely coupled Robin-Robin schemes for thick structures suggests that it should behave as $\sqrt{\rho_{\mathrm{b}} E}$, which may explain which we need to take a higher value for α in this test case with respect to the previous one where the Young's modulus was smaller.

5.3.3 Multiple beams immersed in an incompressible flow

As last example, we consider the numerical test case of Section 2.4.3 involving 75 circular beams of radius $\varepsilon = 0.05$, arranged with 5 along the y-axis and 15 along the x-axis. The

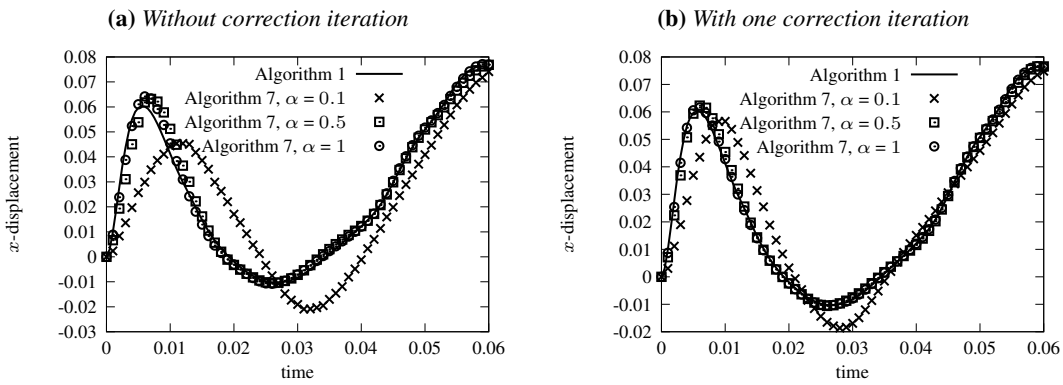

Figure 5.2: *Displacement of the last beam cross-section computed with Algorithm 1 and Algorithm 7 with or without correction iteration over the interval* $[0, 0.06]$ *- fluid sub-problem solved with Navier-Stokes equations.*

beam is modeled by a non-linear co-rotational formulation that allows for large deformations (see [Krenk, 2009, Chapter 5]) and potential contact are dealt using a ray-tracing algorithm described in Section 2.A.1 of the Appendix. All the beams have the same Young's modulus and density, $E = 10^8$ and $\rho^{\mathrm{b}} = 1$, respectively. The fluid satisfies the Navier-Stokes equations with Reynolds $Re = 480$, density $\rho_{\mathrm{f}} = 1$ and viscosity $\mu_{\mathrm{f}} = 0.05$. The size of the fluid mesh is uniform with $h = 0.035$. Based on the previous results, we take $\alpha = 1$ as Robin coefficient and one correction iteration. In Figure 5.3, we provide snapshots of the fluid velocity magnitude comparing the solution computed with Algorithm 7, $N = 2$ and Algorithm 1, $N = 2$ at times $t \in \{0.05, 0.1, 0.45, 0.6\}$. Using the Robin-based loosely coupled scheme, the duration of the simulation was divided by four and we observe, at least qualitatively, close results for both Algorithm 7 and Algorithm 1, confirming the interest of the explicit method for large-scale simulations.

Conclusion

In this chapter we presented a Robin-based loosely coupled scheme for the simulation of slender structures immersed in a three dimensional flow. Assuming that the contribution of the solid rotations could be neglected in the coupling conditions, we derived from the reduced order coupled model introduced in Chapter 2 a time explicit scheme with interface Robin conditions in both the fluid and the solid sub-problems. The main advantage of this coupling procedure is to reduce the computational cost of the resolution of the coupled problem by calling the fluid solver and solid solver only once per time-step. A major issue of the loosely coupled schemes for slender structures being the added-mass instability, we also proved that our Robin-based loosely coupled scheme was unconditionally stable. However, although stable, the loosely coupled schemes are not necessarily accurate. By

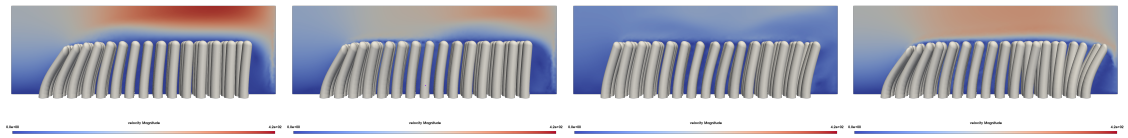

Algorithm 7, $N = 2$

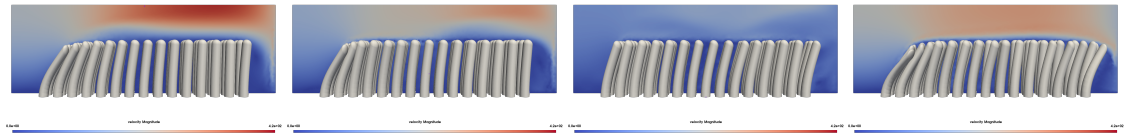

t=0.005 t=0.01 t=0.045 t=0.06

Algorithm 1, $N = 2$

Figure 5.3: *Snapshots of the fluid velocity magnitude for multiple beams immersed in a Navier-Stokes flow with Algorithm 7, $N = 2$ (up) and Algorithm 1, $N = 2$ (down) at time $t \in \{0.005, 0.01, 0.045, 0.06\}$.*

comparing the results obtained on several test cases with respect to the solution of the semi-implicit coupled scheme, we observed that the results strongly depended on the choice of the Robin parameter α. To reduce the variability of the method, by writing the explicit scheme as one step of an Algorithm for the resolution of the semi-implicit scheme, we proposed a correction iteration consisting of reiterating the Robin scheme a second time without updating the time step. We then observed a much smaller variation of the results and solutions close to those obtained with the semi-implicit scheme.

The study presented in this chapter needs to be taken further, in particular by completing it with numerical tests. A first potential improvement of this work would be to include the rotation contributions in the Robin-based coupling conditions, which however may be quite technical due to their dependence on the geometric configuration of the beam interface. Secondly, we also would like to identify if an optimal range for the Robin parameter α may allow to avoid the need of correction iterations.

Conclusion and perspectives

Conclusion

In this PhD dissertation, we introduced a new formulation for the coupling of one or multiple slender structures, described as 1D manifolds, with a surrounding 3D incompressible fluid. In order to overcome the mathematical issues related to the ill-posed trace operators with such dimensional gap, the proposed formulation builds on the introduction of averaged interface conditions (via projection operators onto a Fourier-based finite-dimensional space). Indeed, standard modeling approaches of 3D-1D coupled problems rely on concentrated sources (delta Dirac), whose solution exhibits low regularity, which compromises model well-posedness and the development of accurate and efficient approximation methods.

In two different simplified settings considered in Chapters 4 and 3, we showed that the modeling error can be mitigated in terms of the number of Fourier modes in the projection space, which enables the balance between efficiency and accuracy. Furthermore, the solutions provided by the present approach are regular enough to be approximated by standard numerical methods. A priori error estimates for a fictitious domain finite element method with respect to the thickness and mesh parameters were thus derived. An augmented finite element method was also proposed which partially enables to decouple the modelling error emerging from the mixed-dimensional formulation and the numerical error of the finite element method.

Finally, in Chapters 2 and 5, the proposed reduced modeling approach is extened to the case of 3D-1D fluid-structure interaction problems. Several numerical experiments involving either Stokes or Navier-Stokes flow (with moderate Reynolds) and a single linear Timoshenko beam, indicate that this formulation yields accurate results with respect to the 3D full coupled problem, both in terms of the fluid and solid dynamics. In particular, we

illustrate that by properly choosing the Fourier projection space, both the displacement and rotation dynamics of the beam can be captured. This approach has also been investigated in the the case of multiple nonlinear beams, possibly getting into contact. In order to mitigate the computational complexity of the coupled problems, a Robin-based loosely coupled scheme has been proposed.

Perspectives

Extensions of this work can explore a number of research directions. The results of Chapters 3 and 4 were limited to two spatial dimensions. An interesting problem would be to extend the well-posedness and the model approximation error results to the 3D case, notably for the Stokes problem. For the model approximation error, in the spirit of the analysis of the slender-body theory [Mori and Ohm, 2021], a first step would be to carry out a spectral analysis on the reduced-order Stokes problem, by considering a straight periodic beam in order to obtain closed-form solutions of the eigenvalue problem. The asymptotic behavior with respect to the thickness of the slender body of these explicit solutions could be used to estimate the modeling error with respect to the full 3D model. These explicit solutions could also be leveraged to develop an augmented finite element method, similar to the one proposed in Chapters 2 and 4, which the purpose of mitigating one the main drawbacks of the proposed method, that is, the dependence of the numerical error of the standard finite element method to the ratio h/ε.

Another interesting extension of the present work is to explore the well-posedness of the 3D fluid-beam reduced order model. Though some studies have been devoted to the existence of solutions for elastic slender structures interacting with a 2D Navier-Stokes flow [Grandmont and Hillairet, 2016, Grandmont et al., 2019, Lequeurre, 2011], or shell or plate in 3D [Lengeler, 2014, Muha and Canić, 2013, Grandmont, 2008], the case of the 3D-1D coupling has not been treated so far, to the best of my knowledge. For such coupled problems, full 3D models often suffer from lack of regularity of the solutions in the solid model. Instead, the case of 3D-1D mixed-dimensional coupling equations may improve the situation.

Finally, in this PhD dissertation, we have shown that the proposed method is able to simulate a large number of beams in a efficient way, notably using loosely coupled schemes. We hence plan to apply this methodology to more realistic situations. One example is the simulation of the lung cilia involved in mucociliary clearance [Smith et al., 2007, Alouges et al., 2013]. The cilia have the ability to change their shapes by generating internal stress. This mechanism is based on the strong reciprocal interaction with the surrounding fluid. We are particularly interesting in investigating whether the presented mixed-dimensional model, with an active 1D model of the cilia (see, e.g., [Decoene et al., 2020]), is able to reproduce the so-called metachronal wave [Mitran, 2007]. It is worth noting that, from an algorithmic perspective, when the mesh size is of the same order as

the thickness of the structure (a framework preferred for limiting the computational cost of the simulations), in addition to numerical errors, another limitation is that the matrix system may become ill-conditioned, requiring the construction of efficient iterative algorithms. Subsequently, it would also be interesting to investigate the impact of some recently developed preconditioners for our specific problem [Dimola et al., 2023].

Bibliography

[Abdol Azis et al., 2019] Abdol Azis, M. H., Evrard, F., and van Wachem, B. (2019). An Immersed Boundary method for flows with dense particle suspensions. *Acta mechanica*, 230:485–515.

[Alouges et al., 2013] Alouges, F., DeSimone, A., Giraldi, L., and Zoppello, M. (2013). Self-propulsion of slender micro-swimmers by curvature control: N-link swimmers. *International Journal of Non-Linear Mechanics*, 56:132–141.

[Angot et al., 1999] Angot, P., Bruneau, C.-H., and Fabrie, P. (1999). A penalization method to take into account obstacles in incompressible viscous flows. *Numerische Mathematik*, 81(4):497–520.

[Antoine et al., 2012] Antoine, X., Ramdani, K., and Thierry, B. (2012). Wide frequency band numerical approaches for multiple scattering problems by disks. *Journal of Algorithms & Computational Technology*, 6(2):241–259.

[Arunakirinathar and Reddy, 1993] Arunakirinathar, K. and Reddy, B. D. (1993). Mixed Finite Element methods for elastic rods of arbitrary geometry. *Numerische Mathematik*, 64:13–43.

[Ausas et al., 2022a] Ausas, R. F., Gebhardt, C. G., and Buscaglia, G. C. (2022a). A Finite Element method for simulating soft active non-shearable rods immersed in generalized Newtonian fluids. *Communications in Nonlinear Science and Numerical Simulation*, 108:106213.

[Ausas et al., 2022b] Ausas, R. F., Gebhardt, C. G., and Buscaglia, G. C. (2022b). A Finite Element method for simulating soft active non-shearable rods immersed in generalized

Newtonian fluids. *Communications in Nonlinear Science and Numerical Simulation*, 108:106213.

[Baaijens, 2001] Baaijens, F. P. T. (2001). A Fictitious Domain/mortar element method for fluid-structure interaction. *International Journal for Numerical Methods in Fluids*, 35:743–761.

[Babuška et al., 2017] Babuška, I., Soane, A. M., and Suri, M. (2017). The computational modeling of problems on domains with small holes. *Computer Methods in Applied Mechanics and Engineering*, 322:563–589.

[Badia et al., 2008a] Badia, S., Nobile, F., and Vergara, C. (2008a). Fluid–structure partitioned procedures based on Robin transmission conditions. *Journal of Computational Physics*, 227(14):7027–7051.

[Badia et al., 2008b] Badia, S., Quaini, A., and Quarteroni, A. (2008b). Modular vs. non-modular preconditioners for fluid–structure systems with large added-mass effect. *Computer Methods in Applied Mechanics and Engineering*, 197(49-50):4216–4232.

[Baek and Karniadakis, 2012] Baek, H. and Karniadakis, G. E. (2012). A convergence study of a new partitioned fluid–structure interaction algorithm based on fictitious mass and damping. *Journal of Computational Physics*, 231(2):629–652.

[Banks et al., 2014] Banks, J. W., Henshaw, W. D., and Schwendeman, D. W. (2014). An analysis of a new stable partitioned algorithm for FSI problems. Part I: Incompressible flow and elastic solids. *Journal of Computational Physics*, 269:108–137.

[Barrenechea and González, 2018] Barrenechea, G. R. and González, C. (2018). A stabilized Finite Element method for a Fictitious Domain problem allowing small inclusions. *Numerical Methods for Partial Differential Equations*, 34:167 – 183.

[Belponer et al., 2023] Belponer, C., Caiazz, A., and Heltai, L. (2023). Reduced Lagrange multiplier approach for non-matching coupled problems in multiscale elasticity. *arXiv preprint arXiv:2309.06797*.

[Boffi et al., 2013] Boffi, D., Brezzi, F., Fortin, M., et al. (2013). *Mixed Finite Element Methods and applications*, volume 44. Springer.

[Boffi and Gastaldi, 2015] Boffi, D. and Gastaldi, L. (2015). A Fictitious Domain approach with Lagrange multiplier for fluid-structure interactions. *Numerische Mathematik*, 135:711–732.

[Boilevin-Kayl et al., 2019] Boilevin-Kayl, L., Fernández, M. A., and Gerbeau, J.-F. (2019). Numerical methods for immersed FSI with thin-walled structures. *Computers & Fluids*.

[Bonnaillie-Noël and Dambrine, 2013] Bonnaillie-Noël, V. and Dambrine, M. (2013). Interactions between moderately close circular inclusions: the Dirichlet–Laplace equation in the plane. *Asymptotic Analysis*, 84(3-4):197–227.

[Bonnaillie-Noël et al., 2007] Bonnaillie-Noël, V., Dambrine, M., Tordeux, S., and Vial, G. (2007). On moderately close inclusions for the Laplace equation. *Comptes Rendus Mathématique*, 345(11):609–614.

[Boulakia et al., 2023] Boulakia, M., Grandmont, C., Lespagnol, F., and Zunino, P. (2023). Numerical approximation of the Poisson problem with small holes, using augmented finite elements and defective boundary conditions. working paper or preprint.

[Bouzarth and Minion, 2011] Bouzarth, E. L. and Minion, M. L. (2011). Modeling slender bodies with the method of regularized Stokeslets. *J. Comput. Phys.*, 230:3929–3947.

[Brezzi, 1974] Brezzi, F. (1974). On the existence, uniqueness and approximation of saddle-point problems arising from Lagrangian multipliers. *Publications mathématiques et informatique de Rennes*, 1(S4):1–26.

[Brezzi and Pitkäranta, 1984] Brezzi, F. and Pitkäranta, J. (1984). On the stabilization of finite element approximations of the Stokes equations. In *Efficient Solutions of Elliptic Systems: Proceedings of a GAMM-Seminar Kiel, January 27 to 29, 1984*, pages 11–19. Springer.

[Bringley and Peskin, 2008] Bringley, T. T. and Peskin, C. S. (2008). Validation of a simple method for representing spheres and slender bodies in an Immersed Boundary method for Stokes flow on an unbounded domain. *J. Comput. Phys.*, 227:5397–5425.

[Bukač et al., 2014] Bukač, M., Čanić, S., Glowinski, R., Muha, B., and Quaini, A. (2014). A modular, operator-splitting scheme for fluid–structure interaction problems with thick structures. *International journal for numerical methods in fluids*, 74(8):577–604.

[Bukač et al., 2015] Bukač, M., Čanić, S., and Muha, B. (2015). A partitioned scheme for fluid–composite structure interaction problems. *Journal of Computational Physics*, 281:493–517.

[Burman, 2010] Burman, E. (2010). Ghost penalty. *Comptes Rendus. Mathématique*, 348(21-22):1217–1220.

[Burman et al., 2023] Burman, E., Durst, R., Fernández, M., and Guzmán, J. (2023). Loosely coupled, non-iterative time-splitting scheme based on Robin–Robin coupling: Unified analysis for parabolic/parabolic and parabolic/hyperbolic problems. *Journal of Numerical Mathematics*, 31(1):59–77.

[Burman et al., 2022a] Burman, E., Durst, R., Fernández, M. A., and Guzmán, J. (2022a). Fully discrete loosely coupled Robin-Robin scheme for incompressible fluid–structure interaction: stability and error analysis. *Numerische Mathematik*, 151(4):807–840.

[Burman et al., 2022b] Burman, E., Durst, R., and Guzmán, J. (2022b). Stability and error analysis of a splitting method using Robin–Robin coupling applied to a fluid–structure interaction problem. *Numerical Methods for Partial Differential Equations*, 38(5):1396–1406.

[Burman and Fernández, 2009] Burman, E. and Fernández, M. A. (2009). Stabilization of explicit coupling in fluid–structure interaction involving fluid incompressibility. *Computer Methods in Applied Mechanics and Engineering*, 198(5-8):766–784.

[Burman and Fernández, 2014] Burman, E. and Fernández, M. A. (2014). Explicit strategies for incompressible fluid-structure interaction problems: Nitsche type mortaring versus Robin–Robin coupling. *International Journal for Numerical Methods in Engineering*, 97(10):739–758.

[Burman and Hansbo, 2014] Burman, E. and Hansbo, P. (2014). Fictitious Domain methods using cut elements: III. A stabilized Nitsche method for Stokes' problem. *ESAIM: Mathematical Modelling and Numerical Analysis-Modélisation Mathématique et Analyse Numérique*, 48(3):859–874.

[Canic et al., 2012] Canic, S., Muha, B., and Bukac, M. (2012). Stability of the kinematically coupled\beta-scheme for fluid-structure interaction problems in hemodynamics. *arXiv preprint arXiv:1205.6887*.

[Caubet et al., 2016] Caubet, F., Conca, C., and Godoy, M. (2016). On the detection of several obstacles in 2d Stokes flow: topological sensitivity and combination with shape derivatives. *Inverse Problems & Imaging*, 10(2):327.

[Causin et al., 2005] Causin, P., Gerbeau, J.-F., and Nobile, F. (2005). Added-mass effect in the design of partitioned algorithms for fluid–structure problems. *Computer methods in applied mechanics and engineering*, 194(42-44):4506–4527.

[Chapelle, 1997] Chapelle, D. (1997). A locking-free approximation of curved rods by straight beam elements. *Numerische Mathematik*, 77:299–322.

[Chapelle and Ferent, 2003] Chapelle, D. and Ferent, A. (2003). Modeling of the inclusion of a reinforcing sheet within a 3d medium. *Mathematical Models and Methods in Applied Sciences*, 13:573–595.

[Chen et al., 2006] Chen, J., Lu, X.-Y., and Wang, W. (2006). Non-Newtonian effects of blood flow on hemodynamics in distal vascular graft anastomoses. *Journal of Biomechanics*, 39(11):1983–1995.

[Chesnel and Claeys, 2016] Chesnel, L. and Claeys, X. (2016). A numerical approach for the Poisson equation in a planar domain with a small inclusion. *BIT Numerical Mathematics*, 56(4):1237–1256.

[Chiastra et al., 2014] Chiastra, C., Migliavacca, F., Martínez, M. Á., and Malvè, M. (2014). On the necessity of modelling fluid–structure interaction for stented coronary arteries. *Journal of the mechanical behavior of biomedical materials*, 34:217–230.

[Chouly et al., 2023] Chouly, F., Hild, P., and Renard, Y. (2023). *Finite Element Approximation of Contact and Friction in Elasticity*, volume 48. Springer Nature.

[Claeys and Collino, 2010] Claeys, X. and Collino, F. (2010). Augmented Galerkin schemes for the numerical solution of scattering by small obstacles. *Numerische Mathematik*, 116(2):243–268.

[Cortez et al., 2005] Cortez, R., Fauci, L. J., and Medovikov, A. A. (2005). The method of regularized Stokeslets in three dimensions : Analysis, validation, and application to helical swimming. *Physics of Fluids*, 17:031504.

[Corti et al., 2023] Corti, D., Delay, G., Fernández, M. A., Vergnet, F., and Vidrascu, M. (2023). Low-order Fictitious Domain method with enhanced mass conservation for an interface Stokes problem. *ESAIM: Mathematical Modelling and Numerical Analysis*.

[Cosserat and Cosserat, 1909] Cosserat, E. M. P. and Cosserat, F. (1909). *Théorie des corps déformables*. A. Hermann et fils.

[Dai, 2015] Dai, J. S. (2015). Euler–Rodrigues formula variations, quaternion conjugation and intrinsic connections. *Mechanism and Machine Theory*, 92:144–152.

[Dautray and Lions, 1985] Dautray, R. and Lions, J.-L. (1985). Analyse mathématique et calcul numérique pour les sciences et les techniques. *Collection du Commissariat a l'Energie Atomique. Serie Scientifique*.

[Decoene et al., 2023] Decoene, A., Martin, S., and Méziane, C. (2023). 3D simulation of active thin structures in a viscous fluid and application to mucociliary transport. working paper or preprint.

[Decoene et al., 2020] Decoene, A., Martin, S., and Vergnet, F. (2020). A continuum active structure model for the interaction of cilia with a viscous fluid. *ZAMM-Journal of Applied Mathematics and Mechanics/Zeitschrift für Angewandte Mathematik und Mechanik*, page e202100534.

[Degroote et al., 2008] Degroote, J., Bruggeman, P., Haelterman, R., and Vierendeels, J. (2008). Stability of a coupling technique for partitioned solvers in FSI applications. *Computers & Structures*, 86(23-24):2224–2234.

[Dijkstra and Uittenbogaard, 2010] Dijkstra, J. and Uittenbogaard, R. (2010). Modeling the interaction between flow and highly flexible aquatic vegetation. *Water Resources Research*, 46(12).

[Dimola et al., 2023] Dimola, N., Kuchta, M., Mardal, K.-A., and Zunino, P. (2023). Robust Preconditioning of mixed-dimensional PDEs on 3D-1d domains coupled with Lagrange multipliers. *arXiv preprint arXiv:2307.08431*.

[Donea et al., 1982] Donea, J., Giuliani, S., and Halleux, J.-P. (1982). An arbitrary Lagrangian-Eulerian Finite Element method for transient dynamic fluid-structure interactions. *Computer methods in applied mechanics and engineering*, 33(1-3):689–723.

[Ern and Guermond, 2004] Ern, A. and Guermond, J.-L. (2004). *Theory and practice of finite elements*, volume 159. Springer.

[Ern and Guermond, 2021] Ern, A. and Guermond, J.-L. (2021). *Finite elements I: Approximation and interpolation*, volume 72. Springer Nature.

[Eugster, 2015] Eugster, S. R. (2015). *Geometric continuum mechanics and induced beam theories*. Springer.

[Evans, 1998] Evans, L. C. (1998). *Partial differential equations*, volume 19 of *Graduate Studies in Mathematics*. American Mathematical Society, Providence, RI.

[Feng et al., 1994a] Feng, J., Hu, H. H., and Joseph, D. D. (1994a). Direct simulation of initial value problems for the motion of solid bodies in a Newtonian fluid part 1. Sedimentation. *Journal of Fluid Mechanics*, 261:95–134.

[Feng et al., 1994b] Feng, J., Hu, H. H., and Joseph, D. D. (1994b). Direct simulation of initial value problems for the motion of solid bodies in a Newtonian fluid. part 2. Couette and Poiseuille flows. *Journal of fluid mechanics*, 277:271–301.

[Feng and Michaelides, 2004] Feng, Z.-G. and Michaelides, E. E. (2004). The Immersed Boundary-latticee Boltzmann method for solving fluid–particles interaction problems. *Journal of computational physics*, 195(2):602–628.

[Fernández, 2013] Fernández, M. A. (2013). Incremental displacement-correction schemes for incompressible fluid-structure interaction: stability and convergence analysis. *Numerische Mathematik*, 123(1):21–65.

[Fernández and Gerbeau, 2009] Fernández, M. A. and Gerbeau, J.-F. (2009). *Algorithms for fluid-structure interaction problems*, pages 307–346. Springer Milan, Milano.

[Fernández et al., 2015a] Fernández, M. A., Landajuela, M., and Vidrascu, M. (2015a). Fully decoupled time-marching schemes for incompressible fluid/thin-walled structure interaction. *Journal of Computational Physics*, 297:156–181.

[Fernández and Moubachir, 2005a] Fernández, M. A. and Moubachir, M. (2005a). A Newton method using exact jacobians for solving fluid–structure coupling. *Computers & Structures*, 83(2-3):127–142.

[Fernández and Moubachir, 2005b] Fernández, M. A. and Moubachir, M. (2005b). A Newton method using exact jacobians for solving fluid-structure coupling. *Computers & Structures*, 83:127–142.

[Fernández et al., 2013] Fernández, M. A., Mullaert, J., and Vidrascu, M. (2013). Explicit Robin–Neumann schemes for the coupling of incompressible fluids with thin-walled structures. *Computer Methods in Applied Mechanics and Engineering*, 267:566–593.

[Fernández et al., 2015b] Fernández, M. A., Mullaert, J., and Vidrascu, M. (2015b). Generalized Robin–Neumann explicit coupling schemes for incompressible fluid-structure interaction: Stability analysis and numerics. *International Journal for Numerical Methods in Engineering*, 101(3):199–229.

[Förster et al., 2007] Förster, C., Wall, W. A., and Ramm, E. (2007). Artificial added mass instabilities in sequential staggered coupling of nonlinear structures and incompressible viscous flows. *Computer methods in applied mechanics and engineering*, 196(7):1278–1293.

[Gay, 1968] Gay, N. (1968). The motion of rigid particles embedded in a viscous fluid during pure shear deformation of the fluid. *Tectonophysics*, 5(2):81–88.

[Gee et al., 2011] Gee, M. W., Küttler, U., and Wall, W. (2011). Truly monolithic algebraic multigrid for fluid–structure interaction. *International Journal for Numerical Methods in Engineering*, 85(8):987–1016.

[Gerardo-Giorda et al., 2010] Gerardo-Giorda, L., Nobile, F., and Vergara, C. (2010). Analysis and optimization of Robin–Robin partitioned procedures in fluid-structure interaction problems. *SIAM Journal on Numerical Analysis*, 48(6):2091–2116.

[Gigante and Vergara, 2021] Gigante, G. and Vergara, C. (2021). On the stability of a loosely-coupled scheme based on a Robin interface condition for fluid-structure interaction. *Computers & Mathematics with Applications*, 96:109–119.

[Girault and Glowinski, 1995] Girault, V. and Glowinski, R. (1995). Error analysis of a Fictitious Domain method applied to a Dirichlet problem. *Japan Journal of Industrial and Applied Mathematics*, 12:487–514.

[Girault et al., 2002] Girault, V., Glowinski, R., and Pan, T. W. (2002). *A Fictitious-Domain Method with Distributed Multiplier for the Stokes Problem*, pages 159–174. Springer US, Boston, MA.

[Giroire, 1987] Giroire, J. (1987). *Etude de quelques problemes aux limites extérieurs et résolution par équations intégrales*. PhD thesis, Paris 6.

[Glowinski et al., 1999a] Glowinski, R., Pan, T., Hesla, T. I., and Joseph, D. (1999a). A distributed Lagrange multiplier/Fictitious Domain method for particulate flows. *International Journal of Multiphase Flow*, 25:755–794.

[Glowinski et al., 1999b] Glowinski, R., Pan, T.-W., Hesla, T. I., and Joseph, D. D. (1999b). A distributed Lagrange multiplier/Fictitious Domain method for particulate flows. *International Journal of Multiphase Flow*, 25(5):755–794.

[Glowinski et al., 2001] Glowinski, R., Pan, T.-W., Hesla, T. I., Joseph, D. D., and Periaux, J. (2001). A Fictitious Domain approach to the direct numerical simulation of incompressible viscous flow past moving rigid bodies: application to particulate flow. *Journal of computational physics*, 169(2):363–426.

[Glowinski et al., 1994] Glowinski, R., Pan, T.-W., and Periaux, J. (1994). A Fictitious Domain method for external incompressible viscous flow modeled by Navier-Stokes equations. *Computer Methods in Applied Mechanics and Engineering*, 112(1-4):133–148.

[Gong et al., 2014] Gong, W., Wang, G., and Yan, N. (2014). Approximations of elliptic optimal control problems with controls acting on a lower dimensional manifold. *SIAM journal on Control and Optimization*, 52(3):2008–2035.

[Grandmont, 2008] Grandmont, C. (2008). Existence of weak solutions for the unsteady interaction of a viscous fluid with an elastic plate. *SIAM journal on mathematical analysis*, 40(2):716–737.

[Grandmont and Hillairet, 2016] Grandmont, C. and Hillairet, M. (2016). Existence of global strong solutions to a beam–fluid interaction system. *Archive for Rational Mechanics and Analysis*, 220:1283–1333.

[Grandmont et al., 2019] Grandmont, C., Hillairet, M., and Lequeurre, J. (2019). Existence of local strong solutions to fluid–beam and fluid–rod interaction systems. In *Annales de l'Institut Henri Poincaré C, Analyse non linéaire*, volume 36, pages 1105–1149. Elsevier.

[Griffith and Lim, 2012] Griffith, B. E. and Lim, S. (2012). Simulating an elastic ring with bend and twist by an adaptive generalized Immersed Boundary method. *Communications in Computational Physics*, 12:433–461.

[Groß and Reusken, 2007] Groß, S. and Reusken, A. (2007). An extended pressure finite element space for two-phase incompressible flows with surface tension. *Journal of Computational Physics*, 224(1):40–58.

[Guidoboni et al., 2009] Guidoboni, G., Glowinski, R., Cavallini, N., and Canic, S. (2009). Stable loosely-coupled-type algorithm for fluid–structure interaction in blood flow. *Journal of Computational Physics*, 228(18):6916–6937.

[Guillaume and Idris, 2002] Guillaume, P. and Idris, K. S. (2002). The topological asymptotic expansion for the Dirichlet problem. *SIAM journal on Control and Optimization*, 41(4):1042–1072.

[Guzmán and Neilan, 2014] Guzmán, J. and Neilan, M. (2014). Conforming and divergence-free Stokes elements on general triangular meshes. *Mathematics of Computation*, 83(285):15–36.

[Hagmeyer et al., 2023] Hagmeyer, N., Mayr, M., and Popp, A. (2023). A fully coupled regularized mortar-type finite element approach for embedding one-dimensional fibers into three-dimensional fluid flow.

[Hagmeyer et al., 2022] Hagmeyer, N., Mayr, M., Steinbrecher, I., and Popp, A. (2022). One-way coupled fluid–beam interaction: capturing the effect of embedded slender bodies on global fluid flow and vice versa. *Advanced Modeling and Simulation in Engineering Sciences*, 9.

[Hansbo and Hansbo, 2002] Hansbo, A. and Hansbo, P. (2002). An unfitted Finite Element method, based on Nitsche's method, for elliptic interface problems. *Computer methods in applied mechanics and engineering*, 191(47-48):5537–5552.

[Hansbo, 2005] Hansbo, P. (2005). Nitsche's method for interface problems in computational mechanics. *GAMM-Mitteilungen*, 28(2):183–206.

[Haslinger and Renard, 2009] Haslinger, J. and Renard, Y. (2009). A new Fictitious Domain approach inspired by the extended Finite Element method. *SIAM Journal on Numerical Analysis*, 47(2):1474–1499.

[Heltai and Zunino, 2023] Heltai, L. and Zunino, P. (2023). Reduced Lagrange multiplier approach for non-matching coupling of mixed-dimensional domains. *arXiv preprint arXiv:2303.10600*.

[Henrot and Pierre, 2006] Henrot, A. and Pierre, M. (2006). *Variation et optimisation de formes: une analyse géométrique*, volume 48. Springer Science & Business Media.

[Hirt et al., 1974] Hirt, C. W., Amsden, A. A., and Cook, J. (1974). An arbitrary Lagrangian-Eulerian computing method for all flow speeds. *Journal of computational physics*, 14(3):227–253.

[Hong and Shah, 2018] Hong, K.-S. and Shah, U. H. (2018). Vortex-induced vibrations and control of marine risers: A review. *Ocean Engineering*, 152:300–315.

[Hsiao and Wendland, 2008] Hsiao, G. C. and Wendland, W. L. (2008). *Boundary integral equations*. Springer.

[Hu et al., 1992] Hu, H. H., Joseph, D. D., and Crochet, M. J. (1992). Direct simulation of fluid particle motions. *Theoretical and Computational Fluid Dynamics*, 3(5):285–306.

[Huang et al., 2019] Huang, D. Z., Avery, P., and Farhat, C. (2019). An embedded boundary approach for resolving the contribution of cable subsystems to fully coupled fluid-structure interaction. *International Journal for Numerical Methods in Engineering*, 122:5409 – 5429.

[Huang et al., 2021] Huang, D. Z., Avery, P., and Farhat, C. (2021). An embedded boundary approach for resolving the contribution of cable subsystems to fully coupled fluid-structure interaction. *International Journal for Numerical Methods in Engineering*, 122(19):5409–5429.

[Janela et al., 2005] Janela, J., Lefebvre, A., and Maury, B. (2005). A penalty method for the simulation of fluid-rigid body interaction. In *ESAIM: Proceedings*, volume 14, pages 115–123. EDP Sciences.

[Johnson and Tezduyar, 1997] Johnson, A. A. and Tezduyar, T. E. (1997). 3d simulation of fluid-particle interactions with the number of particles reaching 100. *Computer Methods in Applied Mechanics and Engineering*, 145(3-4):301–321.

[Kallemov et al., 2016] Kallemov, B., Bhalla, A., Griffith, B., and Donev, A. (2016). An Immersed Boundary method for rigid bodies. *Communications in Applied Mathematics and Computational Science*, 11(1):79–141.

[Khristenko et al., 2021] Khristenko, U., Schuß, S., Krüger, M., Schmidt, F., Wohlmuth, B., and Hesch, C. (2021). Multidimensional coupling: A variationally consistent approach to fiber-reinforced materials. *Computer Methods in Applied Mechanics and Engineering*, 382:113869.

[Kirchhoff, 1850] Kirchhoff, G. (1850). Über das Gleichgewicht und die Bewegung einer elastischen Scheibe. *Journal für die reine und angewandte Mathematik (Crelles Journal)*, 1850(40):51–88.

[Kirchhoff, 1859] Kirchhoff, G. (1859). Ueber das gleichgewicht und die bewegung eines unendlich dünnen elastischen stabes.

[Kleinstreuer and Zhang, 2003] Kleinstreuer, C. and Zhang, Z. (2003). Laminar-to-turbulent fluid-particle flows in a human airway model. *International Journal of Multiphase Flow*, 29(2):271–289.

[Kleinstreuer and Zhang, 2010] Kleinstreuer, C. and Zhang, Z. (2010). Airflow and particle transport in the human respiratory system. *Annual review of fluid mechanics*, 42:301–334.

[Kounchev, 2001] Kounchev, O. (2001). *Multivariate polysplines: applications to numerical and wavelet analysis*. Academic Press.

[Krenk, 2009] Krenk, S. (2009). *Co-rotating beam elements*, page 100–144. Cambridge University Press.

[Kuchta et al., 2020] Kuchta, M., Laurino, F., Mardal, K., and Zunino, P. (2020). Analysis and approximation of mixed-dimensional PDEs on 3D-1D domains coupled with Lagrange multipliers. *ArXiv*, abs/2004.02722.

[Kuchta et al., 2021a] Kuchta, M., Laurino, F., Mardal, K.-A., and Zunino, P. (2021a). Analysis and approximation of mixed-dimensional PDEs on 3d-1d domains coupled with Lagrange multipliers. *SIAM Journal on Numerical Analysis*, 59(1):558–582.

[Kuchta et al., 2021b] Kuchta, M., Laurino, F., Mardal, K.-A., and Zunino, P. (2021b). Analysis and Approximation of Mixed-Dimensional PDEs on 3D-1D Domains Coupled with Lagrange Multipliers. *SIAM Journal on Numerical Analysis*, 59(1):558–582.

[Köppl et al., 2018] Köppl, T., Vidotto, E., Wohlmuth, B., and Zunino, P. (2018). Mathematical modeling, analysis and numerical approximation of second-order elliptic problems with inclusions. *Mathematical Models and Methods in Applied Sciences*, 28(5):953–978.

[Ladd, 1994a] Ladd, A. J. (1994a). Numerical simulations of particulate suspensions via a discretized Boltzmann equation. part 1. Theoretical foundation. *Journal of fluid mechanics*, 271:285–309.

[Ladd, 1994b] Ladd, A. J. (1994b). Numerical simulations of particulate suspensions via a discretized Boltzmann equation. part 2. Numerical results. *Journal of fluid mechanics*, 271:311–339.

[Ladd and Verberg, 2001] Ladd, A. J. and Verberg, R. (2001). Lattice-Boltzmann simulations of particle-fluid suspensions. *Journal of statistical physics*, 104:1191–1251.

[Lai et al., 2009] Lai, S. K., Wang, Y.-Y., Wirtz, D., and Hanes, J. (2009). Micro-and macrorheology of mucus. *Advanced drug delivery reviews*, 61(2):86–100.

[Landajuela et al., 2017] Landajuela, M., Vidrascu, M., Chapelle, D., and Fernández, M. A. (2017). Coupling schemes for the FSI forward prediction challenge: Comparative study and validation. *International Journal for Numerical Methods in Biomedical Engineering*, 33.

[Lauga and Powers, 2009] Lauga, E. and Powers, T. R. (2009). The hydrodynamics of swimming microorganisms. *Reports on progress in physics*, 72(9):096601.

[Lengeler, 2014] Lengeler, D. (2014). Weak solutions for an incompressible, generalized newtonian fluid interacting with a linearly elastic koiter type shell. *SIAM Journal on Mathematical Analysis*, 46(4):2614–2649.

[Lequeurre, 2011] Lequeurre, J. (2011). Existence of strong solutions to a fluid-structure system. *SIAM journal on mathematical analysis*, 43(1):389–410.

[Lespagnol et al., 2023] Lespagnol, F., Grandmont, C., Zunino, P., and Fernández, M. A. (2023). A mixed-dimensional formulation for the simulation of slender structures immersed in an incompressible flow. working paper or preprint.

[Li et al., 2010] Li, J., Luo, Q., Xie, Z., Li, Y., and Zeng, Y. (2010). Fatigue life analysis and experimental verification of coronary stent. *Heart and vessels*, 25:333–337.

[Liron and Mochon, 1976] Liron, N. and Mochon, S. (1976). The discrete-cilia approach to propulsion of ciliated micro-organisms. *Journal of Fluid Mechanics*, 75(3):593–607.

[Liu et al., 2007] Liu, W. K., Kim, D. W., and Tang, S. (2007). Mathematical foundations of the immersed Finite Element method. *Computational Mechanics*, 39:211–222.

[Liu et al., 2012] Liu, Z., Liu, Y., and Lu, J. (2012). Numerical simulation of the fluid–structure interaction for an elastic cylinder subjected to tubular fluid flow. *Computers & Fluids*, 68:192–202.

[Love, 2013] Love, A. E. H. (2013). *A treatise on the mathematical theory of elasticity*. Cambridge university press.

[Luhar et al., 2008] Luhar, M., Rominger, J., and Nepf, H. (2008). Interaction between flow, transport and vegetation spatial structure. *Environmental Fluid Mechanics*, 8:423–439.

[Maniyeri and Kang, 2012] Maniyeri, R. and Kang, S. (2012). Numerical study on the rotation of an elastic rod in a viscous fluid using an Immersed Boundary method. *Journal of Mechanical Science and Technology*, 26:1515–1522.

[Marrey et al., 2006] Marrey, R. V., Burgermeister, R., Grishaber, R. B., and Ritchie, R. (2006). Fatigue and life prediction for cobalt-chromium stents: A fracture mechanics analysis. *Biomaterials*, 27(9):1988–2000.

[mathematics for bio-medical applications, 2023] mathematics for bio-medical applications, C. C. (2023). https://gitlab.inria.fr/felisce/felisce.

[Maxian and Peskin, 2020] Maxian, O. and Peskin, C. S. (2020). An Immersed Boundary method with subgrid resolution and improved numerical stability applied to slender bodies in Stokes flow. *SIAM Journal on Scientific Computing*, 42(4):B847–B868.

[Maz'Ya et al., 2000] Maz'Ya, V., Nazarov, S., and Plamenevskij, B. (2000). *Asymptotic theory of elliptic boundary value problems in singularly perturbed domains*, volume 1. Springer Science & Business Media.

[Maz'ya and Nazarov, 1987] Maz'ya, V. G. and Nazarov, S. A. (1987). Asymptotic behavior of energy integrals under small perturbations of the boundary near corner and conic points. *Trudy Moskovskogo Matematicheskogo Obshchestva*, 50:79–129.

[Maz'ya et al., 1984] Maz'ya, V. G., Nazarov, S. A., and Plamenevskii, B. A. (1984). Asymptotic expansions of the eigenvalues of boundary value problems for the Laplace operator in domains with small holes. *Izvestiya Rossiiskoi Akademii Nauk. Seriya Matematicheskaya*, 48(2):347–371.

[Maz'ya and Poborchi, 1998] Maz'ya, V. G. and Poborchi, S. V. (1998). *Differentiable Functions on Bad Domains*. WORLD SCIENTIFIC.

[Meier et al., 2019] Meier, C., Popp, A., and Wall, W. A. (2019). Geometrically exact Finite Element formulations for slender beams: Kirchhoff–Love theory versus Simo–Reissner theory. *Archives of Computational Methods in Engineering*, 26(1):163–243.

[Mitran, 2007] Mitran, S. M. (2007). Metachronal wave formation in a model of pulmonary cilia. *Computers & structures*, 85(11-14):763–774.

[Mori and Ohm, 2021] Mori, Y. and Ohm, L. (2021). Accuracy of slender body theory in approximating force exerted by thin fiber on viscous fluid. *Studies in Applied Mathematics*, 147(1):127–179.

[Mori et al., 2018] Mori, Y., Ohm, L., and Spirn, D. (2018). Theoretical Justification and Error Analysis for Slender Body Theory with Free Ends. *Archive for Rational Mechanics and Analysis*, 235:1905–1978.

[Muddle et al., 2012] Muddle, R. L., Mihajlović, M., and Heil, M. (2012). An efficient preconditioner for monolithically-coupled large-displacement fluid–structure interaction problems with pseudo-solid mesh updates. *Journal of Computational Physics*, 231(21):7315–7334.

[Muha and Canić, 2013] Muha, B. and Canić, S. (2013). Existence of a weak solution to a nonlinear fluid–structure interaction problem modeling the flow of an incompressible, viscous fluid in a cylinder with deformable walls. *Archive for rational mechanics and analysis*, 207:919–968.

[Nazarov, 1999] Nazarov, S. (1999). Asymptotic conditions at a point, selfadjoint extensions of operators, and the method of matched asymptotic expansions. *Translations of the American Mathematical Society-Series 2*, 193:77–126.

[Nazarov and Sokołowski, 2003] Nazarov, S. A. and Sokołowski, J. (2003). Asymptotic analysis of shape functionals. *Journal de Mathématiques pures et appliquées*, 82(2):125–196.

[Nepf and Vivoni, 2000] Nepf, H. M. and Vivoni, E. (2000). Flow structure in depth-limited, vegetated flow. *Journal of Geophysical Research: Oceans*, 105(C12):28547–28557.

[Nobile, 2001] Nobile, F. (2001). Numerical approximation of fluid-structure interaction problems with application to haemodynamics. Technical report, EPFL.

[Nobile and Vergara, 2008] Nobile, F. and Vergara, C. (2008). An effective fluid-structure interaction formulation for vascular dynamics by generalized Robin conditions. *SIAM Journal on Scientific Computing*, 30(2):731–763.

[Ohmori and Saito, 2007] Ohmori, K. and Saito, N. (2007). Flux-free Finite Element method with Lagrange Multipliers for Two-fluid Flows. *Journal of Scientific Computing*, 32:147–173.

[Oyekole et al., 2018] Oyekole, O., Trenchea, C., and Bukac, M. (2018). A second-order in time approximation of fluid-structure interaction problem. *SIAM Journal on Numerical Analysis*, 56(1):590–613.

[Peskin, 1972] Peskin, C. S. (1972). Flow patterns around heart valves: a numerical method. *Journal of computational physics*, 10(2):252–271.

[Polwaththe Gallage et al., 2012] Polwaththe Gallage, P. G. H., Gu, Y., Saha, S., Senadeera, W., and Oloyede, A. (2012). Numerical simulation of red blood cells' motion: a review. In *Proceedings of the 4th International Conference on Computational Methods*, pages 1–8. Queensland University of Technology.

[Reissner, 1972] Reissner, E. (1972). On one-dimensional finite-strain beam theory: the plane problem. *Zeitschrift für angewandte Mathematik und Physik ZAMP*, 23(5):795–804.

[Richter, 2015] Richter, T. (2015). A monolithic geometric multigrid solver for fluid-structure interactions in ALE formulation. *International journal for numerical methods in engineering*, 104(5):372–390.

[Roussel et al., 2007] Roussel, N., Geiker, M. R., Dufour, F., Thrane, L. N., and Szabo, P. (2007). Computational modeling of concrete flow: General overview. *Cement and Concrete research*, 37(9):1298–1307.

[Sarrate et al., 2001] Sarrate, J., Huerta, A., and Donea, J. (2001). Arbitrary Lagrangian–Eulerian formulation for fluid–rigid body interaction. *Computer methods in applied mechanics and engineering*, 190(24-25):3171–3188.

[Scott and Zhang, 1990] Scott, L. R. and Zhang, S. (1990). Finite element interpolation of nonsmooth functions satisfying boundary conditions. *Mathematics of Computation*, 54(190):483–493.

[Sid Idris, 2001] Sid Idris, K. (2001). *Sensibilité topologique en optimisation de forme*. PhD thesis, Toulouse, INSA.

[Simo, 1985] Simo, J. C. (1985). A finite strain beam formulation. the three-dimensional dynamic problem. Part I. *Computer methods in applied mechanics and engineering*, 49(1):55–70.

[Simo and Vu-Quoc, 1986] Simo, J. C. and Vu-Quoc, L. (1986). A three-dimensional finite-strain rod model. Part II: Computational aspects. *Computer methods in applied mechanics and engineering*, 58(1):79–116.

[Smith et al., 2007] Smith, D., Gaffney, E., and Blake, J. (2007). Discrete cilia modelling with singularity distributions: application to the embryonic node and the airway surface liquid. *Bulletin of mathematical biology*, 69:1477–1510.

[Steinbrecher et al., 2020] Steinbrecher, I., Mayr, M., Grill, M. J., Kremheller, J., Meier, C., and Popp, A. (2020). A mortar-type finite element approach for embedding 1D beams into 3D solid volumes. *Computational Mechanics*, 66:1377–1398.

[Takashi and Hughes, 1992] Takashi, N. and Hughes, T. J. (1992). An arbitrary Lagrangian-Eulerian Finite Element method for interaction of fluid and a rigid body. *Computer methods in applied mechanics and engineering*, 95(1):115–138.

[Tezduyar, 1991] Tezduyar, T. (1991). *Stabilized Finite Element Formulations for Incompressible Flow Computations*, volume 28. Elsevier.

[Timoshenko, 1921] Timoshenko, S. P. (1921). On the correction for shear of the differential equation for transverse vibrations of prismatic bars. *Phil Mag Ser*, 41:744–764.

[Timoshenko, 1922] Timoshenko, S. P. (1922). X. on the transverse vibrations of bars of uniform cross-section. *The London, Edinburgh, and Dublin Philosophical Magazine and Journal of Science*, 43(253):125–131.

[Tornberg and Gustavsson, 2006] Tornberg, A.-K. and Gustavsson, K. (2006). A numerical method for simulations of rigid fiber suspensions. *J. Comput. Phys.*, 215:172–196.

[Tornberg and Shelley, 2004] Tornberg, A.-K. and Shelley, M. J. (2004). Simulating the dynamics and interactions of flexible fibers in Stokes flows. *Journal of Computational Physics*, 196:8–40.

[Tschisgale and Fröhlich, 2020] Tschisgale, S. and Fröhlich, J. (2020). An Immersed Boundary method for the fluid-structure interaction of slender flexible structures in viscous fluid. *J. Comput. Phys.*, 423:109801.

[Tu et al., 2012] Tu, J., Inthavong, K., and Ahmadi, G. (2012). *Computational fluid and particle dynamics in the human respiratory system*. Springer Science & Business Media.

[Tuković et al., 2019] Tuković, Ž., Bukač, M., Cardiff, P., Jasak, H., and Ivanković, A. (2019). Added mass partitioned fluid–structure interaction solver based on a robin boundary condition for pressure. In *OpenFOAM®: Selected Papers of the 11th Workshop*, pages 1–22. Springer.

[Uhlmann, 2005] Uhlmann, M. (2005). An Immersed Boundary method with direct forcing for the simulation of particulate flows. *Journal of computational physics*, 209(2):448–476.

[Van Brummelen, 2011] Van Brummelen, E. (2011). Partitioned iterative solution methods for fluid–structure interaction. *International Journal for Numerical Methods in Fluids*, 65(1-3):3–27.

[Vanaki et al., 2020] Vanaki, S. M., Holmes, D., Saha, S. C., Chen, J., Brown, R. J., and Jayathilake, P. G. (2020). Muco-ciliary clearance: A review of modelling techniques. *Journal of biomechanics*, 99:109578.

[Västilä and Järvelä, 2018] Västilä, K. and Järvelä, J. (2018). Characterizing natural riparian vegetation for modeling of flow and suspended sediment transport. *Journal of Soils and Sediments*, 18:3114–3130.

[Veeramani et al., 2007] Veeramani, C., Minev, P. D., and Nandakumar, K. (2007). A Fictitious Domain formulation for flows with rigid particles: a non-Lagrange multiplier version. *Journal of Computational Physics*, 224(2):867–879.

[Wagner et al., 2003] Wagner, G. J., Ghosal, S., and Liu, W. K. (2003). Particulate flow simulations using lubrication theory solution enrichment. *International Journal for Numerical Methods in Engineering*, 56(9):1261–1289.

[Wagner et al., 2001] Wagner, G. J., Moës, N., Liu, W. K., and Belytschko, T. (2001). The extended Finite Element method for rigid particles in Stokes flow. *International Journal for Numerical Methods in Engineering*, 51(3):293–313.

[Wang et al., 2022] Wang, C., Ren, B., and Lin, P. (2022). A coupled flow and beam model for fluid–slender body interaction. *Journal of Fluids and Structures*, 115:103781.

[Wang et al., 2015] Wang, C., Zheng, S.-s., Wang, P.-f., and Hou, J. (2015). Interactions between vegetation, water flow and sediment transport: A review. *Journal of Hydrodynamics*, 27(1):24–37.

[Wang and Xiao, 2016] Wang, E. and Xiao, Q. (2016). Numerical simulation of vortex-induced vibration of a vertical riser in uniform and linearly sheared currents. *Ocean Engineering*, 121:492–515.

[Wang et al., 2019] Wang, M., Avital, E. J., Bai, X., Ji, C., Xu, D., Williams, J. J. R., and Munjiza, A. (2019). Fluid–structure interaction of flexible submerged vegetation stems and kinetic turbine blades. *Computational Particle Mechanics*, 7:839 – 848.

[Weinbaum et al., 1990] Weinbaum, S., Ganatos, P., and Yan, Z. (1990). Numerical multipole and boundary integral equation techniques in Stokes flow. *Annual review of fluid mechanics*, 22(1):275–316.

[Wiens and Stockie, 2015] Wiens, J. K. and Stockie, J. M. (2015). Simulating flexible fiber suspensions using a scalable Immersed Boundary algorithm. *Computer Methods in Applied Mechanics and Engineering*, 290:1–18.

[Wu et al., 2012] Wu, X., Ge, F., and Hong, Y. (2012). A review of recent studies on vortex-induced vibrations of long slender cylinders. *Journal of Fluids and structures*, 28:292–308.

[Yashiro et al., 2011] Yashiro, S., Okabe, T., and Matsushima, K. (2011). A numerical approach for injection molding of short-fiber-reinforced plastics using a particle method. *Advanced Composite Materials*, 20(6):503–517.

[Ye et al., 2016] Ye, T., Phan-Thien, N., and Lim, C. T. (2016). Particle-based simulations of red blood cells—A review. *Journal of biomechanics*, 49(11):2255–2266.

[Yeo and Maxey, 2010] Yeo, K. and Maxey, M. R. (2010). Simulation of concentrated suspensions using the force-coupling method. *Journal of computational physics*, 229(6):2401–2421.

[Zhang et al., 2004] Zhang, L., Gerstenberger, A., Wang, X., and Liu, W. K. (2004). Immersed Finite ElementMethod. *Computer Methods in Applied Mechanics and Engineering*, 193(21-22):2051–2067.

[Zunino et al., 2016] Zunino, P., Tambača, J., Cutrì, E., Čanić, S., Formaggia, L., and Migliavacca, F. (2016). Integrated stent models based on dimension reduction: review and future perspectives. *Annals of biomedical engineering*, 44:604–617.

[Zygmund, 2002] Zygmund, A. (2002). *Trigonometric series*, volume 1. Cambridge university press.